ALMA MATER STUDIORUM
UNIVERSITÀ DI BOLOGNA

Facoltà di Scienze Matematiche Fisiche e Naturali
Dipartimento di Astronomia

DOTTORATO DI RICERCA IN ASTRONOMIA

CICLO XXII (2007-2009)

RR LYRAE STARS IN M31 FIELD AND GLOBULAR CLUSTERS: HOW DID ANDROMEDA FORM?

Tesi di Dottorato
di

Rodrigo Contreras Ramos

COORDINATORE:	**Chiar.mo Prof. Lauro Moscardini**
RELATORE:	**Chiar.mo Prof. Bruno Marano**
CO-RELATORI:	**Dott.ssa Gisella Clementini** **Dott.ssa Luciana Federici**

Esame Finale Anno 2010

SCUOLA DI DOTTORATO IN SCIENZE MATEMATICHE, FISICHE E ASTRONOMICHE
SETTORE SCIENTIFICO DISCIPLINARE: AREA 02 - SCIENZE FISICHE
FIS/05 ASTRONOMIA E ASTROFISICA

A la BuiBui, al Pitufon y a Bebuisina

Contents

1 How do galaxies form? The case of the Milky Way 6

1.1 Cloud Collapse Model for the Milky Way 8

1.2 Hierarchical Model for the Milky Way 10

1.3 "Building Blocks" of The Milky Way 14

1.3.1 RR Lyrae Stars: Real Eyewitnesses of galaxy formation 17

1.3.2 New Pieces of the Puzzle, New Clues 19

2 Variable Stars as Tools. 23

2.1 Classical Cepheids 25

2.2 Type II Cepheids 26

2.3 Anomalous Cepheids 29

2.4 RR Lyrae stars 30

2.4.1 The Oosterhoff Dicothomy 32

2.4.2 Physical Origin of the Oosterhoff Dicothomy 35

2.4.3 What causes the Oosterhoff dichotomy in the MW? 37

2.4.4 The Oosterhoff dichotomy: a formation dichotomy? 38

3 The Andromeda Galaxy 40

3.1 A bit of History 41

3.2 Canonical Structure 41

3.2.1 Nucleus & Disk 42

3.2.2 The Spheroid (Bulge & Halo) 43

3.2.3 The Globular Cluster system 45

3.2.4 Scars of a Violent History 47

3.3 RR Lyrae stars in Andromeda: Previous Works 50

4 Variable stars in M31: Globular Clusters 57

4.1 Observations 58

4.2 Data Reduction: HSTphot & DOLPHOT 61

4.3 Variable star identification and Period Search 62

4.4 The case of Bologna 514 (B514) 64

4.4.1 Variable Stars 66

4.4.2 CMD and Distance 72

4.5 RR Lyrae stars in G11, G33, G76, G105 and G322 75

4.5.1 CMDs, Variable Stars, and Distances 76

4.5.2 Oosterhoff Classification 81

5 Variable Stars in M31: Halo Fields 88

5.1 Observations and Data Reduction 91

5.2 Color Magnitude Diagrams 95

5.3 Variable Stars 104

5.3.1 Comparison with previous variability studies in M31 112

6 Summary, Conclusions & Future works 115

6.1 M31 globular clusters 115

6.2 M31 fields 118

7 Appendix A **121**

8 Appendix B **125**

9 Appendix C **131**

10 Appendix D **147**

11 Appendix E **161**

12 Appendix F **167**

13 Appendix G **179**

14 Appendix H **185**

15 Appendix I **193**

Introduction

As the nearest giant spiral galaxy, Andromeda (M31) provides a unique opportunity to study the structure and evolution of a massive galaxy and, by comparison with the Milky Way (MW), to address the question of variety in the evolutionary histories of massive spirals. Our external view of this system offers a significant advantage, since it reduces complications due to projection and/or line-of-sight effects, that plague the MW studies and, as a result, the structures observed in M31 are easier to study, thus making Andromeda the best current laboratory for investigating faint stellar structures around galaxies.

At a distance of about 800 kpc, M31 is close enough that individual stars in the galaxy field can be resolved and measured with 8m-class telescopes like the Large Binocular Telescope (LBT), reaching the horizontal branch (HB) of the old stellar populations with less than half an hour exposures. Resolving individual stars in the M31 globular clusters (GCs) or in crowded fields requires instead the Hubble Space Telescope (HST).

van den Bergh (2000, 2006) suggested that Andromeda originated as an early merger of two or more relatively massive metal-rich progenitors. This would account for the wide range in metallicity (Durrell, Harris, & Pritchet 2001) and age (Brown et al. 2003) observed in the M31 halo, compared to the MW. M31 hosts spectacular signatures of present and past merging events like the giant tidal stream (Ibata et al. 2001) extending several degrees from the center of the galaxy (McConnachie et al. 2003), and the arc-like overdensity connecting the galaxy to its dwarf elliptical companion NGC205 (McConnachie et al. 2004).

Ferguson et al. (2002) and Ibata et al. (2007) presented the first panoramic views of the Andromeda galaxy, based on deep Isaac Newton Telescope (INT) and Canada-France-Hawaii Telescope (CFHT) photometric observations that cover respectively the galaxy inner 55 kpc, and the southern quadrant out to about 150 kpc, with an extension that reaches M33 at a distance of about 200 kpc. Their data show the giant stream in all its extension and reveal also a multitude of streams, arcs and many other large-scale structures of low surface brightness, as well as two new M31 dwarf companions (And XV and And XVI).

The primary tool to understand the formation history of a galaxy is the analysis of color magnitude diagrams (CMDs) deep to the main-sequence turn-off (TO) of the oldest populations. However, the TO of the oldest stars in M31 ($V \sim 28.5$ mag) is still unreachable by the largest ground-based telescopes, and required hundred orbits of HST/ACS time entirely devoted to "tiny" ($3'.5 \times 3'.7$) portions of the galaxy (Brown et al. 2003, 2006, 2008).

The pulsating variable stars may offer a powerful alternative tool to trace stars of different age in a galaxy since variables of different types arise from parent populations of different age (old: RR Lyrae stars and Population II Cepheids; intermediate age: Anomalous Cepheids – ACs –; young: Classical Cepheids). The RR Lyrae stars, in particular, belonging to the oldest stellar population (t > 10 Gyr), have eyewitnessed the formation of their host galaxies, and thus can allow to reconstruct the star formation history (SFH) back to the first epochs of galaxy formation. These variables are also about 3 magnitude brighter, hence much more easy to observe, than coeval TO stars, and the typical form of their light variation makes them much more easy to recognize than old non-variable stars, in crowded fields dominated by younger stars.

My PhD thesis is part of a large project aimed at studing the variable star population in properly selected fields and globular clusters of the Andromeda galaxy. The Wide Field Planetary Camera 2 (WFPC2) on board the HST has been used to resolve and study variable stars in six M31 globular clusters (GCs), and the wide field capabilities of the LBT were used to study the field star population in selected areas of the M31 halo and giant stream. The study of the M31 variable stars, and in particular the study of the pulsation properties of the RR Lyrae stars holds a crucial role for identifying the "building blocks" of galactic halos and for understanding which galaxy formation scenario (merger/accretion or cloud collapse) is dominant. In the MW almost all GCs which contain significant numbers of RR Lyrae stars sharply divide into two very distinct classes, the Oosterhoff types (Oosterhoff 1939), according to the mean pulsation periods of their RR Lyrae stars, and it is likely that this dichotomy reflects conditions within the MW halo at the time of GC formation.

In M31 the situation is completely unknown. We do not really know whether the M31 GCs show the Oosterhoff dichotomy, or whether indeed they can be placed into Oosterhoff groups at all, since no studies have been yet made that define the properties of RR Lyrae stars in the GCs of M31, and the RR Lyrae that have been identified so far in M31 both from ground-based and HST studies (Pritchet & van den Bergh 1987, Dolphin et al. 2004, Brown et al. 2004, Vilardell et al. 2007, Joshi et al. 2009, Sarajedini et al. 2009) all belong to the field population. Based on our HST and LBT data, this thesis work will try to answer the following questions: *i)* Is the Oosterhoff dichotomy a general characteristic of old cluster populations in spiral galaxies similar to our own, or it is a peculiar phenomenon due to the particular evolutionary history of the MW? *ii)* Do the pulsation properties of the RR Lyrae stars in the M31 GCs correlate with metallicity as in the Galactic GCs? *iii)* Can we demostrate that the RR Lyrae stars in the MW and M31 field and GCs share the same properties, and assume this properties as universal in the definition and calibration of the Population II distance scale?

The thesis is organized in 6 chapters and 9 Appendices. The first 3 chapters describe the thesis scientific background. In particular, in Chapter 1, we present a general overview of the 2 main galaxy formation scenarios for the case of the Milky Way. Then, in Chapter 2 we describe the main properties of different types of intrinsic variable stars, and discuss how they can be used in the context of the present thesis. Finally, in Chapter 3 we give a general picture of Andromeda (M31), the galaxy that hosts the targets selected of our study. We also include a brief summary of the works found in literature concerning the study of the RR Lyrae stars in

Andromeda, and conclude the chapter giving the scientific motivations of this thesis work. The second block of 3 chapters forms the heart of the thesis. These chapters describe all the work done and the results obtained in the thesis. Specifically, Chapter 4 describes the study of the variable stars, in particular of RR Lyrae type, in 6 properly selected globular clusters in M31, for which time-series photometry was obtained with the Hubble Space Telescope. In Chapter 5, we focus on the variability study of 2 selected M31 fields, sampling respectively a region close to the giant stream, and the galaxy halo, for which time-series data were obtained with the Large Binocular Telescope. Finally, Chapter 6 gathers the main conclusions of this study, and the related future work. At the end of the thesis, 9 Appendices present the atlas of light curves for each of our selected targets.

Chapter 1

How do galaxies form? The case of the Milky Way

One of the greatest unanswered questions in astrophysics concerns the formation and evolution of galaxies in the Universe. Today it is believed that galaxies, as well as other structures in the Universe, have been formed out of primordial density fluctuations that have grown under the influence of gravity. As the Universe expanded the average density of the cosmic gas would have declined, however, some density enhancements of sufficient size, became more pronounced, thanks to their own gravitational attraction. This attracted matter from surrounding regions, increased still further the lumpiness of the Universe. This process, known as gravitational instability, was therefore responsible for the production of localized regions in which clouds of cosmic gas collapsed despite the general background of expansion (see Fig. 1.1). These collapsing clouds are the supposed seeds of the galaxies and clusters of galaxies.

So, how did these collapsing clouds give rise to the galaxies that we see today? The simplest scenario for galaxy formation is that the collapse of a single over-dense region gives rise to a single galaxy. The mass contained in such a region would therefore correspond to the mass of the resulting galaxy. This type of formation process is often referred to as monolithic collapse

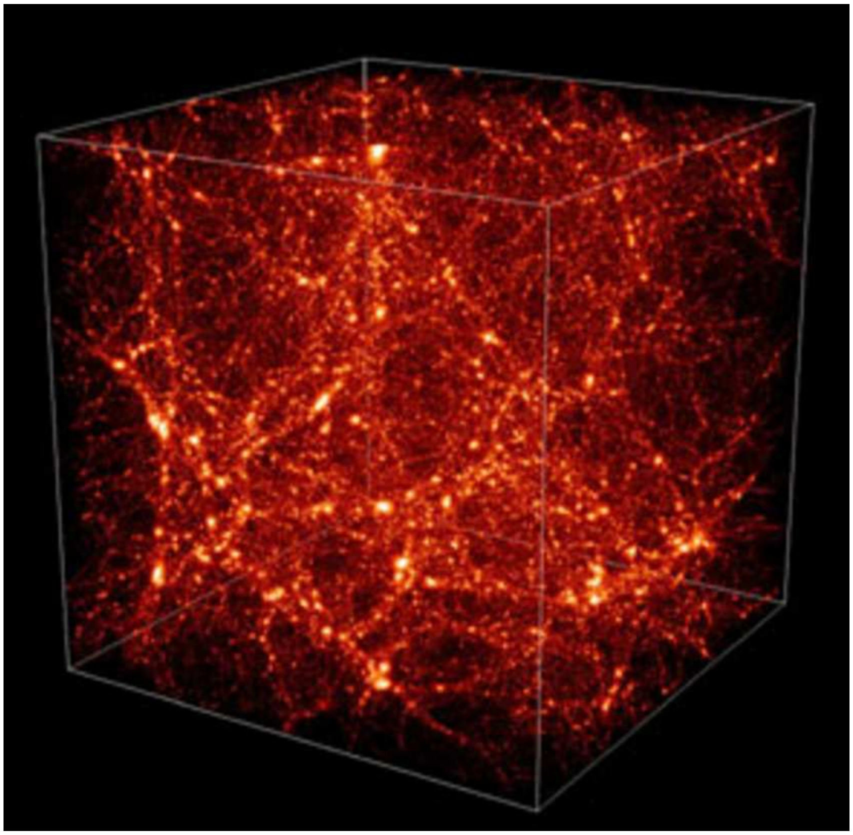

Figure 1.1: The effect of gravitational instabilities in a region of the expanding Universe dominated by dark matter. Regions of enhanced density tend to grow along with the general cosmic expansion, but if sufficiently dense they may eventually defy the expansion and collapse.

scenario. However, the way in which gravitational collapse proceeds depends on the distribution of mass, therefore the most dominant form of matter in the Universe, the dark matter, should play the key role in this process. From the theoretical point of view, two different dynamical behaviors of the dark matter may affect the growth of gravitational instabilities. In one, dark matter consists of slow moving, massive particles. This kind of dark matter is referred as cold dark matter (CMD). The term cold refers to the fact that the hypothetical dark matter particles have random speeds that are small compared with the speed of light. Simulations of gravitational collapse, in a Universe dominated by CDM, reveal that the first structures to form have masses of the order of $10^6 M_\odot$, which is 5 orders of magnitude lower than those typically found for galaxies in the present-day Universe. As time progresses, large scale features develop by further collapse and by merger of the lower mass structures that were form previously. The overall picture is one in which proto-galactic fragments form early in the history of the Universe and many of the galaxies we see today are the results of merging events. This type of process is termed hierarchical scenario or bottom-up scenario, since galaxies are generally formed by amalgamation of smaller entities. The other extreme behavior is one in which the dark matter particles are rapidly moving, and goes under the name of hot dark matter (HDM). The term hot refers to the fact that dark matter particles have speeds that are comparable to the speed of light. One effect of these high speeds is to remove small scale density fluctuations. In this case, the model prediction is that the first entities to form in the Universe would have much larger masses than individual galaxies. Structures with masses similar to the present-day galaxies would form by the fragmentation of these large entities. This type of process is called top-down scenario.

The currently favored theory is that structures in the Universe formed in a bottom-up scenario under the influence of CDM. In such a scenario the first objects formed might be very high mass stars, followed by structures on the scale of GCs and small systems like the dwarf spheroidal galaxies (dSphs). Large galaxies would then form by merging of these smaller components.

1.1 Cloud Collapse Model for the Milky Way

The general notion that the MW reached its present form after a gravity collapse from a more dispersed state dates back at least to Kant (1755). This classical view of the formation of the Galaxy has been given a modern interpretation and quantification by Eggen, Lynden-Bell and Sandage (ELS), after having studied the motion of a sample of high velocity stars in the MW halo (Eggen et al. 1962). They found a correlation between ultraviolet excess and eccentricities

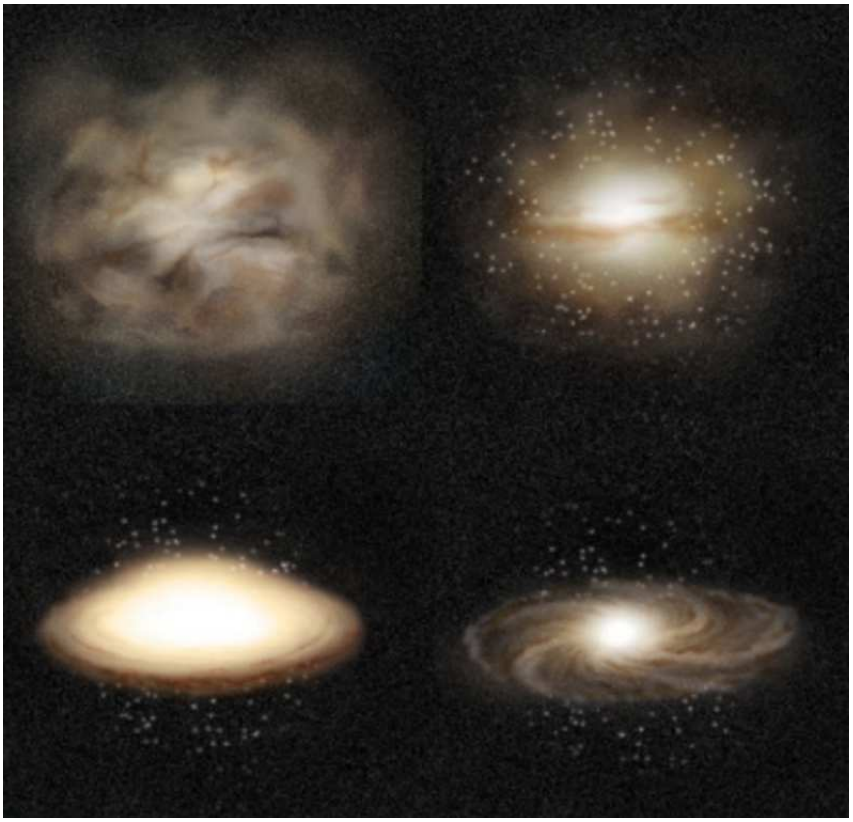

Figure 1.2: Schematic figure showing the Cloud Collapse scenario in four stages, from upper left to lower right (taken from Krauss & Chaboyer 2003).

in the sense that stars with the largest UV excess (i.e., lowest metal abundance) are moving in highly elliptical orbits, whereas stars with little or no UV excess move in nearly circular orbits. A correlation between UV excess and angular momentum was also found: stars with large UV excesses have small angular momentum.

Based on these correlations they proposed that the original proto-Galaxy consisted of a single large spinning, metal poor gas cloud with a radius (in present day coordinates) of about 100 kpc. This cloud, unable to support itself by gas pressure, once its mass had stopped the local Hubble expansion, immediately underwent a free-fall collapse (see Fig. 1.2). Stars that formed in the early stages of the collapse of the protogalactic gas cloud inherit the low metallicity and predominantly radial motion of the inward falling gas, and are seen today as randomly oriented, elliptical orbiting, small angular momentum metal-poor halo stars. The GC and field halo stars are supposed to have formed in condensations embedded within the intra-Galactic medium during this free-fall phase. As the cloud collapsed, its rate of spin increased to conserve its angular momentum, and at the same time, supernova explosions increased slowly the content of metals in the cloud. As a consequence, successive generations of stars formed by this enriched gas, are both closer to the center of the galaxy and increasingly metal rich (radial metallicity gradient). Finally, when the gas achieved a density which allowed pressure support, and dissipation therefore began to become important, it was able to radiate away its kinetic energy; residual angular momentum then forced it to settle into a rotating disk, where all subsequent star and cluster formation has taken place. Metal-rich stars would form in this disk as the interstellar medium is enriched with the products of nucleosynthesis during stellar evolution. In contrast to the gas, the disipationless halo field stars and GCs have retained the kinetic energies, angular momenta, and general spatial distribution that they possessed at the instant the gaseous collapse ceased. According to this scenario, the collapse was very quick, with a duration that could have not exceeded a few times 10^8 years, which translates in a very small spread in age among halo stars and GCs.

1.2 Hierarchical Model for the Milky Way

An alternative scenario for the formation of the MW was proposed by Searle & Zinn (SZ) in 1978. They measured and compiled the most up-to-date and reliable metal abundances and horizontal branch (HB) morphologies[1] available at the time for about 50 Galactic GCs, and

---

[1] The HB morphology is characterized by HB-type defined as: HB-type=$(B-R)/(B+V+R)$, where V is the number of RR Lyrae stars, and B and R are the numbers of HB stars respectively bluer and redder than the RR Lyrae instability strip.

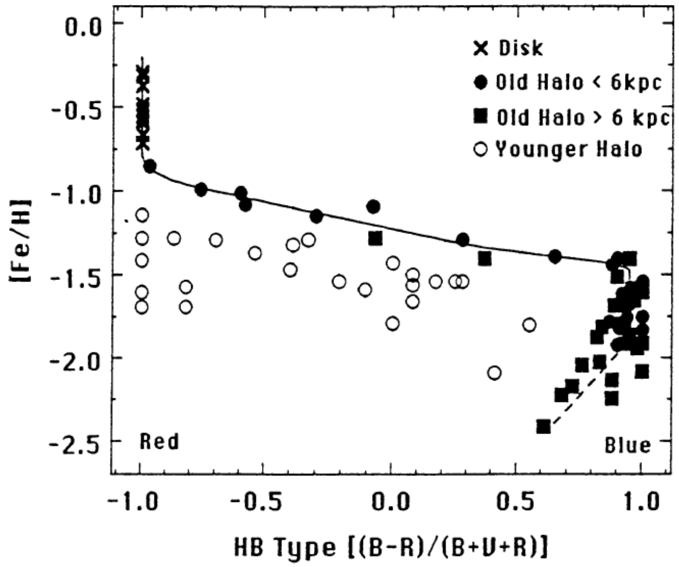

Figure 1.3: Subdivision in the HB morphology versus metal abundance plane of the MW halo GCs ([Fe/H<-0.8) (taken from Zinn 1993).

investigated these properties as a function of galactocentric distance, R_{GC}. Surprisingly, they found no radial abundance gradient in the cluster system in the outer halo ($R_{GC} \gtrsim 8$ kpc), as would be expected for the cloud collapse model. They also found significant differences in HB morphology between inner and outer halo GCs. This effect is shown in Fig. 1.3, where it is clearly visible that GCs in the inner regions of the Galaxy follow a tight relationship between HB morphology and metallicity, whereas clusters at larger galactocentric radii have in the mean, more red HB types at a given metallicity (the so called "second parameter problem") and exhibit a considerable scatter between these 2 quantities[2]. This body of evidence points towards the possibility of two populations of halo GCs. Note that the inner/outer halo dichotomy appears

---

[2] From this plot arose one of the most successful classification scheme for the Galactic GCs: those systems that follow the fiducial line which traces the relationship between HB-type and [Fe/H] for the inner halo clusters are called "old" GCs, while those that clearly deviate form the "young" halo components.

to be well-supported by field stars as well (Carollo et al. 2007). According to early HB models, the observed range in HB morphological types would require that the epoch of GC formation has lasted much more than 1 Gyr, and therefore the formation of the Galactic halo could not have been as rapid as a free-fall collapse. Thus, as suggested by SZ, the large spread in HB-type is best understood as a difference in age, with the red HB outer halo GCs several Gyrs younger than the blue HB counterpart at large radii, as well as the inner halo clusters. In order to explain the required prolonging of cluster formation time, SZ adopted a model assuming that the outer halo formed over a longer period of time via the capture of external systems or "protogalactic fragments", and that the red HB outer halo clusters originated in satellite systems that were subsequently accreted by the MW. This model is known today as the hierarchical picture, since big galaxies form by merging and accretion of small entities or "building blocks" (see Fig. 1.4). The spread in HB morphology of GCs can be explained by different star formation histories in the accreted systems. It is also theorized that a significant fraction of halo field stars were once members of a GC. We now know that GCs do indeed disrupt, the most clear example being that of Pal 5 (Odenkirchen et al. 2003). As noted by Zinn (1980), obvious candidates for these "building blocks" are the present-day dwarf spheroidal (dSph) and dwarf irregular (dIrr) galaxies. Such galaxies are the most numerous in the Universe and the dSphs in particular are found to surround both the MW and M31 in large numbers (although their numbers fail by an order of magnitude or more to match those predicted by ΛCDM theories (Klypin et al. 1999). There are undoubtedly other faint dwarfs still to be found, and the Sloan Digital Sky Survey has recently allowed to discover several of them around the MW (see e.g., Willman et al. 2005; Kleyna et al. 2005; Belokurov 2006, Belokurov et al. 2007). However, it is unlikely that the numbers required by the ΛCDM theories really exist, although the most recent estimate (Simon & Geha 2007) suggests that there is only a factor of 4 too few dwarf galaxies currently known. Many of the newly discovered MW dSph satellites are known to contain a sizeable fraction of stars that are similar to those in the MW halo, namely old and metal-poor.

Indeed, there is at least one well-documented example of a dwarf galaxy, the Sagittarius dSph,

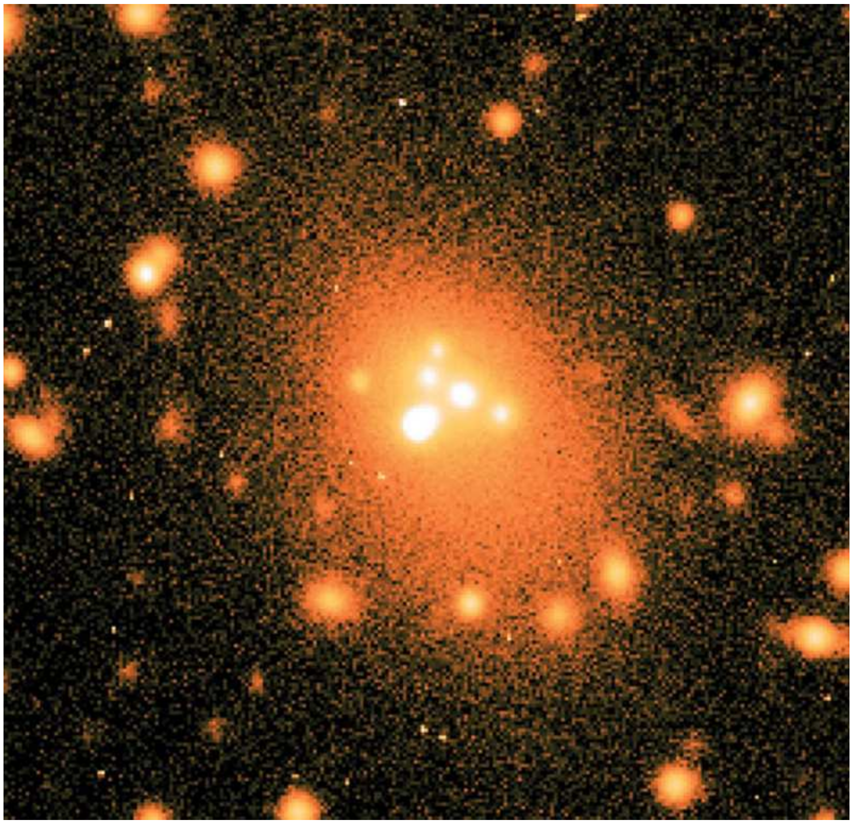

Figure 1.4: A giant elliptical galaxy in the cluster Abell 3287 in the process of hierarchical growing. The partially digested remnants of several cannibalized galaxies are visible in the central region (taken from West et al. 2004).

which is currently being accreted by the MW (Ibata et al. 1995). This dwarf galaxy is not only contributing to the Galaxy with field stars, but also with a handful of GCs; some of which showing a quite young age. This example of recent "cannibalism" suggests that the Galaxy is still in the process of formation an that young GCs in the outer halo can also be accounted for if the SZ model is invoked. Less evident but equally suggestive is the case of ω Centauri, both the brightest and the largest GC associated with our Galaxy, known so far. It has been speculated that this peculiar cluster may be the core of a dwarf galaxy which was disrupted and absorbed by the MW (see, e.g. Villanova et al. 2007). Also interesting is the case of Terzan 5. Very recently Ferraro et el. (2010) have claimed that this GC could be the surviving remnant of one of the primordial "building blocks" that are thought to have merged to form the Galactic bulge. This case is particularly interesting since it suggests that the subsystems hypothesized by SZ may actually have been the "building blocks" not just of the Galactic halo, but of the entire Galaxy.

1.3 "Building Blocks" of The Milky Way

In order to probe the predictions of the SZ theory for the Galaxy formation, an obvious test is to compare the main properties of the present-day dSph or dIrr systems surrounding the MW with those of the MW halo stars. If the MW halo was indeed made up in large part by dissolved systems initially resembling the dSphs or dIrrs we see today, one would expect to find many similarities in their stellar populations.

One approach is the direct comparison of the detailed chemical composition of stars from the two environments, based on spectroscopy. If the halo formed from dSphs or dIrrs or objects like them, their chemical makeups should be similar. Such a study has been dubbed "chemical tagging" by Freeman & Bland-Hawthorn (2002). The catchphrase "near-field cosmology" also applies, as we are probing cosmological galaxy formation theories using the nearest galaxies as our testbeds. The alpha-elements (e.g., O, Mg, Si, Ca, and Ti) are specially useful for this purpose because their abundance is an indicator of the star's enrichment history. The production of these elements is dominated by Type II supernovae, while iron has important contributions by both Type II and Type Ia supernovae. Thus, the ratio of alpha-elements to iron, [α/Fe], is commonly used to trace the star-formation timescale in a system, because it is sensitive to the ratio of SNe II (massive stars) to SNe Ia (intermediate-mass binary systems with mass transfer) that have occurred in the past. The salient feature of these comparisons is that the halo abundances are essentially unique. The general α vs. [Fe/H] pattern of most of the dwarf galaxies

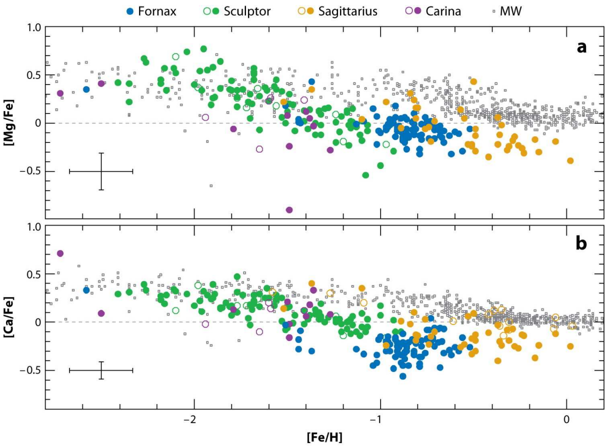

Figure 1.5: [Mg/H] and [Ca/H] vs. [Fe/H] for samples of stars in four different dwarf galaxies. α-elements in extragalactic samples are generally depleted with respect to their Galactic counterparts (taken from Tolstoy et al. 2009).

studied are very different from that of the MW halo stars. More specifically, the [α/Fe] ratios of stars in dSph galaxies are generally lower than those of similar metallicity Galactic stars (see Fig.1.5). In the same vein, the Galactic halo contains a significant fraction of stars more metal-poor than [Fe/H] ~ -2.5 (see, e.g., Christlieb et al. 2004; Beers et al. 2005), including a not negligible tail of stars with metal abundances even lower than -3.0 (see Helmi et at. 2006 and references therein), while the dSphs, on the other hand, contain very few metal-poor stars (see, e.g., Tolstoy et al. 2004; Koch & Grebel 2006), with a significant lack of stars with metallicities below [Fe/H] ~ -3.0 (Helmi et al. 2006; Aoki et al. 2009).

Another approach is the comparison of the stellar populations. In trying to relate the young, metal-rich populations observed in the halo with the stellar population of the present-day dSphs, Unavane et al. (1996) recognized that the Galactic halo contains a negligible amount of young stars in comparison with the vast majority of old components, unlike most of the MW's satellite dSph galaxies which often do contain sizeable numbers of young stars. Thus, they estimate that, at the most, only 6 Fornax-type progenitors or 60 Carina's could have been accreted by the Galaxy. This is in contradiction to the predictions of the hierarchical model, in terms of both the number and the mass spectrum of the contributors needed to produce a MW-type halo (Unavane et al. 1996; Gilmore & Wyse 1998). Similar discrepancies between stellar populations in the dSphs satellites and the MW halo are found when comparing the numbers of intermediate-age giant carbon stars, since the Galatic halo is apparently less abundant in these stars than the present-day dwarf satellites (van den Bergh 1994).

All the arguments mentioned above cast some doubts on the possibility that the dwarf galaxies we see today in the surrounding of the MW and M31 could be the hierarchical protogalactic fragment candidates. However, these arguments hide some obvious limitations; the younger and intermediate-age stars we see today were not present when the bulk of the halo formed. In fact, the halo progenitors or Galactic "building blocks" may not be replicas of present-day satellite galaxies. As pointed out by Mateo (1996), the present-day dSphs are survivors, and therefore special conditions must have precluded them from disruption (late accretion and/or less-radial orbital characteristics). These conditions could have allowed the present-day dSphs to follow a different evolutionary path than the original "building blocks". A difference in time of formation alone, for example, could explain the lack of intermediate and young populations in the halo relative to the present-day satellites (van den Bergh 1994; Majewski et al. 2002). In the same vein, the satellites that have survived may have undergone additional chemical enrichment over a prolonged time span. Running the clock back to the time when the MW halo was forming, a Sculptor-type galaxy would have looked very different. Accordingly, these arguments concerning the role of dwarf galaxies in the assembling of the Galaxy only provides us with information about a "relatively recent" part of the overall history.

Thus, in order to place meaningful constraints on the way our undoubtedly old Galactic halo formed, one should really compare those stars which saw what really happened at the beginning, and survived to this day to tell us the whole truth about the matter. In other words, we should compare the very oldest stars in both the present-day halo and the MW dwarf companions. Unmistakable old, with ages comparable to the age of the Universe, the RR Lyrae stars are ideal candidates to this purpose. If the Galaxy formed by the accretion of protogalactic fragments that resembled the MW dwarf satellites as they were $\sim$ 10 Gyr ago, then the pulsation properties of the RR Lyrae stars in the Galactic halo and in the dwarf galaxies should be basically indistinguishable.

1.3.1 RR Lyrae Stars: Real Eyewitnesses of galaxy formation

In the present section we compare the properties of the RR Lyrae stars in the Galactic GCs with the properties of the RR Lyrae stars belonging to GCs and general field of the MW dwarf satellites. The left panel of Figure 1.6 presents the distribution of the mean periods of the ab-type RR Lyrae (RRab) stars for Galactic GCs containing at least 5 RR Lyrae as a function of the cluster's metallicities. Except for the peculiar positions of the clusters NGC 6441 and NGC 6388, labeled as OoIII in the figure, it is clear from this plot that the MW globulars present the so called Oosterhoff dichotomy (Oosterhoff 1939), i.e. the lack of systems with average period of the RRab stars in the range from 0.58 days to 0.62 days. Only four GCs out of 41, or less than 10%, are found inside the "Oosterhoff gap", two of which are quite peculiar: M75 has a trimodal horizontal branch (Corwin et al. 2003), whereas the metal poor cluster Rup106 appears younger than other typical metal-poor Galactic globulars by about 4-5 Gyr (Buonanno et al. 1990) and is suggested to be connect with the stream of the Sagittarius dSph (Bellazzini et al. 2003). The right panel of Fig. 1.6, on the other hand, shows those nearby extragalactic system possessing their own GC systems, namely, the Large and Small Magellanic Cloud (LMC and SMC, respectively) dIrr's, the Fornax and Sagittarius dSphs, and the recently discover Canis Major overdensity and its suggested GC system[3] (Martin et al. 2004). From the plot, it becomes clear that these massive dwarf galaxies in the immediate vicinity of the MW show a very different picture. For instance, the LMC GCs show a continuous trend in RR Lyrae properties rather than an Oosterhoff dichotomy. In the case of Fornax (see e.g., Greco 2007), the GCs preferentially

---

[3] The true nature of the Canis Major overdensity, whether an actual dwarf galaxy or the MW warp, is still matter of debate (see e.g., Mateu et al. 2009, and references therein).

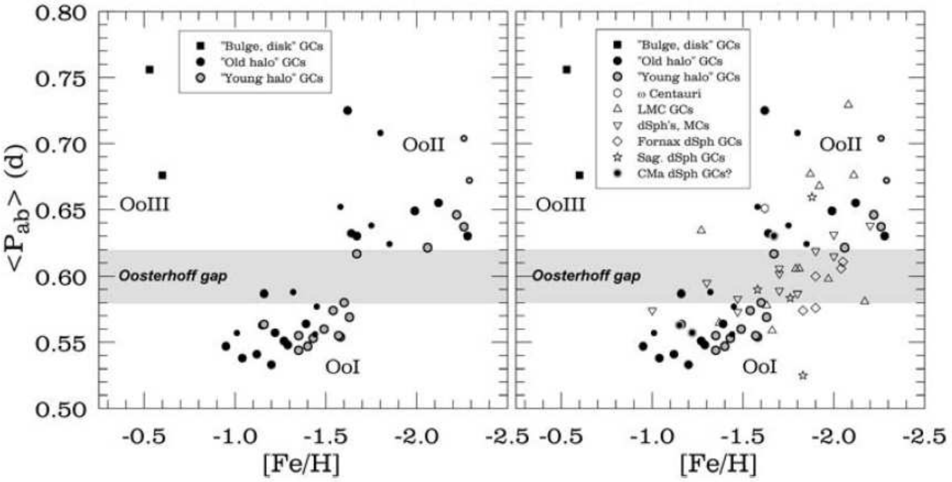

Figure 1.6: Left panel: Oosterhoff type I, II and III Galactic GCs in the $\langle Pab\rangle$ versus [Fe/H] diagram. Clusters containing relatively small numbers of RR Lyrae are plotted using smaller dots. Right panel: same as in the previous plot, but now including dwarf satellites of the MW and their GCs. These extragalactic objects preferentially occupy the Oosterhoff gap region, in stark contrast with the Galactic GCs (taken from Catelan 2009).

occupy the Oosterhoff intermediate region which is almost avoided by the Galactic GCs. This immediately rules out the possibility that any building blocks of the MW may have resembled the LMC or Fornax some 13 Gyr ago, otherwise the Oosterhoff dichotomy would not exist. In fact, in the case of external systems, almost 50% of them are found inside the "Oosterhoff gap". Similar conclusions may be reached when considering the stellar fields of the remaining 7 less massive dwarf MW companions: Ursa Minor, Draco, Carina, Leo II, Sculptor, Leo I and Sextans. All of them, but Ursa Minor, have been classified as Oosterhoff intermediate objects (see eg., Catelan 2009 and references therein). In summary, the distribution of mean periods of the RRab stars for the Galactic and nearby extragalactic systems is undoubtedly different. The Oosterhoff dichotomy is not present among the satellite companions of the MW. Thus, these results seems to definitely ruled out the present-day dSph galaxies as the possible protogalactic fragments invoked by SZ. While we do see evidence of ongoing mergers between some dSphs (e.g., Sagittarius, Ibata et al. 1995) and the Galaxy, the Oosterhoff argument suggests that these must not have provided a major contribution to the stellar content of the MW halo.

1.3.2 New Pieces of the Puzzle, New Clues

Prior to the Sloan Digital Sky Survey (SDSS; York et al. 2000), the number of known MW dSph satellites had been increasing at a rate of one or two per decade, reaching the total number of only ten widely accepted MW dSph satellites. The small number of known companions surrounding the Galaxy is one of the biggest problems of the ΛCMD model, often referred as the "missing satellite problem" (Klypin et al. 1999, Moore et al. 1999). Indeed, in the current ΛCMD paradigm of structure formation, dark matter halos of the mass of the MW dSph galaxies outnumber the known dSphs by a factor of 10-100 (Penarrubia, Navarro, & McConnachie 2000, and references therein). Since 2005, 17 new dSph satellites of the MW have been discovered, primarily from the analysis of images obtained by the SDSS: Willman I, Ursa Major I (UMa I), Ursa Major II (UMa II), Bootes I, Coma Berenices (Coma), Segue I, Canes Venatici I (CVn I), Canes Venatici II (CVn II), Leo IV, Hercules, Leo T, Bootes II, Leo V, Bootes III, Segue II, Pisces I, and Pisces II (Willman et al. 2005a, 2005b; Zucker et al. 2006a, 2006b; Grillmair 2006, 2009; Belokurov et al. 2006, 2007, 2008, 2009; Irwin et al. 2007; Walsh et al. 2007; Watkins et al. 2009; Belokurov et al. 2010). They have eluded previous discovery because they all have very low surface brightness ($\mu_v \gtrsim 28$ mag arcsec^{-2}). Being so faint they have been named "ultra-faint" dSphs (UFDs). The new galaxies are mainly concentrated around the North Galactic pole, as this is the region observed by the SDSS. After the discovery of the new systems, the dSph galaxies surrounding the MW have been divided into two main groups: "bright" or "classical" dSphs, already known before 2005, and "ultra-faint" dSphs, discovered in the last three-four years. Classical and ultra-faint dSphs lie in two separate regions in the absolute magnitude versus half-light radius plane (see Figure 1.7). UFDs have small velocity dispersions,

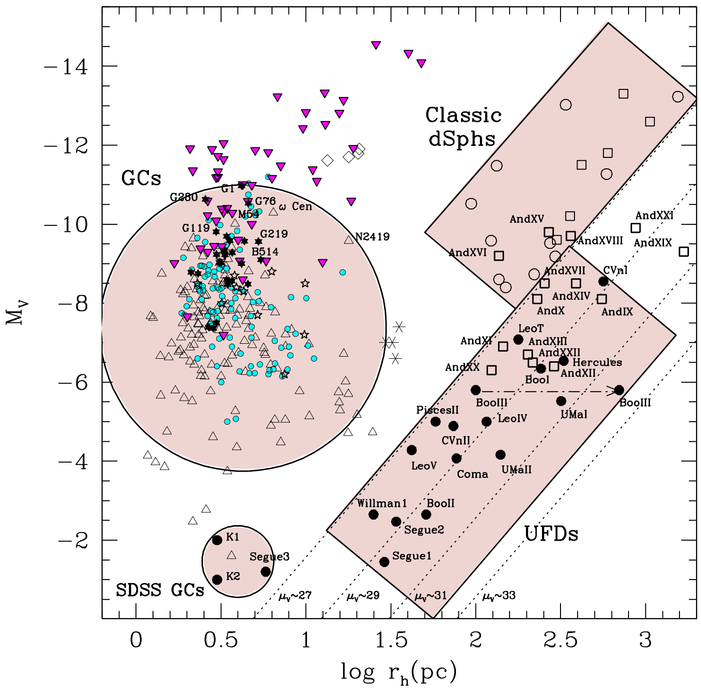

Figure 1.7: Location of different classes of objects in the plane of absolute magnitude vs half-light radius. Lines of constant surface brightness are marked. Open circles and open squares are the bright dSphs surrounding the MW and M31, respectively. Filled circles are the "ultra-faint" Milky Way (MW) dSphs satellites, and two extremely low luminosity globular clusters, discovered after 2005, mainly from the analysis of SDSS data (see text). Bold open squares are new M31 dSph satellites discovered after 2004 (see Chapter 3). Open triangles are Galactic globular clusters (GCs) from Harris (1996), and Mackey & van den Bergh (2005). Filled stars are GCs of the Andromeda galaxy, from Federici et al. (2007). Open stars are GCs in the outer halo of M31, from Mackey et al. (2007) and Martin et al. (2006). Asteriscs are extended M31 GCs, from Huxor et al. (2005) with parameters measured by Mackey et al. (2006). Cyan filled circles are GCs of NGC5128, from McLaughlin et al. (2008). Magenta filled inverted triangles are nuclei of dwarf elliptical galaxies in the Virgo cluster, from Cote et al. (2006). Diamonds are ultra-compact dwarfs in the Fornax cluster, from De Propris et al. (2005). (taken from Clementini 2010).

Table 1.1: Oosterhoff properties of RR Lyrae stars in the "ultra-faint" MW dSphs

Name	Distance[1] (kpc)	$\langle$[Fe/H]$\rangle$	N(RRab+c+d)[1]	$\langle Pab \rangle$[1] (days)	Oo Type[1]
Bootes I	$66\,^{+3}_{-2}$	−2.5	7+7+1	0.69	Oo II
Canes Venatici I (CVn I)	$210\,^{+7}_{-5}$	−2.1	18+5	0.60	Oo Int
Canes Venatici II (CVn II)	$160\,^{+4}_{-5}$	−2.3	1+1	0.74	Oo II?
Coma Berenices (Coma)	$42\,^{+2}_{-1}$	−2.3	1+1	0.67	Oo II?
Leo IV	154 ±5	−2.3	3	0.66	Oo II?
Ursa Major II (UMa II)	34.6±0.7	−2.4	1	0.66	Oo II?
Ursa Major I (UMa I)	95 ±4	−2.2	3	0.64	Oo II?

[1] Distances and properties of the RR Lyrae stars are from Dall'Ora et al. (2006) for Bootes I; from Kuehn et al. (2008) for CVn I; from Greco et al. (2008) for CVn II; from Musella et al. (2009) for Coma, from Moretti et al. (2009) for Leo IV; from Dall'Ora et al. (2009) for UMa II; and from Garofalo (2009) for UMa I. Question marks indicate the difficulty of classifying these galaxies due the small number of variables they contain (taken from Clementini 2010).

3-4 km/s, showing dark matter dominance, and have distorted morphologies, probably due to the tidal interaction with the MW. They all host an ancient stellar population with chemical properties similar to that of external Galactic halo stars (Simon & Geha 2007; Kirby et al. 2008; Frebel et al. 2009). Several of the UFDs have mean metallicities as low or lower than the most metal-poor GCs and, generally, much lower than those of the classical dSphs. Furthermore, the α/Fe ratios of extremely metal-poor stars in the ultra-faint dwarf spheroidals are as high as those found in the bulk of Galactic halo stars (Frebel et al. 2009), while the abundance ratios between α-elements and iron in the most metal-poor stars found in the classical dSphs are lower than those found in Galactic halo stars (Aoki et al. 2009). Seven of the UFDs have been searched for variable stars so far (namely, Bootes I, Dall'Ora et al. 2006, Siegel 2006; CVn I, Kuehn et al. 2008; CVn II, Greco et al. 2008; Coma, Musella et al. 2009; Leo IV, Moretti et al. 2009; UMa I, Dall'Ora et al. 2009; and UMa II, Garofalo 2009) and only with the exception of CVn I, were all found to contain RR Lyrae stars with properties resembling those of the MW Oosterhoff II GCs, although one must be aware that this Oosterhoff classification is more insecure than in the case of the classical dSphs, given the few RR Lyrae stars found in the UFDs. All of the above characteristics suggest that a much larger population of objects similar to the present-day UFDs, as they were at earlier times, may have been the “building blocks” of the halos of large galaxies such as the MW. The association is particularly clear with the outer halo of the MW, which Carollo et al. (2007) have demonstrated to exhibit a peak metallicity of [Fe/H]$= -2.2$, substantially lower than the inner halo, whose metal abundance peaks at [Fe/H]$= -1.6$, and which is the dominant population at Galactocentric distances beyond 15-20 kpc. Last but not least, the SDSS discoveries could have a bearing on the “missing satellite” problem. In fact, the SDSS present-day sky coverage is only about 1/4 of the celestial sphere, simple statistical arguments suggest that many more UFDs likely exist at latitudes not yet explored and could potentially fill the gap between theoretical expectations and observational evidence. In conclusion, it seems plausible that a population of ultra-faint, dark dwarf galaxies really does surround the MW. Only after a complete census of these objects has been obtained will we be able to assess whether their number and properties are consistent with the predictions of the simulations.

Chapter 2

Variable Stars as Tools.

All stars display variations of brightness and color in the course of their evolution. Variable stars are traditionally devided into two main categories: intrinsic and extrinsic variables. The former vary due to causes internal to their structure and, among them, pulsating stars are characterized by periodic or cyclic variations. In particular, radially pulsating stars have pulsation periods typically ranging from hours to hundreds of days, and pulsation amplitudes of hundredths to ~ 1 mag. They share a common locus that runs almost vertical in the HR diagram, named instability strip (IS), due to the fact that they also share the same pulsation mechanism, associated to opacity variations in the ionization regions of H, He and HeI.

Pulsating stars obey to a period- mean density relation that is at the basis of their use as stellar population tracers and distance indicators. In fact, assuming the Stephan Boltzman law combined with the period-mean density relation one obtains a relation between the period, the mass, the luminosity and the effective temperature. If the mass and the luminosity are related to each other, as in the case of Classical Cepheids, a period-luminosity-color relation is expected. Moreover neglecting the color dependence, or averaging over the color extension, one obtains a period-luminosity relation. This implies that the study of the pulsation properties of variable stars can help us to constrain the distance of the host systems, as well as the intrinsic

Table 2.1: Main characteristics of different types of pulsating variables found in the Classical Instability strip

Type	Period (days)	M_v (mag)	A_v	Population	Evolutionary Phase
δ Scuti	$0.02\div0.25$	$2\div3$	≤ 0.5	I	MS
SX Phoenicis	≤ 0.1	$2\div3$	≤ 1.5	II	MS
RR Lyrae ab-type	$0.4\div1.0$	$0\div1$	$\geq 0.6 \div 1$	II	HB
RR Lyrae c-type	$0.2\div0.4$	$0\div1$	$0.4 \div 0.6$	II	HB
Anomalous Cepheids	$0.2\div2.0$	$-2 \div 0$	≤ 1.5	Int	HB turnover
δ Cepheids	$1\div100$	$-7 \div -2$	≤ 1.5	I	Blue loop
BL Herculis	$1\div5$	$-1 \div 0$	≤ 1.5	II	post-HB
W Virginis	$12\div20$	$-3 \div -1$	≤ 1.5	II	post-HB
Rv Tauri	$20\div50$	$-3 \div -1$	....	II	post-HB

evolutionary properties of the investigated stars. The study of pulsating variables based on times series may allow to map the 3D structures and to characterize the spatial distribution of the different types of variables in a galaxy, providing information on the spatial distribution and time confinement of the burst of their parent populations. Furthermore, since different types of variables in the classical instability strip are in different evolutionary phases and belong to different stellar populations, they can be used as tracers of the different components in a stellar system: RR Lyrae stars and the Type II Cepheids tracing the oldest stars ($t > 10$ Gyr); the Anomalous Cepheids (ACs) tracing the intermediate-age component ($\sim 1-5$ Gyrs); and the Classical Cepheids representing the young stellar population (50-200 Myrs). The role of these variable stars can become crucial when the stellar population is not as simple as in a globular cluster (GC), and stars with different ages and metallicities share the same region of the CMD. The detection of different classes of pulsating variables may allow to identify different star formation episodes that have occurred in the host stellar system. Table 2.1 shows and owerview of the currently known major types of pulsating variables, along with their main characteristics and Fig. 2.1 illustrates the loci occupied by them in the HR diagram. In the following subsections, we present a briefly description of the variable stars that we have detected in this thesis.

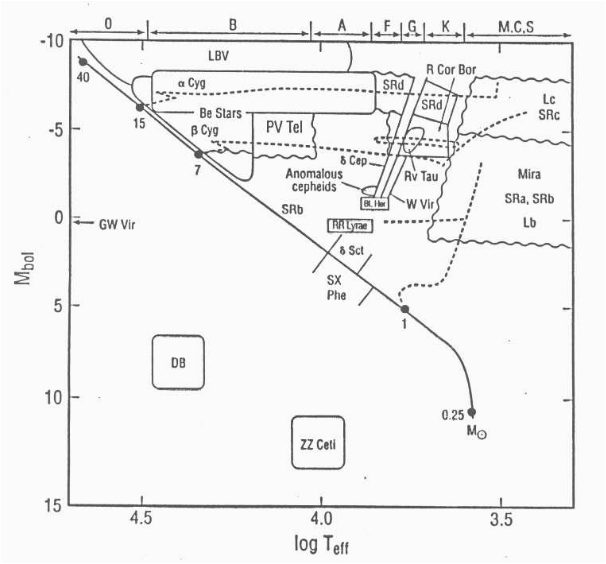

Figure 2.1: Position of different types of pulsating stars in the HR diagram.

2.1 Classical Cepheids

Cepheids are high-luminosity, radially pulsating variable stars, with periods ranging between 1-100 days, and commonly associated with relatively young stellar populations like those found in open clusters, disk of spiral galaxies or in irregular galaxies. Their presence in star clusters allows their ages to be estimated as up to about 10^8 yr. From the stellar evolution point of view, these variables are intermediate-mass ($3 - 12 M_\odot$) stars that cross the instability strip during the helium burning phase. In particular, after the quiescent ignition of He at the core by the 3α reaction, these stars may make an excursion toward higher effective temperature and, subsequently come back toward the asymptotic giant branch in the HR diagram. This "loop" may extend to sufficiently high temperature (or blue color) to intersect the instability strip in which case the stars become classical Cepheids. Their intrinsic brightnesses range from $-2 > M_V > -7$, making them ideal distance indicators on Galactic and extragalactic scales. In fact, they are observable up to distances of 20-30 Mpc (see e.g. Freedman et al. 2001). The close relationship between period and luminosity which was found by Henrietta S. Leavitt in 1912, has given the Classical Cepheids a unique role in establishing the distances to the nearer galaxies, and hence the distance scale of the Universe. On this basis they provide the absolute calibration of important secondary distance indicators, such as the maximum luminosity of supernovae Ia, the Tully-Fisher relation, surface brightness fluctuations, and the planetary nebulae luminosity function, that are the basis for measurement of the Hubble constant (Freedman et al. 2001; Saha et al. 2001). A very debated issue is the universality of the period-luminosity relation and in particular the effect of the metallicity on its coefficients, because any systematic effect affecting the Cepheid period-luminosity is expected to have relevant consequences on the extragalactic distance scale and the estimate of the Hubble constant. Cepheids are also good tracers of intermediate-mass stars in the Galactic disk (Kraft & Schmidt 1963), and star-forming regions in extragalactic systems (Elmegreen & Efremov 1996). The use of Cepheids as tracers of young stellar populations was soundly supplemented by the evidence that if these objects obey to a PL relation, and to a Mass-Luminosity relation, they also obey to a Period-Age relation. In particular, an increase in period implies an increase in luminosity, i.e., an increase in the stellar mass, and in turn a decrease in the Cepheid age.

2.2 Type II Cepheids

Type II Cepheids have periods between 1 and 26 d and are observed in GCs with few RR Lyrae stars. They are brighter than the RR Lyrae stars with similar metal content and are often divided into two classes: BL Her stars ($P < 1$) and W Vir ($P > 1$). As reviewed by Wallerstein (2002) they originate from hot, low mass stellar structures that started the main central He burning phase bluer than the RR Lyrae gap and now evolve toward the AGB crossing the pulsation region with luminosity and effective temperature that increase with decreasing the mass (see also Di Criscienzo, Marconi, Caputo, Cassisi 2007).

Type II Cepheids are widely believed to be the immediate progeny of low mass HB stars ($M \sim 0.53 M_{\odot}$), but with mass still enough to reach the AGB stage, i.e., blue HB stars. This is supported both by the observational record, which shows that type II Cepheids are present only when a sizeable blue HB component is also present (Wallerstein 1970; Smith & Wehlau 1985), seemingly irrespective of the metallicity (Pritzl et al. 2002; 2003); and by theoretical models (Schwarzschild & Harm 1970; Gingold 1976; 1985). Accordingly, detection of type II Cepheids should immediately imply the presence of a sizeable blue HB component.

These pulsating variable stars consist of three subclasses in different evolutionary stages, namely, BL Herculis (BL Her), W Virgins (W Vir) and RV Tauri (RV Tau) stars. Their evolutionary status can be summarized as follows: Stars on the horizontal branch, bluer than the RR Lyrae gap, evolve toward higher luminosity and larger radius (just like stars leaving the main sequence) as they deplete the helium in their cores. In doing so they cross the instability strip at a luminosity that corresponds to a period between roughly 1 and 5 days. This accounts for the short-period group, namely, BL Her of low metallicity. The origin of BL Her of near-solar metallicity remains uncertain, since they are likely to originate from the red horizontal branch. After reaching the AGB they advance to higher luminosity and begin to suffer helium shell flashes, which cause the star to make an excursion into the instability strip. The luminosity at which this occurs results in stars having periods between 12 and about 20 days. These are the so called W Vir variable stars. The paucity of Type II Cepheids with periods between 5 and 12 days, especially in the globular clusters, can be understood as the lack of shell flashes until the star's luminosity reaches that which corresponds to a 12 day period. As the star becomes more luminous, mass loss reduces the remaining hydrogen shell to around $0.01 M_{\odot}$, whereupon the star begins its travel across the top of the HR diagram around $M_V = -3.5$ to -4.5, heading to the white dwarf cooling sequence. While doing so it passes through the instability strip once again, now with a period of 20-50 days (which is often listed as twice that because of their behavior of alternating deep and shallow minima). These are the RV Tau stars, and are easily recognizable by their alternating deep and shallow minima of their light curves. (Wallerstein 2002; Soszynski

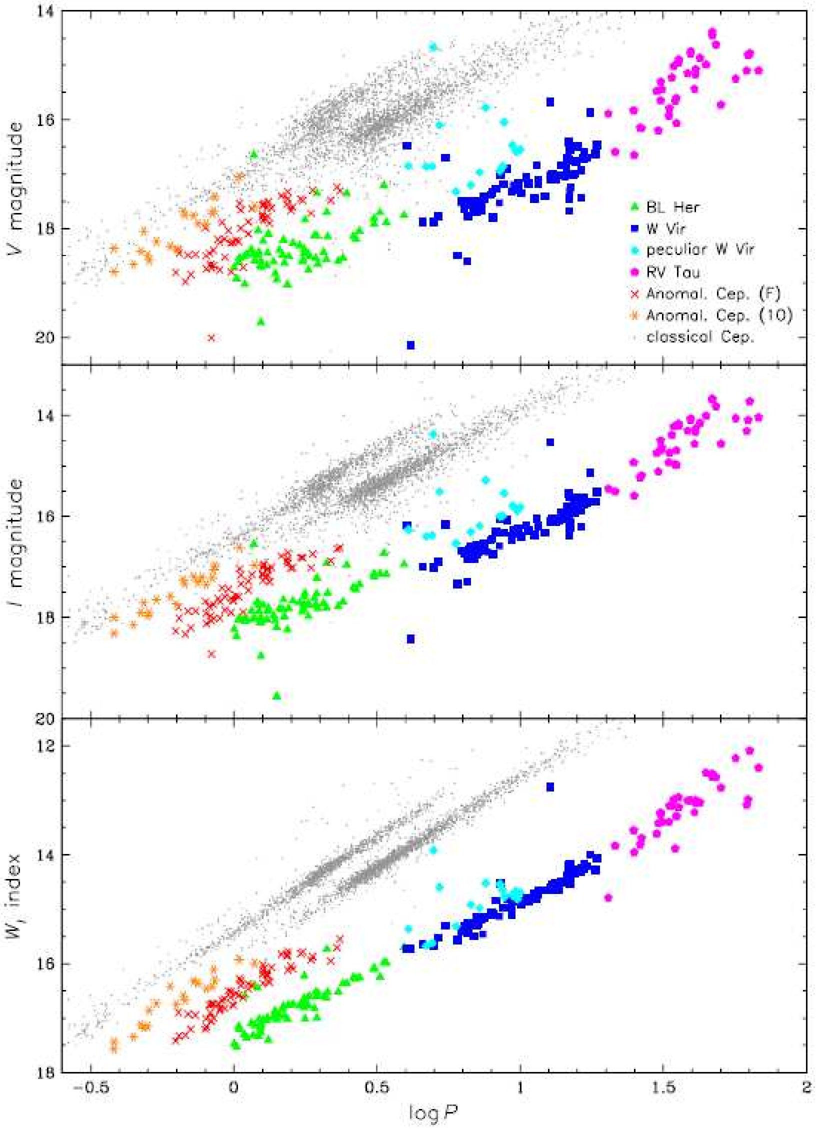

Figure 2.2: Period-Luminosity diagrams for Cepheids in the LMC. Green, blue, cyan and magenta symbols show type II Cepheids; red and orange symbols represent anomalous Cepheids; and grey points Classical Cepheids (taken from Soszynski et al. 2008)

et al. 2008). Since these variables obey a P-L relation, they can be used as standard candles to find distances (see Fig. 2.2). However, as illustrated in the plots, the P-L relation is not linear for the whole range of periods covered by type II Cepheids, and actually the P-L relations should be fitted separately for BL Her, W Vir and RV Tau stars. This is is especially valid for RV Tau stars which seem to be much brighter than would be expected from the extrapolated relation fitted to shorter-period type II Cepheids (e.g., Demers and Harris 1974, Alcock et al. 1998).

2.3 Anomalous Cepheids

Anomalous Cepheids (ACs) are radialy pulsating variable stars commonly observed in Local Group galaxies containing metal poor stellar populations. Their pulsation periods range from ~ 0.2 to 2 days and they are typically 0.5-1.5 mag brighter than the RR Lyrae stars in a system. The origin of their anomaly lies in the evidence of being more luminous, for the same period, than Type II Cepheids tipically observed in old and metal poor stellar clusters, like GCs. The ACs follow their own P-L relation, both for fundamental mode pulsators and first overtone ones (Pritzl et a. 2002), which runs between the type I and type II Cepheid P-L relations (see Fig. 2.2).

A general consensus exists in the literature (see, e.g., Bono et al. 1997, Caputo 1998, and references therein) on the fact that AC variables, like RR Lyrae stars and Population II Cepheids, are metal-poor He-burning stars in the post Zero Age Horizontal Branch (ZAHB) evolutionary phase. As reviewed by Caputo (1998), for low metal abundances ($Z < 0.0004$) and relatively young ages (< 4 Gyr) the effective temperature of ZAHB models reaches a minimum ($\log Te \sim 3.764$) for a mass of about 1.0-1.2 $M_\odot$, while if the mass increases above this value, both the luminosity and the effective temperature start increasing, forming the so called ZAHB turnover. For larger metallicities, the more massive ZAHB structures have brighter luminosities but effective temperatures rather close to the minimum effective temperature. Within such an evolutionary scenario, the ACs appear to belong to the post-turnover portion of the ZAHB which crosses the instability strip at luminosity higher than the RR Lyrae pulsators. Their origin is still debated and the most widely accepted interpretations are: (1) they are young ($\sim$5 Gyr) single stars due to recent star formation; (2) they formed from mass transfer in binary systems as old as the other stars in the same stellar system. Their pulsation properties allow us to use them as distance indicators and tracers of intermediate age stellar populations (see Marconi, Fiorentino, & Caputo 2001).

While ACs are almost nonexistent in GCs, they are common in dSph galaxies. Every dSph surveyed for variable stars has been shown to include at least one AC. As recently suggested by Dolphin et al. (2002) and theoretically confirmed by Caputo et al. (2004) ACs are indeed the extension to the lowest metallicities of the short period Classical Cepheids observed for example in the Magellanic Clouds.

2.4 RR Lyrae stars

RR Lyrae are low mass He burning stars on the HB evolutionary phase. They are important distance indicators and tracers of the properties of the old stellar populations. Their role as standard candles is twofold: i) their absolute visual magnitude is a relatively well known function of the metal content; ii) they obey to a PL relation in the near infrared bands. Their periods range between about 0.2 days and 1 day, and since Bailey (1902) they are divided in two main classes: RRab with relatively high amplitude ($0.4 < A_v < 1.5$) decreasing with the period, periods ranging from $\sim$ 0.4 to 1 day, and asymmetric light curve shapes; and RRc, with amplitudes ranging from $0.2 < A_v < 0.6$ mag, periods around 0.2-0.4 days, and sinusoidal light curve shapes. The theory of pulsation has shown that RRab pulsate in the fundamental mode, while RRc pulsate in the first overtone. In addition there are also double-mode variables, pulsating simultaneously in the fundamental and first overtone modes, and it has also been suggest that RR Lyrae stars may pulsate in the second overtone (e.g., Alcock et al. 1996,; Clement &

Rowe 2000). An intriguing and not well understood phenomenon is the so called Blazhko effect present in some RR Lyrae, and consisting in a periodic modulation, on a much longer timescale than the primary period, of the light curve shape. The Blazhko period falls in the range between $\sim$ 5 days and 530 days. Fig. 2.3 illustrated the different types of RR Lyrae stars. According to evolutionary models, these variables are the progeny of stars that begin their life in the main sequence with a mass near 0.8 $M_{\odot}$. Like other low-mass stars, they spend most of their lifetime in this sequence burning H into He in their cores and, after perhaps $\sim$ 10 Gyr, they climb the RGB where the core temperature becomes high enough to initiate helium fusion with a flash. Via the 3α reactions helium burning is ignited in a degenerate core and these reactions induces a violent re-adjustment in the giant structure, and the stars will contract toward their ZAHB location, where a new equilibrium is attained burning helium into carbon at the centre, and hydrogen into helium in a shell surrounding the helium-rich core. According to this scenario, RR

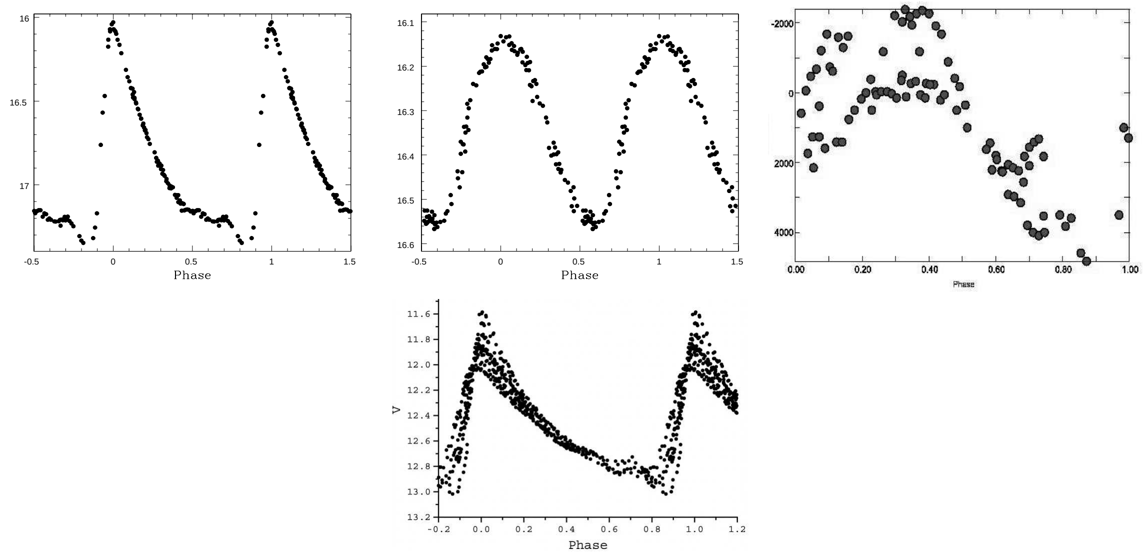

Figure 2.3: Examples of RR Lyrae star light curves: RRab, upper left; RRc, upper center; RRd, upper right; and Blazhko RR Lyrae, lower center.

Lyrae variables are unanimously recognized as HB stars that cross the instability strip during their central He-burning evolutionary phase.

Being part of the oldest stars in the Universe, they have long been known to be present in large numbers in GCs, and to represent the ancient population in systems composed by stars of different ages and compositions. Accordingly, they can be used as ideal tracers of the old component ($t > 10$) in the MW and external galaxies. On the other hand, as stated above, they are important primary distance indicators due to their characteristic variability and to the fact that their mean brightness has been known to be nearly constant in any given GC since a century ago. Nowadays, it is widely accepted that the RR Lyrae visual magnitude has an approximately linear dependence on metallicity (see Caputo et al. 2000, for a non linear dependence) and that evolutionary effects must also be take into account. For our purposes, we assume that the $M_v(RR) - [Fe/H]$ is linear, with the slope value estimated by Clementini et al. (2003) and Gratton et al. (2004), and the zero point value consistent with a distance modulus for the LMC of 18.52± 0.09 mag (Clementini et al. 2003), i.e. $M_v(RR) = (0.214 \pm 0.047)[Fe/H] + (0.86 \pm 0.12)$. Fiinally, as already mentioned, RR Lyrae stars are characterized by a quite narrow PL relation in the near-infrared bands that has been found to be sensitive to metallicity (see e.g. Bono et al. 2003, Sollima et al. 2006.)

2.4.1 The Oosterhoff Dicothomy

Seventy years ago, P.Th.Oosterhoff discovered that the Galactic GCs could be divided into two groups according to the mean periods of their RR Lyrae stars. Studying a sample of only 5 GCs, he published a short paper giving just“some remarks on the variable stars in GCs” (Oosterhooff 1939), obviously unaware that his discovery could be hiding a recipe for understanding the formation of the MW. In this paper, he classified those clusters whose fundamental mode RR Lyrae stars showed mean periods, $\langle P_{ab} \rangle$, close to 0.55 days (M3, M5) as Oosterhoff I (OoI), while those with mean periods close to 0.65 days (Omega Centauri, M15, and M53) as Oosterhoff type

II (OoII). Differences in the mean periods of the RRc variables ($\langle P_c \rangle$) in these clusters were also present. Oo I clusters had RRc mean periods near 0.32 days, while those classified as OoII, showed mean periods close to 0.37 days. He also noted that the percentage of c-type variables differed between the two groups, in the sense that the RR Lyrae populations in OoI clusters were largely dominated by ab-type pulsators whereas OoII clusters generally contained a more balanced proportion between c and ab-type pulsators, although he was aware that incompleteness and selection effects may alter this property. Though the sample of clusters originally examined by Oosterhoff was small, subsequent works (Oosterhoff 1944, Sawer 1944) including new RR Lyrae-rich GCs soon confirmed the dichotomy. When in the 1950s metal abundances began to be determined for GCs, it became evident that these two classes were associated with differences in metallicity. OoI clusters were moderately metal-poor, while OoII clusters were very metal-poor. A summary of the Oosterhoff properties of the MW GCs is provided in table 2.4.1. The most recent studies (see e.g., Cetalan 2009, for a review), involving larger samples of GCs, more accurate metallicities, precise periods for the RR Lyrae stars, and better completeness, have fully confirmed the Oosterhoff dichotomy not only for GCs, but also for the halo field stars in the MW. In Figure 2.4, $\langle P_{ab} \rangle$ is plotted against [Fe/H] for GCs containing a significant number (at least 10) of RR Lyrae stars. The separation into two Oosterhoff groups is evident, as well as the so-called "Oosterhoff gap", the region that covers the period range between $0.58 \lesssim \langle P_{ab} \rangle \lesssim 0.62$, that is basically avoided by Galactic GCs. Note that the figure shows also a gap for metallicities between $-1.6 \lesssim$ [Fe/H] $\lesssim -1.9$. The reason for this feature is that GCs with metal abundances in this range generally have horizontal branches which are extremely to the blue of the instability

Table 2.2: General properties of Oofterhoff I and II GCs

Type	$\langle \mathbf{P_{ab}} \rangle$ (days)	$\langle \mathbf{P_c} \rangle$ (days)	$\mathbf{n(c)/n(ab+c)}$	[Fe/H]
OoI	0.55	0.32	0.17	$\gtrsim -1.6$
OoII	0.64	0.37	0.44	$\lesssim -1.6$

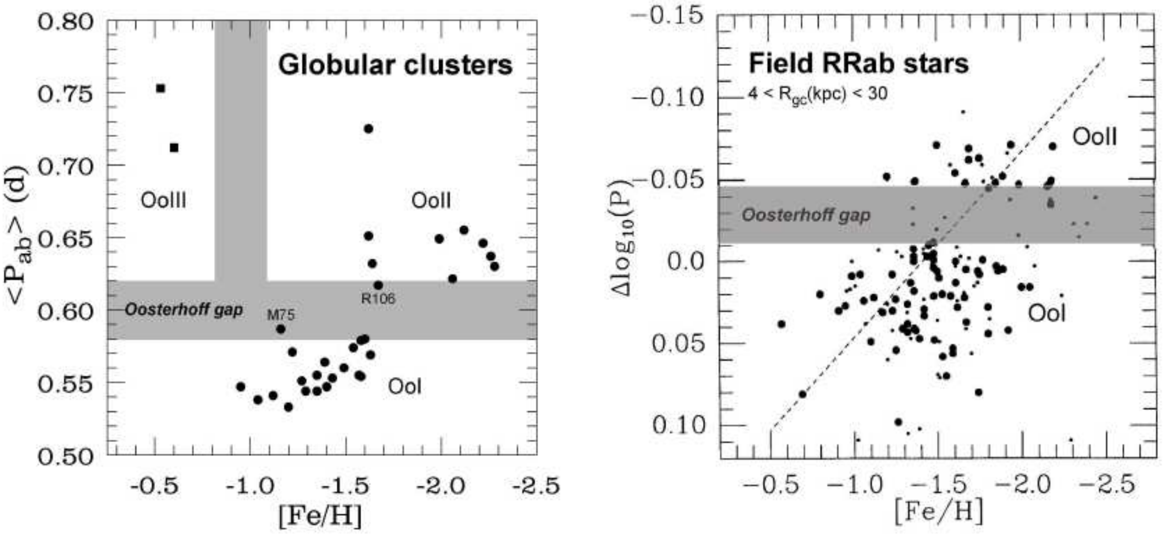

Figure 2.4: Oosterhoff dicothomy in GCs (left) and in the field (right). Only GCs with at least 10 RRab are plotted, except for the OoIII globular cluster NGC 6388 with has only 9 RR Lyrae stars. In the plot with the field variables, period shifts were measured with respect to the M3 RR Lyrae stars (taken from Catelan 2004).

strip, and hence have very few RR L yrae stars. On the other hand, metal-rich glubular clusters such as 47 Tuc ([Fe/H]=-0.7) have most of the time stubby red horizontal branches that fall almost entirely to the red side of the instability strip, and thus have almost no RR Lyrae at all. Interesting however, are the cases of the GCs NGC6388 and NGC6441 which have [Fe/H] values of −0.6 and −0.5 dex, respectively. Despite their high metallicities, they have blue HB components in addition to the red horizontal branch usually seen in GCs of that metallicity. This blue extension crosses the instability strip, so that numerous RR Lyrae stars occur in both clusters, and unexpectedly, their values of $\langle P_{ab} \rangle$ are among the longest known for any cluster. Because of their bizarre position in the [Fe/H]-$\langle P_{ab} \rangle$ diagram, they have defined a new class of objects; the Oosterhoff type III GCs (Pritzl et al. 2000).

The center panel of figure 2.5 shows the run of $\langle P_{ab} \rangle$ as a function of the fraction of c-type RR

Lyrae variables, $f_c \equiv N_c/(N_c + N_{ab})$. This plot suggests that, while there is a trend for OoI clusters to have smaller values of f_c than OoII clusters, practically any value of f_c is allowed for both OoI and OoII clusters, thus suggesting that, f_c is not a good diagnostic of the Oosterhoff status. Likewise, the left panel of Figure 2.5 shows the run of $\langle P_{ab} \rangle$ with the average c-type period $\langle P_c \rangle$. As can be clearly seen from this plot, $\langle P_c \rangle$ does not appear to be a good Oosterhoff indicator either. Note that, since the pioneering work of Oosterhoff (1939, 1944), these two parameters have been considered important indicators of the Oosterhoff status. Finally, the right panel of Figure 2.5 shows the correlation between $\langle P_{ab} \rangle$ and the corresponding shortest period of the ab-type stars $P_{ab,min}$, that indicates the transition period between RRab and RRc variables. As can clearly be seen, there is not only a strong global correlation between these two quantities, but also a strong correlation within each Oosterhoff group. Therefore, it seems that $P_{ab,min}$ along with $\langle P_{ab} \rangle$ are the most important quantities defining the Oosterhoff behavior.

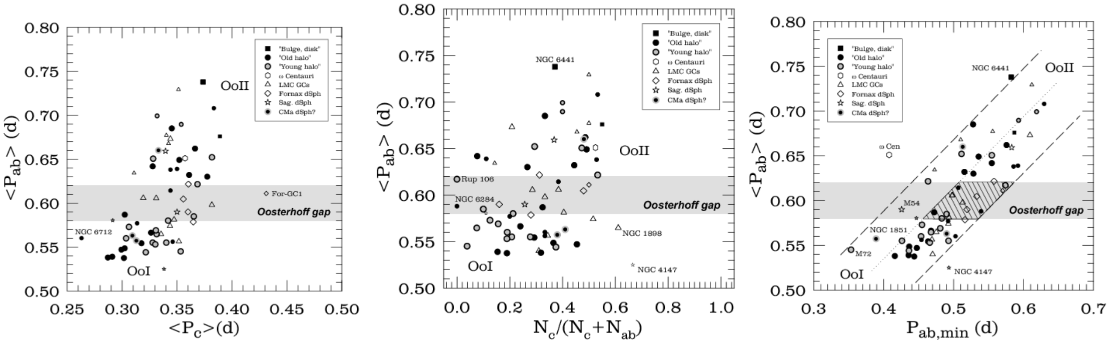

Figure 2.5: The average period of ab-type RR Lyrae stars $\langle P_{ab} \rangle$ as a function of: (Left) average period of c-type stars; (Center) fraction of c-type pulsators with respect to the total number of RR Lyrae stars; and (Right) as a funtion of the minimum period of the RRab stars, $P_{ab,min}$. The only clear correlation exists for $\langle P_{ab} \rangle$ vs. $P_{ab,min}$ (taken from Catelan et al. 2010, in preparation).

2.4.2 Physical Origin of the Oosterhoff Dicothomy

Although much time has passed since the discovery of the dichotomy in Galactic GCs, its physical origin is still controversial. According to Sandage (1993) the dichotomy was due to a difference in period between individual ab pulsators at fixed effective temperature. Taking into account the van Albada & Backer equation (1971), this implied a difference in luminosity higher than what expected on the basis of the canonical evolutionary scenario, and with the unpleasant consequence that Y should be anti-correlated with Z (see Bono et al. 1995, for a discussion). The favored theoretical explanation for the Oosterhoff phenomenon is related to a sort of *hysteresis mechanism* (van Albada & Backer 1973). According to this explanation, the Oosterhoff dichotomy is due to a different distribution of ab and c pulsators in the OR region, that is the region of intersection between the fundamental and the first overtone in the instability strip, where in principle both pulsation modes are efficient. In particular in OoI GCs the OR region is expected to be mainly populated by RRab, whereas in OoII GCs it should be mainly populated by RRc. This different behavior should be caused by an hysteresis mechanism according to which in the OR region the pulsation mode is determined by the star's previous evolutionary path (see left panel of Fig. 2.6). Thus, RRab stars entering the OR region from the red side continue to pulsate in the fundamental mode until they reach the blue edge of the fundamental mode, and then become RRc stars. On the other hand, RRc variables entering the OR region from the blue side, continue to pulsate in the first overtone mode until they reach the red edge of the first overtone mode, where they start to pulsate in the fundamental mode. This mechanism would naturally explain the Oosterhoff groups if RR Lyrae stars in OoII clusters are evolving redward from a position mainly on the blue side of the HB, whereas those RR Lyrae stars in OoI clusters contain a mix of unevolved and blueward evolving stars. The right panel of Fig. 2.6, shows schematically the situation for a single evolutionary track. As one can see, in cases a), b) and c) periods come from both low (unevolved) and high (evolved) luminosity pulsators, while in c) and d) an abrupt increase in mean periods of the fundamental pulsators is expected

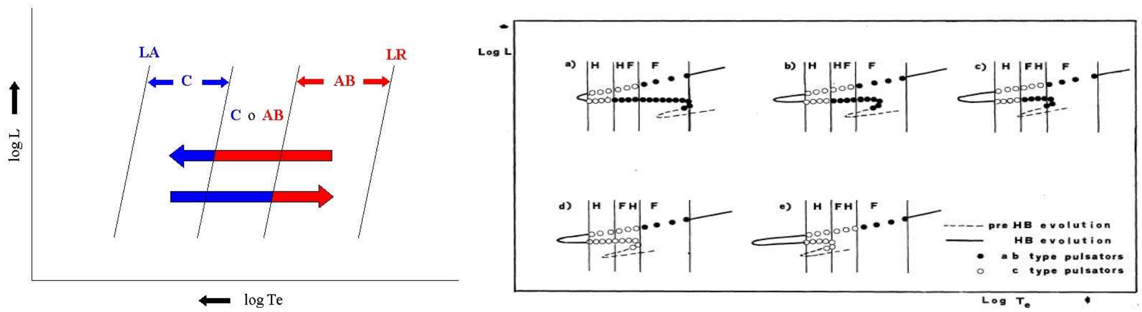

Figure 2.6: Left panel: Schematic diagram illustrating the pulsation zones inside the instability strip under the hysteresis mechanism proposed by van Albada & Backer. Right panel: An example of how the instability region is populated by RRab (filled dots) and RRc (open dots) during the main phase of the HB evolution, under the hysteresis mechanism (taken from Caputo et al. 1978).

because the contribution of lower (unevolved) luminosity ab-type pulsators suddenly disappears. We note that the Hysteresis scenario is supported by the results of nonlinear convective pulsation models (see Bono et al. 1995, Bono et al. 1997).

2.4.3 What causes the Oosterhoff dichotomy in the MW?

Sandage et al. (1981) argued that RR Lyrae stars in OoII clusters had longer periods mainly because they were more luminosus than those in OoI clusters. The higher luminosity in OoII group should be caused by the low metallicity of these clusters, even if the amount of overluminosity required to explain the Sandage period effect was to high to be explained by the canonical evolutionary scenario. This has been generalized to a relation between [Fe/H] and absolute V magnitude $\langle M_v \rangle$, for the RR Lyrae stars, with the more metal poor pulsators also being intrinsically brighter. On the other side, Lee et al. (1990) concluded, from the study of horizontal branch models, that the Oosterhoff dichotomy is instead a morphological issue: RR Lyrae variables in OoII GCs, with their predominantly blue HB types, are evolved away from a position on the blue zero-age horizontal branch (ZAHB), and therefore, they cross the instability strip at higher luminosities (and lower masses) and thus their periods are longer. Conversely, RR Lyrae stars in OoI clusters, with their uniformly populated or red HB morphologies, are mostly “unevolved” or ZAHB objects, which translates into lower luminosities and therefore lower periods. Thus the Oosterhoff type, is determined not by the metallicity of the cluster but rather by the HB type. Whether the metallicity or the HB morphology or a combination of both effects is controlling the Oosterhoff status of a GC is still unclear. While Lee & Carney (1999) showed that for the case of GCs with similar metallicities but very different horizontal branch morphologies, the Oosterhoff classification is determined by the latter, Contreras et al. (2005; 2010), on the other hand, concluded that metallicity, at a fixed HB type, is a key parameter determining the Oosterhoff status of a GC. Consequently, both [Fe/H] and HB type are responsible for the observed period dichotomy, as the evolutionary effects are crucial in determining the Oo type.

2.4.4 The Oosterhoff dichotomy: a formation dichotomy?

Further studies on the Oosterhoff dichotomy have revealed that the well defined Oosterhoff groups have also differences in age, spatial distributions, kinematics and even origin. Lee & Carney (1999) discussed the kinematic differences between Oosterhoff group I and II clusters (see left panel of Fig. 2.7). Their results showed that the OoI clusters have zero or retrograde rotation, while the OoII clusters have prograde rotation, confirming a similar conclusion of van den Bergh (1993). In their opinion, the difference in kinematics and ages between Oosterhoff group I and II clusters suggests that they may have different origins: the Oosterhoff II clusters were formed very early in the proto-Galaxy while the Oosterhoff I clusters were formed at different locations and at a later time, and were probably the result of merging events. Independently, De Angeli et al. (2005) found that nearly all the MW clusters with [Fe/H]< -1.7 are older (by about 1.5 Gyr) than the intermediate metallicity ($-1.7 < [Fe/H] < -0.8$) (see right panel of Fig. 2.7), confirming that OoII clusters would be, on average, older than OoI clusters. In the same vein, Yoon & Lee (2002) found evidence that most of the lowest metallicity ([Fe/H] < -2.0) OoII clusters have a very peculiar spatial distribution; they seem to display a planar alignment in the outer halo. This alignment, combined with evidence from kinematics and stellar population, indicates a captured origin from a satellite galaxy, at odds with Lee & Carney's conclusions. Whatever the true hypothesis, it is logical to guess that each Oosterhoff group possibly originated in a different event in the halo, since the Oosterhoff dichotomy reflects conditions within the MW halo at the time of GC formation.

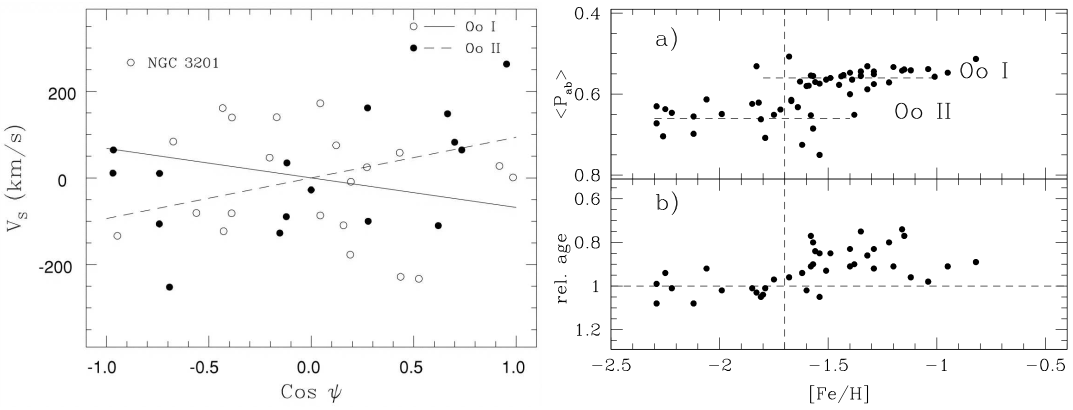

Figure 2.7: Right panel: The mean rotation velocity $\langle V_{rot} \rangle$ is given by the slope of the straight lines. The fit for the OoI clusters is represented by the solid line and indicates that this group have retrograde rotation, while OoII clusters, fitted by the dashed line have prograde rotation (taken from Lee & Carney 1999). Right panel: a) The Oosterhoff diagram for Galactic GCs; b) Distribution of relative ages vs. metallicity for the same Galactic GCs, showing evidence of an older age for OoII clusters.

Chapter 3

The Andromeda Galaxy

The Andromeda galaxy (R.A.=$00^h42^m44.3^s$, Dec=$41^o16'09''$) is the closest giant spiral galaxy to our own and the only other giant galaxy in the Local Group, which includes besides Andromeda, the Milky Way (MW), the Triangulum galaxy (M33), and about 40 dwarf satellite galaxies, a number that is continuosly increasing thanks to new and deep surveys such as the Sloan Digital Sky Survey (SDSS; York et al. 2000) of the MW surroundings, and the Isaac Newton Telescope (INT) and the Canada-France-Hawaii Telescope (CFHT) panoramic surveys of Andromeda by Ferguson et al. (2002), Ibata et al. (2007), and McConnachie et al. (2009). In many ways Andromeda is the "sister" to the MW, having very similar total mass (including the dark matter, Evans et al. 2000; Ibata et al. 2004), having shared a common origin, and probably sharing the same ultimate fate when they finally merge in the distant future (Ibata et al. 2007). The Andromeda galaxy is also known as M31, NGC 224 and often referred to as the Great Andromeda Nebula.

3.1 A bit of History

The first known record of M31 is by the Persian astronomer al-Sufi (903-986), however, a first description was given by Marius in 1612, who was the first person to view Andromeda through a telescope. In 1764, the Andromeda galaxy was catalogued by Messier as M31 because it was the 31^{st} object in his catalogue of diffuse objects, that he found not to be a comet. The stellar nature of Andromeda was deduced by Huggins studying its spectra in 1864, while the spiral nature was first clearly shown in photographs obtained by Roberts (1887) with a 0.5-m reflector. In 1923, Edwin Hubble found the first Cepheid variable in the Andromeda galaxy, and thus demonstrated conclusively that this diffuse object was not a cluster of stars and gas within our Galaxy, but an entirely separate galaxy located a significant distance from our own. Because he was not aware of the two Cepheid classes, his distance was incorrect by a factor of more than two, though. Hubble published his epochal study of the Andromeda "nebula" as an extragalactic stellar system (galaxy) in 1929 (Hubble 1929). In 1943, Walter Baade was the first to resolve stars in the central region of the Andromeda Galaxy. Based on his observations of this galaxy, he was able to discern two distinct populations of stars based on their metallicity, Population I (young metal rich) and Population II (old metal poor) stars. This nomenclature was subsequently adopted for stars within the MW, and elsewhere. Baade also discovered that there were two types of Cepheid variables, which resulted in a doubling of the distance estimate to M31, as well as the whole Universe.

3.2 Canonical Structure

M31 is a galaxy of SA(s)b type in the de Vaucouleurs-Sandage extended classification system of spiral galaxies. "SA" stands for spiral galaxy without bars, (s) indicates the absence of ring-like structures and finaly "b" denotes that the spiral arms are not significantly tightly-wound. Note that this classification is not longer entirely correct since recently a near-infrared survey from

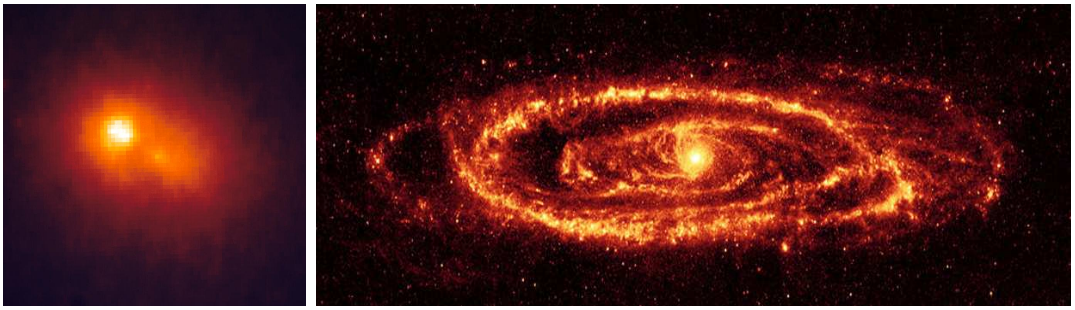

Figure 3.1: Left panel: HST image of the Andromeda core showing a possible double structure (NASA/ESA photo). Right panel: M31 observed with IRAC, on board the Spitzer Space Telescope, at a wavelength of 8μm, showing the famous outer dust ring at ~ 10 kpc from the center (Block et al. 2006).

the 2MASS (Beaton et al. 2007) has confirmed earlier suggestions from optical studies: M31 is a barred spiral galaxy like the MW. The basic components of M31 are similar to those of our own Galaxy. These components, including the M31 GC system, will be briefly described in the following sections.

3.2.1 Nucleus & Disk

The nucleus of Andromeda consists of two concentrations separated by 0.49 arcsec (Lauer et al. 1993, see left panel of Fig. 3.1). The brighter concentration is offset from the center of the galaxy. The dimmer concentration falls at the true center of the galaxy and contains a $\sim 3-5\times 10^7 M_\odot$ black hole (Lauer et al. 1993). Several explanations have been proposed as the cause of this structure, including an accreted small satellite galaxy (Corbin et al. 2001), a few blue horizontal branch globular clusters tidally disrupted and a large nuclear star cluster partially obscured by a ring of gas. However, the solution with larger acceptance has been proposed by Tremaine (1995) who argued that the nucleus of M31 may be a thick eccentric disk, composed of stars traveling on nearly Keplerian orbits around a black hole. The eccentricity is such that stars linger at the orbital apocenter, creating the brighter concentration of stars. In 2005, Hubble Space Telescope data have confirmed and improved Tremaine's solution, adding that the two bright blobs are actually composed of an elliptical ring of older red stars and a smaller, brighter, and denser disk of young blue stars about 200 million years old around the galaxy's central black hole. Binary nuclei have also been found in other galaxies (see e.g., Lauer et al. 1996 for the particular case of NGC 4484B) suggesting that such objects may not be particularly rare.

Andromeda shows a bright visible disk with two spiral arms embedded into it that are outlined by a series of HII regions and OB associations. This visible disk extends $\sim$ 25 kpc from the center. However, new studies (Ibata et al. 2005) support the hypothesis of a huge rotating structure that follows an exponential density law with scale length of 5.1 kpc out to a deprojected distance of $\sim$ 40 kpc, with substructures continuing out even further in radius ($\sim$ 70 kpc). This scale length is similar to that of the inner disk, so it appears that the large-scale properties of the outer disk structure follow on smoothly from those of the inner disk. The stars that belong to this structure show a wide metallicity range, with a mean metallicity of [Fe/H] = -0.9 dex. When observed in the infrared, what optical telescopes interpret as a big galaxy typically spiral-shaped, turns out to be structured in multiple concentric rings. In fact, images taken with the Spitzer Space Telescope confirm that a $\sim$ 10 kpc ring is the most evident feature on the disk (Block et al. 2006; see right panel of Fig. 3.1). A large fraction of the dust and most of the gas of the galaxy gathers on this ring. Analysis of the cross-sectional shape of the galaxy appears to demonstrate a pronounced, S-shaped warp, rather than just a flat disk. Andromeda's warp is especially pronounced on the northeast side of its major axis. A possible cause of such a warp could be gravitational interaction with the satellite galaxies near M31 (see section 3.2.4 for more details).

3.2.2 The Spheroid (Bulge & Halo)

At first glance, Andromeda and the Milky Way appear to be very similar; both are of similar Hubble type, luminosity, size (van den Bergh 1992, 2000; Klypin et al. 2002), and total mass (including dark matter; Evans et al. 2000; Ibata et al. 2004; Watkins et al. 2010). However, comparison has also revealed several notable differences between the two galaxies. The stellar density of the M31's spheroid appears to be 10 times higher than that at a comparable location in the Milky Way (Reitzel et al. 1998). Mould & Kristian (1986) surprisingly found that the "halo" of M31 at R$\sim$ 7 kpc is also 10 times more metal-rich than the Milky Way's, and Brown et al. (2003) found at similar distances that in the mean the stellar population in M31 is intermediate-age. Further studies of the metallicity distribution function in M31 not only confirmed this result, but also showed that there is no evidence for an abundance gradient out to 30 kpc (Durrell et al. 2001, 2004; Bellazzini et al. 2003), a result at odds with model predictions. The canonical picture of an old, metal-poor population simply does not appear to describe the M31's halo. Until recently, there appeared to be another striking structural difference between the Milky Way and M31 spheroids. Whereas the Milky Way shows a de Vaucouleurs $R^{1/4}$ (de Vaucouleurs 1958) surface brightness profile in the inner regions of the Galaxy (bulge) and a power-law R^{-2} projected profile for the halo in the outer parts (halo), Pritchet & van den Bergh (1994) found that the entire spheroid of M31 could be fit by a single $R^{1/4}$ profile. Their star-count measurements extended out to R $\sim$ 20 kpc along the southeast minor axis of M31. Similarly, Durrell et al. (2004) found that an $R^{1/4}$ law is consistent with the M31's surface brightness profile out to 30 kpc.

Ostheimer (2003) carried out a survey that was a significant improvement over previous works in terms of spatial coverage (R$\sim$ $10-165$ kpc). His M31 surface brightness profile showed the first sign of a flattening (e.g., deviation of the slope from a de Vaucouleurs profile) finding preliminary evidence of a metal-poor stellar halo in M31. Guhathakurta et al. (2006) showed that M31 does possess a stellar component that is structurally distinct from its bulge and whose radial extent (R $>$ 160 kpc) and surface brightness profile ($\sim R^2$) resemble those of our Galaxy's stellar halo. Finally, Kalirai et al. (2006) showed that this newly discovered stellar halo in M31 is chemically distinct from its bulge and is in fact quite metal-poor: [Fe/H] $= -1.5$. Moreover, they showed that the crossover between the metal-rich and metal-poor components occurs at a minor-axis distance of ~ 30 kpc, in excellent agreement with the transition radius that separates the discovered halo of M31 from the inner de Vaucouleurs ($R^{1/4}$) bulge. Taken together, these results clarify that the actual structural disparities between the Milky Way and M31 may not lie in the properties of their halo populations, but rather in the relative sizes of the bulges of the two systems. It is possible that previous studies had mistakenly identified the outer parts of Andromeda's central bulge as its halo. The discovery of this metal-poor stellar halo also provides a powerful confirmation of galaxy formation models.

3.2.3 The Globular Cluster system

As first recognized by Hubble (1932), the M31 globular clusters (GCs) occupy a unique place in the study of these systems since they provide a bridge between the Galactic GCs, where observations allow to study the individual stellar properties, and the extragalactic clusters, where the integrated properties are the only observables. Indeed, Andromeda is perhaps the only case in which the integrated properties of GCs can be compared with their actual resolved stellar populations. Perhaps, the main difference between the M31 and MW GC systems is that the former is more populous with an estimated total number of ~ 600 members (Barmby et al. 2000; Perrett et al. 2002; Huxor et al. 2008; Caldwell et al. 2009; and the Revised Bologna Catalogue V.4 available at www.bo.astro.it/M31) and may contain a significant population of intermediate-age (3-6 Gyr) globular clusters (Beasley et al. 2005). Otherwise M31 and MW GCs share many similarities: a Gaussian-like luminosity function that peaks around $M_V = -7.62$ mag with a dispersion of 1.06 mag (Barmby, Huchra & Brodie 2001); two subpopulations with mean metallicities [Fe/H]=-1.57 and -0.61, associated respectively with the halo and bulge (Barmby, Huchra & Brodie 2001; Forbes, Brodie & Larsen 2001), and similar structural properties (Barmby et al. 2007). Outer halo globular clusters have also been discovered recently in M31 beyond a projected radius of 70 kpc, but remain rare. There also significant differences, though: Huxor et al. (2005) discovered a new class of GCs in the M31 halo which, although having globular-like colors and luminosities, have unusually large half-light radii of ~ 30 pc. These objects start to fill the gap in parameter space between (negligible dark matter) classical GCs and (dark matter dominated) dwarf spheroidals, and have no known analogues in the MW, where such clusters would certainly have been discovered if they existed, unless hidden by the Galactic plane. In the same vein, Fusi Pecci et al. (2005) have claimed the presence in M31 of stellar systems similar to the MW GCs in luminosity and shape, but with integrated colors significantly bluer (BLCCs: Blue Luminous Compact Clusters) than the bluest MW counterparts. They provided some evidence suggesting that clusters of similar age ($\lesssim 2$ Gyr) and total luminosity may be lacking in the MW. While the luminosity range spanned by the BLCCs is within that of ordinary GCs, the age distribution of the present-day MW GCs is not consistent with the young age of the BLCCs. On the other hand, Galactic open clusters are comparably young, but they appear less luminous on average than the BLCCs. From a photometric study of 10 GCs, Rich et at. (2005) concluded that the HB morphology of the M31 GCs follow the same behavior with metallicity as for the Galactic globulars, with indications that the second-parameter effect can be present in some clusters of their sample, but with a difference: while in the MW the second-parameter phenomenon affects only clusters in the metallicity range approximately between [Fe/H] = -1.1 and -1.6, in M31 the effect would appear to occur at a lower metallicity ([Fe/H] $=\sim -1.7$) resembling what is found for the GCs in the Fornax dwarf spheroidal galaxy. We note that "The Osservatorio Astronomico di Bologna" (OAB) M31 team, in collaboration with other scientists, is carrying out the exhaustive systematic census of M31 GC candidates, using both photometry and spectroscopy. As a result, a continuously updated catalogue of globular clusters in M31 is avaliable in electronic form[1].

---

[1] www.bo.astro.it/M31

3.2.4 Scars of a Violent History

Within the framework of hierarchical structure formation, large spiral galaxies arose from the merger of many small galaxies and protogalactic systems. Theory predicts that the complete destruction of these “building blocks” is usually progressive, and may take several orbits. The stellar debris from the destroyed dwarf galaxy follow a similar orbital trajectory than the progenitor, and so the tidally disrupted matter tends to be deposited over a broad range in distances from the larger accreting galaxy. Over time, with the accumulation of many such mergers, large galaxies develop an extensive stellar and dark-matter halo, the latter being by far the most massive component of the galaxy. If this prediction is correct, then the haloes of the large galaxies should contain significant amounts of substructures all around their main bodies. In the Milky Way, the Sagittarius stream (Ibata et al. 1994; Majewski et al. 2003), the Magellanic stream (Mathewson et al. 1974), the Monoceros stream (Yanny et al. 2003), the phase-space clumping of halo stars in the solar neighborhood (Helmi et al. 1999), and the tidal tails emanating from halo globular clusters (e.g., Grillmair et al. 1995; Odenkirchen et al. 2001; Leon, Meylan, & Combes 2000) and dwarf spheroidal galaxies (e.g., Irwin & Hatzidimitriou 1995; Majewski et al. 2000), are clear signatures that merging processes are prominent in massive galaxies and are still occurring today. Then, the question that arises naturally is, are these cannibalized substructures as common in the haloes of galaxies as predicted by galaxy-formation theory? The answer is still not clear, however, in the particular case of Andromeda, stars and coherent structures have been detected that are almost certainly remnants of dwarf galaxies destroyed by the tidal forces. van den Bergh (2000, 2006) suggested that M31 originated as an early merger of two or more relatively massive metal-rich progenitors. This would account for the wide range in metallicity (Durrell, Harris, & Pritchet 2001) and age (Brown et al. 2003) observed in the M31 halo, compared to the MW. Among the most spectacular signatures of present and past interactions in M31 is a giant stream of metal-rich stars (Ibata et al. 2001) extending several degrees from the M31 center (McConnachie et al. 2003) along a line connecting the galaxy to its dwarf companions

M32 and NGC205 (McConnachie et al. 2004), thus suggesting a connection between the giant stream and these two dwarf galaxies. If this is the case, it is possible that this kind of complex interactions may explain the extreme warp in the stellar disk as well (Ibata 2001). Metallicity, luminosity, and alignment with M32 are consistent with the M31 stream being tidally extracted from M32 (Ibata e al. 2001, Choi et al. 2002, Ferguson et al. 2002). Its low velocity dispersion (11 km/sec) supports the notion that it is a coherent interaction remnant, but Keck/DEIMOS spectroscopic studies tend to disfavor M32 as the stream progenitor (Font et al. 2006). The M31 disk appears to have irregular shape at large radii and shows a wealth of substructures that must be transitory in nature and are almost certainly tidal debris (Ibata et al. 2005). The infrared photometry of the M31 disk obtained by IRAS (Habing et al. 1984) and by the Spitzer Space Telescope (Barmby et al. 2006) revealed the two unusual rings of star formation off-centered from the M31 nucleus (Block et al. 2006, and references therein) already mentioned in section 3.2.1. They appear to be density waves propagating in the disk. Numerical simulations show that both rings may result from a companion galaxy plunging head-on through the center of the M31 disk about 210 Myr ago (Block et al. 2006). Similar hypotheses have been suggested to explain the peculiar double nucleus of M31 who might be caused by a smaller satellite galaxy that was "eaten" by Andromeda (Corbin et al. 2001).

Ferguson et al. (2002) and Ibata et al. (2007) presented the first panoramic views of the Andromeda galaxy, based on deep INT and CFHT photometric observations that cover respectively the galaxy inner 55 kpc, and the southern quadrant out to about 150 kpc, with an extension that reaches M33 at a distance of about 200 kpc. Their data show the giant stream in all its extension and reveal also a multitude of streams, arcs and many other large-scale structures of low surface brightness, as well as two new M31 dwarf companions (And XV and And XVI). Twelve dwarf galaxies were known to be M31 companions until 2004, among which only 6 classical, bright dSphs (namely, And I, II, III, V, VI and VII; see, e.g. McConnachie et al. 2006, and references therein), but an additional 12 new, fainter M31 dSph satellites were discovered in the last five years mainly based on the INT and CFHT data. The most recent census is reported by Martin

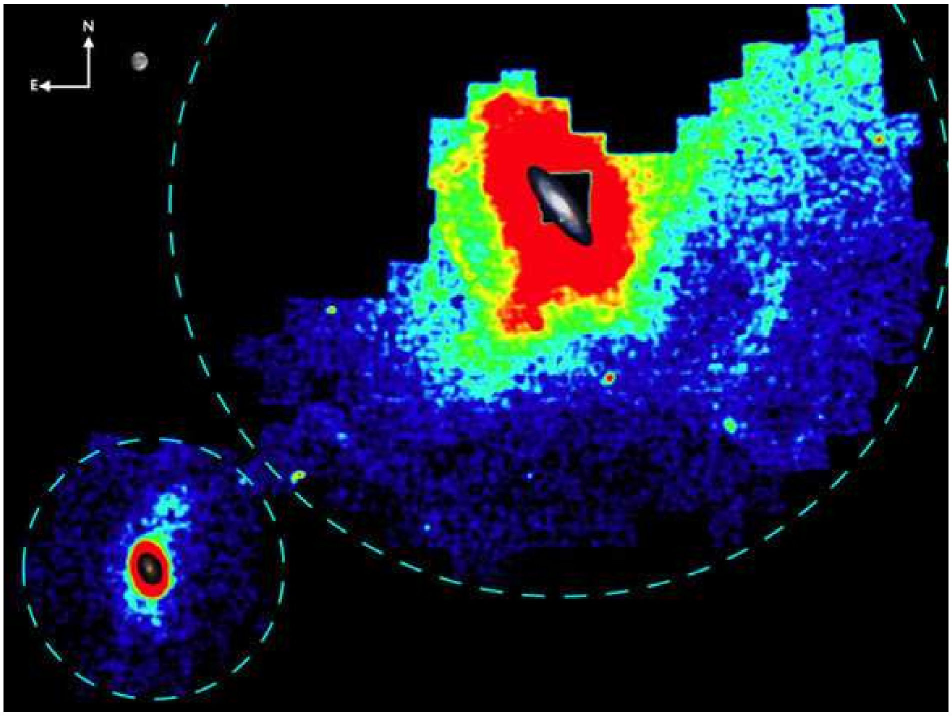

Figure 3.2: Stellar density map of the Andromeda-Triangulum pair highlighting the largest and most obvious substructures as evidences of merging, accretion and tidal interactions (taken from McConnachie et al. 2009).

et al. (2009) along with the discovery of two new M31 dSph satellites: And XXI and And XXII, as a result from the first year data of the "PanAndromeda Archeaeological Survey" (PAndAS; McConnachie et al. 2009). Started in August 2008, the PAndAS survey is extending the global view of M31 and of its companion M33 by collecting data with MegaPrime/MegaCam on the 3.6 m CFHT, for a total area of 300 square degrees and out to a maximum projected radius from the M31's centre of about 150 kpc. This survey will likely detect several other M31 faint satellites. Bright and faint M31 dSphs are shown by open square in Fig. 1.7. Not only new structures have been discovered (McConnachie et al. 2009) including a radial overdensity along the northwest minor axis extending nearly 100 kpc from M31 (see Fig. 3.2), a diffuse structure to the southwest coherent over an arc spanning ~ 40 kpc at a distance of ~ 100 kpc from M31, and an apparent continuation of a previously known stream in the east, $\sim$ 50 kpc from M31 that loops around to the north of the galaxy, but even more intriguing are two prominent stellar structures extending from M33 in the direction of M31 (see left bottom corner of Fig. 3.2), suggestive evidence of a tidal disturbance excited as this galaxy orbits around M31. Finally, as in the MW, some of the M31 GCs have been suggested to be the remnants of dSph galaxies "cannibalized" by M31. This is the case of G1, the brightest globular star cluster in the Local Group (see Fig. 1.7). G1 is metal rich ([Fe/H]= -0.73, Galleti et al. 2009), and presents a significant metallicity spread, a mass three times the total mass of ω Centauri and several structural parameters that suggest that it may actually be the stripped core of a dwarf spheroidal galaxy (Meylan et al. 2001). Supporting this idea is the proximity of the cluster to a significant stellar overdensity known as the G1 clump, located at a project distance of $\sim$ 35 kpc from the center, along to the southwestern major axis of the galaxy (Ferguson et al. 2002). Recently, Perina et al. (2009), based on different empirical evidences, hypothesized that the globular clusters B407 and B403 are both relics of a merging event as well.

Having in mind the rich harvest of merging evidences described above, the obvious further step is to understand whether these signatures are showing us just the most recent history of the Andromeda galaxy, or are, instead, a sign of an even more violent past, where the dwarf galaxies we see today orbiting around M31 are surviving replicas of the hierarchical formation process. There are different manners to try and answer this question, however, the last word belongs to the stars who really were there at the time of the M31 formation. Thus, one aim of this thesis is to use variable stars, in particular the RR Lyrae stars, which trace the oldest galaxy's populations, as probes to put constraints on the assembling history of the Andromeda galaxy.

3.3 RR Lyrae stars in Andromeda: Previous Works

RR Lyrae stars have not been widely studied in our nearest large neighbor galaxy, Andromeda, nor in its spheroidal and elliptical companion satellites.

Pritchet & van den Bergh (1987) made one of the first attemps to detect RR Lyrae stars in M31, using the Canadian-France-Hawaii 3.6m telescope (CFHT) to observe a field at a distance of 9 kpc from the center of M31 along the minor axis. They identified 30 RR Lyrae candidates and estimates periods for 28. All these variables are ab-type RR Lyrae stars (RRab) and have a mean period of $\langle P_{ab} \rangle = 0.548$ days, which suggests that the properties of the halo of M31 belong to a population having Oosterhoff type I properties. However, the phase coverage and photometric accuracy of Pritchet & van den Bergh (1987) data are such that periods are not univocally defined, nor the c-type RR Lyrae stars could be identified due to the photometric uncertainties and the lower amplitudes compared to the RRab variables.

Dolphin et al. (2004) observed the same field of Pritchet & van den Bergh (1987) with the 3.5m WIYN Telescope, and found 37 variable star candidates, of which 24 are likely RR Lyrae stars, and the remaining 13 are a mixture of Anomalous Cepheids, population II Cepheids, and blended RR Lyrae stars. With a window of only 8 hours of observations they had a very poor phase coverage for stars with periods near half a day, as is the case of RR Lyrae stars. The lack of adequate phase coverage produced aliases in the determination of periods. Many RR Lyrae stars could equally have periods of one-half or one-third of a day; a degeneracy very unfortunate given that an RR Lyrae can have either periods. For these reasons they were unable to classify the variable stars and therefore no mean periods nor Oosterhoff classification was possible for the RR Lyrae stars they had found.

The first definitive work on the RR Lyrae stars of M31 was published by Brown et al. (2004) and made use of 84 hours of imaging (250 exposures over 41 days) with the Advance Camera for Surveys/Wide Field Channel (ACS/WFC) on board the HST. They searched in a field located along the minor axis of M31 approximately 11 kpc from the center. Their analysis revelead a sample of RR Lyrae stars consisting of 29 RRab stars with a mean period of $\langle P_{ab} \rangle = 0.594$ days, and 25 RRc variables with a mean period of $\langle P_c \rangle = 0.316$ days. These values make it difficult to clearly place the old population in Andromeda into one of the two Oosterhoff classes (see section 2.4.1): the ratio of $\mathrm{RR}_c/(\mathrm{RR}_{ab}+\mathrm{RR}_c) \equiv f_c$ stars is within the range seen in Oosterhoff type II

(OoII) MW GCs, the mean period of the RRab variables is in the gap between Oosterhoff types, and the mean period of the RRc stars is in the range seen in Oosterhoff I (OoI) GCs. However, as discussed in Catelan et al. (2010, in preparation), neither f_c nor $\langle P_c \rangle$ are particulary reliable indicators of the Oosterhoff type, which would suggest rather an intermediate type for this field if we based the classification only on $\langle P_{ab} \rangle$.

Very recently, Sarajedini et al. (2009) used HST observations taken with the ACS/WFC to search for RR Lyrae stars of two fields in the M31 spheroid, between 4 and 6 kpc from the galaxy center and close to M32. They found 681 RR Lyrae variables of which 555 are ab-type with a mean period of $\langle P_{ab} \rangle = 0.557$ days and 126 are c-type with a mean period of $\langle P_c \rangle = 0.327$ days with light curves of excellent photometric and temporal coverage. The location of the RR Lyrae stars in the Period-Amplitude (Bailey) diagram, the ratio of c-type RR Lyrae to all types, the mean periods and the period distribution are all closer to RR Lyrae in Oosterhoff type I GCs in the MW, as compared to OoII clusters. It's important to note that these RR Lyrae stars are roughly equally distributed between the two fields, have same average magnitudes, metallicities and Oosterhoff types, thus suggesting that both fields are minimally contaminated by M32 RR Lyrae stars.

Moving to the M31 satellites, in a series of papers published between 2002 and 2005, Pritzl and collaborators studied the variable star component in 4 classical dSph galaxies surrounding M31 using Wide Field Planetary Camera 2 on board HST (WFPC2/HST) observations. In their first paper, Pritzl et al. (2002) presented the study of variable stars in Andromeda VI (hereafter And VI). A total of 118 variables were found, including 111 RR Lyrae stars that lie close to the Oosterhoff type I Galactic GCs in the Period - Amplitude diagram, although the mean period of the RRab stars, $\langle P_{ab} \rangle = 0.588$ is slightly longer than that of the typical MW Oosterhoff type I clusters, and the mean period of the RRc stars, $\langle P_c \rangle = 0.382$ suggests an Oosterhoff type II classification. In Pritzl et al. (2004) results were presented of a variability star search in Andromeda II (And II). They found 72 RR Lyrae stars in their field of view, with 64 pulsating in the fundamental mode, and 8 pulsating in the first-overtone mode. The mean periods are 0.571

Table 3.1: Oosterhoff properties of RR Lyrae stars in the M31 classical dSphs

Name	Distance[1] (kpc)	⟨[Fe/H]⟩	N(RRab+c+d)[1]	$\langle Pab \rangle^1$ (days)	Oo Type[1]
And I	765±25	−1.5	72+26	0.575	Oo I/Int
And II	665±20	−1.5	64+8	0.571	Oo I
And III	740±20	−1.9	39+12	0.657	Oo II
And V	820±16	−2.2	7+3	0.685	Oo II
And VI	815±25	−1.6	91+20	0.588	Oo Int

[1] Distances and properties of the RR Lyrae stars are from Pritzl et al. (2002) for And VI; from Pritzl et al. (2004) for And II; from Pritzl et al. (2005) for And I and III; and from Mancone & Sarajedini (2008) and Sarajedini (2009, private communication) for And V, (taken from Clementini 2010).

and 0.363 days for the RRab and RRc, respectively. All these values are consistent with an Oosterhoff type I classification for And II. Pritzl et al. (2005) presented the results of variable star searches in Andromeda I (And I) and Andromeda III (And III). A total of 100 variable stars were found in And I, while 56 were found in And III. These samples include 72 fundamental mode and 26 first-overtone RR Lyrae stars in And I, giving mean periods of 0.575 and 0.388 days, respectively. For And III, 39 RR Lyrae stars are pulsating in the fundamental mode, with a mean period of 0.657 days, and 12 are in the first-overtone mode with a mean period of 0.402 days. Following the mean period of the RRab variables, And I can be classified as Oosterhoff type I, while And III seems to belong to Oosterhoff type II class. Finally, using archival imaging from the WFPC2 onboard the HST, Mancone et al. (2008) investigate the stellar population of Andromeda V (And V). Their analysis of the variable star population of And V revealed the presence of 28 potential variables. Of these, 7 are certainly fundamental mode pulsators with $\langle P_{ab} \rangle = 0.685$, and 3 first overtone RR Lyrae stars. From these values they classified And V as an Oosterhoff type II system (Sarajedini 2009, private comunication). Results for these galaxies are summarized in table 3.1. Detection of RR Lyrae stars, without reliable period determination, is also reported for three of the big M31 dSphs, namely, NGC147, NGC185, and NGC205, which were found to contain, respectively, 36 (Yang & Sarajedini 2010, and references therein), 151 (Saha et al. 1990), and 30 (Saha et al. 1992) candidate RR Lyrae stars.

Alonso-Garcia et al. (2004) were the first to attempt and directly detect RR Lyrae stars in fields near the dwarf galaxy M32, an elliptical satellite companion of M31. They imaged a field $\sim 3.5'$ to the east of M32 with WFPC2/HST and compared it with a control field well away from M32, that should sample the M31 field stars. They identified variable stars which claimed to be RR Lyraes belonging to M32, however they were unable to derive periods and amplitudes, hence classify them in types. Very recently, Fiorentino et al. (2010) observed two fields near M32 with the ACS/High Resolution Channel (ACS/HRC) on board HST. They detected 17 RR Lyrae stars in the field closest to M32, and 14 RR Lyrae stars in the background field that samples the M31 disk. They found the same mean period for the RRab stars, $\langle P_{ab} \rangle = 0.59$ in the two fields, a value that may suggest an Oosterhoff intermediate (Oo-Int) classification, however, this conclusion must be taken with some caution since only one RR Lyrae star with a period within the Oosterhoff gap ($0.58 \lesssim \langle P_{ab}(\mathrm{d}) \rangle \lesssim 0.62$) is present in their data sample. They used completness arguments to infer that part of the RR Lyrae stars discovered in the field close to M32 are representative of the ancient population present in this galaxy, that seems to be indistinguishable from the ancient population of M31. In fact, they compared the pulsation properties of the RR Lyrae stars detected in the two fields and concluded that the two groups of variable stars do not present any significant differences. However, the color distributions in the two fields are different, with a population of red RRab variables not seen in the field characterizing M31. These red RRab stars might represent the M32 RR Lyrae population, but the small number of stars makes it impossible a definitive claim. Thus, it is still an open question the precise nature or even the confirmed presence of RR Lyrae stars in M32. Concerning the "dwarf spiral" M33, Sarajedini & Yang (2010) published an update review summarazing the situation. Although the study of RR Lyare stars in M33 began almost 25 years ago (Pritchet 1988), only recently (Sarajedini et al. 2006) has been unequivocally confirmed the presence of RR Lyrae stars in M33 halo (and probably also in the disk), suggesting that this component formed early in the history of M33, and accordingly the halos of M33, M31, and the MW are similar in this regard. Furthermore, they concluded that the RR Lyrae stars present in M33 have pulsational properties that are consistent with those in Oosterhoff type I Galactic GCs.

So far, there was only one previous attempt at detecting RR Lyrae stars in the GCs of Andromeda. Clementini et al (2001) investigated variability in clusters using WGPC2/HST archival data and made the first tentative detection of RR Lyrae stars in 4 M31 GCs, namely, G11, G33, G64 and G322. They used 4 F555W (V) and 4 F814W (I) frames per cluster, reduced them individually and identified RR Lyrae candidates from the comparison of their photometric variations with template light curves. A number of RR Lyrae candidates were identified in each cluster (2, 4, 11 and 8 respectively), but the small number of available data points and the short time baseline did not allow a definition of the light curves and hence periods.

This review of the literature reveals a significant deficiency in the study of the RR Lyrae stars in the M31 field and GCs. The situation before this work may be summarized in Fig. 3.3, which shows the classical Oosterhoff diagram (see section 2.4.1) for M31 objects. This figure clearly illustrated that the current knowledge concerning the Oosterhoff classification of Andromeda is based only on five M31 classical dSph galaxies, since no conclusive studies have been done so far on the GCs and, on the other hand, there is no general consensus regarding the classification of the M31 field, due to the relatively small areas covered in previous studies. In spite of the small number of M31 dSph galaxies studied so far, all Oosterhoff types (OoI, OoII, and Oo-Int) have been found and the M31 dSphs seem to be almost evenly distributed among the three types (see left panel of Fig. 3.3). The classical dSph galaxies in the MW, instead, seem to prefer the Oo-Int type ($\sim 70\%$) and occupy the Oo gap (see right panel of Fig. 3.3). Given the great astrophysical utility of the RR Lyrae variables and the large size on the sky of the Andromeda galaxy, a survey of these stars sampling a variety of regions and GCs in M31 is highly demanded, and can provide very valuable insights to re-construct the star formation and chemical enrichment histories of our nearest spiral neighbor.

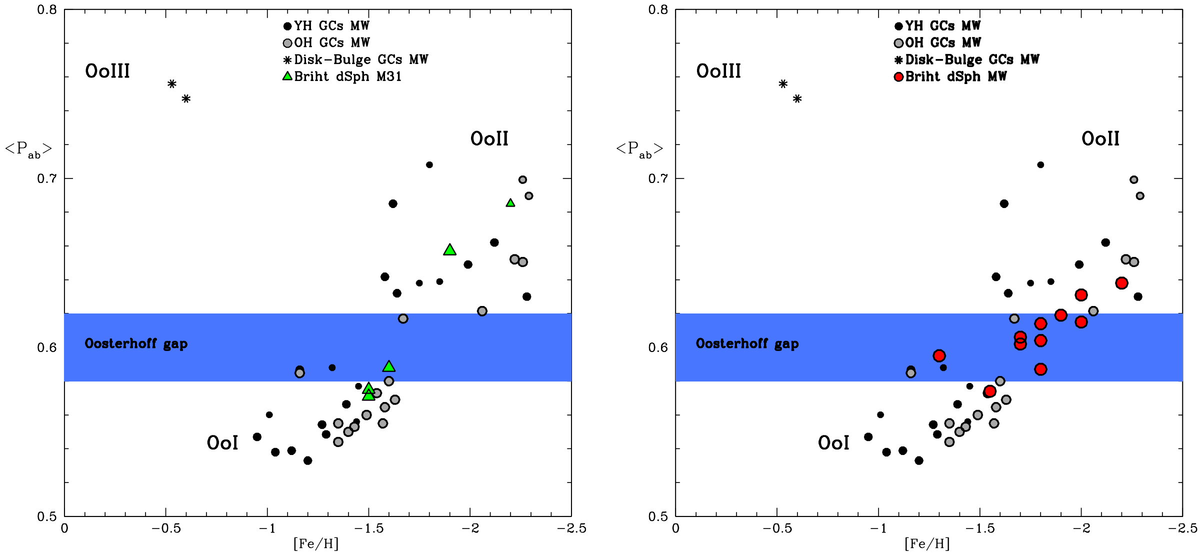

Figure 3.3: Left panel: Distribution of $\langle P_{ab} \rangle$ vs. metallicity for the MW GCs (filled and open circles), with overploted as green filled triangles the classical M31 dSphs. Right panel: Same as in the left panel but showing the distribution of the MW classical dSph galaxies (red filled circles)

Chapter 4

Variable stars in M31: Globular Clusters

Among the Local Group galaxies, M31 has the largest population of globular clusters (more than $\sim$ 600, according to the Revised Bologna Catalogue V.4, and is the nearest analog of the Milky Way. Its distance from the MW, $\sim$780 kpc (McConnachie et al. 2005), is large enough that the dispersion of the distance moduli of the M31 GCs can be considered small (50 kpc correspond to $\Delta(M-m)$ $\sim$0.15 at the distance of M31), hence the M31 GCs can be considered to be nearly at the same distance from us. Also, their almost stellar appearance (10 pc correspond to$\sim$ $2.''6$) allows an easy study of their integrated properties from the ground. On the other hand, the high resolution capabilities of the Hubble Space Telescope (HST), are needed to resolve individual stars in these distant GCs and identify stars on the different evolutionary paths, including their RR Lyrae variable stars.

The M31 GCs we have studied for variability were appropriately selected out of the about 40 clusters already observed with HST. All of them have well defined CMDs, metallicities compatible with the existence of RR Lyrae stars, and populous HBs stretching across the instability strip to provide a good probability of having RR Lyrae stars. Three of our GC targets have a metallicity that, in the MW, would place them in the Oo I group, whereas the others are more metal-poor and, in the MW, would be expected to be Oo II. Some of the chosen clusters could in principle be in the Oosterhoff-intermediate range, and therefore provided a further check of the RR Lyrae pulsation properties in M31. The selected clusters also allowed us to probe different areas in M31, from the galaxy's unperturbed halo to regions close to the giant stream. We also selected our targets taking into account whether they had HST-archive which could be used to extend the time baseline of our observations, which is especially important for a better definition of the periods of the variable stars.

Our goal was to determine, for the first time, the detailed pulsation properties of RR Lyrae stars in these carefully selected M31 GCs. We are aware that the selected clusters may not characterize the entire GC ensemble of M31, nevertheless they have allowed us to check for the first time whether the properties of the RR Lyrae stars in the M31 GCs are compatible with the Oosterhoff dichotomy, and whether they show the same correlations with HB morphology as seen in the MW. It is noteworthy that the basic knowledge of the MW GCs showing an Oosterhoff dichotomy was set by Oosterhoff about 70 years ago by studying the RR Lyrae properties in only 5 MW clusters, of which 3 turned out to be Oosterhoff type II, and 2 Oosterhoff type I clusters! Thus, in M31 we are practically in the same position as Oosterhoff 70 years ago. In fact, although our sample is smaller taking into account that the GC system in M31 is about three times bigger than in the MW, we, on the other hand, could properly select the GCs to study on.

4.1 Observations

The M31 clusters selected for our study are: G322, G33 and B514, all three along the galaxy major axis, the first two projected on the optical disk and the latter in the outermost part of M31; G76 and G105, which are relatively close to the M31 giant stream and G11 in the galaxy's unperturbed halo. The positions of the six clusters with respect to the nucleus of M31 are

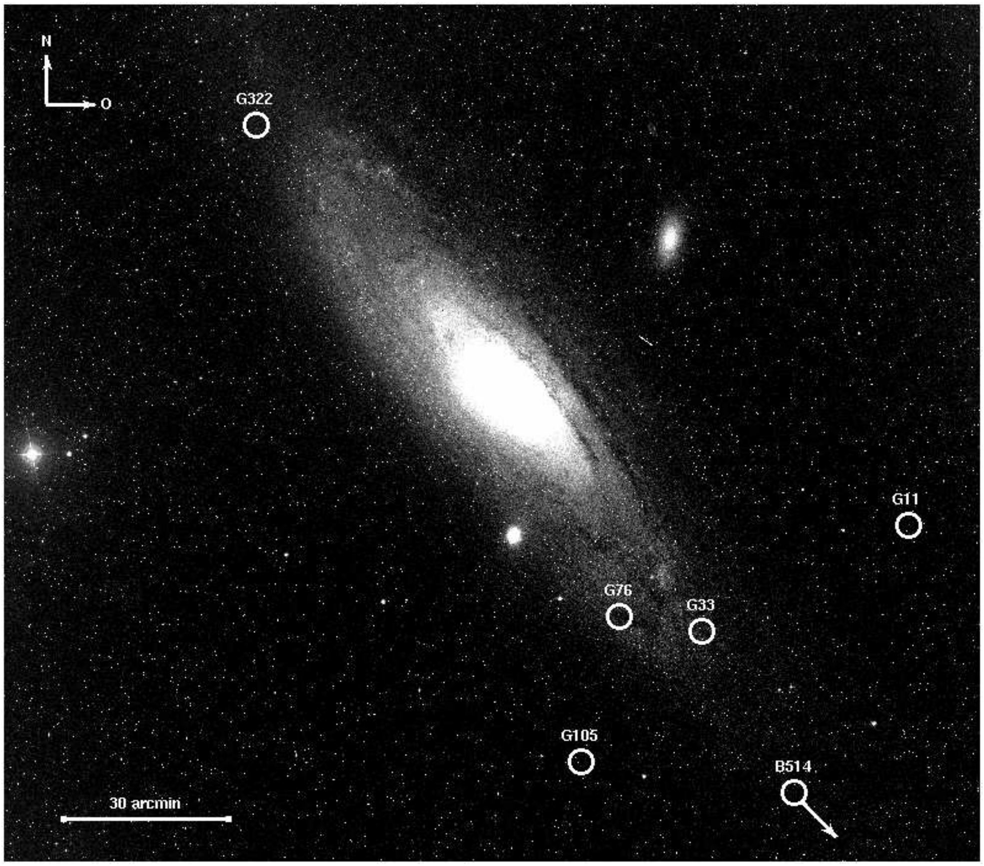

Figure 4.1: Location of our target GCs with respect to the M31 main body.

shown in Fig. 4.1, and their main properties are summarized in Table 4.1. Observing time for this project was obtained in HST Cycle 15, under program GO 11081 (PI: G. Clementini), using the WFPC2 on board HST. Observations were executed in the second half of 2007. The selected WFPC2 filters were F606W (broad V) and F814W (broad I) to be directly comparable with most previous studies of GCs and field stellar populations in the MW and in M31, including the M31 field RR Lyrae studies by Brown et al. (2004) and Sarajedini et al. (2009). The clusters were all centered on the Planetary Camera of the WFPC2 that provides better spatial

Table 4.1: Information on the six target GCs

G Name	Bo Name	RA J2000	DEC J2000	[Fe/H] dex	[Fe/H] dex	V_{HB} mag	V Integrated	E(B-V) mag	M_V mag
11......	293	00:36:20.865	40:53:37.25	−1.80	-1.59 ± 0.23	25.23	16.29	0.09	$\simeq -8.46$
33......	311	00:39:33.725	40:31:14.68	−1.78	-1.71 ± 0.53	25.49	15.44	0.29	$\simeq -9.93$
76......	338	00:40:58.870	40:35:47.79	−1.28	-1.23 ± 0.22	24.94	14.25	0.14	$\simeq -10.65$
105.....	343	00:41:43.102	40:12:22.50	−1.44	-1.28 ± 0.15	25.47	16.31	0.06	$\simeq -8.34$
322.....	386	00:46:27.016	42:01:52.75	−1.08	-1.09 ± 0.12	25.10	15.55	0.21	$\simeq -9.58$
....	514	00:31:09.821	37:54:00.09	−1.80	-2.06 ± 0.16	25.25	15.76	0.07	$\simeq -8.93$

resolution.

The time series observations of G11, G33, and G322 were executed in July 2007, and consist of 11 individual exposures of 1100s length in each band, taken by alternating the filters. The length of our exposures represented the best compromise to have reasonably good S/N even for measurements corresponding to the minimum light of the M31 RR Lyrae stars ($V \sim 25.5 - 25.7$ mag) and avoid smearing the light curves. At the same time these were also the longest possible exposures allowing us to fit an F606W, F814W image pair into one orbit. Exposures of these three GCs were scheduled in one 11-orbit block with a 50 minutes gap between each pair of observations, for total exposure times on target of 3 hr and 22 minutes in each band, spanning a total time-window of $\sim$ 16 hr. In the case of G76, G105, and B514, the time series data were obtained in June 2007 for B514, and in September 2007, for G76 and G105. The data consist on 15 individual exposures in each filter, of 1100s length and taken by alternating the filters as in the previous case. They were scheduled in two blocks of 5 and 10 orbits respectively with a 50 minutes gap occurring between each pair of observations, and a separation of 9 hours between the two blocks, for total exposure times of 4 hr and 35 minutes in each band. The total time-window spanned for these clusters is of $\sim$ 30 hr. Unfortunately, two orbits-data of cluster G76 were lost for technical problems, thus for this cluster we obtained only 13 phase points useful for further analysis, in each filter. For all the clusters we also retrieved from the HST archive additional WFPC2 data, for B514 additional data come instead from previous ACS observations.

The archive data of G11, G33, G76, and G322 come from program GO 6671 (PI: Rich) taken between 1999-2000 and consist of four F555W (V) and four F814W (I) frames. For each cluster, individual exposures of the archive data are about 20 minutes long and taken consecutively over a total time interval of 5 hr 15 minutes. The archive data of G105 stem from observations under program GO 5112 (PI: Westphal) executed in February 1994 and consist of two F555W (V) and two F814W (I) frames of 1000s length each. For B514, the WFPC2 proprietary data were combined with ACS/WFC archive data from program GO 10394 (PI: N. R. Tanvir), covering the period 2005 July 19-20, and from program GO 10565 (PI: S. Galleti) obtained in 2006 June 10, making a total of 20 phase points in the F606W band, and 21 phase points in the F814W band.

4.2 Data Reduction: HSTphot & DOLPHOT

We have performed the stellar photometry of our data with HSTphot (Dolphin 2000) and using the ACS module of DOLPHOT[1], which are photometry packages specifically designed to handle the undersampled Point Spread Function (PSF) of the WFPC2/HST and ACS/HST data, respectively. As PSF fitting stellar photometry packages, HSTphot and DOLPHOT are not significantly different in concept from the well known DAOPHOT (Stetson 1987) and DoPHOT (Schechter, Mateo, & Saha 1993) packages. The Stetson's (1987) introduction to DAOPHOT, gives a very detailed description of techniques of stellar photometry.

A number of initial preprocessing steps are required before running the photometry procedure.

---

[1] DOLPHOT is a photometry package that was adapted from HSTphot for general use and as been referenced in the literature as "a modified version of HSTphot". Both photometry softwares may be free downloaded from: http://purcell.as.arizona.edu/

First, image defects such as bad columns and saturated pixels are masked using the data quality files. All masked pixels are set to the bad data value, -100 ADU, and are ignored for the remainder of the photometry. Next, cosmic rays and hot pixels are flagged automatically and sky images are created in order to provide an initial guess of the background. At the same time, the positional offsets between each image and a reference image are measured using the IMEXAMINE task in IRAF. These values are input into the multiphotometry mode of HSTphot/DOLPHOT in order to measure the magnitudes of all detected objects on each image. The photometric measurements were done using PSFs employing the "weighted PSF fitting mode" which places more weight on the central pixels in a profile and less on the outer pixels. The photometric procedure automatically applies aperture and CTE corrections and transforms the instrumental magnitudes to the VEGAmag system as well as to the Johnson-Cousins system using equations included in the packages based on the calibration formulas by Holtzman et al. (1995) and Sirianni et al. (2005). In addition to position, magnitudes and errors, a variety of quality information is provided for each detected object in the output photometry file. This information can be used to select stars with high-quality measurements and includes: the "object type" (stellar, extended, bad, etc.), χ^2 which simply gives the quality of the the PSF fit; "sharpness" used to eliminate cosmic rays and extended objects, "roundness", "S/N", and a "crowding" parameter which describes the change in brightness in the star if neighbors are not subtracted. Generally this parameter is zero if the star has no close companions or positive if the star has neighbors.

4.3 Variable star identification and Period Search

For all our target GCs we have followed the same procedure to identify the variable stars, which is based exclusively on our observations from Cycle 15. The archive data, were only used for the purpose of improving the period definition. Only in the case of the cluster B514 the identification of the variable stars was done on both the WFPC2 proprietary data and the ACS archive data, since the latter cover a larger area around the cluster. Identification of the variable stars time-series was carried out using 2 different approaches. First, variable star candidates were identified from the scatter diagrams of the F606W and F814W data sets, using VARFIND, custom software developed at the Bologna Observatory by P. Montegriffo. Briefly, VARFIND computes the standard deviation of the mean magnitude of each source over the entire set of its individual values and plots the standard deviations against magnitudes (scatter diagram). It is quite easy to identify variable star candidates on this plot, since they clearly deviate (i.e. have large standard deviations due to the light variation) from the tendency of the rest of the normal stars. Fainter stars will have larger standard deviation too due to the photon noise, so it's advisable to proceed with caution at low luminosity levels.

Our second approach was to compute the Welch-Stetson variability index (see Stetson 1996 for a detailed definition and description) for each photometrized object. Basically, for each star the residual of each magnitude measurement with respect to the weighted mean magnitude in each photometric band is calculated and normalized by the photometric error ($R = \frac{x-\bar{x}}{err}$). Then, residuals corresponding to pairs of V and I observations closely spaced in time are multiplied and finally added ($\sum_{i=1}^{n}(R_{V_i} * R_{I_i})$). The basic idea here is that if a star is truly variable, it will be brighter than usual in V when it is also brighter than usual in I, and vice versa. Therefore, the total sum of the residual-products will be positive. On the other hand, if the star is constant, and there are only small random errors in each recorded magnitude, then one expects the V-band and I-band residuals to have the the same sign half the time, and opposite signs the other half of the time, leaving the overall sum of the residual product close to zero.

Period search and study of the light curves was performed using two different methods. A first verification of variability and guess of the star periodicity was obtained using the phase dispersion minimization (PDM) method (Stellingwarf 1978) as implemented in IRAF. PDM is a generalization of the Lafler & Kinman (1965) algorithm, and essentially attempts to identify the phased light curve that produces the minimum scatter in phase. The period refinement was then obtained with the Grafical Analyser of Time Series (GRATIS), a private software developed at the Bologna Observatory by P. Montegriffo (see e.g. Clementini et al. 2000), which uses both the Lomb periodogram (Lomb 1976) and the best fit of the data with a truncated Fourier series (Barning 1963). In the following Sections we describe the results we have obtained for the 6 M31 GCs in our program.

4.4 The case of Bologna 514 (B514)

Within our selection of M31 GCs, Bologna 514 (B514) is of special interest because it is a very bright (Mv $\simeq -8.9$) GC, and it has been widely suggested that bright GCs may be the remnants of disrupted nucleated dwarf galaxies (Freeman & Bland-Hawthorn 2002, and references therein). On the other hand, B514 is one of the outermost GC in the Andromeda galaxy known at present, which makes the probabilities of finding observational fingerprints of any accretion phenomena, if any, much higher because at such large distance from the parent galaxy, substructures may survive for longer times, and the overall stellar density is very low. In this context GCs may serve as excellent tracers of substructures in the outer region of their parent galaxy. For instance, Bellazzini et al. (2003a) were able to identify a signature of the Sagittarius dSphs accretion among the GCs in the outer halo of the Milky Way. In the particular case of B514, Federici et al. (2007) by means of a surface brightness distribution analysis based on HST/ACS observations, found evidence for extra tidal stars around the cluster, that may be interpreted as tidally stripped stars, or alternatively, one might hypothesize that the cluster is embedded in a very low surface brightness stellar system, such as an unknown dwarf galaxy. In addition, they also showed that B514 has a significantly larger half-light radius ($R_h = 1.6$ arcsec, corresponding to ~ 6 pc at the distance of M31) than ordinary GCs of the same luminosity, a feature that is shared by other peculiar globular clusters, like ω Cen, NGC2419, M54 and G1, as well as by the nuclei of dwarf elliptical galaxies.

B514 was independently identified by Huxor et al. (2004) and Galleti et al. (2005). As mentioned above, one of the most remarkable characteristic of this cluster is its position within the M31 system. B514 is located at $R \simeq 4^o$ from the center of M31, corresponding to a projected distance $R_p = 54.7$ kpc. Hence, it is one of the most distant M31 cluster presently known (Mackey et al. 2007). Interestingly too, the cluster lies about $\simeq 14'$ apart of the M31 major axis, on the south-western extension of the disc. Moreover, its "M31-centric" line-of-sight velocity ($V_{\rm M31} = -155 \pm 23$ km s-1) places it close to the extrapolation at large distances of the HI-disc velocity curve (Galleti et al. 2005). On the other hand, several authors have proposed that the stellar population of the Andromeda galaxy (as sampled from Earth-centered line of sights) is dominated by an extended disc component that provides the large majority of the sampled stars out to $R_{\rm p} \simeq 35$ kpc (Sarajedini & Van Duyne 2001; Ferguson & Johnson 2001; Worthey et al. 2005). Moreover, Morrison et al. (2004) showed that, at odds with the case of the MW, a significant fraction of the M31 GCs share the positional and kinematical properties of the dynamically-cold thin disc of the galaxy. All the B514's properties mentioned above are fully compatible with the hypothesis that the cluster belongs to this thin disc. If this will be confirmed by further observations it would imply a really huge size for the M31 disc, with far reaching consequences on our ideas on the formation and evolution of galactic discs.

As a further step to characterize the main features of this particular globular cluster, we have focused on the study of its variable stars. The Oosterhoff classification of the B514 RR Lyrae stars and the comparison with the properties of variables in the MW GCs, will provide important hints on the formation of the Andromeda galaxy. In what follows, we present results of our search for variable stars which lead us to the discovery of about a hundred RR Lyrae stars in B514. This number is larger than found in the vast majority of the MW GCs, and since we are not able to resolve the cluster's core, there are likely many more RR Lyrae stars in B514. This is the first time that a large sample of RR Lyrae stars is discovered in an M31 GC and that their pulsation properties (periods, amplitudes, etc.) are fully characterized, thus allowing to establish the cluster's Oosterhoff type.

4.4.1 Variable Stars

After the photometric reduction of the individual prereduced images of B514 supplied by the STScI pipeline, using HSTphot and DOLPHOT/ACS (see section 4.2), variable star candidates were identified from the scatter diagrams of the F606W and F814W data sets, using VARFIND and by computing the Welch-Stetson variability index (see section 4.3). The typical errors of the combined photometry (eight ACS frames) for non-variable stars at the magnitude level of the B514 horizontal branch (HB; V ∼ 25.2 mag) are rather small ($\sigma_V = 0.017$ mag and $\sigma_I = 0.015$ mag for the ACS data set, and $\sigma_V = 0.019$ mag and $\sigma_I = 0.032$ mag for the WFPC2 data), hence variable stars on the cluster HB show up quite clearly in the scatter diagrams of B514. We first analyzed the WFPC2 proprietary data, whose extended time series are optimized for the detection of variables of RR Lyrae type. The WFPC2 candidate variables were then counter-identified on the ACS data. A further search with VARFIND was later performed on the ACS archive data, and the counter-identification with the WFPC2 data was iteratively repeated. The search procedure returned a final catalog of 161 candidate variables, most of which are located on the cluster HB. We expect many more variable to exist in the core region of the cluster, that is not resolved in our photometry. Periods and classification in type of the candidate variables were derived from the study of the light curves with the PDM and GRaTiS (see Clementini et al. 2000). We obtained reliable periods and light curves for 89 RR Lyrae stars: 82 fundamental-mode (RRab) and 7 first-overtone (RRc) pulsators. For the remaining 72 candidates, we still lack a firm classification, mostly because of scatter in the data. The total exposure time on target of our proprietary data is 4 hr and 35 minutes in each band, spread over a total time interval of about 30 hours. In addition, we have six epochs of archive data spaced by 694 and 368 days. This ensures that all possible periods of RR Lyrae stars are well sampled and no bias or alias effects are present, and allows us to derive accurate periods mostly to the 3rd-4th decimal digit. The characteristics of the B514 confirmed variable stars (identification, period, V amplitude, V mean magnitude and RR Lyrae type) are summarized in Table 4.2 and 4.3.

Table 4.2: Characteristics of B514 confirmed variable stars

ID	Period(d)	A_V	$\langle V \rangle$	Type
V150	....	.....	......	?
V165	0.22?	1.269	24.670	?
V208	0.737	0.358	23.920	?
V330	1.32	0.267	24.660	?
V376	0.604	0.501	24.724	RRab
V383	0.497	0.988	25.072	RRab
V393	0.366	0.292	24.784	RRc
V396	0.523	0.990	24.863	RRab
V397	0.503	0.830	24.915	RRab
V406	0.608	0.435	24.910	RRab
V410	0.629	0.460	24.877	RRab
V415	0.644	0.469	25.062	RRab
V430	0.675	0.398	25.211	RRab
V433	0.537	0.996	25.012	RRab
V438	0.552	0.805	25.101	RRab
V439	0.593	0.657	25.037	RRab
V443	0.592	0.735	25.153	RRab
V444	0.629	0.881	25.105	RRab
V452	0.528	1.132	25.073	RRab
V455	0.477	0.847	25.180	RRab
V459	0.563	1.011	25.249	RRab
V462	0.574	0.591	24.947	RRab
V463	0.354	0.402	25.063	RRc
V465	0.556	0.713	25.138	RRab
V468	0.544	1.170	25.147	RRab
V470	0.551	0.620	25.157	RRab
V478	0.494	0.994	24.892	RRab
V486	0.308	0.502	25.130	RRc
V487	0.501	1.159	25.272	RRab
V490	0.572	0.916	25.175	RRab
V492	0.731	0.472	25.230	RRab?
V493	0.719	0.680	25.188	RRab
V496	0.563	1.207	25.166	RRab
V504	0.658	0.688	24.999	RRab
V505	0.533	0.903	25.087	RRab
V508	0.491	1.052	25.159	RRab
V512	0.644	0.603	25.101	RRab
V513	0.618	0.442	25.201	RRab
V517	0.555	0.841	25.203	RRab
V520	0.573	0.996	25.234	RRab
V523	0.595	0.555	24.988	RRab

ID	Period(d)	A_V	$\langle V \rangle$	Type
V525	0.620	0.840	25.200	RRab
V527	0.291	0.436	25.158	RRc
V529	0.379	0.452	25.192	RRc
V532	0.618	0.432	25.196	RRab
V534	0.417	0.416	25.222	RRc
V537	0.561	0.758	25.139	RRab
V539	0.601	1.099	25.110	RRab?
V541	0.577	0.813	25.298	RRab
V542	0.568	0.617	25.259	RRab
V544	0.557	1.018	25.290	RRab
V549	0.621	0.558	25.283	RRab
V551	0.586	0.809	25.233	RRab
V557	0.616	1.376	25.112	RRab
V572	0.654	0.769	25.185	RRab
V573	0.358	0.391	25.200	RRc?
V575	0.572	0.531	25.290	RRab
V577	0.553	0.985	25.347	RRab
V578	0.615	0.679	25.251	RRab
V580	0.520	0.876	25.235	RRab
V583	0.493	0.842	25.243	RRab
V585	0.530	0.970	25.249	RRab
V588	0.795	0.530	25.313	RRab?
V591	0.546	0.875	25.348	RRab
V592	0.575	1.146	25.249	RRab
V596	0.664	0.656	25.345	RRab
V601	0.617	0.819	25.310	RRab
V611	0.358	0.541	25.390	RRc?
V622	0.519	1.104	25.425	RRab
V633	0.483	1.064	25.515	RRab
V4718	0.547	0.735	25.172	RRab
V4721	0.549	1.124	25.170	RRab
V9549	0.512	0.223	24.920	RRab?
V9565	0.561	0.872	25.164	RRab
V15053	0.618	0.558	25.261	RRab
V15056	0.310	0.380	25.261	RRc

Table 4.3: Characteristics of B514 confirmed variable stars

Figure 4.2 shows the V, V-I CMD of B514, obtained from the ACS data, for stars in four separate regions at increasing distance from the cluster center. Only sources with object type flag=1 (i.e., best measured stars), crowding < 0.3, $-0.5 <$ sharpness < 0.5, $\chi^2 < 1.5$ for V > 24

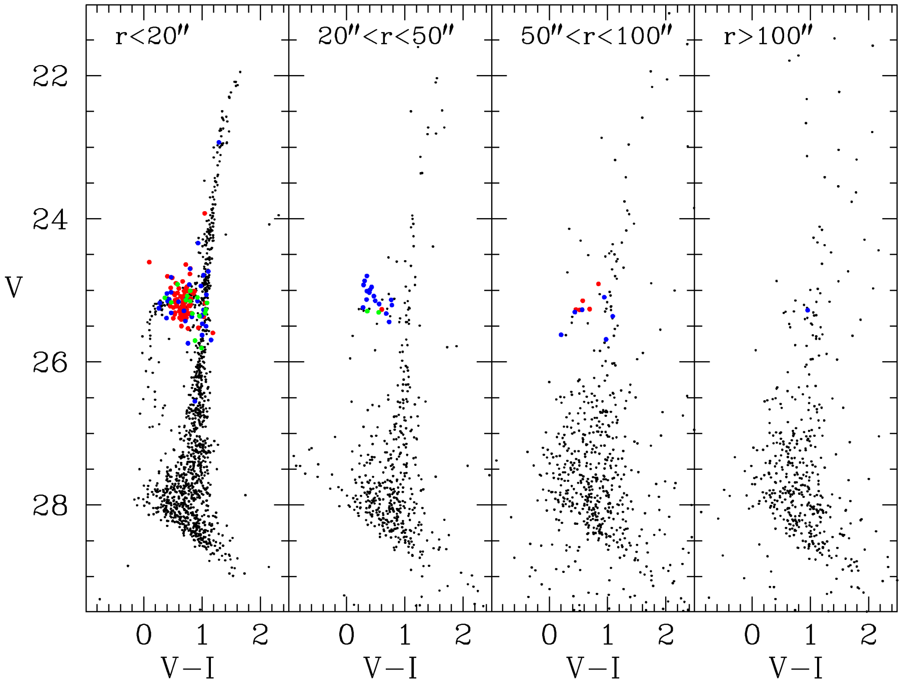

Figure 4.2: V, V-I CMD of B514 in four regions with increasing the distance from the cluster center, based on our reductions of the ACS archive photometry. Bona fide RR Lyrae stars are marked by filled red circles, candidate variable stars by blue and gree filled circles depending on the reliability of the classification (see text; taken from Clementini et al. 2009).

mag and $\chi^2 < 2.5$ for brighter stars are shown in the figure. Confirmed variable stars are plotted as red filled circles, candidate variables with sufficient light curve sampling as blue filled circles, and less reliable candidates as green filled circles. According to their position on the CMD, the vast majority of the candidate variables discovered in B514 are likely RR Lyrae stars. However, our candidate's list also includes a number of binaries and a few objects above and below the HB. Variable stars are plotted in the CMD using mean magnitudes and colors computed as simple averages of the available photometric measurements. The scatter observed around the average level of the HB is therefore largely due to variable stars with uneven coverage of the light curve,

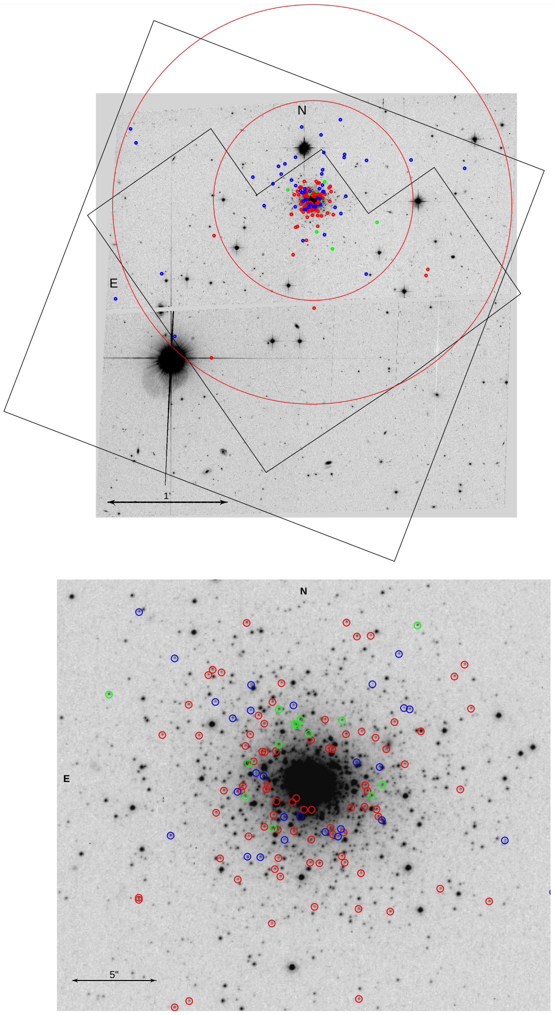

Figure 4.3: Upper panel: Location of the B514 confirmed (red circles) and candidate (blue and green circles) variable stars on a 3′22″ × 3′22″ map of the cluster, corresponding to the fiels of view covered by the ACS observations of HST GO 10565 (see Galleti et al. 2006). Also shown are the field of view covered by the ACS observations of HST GO 10394 (see Mackey et al. 2007; tilted square) and the field of view of our WFCPC2 observations. The two large red circles correspond to radii of $r = 50''$ and $r = 100''$ from the center of B514. Lower panel: enlargement of the variable stars map showing a 30″ × 30″ region centered on the cluster (taken from Clementini et al. 2009)

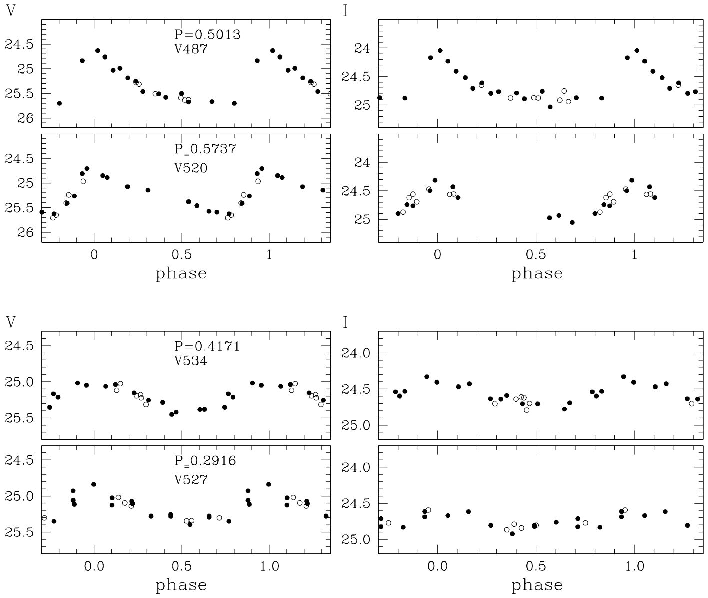

Figure 4.4: V (left) and I (right) light curves of RR Lyrae stars identified in B514. Two upper rows: fundamental-mode pulsatiors. Two lower rows: first-overtone pulsatiors. Filled and open circles indicate WFPC2 and ACS data, respectively. Typical error of a single data point at the magnitude level of the HB is about 0.06 mag (taken from Clementini et al. 2009).

and will likely be significantly reduced when the mean magnitudes will be derived averaging over the full pulsation cycle. The upper panel of Fig. 4.3 shows the location of the B514 variable stars on the $3'22'' \times 3'22''$ field of view covered by the ACS observations of Galleti et al. (2006). The lower panel of Fig. 4.3 shows an enlargement of the map in the upper panel, corresponding to a $30'' \times 30''$ region around the cluster center. As noted in Federici et al. (2007), B514 is rather extended (see their Figure 6) and its tidal radius was estimated as 17 arcsec ($\sim$ 65 pc) from the analysis of the distribution of the integrated light and star counts. However, we have detected variables well beyond this distance, in particular five RR Lyrae stars are located farther than 50 arcsec and as far as 90 arcsec from the cluster center (see Fig. 4.3). Although they are likely field stars, the CMD shown in Fig. 4.2 indicates that a non-negligible fraction of the cluster population is still present in the annulus 50-100 arcsec, suggesting the possibility that at least a few of these distant variables may belong to the cluster. Radial velocity membership will be the most reliable way to assess to which population they belong. Examples of light curves for two fundamental-mode and two first-overtone RR Lyrae stars we have identified in B514 are shown in Fig. 4.4. Typical errors of the individual data points are of about 0.06 mag, both in V and I. The complete atlas of V-band light curves is presented in Appendix A. The mean periods of the 89 confirmed RR Lyrae stars in B514 are $\langle P_{ab} \rangle = 0.58$ days and $\langle P_c \rangle = 0.35$ days for fundamental-mode and first-overtone variables, respectively, suggesting a possible dominance of Oo I. The period distribution of the B514 RR Lyrae population is shown in the upper panel of Fig. 4.5, where best-fit model Gaussian curves are also superposed. Clement & Shelton (1999) found that the V-band period-amplitude diagram A_V-log P provides a very useful tool to define the Oosterhoff type of a GC. How does this diagram look in the case of B514? The bottom panel of Figure 4.5 shows the V-band period-amplitude diagram of the B514 RR Lyrae stars, along with the Oosterhoff loci defined by the Galactic GCs from (Clement & Rowe 2000; linear relations), and the period-amplitude distributions of bona fide regular and evolved RRab stars in M3 (quadratic relations), from Cacciari et al. (2005). The B514 RR Lyrae stars are close to the loci of OoI systems and regular RRab stars in M3. In conclusion, according to both the average period of the fundamental mode pulsators and the period-amplitude diagram of its RR Lyrae stars B514 appears to be a somewhat borderline OoI cluster, and seems to follow a different rule than what is found in the MW, where metal-poor ([Fe/H] $\lesssim 1.7$) GCs containing RR Lyrae stars show OoII properties.

4.4.2 CMD and Distance

We obtained reliable photometry of individual stars in B514 down to V $\sim$ 28 mag. This is about half a magnitude fainter than in previous studies of the cluster (see Galleti et al. 2006 and Mackey et al. 2007). From the CMDs corresponding to different radial annuli around the

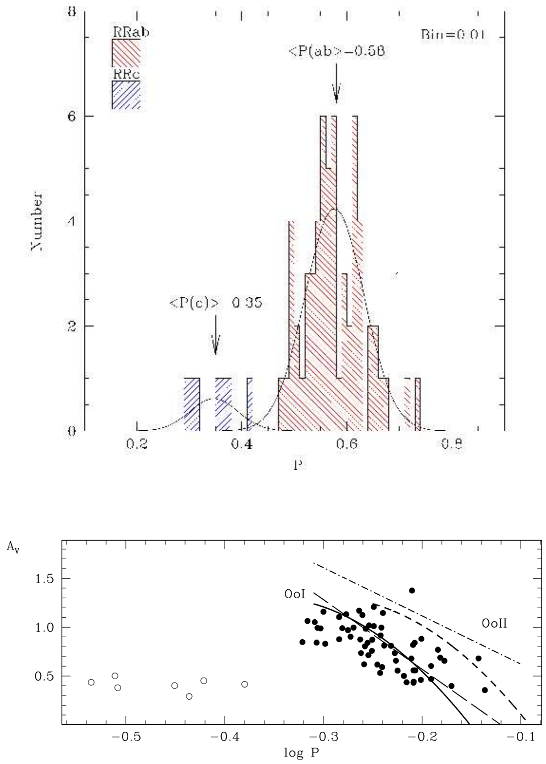

Figure 4.5: Upper panel: Period distribution histogram for RR Lyrae stars in B514. The peak of the distribution, at ~ 0.58 match the average period of the ab-type RR lyrae stars. Bottom panel: Period-amplitude distribution in the V band. RRab variables are plotted as filled circles; RRc stars are shown by open circles. The linear relations show the period-amplitude distributions of Galactic OoI and II GCs (Clement & Rowe 2000). The quadratic relations show the bona fide regular (Ooi) and evolved (OoII) RRab stars in M3, from Cacciari et al (2005), for comparison.

cluster center (see Fig. 4.2), it is evident that field star contamination is not a significant issue for B514. In all panels of figure Fig. 4.2 the main sequences of the cluster are very clearly visible, without need for sophisticated statistical subtraction of the field. The large majority of the cluster stars are obviously in the innermost region, accordingly the left-most diagram of Fig. 4.2 shows more clearly the main evolutionary sequences of B514. Going from V $\sim$ 21.7

and V-I $\sim$ 1.8 down to the limiting magnitude level at V-I $\sim$ 1.2, the CMD is dominated by an extended and steep red giant branch (RGB), indicating that B514 is a metal-poor cluster. The metal abundance of B514 has been calculated photometrically and spectroscopically and results agree on a low amount of metals in this cluster. In the following we have adopted the most recent re-evaluation of the cluster metaliicity by Galleti et al. (2009): [Fe/H]=-2.06 ± 0.16. The RGB does not exhibit significant scatter, thus ruling out a metallicity spread in B514. A small overdensity corresponding to the RGB bump is discernible at V $\sim$ 24.3. A RGB bump brighter than the HB level is typical of metal-poor globular cluster (see Ferraro et al. 1999 for more details). The HB of B514 appears quite extended in color. It stretches across the RR Lyrae instability strip, which is entirely filled by the large number of confirmed and candidate RR Lyrae stars, and extends significantly to the blue through a blue tail that reaches V $\sim$ 27 mag at V-I $\sim$ 0.1 mag. The mere presence of blue HB stars and RR Lyrae indicates that the cluster is older than 10 Gyr.

The mean magnitude of the B514 RR Lyrae stars is $\langle V \rangle = 25.18 \pm 0.02$ mag (with a dispersion of 0.16 mag among the 81 stars). We adopt an absolute magnitude of $M_V = 0.42 \pm 0.14$ mag for RR Lyrae stars with the metallicity [Fe/H] = -2.06 ± 0.16 dex of B514 (see section 2.4), which is consistent with an LMC distance modulus of 18.52 mag. Using the reddening value of E(B-V) = 0.07 ± 0.02 mag estimated from Schlegel et al. (1998), we find a distance modulus of $\mu_0 = 24.54 \pm 0.15$ mag, which corresponds to a distance of about 810 ± 56 kpc. Alternately, one may use the formula determined by Alcock et al. (2000) that relates the metallicity of an RRab star to its period and V-band amplitude, for determining the metallicity of the B514 RR Lyrae stars. This relation: $[\mathrm{Fe/H}]_{\mathrm{ZW}} = -8.85(\log P_{ab} + 0.15 A_V) - 2.60$, was calibrated using the RRab stars in M3, M5, and M15, and provides metal abundances in the Zinn & West (1984) metallicity scale for individual RR Lyrae stars, with accuracy of $\sigma_{[Fe/H]} = 0.31$ per star. The large error makes the determination of individual stellar metallicities unreliable, but the formula can be useful to estimate the mean abundance of a population of RR Lyrae stars. As a matter of fact, this formula provided metallicity estimates in good agreement with independent determinations for RR Lyrae stars in the LMC (Alcock et al. 2000), And IV (Pritzl et al. 2002), and And II (Pritzl et al. 2004). Applying Alcock et al.'s relation to the RR Lyrae variables in B514 we find a significantly higher mean value of the metal abundance: $\langle[\mathrm{Fe/H}]\rangle = -1.52 \pm 0.03 \pm 0.31$ dex. Here, the first error takes into account the uncertainties on both periods and amplitudes, whereas the second error is the standard deviation from the mean value. Such a high value is at odds with the literature metal abundances for B514 [namely,-1.8 ± 0.3, integrated-light spectra (Galleti et al. 2005); -1.8 ± 0.15, using ΔV_{HB}^{bump} method in the CMD (Galleti et al. 2006); -2.14 ± 0.15, photometric metallicity from CMD (Mackey et al 20060; and -2.06 ± 0.16, integrated-light spectroscopy, (Galleti et al. 2009)], which all consistently point to a very low metal abundance for the cluster. Incidentally, if the high metallicity inferred with Alcock et al. formula were correct, it would make the classification of B514 as a borderline OoI cluster less surprising.

4.5 RR Lyrae stars in G11, G33, G76, G105 and G322

In this section we present preliminary results on the study of the variable stars in the other five clusters of our sample. We notice that for all 5 clusters we have not yet completed the analysis of the light curves, and thus hope to further increase the statistics of RR Lyrae stars. We also hope to improve the periods for those variables that we have already detected, above the present accuracy of ~ 0.01 days, by adding archive data which will allow us to significantly extend the time baseline of our observations. This will also allow us to classify the candidate long period variables we have found, since the short time coverage of the proprietary observations did not allow us to properly analyze variables with periods longer than 16 hrs in the case of G11, G33 and G322; and $\sim$ 30 hrs for G76 and G105. In any case, the main conclusions concerning the cluster's classification in Oosterhoff types that we present in this chapter are likely to remain unchanged, since the current ~ 0.01 accuracy of our period determinations is already sufficient to discriminate between Oo I and OoII types. Finally, it is worth mentioning that, since we started our project the metal abundance of our target GCs have partially changed due to improved metallicity studies. Fortunately, these changes did not affect our primary aim: to study the variable stars in M31 GCs spanning the full range of metallicities found among their MW counterparts.

4.5.1 CMDs, Variable Stars, and Distances

The time series data of all 5 GCs were processed with HSTphot according to the procedures described in section 4.2, and produced calibrated photometric catalogs which were used to compute the variability index and to create scatter diagrams in order to select variable star candidate (see 4.3) which were then analyzed using both the PDM and the GRATIS packages. The left panels of Figs. 4.6 and 4.7 show the CMDs we have obtained for the five GCs. Only sources with object type flag=1 (i.e., best measured stars), crowding < 0.25, $-0.3 <$, sharpness < 0.3, $\chi^2 < 1.5$ for V > 24 mag and $\chi^2 < 2.5$ for brighter stars, are shown in the figures. We have also isolated each cluster from the surrounding field population by imposing a radial cut. For G33, G76, and G322 which are radially projected fairly close to the main body of M31, and hence suffer from heavy background contamination, we set the selection radii to be smaller than $7.5''$. We found this sufficient to obtain clean CMDs with considerable number of stars still available to define the primary sequences. For the two clusters located in regions less affected by field contamination (G11, G105), we have relaxed the above condition imposing limiting radii closer to the typical cluster's tidal radii, ~ 60 pc, which corrisponds to $\sim 15''$ if we adopt the canonical distance modulus of $(m-M)_0 = 24.47$ mag (~ 780 kpc) for M31 by McConnachie et al. (2005). The right pannels of Figs. 4.6 and 4.7 show the corresponding field CMDs for each cluster. The limiting magnitudes of our photometry, defined as 4 σ detection, range from $V, I \sim 26.5$ mag in the worst crowding case (i.e., G76) to $V, I \sim 27.5$ mag in the best case (i.e., G105). The internal photometric errors in magnitude and color were estimated from the photometric errors provided by HSTphot. It is found that $\epsilon(V)$ and $\epsilon(V-I)$ are ~ 0.01 mag

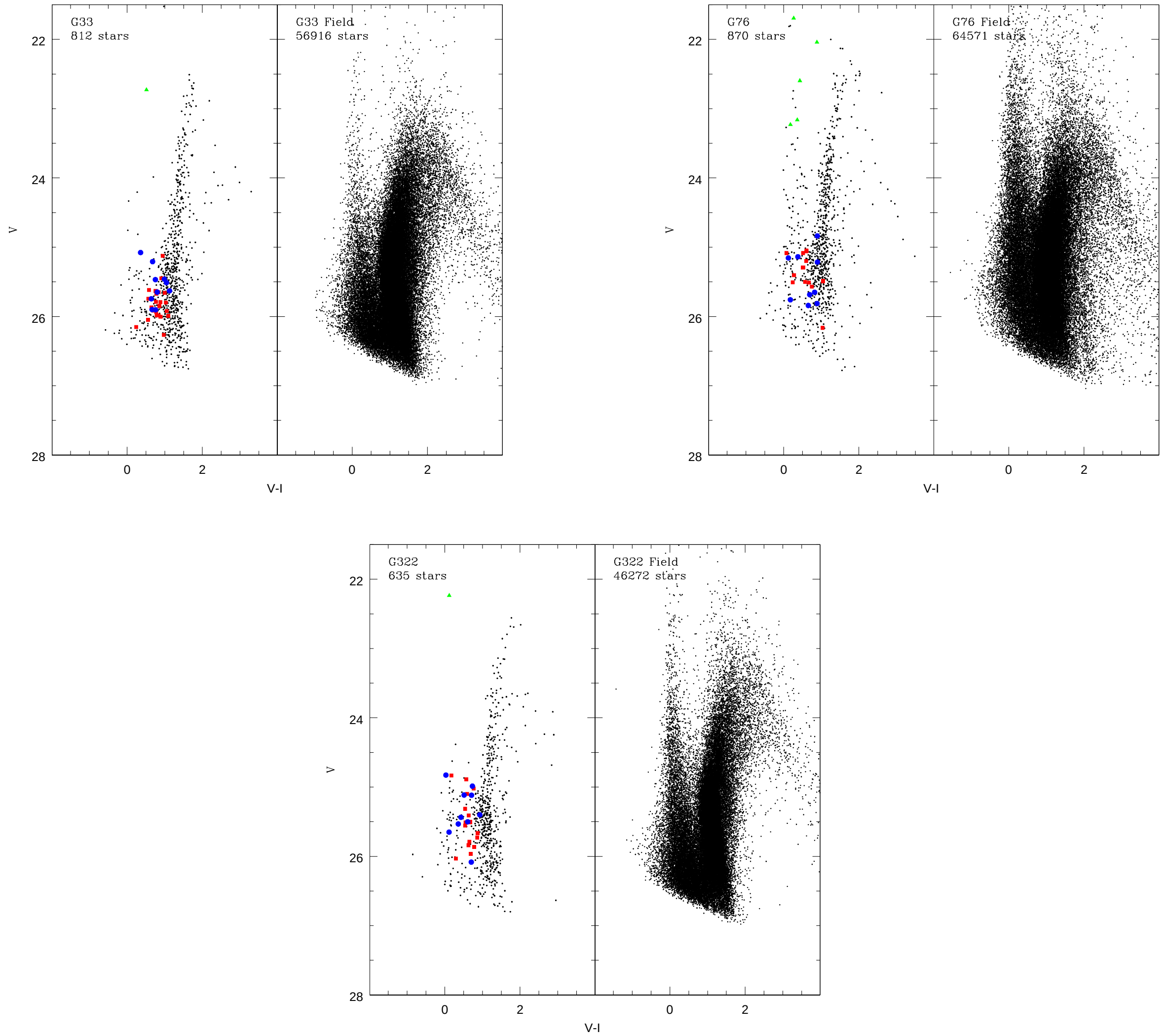

Figure 4.6: $V, V-I$ CMDs of G33, G76, G322 and their surrounding fields, obtained in the present study. In each plot the left panel shows the cluster CMD obtained from the photometry of the PC data, while the right panel shows the CMD of the surrounding field stars imaged on the other 3 cameras of WFPC2. Red and blue filled circles show respectively the ab and c-type RR Lyrae stars identified in the cluster, green triangles mark other types of variables. Each CDM is labeled with the cluster name and the number of stars displayed.

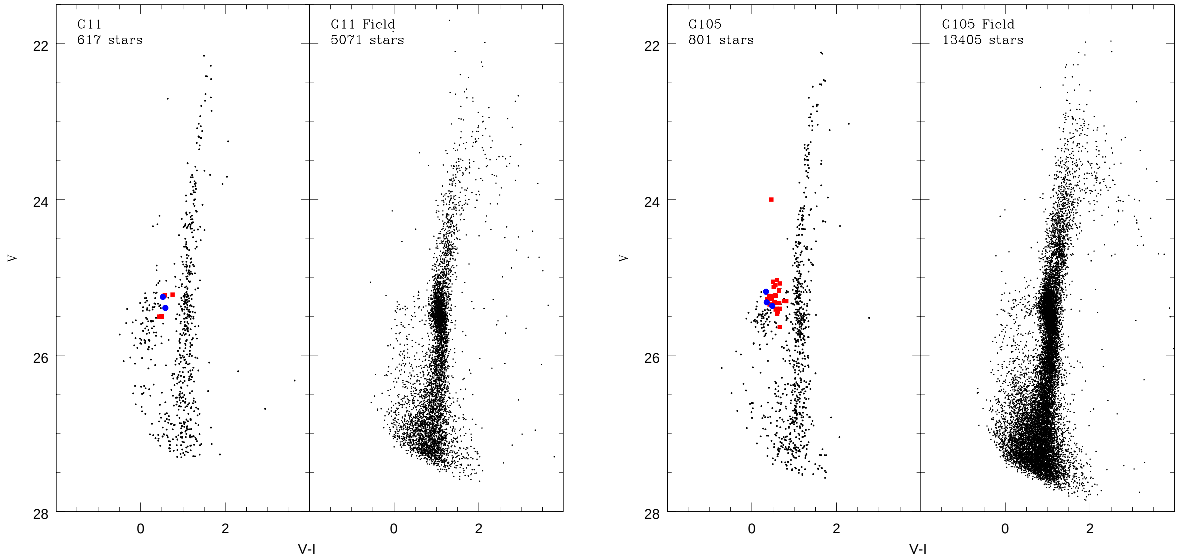

Figure 4.7: Same as Fig. 4.6 for G11 and G105.

down to $V \backsimeq 24$ mag; then $\epsilon(V)$ and $\epsilon(V-I)$ increase continuously up to ~ 0.1 and 0.18 mag respectively, from $V \backsimeq 24$ to 27.5 mag. At the level of the HB ($V \backsimeq 25$) the photometric errors are typically $\epsilon(V) \sim 0.02$ mag and $\epsilon(V-I) \sim 0.04$ mag.

In our study we have unequivocally identified candidate variable stars in all the M31 GCs in our sample, and were able to obtain well sampled light curves for most of our candidates. The variables we have identified are mainly RR Lyrae stars, but we also found a few candidates above the HB, likely Anomalous and/or Population II Cepheids. Examples of the light curves for RR Lyrae stars identified in G11, G33, G76, G105, and G322 are shown in Fig. 4.8. The complete atlas of V-band light curves for each GC are presented in Appendices B, C, D, E and F respectively. Table 4.4 summarizes the statistics of candidates detected in each GC, along with their classification and a number of pulsation parameters (namely, average period of the fundamental and first overtone pulsators, minimum period of the fundamental mode variables, frequency of c-type pulsators) for those that we have confirmed as variables. We also list in

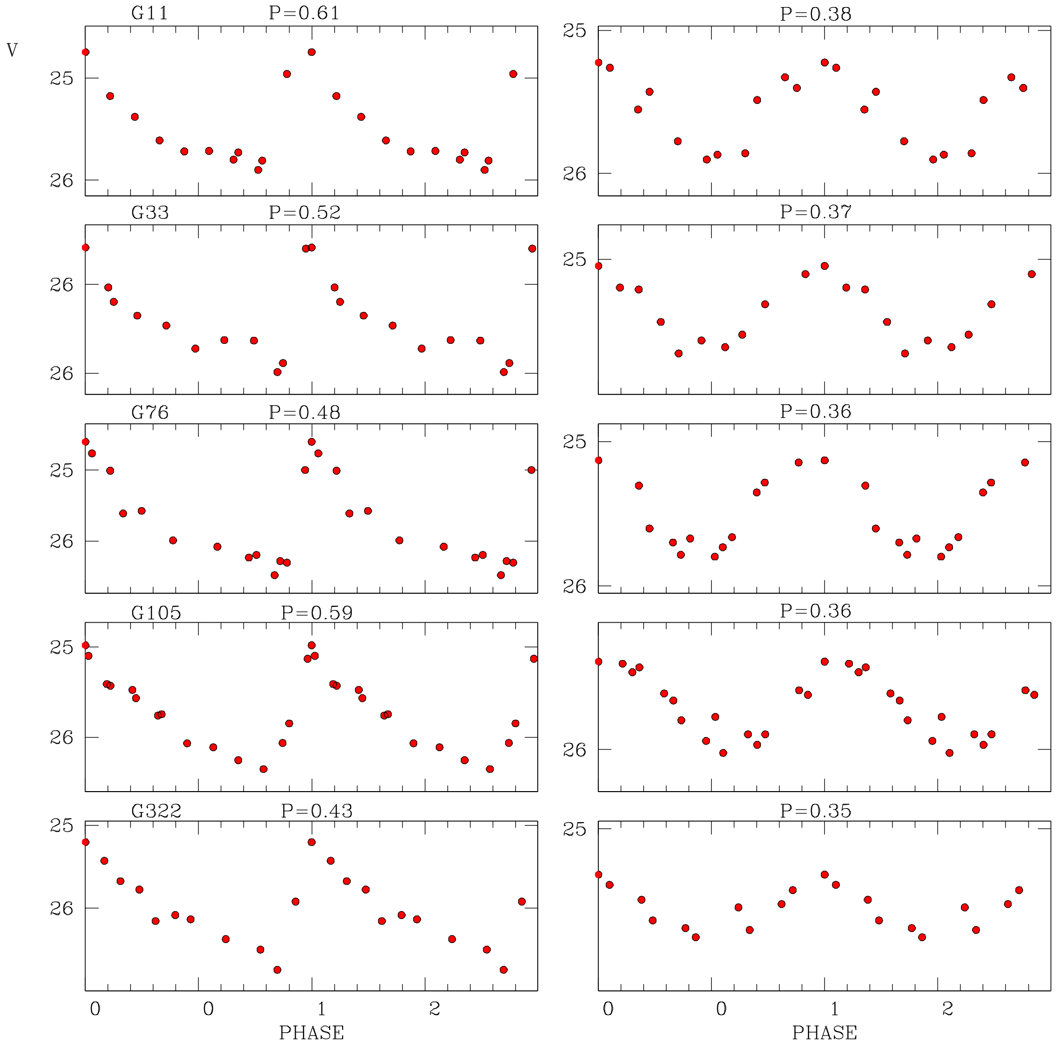

Figure 4.8: Examples of V-band light curves for fundamental mode (left panels) and first overtone RR Lyrae stars (right panels) in (from top to bottom) G11, G33, G76, G105, and G322. Typical internal errors of the individual data points are of 0.02-0.05 mag.

Table 4.4: Number and properties of the variables identified in G11, G33, G76, G105 and G322

Name	[Fe/H]	Candidates	Confirmed	N(RRab+c)	N(others)	$\langle P_{ab}\rangle$ (days)	$\langle P_c\rangle$ (days)	$P_{ab,min}$ (days)	f_c
G11	-1.59 ± 0.23	28	6	4+2	0	0.547	0.370	0.434	0.33
G33	-1.71 ± 0.53	177	44	23+10	1	0.590	0.383	0.510	0.30
G76	-1.23 ± 0.22	147	21	13+3	5	0.543	0.303	0.482	0.18
G105	-1.28 ± 0.15	57	26	23+3	0	0.598	0.330	0.512	0.11
G322	-1.09 ± 0.12	123	27	16+10	1	0.618	0.334	0.431	0.38
B514	-2.06 ± 0.16	161	89	82+7	0	0.580	0.350	0.477	0.08

Column 2 of the table the most recent metallicity estimates for the 6 clusters in our sample, taken the Revised Bologna Catalogue V.4 (Galleti et al. 2009). We show the confirmed variable stars in the CMD of Fig. 4.6 and 4.7, plotting ab-type and c-type RR Lyrae stars as red and blue filled circles, respectively, and candidate Cepheids as green filled triangles. Note that in some cases, most noticeable for G76 and G322, there is a large spread in the magnitude and color of the variables around the HB level. This is likely cause because we have plotted the variable stars according to their mean magnitudes and colors computed as simple averages of the available photometric measurements. This scatter will reduce significantly when the mean magnitudes will be derived averaging over the full pulsation cycle.

We can derive estimates of the cluster's distances using the mean magnitude of their RR Lyrae stars as distance indicator. As an example, given the large spread around the HB of some clusters, we have applied this technique to the clusters with least scatter, namely, G11 and G105, been aware that even for these two clusters we'll need to properly re-evaluate mean magnitudes and colors of their RR Lyrae stars averaging over the full pulsation cycle. Adopting the metallicities listed in table 4.4 and the absolute magnitude-metallicity relation provided in section 2.4, we find $M_V(RR) = 0.52 \pm 0.13$ and $M_V(RR) = 0.59 \pm 0.11$ for G11 and G105 respectively. Using the reddening values in table 4.1 and a standard estinction law ($A_V =$

$3.1E(B-V)$), we obtain de-reddened mean apparent magnitudes ($\langle V\rangle_0 = \langle V\rangle - A_V$) of the RR Lyrae stars of 25.06 ± 0.08 mag and 25.08 ± 0.04 mag (standard error of the mean), giving preliminary true distance moduli of $(m-M)_0 = 24.54 \pm 0.15$, and $(m-M)_0 = 24.50 \pm 0.12$, for G11 and G105, respectively. These values correspond to distances of about 809 ± 55 kpc for G11 and 650 ± 33kpc for G105. Giving the large error bars (which are mainly due to uncertainties in the cluster's metallicities and in the zero point error from the adopted [Fe/H]-M_v relation), these estimates are not inconsistent with the moduli reported for these two GCs by Rich et al. (2005).

4.5.2 Oosterhoff Classification

There are several quantities useful to discriminate the Oosterhoff type of a globular cluster, some are more reliable than others (see section 2.4.1 and Catelan et al. 2010, in preparation). In the present case, as we are presenting results that need to be further verified and re-analyzed, the Oosterhoff classification of our M31 GC sample will be mainly based on the average period of the variables that have been so far confirmed to be ab-type RR Lyrae stars, and on the location of the variables in the Oosterhoff diagram showing the relationship between average period of the ab-type RR Lyrae stars and the metallicity. In the following we discuss the Oosterhoff classification of G11, G33, G76, G105 and G322, based on the preliminary values of $\langle P_{ab}\rangle$.

G76: This is one of the brightest globulars being second only to G1 in M31, and also brighter than ω Centauri in the MW. In the $M_v - R_h$ plot (see Federici et al. 2007, and Fig. 1.7), it shares the region inhabited by peculiar clusters like ω Cen, G1, NGC2419, and M54. A region generally avoided by ordinary GCs, where GCs mimic the properties of dwarf elliptical galaxies nuclei. Despite the above unusual properties, our preliminary mean period of the fundamental mode RR Lyrae stars, based on a sample of 13 variables, suggests that G76 follows the rule of the classical MW GCs with similar metallicity, being classified as OoI.

G322: It is a very bright GC (Mv $\backsimeq -9.5$). Its metallicity, ([Fe/H]= -1.09 ± 0.12 dex), makes G322 the most metal rich cluster of our sample. In the MW, GCs with such a high metall content are all, but NGC6388 and NGC 6441, classified as Oosterhoff type I (see Fig. 2.4). Following the peculiar behavior of NGC 6388 and NGC 6441, G322 shows a mean period of the ab-type RR Lyrae stars that deviates significantly from the Oo-type *versus* metallicity trend followed by metal-rich Galactic GCs. The current precision of our period determinations for this cluster does not allow us to clearly decide whether G322 belongs to the Oo-Int or Oo II group. Whatever the case, both possibilities make this cluster an object out of the classical MW trend, and an interesting target for future analysis.

G11: Only 4 ab-type RR Lyrae stars were found in this GC. This low number, however, is quite consistent with the very blue HB morphology exhibited by G11 (see Fig. 11 in Rich et al. 2005), and in very good agreement with Clementini et al. 's (2001) identification of "only two" likely RR Lyrae star candidates in the cluster. Thus, although we still have a list of several candidates to analyze, it is unlikely that the number of RRab stars in G11 will increase significantly. Using such small statistics, G11 would be classified as an Oosterhoff type I GC, according to the mean period of its fundamental-mode RR Lyrae stars, $\langle P_{ab} \rangle = 0.547$. However, there is something quite peculiar in this cluster that makes it a very intriguing object. With a metallicity value around -1.6 dex, this GC falls into the region where, in the MW, one finds GCs on each side of the Oosterhoff-gap, i.e., GCs which have almost same metal abundance, yet very different values of $\langle P_{ab} \rangle$ (see left panel of Fig. 2.4). Looking at this plot, one immediately wonders: if not the metallicity, what it the "second" parameter responsible for the different periods seen in these globular clusters? Different models suggest (see Lee & Zinn 1990) and observational evidence supported (see Lee & Carney 1999) that the HB morphology is a key factor, besides the metal abundance, in controlling the Oosterhoff dichotomy. Under this hypothesis, Oo type I GCs are characterized by red HB in which the RR Lyrae variables are, mostly, not evolved ZAHB stars. On the other hand, RR Lyrae stars in Oo II clusters would be the progeny of stars evolved from the blue side of the HB and, accordingly they cross the instability strip at higher luminosities producing therefore longer periods. Within this scheme, G11, with its blue HB should have properties consistent with an Oo II classification, at odds with what we have found in our study.

G33: This is the cluster with the least clear classification due to the large uncertainty affecting its metallicity estimate (±0.5). With a mean period of the ab-type RR Lyrae stars close to $\langle P_{ab} \rangle = 0.59$, G33 is the first clear case (the second if we consider G322 as well) of an intermediate Oosterhoff type GC in M31. Giving the large error in the metalicity estimate, we have considered the two most extreme cases respectively of a metal abundance around ~ -1.2 dex, and around ~ -1.7 dex. In the former case G33 would be a fairly "normal" Oo-Int GC, a classification interesting by its own since the MW GCs practically avoid these $\langle P_{ab} \rangle$ values, but otherwise not at all rare outside the MW (see right panel of Fig. 3.3). On the other hand, the situation becomes much more interesting if the cluster would have metal abundance around -1.7, since we would find the second case in Andromeda, besides B514, of a low metallicity cluster which does not have Oo type II properties. In the following we try to speculate on whether there is a way to produce such an unusual classification. Rich et al. (2005) have suggested that a number of clusters in M31 have HB morphologies too red for their low metallicities (~ -1.7 dex). More specifically there seems to be several GCs in M31 presenting the so called "second parameter effect", and a possible explanation is that these GCs are a few Gyr younger than the MW GCs of similar metallicity. If indeed a number of the metal-poor GCs in M31 are coeval or even younger than the intermediate metallicity GCs, then the Oosterhoff dichotomy should not exist in M31. G33 has an HB that seems to contain a rather balanced proportion between red and blue stars (Rich et al 2005), hence, perhaps, most of the G33 RR Lyrae stars come from the red side of the HB, and the contribution of RR Lyrae stars evolved from the blue side of the HB is minor, thus resulting in a short mean period of the ab-type RR Lyrae stars, and in classification more towards the Oo-type I, as we indeed find for G33.

G105: Is the most intriguing case in our sample. With a metallicity close to -1.28, one would expect an OoI classification if G105 were a MW GC. However, the mean period of its fundamental-mode RR Lyrae stars, $\langle P_{ab} \rangle = 0.598$, qualifies the cluster as an Oosterhoff-intermediate type, and puts G105 right in the middle of the Oosterhoff-gap avoided by the MW GCs. Moreover, the period distribution of G105 does not show a marked peak around $\langle P_{ab} \rangle \sim 0.6$ that usually characterized this type of clusters, but instead iseems to result from the superposition of two separate groups of variables having of $\langle P_{ab} \rangle \backsimeq 0.55$ and $\langle P_{ab} \rangle \backsimeq 0.66$, respectively. If this feature will be confirmed, G105 along with NGC 1835 in the Large Magellanic Clouds (Soszynski et al. 2003), would be the only two cases known so far of "hermaphrodite" Oo-int globular custers. Figure 4.9 (left) shows the period histogram of the ab-type RR Lyrae stars in G105. It is worth mentioning that the period uncertainty (±0.01) is lower that the bin used to create the figure (0.02 d); thus the observed bi-modality might be real. We have performed a Kolmogorov-Smirnov test to verify whether the two distribution differ significantly. We find a Kolmogorov-Smirnov value of $D_{ks} \sim 1$, implying a probability of only $P_{ks} \sim 10^{-5}$ that the 2 groups were drawn from the same parent distribution.

The right panel of Fig. 4.9 shows the Bailey diagram for the G105 RR Lyrae stars. In the figure, RRc variables are plotted as blue filled circles, while the RRab variables have been divided according to the period-group they belong to. Longer period RRab stars appear as green squared, whereas red squares represent the RRab group with shorter periods. For comparison, we have also plotted the reference lines for regular and evolved RR Lyrae stars in M3 from Cacciari et al. (2005), which mimic quite well the distributions of the OoI and OoII Galactic GCs (see Fig. 4, in Cacciari et al. 2004). Sandage et al (1981), have shown that the B amplitude of an RRab variable is related to its effective temperature; the larger the amplitude, for a given metallicity, the higher the temperature. Thus, the location of the RR Lyrae stars in the period-amplitude plane is a measure of their average luminosity and temperature. The period-amplitude distribution in

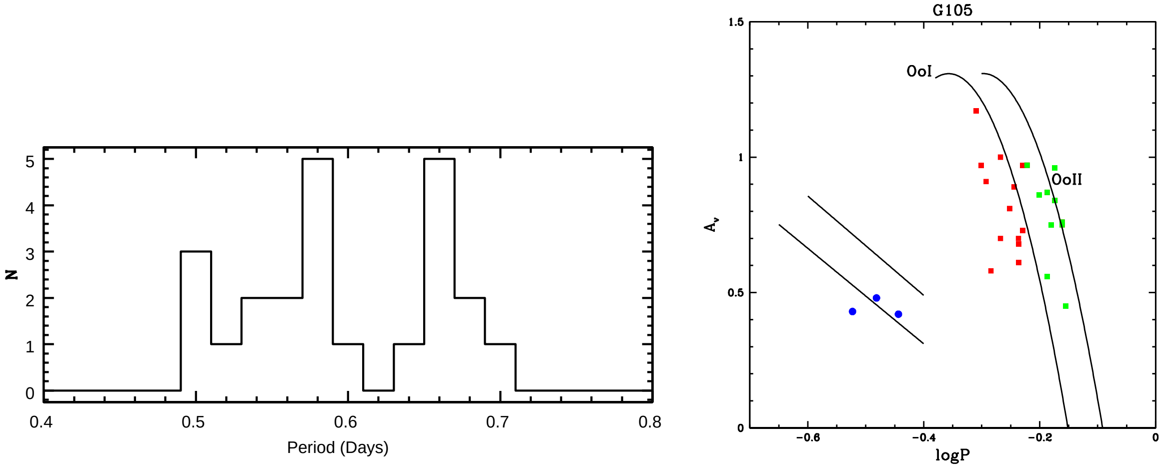

Figure 4.9: Left panel: period histogram of the fundamental mode RR Lyrae stars in G105. Right panel: period-amplitude diagram of G105 RR Lyrae stars.

the right panel of Fig. 4.9 shows that, while there are a couple of long period stars that appear at lower amplitude (lower temperature, although this feature could also be cause by Blazhko effectl, see, e.g., Contreras et al. 2010, submitted, and references therein), the bi-modality found in G105 seems mainly due to a difference in luminosity between the two groups, thus suggesting that the cluster might be a combination of two independent populations, each one represented by a different Oosterhoff type. However, our results are still preliminary and must be taken with caution, because of the current uncertainties in our estimates of periods and amplitudes of the G105 RR Lyrae stars. These uncertainties will be definitely cut down by the re-analysis of the light curves and the addition of the archive data, which is in progress. A further check on the origin of this bi-modality will also be to verify whether the bi-modal grouping seen in the period histogram and in the Bailey diagram reflects also into a different position in the cluster CMD of variables belonging to the two different groups, as well as into a different spatial distribution within the cluster.

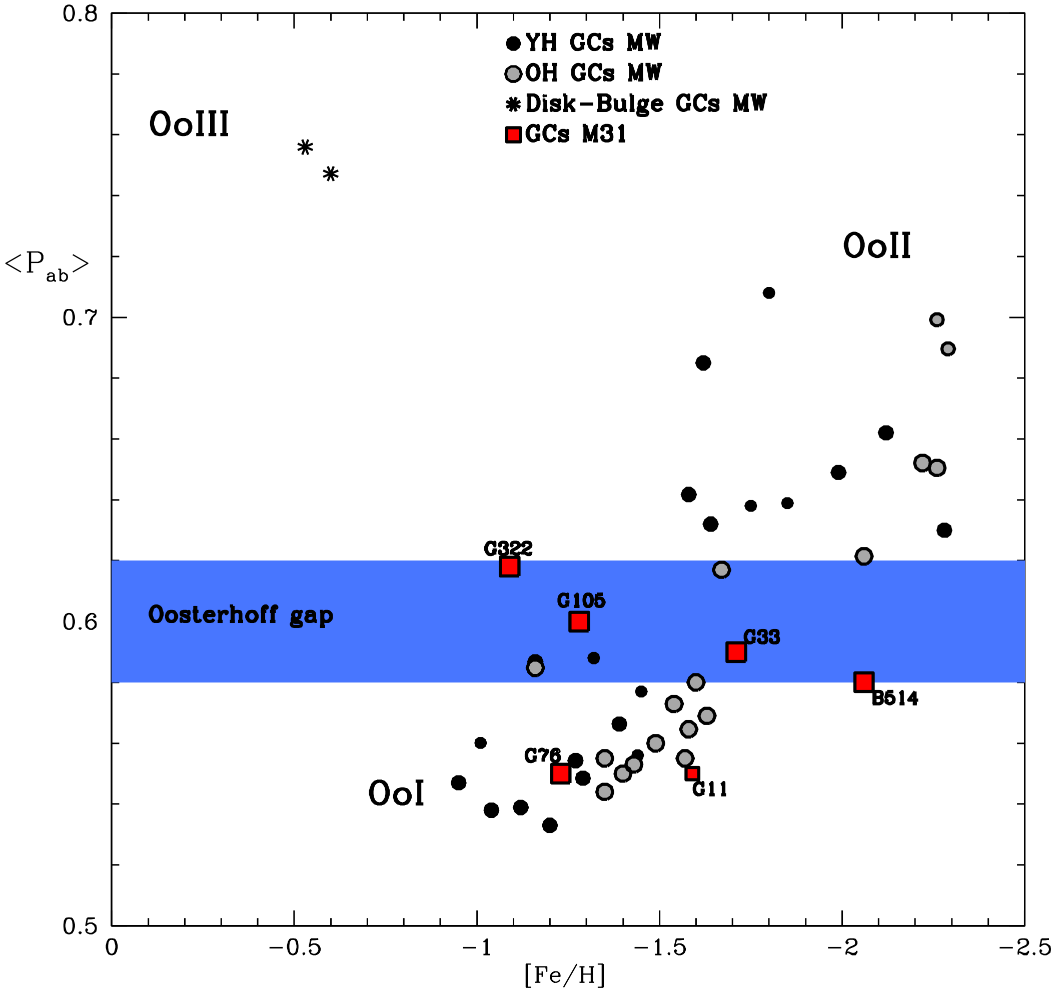

Figure 4.10: Distribution of $\langle P_{ab} \rangle$ vs. metal abundances for the Galactic GCs (from Clement et al. 2001; filled and open circles); for the classical M31 dSphs (green triangles; from Pritzl et al. 2002, 2004, 2005; Macone & Sarajedini 2008; and Sarajedini 2009, private comunication),; and for the six M31 GCs we have analyzed in the present work (red squares). Smaller symbols refer to systems containing less than 10 fundamental mode RR Lyrae stars.

The main results on the Oosterhoff classification of the 6 M31 GCs analyzed in this thesis work are illustrated in Fig. 4.10 and can be summarized as follows: 1) we have found that three, out of the 6 M31 GCs in our sample, likely have Oo-Intermediate characteristics. Such kind of GCs are almost inexistent among MW GCs, but are fairly common among the MW dSph satellites; 2) among the 3 Oo-Int clusters G105, looks particularly intriguing due to the possible bimodal distribution of its RRab stars; Thus, it represents indeed a "non-genuine" type of Oo-Int globular cluster. 3) the remaining three GCs RR Lyrae star properties consistent with an Oosterhoff I classification. However, among them, G11 possess a combination of metallicity and HB morphology at odds with its Oosterhoff classification; 4) we have not found any Oo type II cluster in our M31 sample, despite the low metallicity of B514 and, possibly G33, would make them both Oo II systems if they were in the MW. In fact, B514 and likely G33 if a low metallicity for it is confirmed, might conformed a class of objects with no counterparts in the MW, characterized by a deficient metal content and RR Lyrae stars with relatively low periods. With such a small sample and preliminary results, we cannot definitely conclude whether the M31 GCs follow a different pattern than the MW ones, thus pointing to a different formation and evolution history, but at least we may suggest that the division into metal-poor long-period, and metal-rich short-period RRab variables seems not to be present in M31. Indeed, the sample of M31 clusters observed in our Cycle 15 program is being analyzed more carefully (see R. Contreras et al. 2010, in preparation) to reach much firmer conclusions on the Oosterhoff properties of the M31 GCs. On the other side, if these preliminary results will hold and be confirmed by further studies, then would indicate a fundamental difference between halo GC populations in the MW and M31, and would imply that the events of halo formation that resulted in the Oosterhoff gap are peculiar to the Milky Way, and are not general to the formation of the halos of large spiral galaxies; i.e., the halo of M31 formed differently.

Chapter 5

Variable Stars in M31: Halo Fields

Our current knowledge concerning the properties of the RR Lyrae stars in the field of the Andromeda galaxy resides in two relatively recent studies (see section 3.3). In their deep HST/ACS survey of the M31 halo Brown et al. (2004) concluded that the old population in the Andromeda halo doesn't conform to the sharp subdivision in Oosterhoff I and Oosterhoff II types followed by the MW globular clusters. In this respect the M31 halo field would thus be different from the MW halo field, and this would point to a different formation/evolution history. However, a different conclusion was reached by Sarajedini et al. (2009) who concluded that their M31 studied fields have Oosterhoff I properties. However, how general are these results given the small areas covered by thses studies? Another open question is whether there are any RR Lyrae stars in the M31 giant stream. If present, they could either belong to the merged satellite, for instance to M32 where RR Lyrae stars have likely been found (Javier, Mateo & Worthey 2004, Fiorentino et al. 2010), or have formed during the merger, in which case the merging event would have occurred at least 10 Gyr ago. In any case, their pulsation properties could provide hints to identify the progenitor stream stars.

As a complement of the GC study described in chapter 4 we have obtained time series photometry using the Large Binocular Camera at the Large Binocular Telescope (LBC@LBT) of 4 fields carefully selected in the halo and in the giant tidal stream of the Andromeda galaxy, to study the variable stars in the M31 field. The main goal with is to find out whether the Oosterhoff dichotomy is present in the M31's halo and join these results with the cluster's results to obtain a more complete picture. A direct comparison of the properties of variables in GCs and in the adjacent fields can provide a very interesting diagnostic as to whether the spheroid and the GC system share a common origin. We are also interested in reconstructing the star formation history and the merging episodes that lead to the early assembling of M31. The study of different types of pulsating variables expected to be present in the field of M31, based on times series data, allow us to characterize the different stellar populations and to trace the oldest populations in the M31 halo and stream, overcoming the need for reaching their faint main sequence turn-offs.

Figure 5.1 shows the location of our target fields (large squares) on a schematic map of the Andromeda galaxy. We have also plotted, as filled circles, our GC targets, to provide an overall picture of our survey. Also shown in the figure, as crosses, are the fields studied for variability by Brown et al. (2004) and Sarajedini et al. (2009) using ACS/HST time-series data, and as diamonds the fields studied for variability by Vilardell et al. (2006, 2007) and Joshi et al. (2009). Identification and coordinates of the M31 fields we have observed with the LBT are provided in Table 5.1. Our stream fields were chosen as to monitor both the stream portion that enters into the M31 disk (field S1 in Fig. 5.1) and a region towards the North-East portion of the stream that exits from the disk (field S2 in Fig. 5.1). The halo field H2 was centered instead on the newly discovered M31 dSph satellite And XXI (Martin et al. 2009). Results on the cluster variables show that RR Lyrae stars in the M31 GCs tend to have different properties than their MW counterparts (section 4.5.2), thus supporting Brown's et al conclusions. The LBT is the ideal tool to carry out the study of the pulsating variable stars in the M31 halo and stream to the same level of accuracy reached by the HST/ACS studies, but on a much larger area, thus attaining a statistical significance never reached before for an external galaxy, as each LBT field covers an area about 37 times larger than an HST/ACS field.

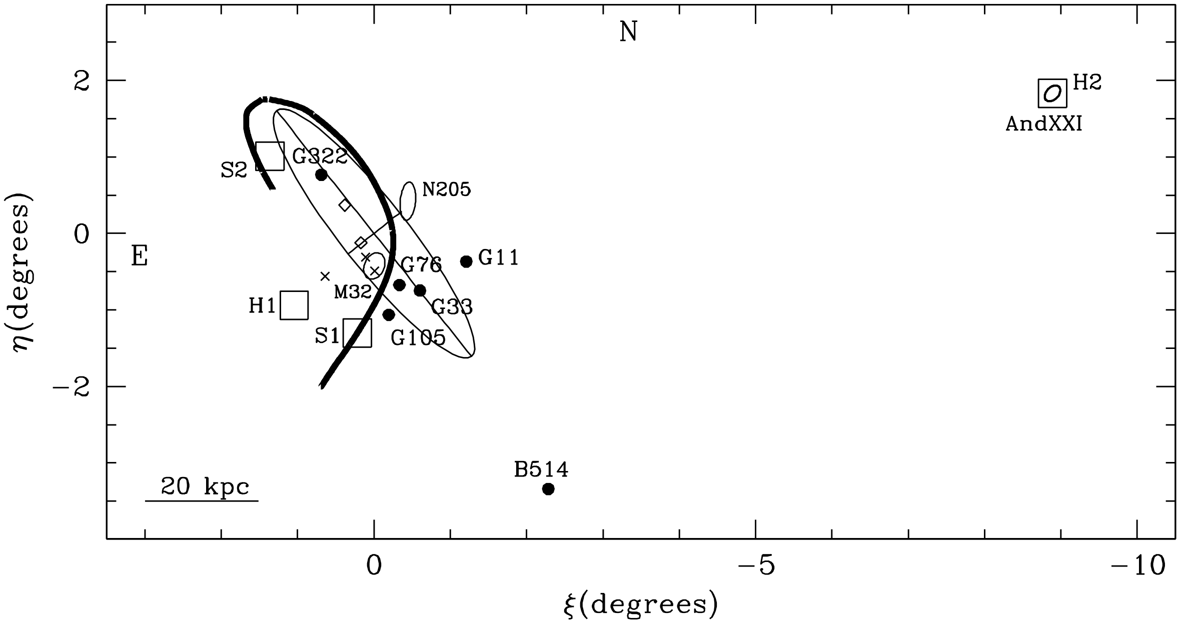

Figure 5.1: A schematic map of the Andromeda galaxy showing the location of the fields observed with the LBT/LBC-blue and the GCs observed with HST. The heavy-solid lines shows the approximate location of the M31 giant stream according to Ferguson et al. (2002). Crosses show the centers of the M31 fields studied by Brown et al. (2004) and Sarajedini et al. (2009) using ACS/HST time-series data. Diamonds mark the center positions of the M31 fields studied for variability by Vilardell et al. (2006, 2007) and Joshi et al. (2009), respectively.

In this chapter we present results from the observation of fields S2 and H1 while the analysis of fields S1 and H2 is still in progress. Data for the four fields was obtained with the blue channel of the Large Binocular Camera (LBC-blue) mounted at the prime focus of the first unit of the LBT (Giallongo et al. 2008). Each of these fields covers a $23' \times 23'$ area. We have obtained B, V CMDs to $V \sim 26$ mag for both fields. The large field of view along with the depth capabilities of LBT/LBC-blue allowed us to bridge in a single shot of field S2 portions of the M31 disk to traces of the galaxy giant stream. We present first results of a search for variable stars in these regions of the Andromeda galaxy, that allowed us to identify Classical Cepheids with periods in the range from 3 to 10 days, Anomalous Cepheids and/or short-period Classical Cepheids with

Table 5.1: Identification and coordinates of our LBT fields in M31.

Name	Object type	α	δ	ξ	η	$D_{M31\ center}$	N_B	N_V
H1	Halo field	00 48 13.11	+40 19 09.4	1.04	−0.94	18.9	48	3
H2	And XXI	23 54 47.71	+42 28 15.0	...	...	...	12	10
S1	Stream field	00 43 51.51	+39 58 09.4	...	...	...	6	3
S2	Stream field	00 49 08.31	+42 16 09.4	1.18	1.01	20.9	59	8

[a] Each image of fields S2 and H1 corresponds to a 300^s exposure.

periods around 1 day, as well as RR Lyrae stars. These results demonstrated the big capabilities of the LBT instrument, and confirmed that it is possible to perform the study of the M31 field RR Lyrae stars from the ground.

5.1 Observations and Data Reduction

B, V photometry of the M31 fields S2 and H1 (see Table 5.1) was obtained with the LBT/LBC-blue, during ten hours of Science Demonstration Time of the Blue Channel in 2007, October 11-18. According to the LBT/LBC-blue scale (0.225 arcsec/pixel and total field of view (FOV, $23' \times 23'$) each of these fields covers an area roughly corresponding to 5.1×5.1 kpc^2, at the distance of M31 ($\mu_{M31} \sim 24.4$ mag). Fig. 5.2 shows the location of field S2 and H1 over a 3.5×3.5 deg^2 image of the Andromeda galaxy obtained from the combination of the 3.4 μ, 4.6 μ, 12 μ and 22 μ fluxes measured by the NASA's Wide-field Infrared Survey Explorer (WISE; Image Credit: NASA/JPL-Caltech/UCLA), along with a schematic view of the M31 giant tidal stream (heavy dashed line). Both our fields are contained in the area surveyed by Ferguson et al. (2002) with the INT, reaching a limiting magnitude $V \sim 24.5$ mag, i.e. 1.5 mag shallower than our observations. These areas are also planned to be observed by the PAndA Survey (McConnachie et al. 2009), with limiting magnitude $g_0 \sim 25.5$ mag, however, no CMDs of the regions sampled

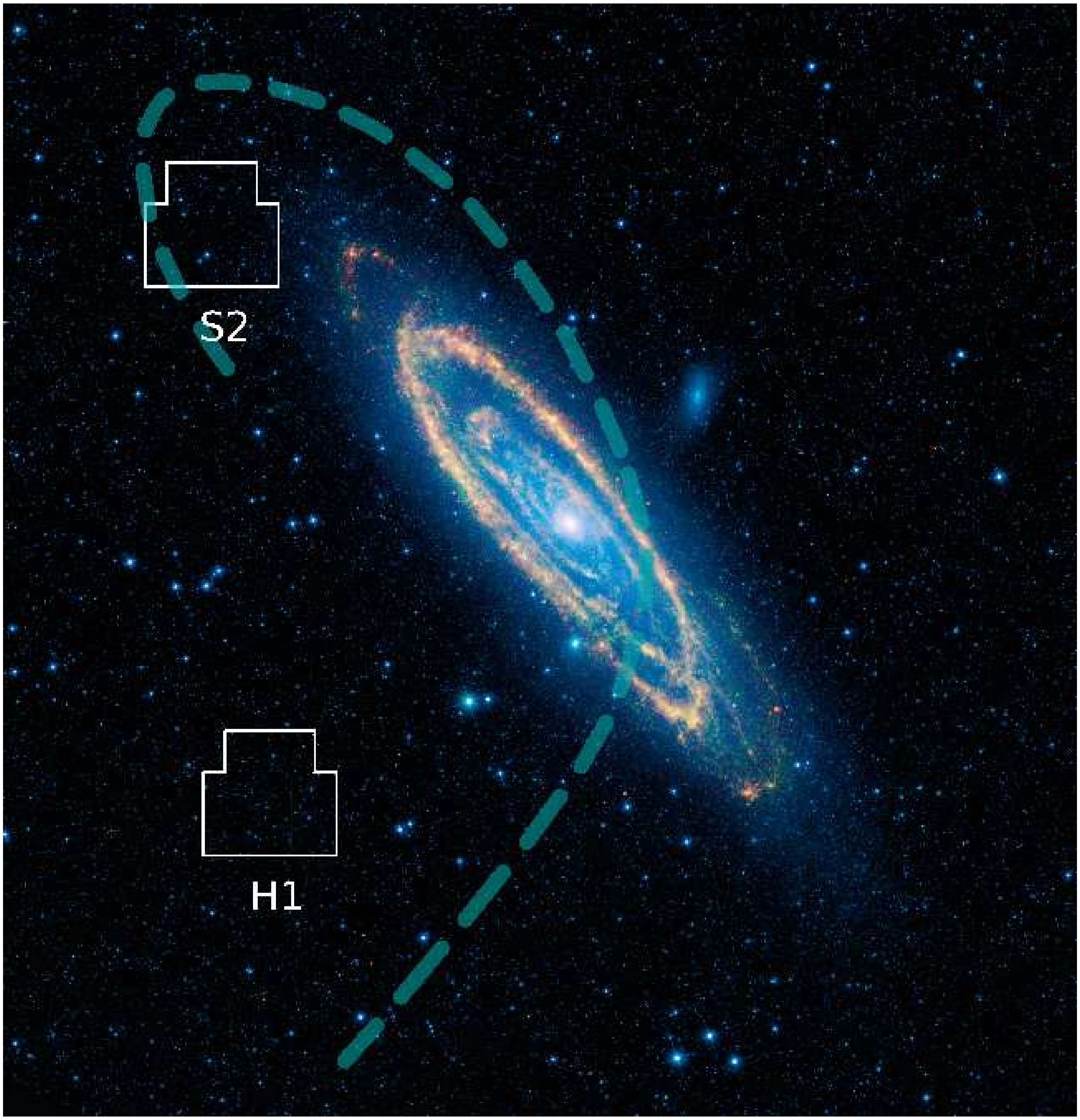

Figure 5.2: 3.5×3.5 deg^2 image of the Andromeda galaxy obtained from the combination of the 3.4 μ, 4.6 μ, 12 μ and 22 μ fluxes, measured by the NASA's Wide-field Infrared Survey Explorer (WISE; Image Credit: NASA/JPL-Caltech/UCLA), showing the location of fields S2 and H1 and a schematic view of the M31 giant tidal stream (heavy dashed line).

by fields S2 and H1 have been published yet. Field H1 contains the two HST/ACS fields of the M31 "Minor axis" observed by Richardson et al. (2008; see their table 1).

RR Lyrae stars in M31 are expected to have average magnitudes around $V \sim 25.3$-25.5 mag. Taking into account their typical intrinsic colors, amplitudes and periods ($B - V \sim 0.2 - 0.4$, $A_v \sim 0.3$-0.5 and 0.6-1.2 mag, P$\sim$ 0.2-1 day, for first overtone and fundamental mode pulsators, respectively) we aimed at reaching a limiting magnitude of B ~26 mag (corresponding to the minimum light of these variables in M31) in no longer than 15-20 min to avoid smearing the light curve and to have an acceptable S/N even at the light curve minimum. Based on the LBT exposure time calculator we had estimated that in dark time, with a 15 min exposure we would obtain S/N~6 for B=26 mag, and V=25.5 mag with S/N~9. This would have been perfectly adequate for our purposes. Unfortunately, seeing conditions varied significantly during our observing run, ranging from 0.8 to 2.7 arcsec. We also experienced a number of severe problems with the telescope focus and tracking which did not allowed us to make individual exposures longer than 300^s. Our observations, acquired in time-series mode, consist of 59 B and 8 V frames of field S2, and 48 B and 3 V frames of field H1, each frame corresponding to a 300^s exposure, and we obtained S/N~2 for $B \sim 26$ mag in our best image with FWHM~0.8 arcsec. Nevertheless, we managed to obtain 30 B and 6 V images of field S2, and 33 B and 1 V image of field H1 with FWHM < 1.3 arcsec, which, using the Image Subtraction Technique, turned out to be adequate to identify variable stars as faint as $\sim$ 25.5 mag. It should also be noted that, due to technical problems, the V images of both field S2 and H1 were trimmed during the read-out of the CCDs, as a consequence the upper 500 pixels of each CCD in the V images were lost.

Pre-reduction of the entire dataset (bias-subtraction and flat-fielding) through the LBC dedicated pipeline was provided by the LBC team[1], while bad pixel mask correction was performed by us using the task FIXPIX in the IRAF environment. PSF-photometry of the pre-reduced

---

[1] http://lbc.oa-roma.inaf.it/

images of each chip of the LBC mosaic, separately, was then performed using two different packages. We used DoPHOT (Schechter et al. 1993) to process images obtained in best observing conditions (1B and 1V with FWHM$\sim$ 0.8 - 1 arcsec for each of the two fields), and produce the CMDs, and DAOPHOTII/ALLSTAR/ALLFRAME (Stetson 1987, 1994) to process the individual time-series data and produce light curves on a magnitude scale for the variables stars. A 2MASS catalogue[2] was used to identify astrometric standards in the LBC field of view. More than a thousand stars were used to find an astrometric solution for each of the four LBC CCDs, with an accuracy of the order of $\sim$ 0.3 arcsec in both right ascension and declination. The absolute photometric calibration of the S2 and H1 photometry was obtained using a set of 192 local secondary standard stars with B, V photometry in the Johnson-Cousins system, extracted from Massey et al. (2006) catalogue, which fall in the region of field S2 covered by CCD 1. Aperture corrections were calculated for each of the 4 CCD mosaics of field S2 and H1, separately, by performing aperture photometry in each photometric band with the SExtractor package (Bertin et al. 1996). The calibration equations so derived are:

$$B = b - 0.0635(b - v) + 27.78 - K_b X_b$$

and

$$V = v + 0.0107(b - v) + 28.12 - K_v X_v$$

where B and V are the standard magnitudes and b, v are the instrumental magnitudes normalized to 1 sec and corrected for aperture corrections. K_b and K_v are the extinction coefficients in B and V for which we adopted values of 0.22 and 0.15 mag, respectively, as provided on the LBC commissioning web page (available at http://lbc.oa-roma.inaf.it/commissioning/standards.html). Typical errors of our photometry for non-variable stars at the level of the M31 horizontal branch ($V \sim$ 25.5 mag) are σ_V= 0.17 mag, and σ_B= 0.26 mag, respectively.

---

[2] http://irsa.ipac.caltech.edu/

5.2 Color Magnitude Diagrams

Figures 5.3, 5.4, 5.5, 5.6 show the $V, B-V$ and $B, B-V$ CMDs of the 4 CCD mosaics of field S2 and H1, respectively, obtained at the end of the reduction and calibration processes, from the DoPHOT photometry of pairs of B, V images of each field, corresponding to 300^s exposures obtained with FWHM of about 0.8-1.0 arcsec. The photometric catalogues producing these CMDs were cleaned from stars with photometric errors larger than twice the mean error at each magnitude, and by manually removing “spurious stars” produced by ghosts and spikes of saturated sources and background galaxies. In each figure the CMDs are arranged according to the geometry of the 4 CCDs composing the LBC-blue mosaic, and each CCD was divided in 2 equal parts, namely, North and South parts for CCDs 1, 2 and 3, and East and West parts, for CCD 4. Accordingly, CMDs corresponding to the four different CCDs of each field were labeled as follows: C1 N for CCD1 North part, C1 S, for CCD1 South part, etc., while the CMDs corresponding to the two parts of CCD4 were labeled as C4 E for CCD4 part East, and C4 W for CCD4 part West. We recall that each CCD of the LBT/LBC-blue mosaic covers about a 1.7×3.9 kpc^2 area of M31, however, because of the trimming of the V images, CMDs corresponding to individual CCDs in fact, cover a reduced, but still remarkable, area roughly of 1.7×3.4 kpc^2. We have accounted for this problem when dividing CCDs and corresponding CMDs in parts, in other words, each CMD in Figures 5.3, 5.4, 5.5, 5.6 samples the same area of M31. The more striking feature in the CMDs of field S2 is a conspicuous blue plume observed in panels C1 N, C1 S and C4 W of Figs. 5.3 and 5.4 at $V \leq 25.0$ mag and $B-V \leq 0.4$ mag of field S2. This blue plume is barely discernible in C2 N, and eventually disappears moving eastward, from CCD2 to CCD 3. Also intriguing is a feature seen in C2 N and S, C3 N and S, and C4 E at $V \leq 25.0$ mag and $0.2 < B-V < 0.4$ mag. Finally, all CMDs show a bright red plume, variably populated, and a sparse distribution of bright stars of intermediate colors. We believe this blue-plume is produced by young stars possibly associated to the galaxy disk (see below). The CMDs of field H1 (see Figs.5.5, 5.6) are much less populated than those of field S2, and

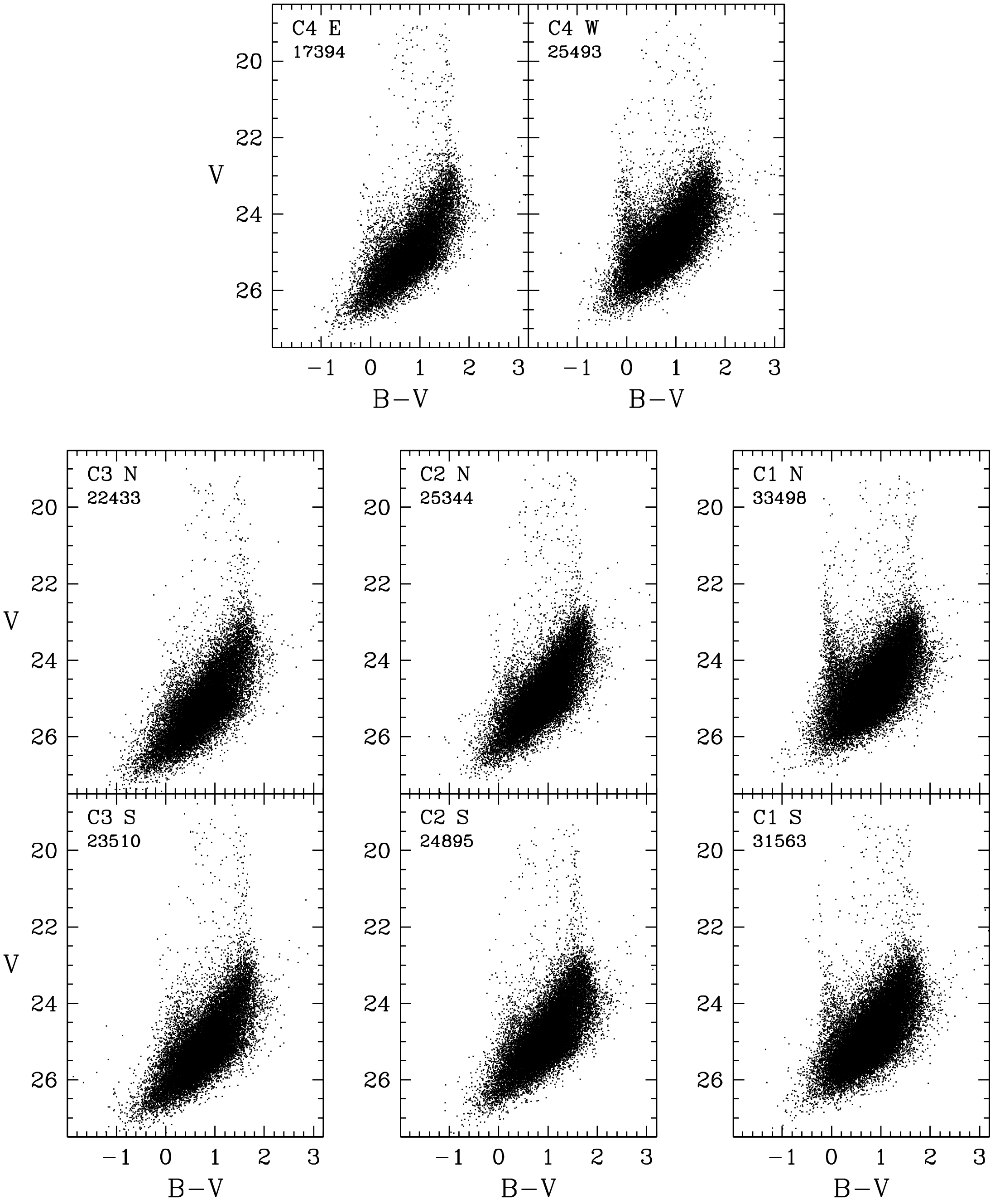

Figure 5.3: $V, B-V$ CMDs of field S2, from a pair of B, V images of 300^s exposure time, obtained in optimal observing conditions (FWHM ∼ 0.8-1.0 arcsec).

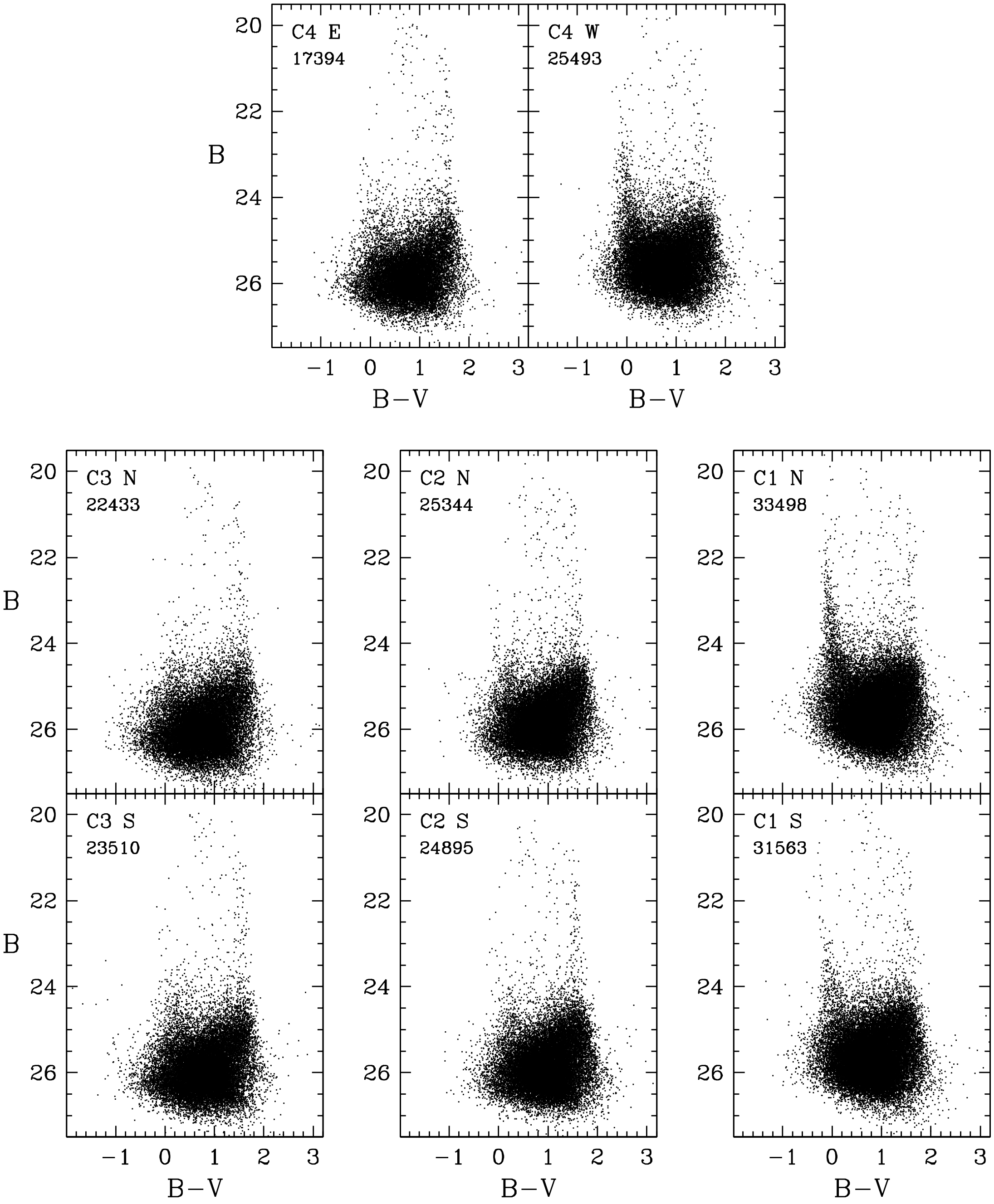

Figure 5.4: $B, B-V$ CMDs of field S2, from a pair of B, V images of 300^s exposure time, obtained in optimal observing conditions (FWHM ∼ 0.8-1.0 arcsec).

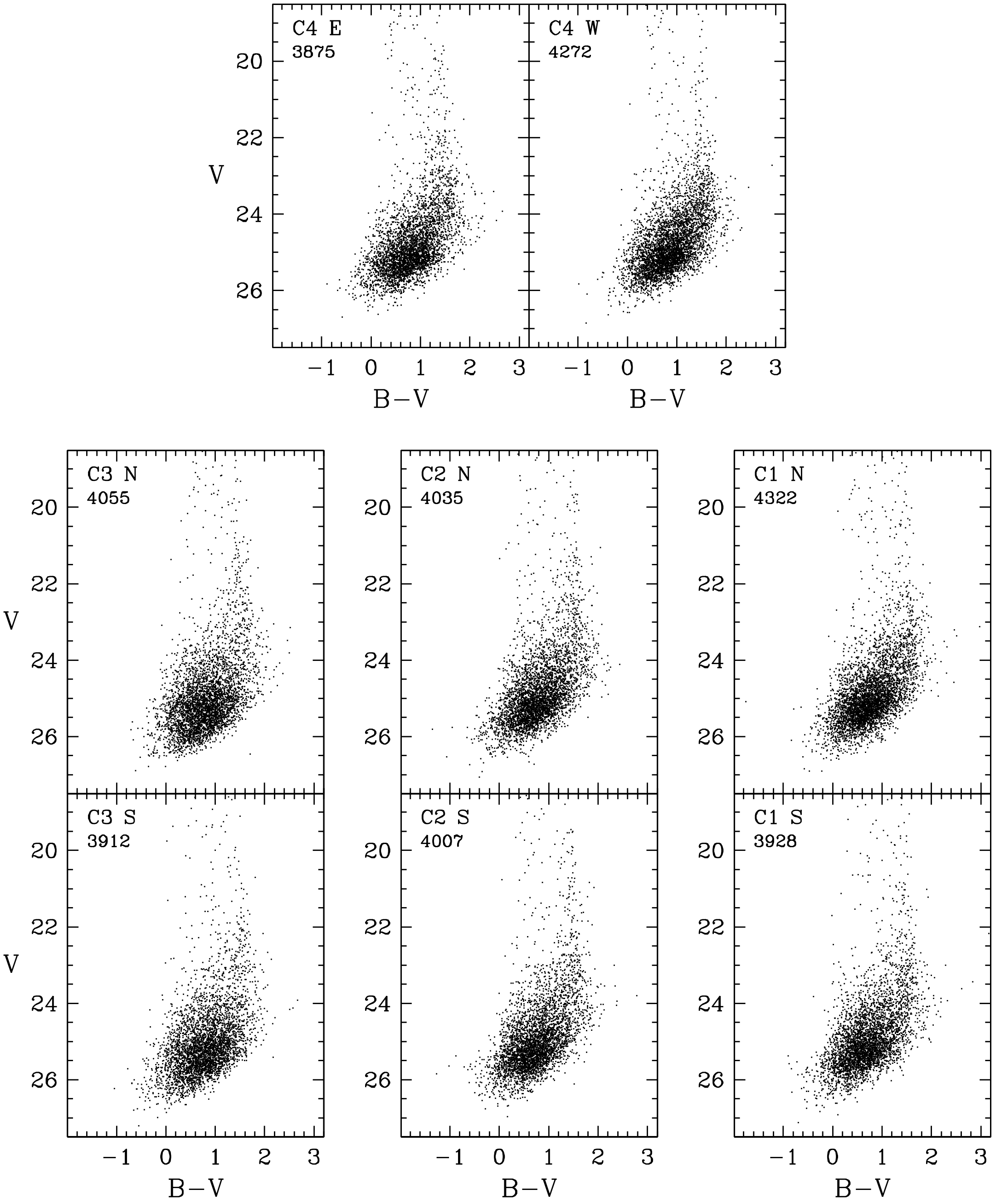

Figure 5.5: $V, B-V$ CMDs of field H1, from a pair of B, V images of 300^s exposure time, obtained in optimal observing conditions (FWHM $\sim$ 0.8-1.0 arcsec).

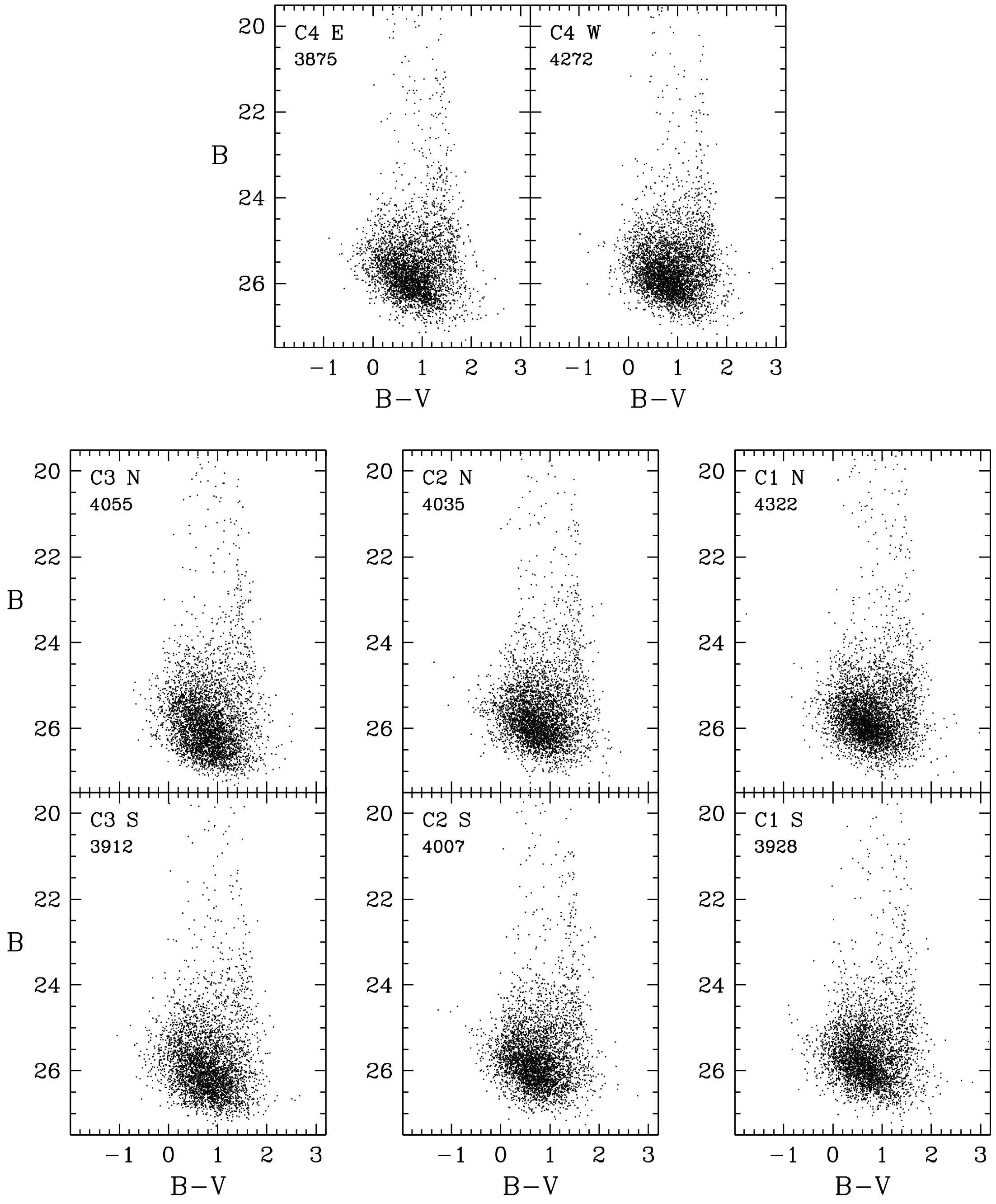

Figure 5.6: $B, B-V$ CMDs of field H1 from a pair of B, V images of 300^s exposure time, obtained in optimal observing conditions (FWHM ~ 0.8-1.0 arcsec).

the blue-plume is totally absent, which is not surprising if our interpretation of the blue-plume in field S2 as due to disk stars, since field H1 is instead more a representation of the M31 halo population.

In order to correctly interpret the features we see in the CMDs in terms of star formation history and structure of M31, a reliable evaluation of the foreground contamination due to our Galaxy is necessary. To approach this problem, we have run simulations using a well-tested star-count code for our Galaxy (see Cignoni et al. 2008 and Castellani et al. 2002). In this code the Galaxy is divided into three major Galactic components, namely the thin disk, the thick disk and the halo. For each of these three components an artificial population is created by a random choice of mass and age from the assumed initial mass function and star formation law, interpolating on a grid of evolutionary tracks (from the zero age main sequence the white dwarf phase), whose metallicity is determined by the adopted age-metallicity relation. Finally, reddening and photometric errors are convolved with the synthetic photometry producing a realistic CMD. The following ingredients were adopted in the present simulation: the thin disk and the thick disk density laws were modeled by a double exponential with same scale length (3500 pc) but different scale height (1 kpc for the thick disk, 300 pc for the thin disk). The halo followed a power law decay with exponent 3.5 and an axis ratio of 0.8. A local spatial density of 0.11 stars pc^{-3} was adopted for the thin disk, whereas thick disk and halo normalizations were respectively 1/10 and 1/500 relative to the thin disk. The metallicity of each Galactic component was fixed at Z=0.02, Z=0.006 and Z=0.0002 for thin disk, thick disk and halo, respectively. In order to establish quantitative limits to the Galactic star counts in field S2, all free model parameters were varied. In particular, the thin-disk scale height was let vary between 250 and 300 pc, whereas thick disk and halo normalizations were, respectively, tested between 1/10 and 1/20 and between 1/500 and 1/850 relative to the thin disk. Left panel of Fig. 5.7 summarizes the predicted star counts as a function of magnitude and color, while the right panel shows a typical simulated CMD for the foreground contamination in field S2, obtained by assuming $E(B-V)$=0.08 mag, and the typical internal errors of our photometry (0.007< σ_B <0.296 and 0.008< σ_V <0.252,

	$0 < (B - V) < 0.5$	$0.5 < (B - V) < 1$
$V < 20$	2 – 3	43 – 78
$20 < V < 21$	0 – 1	6 – 10
$21 < V < 22$	0 – 1	3 – 9
$22 < V < 23$	0 – 1	3 – 7
$23 < V < 24$	1 – 3	3 – 8

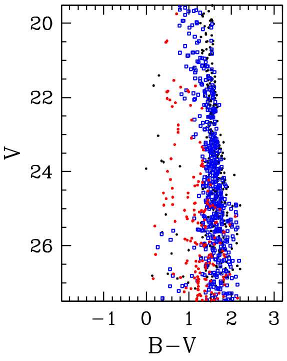

Figure 5.7: (Left) Range of expected Galactic contaminating stars as a funtion of magnitude and color. (Right) Foreground simulation for S2 including thin disk (black stars), thick disk (blue diamonds) and halo (red filled circles) stars. Notice that this CMD is on the same scale as those of Fig. 5.3 to allow for a direct comparison.

for 20.0< V <26.0). The simulation describes the contamination by Galactic stars, affecting each of the CMDs shown in the 8 panels of Figs. 5.3 and 5.5. This simulation demonstrates that the blue plume observed in the CMDs of panels C1 N, C1 S and C4 W is produced by M31 stars, and is not due to contamination by Galactic stars. Viceversa all the bright stars with intermediate colors are likely MW stars (of the halo and thick disk), while most of the bright red plume stars are MW thick disk objects. In Figures 5.8 and 5.9 we show, respectively, a B image of field S2 and a B image of field H1 where we have overploted in red stars having $V \leq 25.0$ mag and $B - V \leq 0.2$ mag, which correspond to sources populating the blue plume of the CMDs, and in cyan stars having $V \leq 25.0$ mag and $0.2 < B - V \leq 0.4$ mag, corresponding to the intermediate-color features we see in Figs. 5.3 and 5.5. We recall that for stars located on the upper 500 pixels of each CCD of the mosaic we only have B magnitudes, because of the unfortunate trimming of the V images. This is why all these stars are missing in the CMDs of Figs. 5.3, 5.4, 5.5, 5.6 and in the images showns in Figs. 5.8 and 5.9. Nevertheless, while the intermediate-color sources (cyan points) are almost homogeneously widesperad on all 4 CCDs,

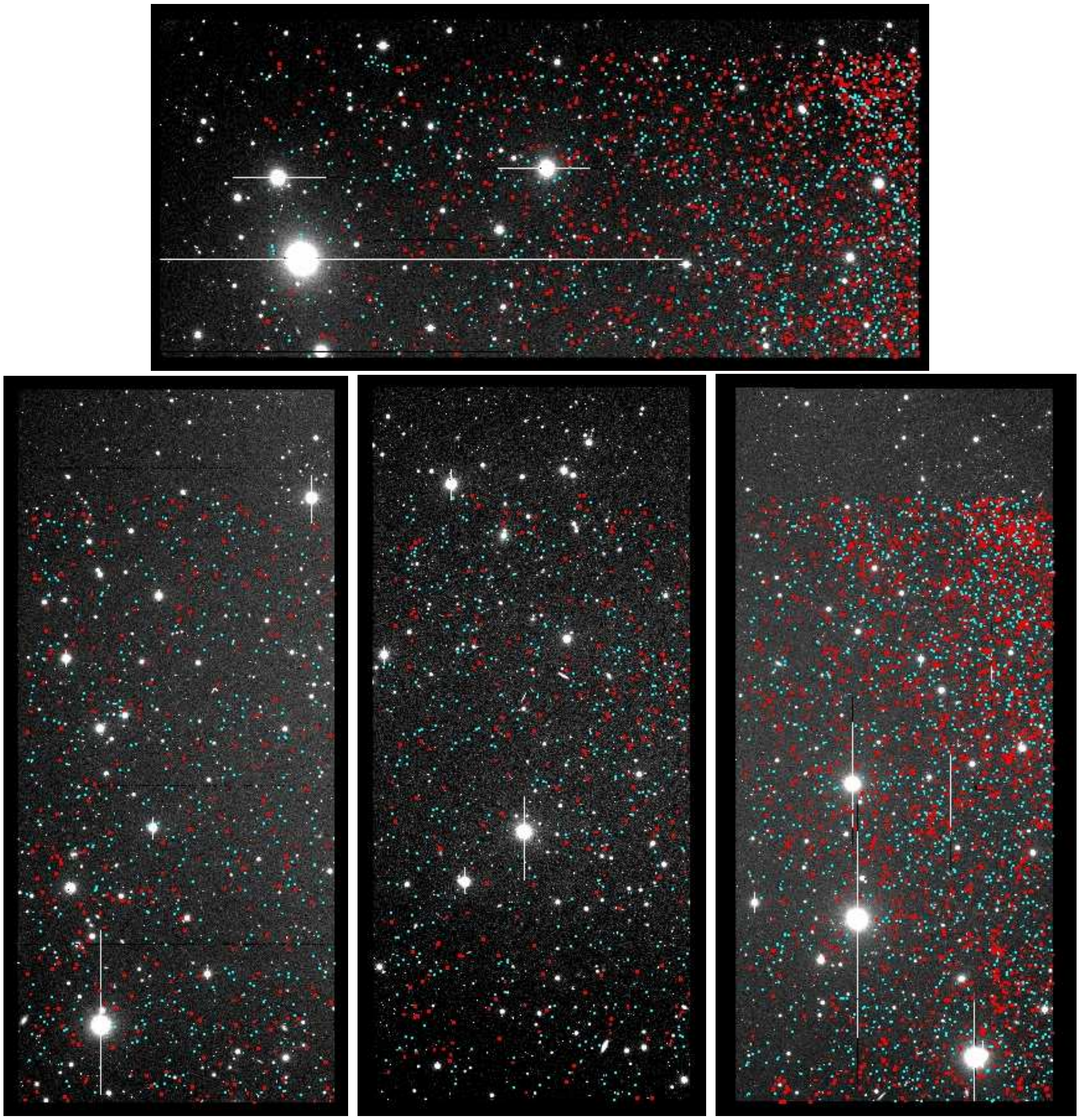

Figure 5.8: Position on the 4 CCDs mosaic of field S2 of stars in the blue plume of the CMD (see Figs. 5.3 and 5.4). Red dots are stars with $V \leq 25.0$ and $B-V \leq 0.2$ mag; cyan dots are stars with $V \leq 25.0$ and $0.2 < B-V \leq 0.4$ mag.

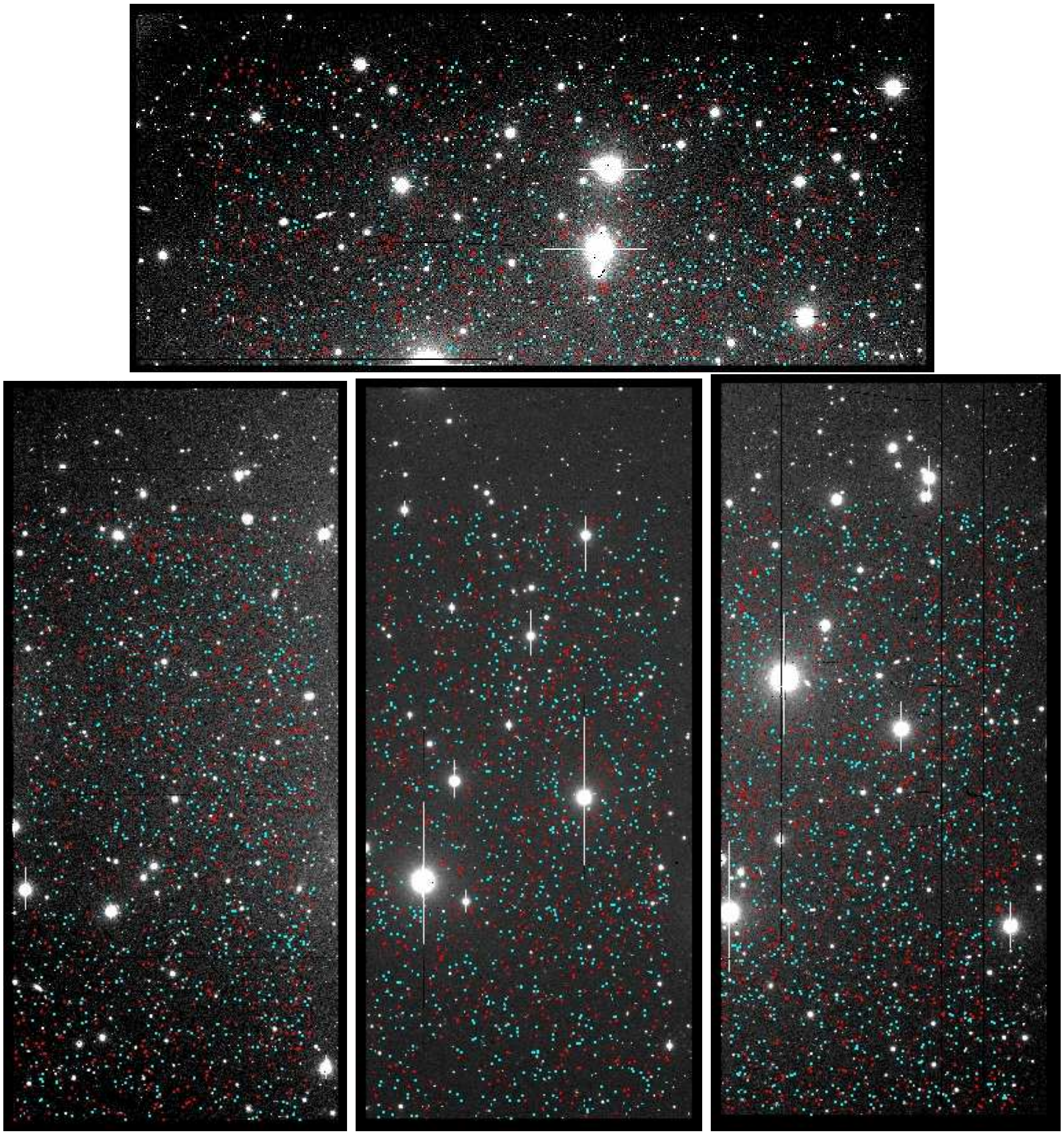

Figure 5.9: Position on the 4 CCDs mosaic of field H1 of stars in the CMD (see Figs. 5.5 and 5.6) with $V \leq 25.0$ and $B - V \leq 0.2$ mag (red dots); and with $V \leq 25.0$ and $0.2 < B - V \leq 0.4$ mag (cyan dots).

both in field S2 and in field H1, and could thus trace the halo component, the blue-plume stars (red points) appear to be mainly concentrated in the upper-right (North-West) part of CCD1 and in the right (West) portion of CCD4 of field S2, thus likely tracing the disk of M31.

5.3 Variable Stars

As discussed in Section 5.1, the poor seeing conditions and technical problems which affected our data, made it rather difficult to use them for our original purpose: the identification of variable stars in these regions of M31. A further complication came from the significant optical distortions of the LBT/LBC-blue camera (see Giallongo et al. 2008, Figure 4). We had to implement a number of different procedures and make several trails to detect the variable stars. Hence, the numbers of confirmed variables we were able to identify are very likely lower limits. Nevertheless, this exercise definitely proved that a telescope and camera like LBT/LBC can reach the M31 RR Lyrae stars. In the following we briefly describe the procedures we have implemented and the results we have obtained from the search for variable stars in CCD2 and in the upper half portion of CCD1 of field S2, and in the upper half portion of CCD2 of field H1.

To identify candidate variables in our B time series images of fields S2 and H1 we used the Optimal Image Subtraction technique and the package ISIS2.1 (Alard 2000), which is known to be very efficient in identifying variables with amplitudes as low as ΔB <0.1 mag in crowded fields. The package was run on the B time series of CCD1 and 2 of field S2 and CCD 2 of field H1. We encountered several difficulties to align and interpolate with ISIS the images of our LBT/LBC-blue time series data, likely because of the significant distortions of LBT/LBC-blue. Since the regions of the LBC mosaic less affected by optical distortions are those covered by CCD2, and the better observing conditions occurred during the observations of field S2, we managed to properly align and interpolate with ISIS, and then make the subsequent search for variable stars, of a subset of 43 B images of the entire CCD2 of field S2. Interpolation didn't succeeded instead for the entire CCD1: we had to divide it in two halves and only images corresponding to the upper half of CCD1 of field S2 were successfully aligned. We encountered even more problems with the images of field H1, since they were generally obtained under worse seeing conditions. We divided the CCD in two parts and were able to align and interpolate only a subset of 33 images corresponding to the upper half of CCD2. After aligning and interpolating the images we built reference images of CCD2 - S2, CCD1 - S2 upper part, and CCD2 - H1 upper part, subtracted them out from the respective time series and summed the difference images to obtain var.fits images, which, according to ISIS are the maps of variable sources in the frames under study. From each set of CCD1 - S2, CCD2 - S2, and CCD2 - H1 aligned images we built two different var.fits images, by varying the number of stacked images. Specifically we used 19 and 28 frames to build two var.fits images of CCD2 of Field H1, 17 and 28 images for CCD2 of field S2, and 20 and 43 images for CCD1 of field S2. In order to be able to pick up on the var.fits images candidate variables as faint as the RR Lyrae stars, that at minimum light in our frames are expected to have S/N$\sim$ 2, we had to use a very low detection threshold of 0.33. We ended up with rather large lists of about 4000 candidate variables from each var.fits frames. Lists corresponding to the pair of var.fits frames of each field were cross-correlated, thus obtaining a list of about 2000 common candidate sources per each set of images. Visual inspection of these stars returned a final catalogue of 161 bona fide candidate variables in CCD2 of field S2, 100 candidates in the upper portion of CCD1 of field S2, and 38 candidates in the upper portion of CCD2 of field H1. We note that many of the original candidates we checked should be real variables, but we only retained for further analysis those candidates which have more coherent and unquestionable light curves. We also note that only a fraction of our candidates have a counterpart in the ALLFRAME catalogues, hence have a light curve on a magnitude scale, while all the others only have differential flux light curves. For instance, out of the 161 candidates we found in CCD2 of field S2 only 48 have a counterpart on the ALLFRAME catalogue.

In field H1, variable stars were also searched on the catalogues produced by the ALLFRAME reductions of the B time series of the entire CCD2 using the Stetson variability index within

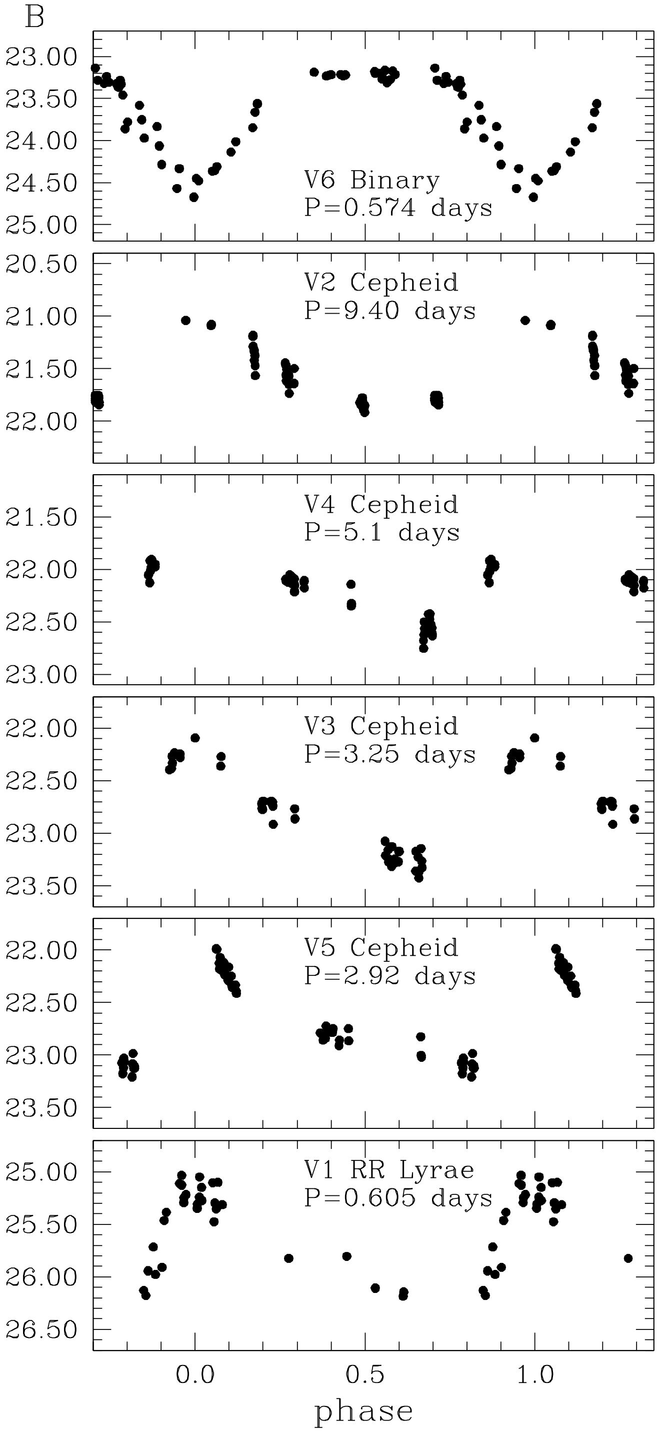

Figure 5.10: Examples of *B* light curves for 4 Cepheids, one RR Lyrae star, and binary system detected in field S2 Chip 1. Each data point corresponds to a 300 sec exposure. Typical error bars of the individual data points are in the range from 0.01 to 0.02 mag for the Classical Cepheids, 0.11-0.17 mag for the candidate ACs/spCCs, and from 0.13 to 0.38 mag for the RR Lyrae stars.

ALLFRAME, and obtaining a list of 200 candidates. However, visual inspection of the images of several of these candidates showed that they often have extended PSFs. Thus, although the variability of the light curve seems rather secure, a deeper analysis is in progress to ascertain the actual nature of these sources. Work is also in progress to identify candidate variables in the other CCDs of fields S2 and H1.

As with the cluster variables, the study of the light curves of the bona fide candidate variables was performed with the GRATIS package. Although our observing strategy was mainly devised to optimize the detection of RR Lyrae stars, it turned out to be adequate also to identify and characterize longer period variables such as Anomalous and Population II Cepheids, and short and intermediate period Classical Cepheids. In Figure 5.3 we show examples of the *B* light curves of the variables stars we have detected in field S2, while in Table 5.2 we summarized their main properties. They include four pulsating stars with periods of 9.9, 4.9, 3.3 and 2.92 days, that we have classifed as Classical Cepheids on the basis of their brightness and position in the CMD (see below), an RR Lyrae star with period of 0.605 days, and a binary system with period of 0.574 days. The catalogues of light curves, in *B*-band differential flux, for all

Table 5.2: Identification and properties of some confirmed variable stars in the M31 field S2

Name	Id	α (2000)	δ (2000)	Type	P (days)	Epoch (-2450000)	N_V	N_B	⟨B⟩ (b)	A_B (mag)	⟨V⟩ (c)
V1	54011	00 48 36.39	42 14 57.7	RRab	0.605	4386.822	4	31	25.75	1.03	25.36
V2	390	00 48 38.17	42 15 44.7	Cepheid	9.40	4385.200	5	53	21.48	0.88	20.62
V3	933	00 48 21.60	42 16 55.3	Cepheid	3.22	4387.942	5	49	22.74	1.07	22.03
V4	427	00 48 31.74	42 16 31.9	Cepheid	5.1 :	4388.400 :	5	51	22.13 :	0.84 :	21.47 :
V5	480	00 48 10.19	42 16 30.3	Cepheid	2.92	4383.700	5	51	22.58	1.29	21.97
V6	3836	00 48 20.94	42 19 38.7	Binary	0.574	4389.790	3	49	23.52	1.35	23.36

[a] Epochs correspond to the time of maximum light for the pulsating variables, to the time of the main minimum light for the binary system.

[b] ⟨B⟩ values are intensity-averaged mean magnitudes.

[c] The ⟨V⟩ values were derived scaling from the *B* light curves according to the procedure described in the text.

the candidate variables discussed in this chapter are presented in the Appendices G, H, and I. While the sampling of the B-band light curves was adequate to obtain a reliable estimate of the B amplitude and average magnitude of the variable stars, coverage of the V-band light curve is very sparse. To recover the average magnitudes in the visual band, and thus be able to plot the variable stars on the CMDs, we used the star's B band light curve as a template, and properly scaled it in amplitude to fit the few available V data-points. To constrain the scaling factor for the RR Lyrae stars we used amplitude ratios $A(B)/A(V)$ computed using literature B, V light curves of RR Lyrae stars with good light curve parameters, selected from a number of Galactic globular clusters (see Di Criscienzo et al. 2010, in preparation, for details) and, for the Cepheids, we used amplitude ratios and phase lags taken from Freedman (1988) and Wisniewski & Johnson (1968). Finally, for the binary system we used amplitude ratio of 1, since for binaries we do not expect significant cromatic effects.

The $\langle B\rangle$, $\langle V\rangle$ magnitudes obtained with the procedures described above were used to place the variable stars on the CMDs. This is shown in Figure 5.11 where we have zoomed the $V, B-V$ CMD of the portion of field S2 images on CCD1 (corresponding to the sum of the CMDs of C1 N and C1 S in Fig. 5.3), and plotted as large open stars 5 pulsating variables and one binary system whose B light curves are shown in Fig. 5.3. Since the $\langle V\rangle$ magnitudes and $\langle B\rangle$ - $\langle V\rangle$ colors of these variables were obtained averaging over the full pulsation cycle, the pulsating stars are found to populate in the CMD the rather narrow region corresponding to the classical instability strip (IS) of Cepheids and RR Lyrae stars (see below). In the CMD we have also plotted as filled dots a few other variables detected in this region, namely, according to their magnitude level: RR Lyrae stars at $V \sim$ 25-25.2 mag, short period Classical Cepheids or Anomalous Cepheids at $V \sim 24$ mag, Classical Cepheids at $V \geq 22$ mag. These variables were plotted using magnitudes and colors arising from only the pair of B, V images used to build the CMD, hence sampling random phases of the B, V light curves. As expected, because of the decoupling of their B,V magnitudes some of these variables fall outside the IS. In the upper panel of Fig. 5.11 the long-dashed black lines show the boundaries of the theoretical instability strips for RR Lyrae stars (Di Criscienzo, Marconi, Caputo 2004), and for Anomalous Cepheids with Z=0.0004 and 1.3 $<$ M$<$ 2.2 M$\odot$ (Marconi et al. 2004). The dotted heavy lines represent instead the first overtone and fundamental blue edges (blue lines) and the fundamental red edge (red line) for Classical Cepheid models with Z=0.008, Y=0.25 and 3.25 $<$ M/M$_\odot$ $<$ 11 (Bono, Marconi, Stellingwerf 1999; Bono et al. 2002). We note that the two variables at $V \sim 24$ mag (red filled dots) although plotted with their V and $B-V$ values from the Dophot photometry only (i.e. with random phase values corresponding to their magnitudes in the pair of images with FWHM=0.8 arcsec only) fall very well within the instability strip of Anomalous Cepheids. From the study of the light curves in differential flux obtained with ISIS we have derived for both stars periods around 1.2, 1.3 days, which is also consistent with them being Anomalous Cepheids, that is the extension to low metallicity of “classical” (i.e. metal-intermediate) short-period Cepheids (see Dolphin et al. 2002, Caputo et al. 2004). Also shown, for a comparison are isochrones by Girardi et al. (2000, and following updates) for Z=0.008 and ages of 63 and 141 million years, and for Z=0.0004 and age of 700 million years, which well fit respectively the young and intermediate-age stellar components in the CMD, and the mean ridge lines of the Galactic globular clusters (GCs) M15, M3, 47 Tuc and NGC6553 (drawn from the B, V database of Galactic GCs collected by Piotto et al. 2002) for the old (t$>$ 10 Gyr) stellar component. To plot on our CMD the GCs ridgelines, the theoretical IS boundaries, and the Girardi et al. (2000) isochrone we have assumed: $E(B-V)$=0.08 mag from Schlegel et al. (1998), computed running the program provided by the authors to interpolate on their maps, A$_V$=3.315 $E(B-V)$ from Schlegel et al. (1998), and μ_0(M31)= 24.43 mag. The latter value was obtained correcting the distance modulus measured by McConnachie et al. (2005) from the M31 red giant branch tip for $E(B-V)$=0.06 mag and A$_I$=1.94 $E(B-V)$ (Schlegel et al. 1998) to our adopted reddening of $E(B-V)$=0.08 mag.

The comparison shown in this figure demonstrates how powerful is the approach of combining informations coming from the CMD of a given field, to informations obtained from the variable star population present in the field. In fact, while the presence of an old (t$>$10 Gyr) population

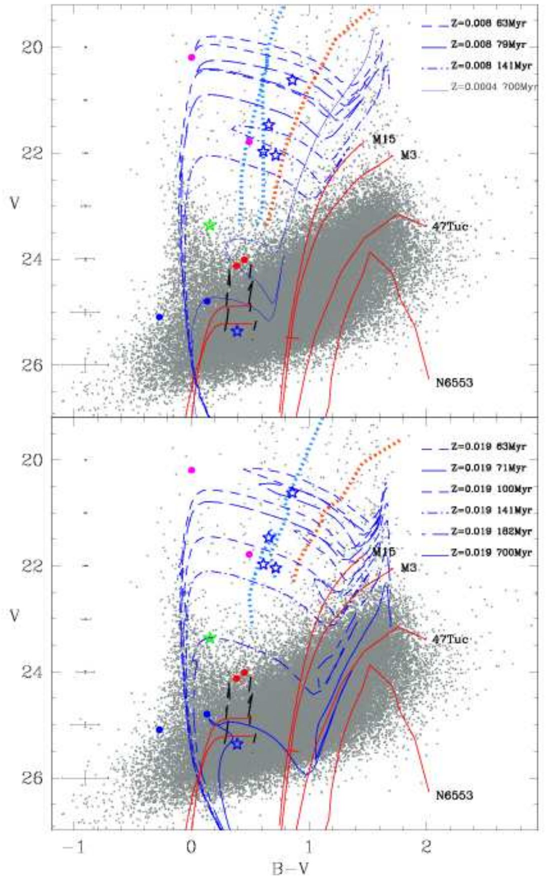

Figure 5.11: Zoom of the $V, B-V$ CMD of the portion of field S2 imaged on CCD1, showing the comparison with isochrones from Girardi et al. (2000, and following updates) for ages in the range from 63 to 700 million years and different choices of metal content (Z=0.008 and 0.0004 in the upper panel, and Z=0.019 in the lower panel) to fit the young and intermediate-age stellar components, and with the mean ridge lines of the Galactic globular clusters M15, M3, 47 Tuc and NGC6553 for the old (t> 10 Gyr) stellar component. Examples of the different types of variable stars detected in this portion of the field S2 are shown by large filled dots; they include RR Lyrae stars (at $V \sim$ 25-25.2 mag, blue dots), candidate ACs/spCCs (at $V \sim$ 24 mag, red dots), Classical Cepheids ($V \geq$ 22 mag, magenta dots). These variables were plotted according to their random phase magnitudes and colors. Large open stars mark 5 pulsating variables (blue stars) and 1 binary system (green star) for which we have a good sampling of the B light curves (see Fig. 5.3), their magnitudes and colors correspond to the average values along the full light cycle. The long-dashed black lines show the boundaries of the theoretical instability strips for RR Lyrae stars, and for Anomalous Cepheids with Z=0.0004 and 1.3 < M< 2.2 $M_\odot$ (Marconi et al. 2004). The dotted heavy lines represent the first overtone and fundamental blue edges (blue lines) and the fundamental red edge (red line) for Classical Cepheid models with Y=0.25 and 3.25 < $M/M_\odot$ < 11 and Z=0.008 in the upper panel, and Z=0.019 in the lower panel (Bono, Marconi, Stellingwerf 1999; Bono et al. 2002).

in this M31 field cannot be proven by the fitting with the GC ridgelines because of the confusion by stars with different ages and metal content, and the contamination by Galactic stars at red colors, nor can the horizontal branch (HB) of such an old population, if any, be disentangled, since buried into the overwelming young population, the mere presence of RR Lyrae variable stars, and their average magnitudes being consistent with them belonging to M31, definitely proves that such an old population exists in this regions of M31. Such an old population could, perhaps, be similar to the population of the Galactic GC M3, since the fitting with the GC ridgelines shows that the average magnitude of the RR Lyrae star appears to be more consistent with the average magnitude of the HB in M3 rather than the with the HB of M15, while the period would point to an Oosterhoff intermediate type, consistently with what found by Brown et al. (2004) in their study of the M31 field RR Lyrae stars based on ACS/HST data. The two panels of Fig. 5.11 also show that the isochrone fitting of the CMD does not allow to discriminate between the Z=0.008 and Z=0.019 metal abundances for the younger populations, but the position on the CMD of the variables of Cepheid type and the comparison with the edges of the theoretical IS for the different metal abundances, do indeed allow to discriminate between the two possibilities. In fact, Cepheids are intermediate-mass ($3 \leq M/M_{\odot} \leq 13$) stars that cross the IS during the blueward excursion of the helium burning phase predicted by theory in this mass range, referred to as blue loop. Fig. 5.11 shows that only for Z=0.008 do the blue loops extend blueward enough to produce the 4 Classical Cepheids in our sample, although the 9.4 days Cepheid could be produced by both isochrone sets. The comparison of the position of the 4 variables on the CMD and the boundaries of the IS also favors the lower metal abundance of Z=0.008 for our variables. Indeed, the four variables classified as Cepheids appear to lie close to the blue edge of the instability strip for $Z = 0.02$. In particular at this metallicity the two bluest Cepheids are located between the blue edge of the fundamental mode and the blue edge of the first overtone mode. This occurrence suggests that if Z=0.02 the two bluest Cepheids are first overtone pulsators, whereas the other two Cepheids are at the fundamental blue edge. Cepheids at the first overtone blue edge are expected to have low pulsation amplitudes. At the same time the brightest Cepheid is at a luminosity for which only the fundamental mode of pulsation is efficient, so that its closeness to the blue edge again implies a quite low pulsation amplitude (see e.g. Bono, Castellani, Marconi 2000). These predictions are at variance with the observed pulsation amplitudes that range between 0.84 to 1.29 mag in the B band, in better agreement with the values expected if $Z = 0.008$ and the Cepheids are in the middle of the instability strip. Finally, the presence of a metal poor (Z=0.0004), intermediate-age (of about 700 Myr age, according to Girardi et al. isochrones) population is required to explain the possible Anomalous Cepheids(ACs)/short period Classical Cepheids (spCCs) we have observed in this field, such a population would never be guessed based on the isochrone fitting alone. It is also worth of notice that the predicted gap in magnitude between the RR Lyrae level and the faintest Cepheid pulsators at a metallicity of 0.004 is of about 0.8 mag (Caputo et al. 2004) in excellent agreement with the difference in magnitude between the RR Lyrae and the two AC/spCC pulsators we see in Fig. 5.11. It is obviously very premature to draw any conclusions based on one RR Lyrae star and the very few other variables presented here, still we want to point out what will be achievable based on the analysis of the entire sample of M31 variable stars we have detected in this study (Contreras et al. 2010, in preparation).

5.3.1 Comparison with previous variability studies in M31

We have compared our results for the Cepheids with previous studies of these variable stars in M31. In particular, we have made the comparison with Vilardell et al (2007) and Joshi et al. (2009). The position of the M31 regions observed by these authors are shown by diamonds in Fig. 5.1. For the metal abundances Vilardell et al. (2007) assume the metallicity gradient as a function of the Galactocentric distance by Zaritsky et al. (1994) and an empirical metallicity correction of the Cepheid Period-Luminosity (PL) relation. According to their resulting corrections and to the reported Galactocentric distances we estimate that the Cepheids in their sample have [O/H] in the range -0.2 $\div$ 0.2. As we are exploring quite external regions of M31

Table 5.3: Individual distances for the four Classical Cepheids

P	μPL	μWes	$\mu_{\mathrm{ogle}_{\mathrm{HST}}}$	$\mu PL02$	$\mu Wes02$
9.4	24.42	24.24	24.52	24.15	24.42
3.22	24.55	24.40	24.64	24.53	24.60
5.1	24.54	24.73	24.63	24.41	24.92
2.92	24.37	24.50	24.46	24.38	24.70

(see Fig. 5.1, and Column 7 of Table 5.1) we expect that the metallicity of our Cepheid pulsators is close to [O/H]=-0.2 that implies $Z \sim 0.01$, in agreemnt with the value inferred from inspection of the CMD. Vilardell et al. (2007) also assume a distance modulus of 18.4 mag for the Large Magellanic Cloud (LMC) that combined with the adopted metallicity correction explains at least in part the discrepancy between their distance estimate and the results presented here (see below). As for the comparison with Joshi et al. (2009) we note that these authors have identified Cepheids with periods as short as 3.4 days with a frequency-period distribution that peaks at $\log P \sim 0.9$ and 1.1 days. Moreover most of their Cepheids are found with $\langle R \rangle \sim$ 20-21 mag. The sample we discuss here is much poorer, nevertheless our magnitudes and periods are consistent with their results. In particular for the Cepheid at 9.4 d we find $\langle V \rangle$=20.62 mag and in the same period range they find consistent R magnitudes, assuming a typical $V - R$ color and taking into account the uncertainties related to reddening corrections.

To derive a distance estimate for the four Classical Cepheids listed in Table 5.2 and confirm that they are M31 members, we adopted the theoretical Wesenheit relations for Z=0.008 and Z=0.02 (see Caputo, Marconi, & Musella 2000) and the PL relation by Udalski et al. (1999), assuming a distance modulus for the LMC of 18.5 mag. The resulting individual (from the Wesenheit relations) and mean (from the PL) distances are reported in Table 5.3. We attach to individual distance moduli from the Wesenheit relations an uncertainty of ± 0.1, while the average distance modulus obtained from the Udalski et al. (1999) PL is 24.56± 0.2 mag. The errors on the estimated distances take into account both the observational errors in B and V and the intrinsic dispersion of the adopted relations.

Chapter 6

Summary, Conclusions & Future works

In this thesis we have studied the variable stars in properly selected globular clusters (GCs) and fields of the Andromeda galaxy (M31), on the basis of time-series data specifically obtained for this project with the Hubble Space Telescope (HST) and the Large Binocular Telescope (LBT). The the final goal is to get hints on the M31 formation mechanisms from the properties of the galaxy variable stars . The main results obtained from the present study are summarized below.

6.1 M31 globular clusters

We have obtained HST time-series data to study the RR Lyrae stars in six M31 GCs (namely, G11, G33, G76, G105, G322, nad B514) that were selected in metallicity as to detect the existence of the Oosterhoff dichotomy in M31, if any. Preliminary results from this study (see section 4.5.2) show that 3 of the clusters in our M31 sample have Oosterhoff type I (OoI) characteristics, while the remaining 3 have Oosterhoff-intermediate (Oo-Int) properties, although for one of latter the Oo-Int type might result from the superposition of two distinct populations respectively with OoI and OoII characteristics. In any case, none of these six clusters has pure Oo type II properties (long-periods and low metal abundances), even though clusters as metal-poor as B514 (and perhaps G33) would, in the MW, be expected to belong to the OoII group. In other words, our M31 GC sample do not seem to conform to the Oosterhoff dichotomy observed in the MW, and this may indicate that a fundamental difference exists between the halo GC populations of the MW and M31. **If these results hold, they would imply that the events of halo formation that resulted in the Oosterhoff gap are peculiar to the Milky Way and are not general to the formation of the halos of large spiral galaxies; i.e., the halo of M31 formed differently.** By contrast, the processes responsible for the RR Lyrae properties of at least the larger dwarf spheroidal galaxies (dSphs) are similar for the MW and M31 (Pritzl et al. 2004). In neither the MW nor M31 do we find the RR Lyrae properties of the dSphs mimicking those of the globular cluster systems, thus ruling out these dwarf galaxies as possible building blocks of their host galaxy. A detailed and careful re-analysis of the variable stars we have detected in these six M31 GCs is in progress, based on additional data available on the HST archive, and will allow us to put on a firmer basis our preliminary results, that will soon be published in a series of papers (Contreras et al. 2010a,b,c).

However, given the much larger population of old GCs in M31, ~ 500, compared to the sample of about 150 in the MW, are our results statistically significant? The possibility that the RR Lyrae populations of GCs in M31 are different from those in the MW peeps out, but a larger sample is needed to either confirm or disprove it. Results for additional clusters of low metal abundance which, in the MW, would be expected to have Oo II properties, are crucial in this regard. With this in mind, we have submitted an HST proposal for Cycle 18 requesting time to determine the detailed pulsation properties of RRL stars in an additional 5 carefully selected M31 GCs, in order to extend the parameter space covered by the targets observed in the present study, with particular emphasis on the low metallicity part of the distribution. These new clusters have a metallicity that, in the MW, would definitely place them in the Oo II group. Our target GCs include (see Fig. 6.1): GC10, which lies possibly on the far extension of the M31 giant

Name	⟨V(HB)⟩ (mag)	[Fe/H]
GC2	25.1	−1.9
GC10	25.2	−2.1
EC1	25.2	−1.8
EC3	25.0	−2.1
G64	24.9	−1.9

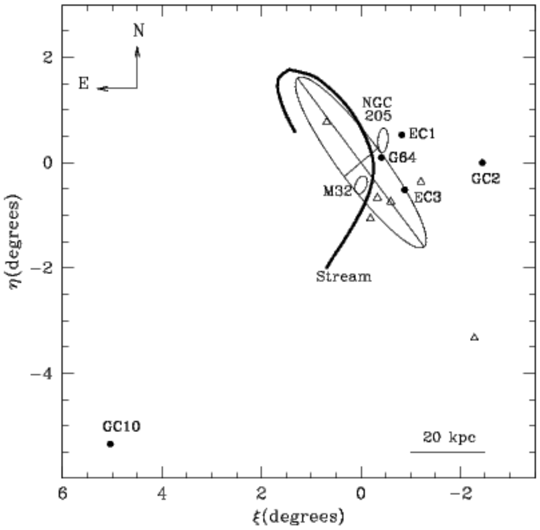

Figure 6.1: (Left) Main properties of the target GCs. $\langle V(HB)\rangle$ values and metallicities for GC2 and GC10 are from Mackey et. al (2007); for EC1 and EC3 from Mackey et al. (2006); and for G64 $\langle V(HB)\rangle$ and metallicity values are from Rich et al. (2005) and Galletv et al. (2009), respectively. (Right) Location of the target globular clusters on a schematic view of M31. Filled circles mark the 5 selected clusters in the new proposal, open triangles show the 6 GCs observed in cycle 15.

stream (Mackey et al. 2007, Ibata et al. 2007); EC1 which is projected along the M31 minor axis beyond NGC205; EC3 and G64 which lie on the North-West edge of the visible disk; and GC2 that is located in the galaxy's unperturbed halo. In particular, the very low metallicity (see table above) makes clusters GC10 and EC3 (Mackey et al. 2006, 2007) the counterparts of MW clusters such as M92 and M15, perhaps te best known Oosterhoff type II Galactic globular clusters. Some of the chosen clusters could be in the Oo-intermediate range, and therefore provide a further check of the RRL pulsation properties in M31. The target clusters also allow us to probe different areas in M31, from the galaxy's unperturbed halo to regions close to the giant stream and galaxy disk. The clusters selected for the new proposal, along with the six clusters we have already studied, will provide a better sampling and characterization of the entire GC ensemble of M31, and will allow us to establish on a firmer basis whether the M31 cluster RRL properties are compatible with the Oosterhoff dichotomy and whether they show the same correlation with HB morphology as seen in the MW.

6.2 M31 fields

B, V photometry down to $V \sim 26$ mag has been obtained for four $23' \times 23'$ fields of the Andromeda galaxy which were observed with the blue channel camera of the Large Binocular Telescope (LBT/LBC-blue) during the Science Demonstration Time. Each field covers an area of about 5.1×5.1 kpc^2, at the distance of M31 ($\mu_{\rm M31} \sim 24.4$ mag), sampling respectively regions close to the M31 giant stream, and portions of the galaxy unperturbed halo. In this thesis work we have described results from the study of the field sampling a North-East region close to the M31 giant stream, and of the field sampling an Eastern portion of the galaxy halo in the direction of the M31 minor axis. The stream field revealed substructures in the color magnitude diagrams of the region which likely bridges the disk of Andromeda to a region of the galaxy crossed by the giant stream. The B photometry, acquired in time-series mode, allowed the identification of variable stars which populate the instability strip from the Classical Cepheids down to the RR Lyrae stars, thus tracing the different stellar generations in this region of M31 down to the horizontal branch of the oldest ($t \sim 10$ Gyr) component.

Our study is the first large-area and deep variability survey of M31 fields, reaching with a ground-based telescope the galaxy RR Lyrae stars at $B \sim$ 25.5-26 mag. We will complete the study of the variable stars detected in these M31 regions and will publish the related catalogues. The CMDs will be used to derive informations on the SFH of the observed fields by applying synthetic CMD techniques. Combined with the ages of the variable stars, this will allow us to obtain the overall scenario of the evolution of these portions of the M31 halo and stream and to put stringent constraints on the characteristics of their formation. One of the fields Observed with the LBT contains Andromeda XXI (And XXI), a new M31 dSph satellite. In

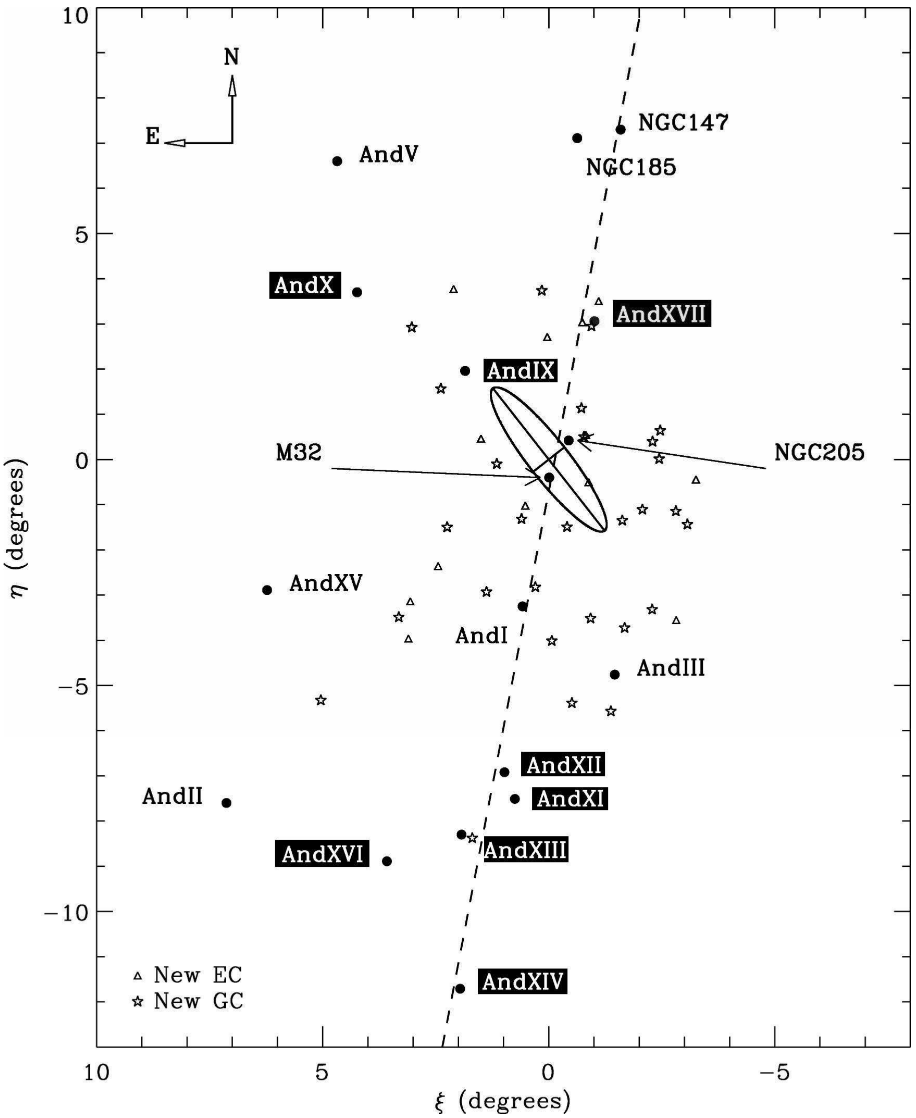

Figure 6.2: Location of recently discovered M31 dSph satellites on a schematic view of the Andromeda galaxy (taken from Irwin et al. 2005). We have outlined the galaxies for which we already have, or have requested data, to study variable stars. And XXI, for which we already have LBT time series data, is located outside this map (see Fig. 5.1.)

the $M_V - \log r_h$ plane (see Fig. 1.7), And XXI locates at the bright end of the distribution of "ultra-faint" dSphs recently discovered around M31 and the MW. All these new galaxies are fainter, and generally more extended than the "classical" dSphs surrounding M31 and the MW. It will be particularly important to study the properties of the RR Lyrae population in And XXI, to check whether And XXI conforms to the classical M31 satellites (e.g. And I, II, III, V, VI and VII) where examples of all three Oosterhoff types (Oo I, Oo II, and Oo-Int) are present, or instead resembles the M31 GCs, which, according to our study, seem to lack the Oosterhoff type II. We also have already available HST time series data to study the variable stars of other 3 new M31 satellites (namely, And Xi, XII and XIII) and to further extend our survey of the variable stars in the new M31 companions, have requested time to observe And IX, X, XIV, XVI and XVII with the GranTeCan and Subaru telescopes. Fig. 6.2 show the location of our M31 dSph targets on a schematic map of M31.

Chapter 7

Appendix A

ATLAS OF LIGHT CURVES: B514

Atlas of the V-band light curves of the B514 variable stars listed in Tables 4.2 and 4.3 For each variable identification and period are provided on top of the plot.

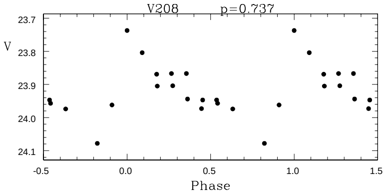
V208 p=0.737
V
23.7
23.8
23.9
24.0
24.1
-0.5
0.0
0.5
1.0
1.5
Phase

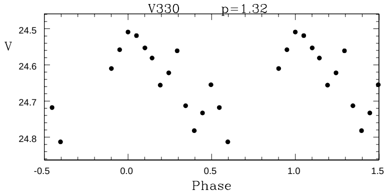
V330 p=1.32
V
24.5
24.6
24.7
24.8
-0.5
0.0
0.5
1.0
1.5
Phase

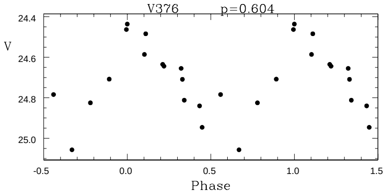
V376 p=0.604
V
24.4
24.6
24.8
25.0
-0.5
0.0
0.5
1.0
1.5
Phase

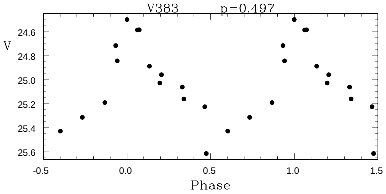
V383 p=0.497
V
24.6
24.8
25.0
25.2
25.4
25.6
-0.5
0.0
0.5
1.0
1.5
Phase

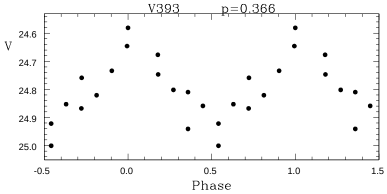
V393 p=0.366
V
24.6
24.7
24.8
24.9
25.0
-0.5
0.0
0.5
1.0
1.5
Phase

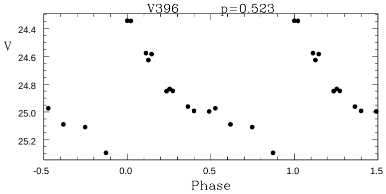
V396 p=0.523
V
24.4
24.6
24.8
25.0
25.2
-0.5
0.0
0.5
1.0
1.5
Phase

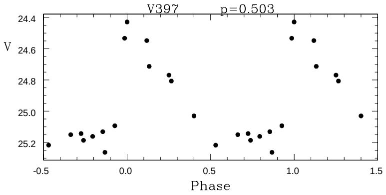
V397 p=0.503
V
24.4
24.6
24.8
25.0
25.2
-0.5
0.0
0.5
1.0
1.5
Phase

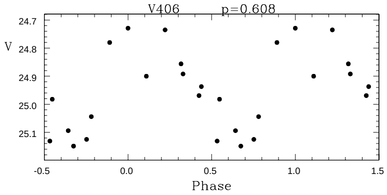
V406 p=0.608
V
24.7
24.8
24.9
25.0
25.1
-0.5
0.0
0.5
1.0
1.5
Phase

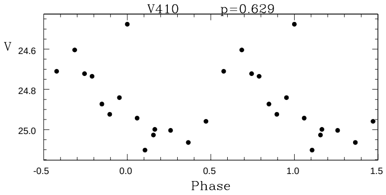
V410 p=0.629
V
24.6
24.8
25.0
-0.5
0.0
0.5
1.0
1.5
Phase

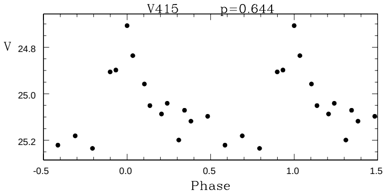
V415 p=0.644
V
24.8
25.0
25.2
-0.5
0.0
0.5
1.0
1.5
Phase

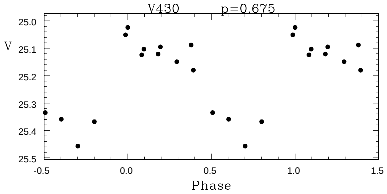
V430 p=0.675
V
25.0
25.1
25.2
25.3
25.4
25.5
-0.5
0.0
0.5
1.0
1.5
Phase

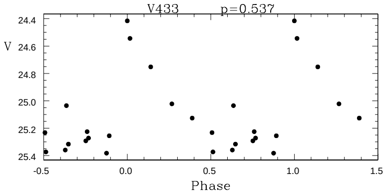
V433 p=0.537
V
24.4
24.6
24.8
25.0
25.2
25.4
-0.5
0.0
0.5
1.0
1.5
Phase

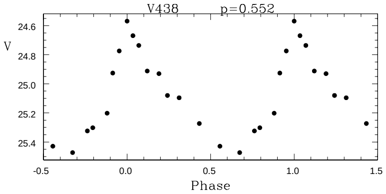
V438 p=0.552
V
24.6
24.8
25.0
25.2
25.4
-0.5
0.0
0.5
1.0
1.5
Phase

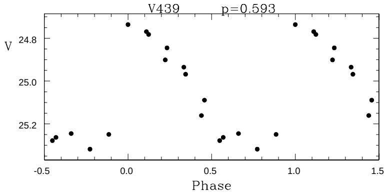
V439 p=0.593
V
24.8
25.0
25.2
-0.5
0.0
0.5
1.0
1.5
Phase

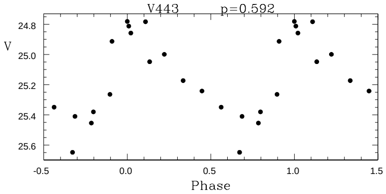
V443 p=0.592
V
24.8
25.0
25.2
25.4
25.6
-0.5
0.0
0.5
1.0
1.5
Phase

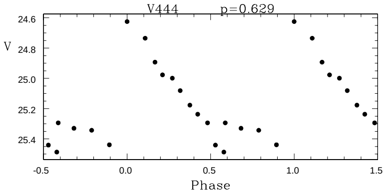
V444 p=0.629
V
24.6
24.8
25.0
25.2
25.4
-0.5
0.0
0.5
1.0
1.5
Phase

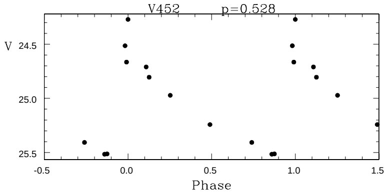
V452 p=0.528
V
24.5
25.0
25.5
-0.5
0.0
0.5
1.0
1.5
Phase

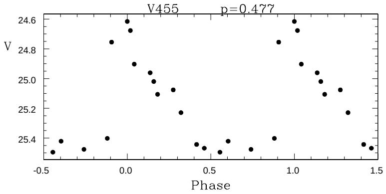
V455 p=0.477
V
24.6
24.8
25.0
25.2
25.4
-0.5
0.0
0.5
1.0
1.5
Phase

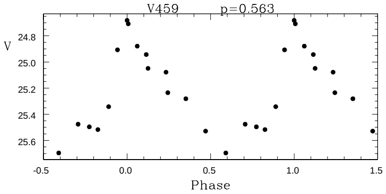
V459 p=0.563
V
24.8
25.0
25.2
25.4
25.6
-0.5
0.0
0.5
1.0
1.5
Phase

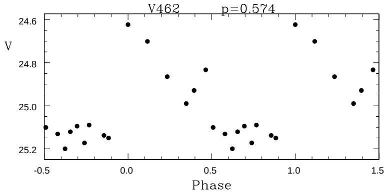
V462 p=0.574
V
24.6
24.8
25.0
25.2
-0.5
0.0
0.5
1.0
1.5
Phase

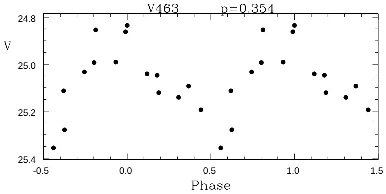
V463 p=0.354
V
24.8
25.0
25.2
25.4
-0.5
0.0
0.5
1.0
1.5
Phase

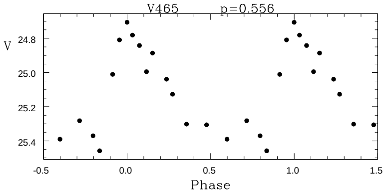
V465 p=0.556
V
24.8
25.0
25.2
25.4
-0.5
0.0
0.5
1.0
1.5
Phase

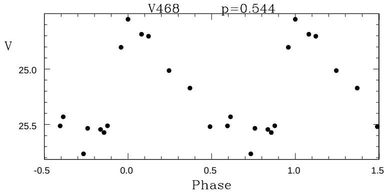
V468 p=0.544
V
25.0
25.5
-0.5
0.0
0.5
1.0
1.5
Phase

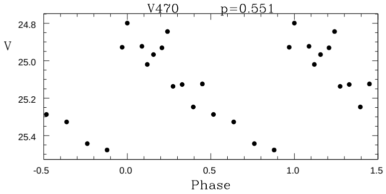
V470 p=0.551
V
24.8
25.0
25.2
25.4
-0.5
0.0
0.5
1.0
1.5
Phase

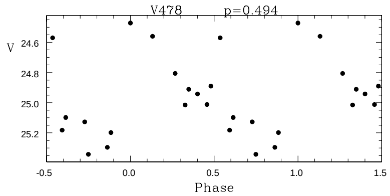
V478 p=0.494
V
24.6
24.8
25.0
25.2
-0.5
0.0
0.5
1.0
1.5
Phase

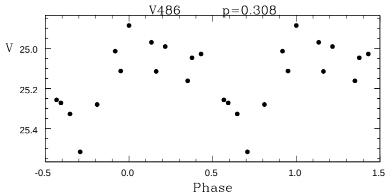
V486 p=0.308
V
25.0
25.2
25.4
-0.5
0.0
0.5
1.0
1.5
Phase

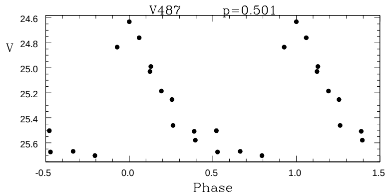
V487 p=0.501
V
24.6
24.8
25.0
25.2
25.4
25.6
-0.5
0.0
0.5
1.0
1.5
Phase

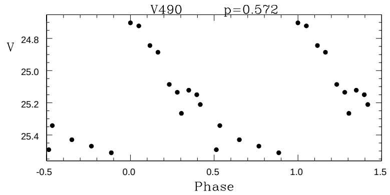
V490 p=0.572
V
24.8
25.0
25.2
25.4
-0.5
0.0
0.5
1.0
1.5
Phase

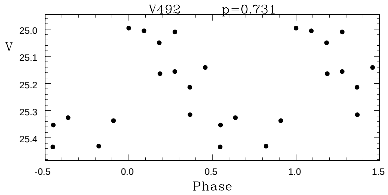
V492 p=0.731
V
25.0
25.1
25.2
25.3
25.4
-0.5
0.0
0.5
1.0
1.5
Phase

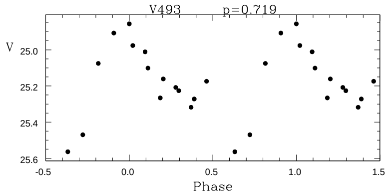
V493 p=0.719
V
25.0
25.2
25.4
25.6
-0.5
0.0
0.5
1.0
1.5
Phase

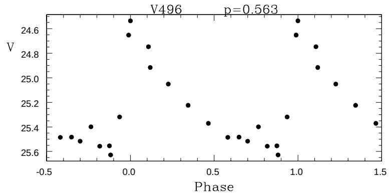
V496 p=0.563
V
24.6
24.8
25.0
25.2
25.4
25.6
-0.5
0.0
0.5
1.0
1.5
Phase

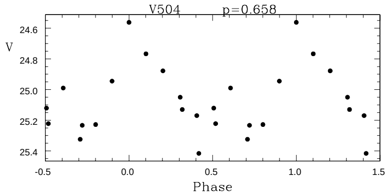
V504 p=0.658
V
24.6
24.8
25.0
25.2
25.4
-0.5
0.0
0.5
1.0
1.5
Phase

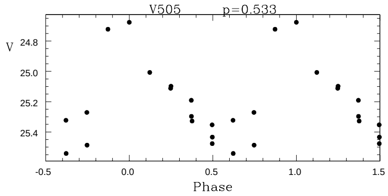
V505 p=0.533
V
24.8
25.0
25.2
25.4
-0.5
0.0
0.5
1.0
1.5
Phase

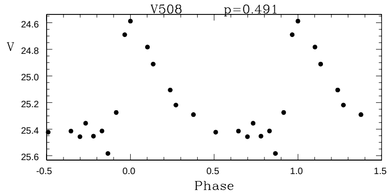
V508 p=0.491
V
24.6
24.8
25.0
25.2
25.4
25.6
-0.5
0.0
0.5
1.0
1.5
Phase

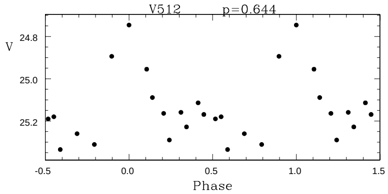
V512 p=0.644
V
24.8
25.0
25.2
-0.5
0.0
0.5
1.0
1.5
Phase

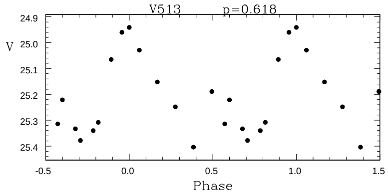
V513 p=0.618
V
24.9
25.0
25.1
25.2
25.3
25.4
-0.5
0.0
0.5
1.0
1.5
Phase

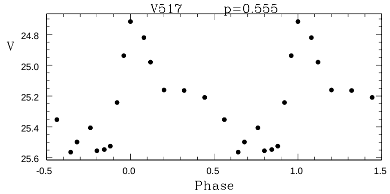
V517 p=0.555
V
24.8
25.0
25.2
25.4
25.6
-0.5
0.0
0.5
1.0
1.5
Phase

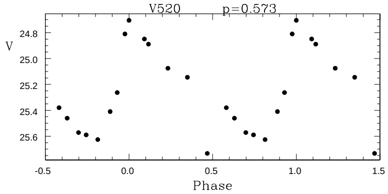
V520 p=0.573
V
24.8
25.0
25.2
25.4
25.6
-0.5
0.0
0.5
1.0
1.5
Phase

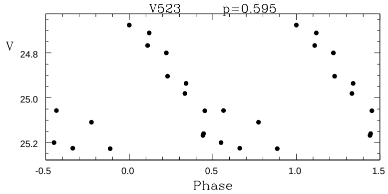
V523 p=0.595
V
24.8
25.0
25.2
-0.5
0.0
0.5
1.0
1.5
Phase

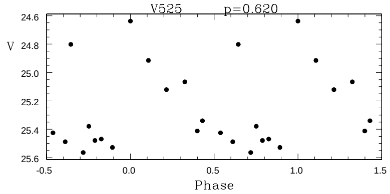
V525 p=0.620
V
24.6
24.8
25.0
25.2
25.4
25.6
-0.5
0.0
0.5
1.0
1.5
Phase

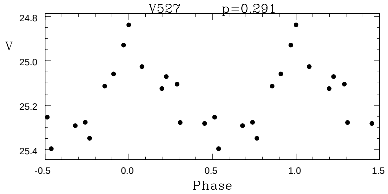
V527 p=0.291
V
24.8
25.0
25.2
25.4
-0.5
0.0
0.5
1.0
1.5
Phase

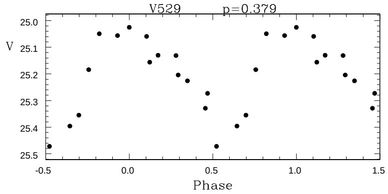
V529 p=0.379
V
25.0
25.1
25.2
25.3
25.4
25.5
-0.5
0.0
0.5
1.0
1.5
Phase

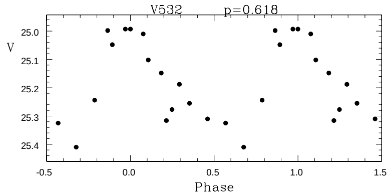
V532 p=0.618
V
25.0
25.1
25.2
25.3
25.4
-0.5
0.0
0.5
1.0
1.5
Phase

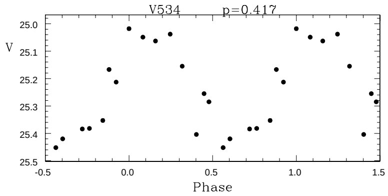
V534 p=0.417
V
25.0
25.1
25.2
25.3
25.4
25.5
-0.5
0.0
0.5
1.0
1.5
Phase

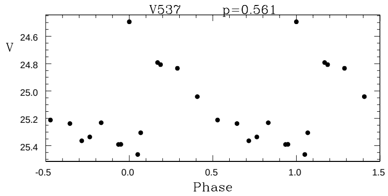
V537 p=0.561
V
24.6
24.8
25.0
25.2
25.4
-0.5
0.0
0.5
1.0
1.5
Phase

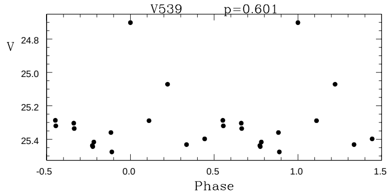
V539 p=0.601
V
24.8
25.0
25.2
25.4
-0.5
0.0
0.5
1.0
1.5
Phase

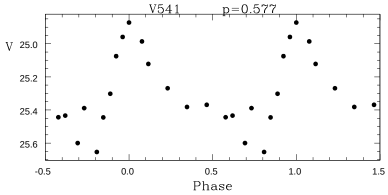
V541 p=0.577
V
25.0
25.2
25.4
25.6
-0.5
0.0
0.5
1.0
1.5
Phase

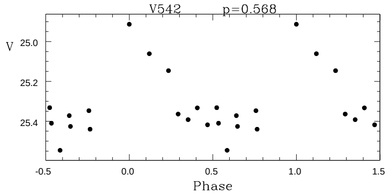
V542 p=0.568
V
25.0
25.2
25.4
-0.5
0.0
0.5
1.0
1.5
Phase

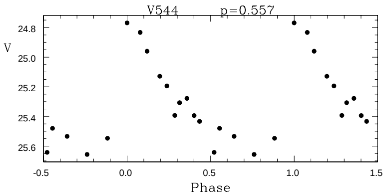
V544 p=0.557
V
24.8
25.0
25.2
25.4
25.6
-0.5
0.0
0.5
1.0
1.5
Phase

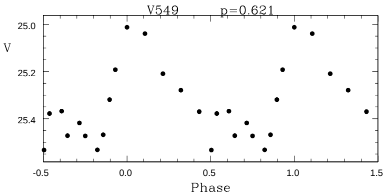
V549 p=0.621
V
25.0
25.2
25.4
-0.5
0.0
0.5
1.0
1.5
Phase

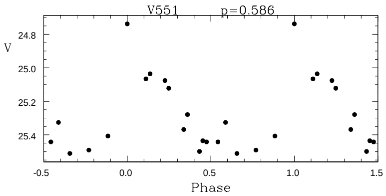
V551 p=0.586
V
24.8
25.0
25.2
25.4
-0.5
0.0
0.5
1.0
1.5
Phase

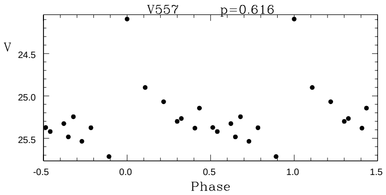
V557 p=0.616
V
24.5
25.0
25.5
-0.5
0.0
0.5
1.0
1.5
Phase

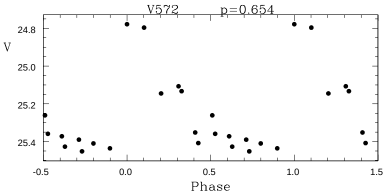
V572 p=0.654
V
24.8
25.0
25.2
25.4
-0.5
0.0
0.5
1.0
1.5
Phase

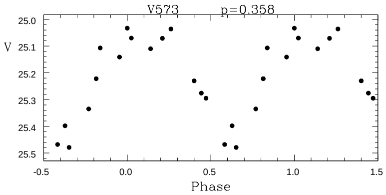
V573 p=0.358
V
25.0
25.1
25.2
25.3
25.4
25.5
-0.5
0.0
0.5
1.0
1.5
Phase

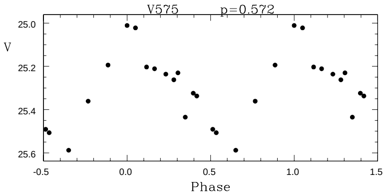
V575 p=0.572
V
25.0
25.2
25.4
25.6
-0.5
0.0
0.5
1.0
1.5
Phase

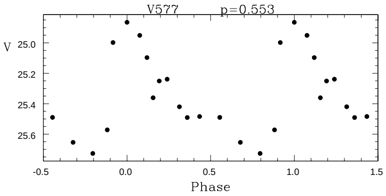
V577 p=0.553
V
25.0
25.2
25.4
25.6
-0.5
0.0
0.5
1.0
1.5
Phase

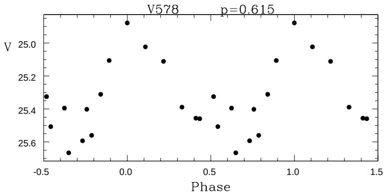
V578 p=0.615
V
25.0
25.2
25.4
25.6
-0.5
0.0
0.5
1.0
1.5
Phase

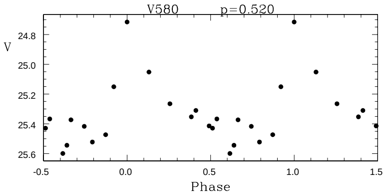
V580 p=0.520
V
24.8
25.0
25.2
25.4
25.6
-0.5
0.0
0.5
1.0
1.5
Phase

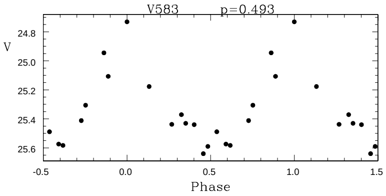
V583 p=0.493
V
24.8
25.0
25.2
25.4
25.6
-0.5
0.0
0.5
1.0
1.5
Phase

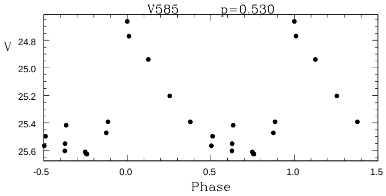
V585 p=0.530
V
24.8
25.0
25.2
25.4
25.6
-0.5
0.0
0.5
1.0
1.5
Phase

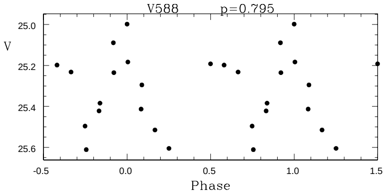
V588 p=0.795
V
25.0
25.2
25.4
25.6
-0.5
0.0
0.5
1.0
1.5
Phase

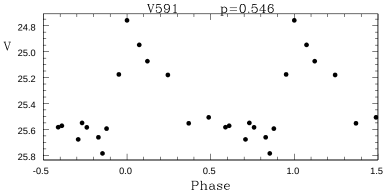
V591 p=0.546
V
24.8
25.0
25.2
25.4
25.6
25.8
-0.5
0.0
0.5
1.0
1.5
Phase

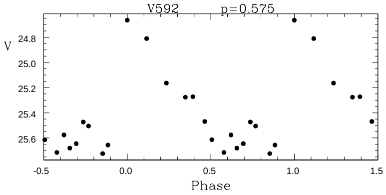
V592 p=0.575
V
24.8
25.0
25.2
25.4
25.6
-0.5
0.0
0.5
1.0
1.5
Phase

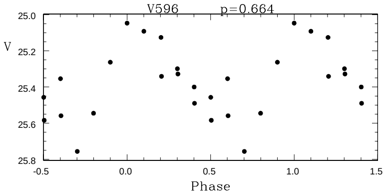
V596 p=0.664
V
25.0
25.2
25.4
25.6
25.8
-0.5
0.0
0.5
1.0
1.5
Phase

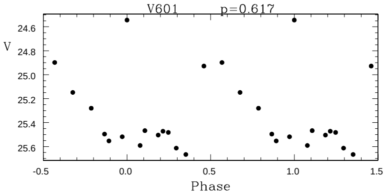
V601 p=0.617
V
24.6
24.8
25.0
25.2
25.4
25.6
-0.5
0.0
0.5
1.0
1.5
Phase

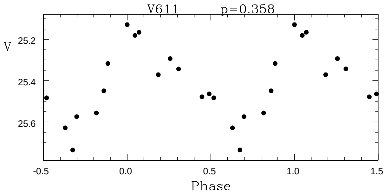
V611 p=0.358
V
25.2
25.4
25.6
-0.5
0.0
0.5
1.0
1.5
Phase

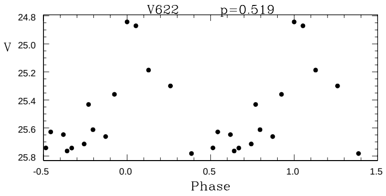
V622 p=0.519
V
24.8
25.0
25.2
25.4
25.6
25.8
-0.5
0.0
0.5
1.0
1.5
Phase

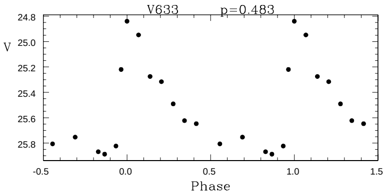
V633 p=0.483
V
24.8
25.0
25.2
25.4
25.6
25.8
-0.5
0.0
0.5
1.0
1.5
Phase

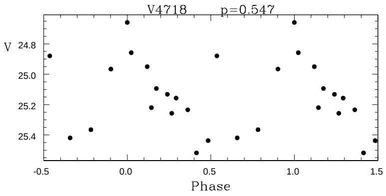
V4718 p=0.547
V
24.8
25.0
25.2
25.4
-0.5
0.0
0.5
1.0
1.5
Phase

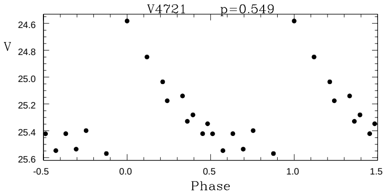
V4721 p=0.549
V
24.6
24.8
25.0
25.2
25.4
25.6
-0.5
0.0
0.5
1.0
1.5
Phase

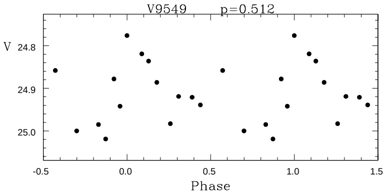
V9549 p=0.512
V
24.8
24.9
25.0
-0.5
0.0
0.5
1.0
1.5
Phase

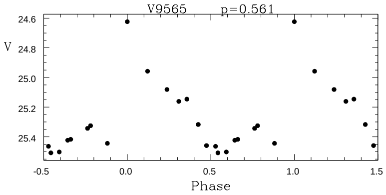
V9565 p=0.561
V
24.6
24.8
25.0
25.2
25.4
-0.5
0.0
0.5
1.0
1.5
Phase

Chapter 8

Appendix B

ATLAS OF LIGHT CURVES: G11

Atlas of the V,I light curves for candidate variable stars identified in G11. For each variable the upper panel shows the I-band light curve, and the lower panel the V-band light curve. Identification, V and I amplitudes, period, average V magnitude and average V−I color, are provided on top labels of the plots.

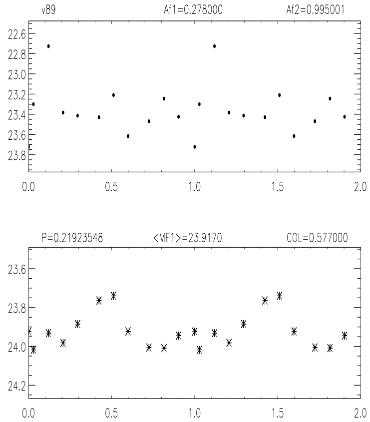
v89
Af1=0.278000
Af2=0.995001
22.6 22.8 23.0 23.2 23.4 23.6 23.8
P=0.21923548
<MF1>=23.9170
COL=0.577000
23.6 23.8 24.0 24.2
0.0 0.5 1.0 1.5 2.0

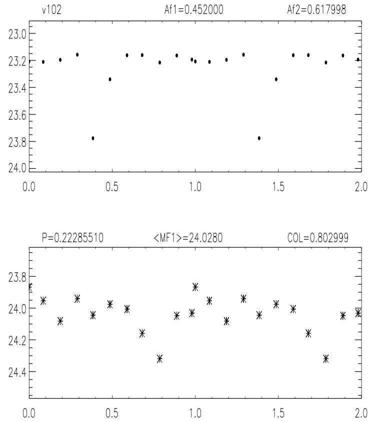
v102
Af1=0.452000
Af2=0.617998
23.0 23.2 23.4 23.6 23.8 24.0
P=0.22285510
<MF1>=24.0280
COL=0.802999
23.8 24.0 24.2 24.4
0.0 0.5 1.0 1.5 2.0

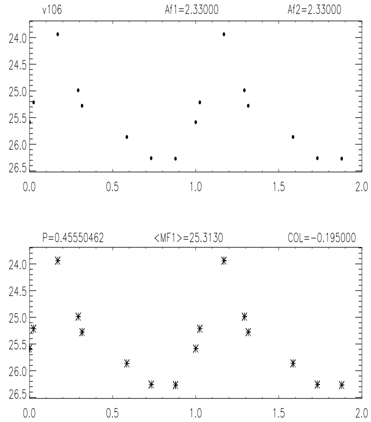
v106
Af1=2.33000
Af2=2.33000
24.0 24.5 25.0 25.5 26.0 26.5
P=0.45550462
<MF1>=25.3130
COL=-0.195000
24.0 24.5 25.0 25.5 26.0 26.5
0.0 0.5 1.0 1.5 2.0

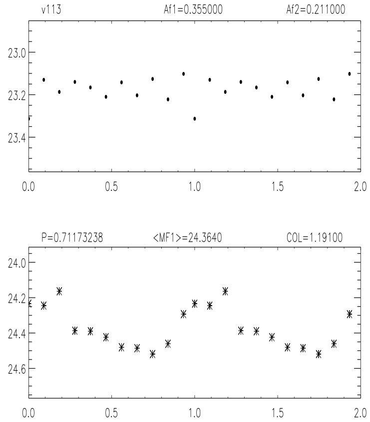
v113
Af1=0.355000
Af2=0.211000
23.0 23.2 23.4
P=0.71173238
<MF1>=24.3640
COL=1.19100
24.0 24.2 24.4 24.6
0.0 0.5 1.0 1.5 2.0

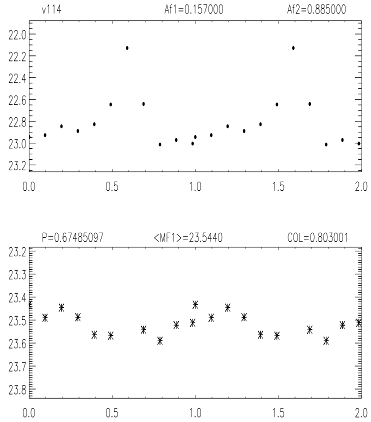
v114
Af1=0.157000
Af2=0.885000
22.0 22.2 22.4 22.6 22.8 23.0 23.2
P=0.67485097
<MF1>=23.5440
COL=0.803001
23.2 23.3 23.4 23.5 23.6 23.7 23.8
0.0 0.5 1.0 1.5 2.0

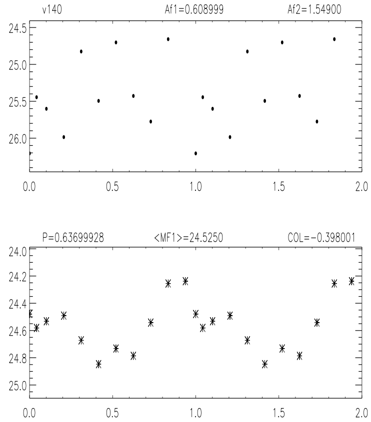
v140
Af1=0.608999
Af2=1.54900
24.5 25.0 25.5 26.0
P=0.63699928
<MF1>=24.5250
COL=-0.398001
24.0 24.2 24.4 24.6 24.8 25.0
0.0 0.5 1.0 1.5 2.0

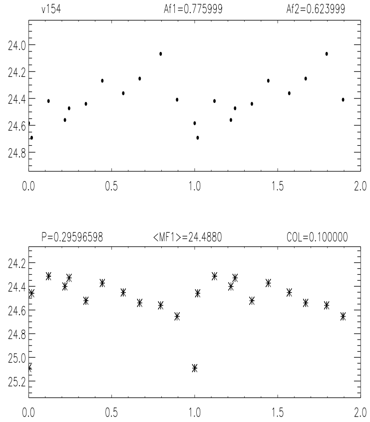
v154
Af1=0.775999
Af2=0.623999
24.0 24.2 24.4 24.6 24.8
P=0.29596598
<MF1>=24.4880
COL=0.100000
24.2 24.4 24.6 24.8 25.0 25.2
0.0 0.5 1.0 1.5 2.0

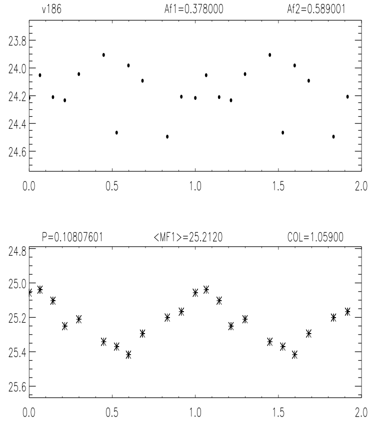
v186
Af1=0.378000
Af2=0.589001
23.8 24.0 24.2 24.4 24.6
P=0.10807601
<MF1>=25.2120
COL=1.05900
24.8 25.0 25.2 25.4 25.6
0.0 0.5 1.0 1.5 2.0

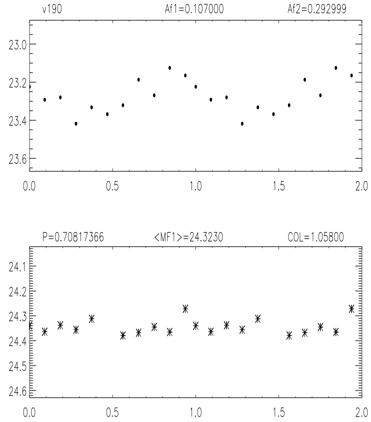
v190
Af1=0.107000
Af2=0.292999
23.0 23.2 23.4 23.6
P=0.70817366
<MF1>=24.3230
COL=1.05800
24.1 24.2 24.3 24.4 24.5 24.6
0.0 0.5 1.0 1.5 2.0

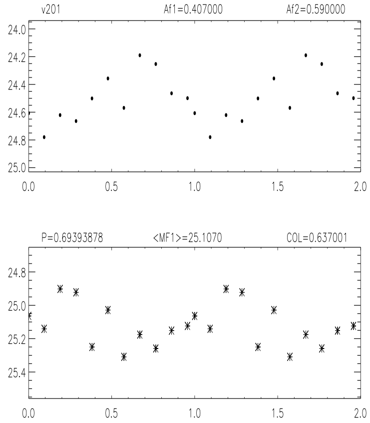
v201
Af1=0.407000
Af2=0.590000
24.0 24.2 24.4 24.6 24.8 25.0
P=0.69393878
<MF1>=25.1070
COL=0.637001
24.8 25.0 25.2 25.4
0.0 0.5 1.0 1.5 2.0

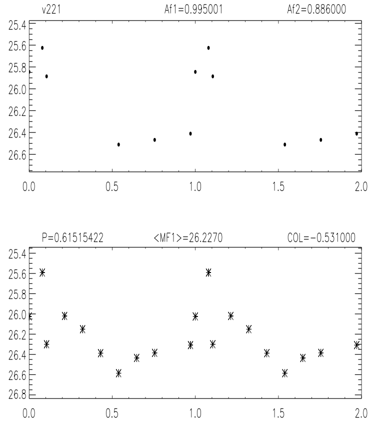
v221
Af1=0.995001
Af2=0.886000
25.4 25.6 25.8 26.0 26.2 26.4 26.6
P=0.61515422
<MF1>=26.2270
COL=-0.531000
25.4 25.6 25.8 26.0 26.2 26.4 26.6 26.8
0.0 0.5 1.0 1.5 2.0

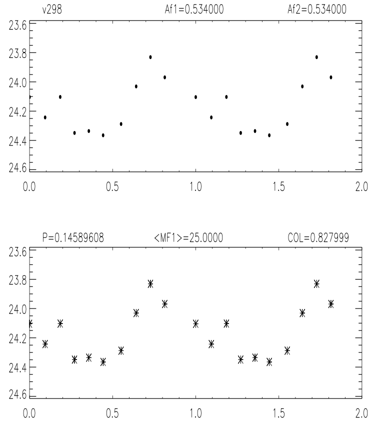
v298
Af1=0.534000
Af2=0.534000
23.6 23.8 24.0 24.2 24.4 24.6
P=0.14589608
<MF1>=25.0000
COL=0.827999
23.6 23.8 24.0 24.2 24.4 24.6
0.0 0.5 1.0 1.5 2.0

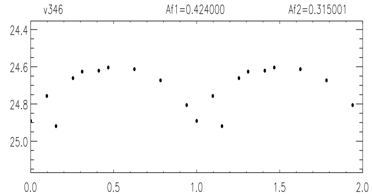
v346
Af1=0.424000
Af2=0.315001
24.4
24.6
24.8
25.0
0.0
0.5
1.0
1.5
2.0

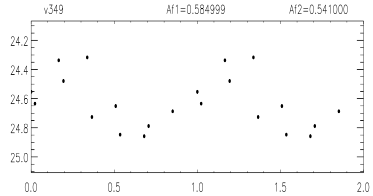
v349
Af1=0.584999
Af2=0.541000
24.2
24.4
24.6
24.8
25.0
0.0
0.5
1.0
1.5
2.0

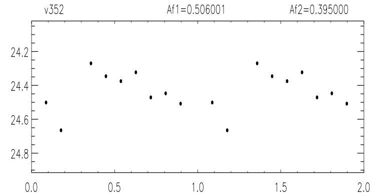
v352
Af1=0.506001
Af2=0.395000
24.2
24.4
24.6
24.8
0.0
0.5
1.0
1.5
2.0

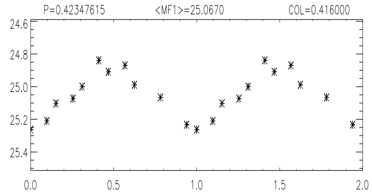
P=0.42347615
<MF1>=25.0670
COL=0.416000
24.6
24.8
25.0
25.2
25.4
0.0
0.5
1.0
1.5
2.0

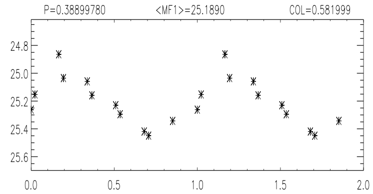
P=0.38899780
<MF1>=25.1890
COL=0.581999
24.8
25.0
25.2
25.4
25.6
0.0
0.5
1.0
1.5
2.0

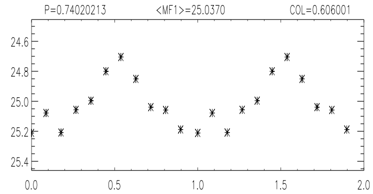
P=0.74020213
<MF1>=25.0370
COL=0.606001
24.6
24.8
25.0
25.2
25.4
0.0
0.5
1.0
1.5
2.0

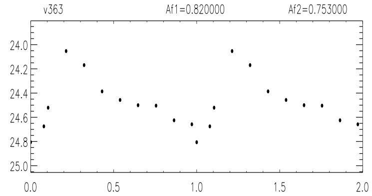
v363
Af1=0.820000
Af2=0.753000
24.0
24.2
24.4
24.6
24.8
25.0
0.0
0.5
1.0
1.5
2.0

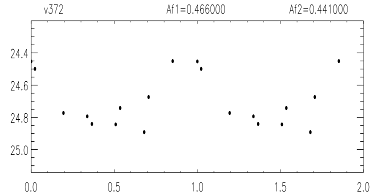
v372
Af1=0.466000
Af2=0.441000
24.4
24.6
24.8
25.0
0.0
0.5
1.0
1.5
2.0

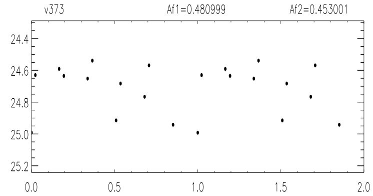
v373
Af1=0.480999
Af2=0.453001
24.4
24.6
24.8
25.0
25.2
0.0
0.5
1.0
1.5
2.0

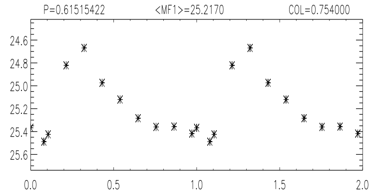
P=0.61515422
<MF1>=25.2170
COL=0.754000
24.6
24.8
25.0
25.2
25.4
25.6
0.0
0.5
1.0
1.5
2.0

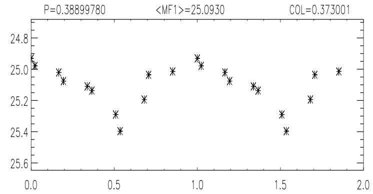
P=0.38899780
<MF1>=25.0930
COL=0.373001
24.8
25.0
25.2
25.4
25.6
0.0
0.5
1.0
1.5
2.0

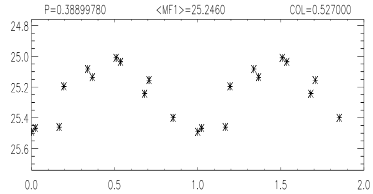
P=0.38899780
<MF1>=25.2460
COL=0.527000
24.8
25.0
25.2
25.4
25.6
0.0
0.5
1.0
1.5
2.0

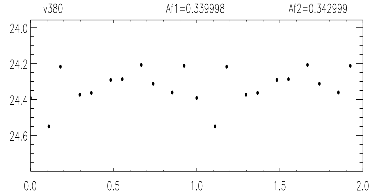
v380
Af1=0.339998
Af2=0.342999
24.0
24.2
24.4
24.6
0.0
0.5
1.0
1.5
2.0

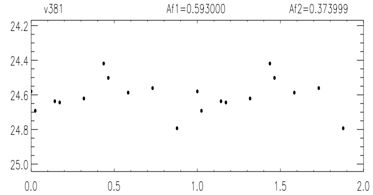
v381
Af1=0.593000
Af2=0.373999
24.2
24.4
24.6
24.8
25.0
0.0
0.5
1.0
1.5
2.0

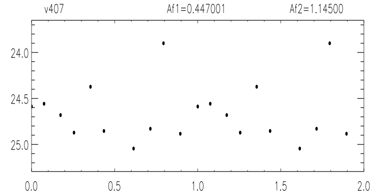
v407
Af1=0.447001
Af2=1.14500
24.0
24.5
25.0
0.0
0.5
1.0
1.5
2.0

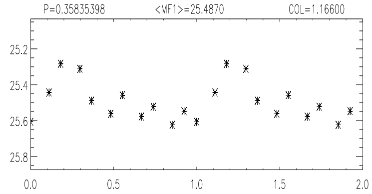
P=0.35835398
<MF1>=25.4870
COL=1.16600
25.2
25.4
25.6
25.8
0.0
0.5
1.0
1.5
2.0

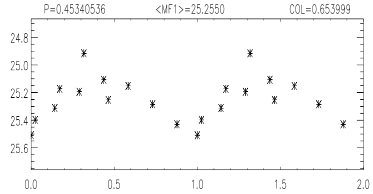
P=0.45340536
<MF1>=25.2550
COL=0.653999
24.8
25.0
25.2
25.4
25.6
0.0
0.5
1.0
1.5
2.0

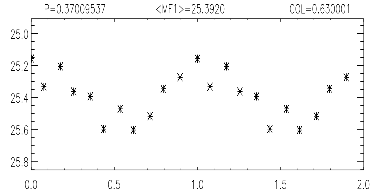
P=0.37009537
<MF1>=25.3920
COL=0.630001
25.0
25.2
25.4
25.6
25.8
0.0
0.5
1.0
1.5
2.0

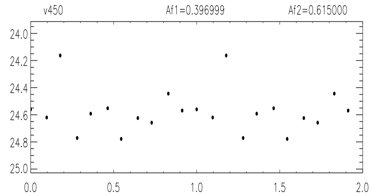
v450
Af1=0.396999
Af2=0.615000
24.0
24.2
24.4
24.6
24.8
25.0
0.0
0.5
1.0
1.5
2.0

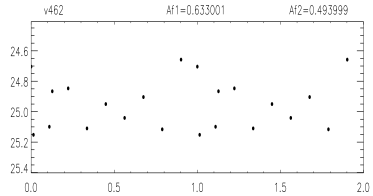
v462
Af1=0.633001
Af2=0.493999
24.6
24.8
25.0
25.2
25.4
0.0
0.5
1.0
1.5
2.0

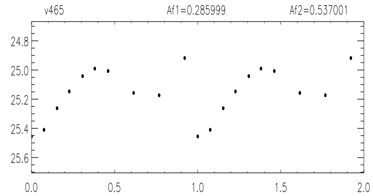
v465
Af1=0.285999
Af2=0.537001
24.8
25.0
25.2
25.4
25.6
0.0
0.5
1.0
1.5
2.0

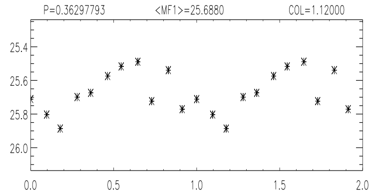
P=0.36297793
<MF1>=25.6880
COL=1.12000
25.4
25.6
25.8
26.0
0.0
0.5
1.0
1.5
2.0

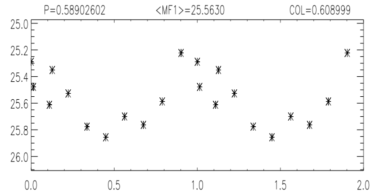
P=0.58902602
<MF1>=25.5630
COL=0.608999
25.0
25.2
25.4
25.6
25.8
26.0
0.0
0.5
1.0
1.5
2.0

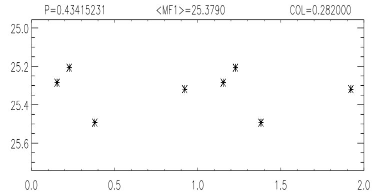
P=0.43415231
<MF1>=25.3790
COL=0.282000
25.0
25.2
25.4
25.6
0.0
0.5
1.0
1.5
2.0

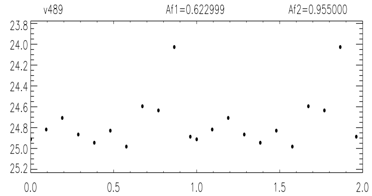
v489
Af1=0.622999
Af2=0.955000
23.8
24.0
24.2
24.4
24.6
24.8
25.0
25.2
0.0
0.5
1.0
1.5
2.0

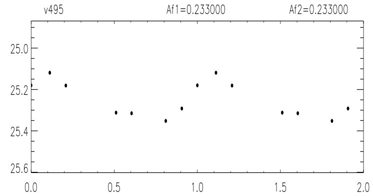
v495
Af1=0.233000
Af2=0.233000
25.0
25.2
25.4
25.6
0.0
0.5
1.0
1.5
2.0

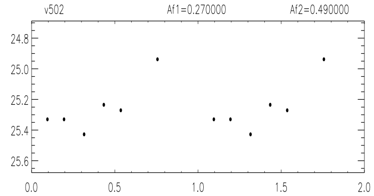
v502
Af1=0.270000
Af2=0.490000
24.8
25.0
25.2
25.4
25.6
0.0
0.5
1.0
1.5
2.0

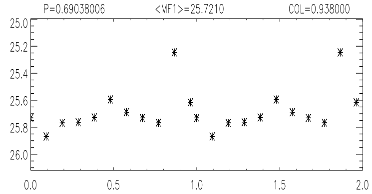
P=0.69038006
<MF1>=25.7210
COL=0.938000
25.0
25.2
25.4
25.6
25.8
26.0
0.0
0.5
1.0
1.5
2.0

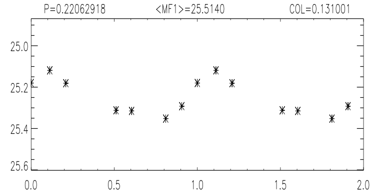
P=0.22062918
<MF1>=25.5140
COL=0.131001
25.0
25.2
25.4
25.6
0.0
0.5
1.0
1.5
2.0

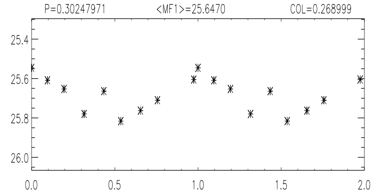
P=0.30247971
<MF1>=25.6470
COL=0.268999
25.4
25.6
25.8
26.0
0.0
0.5
1.0
1.5
2.0

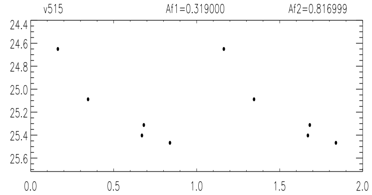
v515
Af1=0.319000
Af2=0.816999
24.4
24.6
24.8
25.0
25.2
25.4
25.6
0.0
0.5
1.0
1.5
2.0

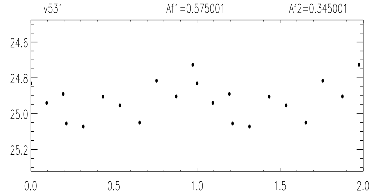
v531
Af1=0.575001
Af2=0.345001
24.6
24.8
25.0
25.2
0.0
0.5
1.0
1.5
2.0

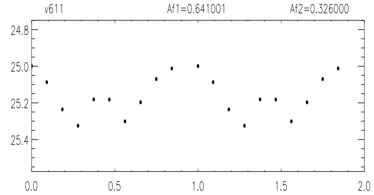
v611
Af1=0.641001
Af2=0.326000
24.8
25.0
25.2
25.4
0.0
0.5
1.0
1.5
2.0

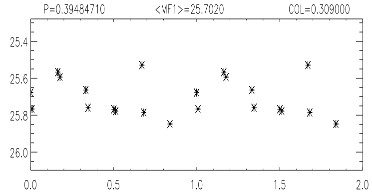
P=0.39484710
<MF1>=25.7020
COL=0.309000
25.4
25.6
25.8
26.0
0.0
0.5
1.0
1.5
2.0

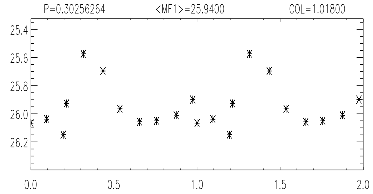
P=0.30256264
<MF1>=25.9400
COL=1.01800
25.4
25.6
25.8
26.0
26.2
0.0
0.5
1.0
1.5
2.0

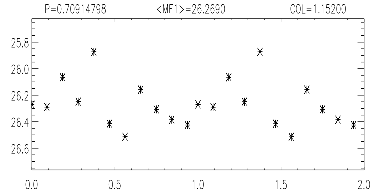
P=0.70914798
<MF1>=26.2690
COL=1.15200
25.8
26.0
26.2
26.4
26.6
0.0
0.5
1.0
1.5
2.0

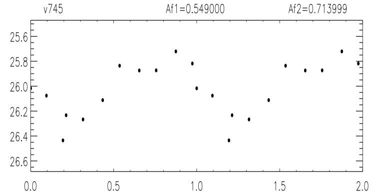
v745
Af1=0.549000
Af2=0.713999
25.6
25.8
26.0
26.2
26.4
26.6
0.0
0.5
1.0
1.5
2.0

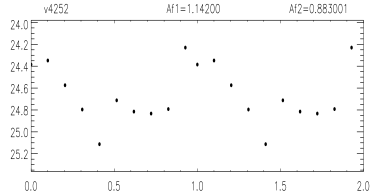
v4252
Af1=1.14200
Af2=0.883001
24.0
24.2
24.4
24.6
24.8
25.0
25.2
0.0
0.5
1.0
1.5
2.0

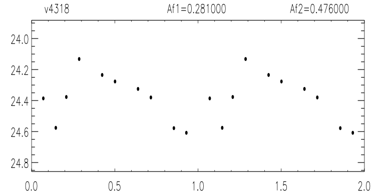
v4318
Af1=0.281000
Af2=0.476000
24.0
24.2
24.4
24.6
24.8
0.0
0.5
1.0
1.5
2.0

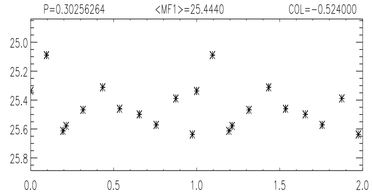
P=0.30256264
<MF1>=25.4440
COL=-0.524000
25.0
25.2
25.4
25.6
25.8
0.0
0.5
1.0
1.5
2.0

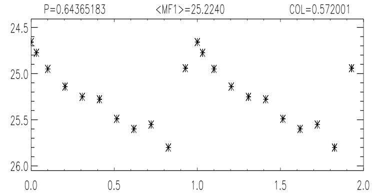
P=0.64365183
<MF1>=25.2240
COL=0.572001
24.5
25.0
25.5
26.0
0.0
0.5
1.0
1.5
2.0

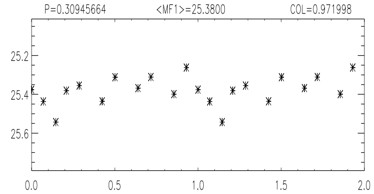
P=0.30945664
<MF1>=25.3800
COL=0.971998
25.2
25.4
25.6
0.0
0.5
1.0
1.5
2.0

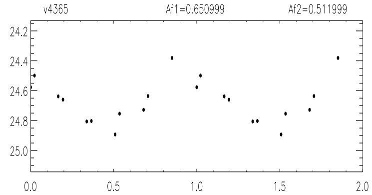
v4365
Af1=0.650999
Af2=0.511999
24.2
24.4
24.6
24.8
25.0
0.0
0.5
1.0
1.5
2.0

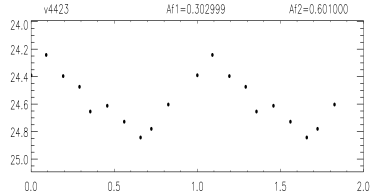
v4423
Af1=0.302999
Af2=0.601000
24.0
24.2
24.4
24.6
24.8
25.0
0.0
0.5
1.0
1.5
2.0

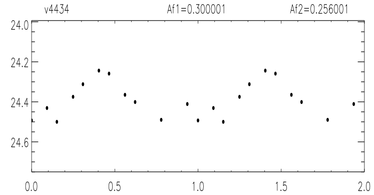
v4434
Af1=0.300001
Af2=0.256001
24.0
24.2
24.4
24.6
0.0
0.5
1.0
1.5
2.0

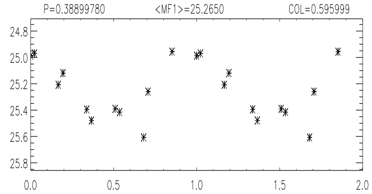
P=0.38899780
<MF1>=25.2650
COL=0.595999
24.8
25.0
25.2
25.4
25.6
25.8
0.0
0.5
1.0
1.5
2.0

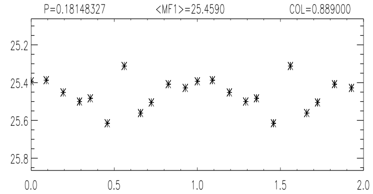
P=0.18148327
<MF1>=25.4590
COL=0.889000
25.2
25.4
25.6
25.8
0.0
0.5
1.0
1.5
2.0

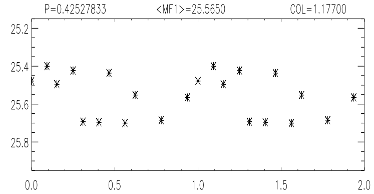
P=0.42527833
<MF1>=25.5650
COL=1.17700
25.2
25.4
25.6
25.8
0.0
0.5
1.0
1.5
2.0

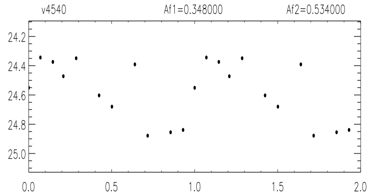
v4540
Af1=0.348000
Af2=0.534000
24.2
24.4
24.6
24.8
25.0
0.0
0.5
1.0
1.5
2.0

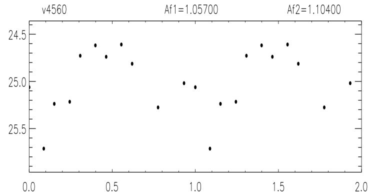
v4560
Af1=1.05700
Af2=1.10400
24.5
25.0
25.5
0.0
0.5
1.0
1.5
2.0

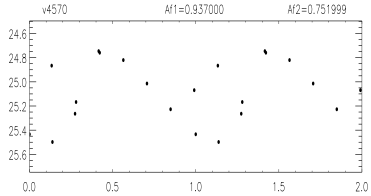
v4570
Af1=0.937000
Af2=0.751999
24.6
24.8
25.0
25.2
25.4
25.6
0.0
0.5
1.0
1.5
2.0

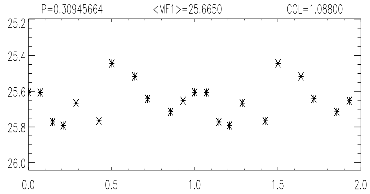
P=0.30945664
<MF1>=25.6650
COL=1.08800
25.2
25.4
25.6
25.8
26.0
0.0
0.5
1.0
1.5
2.0

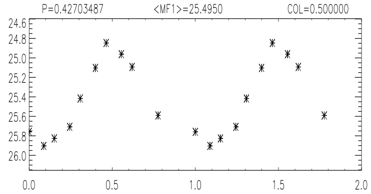
P=0.42703487
<MF1>=25.4950
COL=0.500000
24.6
24.8
25.0
25.2
25.4
25.6
25.8
26.0
0.0
0.5
1.0
1.5
2.0

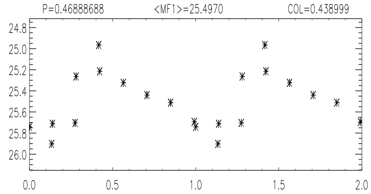
P=0.46888688
<MF1>=25.4970
COL=0.438999
24.8
25.0
25.2
25.4
25.6
25.8
26.0
0.0
0.5
1.0
1.5
2.0

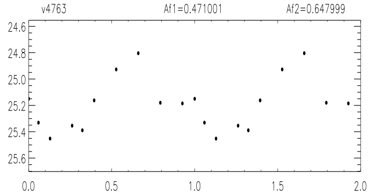
v4763
Af1=0.471001
Af2=0.647999
24.6
24.8
25.0
25.2
25.4
25.6
0.0
0.5
1.0
1.5
2.0

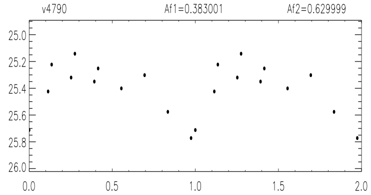
v4790
Af1=0.383001
Af2=0.629999
25.0
25.2
25.4
25.6
25.8
26.0
0.0
0.5
1.0
1.5
2.0

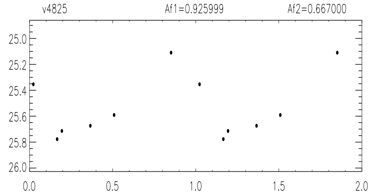
v4825
Af1=0.925999
Af2=0.667000
25.0
25.2
25.4
25.6
25.8
26.0
0.0
0.5
1.0
1.5
2.0

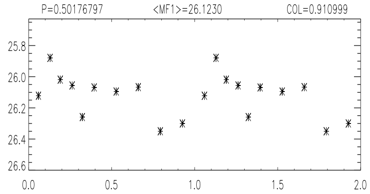
P=0.50176797
<MF1>=26.1230
COL=0.910999
25.8
26.0
26.2
26.4
26.6
0.0
0.5
1.0
1.5
2.0

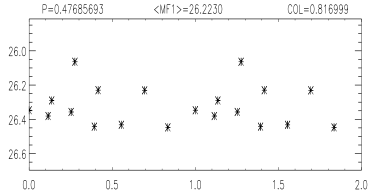
P=0.47685693
<MF1>=26.2230
COL=0.816999
26.0
26.2
26.4
26.6
0.0
0.5
1.0
1.5
2.0

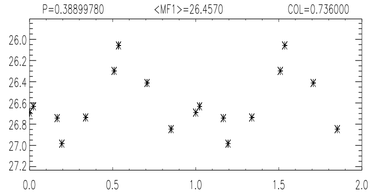
P=0.38899780
<MF1>=26.4570
COL=0.736000
26.0
26.2
26.4
26.6
26.8
27.0
27.2
0.0
0.5
1.0
1.5
2.0

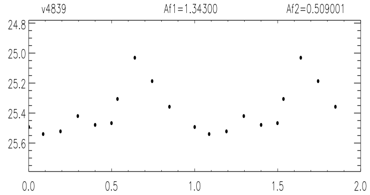
v4839
Af1=1.34300
Af2=0.509001
24.8
25.0
25.2
25.4
25.6
0.0
0.5
1.0
1.5
2.0

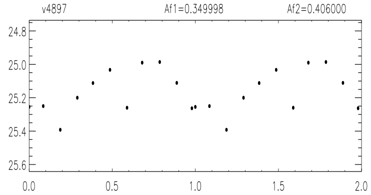
v4897
Af1=0.349998
Af2=0.406000
24.8
25.0
25.2
25.4
25.6
0.0
0.5
1.0
1.5
2.0

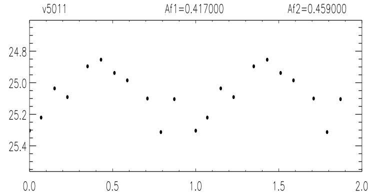
v5011
Af1=0.417000
Af2=0.459000
24.8
25.0
25.2
25.4
0.0
0.5
1.0
1.5
2.0

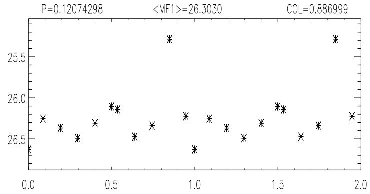
P=0.12074298
<MF1>=26.3030
COL=0.886999
25.5
26.0
26.5
0.0
0.5
1.0
1.5
2.0

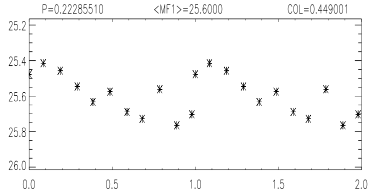
P=0.22285510
<MF1>=25.6000
COL=0.449001
25.2
25.4
25.6
25.8
26.0
0.0
0.5
1.0
1.5
2.0

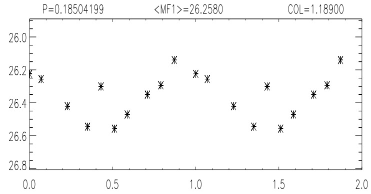
P=0.18504199
<MF1>=26.2580
COL=1.18900
26.0
26.2
26.4
26.6
26.8
0.0
0.5
1.0
1.5
2.0

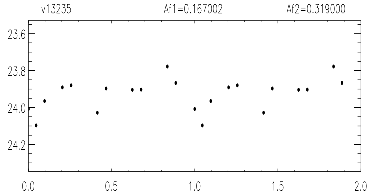
v13235
Af1=0.167002
Af2=0.319000
23.6
23.8
24.0
24.2
0.0
0.5
1.0
1.5
2.0

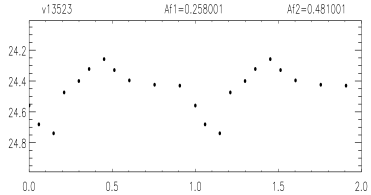
v13523
Af1=0.258001
Af2=0.481001
24.2
24.4
24.6
24.8
0.0
0.5
1.0
1.5
2.0

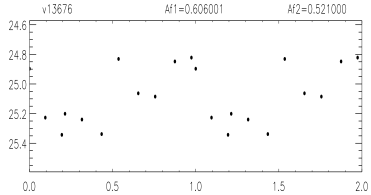
v13676
Af1=0.606001
Af2=0.521000
24.6
24.8
25.0
25.2
25.4
0.0
0.5
1.0
1.5
2.0

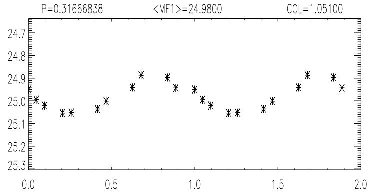
P=0.31666838
<MF1>=24.9800
COL=1.05100
24.7
24.8
24.9
25.0
25.1
25.2
25.3
0.0
0.5
1.0
1.5
2.0

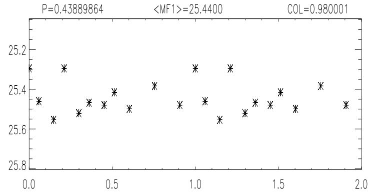
P=0.43889864
<MF1>=25.4400
COL=0.980001
25.2
25.4
25.6
25.8
0.0
0.5
1.0
1.5
2.0

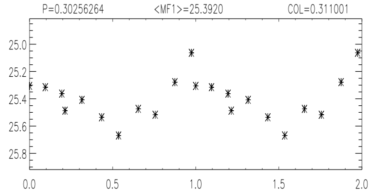
P=0.30256264
<MF1>=25.3920
COL=0.311001
25.0
25.2
25.4
25.6
25.8
0.0
0.5
1.0
1.5
2.0

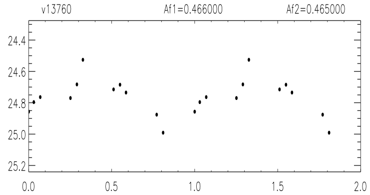
v13760 Af1=0.466000 Af2=0.465000
24.4 24.6 24.8 25.0 25.2
0.0 0.5 1.0 1.5 2.0

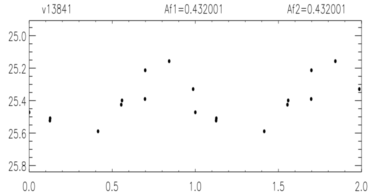
v13841 Af1=0.432001 Af2=0.432001
25.0 25.2 25.4 25.6 25.8
0.0 0.5 1.0 1.5 2.0

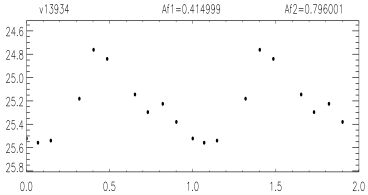
v13934 Af1=0.414999 Af2=0.796001
24.6 24.8 25.0 25.2 25.4 25.6 25.8
0.0 0.5 1.0 1.5 2.0

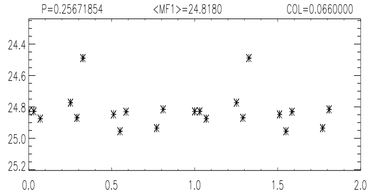
P=0.25671854 <MF1>=24.8180 COL=0.0660000
24.4 24.6 24.8 25.0 25.2
0.0 0.5 1.0 1.5 2.0

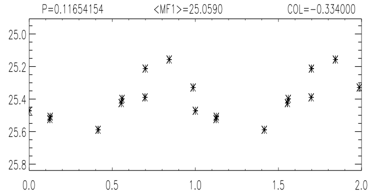
P=0.11654154 <MF1>=25.0590 COL=-0.334000
25.0 25.2 25.4 25.6 25.8
0.0 0.5 1.0 1.5 2.0

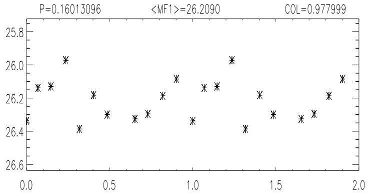
P=0.16013096 <MF1>=26.2090 COL=0.977999
25.8 26.0 26.2 26.4 26.6
0.0 0.5 1.0 1.5 2.0

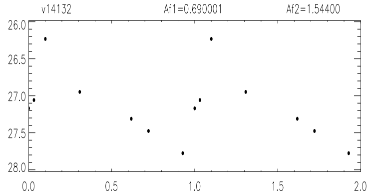
v14132 Af1=0.690001 Af2=1.54400
26.0 26.5 27.0 27.5 28.0
0.0 0.5 1.0 1.5 2.0

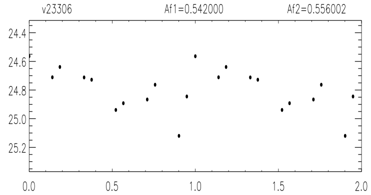
v23306 Af1=0.542000 Af2=0.556002
24.4 24.6 24.8 25.0 25.2
0.0 0.5 1.0 1.5 2.0

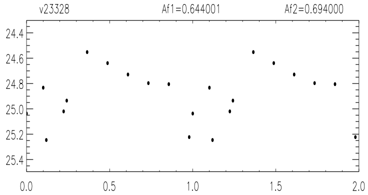
v23328 Af1=0.644001 Af2=0.694000
24.4 24.6 24.8 25.0 25.2 25.4
0.0 0.5 1.0 1.5 2.0

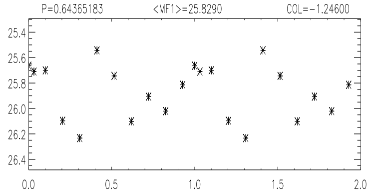
P=0.64365183 <MF1>=25.8290 COL=-1.24600
25.4 25.6 25.8 26.0 26.2 26.4
0.0 0.5 1.0 1.5 2.0

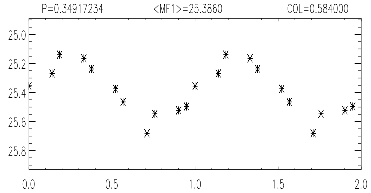
P=0.34917234 <MF1>=25.3860 COL=0.584000
25.0 25.2 25.4 25.6 25.8
0.0 0.5 1.0 1.5 2.0

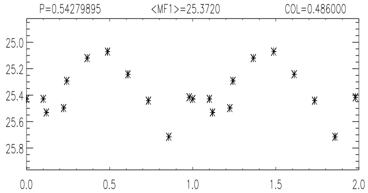
P=0.54279895 <MF1>=25.3720 COL=0.486000
25.0 25.2 25.4 25.6 25.8
0.0 0.5 1.0 1.5 2.0

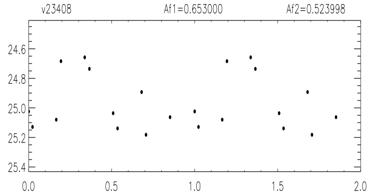
v23408 Af1=0.653000 Af2=0.523998
24.6 24.8 25.0 25.2 25.4
0.0 0.5 1.0 1.5 2.0

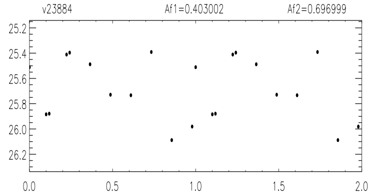
v23884 Af1=0.403002 Af2=0.696999
25.2 25.4 25.6 25.8 26.0 26.2
0.0 0.5 1.0 1.5 2.0

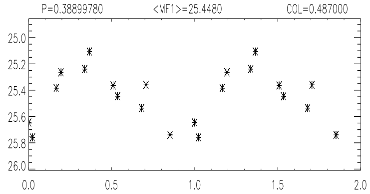
P=0.38899780 <MF1>=25.4480 COL=0.487000
25.0 25.2 25.4 25.6 25.8 26.0
0.0 0.5 1.0 1.5 2.0

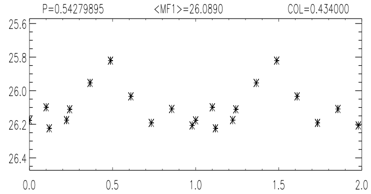
P=0.54279895 <MF1>=26.0890 COL=0.434000
25.6 25.8 26.0 26.2 26.4
0.0 0.5 1.0 1.5 2.0

Chapter 9

Appendix C

ATLAS OF LIGHT CURVES: G33

Atlas of the V,I light curves for candidate variable stars identified in G33. For each variable the upper panel shows the I-band light curve, and the lower panel the V-band light curve. Identification, V and I amplitudes, period, average V magnitude and average V−I color, are provided on top labels of the plots.

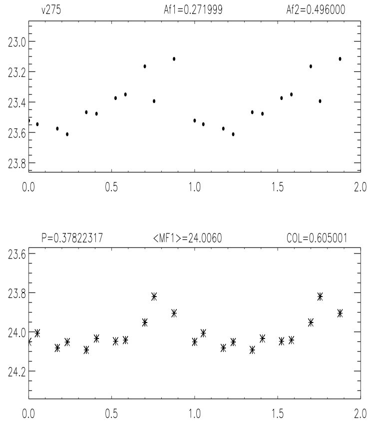
v275 Af1=0.271999 Af2=0.496000
P=0.37822317 <MF1>=24.0060 COL=0.605001

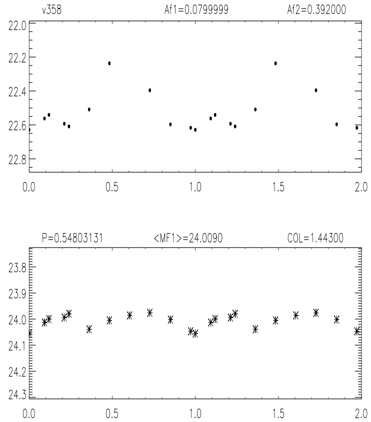
v358 Af1=0.0799999 Af2=0.392000
P=0.54803131 <MF1>=24.0090 COL=1.44300

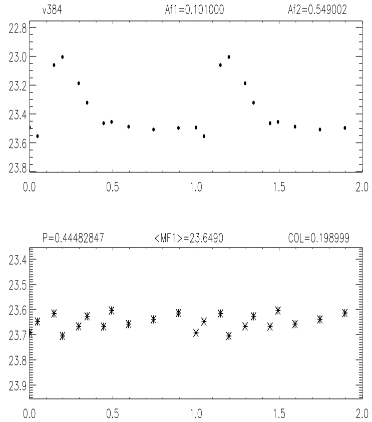
v384 Af1=0.101000 Af2=0.549002
P=0.44482847 <MF1>=23.6490 COL=0.198999

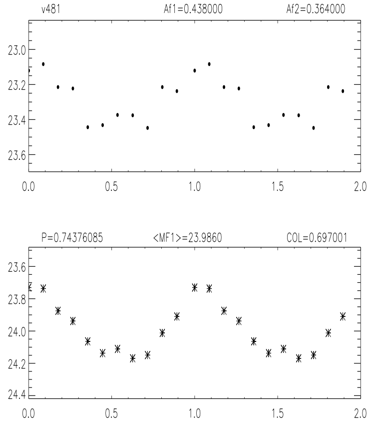
v481 Af1=0.438000 Af2=0.364000
P=0.74376085 <MF1>=23.9860 COL=0.697001

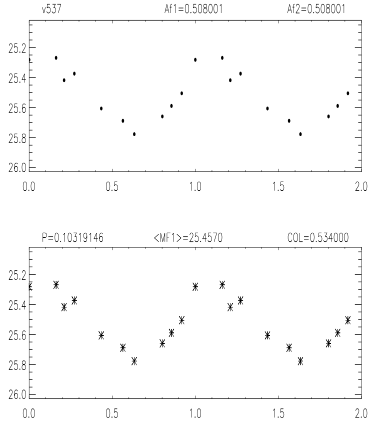
v537 Af1=0.508001 Af2=0.508001
P=0.10319146 <MF1>=25.4570 COL=0.534000

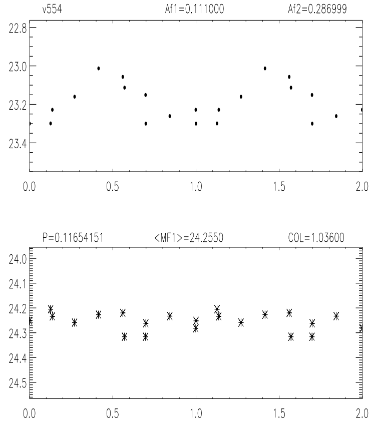
v554 Af1=0.111000 Af2=0.286999
P=0.11654151 <MF1>=24.2550 COL=1.03600

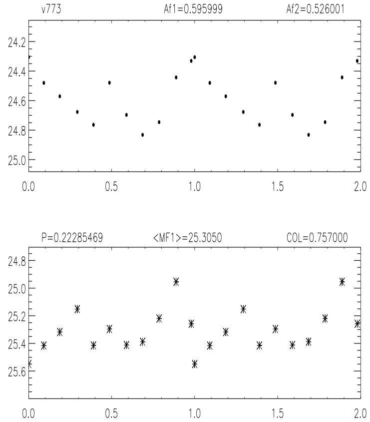
v773 Af1=0.595999 Af2=0.526001
P=0.22285469 <MF1>=25.3050 COL=0.757000

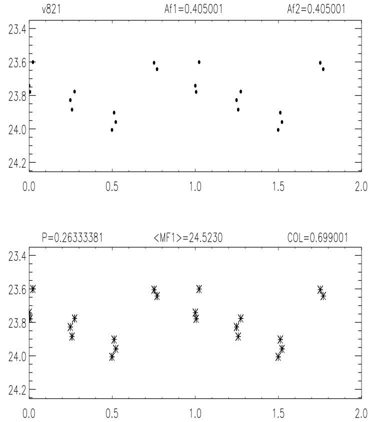
v821 Af1=0.405001 Af2=0.405001
P=0.26333381 <MF1>=24.5230 COL=0.699001

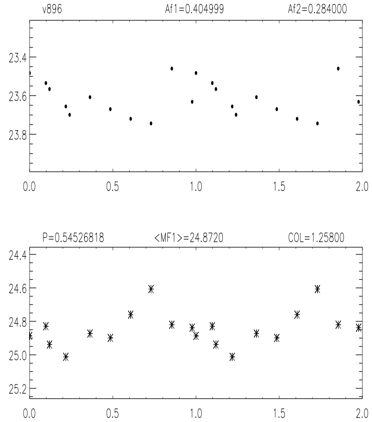
v896 Af1=0.404999 Af2=0.284000
P=0.54526818 <MF1>=24.8720 COL=1.25800

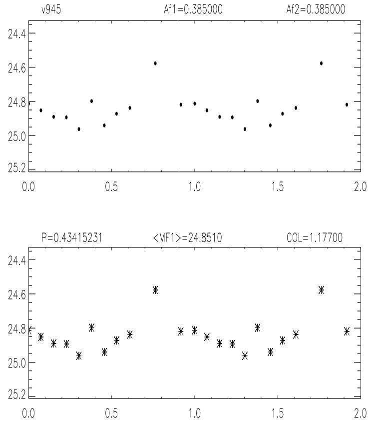
v945 Af1=0.385000 Af2=0.385000
P=0.43415231 <MF1>=24.8510 COL=1.17700

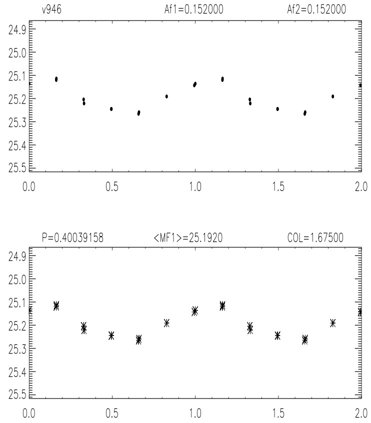
v946 Af1=0.152000 Af2=0.152000
P=0.40039158 <MF1>=25.1920 COL=1.67500

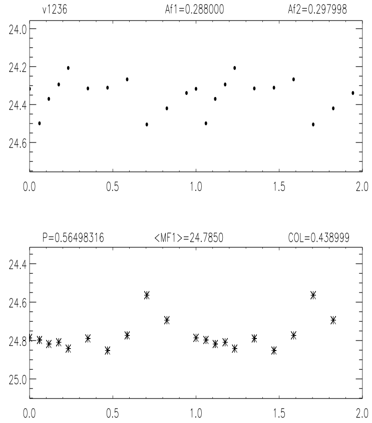
v1236 Af1=0.288000 Af2=0.297998
P=0.56498316 <MF1>=24.7850 COL=0.438999

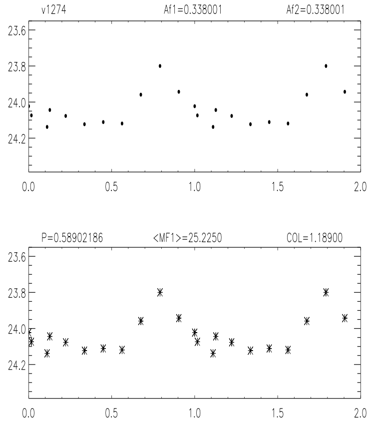
v1274
Af1=0.338001
Af2=0.338001
23.6
23.8
24.0
24.2
P=0.58902186
<MF1>=25.2250
COL=1.18900
0.0
0.5
1.0
1.5
2.0

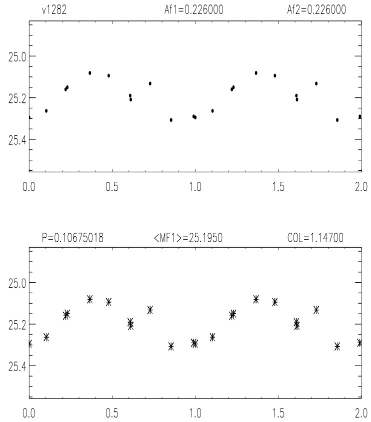
v1282
Af1=0.226000
Af2=0.226000
25.0
25.2
25.4
P=0.10675018
<MF1>=25.1950
COL=1.14700
0.0
0.5
1.0
1.5
2.0

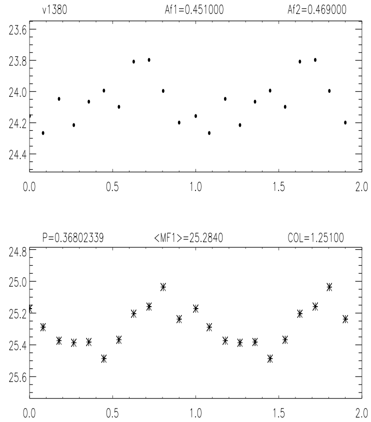
v1380
Af1=0.451000
Af2=0.469000
23.6
23.8
24.0
24.2
24.4
P=0.36802339
<MF1>=25.2840
COL=1.25100
24.8
25.0
25.2
25.4
25.6
0.0
0.5
1.0
1.5
2.0

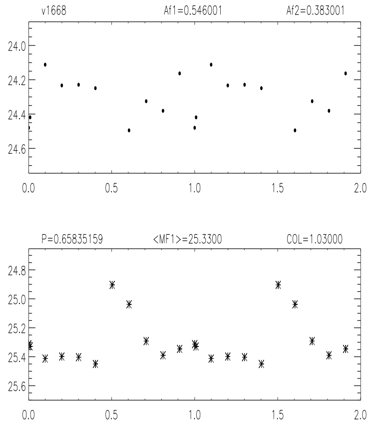
v1668
Af1=0.546001
Af2=0.383001
24.0
24.2
24.4
24.6
P=0.65835159
<MF1>=25.3300
COL=1.03000
24.8
25.0
25.2
25.4
25.6
0.0
0.5
1.0
1.5
2.0

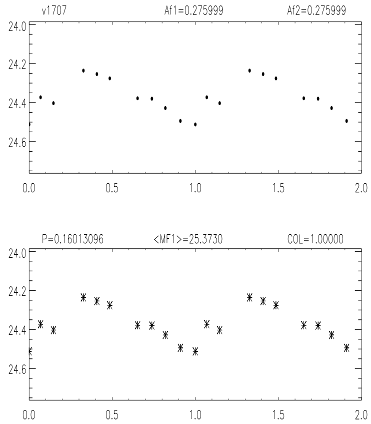
v1707
Af1=0.275999
Af2=0.275999
24.0
24.2
24.4
24.6
P=0.16013096
<MF1>=25.3730
COL=1.00000
0.0
0.5
1.0
1.5
2.0

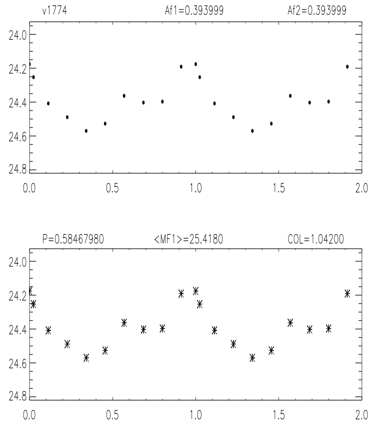
v1774
Af1=0.393999
Af2=0.393999
24.0
24.2
24.4
24.6
24.8
P=0.58467980
<MF1>=25.4180
COL=1.04200
0.0
0.5
1.0
1.5
2.0

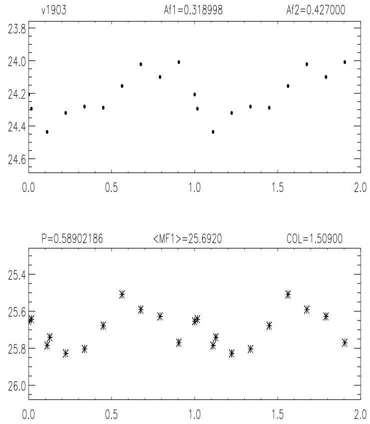
v1903
Af1=0.318998
Af2=0.427000
23.8
24.0
24.2
24.4
24.6
P=0.58902186
<MF1>=25.6920
COL=1.50900
25.4
25.6
25.8
26.0
0.0
0.5
1.0
1.5
2.0

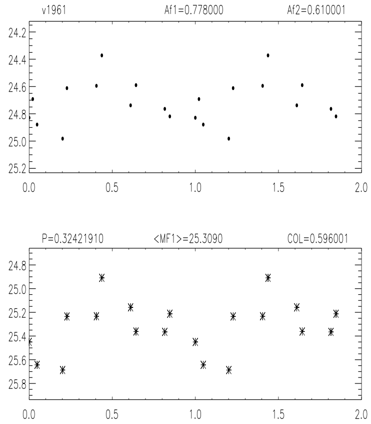
v1961
Af1=0.778000
Af2=0.610001
24.2
24.4
24.6
24.8
25.0
25.2
P=0.32421910
<MF1>=25.3090
COL=0.596001
24.8
25.0
25.2
25.4
25.6
25.8
0.0
0.5
1.0
1.5
2.0

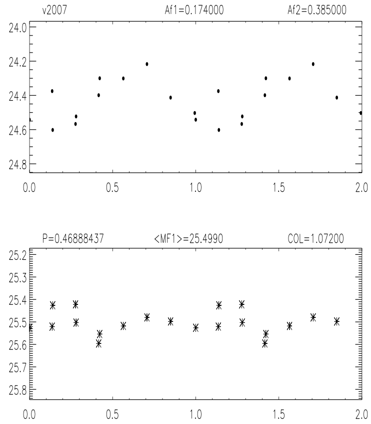
v2007
Af1=0.174000
Af2=0.385000
24.0
24.2
24.4
24.6
24.8
P=0.46888437
<MF1>=25.4990
COL=1.07200
25.2
25.3
25.4
25.5
25.6
25.7
25.8
0.0
0.5
1.0
1.5
2.0

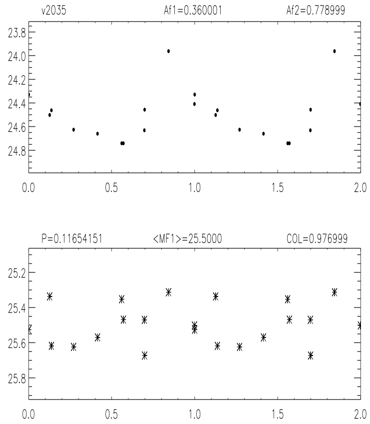
v2035
Af1=0.360001
Af2=0.778999
23.8
24.0
24.2
24.4
24.6
24.8
P=0.11654151
<MF1>=25.5000
COL=0.976999
25.2
25.4
25.6
25.8
0.0
0.5
1.0
1.5
2.0

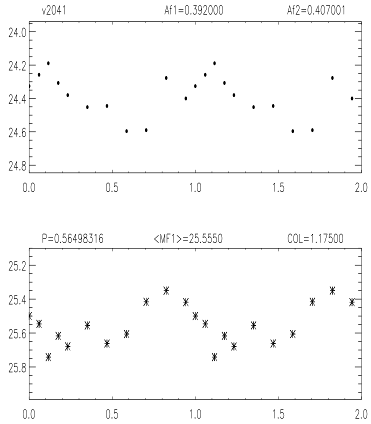
v2041
Af1=0.392000
Af2=0.407001
24.0
24.2
24.4
24.6
24.8
P=0.56498316
<MF1>=25.5550
COL=1.17500
25.2
25.4
25.6
25.8
0.0
0.5
1.0
1.5
2.0

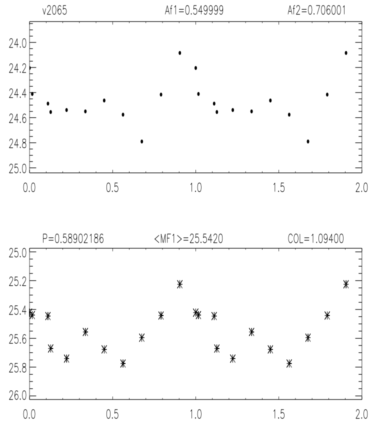
v2065
Af1=0.549999
Af2=0.706001
24.0
24.2
24.4
24.6
24.8
25.0
P=0.58902186
<MF1>=25.5420
COL=1.09400
25.0
25.2
25.4
25.6
25.8
26.0
0.0
0.5
1.0
1.5
2.0

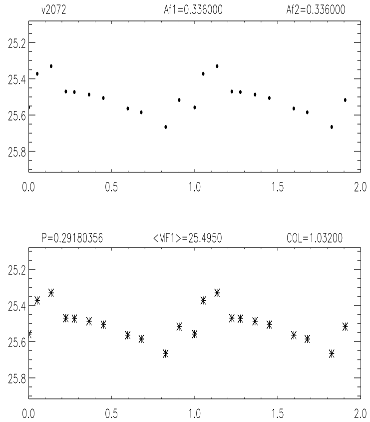
v2072
Af1=0.336000
Af2=0.336000
25.2
25.4
25.6
25.8
0.0
0.5
1.0
1.5
2.0
P=0.29180356
<MF1>=25.4950
COL=1.03200
25.2
25.4
25.6
25.8
0.0
0.5
1.0
1.5
2.0

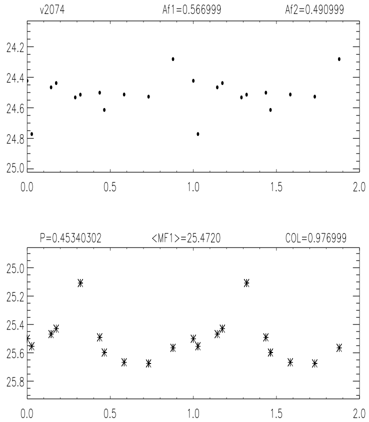
v2074
Af1=0.566999
Af2=0.490999
24.2
24.4
24.6
24.8
25.0
0.0
0.5
1.0
1.5
2.0
P=0.45340302
<MF1>=25.4720
COL=0.976999
25.0
25.2
25.4
25.6
25.8
0.0
0.5
1.0
1.5
2.0

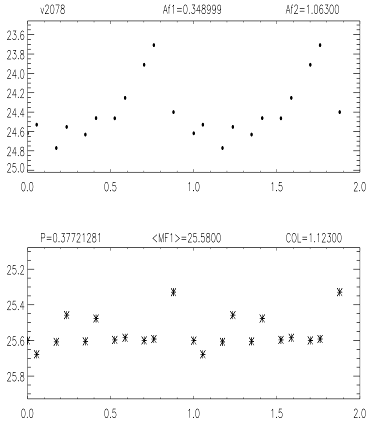
v2078
Af1=0.348999
Af2=1.06300
23.6
23.8
24.0
24.2
24.4
24.6
24.8
25.0
0.0
0.5
1.0
1.5
2.0
P=0.37721281
<MF1>=25.5800
COL=1.12300
25.2
25.4
25.6
25.8
0.0
0.5
1.0
1.5
2.0

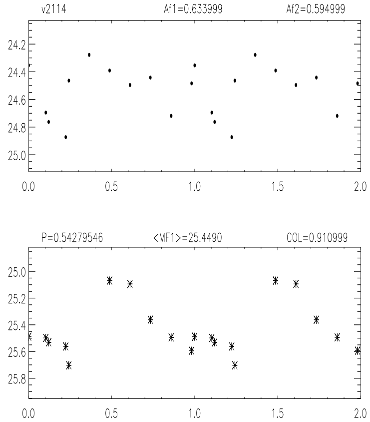
v2114
Af1=0.633999
Af2=0.594999
24.2
24.4
24.6
24.8
25.0
0.0
0.5
1.0
1.5
2.0
P=0.54279546
<MF1>=25.4490
COL=0.910999
25.0
25.2
25.4
25.6
25.8
0.0
0.5
1.0
1.5
2.0

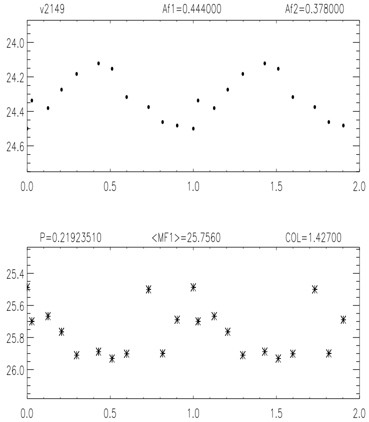
v2149
Af1=0.444000
Af2=0.378000
24.0
24.2
24.4
24.6
0.0
0.5
1.0
1.5
2.0
P=0.21923510
<MF1>=25.7560
COL=1.42700
25.4
25.6
25.8
26.0
0.0
0.5
1.0
1.5
2.0

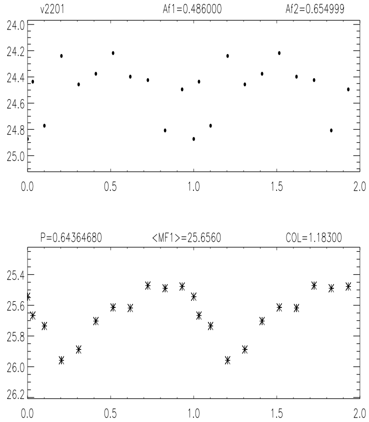
v2201
Af1=0.486000
Af2=0.654999
24.0
24.2
24.4
24.6
24.8
25.0
0.0
0.5
1.0
1.5
2.0
P=0.64364680
<MF1>=25.6560
COL=1.18300
25.4
25.6
25.8
26.0
26.2
0.0
0.5
1.0
1.5
2.0

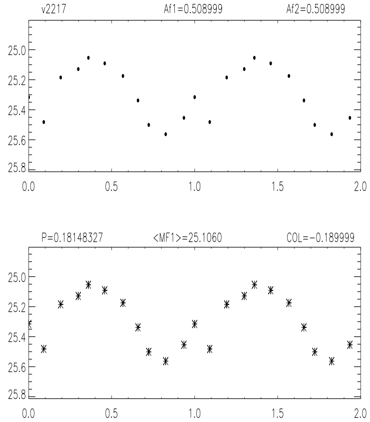
v2217
Af1=0.508999
Af2=0.508999
25.0
25.2
25.4
25.6
25.8
0.0
0.5
1.0
1.5
2.0
P=0.18148327
<MF1>=25.1060
COL=-0.189999
25.0
25.2
25.4
25.6
25.8
0.0
0.5
1.0
1.5
2.0

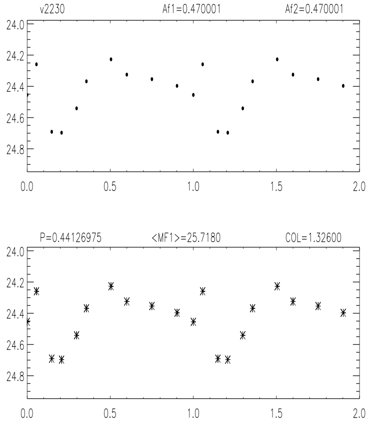
v2230
Af1=0.470001
Af2=0.470001
24.0
24.2
24.4
24.6
24.8
0.0
0.5
1.0
1.5
2.0
P=0.44126975
<MF1>=25.7180
COL=1.32600
24.0
24.2
24.4
24.6
24.8
0.0
0.5
1.0
1.5
2.0

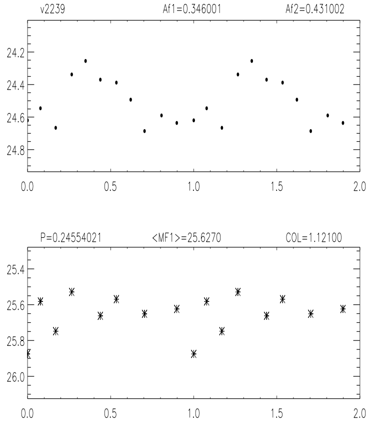
v2239
Af1=0.346001
Af2=0.431002
24.2
24.4
24.6
24.8
0.0
0.5
1.0
1.5
2.0
P=0.24554021
<MF1>=25.6270
COL=1.12100
25.4
25.6
25.8
26.0
0.0
0.5
1.0
1.5
2.0

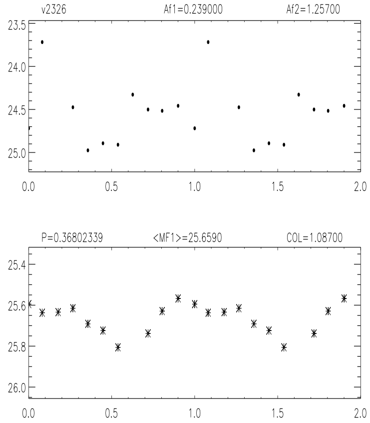
v2326
Af1=0.239000
Af2=1.25700
23.5
24.0
24.5
25.0
0.0
0.5
1.0
1.5
2.0
P=0.36802339
<MF1>=25.6590
COL=1.08700
25.4
25.6
25.8
26.0
0.0
0.5
1.0
1.5
2.0

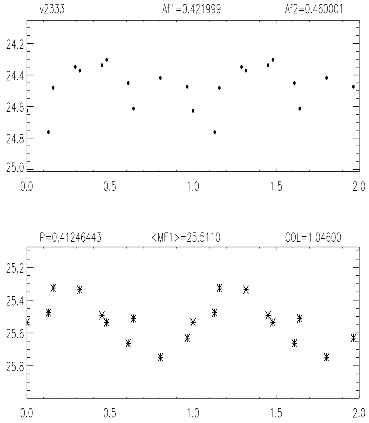
v2333
Af1=0.421999
Af2=0.460001
24.2
24.4
24.6
24.8
25.0
0.0
0.5
1.0
1.5
2.0
P=0.41246443
<MF1>=25.5110
COL=1.04600
25.2
25.4
25.6
25.8
0.0
0.5
1.0
1.5
2.0

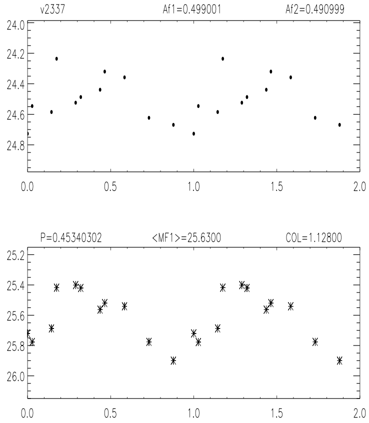
v2337
Af1=0.499001
Af2=0.490999
24.0
24.2
24.4
24.6
24.8
0.0
0.5
1.0
1.5
2.0
P=0.45340302
<MF1>=25.6300
COL=1.12800
25.2
25.4
25.6
25.8
26.0
0.0
0.5
1.0
1.5
2.0

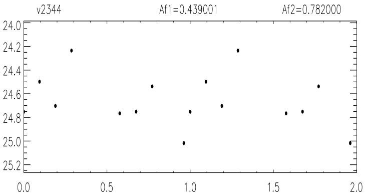
v2344
Af1=0.439001
Af2=0.782000
24.0
24.2
24.4
24.6
24.8
25.0
25.2
0.0
0.5
1.0
1.5
2.0

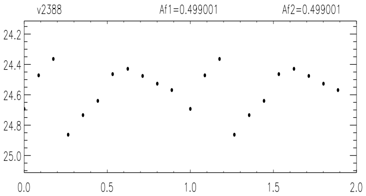
v2388
Af1=0.499001
Af2=0.499001
24.2
24.4
24.6
24.8
25.0
0.0
0.5
1.0
1.5
2.0

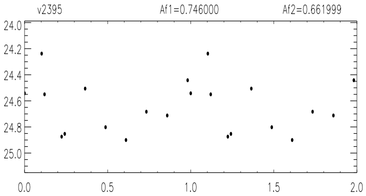
v2395
Af1=0.746000
Af2=0.661999
24.0
24.2
24.4
24.6
24.8
25.0
0.0
0.5
1.0
1.5
2.0

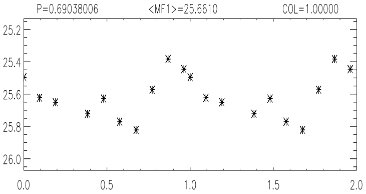
P=0.69038006
<MF1>=25.6610
COL=1.00000
25.2
25.4
25.6
25.8
26.0
0.0
0.5
1.0
1.5
2.0

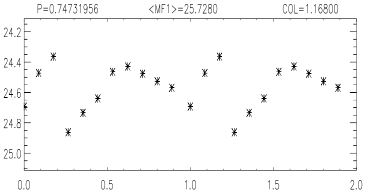
P=0.74731956
<MF1>=25.7280
COL=1.16800
24.2
24.4
24.6
24.8
25.0
0.0
0.5
1.0
1.5
2.0

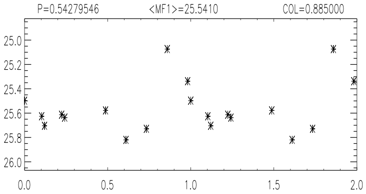
P=0.54279546
<MF1>=25.5410
COL=0.885000
25.0
25.2
25.4
25.6
25.8
26.0
0.0
0.5
1.0
1.5
2.0

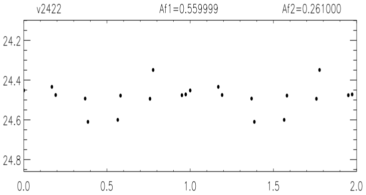
v2422
Af1=0.559999
Af2=0.261000
24.2
24.4
24.6
24.8
0.0
0.5
1.0
1.5
2.0

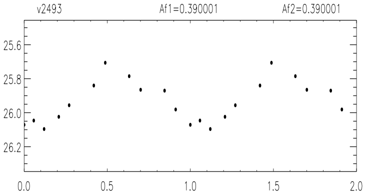
v2493
Af1=0.390001
Af2=0.390001
25.6
25.8
26.0
26.2
0.0
0.5
1.0
1.5
2.0

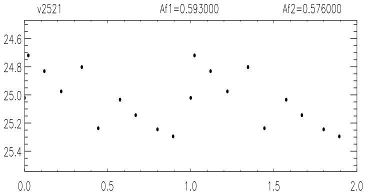
v2521
Af1=0.593000
Af2=0.576000
24.6
24.8
25.0
25.2
25.4
0.0
0.5
1.0
1.5
2.0

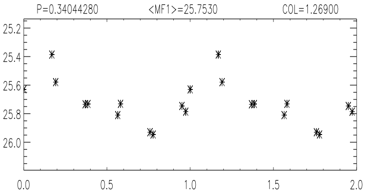
P=0.34044280
<MF1>=25.7530
COL=1.26900
25.2
25.4
25.6
25.8
26.0
0.0
0.5
1.0
1.5
2.0

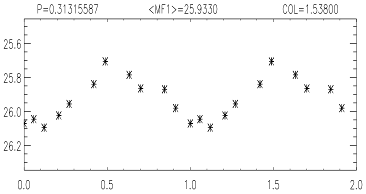
P=0.31315587
<MF1>=25.9330
COL=1.53800
25.6
25.8
26.0
26.2
0.0
0.5
1.0
1.5
2.0

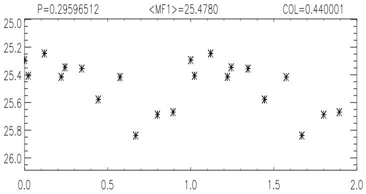
P=0.29596512
<MF1>=25.4780
COL=0.440001
25.0
25.2
25.4
25.6
25.8
26.0
0.0
0.5
1.0
1.5
2.0

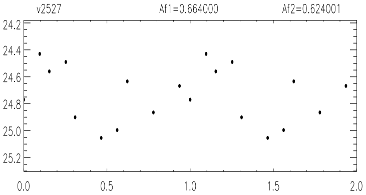
v2527
Af1=0.664000
Af2=0.624001
24.2
24.4
24.6
24.8
25.0
25.2
0.0
0.5
1.0
1.5
2.0

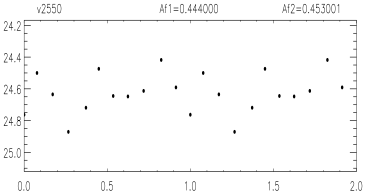
v2550
Af1=0.444000
Af2=0.453001
24.2
24.4
24.6
24.8
25.0
0.0
0.5
1.0
1.5
2.0

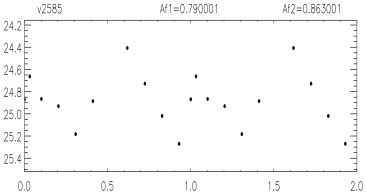
v2585
Af1=0.790001
Af2=0.863001
24.2
24.4
24.6
24.8
25.0
25.2
25.4
0.0
0.5
1.0
1.5
2.0

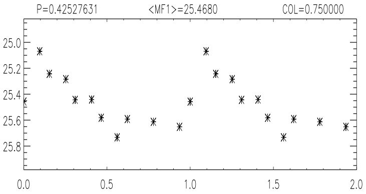
P=0.42527631
<MF1>=25.4680
COL=0.750000
25.0
25.2
25.4
25.6
25.8
0.0
0.5
1.0
1.5
2.0

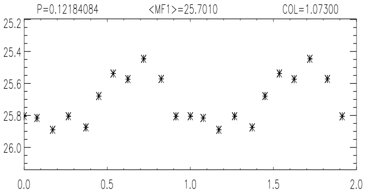
P=0.12184084
<MF1>=25.7010
COL=1.07300
25.2
25.4
25.6
25.8
26.0
0.0
0.5
1.0
1.5
2.0

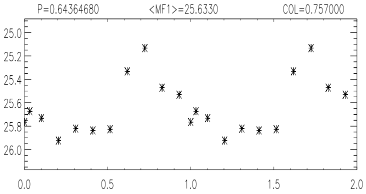
P=0.64364680
<MF1>=25.6330
COL=0.757000
25.0
25.2
25.4
25.6
25.8
26.0
0.0
0.5
1.0
1.5
2.0

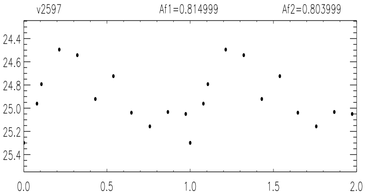
v2597
Af1=0.814999
Af2=0.803999
24.4
24.6
24.8
25.0
25.2
25.4
0.0
0.5
1.0
1.5
2.0

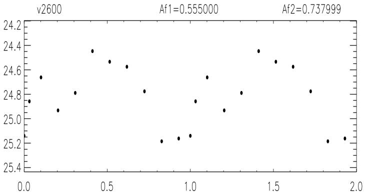
v2600
Af1=0.555000
Af2=0.737999
24.2
24.4
24.6
24.8
25.0
25.2
25.4
0.0
0.5
1.0
1.5
2.0

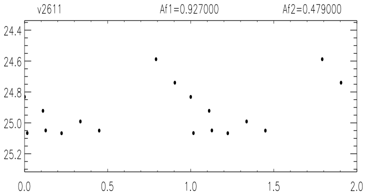
v2611
Af1=0.927000
Af2=0.479000
24.4
24.6
24.8
25.0
25.2
0.0
0.5
1.0
1.5
2.0

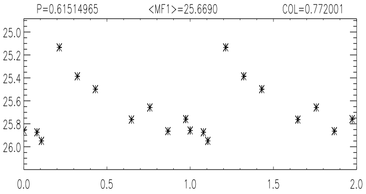
P=0.61514965
<MF1>=25.6690
COL=0.772001
25.0
25.2
25.4
25.6
25.8
26.0
0.0
0.5
1.0
1.5
2.0

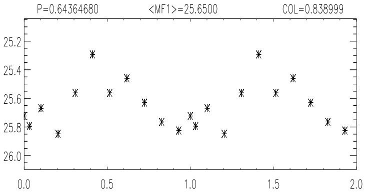
P=0.64364680
<MF1>=25.6500
COL=0.838999
25.2
25.4
25.6
25.8
26.0
0.0
0.5
1.0
1.5
2.0

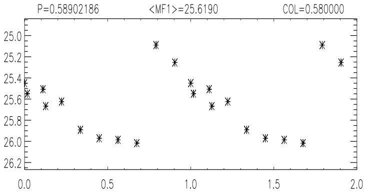
P=0.58902186
<MF1>=25.6190
COL=0.580000
25.0
25.2
25.4
25.6
25.8
26.0
26.2
0.0
0.5
1.0
1.5
2.0

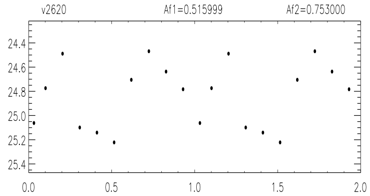
v2620
Af1=0.515999
Af2=0.753000
24.4
24.6
24.8
25.0
25.2
25.4
0.0
0.5
1.0
1.5
2.0

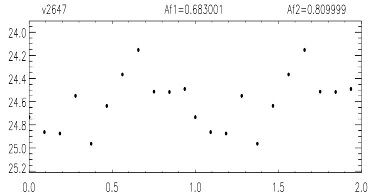
v2647
Af1=0.683001
Af2=0.809999
24.0
24.2
24.4
24.6
24.8
25.0
25.2
0.0
0.5
1.0
1.5
2.0

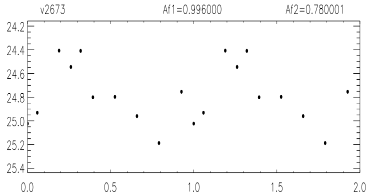
v2673
Af1=0.996000
Af2=0.780001
24.2
24.4
24.6
24.8
25.0
25.2
25.4
0.0
0.5
1.0
1.5
2.0

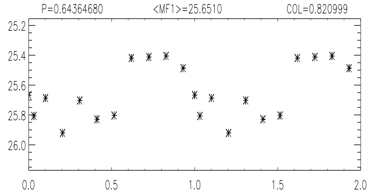
P=0.64364680
<MF1>=25.6510
COL=0.820999
25.2
25.4
25.6
25.8
26.0
0.0
0.5
1.0
1.5
2.0

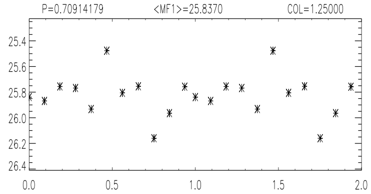
P=0.70914179
<MF1>=25.8370
COL=1.25000
25.4
25.6
25.8
26.0
26.2
26.4
0.0
0.5
1.0
1.5
2.0

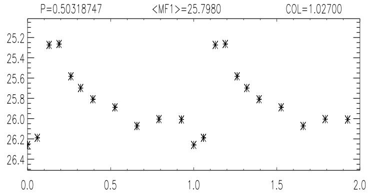
P=0.50318747
<MF1>=25.7980
COL=1.02700
25.2
25.4
25.6
25.8
26.0
26.2
26.4
0.0
0.5
1.0
1.5
2.0

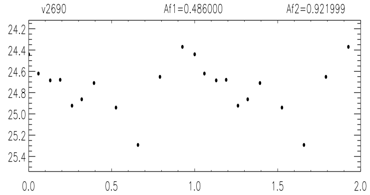
v2690
Af1=0.486000
Af2=0.921999
24.2
24.4
24.6
24.8
25.0
25.2
25.4
0.0
0.5
1.0
1.5
2.0

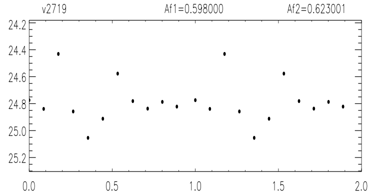
v2719
Af1=0.598000
Af2=0.623001
24.2
24.4
24.6
24.8
25.0
25.2
0.0
0.5
1.0
1.5
2.0

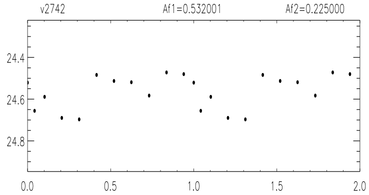
v2742
Af1=0.532001
Af2=0.225000
24.4
24.6
24.8
0.0
0.5
1.0
1.5
2.0

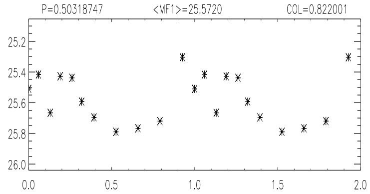
P=0.50318747
<MF1>=25.5720
COL=0.822001
25.2
25.4
25.6
25.8
26.0
0.0
0.5
1.0
1.5
2.0

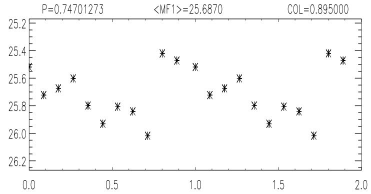
P=0.74701273
<MF1>=25.6870
COL=0.895000
25.2
25.4
25.6
25.8
26.0
26.2
0.0
0.5
1.0
1.5
2.0

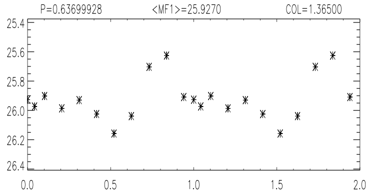
P=0.63699928
<MF1>=25.9270
COL=1.36500
25.4
25.6
25.8
26.0
26.2
26.4
0.0
0.5
1.0
1.5
2.0

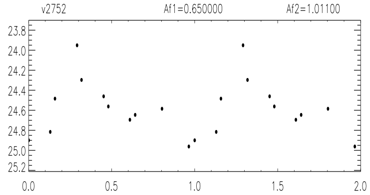
v2752
Af1=0.650000
Af2=1.01100
23.8
24.0
24.2
24.4
24.6
24.8
25.0
25.2
0.0
0.5
1.0
1.5
2.0

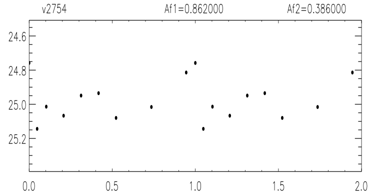
v2754
Af1=0.862000
Af2=0.386000
24.6
24.8
25.0
25.2
0.0
0.5
1.0
1.5
2.0

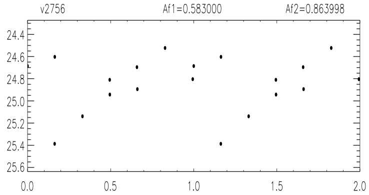
v2756
Af1=0.583000
Af2=0.863998
24.4
24.6
24.8
25.0
25.2
25.4
25.6
0.0
0.5
1.0
1.5
2.0

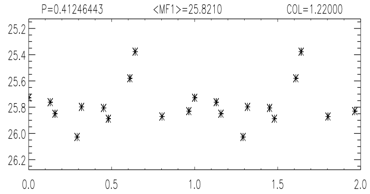
P=0.41246443
<MF1>=25.8210
COL=1.22000
25.2
25.4
25.6
25.8
26.0
26.2
0.0
0.5
1.0
1.5
2.0

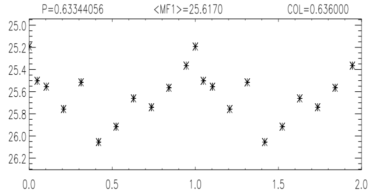
P=0.63344056
<MF1>=25.6170
COL=0.636000
25.0
25.2
25.4
25.6
25.8
26.0
26.2
0.0
0.5
1.0
1.5
2.0

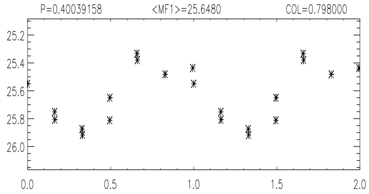
P=0.40039158
<MF1>=25.6480
COL=0.798000
25.2
25.4
25.6
25.8
26.0
0.0
0.5
1.0
1.5
2.0

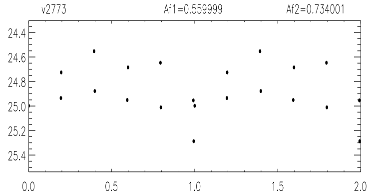
v2773
Af1=0.559999
Af2=0.734001
24.4
24.6
24.8
25.0
25.2
25.4
0.0
0.5
1.0
1.5
2.0

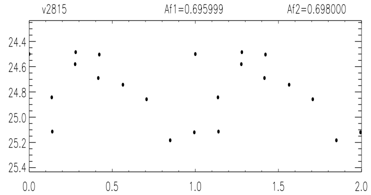
v2815
Af1=0.695999
Af2=0.698000
24.4
24.6
24.8
25.0
25.2
25.4
0.0
0.5
1.0
1.5
2.0

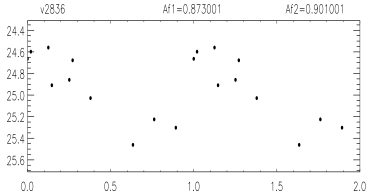
v2836
Af1=0.873001
Af2=0.901001
24.4
24.6
24.8
25.0
25.2
25.4
25.6
0.0
0.5
1.0
1.5
2.0

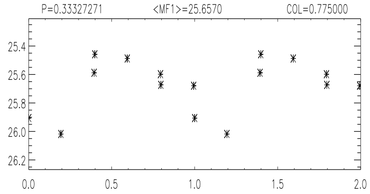
P=0.33327271
<MF1>=25.6570
COL=0.775000
25.4
25.6
25.8
26.0
26.2
0.0
0.5
1.0
1.5
2.0

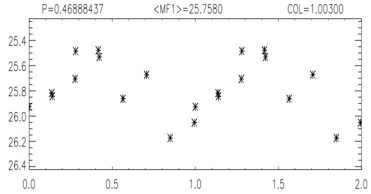
P=0.46888437
<MF1>=25.7580
COL=1.00300
25.4
25.6
25.8
26.0
26.2
26.4
0.0
0.5
1.0
1.5
2.0

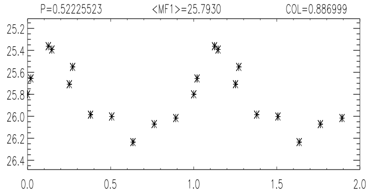
P=0.52225523
<MF1>=25.7930
COL=0.886999
25.2
25.4
25.6
25.8
26.0
26.2
26.4
0.0
0.5
1.0
1.5
2.0

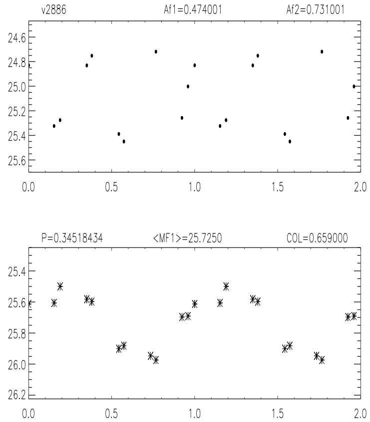
v2886
Af1=0.474001
Af2=0.731001
24.6
24.8
25.0
25.2
25.4
25.6
P=0.34518434
<MF1>=25.7250
COL=0.659000
25.4
25.6
25.8
26.0
26.2
0.0
0.5
1.0
1.5
2.0

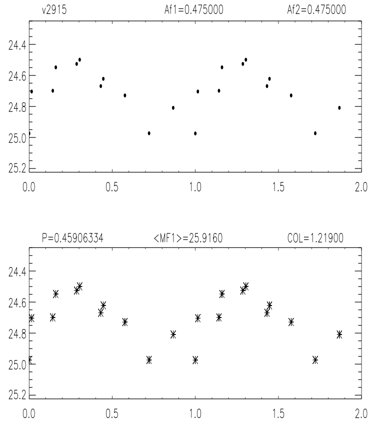
v2915
Af1=0.475000
Af2=0.475000
24.4
24.6
24.8
25.0
25.2
P=0.45906334
<MF1>=25.9160
COL=1.21900
0.0
0.5
1.0
1.5
2.0

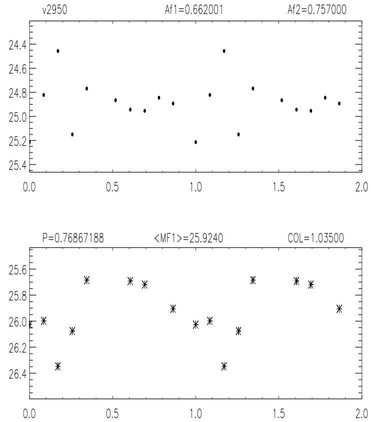
v2950
Af1=0.662001
Af2=0.757000
24.4
24.6
24.8
25.0
25.2
25.4
P=0.76867188
<MF1>=25.9240
COL=1.03500
25.6
25.8
26.0
26.2
26.4
0.0
0.5
1.0
1.5
2.0

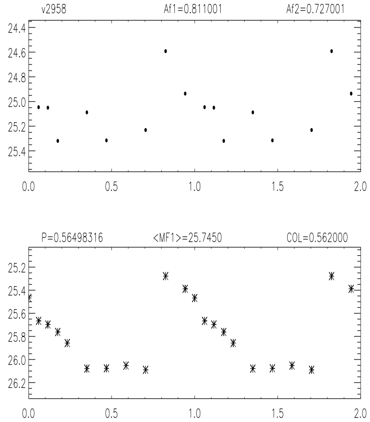
v2958
Af1=0.811001
Af2=0.727001
24.4
24.6
24.8
25.0
25.2
25.4
P=0.56498316
<MF1>=25.7450
COL=0.562000
25.2
25.4
25.6
25.8
26.0
26.2
0.0
0.5
1.0
1.5
2.0

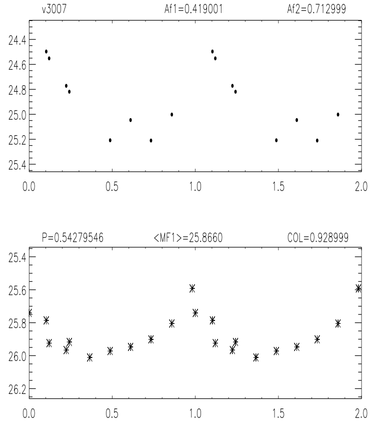
v3007
Af1=0.419001
Af2=0.712999
24.4
24.6
24.8
25.0
25.2
25.4
P=0.54279546
<MF1>=25.8660
COL=0.928999
25.4
25.6
25.8
26.0
26.2
0.0
0.5
1.0
1.5
2.0

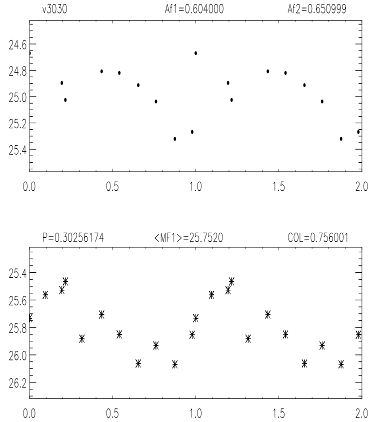
v3030
Af1=0.604000
Af2=0.650999
24.6
24.8
25.0
25.2
25.4
P=0.30256174
<MF1>=25.7520
COL=0.756001
25.4
25.6
25.8
26.0
26.2
0.0
0.5
1.0
1.5
2.0

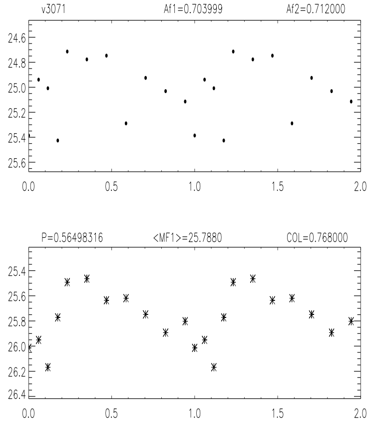
v3071
Af1=0.703999
Af2=0.712000
24.6
24.8
25.0
25.2
25.4
25.6
P=0.56498316
<MF1>=25.7880
COL=0.768000
25.4
25.6
25.8
26.0
26.2
26.4
0.0
0.5
1.0
1.5
2.0

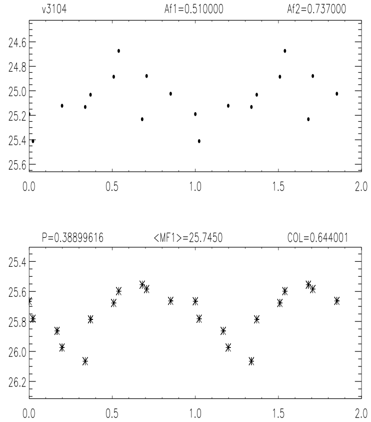
v3104
Af1=0.510000
Af2=0.737000
24.6
24.8
25.0
25.2
25.4
25.6
P=0.38899616
<MF1>=25.7450
COL=0.644001
25.4
25.6
25.8
26.0
26.2
0.0
0.5
1.0
1.5
2.0

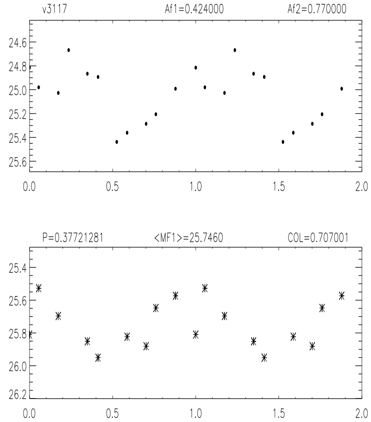
v3117
Af1=0.424000
Af2=0.770000
24.6
24.8
25.0
25.2
25.4
25.6
P=0.37721281
<MF1>=25.7460
COL=0.707001
25.4
25.6
25.8
26.0
26.2
0.0
0.5
1.0
1.5
2.0

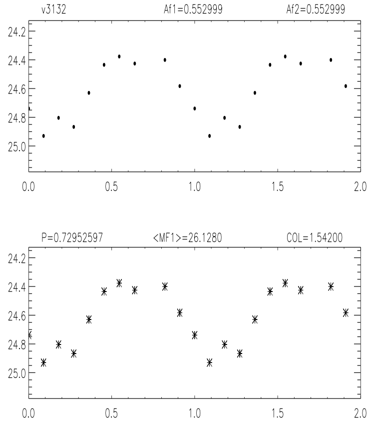
v3132
Af1=0.552999
Af2=0.552999
24.2
24.4
24.6
24.8
25.0
P=0.72952597
<MF1>=26.1280
COL=1.54200
0.0
0.5
1.0
1.5
2.0

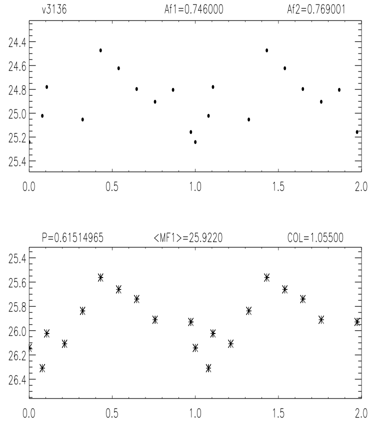
v3136
Af1=0.746000
Af2=0.769001
24.4
24.6
24.8
25.0
25.2
25.4
P=0.61514965
<MF1>=25.9220
COL=1.05500
25.4
25.6
25.8
26.0
26.2
26.4
0.0
0.5
1.0
1.5
2.0

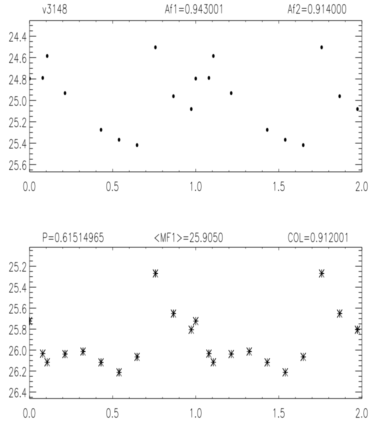
v3148
Af1=0.943001
Af2=0.914000
24.4
24.6
24.8
25.0
25.2
25.4
25.6
P=0.61514965
<MF1>=25.9050
COL=0.912001
25.2
25.4
25.6
25.8
26.0
26.2
26.4
0.0
0.5
1.0
1.5
2.0

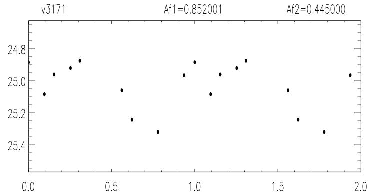
v3171
Af1=0.852001
Af2=0.445000
24.8
25.0
25.2
25.4
0.0
0.5
1.0
1.5
2.0

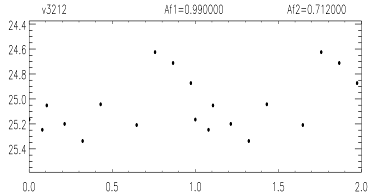
v3212
Af1=0.990000
Af2=0.712000
24.4
24.6
24.8
25.0
25.2
25.4
0.0
0.5
1.0
1.5
2.0

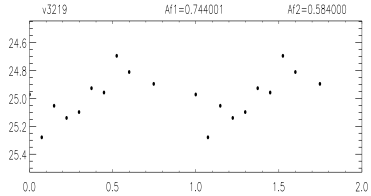
v3219
Af1=0.744001
Af2=0.584000
24.6
24.8
25.0
25.2
25.4
0.0
0.5
1.0
1.5
2.0

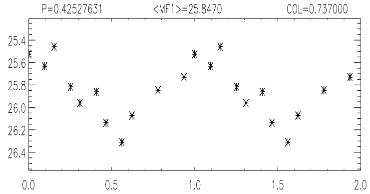
P=0.42527631
<MF1>=25.8470
COL=0.737000
25.4
25.6
25.8
26.0
26.2
26.4
0.0
0.5
1.0
1.5
2.0

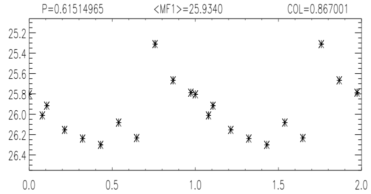
P=0.61514965
<MF1>=25.9340
COL=0.867001
25.2
25.4
25.6
25.8
26.0
26.2
26.4
0.0
0.5
1.0
1.5
2.0

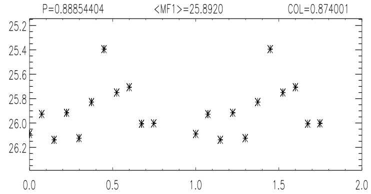
P=0.88854404
<MF1>=25.8920
COL=0.874001
25.2
25.4
25.6
25.8
26.0
26.2
0.0
0.5
1.0
1.5
2.0

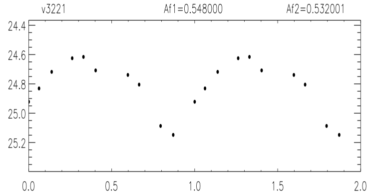
v3221
Af1=0.548000
Af2=0.532001
24.4
24.6
24.8
25.0
25.2
0.0
0.5
1.0
1.5
2.0

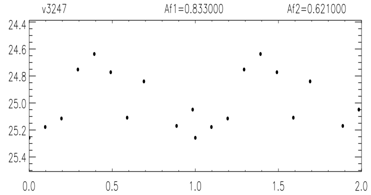
v3247
Af1=0.833000
Af2=0.621000
24.4
24.6
24.8
25.0
25.2
25.4
0.0
0.5
1.0
1.5
2.0

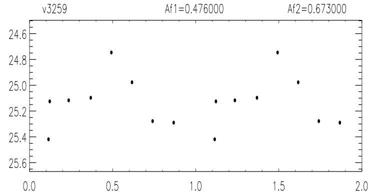
v3259
Af1=0.476000
Af2=0.673000
24.6
24.8
25.0
25.2
25.4
25.6
0.0
0.5
1.0
1.5
2.0

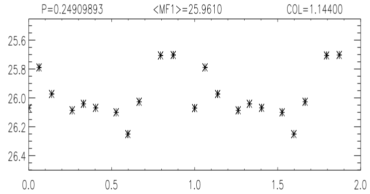
P=0.24909893
<MF1>=25.9610
COL=1.14400
25.6
25.8
26.0
26.2
26.4
0.0
0.5
1.0
1.5
2.0

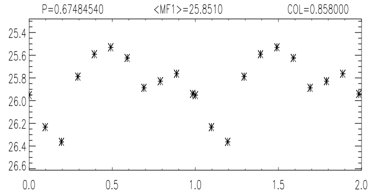
P=0.67484540
<MF1>=25.8510
COL=0.858000
25.4
25.6
25.8
26.0
26.2
26.4
26.6
0.0
0.5
1.0
1.5
2.0

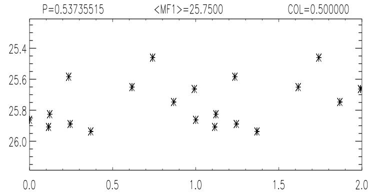
P=0.53735515
<MF1>=25.7500
COL=0.500000
25.4
25.6
25.8
26.0
0.0
0.5
1.0
1.5
2.0

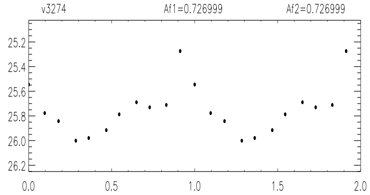
v3274
Af1=0.726999
Af2=0.726999
25.2
25.4
25.6
25.8
26.0
26.2
0.0
0.5
1.0
1.5
2.0

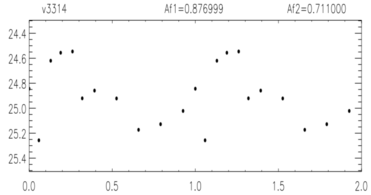
v3314
Af1=0.876999
Af2=0.711000
24.4
24.6
24.8
25.0
25.2
25.4
0.0
0.5
1.0
1.5
2.0

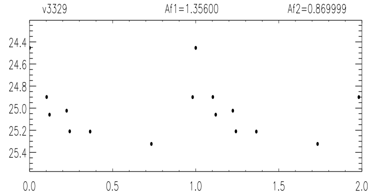
v3329
Af1=1.35600
Af2=0.869999
24.4
24.6
24.8
25.0
25.2
25.4
0.0
0.5
1.0
1.5
2.0

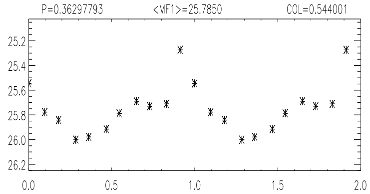
P=0.36297793
<MF1>=25.7850
COL=0.544001
25.2
25.4
25.6
25.8
26.0
26.2
0.0
0.5
1.0
1.5
2.0

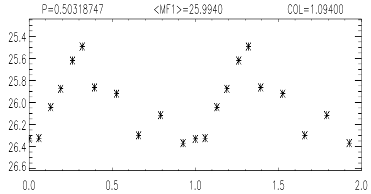
P=0.50318747
<MF1>=25.9940
COL=1.09400
25.4
25.6
25.8
26.0
26.2
26.4
26.6
0.0
0.5
1.0
1.5
2.0

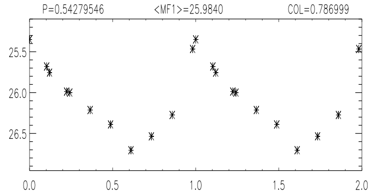
P=0.54279546
<MF1>=25.9840
COL=0.786999
25.5
26.0
26.5
0.0
0.5
1.0
1.5
2.0

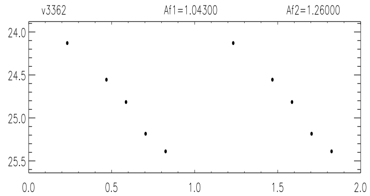
v3362
Af1=1.04300
Af2=1.26000
24.0
24.5
25.0
25.5
0.0
0.5
1.0
1.5
2.0

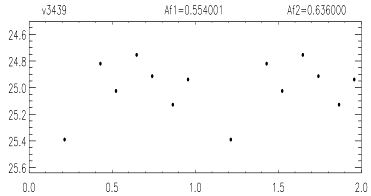
v3439
Af1=0.554001
Af2=0.636000
24.6
24.8
25.0
25.2
25.4
25.6
0.0
0.5
1.0
1.5
2.0

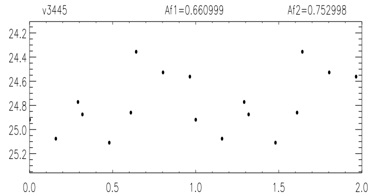
v3445
Af1=0.660999
Af2=0.752998
24.2
24.4
24.6
24.8
25.0
25.2
0.0
0.5
1.0
1.5
2.0

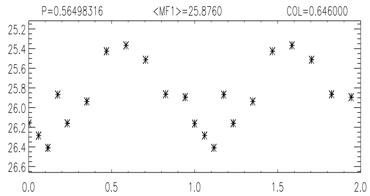
P=0.56498316
<MF1>=25.8760
COL=0.646000
25.2
25.4
25.6
25.8
26.0
26.2
26.4
26.6
0.0
0.5
1.0
1.5
2.0

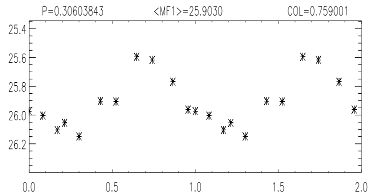
P=0.30603843
<MF1>=25.9030
COL=0.759001
25.4
25.6
25.8
26.0
26.2
0.0
0.5
1.0
1.5
2.0

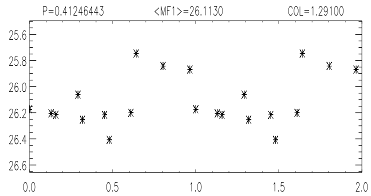
P=0.41246443
<MF1>=26.1130
COL=1.29100
25.6
25.8
26.0
26.2
26.4
26.6
0.0
0.5
1.0
1.5
2.0

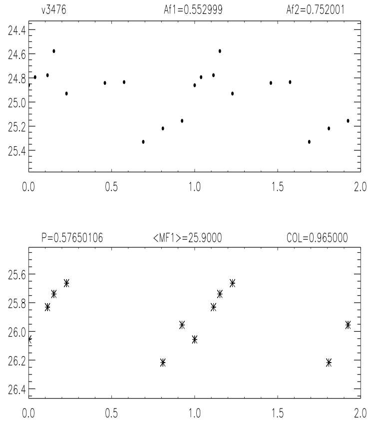
v3476 Af1=0.552999 Af2=0.752001
P=0.57650106 <MF1>=25.9000 COL=0.965000

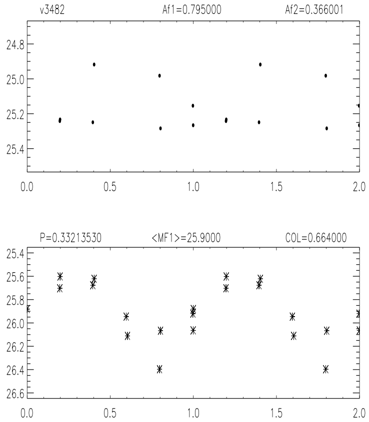
v3482 Af1=0.795000 Af2=0.366001
P=0.33213530 <MF1>=25.9000 COL=0.664000

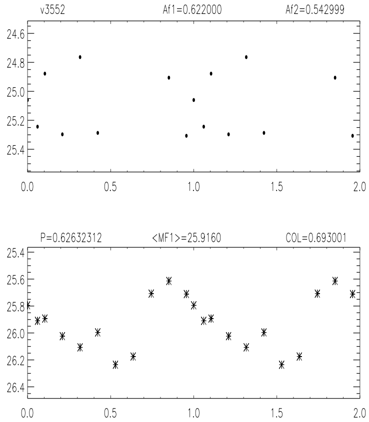
v3552 Af1=0.622000 Af2=0.542999
P=0.62632312 <MF1>=25.9160 COL=0.693001

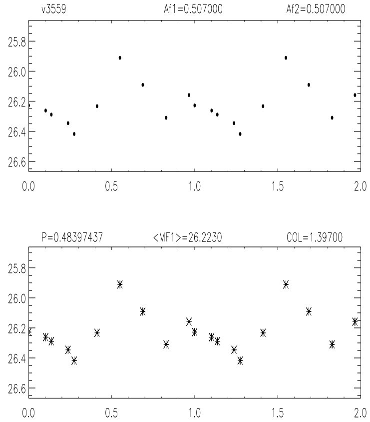
v3559 Af1=0.507000 Af2=0.507000
P=0.48397437 <MF1>=26.2230 COL=1.39700

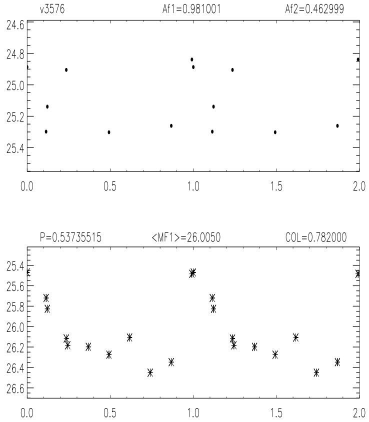
v3576 Af1=0.981001 Af2=0.462999
P=0.53735515 <MF1>=26.0050 COL=0.782000

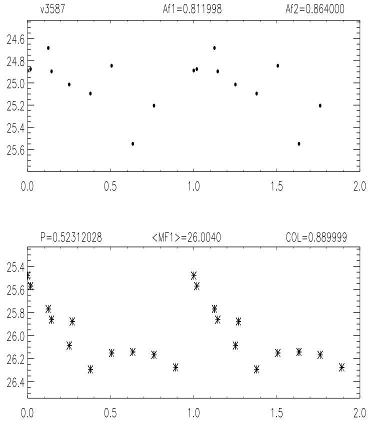
v3587 Af1=0.811998 Af2=0.864000
P=0.52312028 <MF1>=26.0040 COL=0.889999

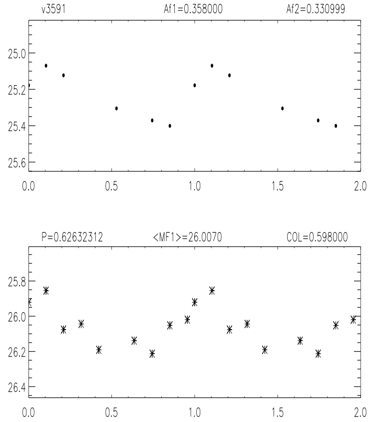
v3591 Af1=0.358000 Af2=0.330999
P=0.62632312 <MF1>=26.0070 COL=0.598000

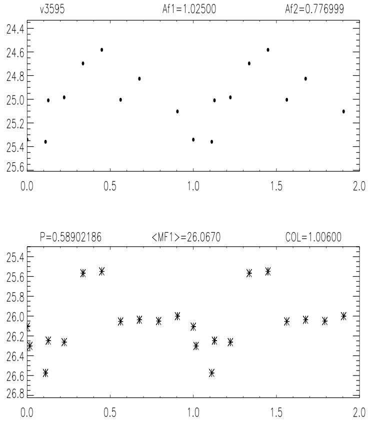
v3595 Af1=1.02500 Af2=0.776999
P=0.58902186 <MF1>=26.0670 COL=1.00600

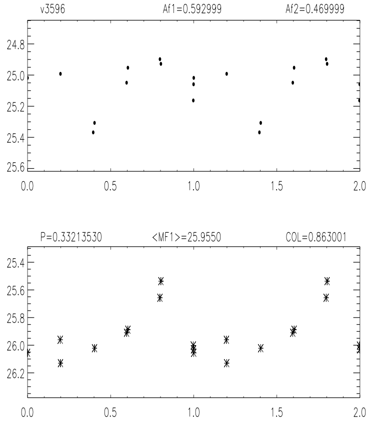
v3596 Af1=0.592999 Af2=0.469999
P=0.33213530 <MF1>=25.9550 COL=0.863001

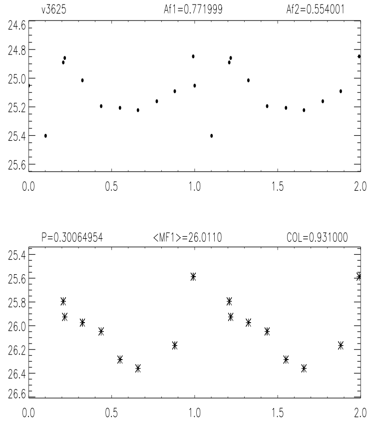
v3625 Af1=0.771999 Af2=0.554001
P=0.30064954 <MF1>=26.0110 COL=0.931000

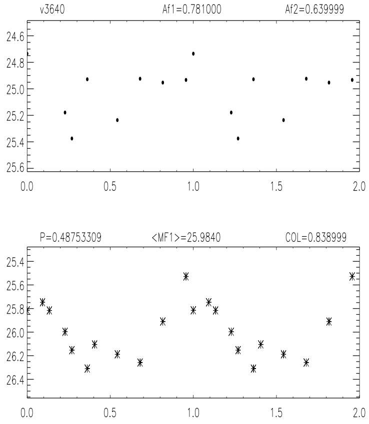
v3640 Af1=0.781000 Af2=0.639999
P=0.48753309 <MF1>=25.9840 COL=0.838999

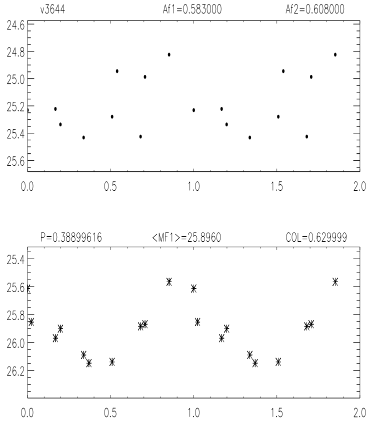
v3644 Af1=0.583000 Af2=0.608000
P=0.38899616 <MF1>=25.8960 COL=0.629999

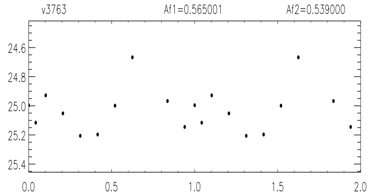
v3763
Af1=0.565001
Af2=0.539000
24.6
24.8
25.0
25.2
25.4
0.0
0.5
1.0
1.5
2.0

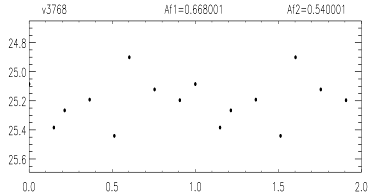
v3768
Af1=0.668001
Af2=0.540001
24.8
25.0
25.2
25.4
25.6
0.0
0.5
1.0
1.5
2.0

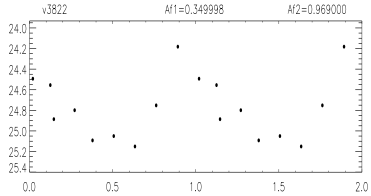
v3822
Af1=0.349998
Af2=0.969000
24.0
24.2
24.4
24.6
24.8
25.0
25.2
25.4
0.0
0.5
1.0
1.5
2.0

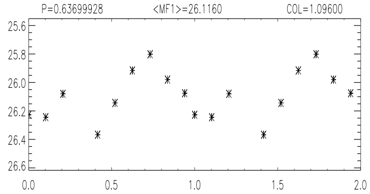
P=0.63699928
<MF1>=26.1160
COL=1.09600
25.6
25.8
26.0
26.2
26.4
26.6
0.0
0.5
1.0
1.5
2.0

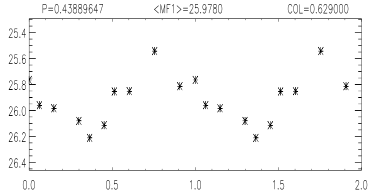
P=0.43889647
<MF1>=25.9780
COL=0.629000
25.4
25.6
25.8
26.0
26.2
26.4
0.0
0.5
1.0
1.5
2.0

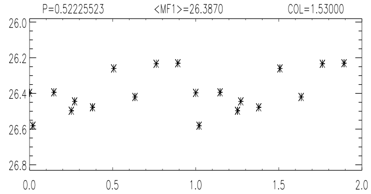
P=0.52225523
<MF1>=26.3870
COL=1.53000
26.0
26.2
26.4
26.6
26.8
0.0
0.5
1.0
1.5
2.0

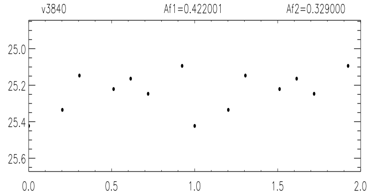
v3840
Af1=0.422001
Af2=0.329000
25.0
25.2
25.4
25.6
0.0
0.5
1.0
1.5
2.0

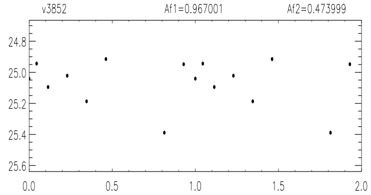
v3852
Af1=0.967001
Af2=0.473999
24.8
25.0
25.2
25.4
25.6
0.0
0.5
1.0
1.5
2.0

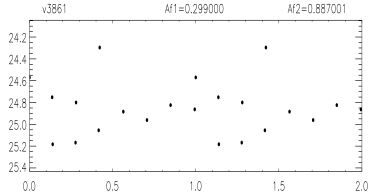
v3861
Af1=0.299000
Af2=0.887001
24.2
24.4
24.6
24.8
25.0
25.2
25.4
0.0
0.5
1.0
1.5
2.0

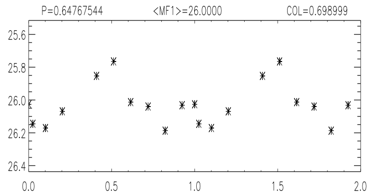
P=0.64767544
<MF1>=26.0000
COL=0.698999
25.6
25.8
26.0
26.2
26.4
0.0
0.5
1.0
1.5
2.0

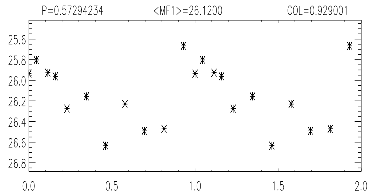
P=0.57294234
<MF1>=26.1200
COL=0.929001
25.6
25.8
26.0
26.2
26.4
26.6
26.8
0.0
0.5
1.0
1.5
2.0

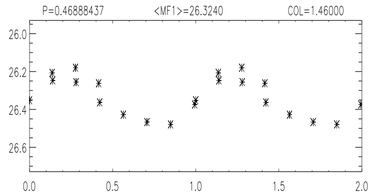
P=0.46888437
<MF1>=26.3240
COL=1.46000
26.0
26.2
26.4
26.6
0.0
0.5
1.0
1.5
2.0

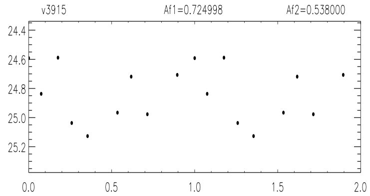
v3915
Af1=0.724998
Af2=0.538000
24.4
24.6
24.8
25.0
25.2
0.0
0.5
1.0
1.5
2.0

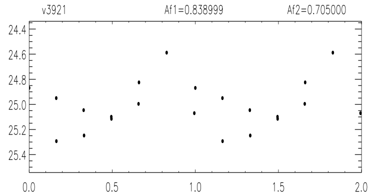
v3921
Af1=0.838999
Af2=0.705000
24.4
24.6
24.8
25.0
25.2
25.4
0.0
0.5
1.0
1.5
2.0

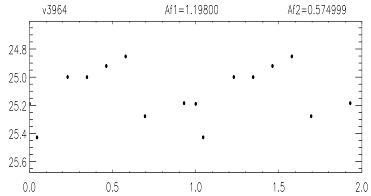
v3964
Af1=1.19800
Af2=0.574999
24.8
25.0
25.2
25.4
25.6
0.0
0.5
1.0
1.5
2.0

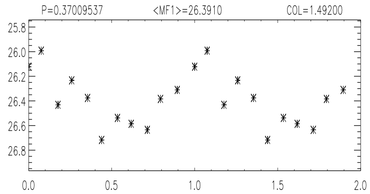
P=0.37009537
<MF1>=26.3910
COL=1.49200
25.8
26.0
26.2
26.4
26.6
26.8
0.0
0.5
1.0
1.5
2.0

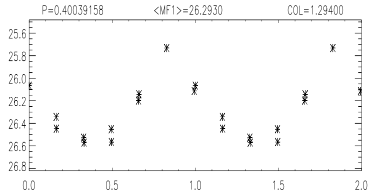
P=0.40039158
<MF1>=26.2930
COL=1.29400
25.6
25.8
26.0
26.2
26.4
26.6
26.8
0.0
0.5
1.0
1.5
2.0

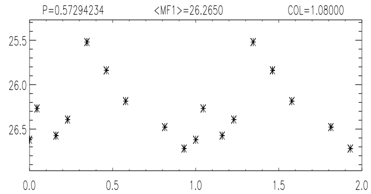
P=0.57294234
<MF1>=26.2650
COL=1.08000
25.5
26.0
26.5
0.0
0.5
1.0
1.5
2.0

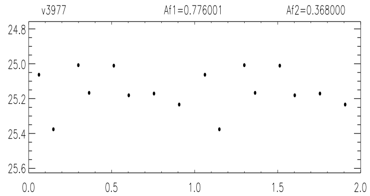
v3977
Af1=0.776001
Af2=0.368000
24.8
25.0
25.2
25.4
25.6
0.0
0.5
1.0
1.5
2.0

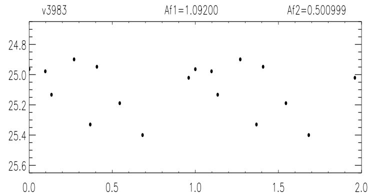
v3983
Af1=1.09200
Af2=0.500999
24.8
25.0
25.2
25.4
25.6
0.0
0.5
1.0
1.5
2.0

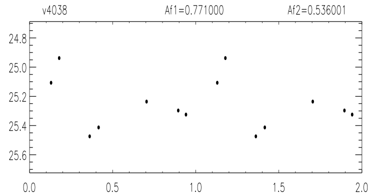
v4038
Af1=0.771000
Af2=0.536001
24.8
25.0
25.2
25.4
25.6
0.0
0.5
1.0
1.5
2.0

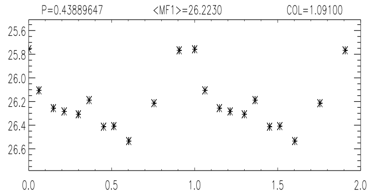
P=0.43889647
<MF1>=26.2230
COL=1.09100
25.6
25.8
26.0
26.2
26.4
26.6
0.0
0.5
1.0
1.5
2.0

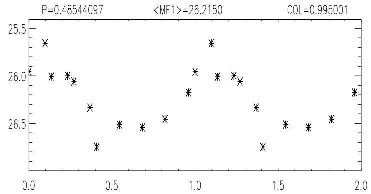
P=0.48544097
<MF1>=26.2150
COL=0.995001
25.5
26.0
26.5
0.0
0.5
1.0
1.5
2.0

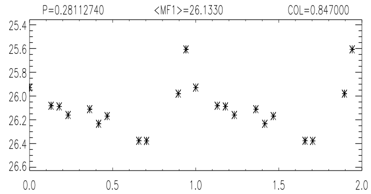
P=0.28112740
<MF1>=26.1330
COL=0.847000
25.4
25.6
25.8
26.0
26.2
26.4
26.6
0.0
0.5
1.0
1.5
2.0

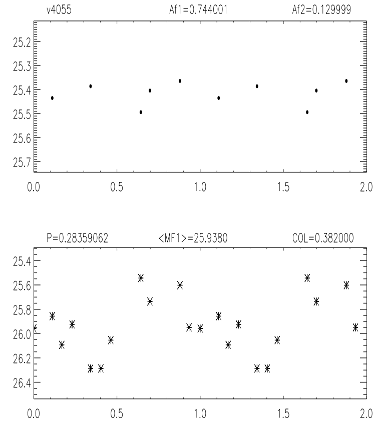
v4055
Af1=0.744001
Af2=0.129999
25.2
25.3
25.4
25.5
25.6
25.7
P=0.28359062
<MF1>=25.9380
COL=0.382000
25.4
25.6
25.8
26.0
26.2
26.4
0.0
0.5
1.0
1.5
2.0

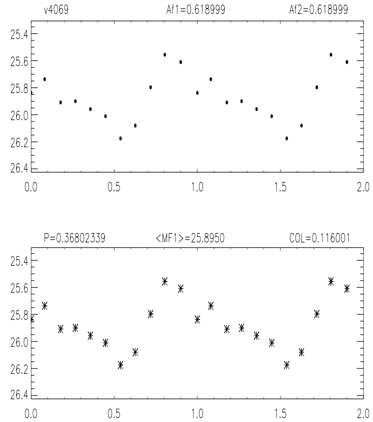
v4069
Af1=0.618999
Af2=0.618999
25.4
25.6
25.8
26.0
26.2
26.4
P=0.36802339
<MF1>=25.8950
COL=0.116001
0.0
0.5
1.0
1.5
2.0

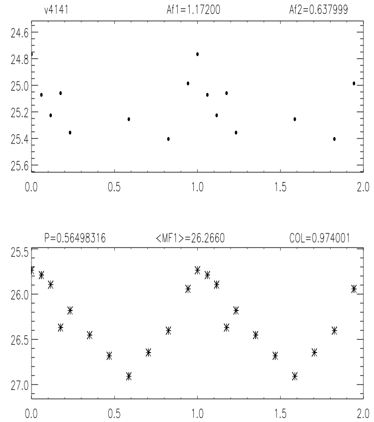
v4141
Af1=1.17200
Af2=0.637999
24.6
24.8
25.0
25.2
25.4
25.6
P=0.56498316
<MF1>=26.2660
COL=0.974001
25.5
26.0
26.5
27.0
0.0
0.5
1.0
1.5
2.0

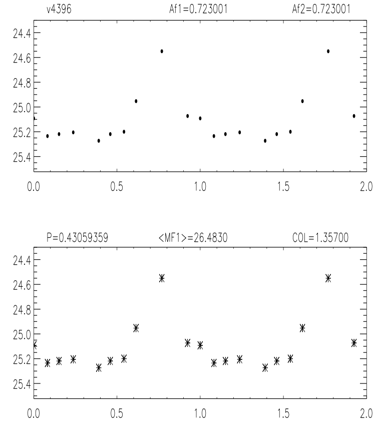
v4396
Af1=0.723001
Af2=0.723001
24.4
24.6
24.8
25.0
25.2
25.4
P=0.43059359
<MF1>=26.4830
COL=1.35700
0.0
0.5
1.0
1.5
2.0

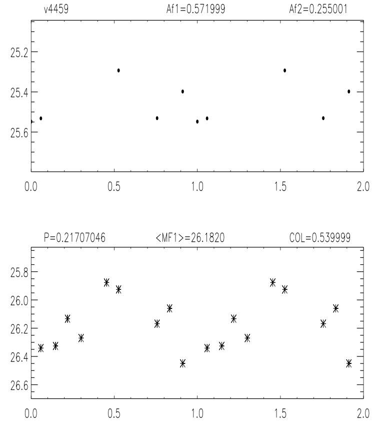
v4459
Af1=0.571999
Af2=0.255001
25.2
25.4
25.6
P=0.21707046
<MF1>=26.1820
COL=0.539999
25.8
26.0
26.2
26.4
26.6
0.0
0.5
1.0
1.5
2.0

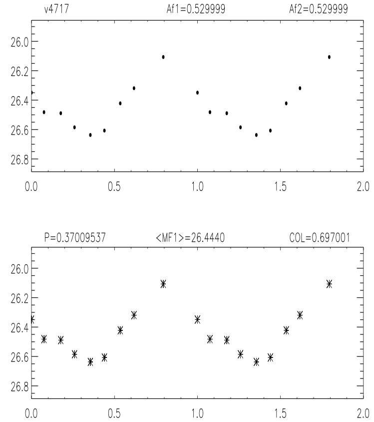
v4717
Af1=0.529999
Af2=0.529999
26.0
26.2
26.4
26.6
26.8
P=0.37009537
<MF1>=26.4440
COL=0.697001
0.0
0.5
1.0
1.5
2.0

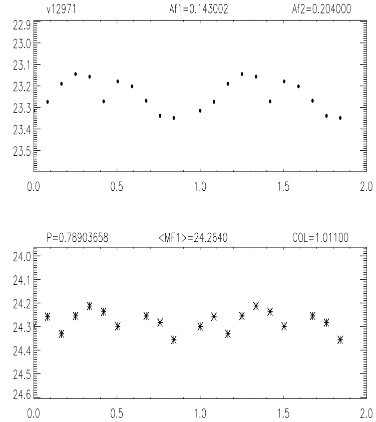
v12971
Af1=0.143002
Af2=0.204000
22.9
23.0
23.1
23.2
23.3
23.4
23.5
P=0.78903658
<MF1>=24.2640
COL=1.01100
24.0
24.1
24.2
24.3
24.4
24.5
24.6
0.0
0.5
1.0
1.5
2.0

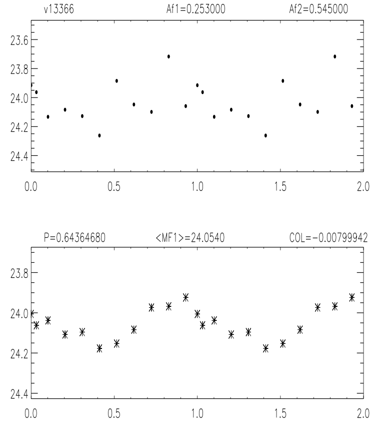
v13366
Af1=0.253000
Af2=0.545000
23.6
23.8
24.0
24.2
24.4
P=0.64364680
<MF1>=24.0540
COL=-0.00799942
0.0
0.5
1.0
1.5
2.0

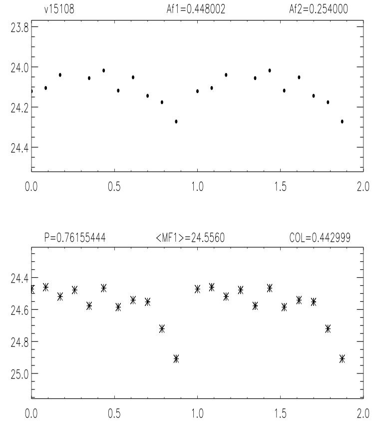
v15108
Af1=0.448002
Af2=0.254000
23.8
24.0
24.2
24.4
P=0.76155444
<MF1>=24.5560
COL=0.442999
24.4
24.6
24.8
25.0
0.0
0.5
1.0
1.5
2.0

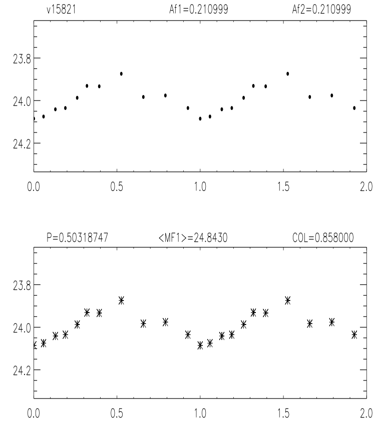
v15821
Af1=0.210999
Af2=0.210999
23.8
24.0
24.2
P=0.50318747
<MF1>=24.8430
COL=0.858000
0.0
0.5
1.0
1.5
2.0

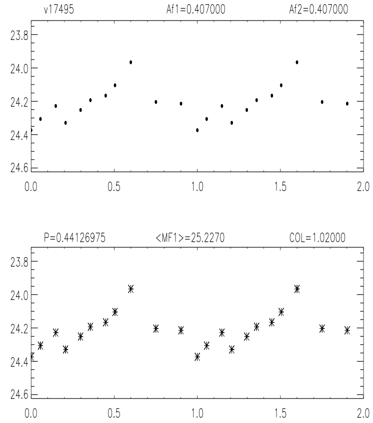
v17495
Af1=0.407000
Af2=0.407000
23.8
24.0
24.2
24.4
24.6
P=0.44126975
<MF1>=25.2270
COL=1.02000
0.0
0.5
1.0
1.5
2.0

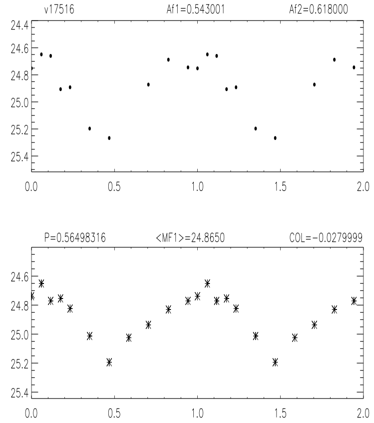
v17516
Af1=0.543001
Af2=0.618000
24.4
24.6
24.8
25.0
25.2
25.4
P=0.56498316
<MF1>=24.8650
COL=-0.0279999
0.0
0.5
1.0
1.5
2.0

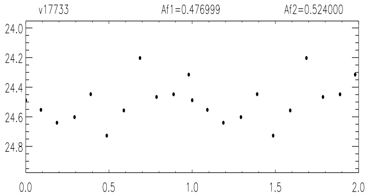
v17733 Af1=0.476999 Af2=0.524000
24.0
24.2
24.4
24.6
24.8
0.0
0.5
1.0
1.5
2.0

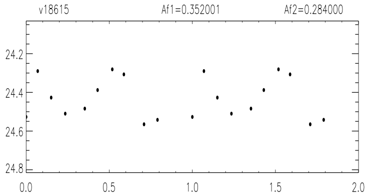
v18615 Af1=0.352001 Af2=0.284000
24.2
24.4
24.6
24.8
0.0
0.5
1.0
1.5
2.0

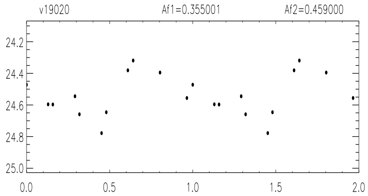
v19020 Af1=0.355001 Af2=0.459000
24.2
24.4
24.6
24.8
25.0
0.0
0.5
1.0
1.5
2.0

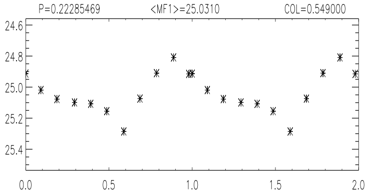
P=0.22285469 <MF1>=25.0310 COL=0.549000
24.6
24.8
25.0
25.2
25.4
0.0
0.5
1.0
1.5
2.0

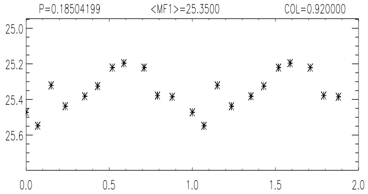
P=0.18504199 <MF1>=25.3500 COL=0.920000
25.0
25.2
25.4
25.6
0.0
0.5
1.0
1.5
2.0

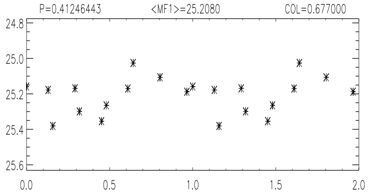
P=0.41246443 <MF1>=25.2080 COL=0.677000
24.8
25.0
25.2
25.4
25.6
0.0
0.5
1.0
1.5
2.0

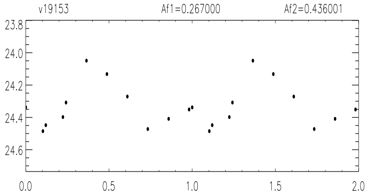
v19153 Af1=0.267000 Af2=0.436001
23.8
24.0
24.2
24.4
24.6
0.0
0.5
1.0
1.5
2.0

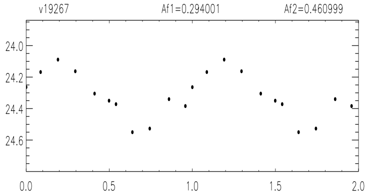
v19267 Af1=0.294001 Af2=0.460999
24.0
24.2
24.4
24.6
0.0
0.5
1.0
1.5
2.0

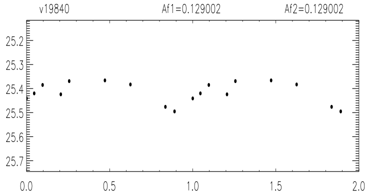
v19840 Af1=0.129002 Af2=0.129002
25.2
25.3
25.4
25.5
25.6
25.7
0.0
0.5
1.0
1.5
2.0

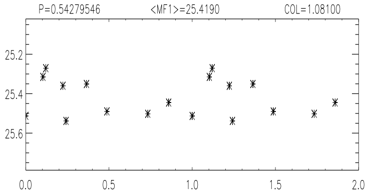
P=0.54279546 <MF1>=25.4190 COL=1.08100
25.2
25.4
25.6
0.0
0.5
1.0
1.5
2.0

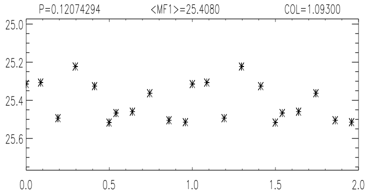
P=0.12074294 <MF1>=25.4080 COL=1.09300
25.0
25.2
25.4
25.6
0.0
0.5
1.0
1.5
2.0

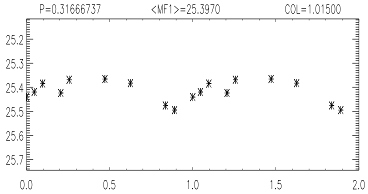
P=0.31666737 <MF1>=25.3970 COL=1.01500
25.2
25.3
25.4
25.5
25.6
25.7
0.0
0.5
1.0
1.5
2.0

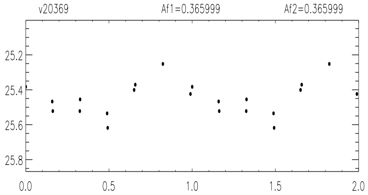
v20369 Af1=0.365999 Af2=0.365999
25.2
25.4
25.6
25.8
0.0
0.5
1.0
1.5
2.0

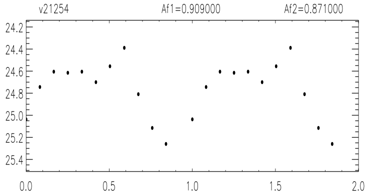
v21254 Af1=0.909000 Af2=0.871000
24.2
24.4
24.6
24.8
25.0
25.2
25.4
0.0
0.5
1.0
1.5
2.0

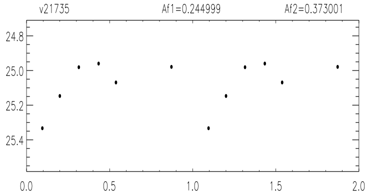
v21735 Af1=0.244999 Af2=0.373001
24.8
25.0
25.2
25.4
0.0
0.5
1.0
1.5
2.0

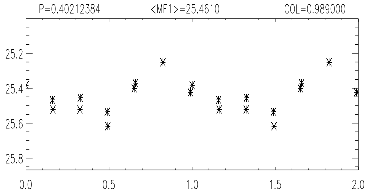
P=0.40212384 <MF1>=25.4610 COL=0.989000
25.2
25.4
25.6
25.8
0.0
0.5
1.0
1.5
2.0

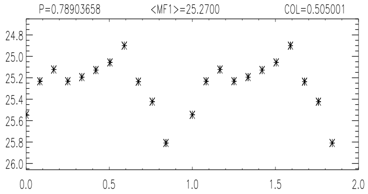
P=0.78903658 <MF1>=25.2700 COL=0.505001
24.8
25.0
25.2
25.4
25.6
25.8
26.0
0.0
0.5
1.0
1.5
2.0

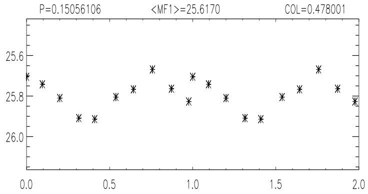
P=0.15056106 <MF1>=25.6170 COL=0.478001
25.6
25.8
26.0
0.0
0.5
1.0
1.5
2.0

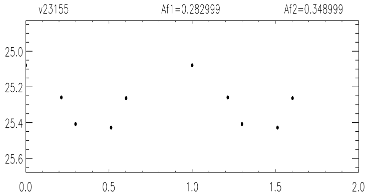
v23155 Af1=0.282999 Af2=0.348999
25.0
25.2
25.4
25.6
0.0
0.5
1.0
1.5
2.0

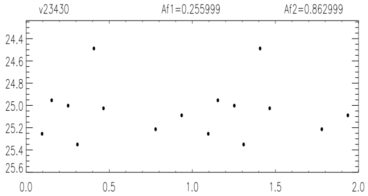
v23430 Af1=0.255999 Af2=0.862999
24.4
24.6
24.8
25.0
25.2
25.4
25.6
0.0
0.5
1.0
1.5
2.0

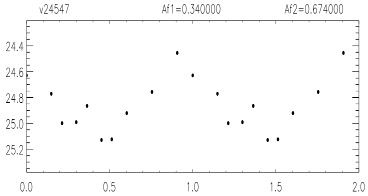
v24547 Af1=0.340000 Af2=0.674000
24.4
24.6
24.8
25.0
25.2
0.0
0.5
1.0
1.5
2.0

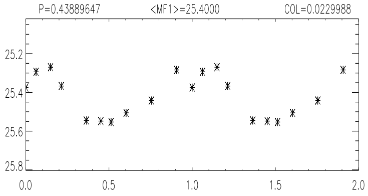
P=0.43889647 <MF1>=25.4000 COL=0.0229988
25.2
25.4
25.6
25.8
0.0
0.5
1.0
1.5
2.0

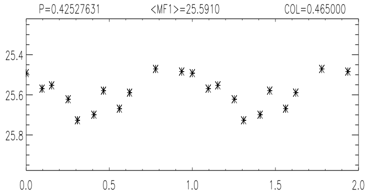
P=0.42527631 <MF1>=25.5910 COL=0.465000
25.4
25.6
25.8
0.0
0.5
1.0
1.5
2.0

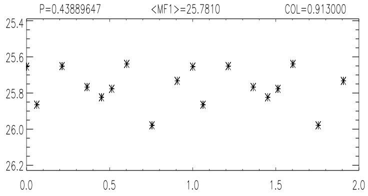
P=0.43889647 <MF1>=25.7810 COL=0.913000
25.4
25.6
25.8
26.0
26.2
0.0
0.5
1.0
1.5
2.0

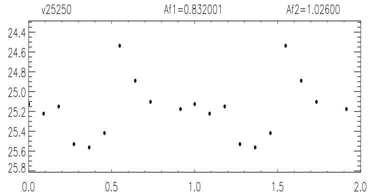
v25250
Af1=0.832001
Af2=1.02600
24.4
24.6
24.8
25.0
25.2
25.4
25.6
25.8
0.0
0.5
1.0
1.5
2.0

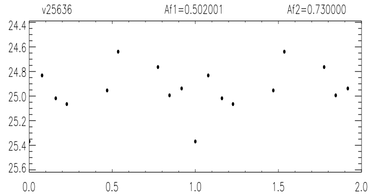
v25636
Af1=0.502001
Af2=0.730000
24.4
24.6
24.8
25.0
25.2
25.4
25.6
0.0
0.5
1.0
1.5
2.0

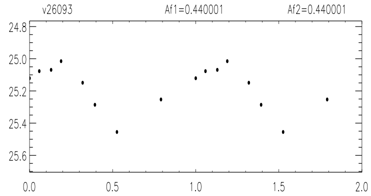
v26093
Af1=0.440001
Af2=0.440001
24.8
25.0
25.2
25.4
25.6
0.0
0.5
1.0
1.5
2.0

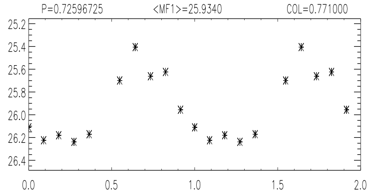
P=0.72596725
<MF1>=25.9340
COL=0.771000
25.2
25.4
25.6
25.8
26.0
26.2
26.4
0.0
0.5
1.0
1.5
2.0

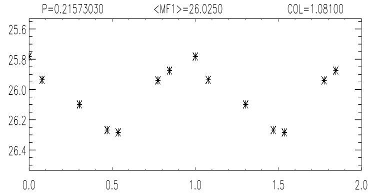
P=0.21573030
<MF1>=26.0250
COL=1.08100
25.6
25.8
26.0
26.2
26.4
0.0
0.5
1.0
1.5
2.0

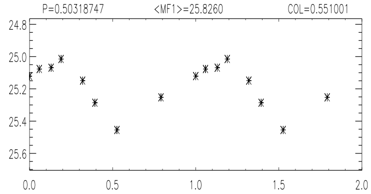
P=0.50318747
<MF1>=25.8260
COL=0.551001
24.8
25.0
25.2
25.4
25.6
0.0
0.5
1.0
1.5
2.0

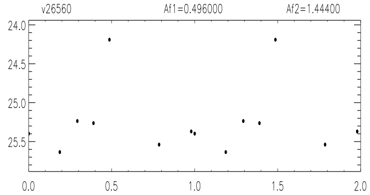
v26560
Af1=0.496000
Af2=1.44400
24.0
24.5
25.0
25.5
0.0
0.5
1.0
1.5
2.0

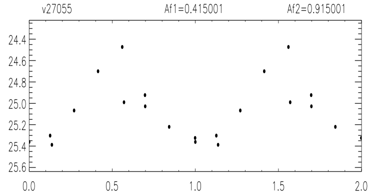
v27055
Af1=0.415001
Af2=0.915001
24.4
24.6
24.8
25.0
25.2
25.4
25.6
0.0
0.5
1.0
1.5
2.0

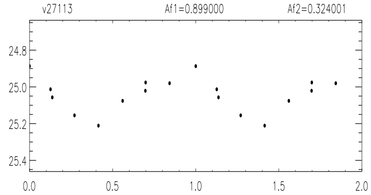
v27113
Af1=0.899000
Af2=0.324001
24.8
25.0
25.2
25.4
0.0
0.5
1.0
1.5
2.0

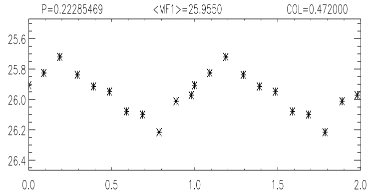
P=0.22285469
<MF1>=25.9550
COL=0.472000
25.6
25.8
26.0
26.2
26.4
0.0
0.5
1.0
1.5
2.0

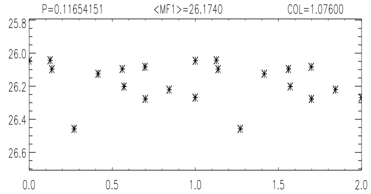
P=0.11654151
<MF1>=26.1740
COL=1.07600
25.8
26.0
26.2
26.4
26.6
0.0
0.5
1.0
1.5
2.0

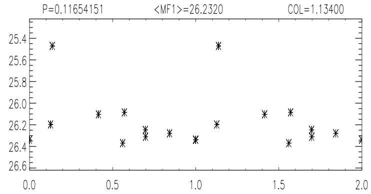
P=0.11654151
<MF1>=26.2320
COL=1.13400
25.4
25.6
25.8
26.0
26.2
26.4
26.6
0.0
0.5
1.0
1.5
2.0

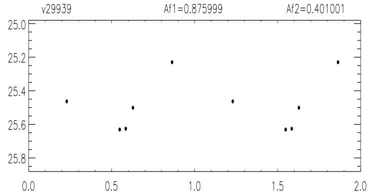
v29939
Af1=0.875999
Af2=0.401001
25.0
25.2
25.4
25.6
25.8
0.0
0.5
1.0
1.5
2.0

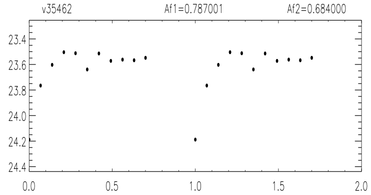
v35462
Af1=0.787001
Af2=0.684000
23.4
23.6
23.8
24.0
24.2
24.4
0.0
0.5
1.0
1.5
2.0

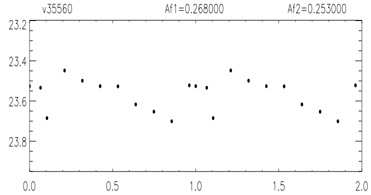
v35560
Af1=0.268000
Af2=0.253000
23.2
23.4
23.6
23.8
0.0
0.5
1.0
1.5
2.0

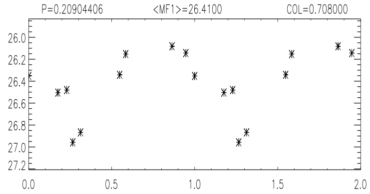
P=0.20904406
<MF1>=26.4100
COL=0.708000
26.0
26.2
26.4
26.6
26.8
27.0
27.2
0.0
0.5
1.0
1.5
2.0

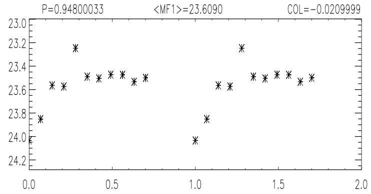
P=0.94800033
<MF1>=23.6090
COL=-0.0209999
23.0
23.2
23.4
23.6
23.8
24.0
24.2
0.0
0.5
1.0
1.5
2.0

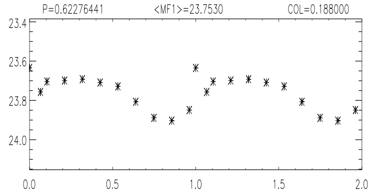
P=0.62276441
<MF1>=23.7530
COL=0.188000
23.4
23.6
23.8
24.0
0.0
0.5
1.0
1.5
2.0

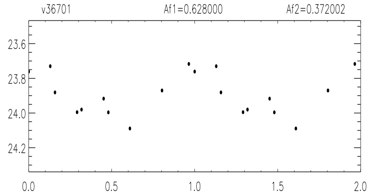
v36701
Af1=0.628000
Af2=0.372002
23.6
23.8
24.0
24.2
0.0
0.5
1.0
1.5
2.0

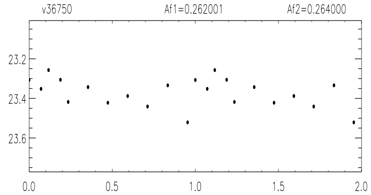
v36750
Af1=0.262001
Af2=0.264000
23.2
23.4
23.6
0.0
0.5
1.0
1.5
2.0

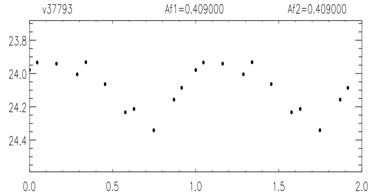
v37793
Af1=0.409000
Af2=0.409000
23.8
24.0
24.2
24.4
0.0
0.5
1.0
1.5
2.0

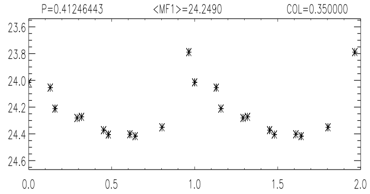
P=0.41246443
<MF1>=24.2490
COL=0.350000
23.6
23.8
24.0
24.2
24.4
24.6
0.0
0.5
1.0
1.5
2.0

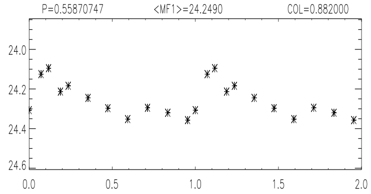
P=0.55870747
<MF1>=24.2490
COL=0.882000
24.0
24.2
24.4
24.6
0.0
0.5
1.0
1.5
2.0

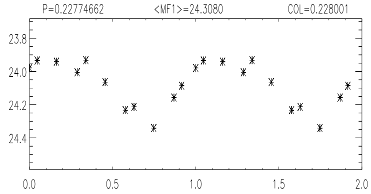
P=0.22774662
<MF1>=24.3080
COL=0.228001
23.8
24.0
24.2
24.4
0.0
0.5
1.0
1.5
2.0

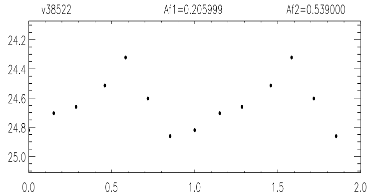
v38522
Af1=0.205999
Af2=0.539000
24.2
24.4
24.6
24.8
25.0
0.0
0.5
1.0
1.5
2.0

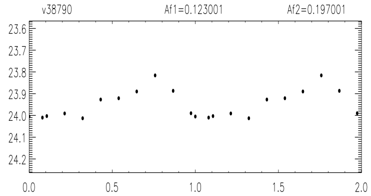
v38790
Af1=0.123001
Af2=0.197001
23.6
23.7
23.8
23.9
24.0
24.1
24.2
0.0
0.5
1.0
1.5
2.0

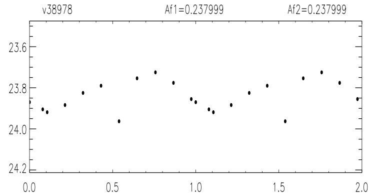
v38978
Af1=0.237999
Af2=0.237999
23.6
23.8
24.0
24.2
0.0
0.5
1.0
1.5
2.0

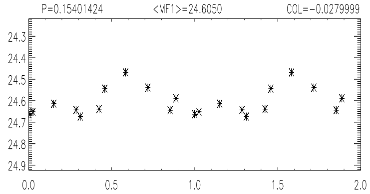
P=0.15401424
<MF1>=24.6050
COL=-0.0279999
24.3
24.4
24.5
24.6
24.7
24.8
24.9
0.0
0.5
1.0
1.5
2.0

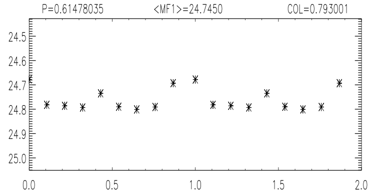
P=0.61478035
<MF1>=24.7450
COL=0.793001
24.5
24.6
24.7
24.8
24.9
25.0
0.0
0.5
1.0
1.5
2.0

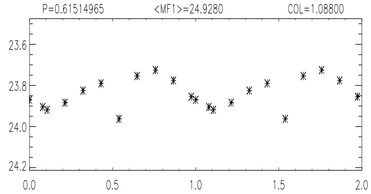
P=0.61514965
<MF1>=24.9280
COL=1.08800
23.6
23.8
24.0
24.2
0.0
0.5
1.0
1.5
2.0

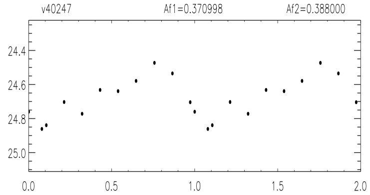
v40247
Af1=0.370998
Af2=0.388000
24.4
24.6
24.8
25.0
0.0
0.5
1.0
1.5
2.0

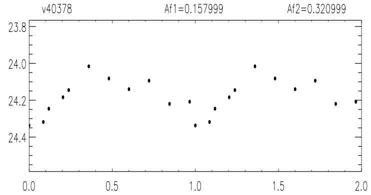
v40378
Af1=0.157999
Af2=0.320999
23.8
24.0
24.2
24.4
0.0
0.5
1.0
1.5
2.0

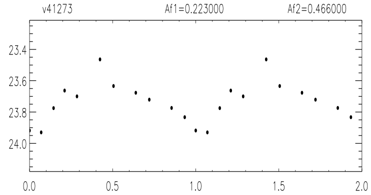
v41273
Af1=0.223000
Af2=0.466000
23.4
23.6
23.8
24.0
0.0
0.5
1.0
1.5
2.0

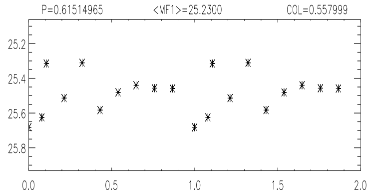
P=0.61514965
<MF1>=25.2300
COL=0.557999
25.2
25.4
25.6
25.8
0.0
0.5
1.0
1.5
2.0

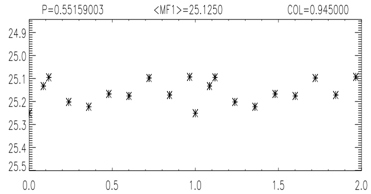
P=0.55159003
<MF1>=25.1250
COL=0.945000
24.9
25.0
25.1
25.2
25.3
25.4
25.5
0.0
0.5
1.0
1.5
2.0

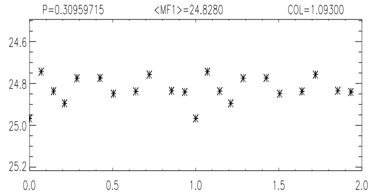
P=0.30959715
<MF1>=24.8280
COL=1.09300
24.6
24.8
25.0
25.2
0.0
0.5
1.0
1.5
2.0

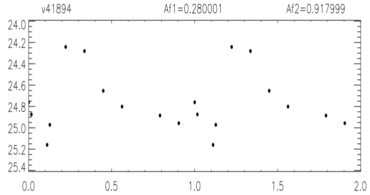
v41894
Af1=0.280001
Af2=0.917999
24.0
24.2
24.4
24.6
24.8
25.0
25.2
25.4
0.0
0.5
1.0
1.5
2.0

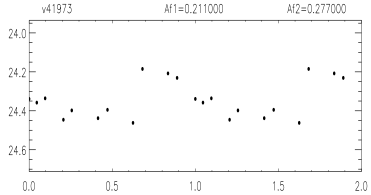
v41973
Af1=0.211000
Af2=0.277000
24.0
24.2
24.4
24.6
0.0
0.5
1.0
1.5
2.0

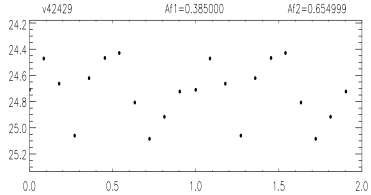
v42429
Af1=0.385000
Af2=0.654999
24.2
24.4
24.6
24.8
25.0
25.2
0.0
0.5
1.0
1.5
2.0

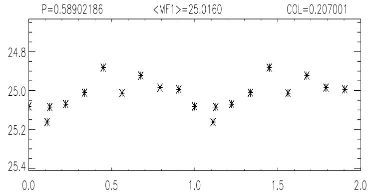
P=0.58902186
<MF1>=25.0160
COL=0.207001
24.8
25.0
25.2
25.4
0.0
0.5
1.0
1.5
2.0

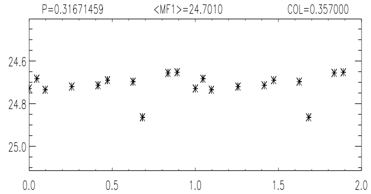
P=0.31671459
<MF1>=24.7010
COL=0.357000
24.6
24.8
25.0
0.0
0.5
1.0
1.5
2.0

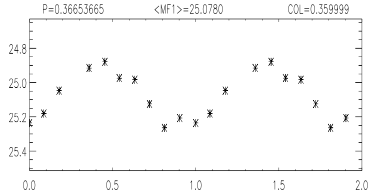
P=0.36653665
<MF1>=25.0780
COL=0.359999
24.8
25.0
25.2
25.4
0.0
0.5
1.0
1.5
2.0

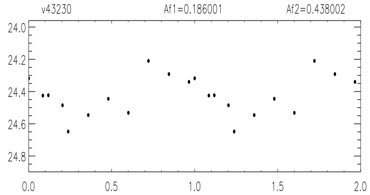
v43230
Af1=0.186001
Af2=0.438002
24.0
24.2
24.4
24.6
24.8
0.0
0.5
1.0
1.5
2.0

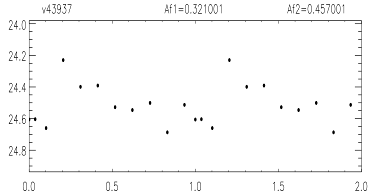
v43937
Af1=0.321001
Af2=0.457001
24.0
24.2
24.4
24.6
24.8
0.0
0.5
1.0
1.5
2.0

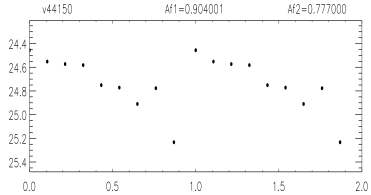
v44150
Af1=0.904001
Af2=0.777000
24.4
24.6
24.8
25.0
25.2
25.4
0.0
0.5
1.0
1.5
2.0

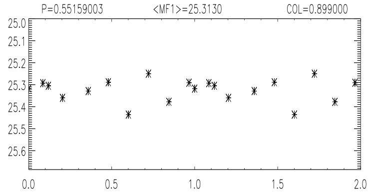
P=0.55159003
<MF1>=25.3130
COL=0.899000
25.0
25.1
25.2
25.3
25.4
25.5
25.6
0.0
0.5
1.0
1.5
2.0

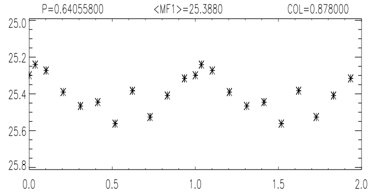
P=0.64055800
<MF1>=25.3880
COL=0.878000
25.0
25.2
25.4
25.6
25.8
0.0
0.5
1.0
1.5
2.0

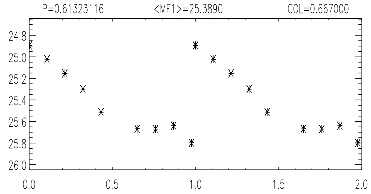
P=0.61323116
<MF1>=25.3890
COL=0.667000
24.8
25.0
25.2
25.4
25.6
25.8
26.0
0.0
0.5
1.0
1.5
2.0

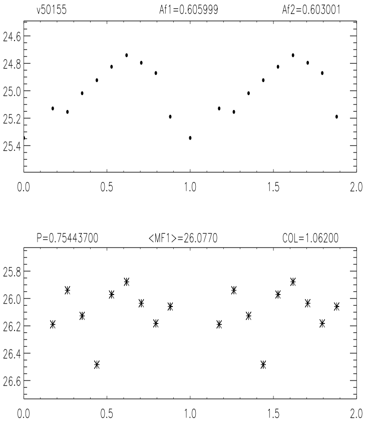
v50155 Af1=0.605999 Af2=0.603001
24.6 24.8 25.0 25.2 25.4
P=0.75443700 <MF1>=26.0770 COL=1.06200
25.8 26.0 26.2 26.4 26.6
0.0 0.5 1.0 1.5 2.0

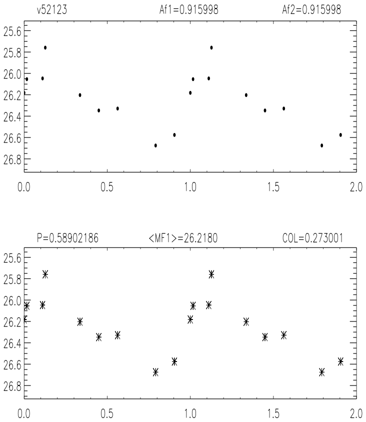
v52123 Af1=0.915998 Af2=0.915998
25.6 25.8 26.0 26.2 26.4 26.6 26.8
P=0.58902186 <MF1>=26.2180 COL=0.273001
25.6 25.8 26.0 26.2 26.4 26.6 26.8
0.0 0.5 1.0 1.5 2.0

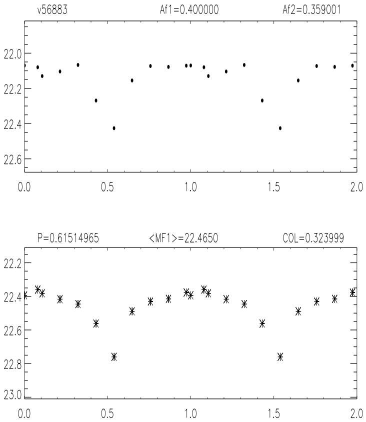
v56883 Af1=0.400000 Af2=0.359001
22.0 22.2 22.4 22.6
P=0.61514965 <MF1>=22.4650 COL=0.323999
22.2 22.4 22.6 22.8 23.0
0.0 0.5 1.0 1.5 2.0

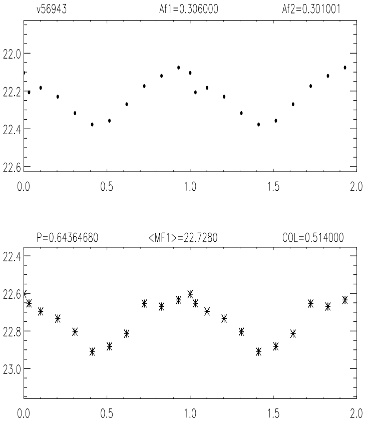
v56943 Af1=0.306000 Af2=0.301001
22.0 22.2 22.4 22.6
P=0.64364680 <MF1>=22.7280 COL=0.514000
22.4 22.6 22.8 23.0
0.0 0.5 1.0 1.5 2.0

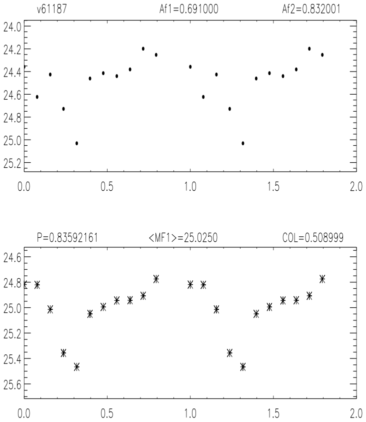
v61187 Af1=0.691000 Af2=0.832001
24.0 24.2 24.4 24.6 24.8 25.0 25.2
P=0.83592161 <MF1>=25.0250 COL=0.508999
24.6 24.8 25.0 25.2 25.4 25.6
0.0 0.5 1.0 1.5 2.0

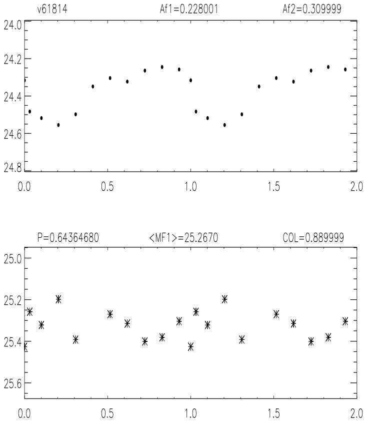
v61814 Af1=0.228001 Af2=0.309999
24.0 24.2 24.4 24.6 24.8
P=0.64364680 <MF1>=25.2670 COL=0.889999
25.0 25.2 25.4 25.6
0.0 0.5 1.0 1.5 2.0

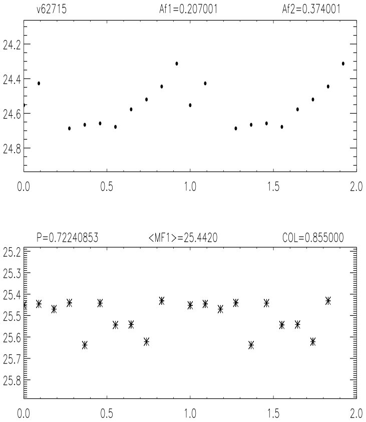
v62715 Af1=0.207001 Af2=0.374001
24.2 24.4 24.6 24.8
P=0.72240853 <MF1>=25.4420 COL=0.855000
25.2 25.3 25.4 25.5 25.6 25.7 25.8
0.0 0.5 1.0 1.5 2.0

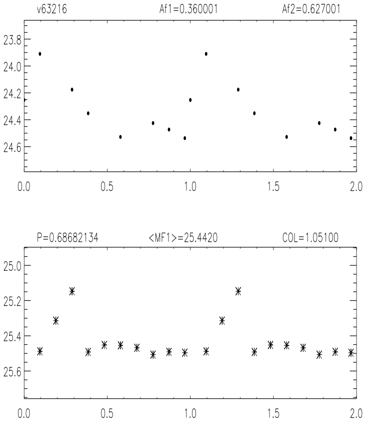
v63216 Af1=0.360001 Af2=0.627001
23.8 24.0 24.2 24.4 24.6
P=0.68682134 <MF1>=25.4420 COL=1.05100
25.0 25.2 25.4 25.6
0.0 0.5 1.0 1.5 2.0

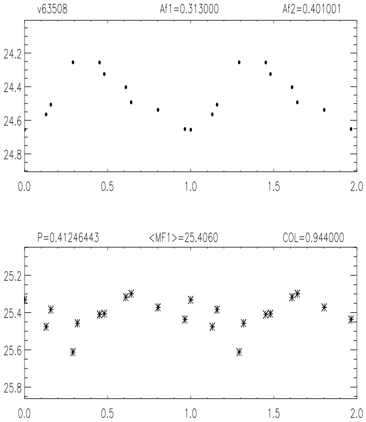
v63508 Af1=0.313000 Af2=0.401001
24.2 24.4 24.6 24.8
P=0.41246443 <MF1>=25.4060 COL=0.944000
25.2 25.4 25.6 25.8
0.0 0.5 1.0 1.5 2.0

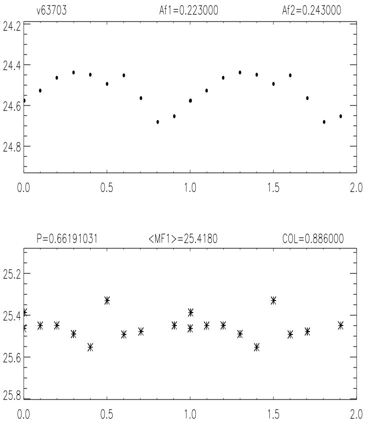
v63703 Af1=0.223000 Af2=0.243000
24.2 24.4 24.6 24.8
P=0.66191031 <MF1>=25.4180 COL=0.886000
25.2 25.4 25.6 25.8
0.0 0.5 1.0 1.5 2.0

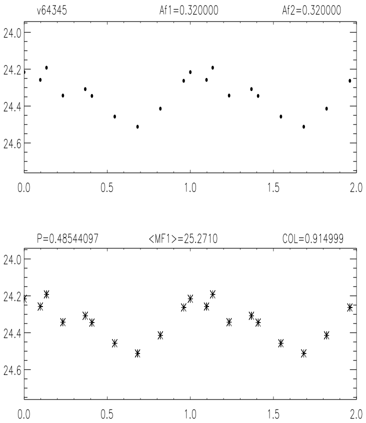
v64345 Af1=0.320000 Af2=0.320000
24.0 24.2 24.4 24.6
P=0.48544097 <MF1>=25.2710 COL=0.914999
24.0 24.2 24.4 24.6
0.0 0.5 1.0 1.5 2.0

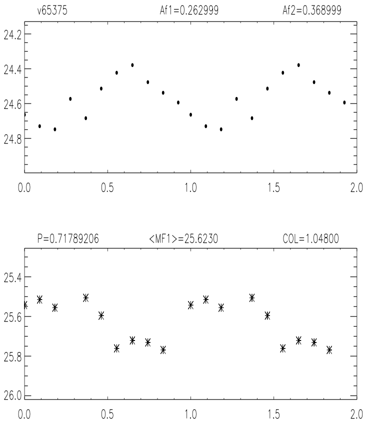
v65375 Af1=0.262999 Af2=0.368999
24.2 24.4 24.6 24.8
P=0.71789206 <MF1>=25.6230 COL=1.04800
25.4 25.6 25.8 26.0
0.0 0.5 1.0 1.5 2.0

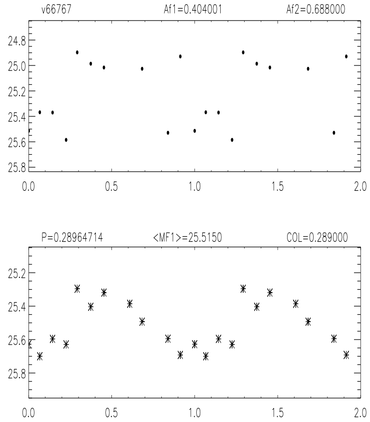
v66767 Af1=0.404001 Af2=0.688000
P=0.28964714 <MF1>=25.5150 COL=0.289000

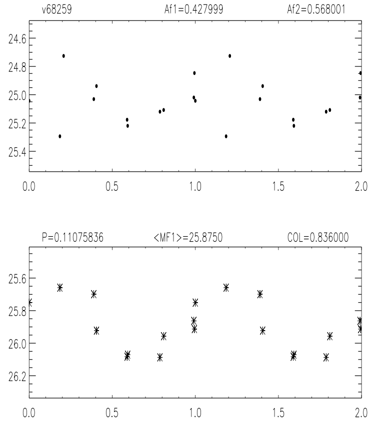
v68259 Af1=0.427999 Af2=0.568001
P=0.11075836 <MF1>=25.8750 COL=0.836000

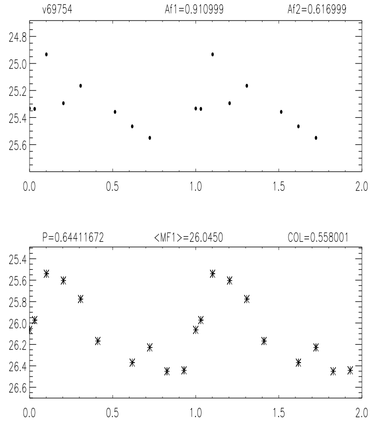
v69754 Af1=0.910999 Af2=0.616999
P=0.64411672 <MF1>=26.0450 COL=0.558001

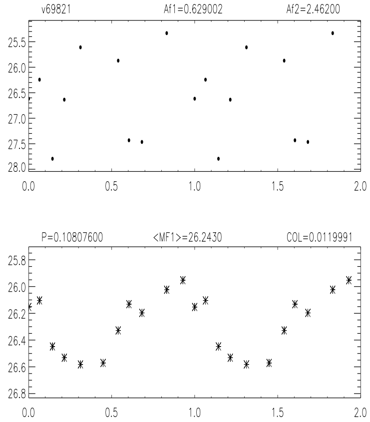
v69821 Af1=0.629002 Af2=2.46200
P=0.10807600 <MF1>=26.2430 COL=0.0119991

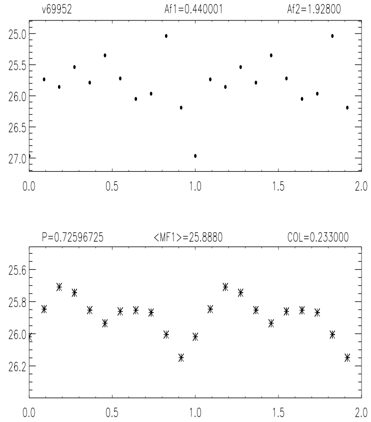
v69952 Af1=0.440001 Af2=1.92800
P=0.72596725 <MF1>=25.8880 COL=0.233000

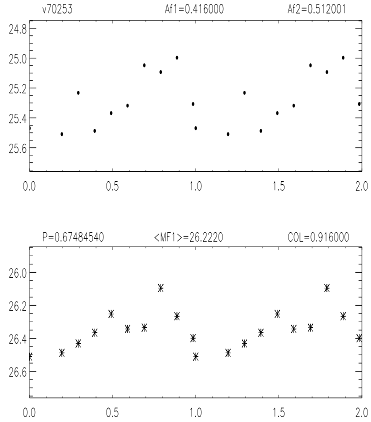
v70253 Af1=0.416000 Af2=0.512001
P=0.67484540 <MF1>=26.2220 COL=0.916000

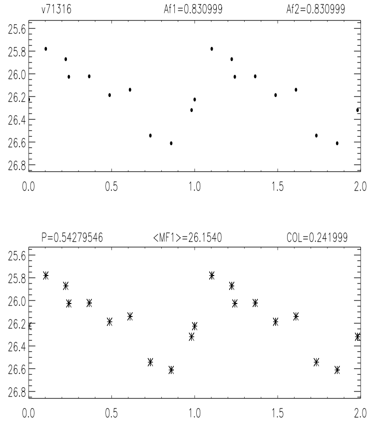
v71316 Af1=0.830999 Af2=0.830999
P=0.54279546 <MF1>=26.1540 COL=0.241999

Chapter 10

Appendix D

ATLAS OF LIGHT CURVES: G76

Atlas of the V,I light curves for candidate variable stars identified in G76. For each variable the upper panel shows the I-band light curve, and the lower panel the V-band light curve. Identification, V and I amplitudes, period, average V magnitude and average V−I color, are provided on top labels of the plots.

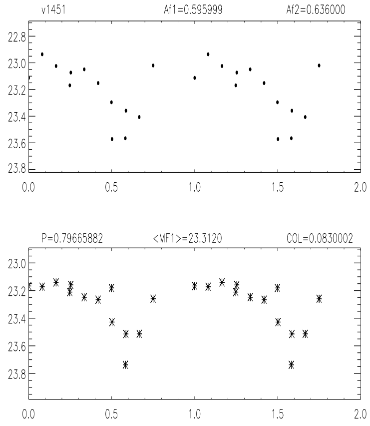
v1451 Af1=0.595999 Af2=0.636000
22.8 23.0 23.2 23.4 23.6 23.8
0.0 0.5 1.0 1.5 2.0
P=0.79665882 <MF1>=23.3120 COL=0.0830002
23.0 23.2 23.4 23.6 23.8
0.0 0.5 1.0 1.5 2.0

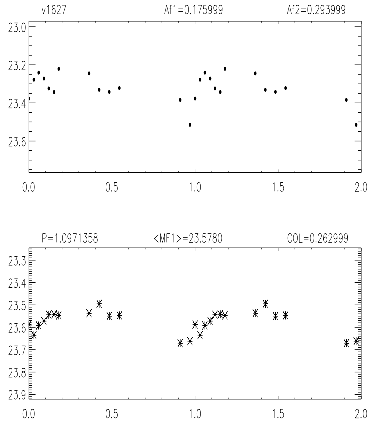
v1627 Af1=0.175999 Af2=0.293999
23.0 23.2 23.4 23.6
0.0 0.5 1.0 1.5 2.0
P=1.0971358 <MF1>=23.5780 COL=0.262999
23.3 23.4 23.5 23.6 23.7 23.8 23.9
0.0 0.5 1.0 1.5 2.0

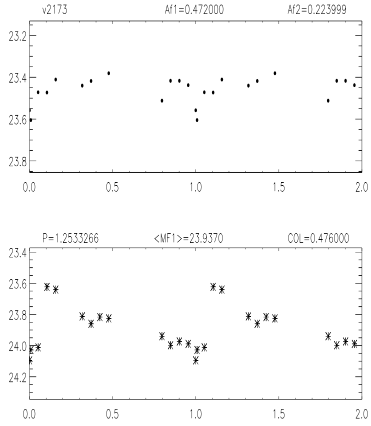
v2173 Af1=0.472000 Af2=0.223999
23.2 23.4 23.6 23.8
0.0 0.5 1.0 1.5 2.0
P=1.2533266 <MF1>=23.9370 COL=0.476000
23.4 23.6 23.8 24.0 24.2
0.0 0.5 1.0 1.5 2.0

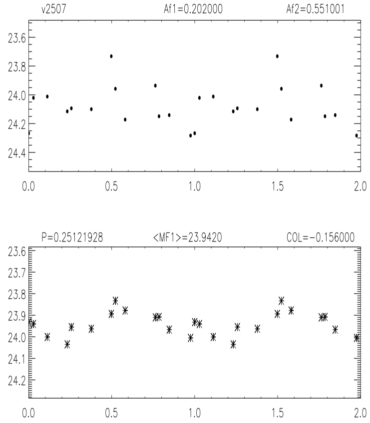
v2507 Af1=0.202000 Af2=0.551001
23.6 23.8 24.0 24.2 24.4
0.0 0.5 1.0 1.5 2.0
P=0.25121928 <MF1>=23.9420 COL=-0.156000
23.6 23.7 23.8 23.9 24.0 24.1 24.2
0.0 0.5 1.0 1.5 2.0

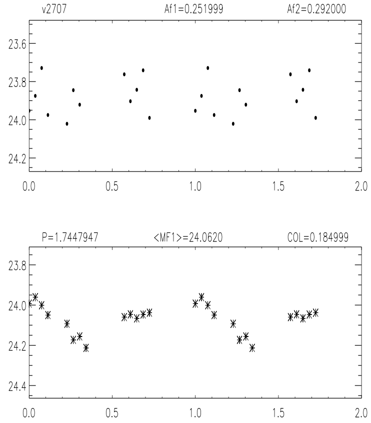
v2707 Af1=0.251999 Af2=0.292000
23.6 23.8 24.0 24.2
0.0 0.5 1.0 1.5 2.0
P=1.7447947 <MF1>=24.0620 COL=0.184999
23.8 24.0 24.2 24.4
0.0 0.5 1.0 1.5 2.0

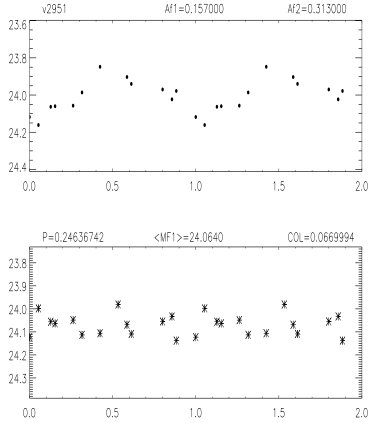
v2951 Af1=0.157000 Af2=0.313000
23.6 23.8 24.0 24.2 24.4
0.0 0.5 1.0 1.5 2.0
P=0.24636742 <MF1>=24.0640 COL=0.0669994
23.8 23.9 24.0 24.1 24.2 24.3
0.0 0.5 1.0 1.5 2.0

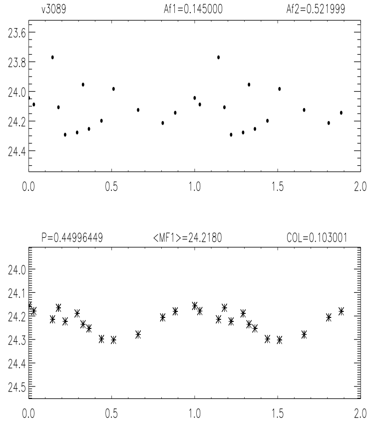
v3089 Af1=0.145000 Af2=0.521999
23.6 23.8 24.0 24.2 24.4
0.0 0.5 1.0 1.5 2.0
P=0.44996449 <MF1>=24.2180 COL=0.103001
24.0 24.1 24.2 24.3 24.4 24.5
0.0 0.5 1.0 1.5 2.0

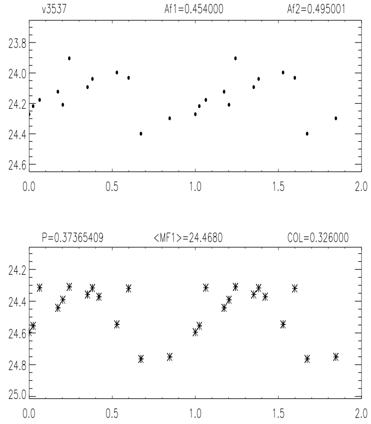
v3537 Af1=0.454000 Af2=0.495001
23.8 24.0 24.2 24.4 24.6
0.0 0.5 1.0 1.5 2.0
P=0.37365409 <MF1>=24.4680 COL=0.326000
24.2 24.4 24.6 24.8 25.0
0.0 0.5 1.0 1.5 2.0

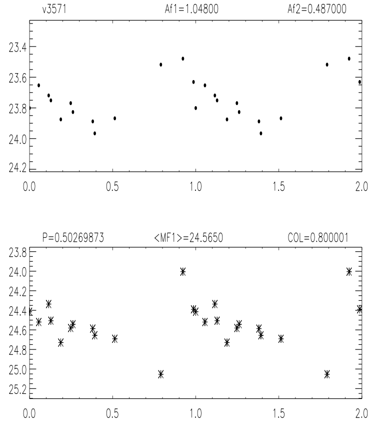
v3571 Af1=1.04800 Af2=0.487000
23.4 23.6 23.8 24.0 24.2
0.0 0.5 1.0 1.5 2.0
P=0.50269873 <MF1>=24.5650 COL=0.800001
23.8 24.0 24.2 24.4 24.6 24.8 25.0 25.2
0.0 0.5 1.0 1.5 2.0

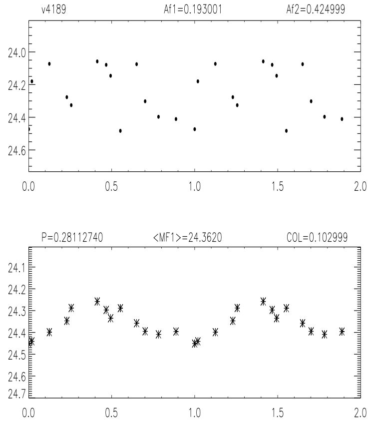
v4189 Af1=0.193001 Af2=0.424999
24.0 24.2 24.4 24.6
0.0 0.5 1.0 1.5 2.0
P=0.28112740 <MF1>=24.3620 COL=0.102999
24.1 24.2 24.3 24.4 24.5 24.6 24.7
0.0 0.5 1.0 1.5 2.0

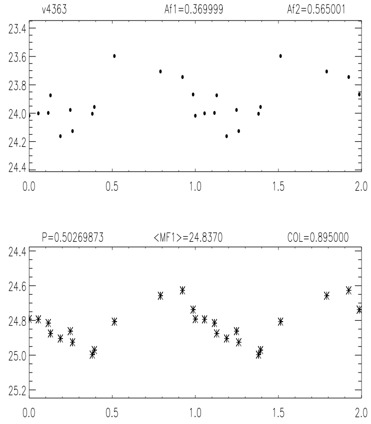
v4363 Af1=0.369999 Af2=0.565001
23.4 23.6 23.8 24.0 24.2 24.4
0.0 0.5 1.0 1.5 2.0
P=0.50269873 <MF1>=24.8370 COL=0.895000
24.4 24.6 24.8 25.0 25.2
0.0 0.5 1.0 1.5 2.0

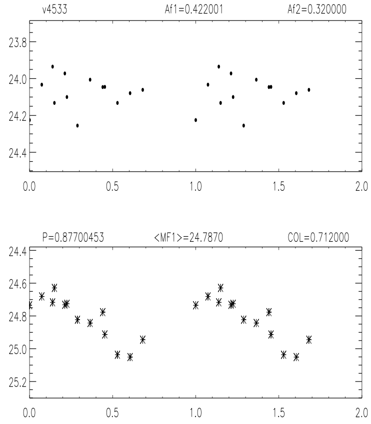
v4533 Af1=0.422001 Af2=0.320000
23.8 24.0 24.2 24.4
0.0 0.5 1.0 1.5 2.0
P=0.87700453 <MF1>=24.7870 COL=0.712000
24.4 24.6 24.8 25.0 25.2
0.0 0.5 1.0 1.5 2.0

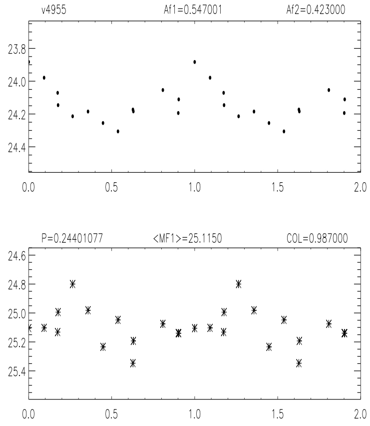
v4955
Af1=0.547001
Af2=0.423000
23.8
24.0
24.2
24.4
0.0
0.5
1.0
1.5
2.0
P=0.24401077
<MF1>=25.1150
COL=0.987000
24.6
24.8
25.0
25.2
25.4
0.0
0.5
1.0
1.5
2.0

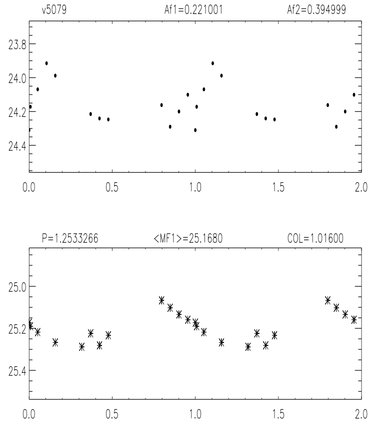
v5079
Af1=0.221001
Af2=0.394999
23.8
24.0
24.2
24.4
0.0
0.5
1.0
1.5
2.0
P=1.2533266
<MF1>=25.1680
COL=1.01600
25.0
25.2
25.4
0.0
0.5
1.0
1.5
2.0

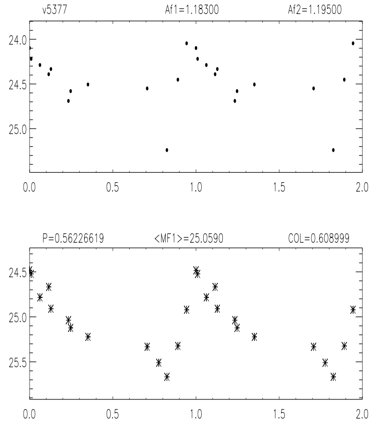
v5377
Af1=1.18300
Af2=1.19500
24.0
24.5
25.0
0.0
0.5
1.0
1.5
2.0
P=0.56226619
<MF1>=25.0590
COL=0.608999
24.5
25.0
25.5
0.0
0.5
1.0
1.5
2.0

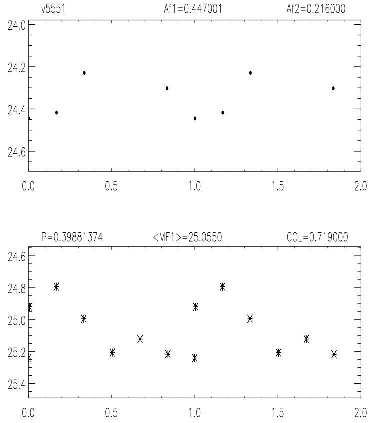
v5551
Af1=0.447001
Af2=0.216000
24.0
24.2
24.4
24.6
0.0
0.5
1.0
1.5
2.0
P=0.39881374
<MF1>=25.0550
COL=0.719000
24.6
24.8
25.0
25.2
25.4
0.0
0.5
1.0
1.5
2.0

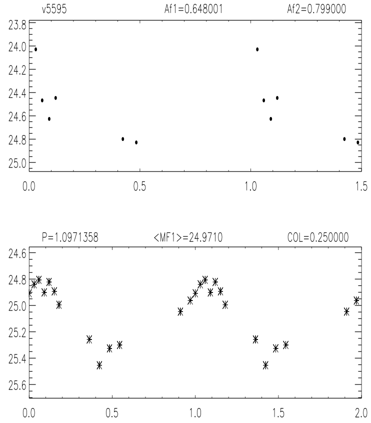
v5595
Af1=0.648001
Af2=0.799000
23.8
24.0
24.2
24.4
24.6
24.8
25.0
0.0
0.5
1.0
1.5
P=1.0971358
<MF1>=24.9710
COL=0.250000
24.6
24.8
25.0
25.2
25.4
25.6
0.0
0.5
1.0
1.5
2.0

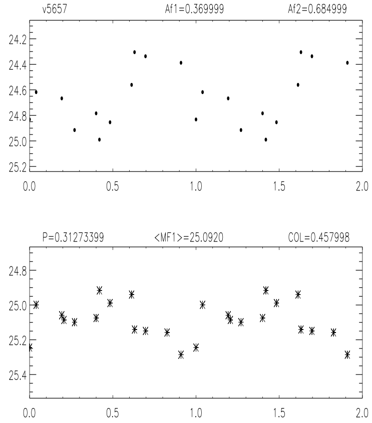
v5657
Af1=0.369999
Af2=0.684999
24.2
24.4
24.6
24.8
25.0
25.2
0.0
0.5
1.0
1.5
2.0
P=0.31273399
<MF1>=25.0920
COL=0.457998
24.8
25.0
25.2
25.4
0.0
0.5
1.0
1.5
2.0

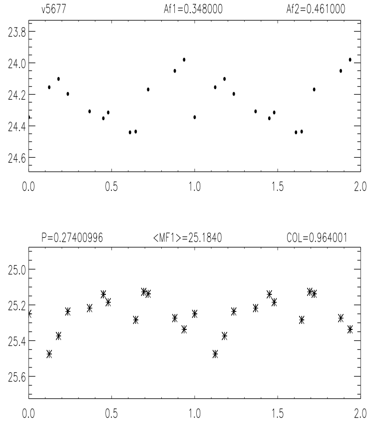
v5677
Af1=0.348000
Af2=0.461000
23.8
24.0
24.2
24.4
24.6
0.0
0.5
1.0
1.5
2.0
P=0.27400996
<MF1>=25.1840
COL=0.964001
25.0
25.2
25.4
25.6
0.0
0.5
1.0
1.5
2.0

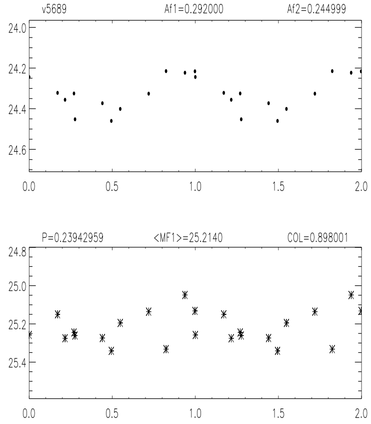
v5689
Af1=0.292000
Af2=0.244999
24.0
24.2
24.4
24.6
0.0
0.5
1.0
1.5
2.0
P=0.23942959
<MF1>=25.2140
COL=0.898001
24.8
25.0
25.2
25.4
0.0
0.5
1.0
1.5
2.0

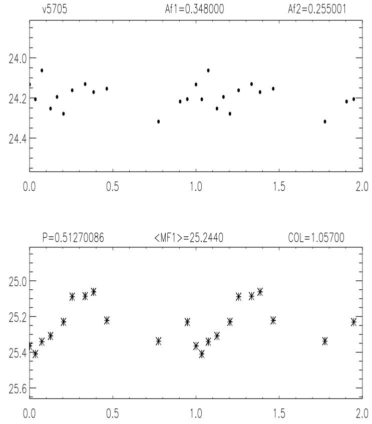
v5705
Af1=0.348000
Af2=0.255001
24.0
24.2
24.4
0.0
0.5
1.0
1.5
2.0
P=0.51270086
<MF1>=25.2440
COL=1.05700
25.0
25.2
25.4
25.6
0.0
0.5
1.0
1.5
2.0

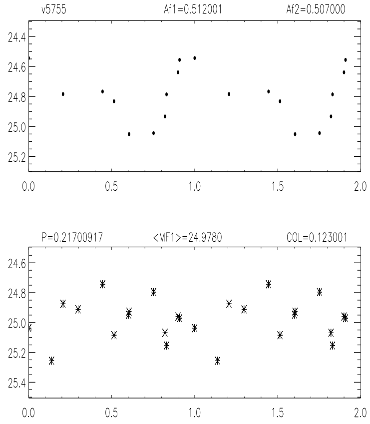
v5755
Af1=0.512001
Af2=0.507000
24.4
24.6
24.8
25.0
25.2
0.0
0.5
1.0
1.5
2.0
P=0.21700917
<MF1>=24.9780
COL=0.123001
24.6
24.8
25.0
25.2
25.4
0.0
0.5
1.0
1.5
2.0

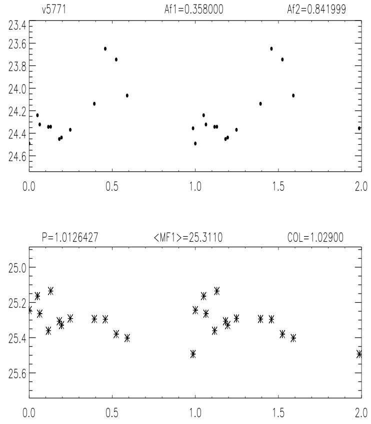
v5771
Af1=0.358000
Af2=0.841999
23.4
23.6
23.8
24.0
24.2
24.4
24.6
0.0
0.5
1.0
1.5
2.0
P=1.0126427
<MF1>=25.3110
COL=1.02900
25.0
25.2
25.4
25.6
0.0
0.5
1.0
1.5
2.0

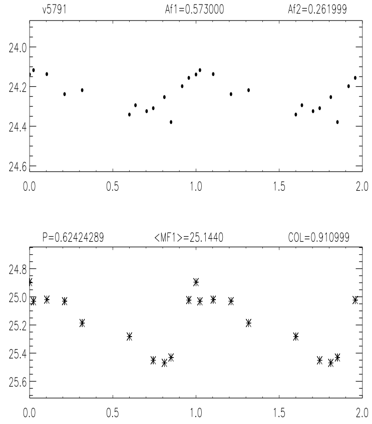
v5791
Af1=0.573000
Af2=0.261999
24.0
24.2
24.4
24.6
0.0
0.5
1.0
1.5
2.0
P=0.62424289
<MF1>=25.1440
COL=0.910999
24.8
25.0
25.2
25.4
25.6
0.0
0.5
1.0
1.5
2.0

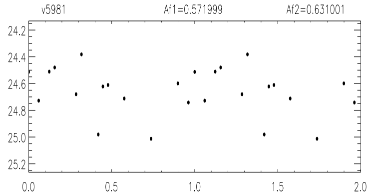
v5981
Af1=0.571999
Af2=0.631001
24.2
24.4
24.6
24.8
25.0
25.2
0.0
0.5
1.0
1.5
2.0

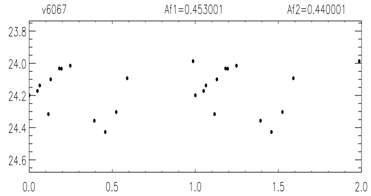
v6067
Af1=0.453001
Af2=0.440001
23.8
24.0
24.2
24.4
24.6
0.0
0.5
1.0
1.5
2.0

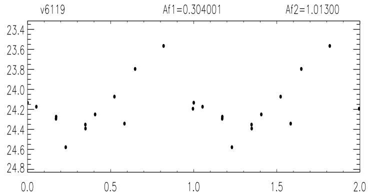
v6119
Af1=0.304001
Af2=1.01300
23.4
23.6
23.8
24.0
24.2
24.4
24.6
24.8
0.0
0.5
1.0
1.5
2.0

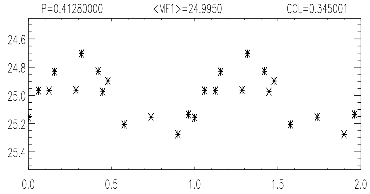
P=0.41280000
<MF1>=24.9950
COL=0.345001
24.6
24.8
25.0
25.2
25.4
0.0
0.5
1.0
1.5
2.0

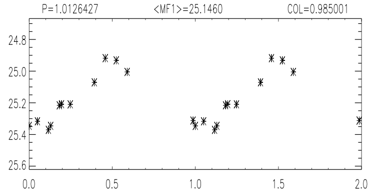
P=1.0126427
<MF1>=25.1460
COL=0.985001
24.8
25.0
25.2
25.4
25.6
0.0
0.5
1.0
1.5
2.0

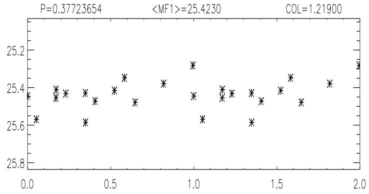
P=0.37723654
<MF1>=25.4230
COL=1.21900
25.2
25.4
25.6
25.8
0.0
0.5
1.0
1.5
2.0

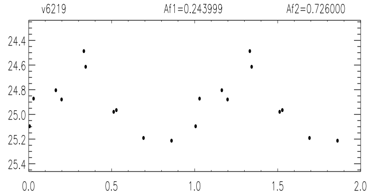
v6219
Af1=0.243999
Af2=0.726000
24.4
24.6
24.8
25.0
25.2
25.4
0.0
0.5
1.0
1.5
2.0

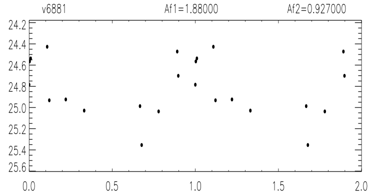
v6881
Af1=1.88000
Af2=0.927000
24.2
24.4
24.6
24.8
25.0
25.2
25.4
25.6
0.0
0.5
1.0
1.5
2.0

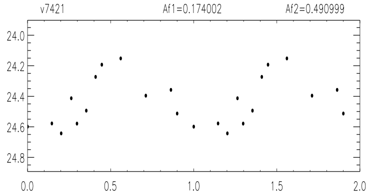
v7421
Af1=0.174002
Af2=0.490999
24.0
24.2
24.4
24.6
24.8
0.0
0.5
1.0
1.5
2.0

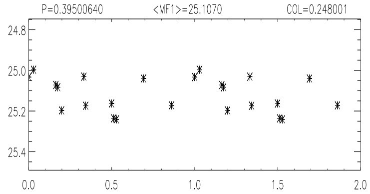
P=0.39500640
<MF1>=25.1070
COL=0.248001
24.8
25.0
25.2
25.4
0.0
0.5
1.0
1.5
2.0

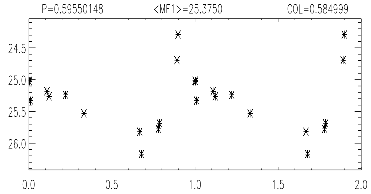
P=0.59550148
<MF1>=25.3750
COL=0.584999
24.5
25.0
25.5
26.0
0.0
0.5
1.0
1.5
2.0

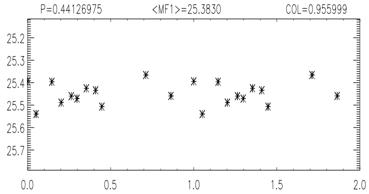
P=0.44126975
<MF1>=25.3830
COL=0.955999
25.2
25.3
25.4
25.5
25.6
25.7
0.0
0.5
1.0
1.5
2.0

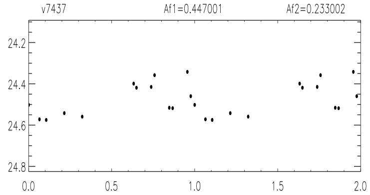
v7437
Af1=0.447001
Af2=0.233002
24.2
24.4
24.6
24.8
0.0
0.5
1.0
1.5
2.0

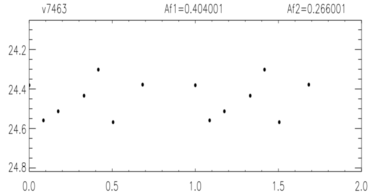
v7463
Af1=0.404001
Af2=0.266001
24.2
24.4
24.6
24.8
0.0
0.5
1.0
1.5
2.0

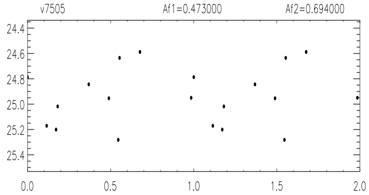
v7505
Af1=0.473000
Af2=0.694000
24.4
24.6
24.8
25.0
25.2
25.4
0.0
0.5
1.0
1.5
2.0

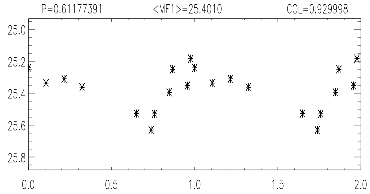
P=0.61177391
<MF1>=25.4010
COL=0.929998
25.0
25.2
25.4
25.6
25.8
0.0
0.5
1.0
1.5
2.0

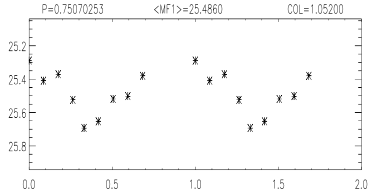
P=0.75070253
<MF1>=25.4860
COL=1.05200
25.2
25.4
25.6
25.8
0.0
0.5
1.0
1.5
2.0

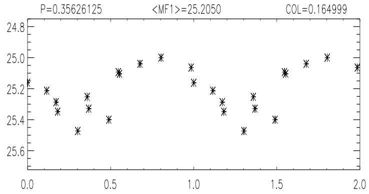
P=0.35626125
<MF1>=25.2050
COL=0.164999
24.8
25.0
25.2
25.4
25.6
0.0
0.5
1.0
1.5
2.0

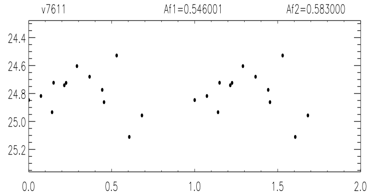
v7611
Af1=0.546001
Af2=0.583000
24.4
24.6
24.8
25.0
25.2
0.0
0.5
1.0
1.5
2.0

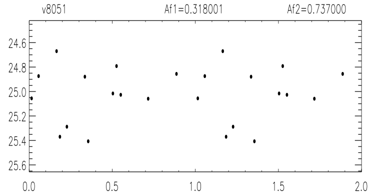
v8051
Af1=0.318001
Af2=0.737000
24.6
24.8
25.0
25.2
25.4
25.6
0.0
0.5
1.0
1.5
2.0

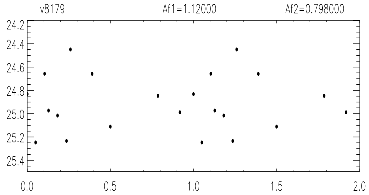
v8179
Af1=1.12000
Af2=0.798000
24.2
24.4
24.6
24.8
25.0
25.2
25.4
0.0
0.5
1.0
1.5
2.0

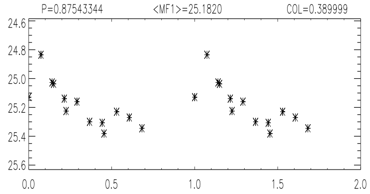
P=0.87543344
<MF1>=25.1820
COL=0.389999
24.6
24.8
25.0
25.2
25.4
25.6
0.0
0.5
1.0
1.5
2.0

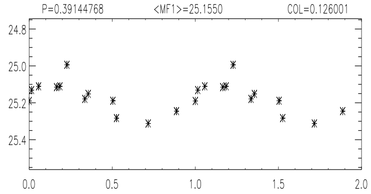
P=0.39144768
<MF1>=25.1550
COL=0.126001
24.8
25.0
25.2
25.4
0.0
0.5
1.0
1.5
2.0

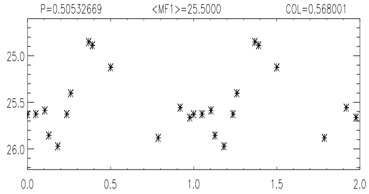
P=0.50532669
<MF1>=25.5000
COL=0.568001
25.0
25.5
26.0
0.0
0.5
1.0
1.5
2.0

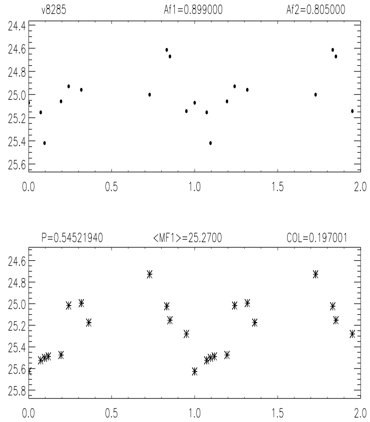
v8285
Af1=0.899000
Af2=0.805000
24.4
24.6
24.8
25.0
25.2
25.4
25.6
0.0
0.5
1.0
1.5
2.0
P=0.54521940
<MF1>=25.2700
COL=0.197001
24.6
24.8
25.0
25.2
25.4
25.6
25.8
0.0
0.5
1.0
1.5
2.0

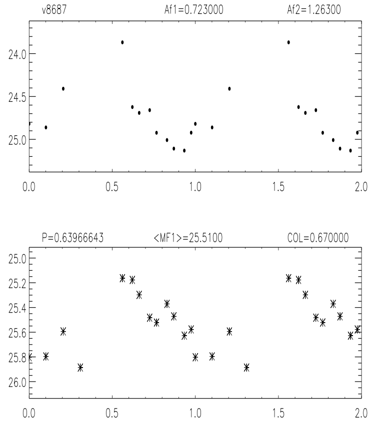
v8687
Af1=0.723000
Af2=1.26300
24.0
24.5
25.0
0.0
0.5
1.0
1.5
2.0
P=0.63966643
<MF1>=25.5100
COL=0.670000
25.0
25.2
25.4
25.6
25.8
26.0
0.0
0.5
1.0
1.5
2.0

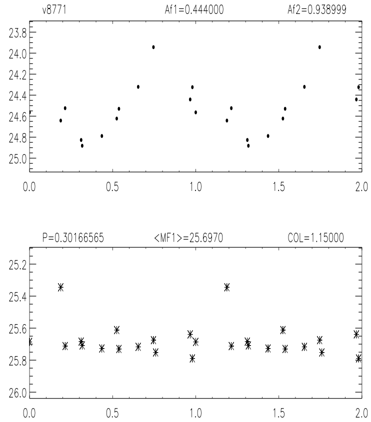
v8771
Af1=0.444000
Af2=0.938999
23.8
24.0
24.2
24.4
24.6
24.8
25.0
0.0
0.5
1.0
1.5
2.0
P=0.30166565
<MF1>=25.6970
COL=1.15000
25.2
25.4
25.6
25.8
26.0
0.0
0.5
1.0
1.5
2.0

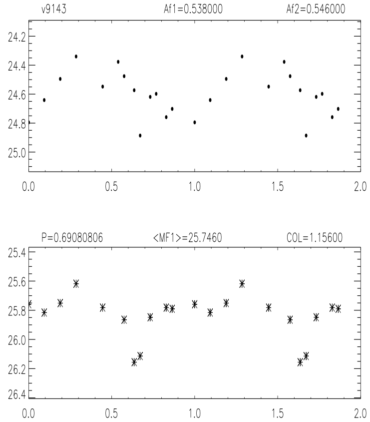
v9143
Af1=0.538000
Af2=0.546000
24.2
24.4
24.6
24.8
25.0
0.0
0.5
1.0
1.5
2.0
P=0.69080806
<MF1>=25.7460
COL=1.15600
25.4
25.6
25.8
26.0
26.2
26.4
0.0
0.5
1.0
1.5
2.0

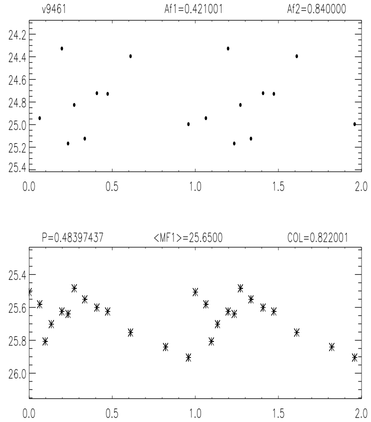
v9461
Af1=0.421001
Af2=0.840000
24.2
24.4
24.6
24.8
25.0
25.2
25.4
0.0
0.5
1.0
1.5
2.0
P=0.48397437
<MF1>=25.6500
COL=0.822001
25.4
25.6
25.8
26.0
0.0
0.5
1.0
1.5
2.0

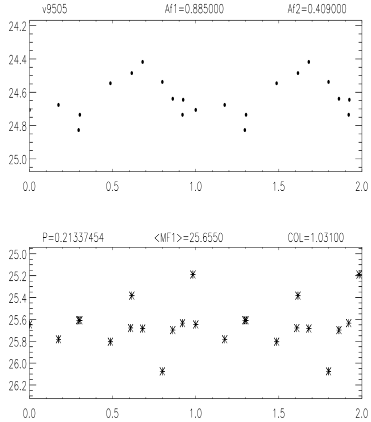
v9505
Af1=0.885000
Af2=0.409000
24.2
24.4
24.6
24.8
25.0
0.0
0.5
1.0
1.5
2.0
P=0.21337454
<MF1>=25.6550
COL=1.03100
25.0
25.2
25.4
25.6
25.8
26.0
26.2
0.0
0.5
1.0
1.5
2.0

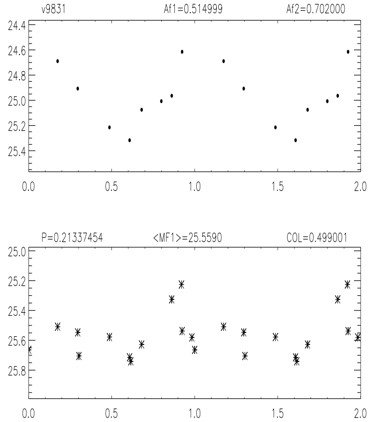
v9831
Af1=0.514999
Af2=0.702000
24.4
24.6
24.8
25.0
25.2
25.4
0.0
0.5
1.0
1.5
2.0
P=0.21337454
<MF1>=25.5590
COL=0.499001
25.0
25.2
25.4
25.6
25.8
0.0
0.5
1.0
1.5
2.0

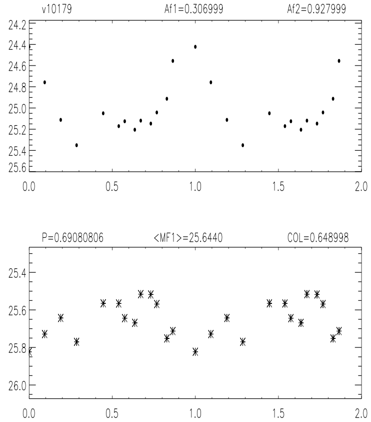
v10179
Af1=0.306999
Af2=0.927999
24.2
24.4
24.6
24.8
25.0
25.2
25.4
25.6
0.0
0.5
1.0
1.5
2.0
P=0.69080806
<MF1>=25.6440
COL=0.648998
25.4
25.6
25.8
26.0
0.0
0.5
1.0
1.5
2.0

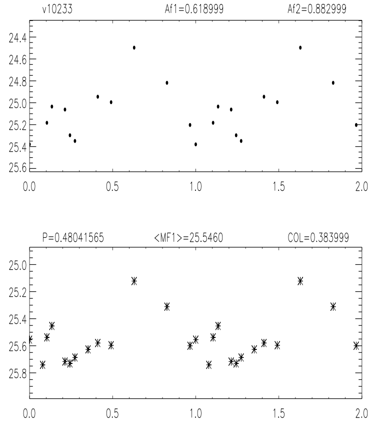
v10233
Af1=0.618999
Af2=0.882999
24.4
24.6
24.8
25.0
25.2
25.4
25.6
0.0
0.5
1.0
1.5
2.0
P=0.48041565
<MF1>=25.5460
COL=0.383999
25.0
25.2
25.4
25.6
25.8
0.0
0.5
1.0
1.5
2.0

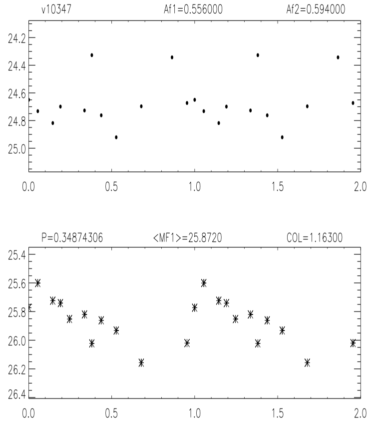
v10347
Af1=0.556000
Af2=0.594000
24.2
24.4
24.6
24.8
25.0
0.0
0.5
1.0
1.5
2.0
P=0.34874306
<MF1>=25.8720
COL=1.16300
25.4
25.6
25.8
26.0
26.2
26.4
0.0
0.5
1.0
1.5
2.0

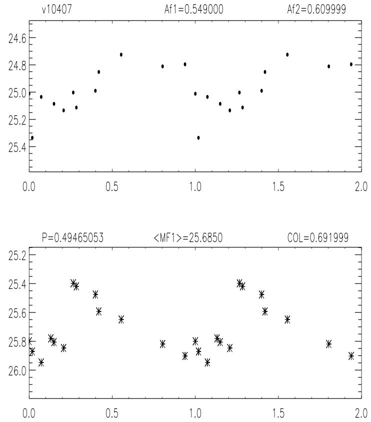
v10407
Af1=0.549000
Af2=0.609999
24.6
24.8
25.0
25.2
25.4
0.0
0.5
1.0
1.5
2.0
P=0.49465053
<MF1>=25.6850
COL=0.691999
25.2
25.4
25.6
25.8
26.0
0.0
0.5
1.0
1.5
2.0

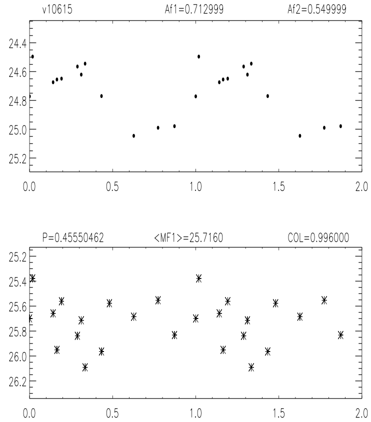
v10615
Af1=0.712999
Af2=0.549999
24.4
24.6
24.8
25.0
25.2
0.0
0.5
1.0
1.5
2.0
P=0.45550462
<MF1>=25.7160
COL=0.996000
25.2
25.4
25.6
25.8
26.0
26.2
0.0
0.5
1.0
1.5
2.0

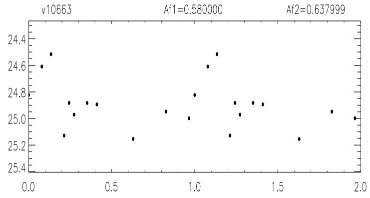
v10663
Af1=0.580000
Af2=0.637999
24.4
24.6
24.8
25.0
25.2
25.4
0.0
0.5
1.0
1.5
2.0

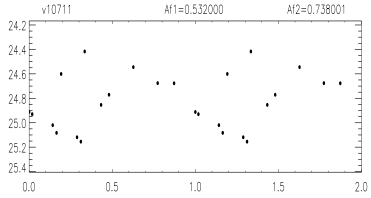
v10711
Af1=0.532000
Af2=0.738001
24.2
24.4
24.6
24.8
25.0
25.2
25.4
0.0
0.5
1.0
1.5
2.0

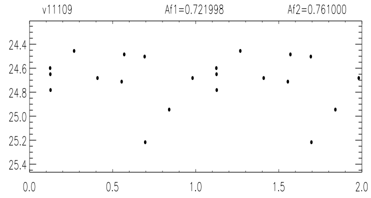
v11109
Af1=0.721998
Af2=0.761000
24.4
24.6
24.8
25.0
25.2
25.4
0.0
0.5
1.0
1.5
2.0

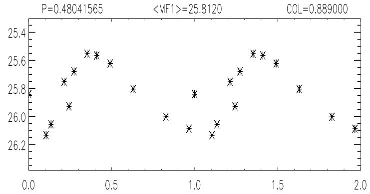
P=0.48041565
<MF1>=25.8120
COL=0.889000
25.4
25.6
25.8
26.0
26.2
0.0
0.5
1.0
1.5
2.0

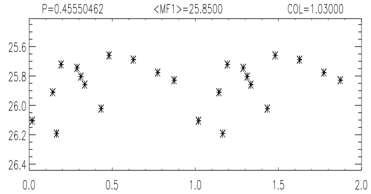
P=0.45550462
<MF1>=25.8500
COL=1.03000
25.6
25.8
26.0
26.2
26.4
0.0
0.5
1.0
1.5
2.0

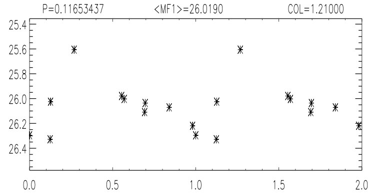
P=0.11653437
<MF1>=26.0190
COL=1.21000
25.4
25.6
25.8
26.0
26.2
26.4
0.0
0.5
1.0
1.5
2.0

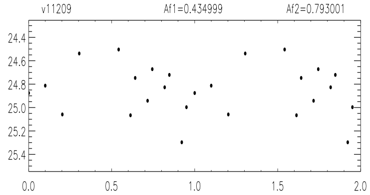
v11209
Af1=0.434999
Af2=0.793001
24.4
24.6
24.8
25.0
25.2
25.4
0.0
0.5
1.0
1.5
2.0

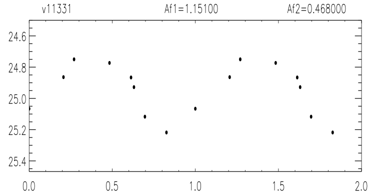
v11331
Af1=1.15100
Af2=0.468000
24.6
24.8
25.0
25.2
25.4
0.0
0.5
1.0
1.5
2.0

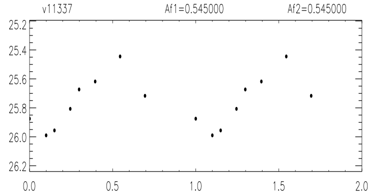
v11337
Af1=0.545000
Af2=0.545000
25.2
25.4
25.6
25.8
26.0
26.2
0.0
0.5
1.0
1.5
2.0

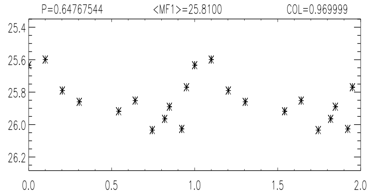
P=0.64767544
<MF1>=25.8100
COL=0.969999
25.4
25.6
25.8
26.0
26.2
0.0
0.5
1.0
1.5
2.0

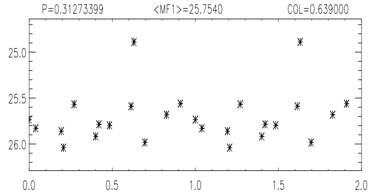
P=0.31273399
<MF1>=25.7540
COL=0.639000
25.0
25.5
26.0
0.0
0.5
1.0
1.5
2.0

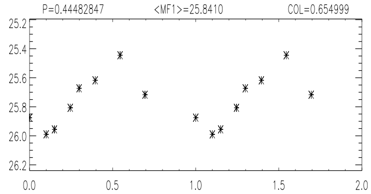
P=0.44482847
<MF1>=25.8410
COL=0.654999
25.2
25.4
25.6
25.8
26.0
26.2
0.0
0.5
1.0
1.5
2.0

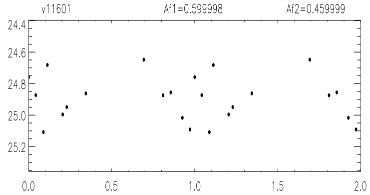
v11601
Af1=0.599998
Af2=0.459999
24.4
24.6
24.8
25.0
25.2
0.0
0.5
1.0
1.5
2.0

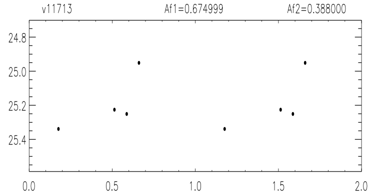
v11713
Af1=0.674999
Af2=0.388000
24.8
25.0
25.2
25.4
0.0
0.5
1.0
1.5
2.0

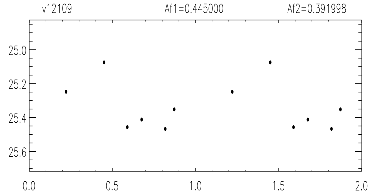
v12109
Af1=0.445000
Af2=0.391998
25.0
25.2
25.4
25.6
0.0
0.5
1.0
1.5
2.0

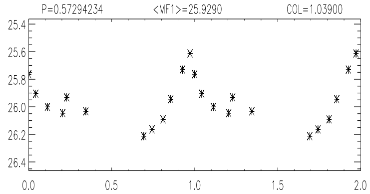
P=0.57294234
<MF1>=25.9290
COL=1.03900
25.4
25.6
25.8
26.0
26.2
26.4
0.0
0.5
1.0
1.5
2.0

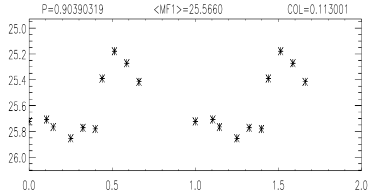
P=0.90390319
<MF1>=25.5660
COL=0.113001
25.0
25.2
25.4
25.6
25.8
26.0
0.0
0.5
1.0
1.5
2.0

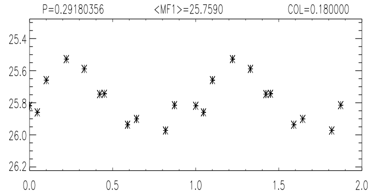
P=0.29180356
<MF1>=25.7590
COL=0.180000
25.4
25.6
25.8
26.0
26.2
0.0
0.5
1.0
1.5
2.0

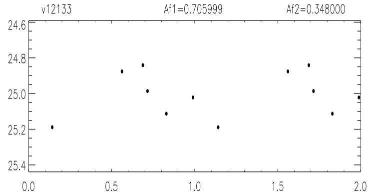
v12133
Af1=0.705999
Af2=0.348000
24.6
24.8
25.0
25.2
25.4
0.0
0.5
1.0
1.5
2.0

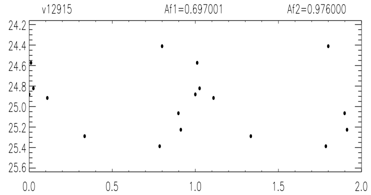
v12915
Af1=0.697001
Af2=0.976000
24.2
24.4
24.6
24.8
25.0
25.2
25.4
25.6
0.0
0.5
1.0
1.5
2.0

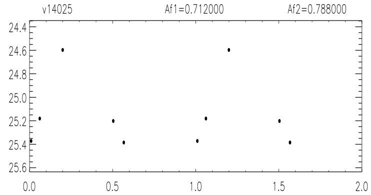
v14025
Af1=0.712000
Af2=0.788000
24.4
24.6
24.8
25.0
25.2
25.4
25.6
0.0
0.5
1.0
1.5
2.0

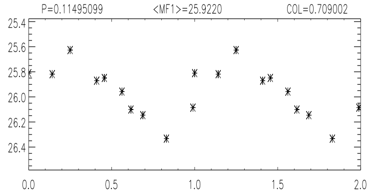
P=0.11495099
<MF1>=25.9220
COL=0.709002
25.4
25.6
25.8
26.0
26.2
26.4
0.0
0.5
1.0
1.5
2.0

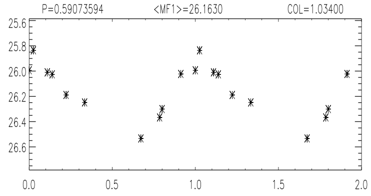
P=0.59073594
<MF1>=26.1630
COL=1.03400
25.6
25.8
26.0
26.2
26.4
26.6
0.0
0.5
1.0
1.5
2.0

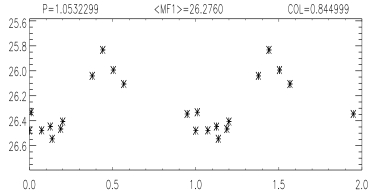
P=1.0532299
<MF1>=26.2760
COL=0.844999
25.6
25.8
26.0
26.2
26.4
26.6
0.0
0.5
1.0
1.5
2.0

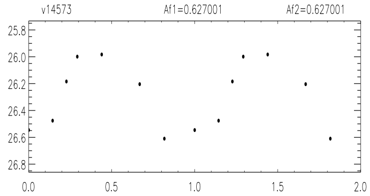
v14573
Af1=0.627001
Af2=0.627001
25.8
26.0
26.2
26.4
26.6
26.8
0.0
0.5
1.0
1.5
2.0

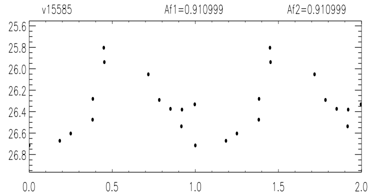
v15585
Af1=0.910999
Af2=0.910999
25.6
25.8
26.0
26.2
26.4
26.6
26.8
0.0
0.5
1.0
1.5
2.0

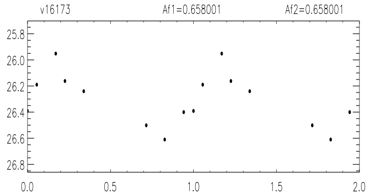
v16173
Af1=0.658001
Af2=0.658001
25.8
26.0
26.2
26.4
26.6
26.8
0.0
0.5
1.0
1.5
2.0

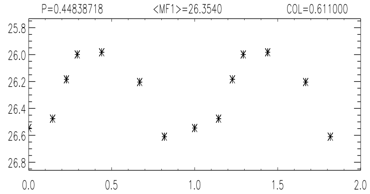
P=0.44838718
<MF1>=26.3540
COL=0.611000
25.8
26.0
26.2
26.4
26.6
26.8
0.0
0.5
1.0
1.5
2.0

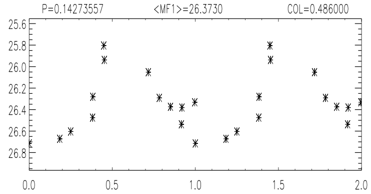
P=0.14273557
<MF1>=26.3730
COL=0.486000
25.6
25.8
26.0
26.2
26.4
26.6
26.8
0.0
0.5
1.0
1.5
2.0

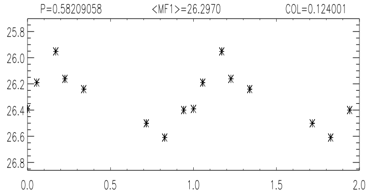
P=0.58209058
<MF1>=26.2970
COL=0.124001
25.8
26.0
26.2
26.4
26.6
26.8
0.0
0.5
1.0
1.5
2.0

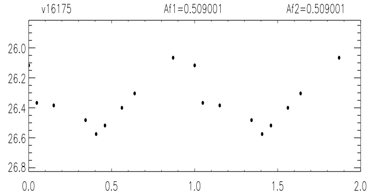
v16175
Af1=0.509001
Af2=0.509001
26.0
26.2
26.4
26.6
26.8
0.0
0.5
1.0
1.5
2.0

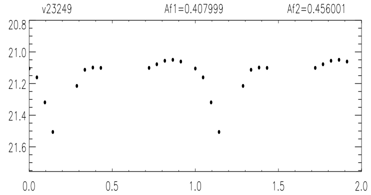
v23249
Af1=0.407999
Af2=0.456001
20.8
21.0
21.2
21.4
21.6
0.0
0.5
1.0
1.5
2.0

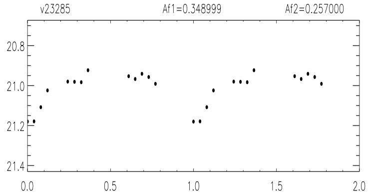
v23285
Af1=0.348999
Af2=0.257000
20.8
21.0
21.2
21.4
0.0
0.5
1.0
1.5
2.0

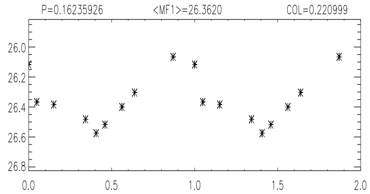
P=0.16235926
<MF1>=26.3620
COL=0.220999
26.0
26.2
26.4
26.6
26.8
0.0
0.5
1.0
1.5
2.0

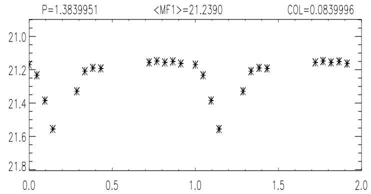
P=1.3839951
<MF1>=21.2390
COL=0.0839996
21.0
21.2
21.4
21.6
21.8
0.0
0.5
1.0
1.5
2.0

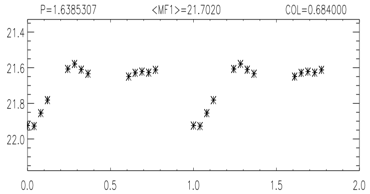
P=1.6385307
<MF1>=21.7020
COL=0.684000
21.4
21.6
21.8
22.0
0.0
0.5
1.0
1.5
2.0

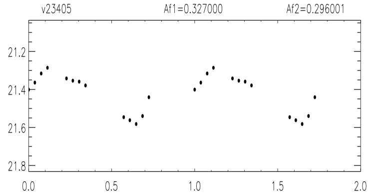
v23405
Af1=0.327000
Af2=0.296001
21.2
21.4
21.6
21.8
0.0
0.5
1.0
1.5
2.0

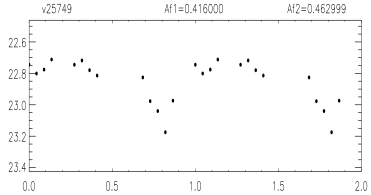
v25749
Af1=0.416000
Af2=0.462999
22.6
22.8
23.0
23.2
23.4
0.0
0.5
1.0
1.5
2.0

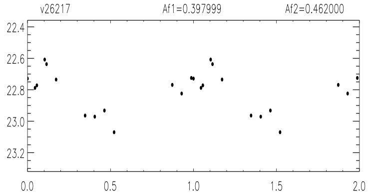
v26217
Af1=0.397999
Af2=0.462000
22.4
22.6
22.8
23.0
23.2
0.0
0.5
1.0
1.5
2.0

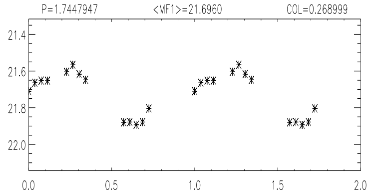
P=1.7447947
<MF1>=21.6960
COL=0.268999
21.4
21.6
21.8
22.0
0.0
0.5
1.0
1.5
2.0

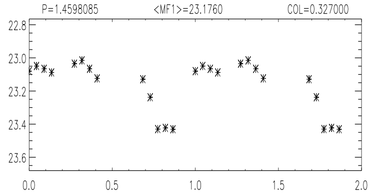
P=1.4598085
<MF1>=23.1760
COL=0.327000
22.8
23.0
23.2
23.4
23.6
0.0
0.5
1.0
1.5
2.0

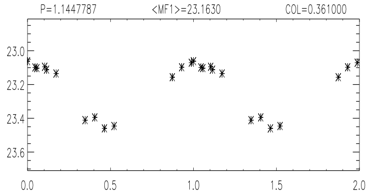
P=1.1447787
<MF1>=23.1630
COL=0.361000
23.0
23.2
23.4
23.6
0.0
0.5
1.0
1.5
2.0

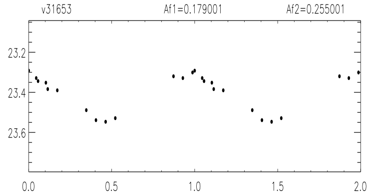
v31653
Af1=0.179001
Af2=0.255001
23.2
23.4
23.6
0.0
0.5
1.0
1.5
2.0

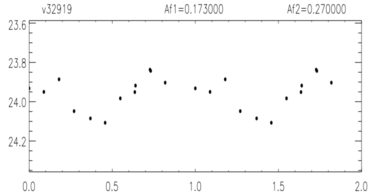
v32919
Af1=0.173000
Af2=0.270000
23.6
23.8
24.0
24.2
0.0
0.5
1.0
1.5
2.0

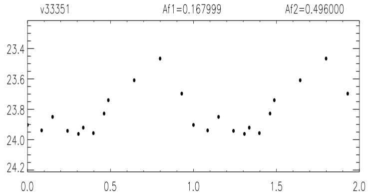
v33351
Af1=0.167999
Af2=0.496000
23.4
23.6
23.8
24.0
24.2
0.0
0.5
1.0
1.5
2.0

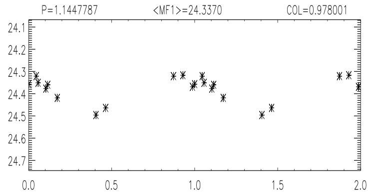
P=1.1447787
<MF1>=24.3370
COL=0.978001
24.1
24.2
24.3
24.4
24.5
24.6
24.7
0.0
0.5
1.0
1.5
2.0

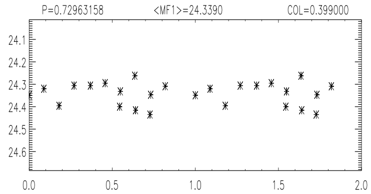
P=0.72963158
<MF1>=24.3390
COL=0.399000
24.1
24.2
24.3
24.4
24.5
24.6
0.0
0.5
1.0
1.5
2.0

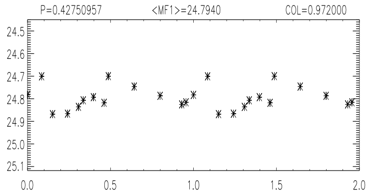
P=0.42750957
<MF1>=24.7940
COL=0.972000
24.5
24.6
24.7
24.8
24.9
25.0
25.1
0.0
0.5
1.0
1.5
2.0

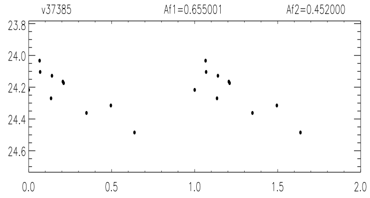
v37385 Af1=0.655001 Af2=0.452000
23.8 24.0 24.2 24.4 24.6
0.0 0.5 1.0 1.5 2.0

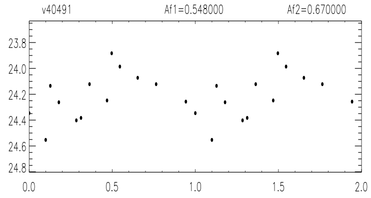
v40491 Af1=0.548000 Af2=0.670000
23.8 24.0 24.2 24.4 24.6 24.8
0.0 0.5 1.0 1.5 2.0

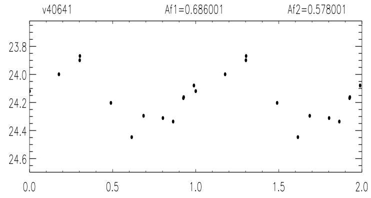
v40641 Af1=0.686001 Af2=0.578001
23.8 24.0 24.2 24.4 24.6
0.0 0.5 1.0 1.5 2.0

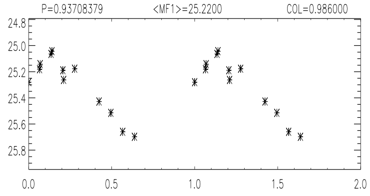
P=0.93708379 <MF1>=25.2200 COL=0.986000
24.8 25.0 25.2 25.4 25.6 25.8
0.0 0.5 1.0 1.5 2.0

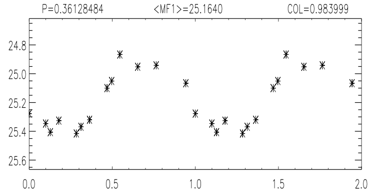
P=0.36128484 <MF1>=25.1640 COL=0.983999
24.8 25.0 25.2 25.4 25.6
0.0 0.5 1.0 1.5 2.0

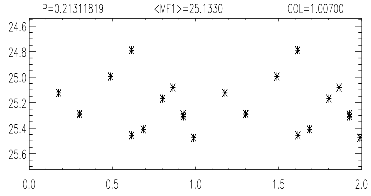
P=0.21311819 <MF1>=25.1330 COL=1.00700
24.6 24.8 25.0 25.2 25.4 25.6
0.0 0.5 1.0 1.5 2.0

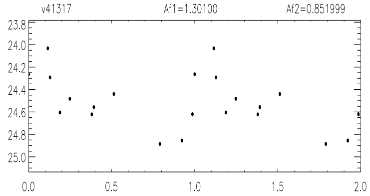
v41317 Af1=1.30100 Af2=0.851999
23.8 24.0 24.2 24.4 24.6 24.8 25.0
0.0 0.5 1.0 1.5 2.0

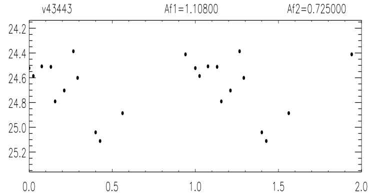
v43443 Af1=1.10800 Af2=0.725000
24.2 24.4 24.6 24.8 25.0 25.2
0.0 0.5 1.0 1.5 2.0

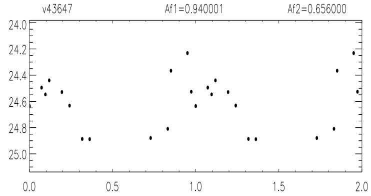
v43647 Af1=0.940001 Af2=0.656000
24.0 24.2 24.4 24.6 24.8 25.0
0.0 0.5 1.0 1.5 2.0

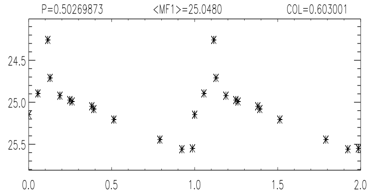
P=0.50269873 <MF1>=25.0480 COL=0.603001
24.5 25.0 25.5
0.0 0.5 1.0 1.5 2.0

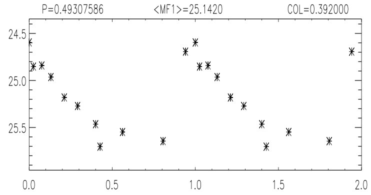
P=0.49307586 <MF1>=25.1420 COL=0.392000
24.5 25.0 25.5
0.0 0.5 1.0 1.5 2.0

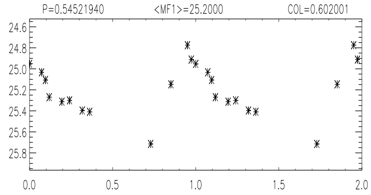
P=0.54521940 <MF1>=25.2000 COL=0.602001
24.6 24.8 25.0 25.2 25.4 25.6 25.8
0.0 0.5 1.0 1.5 2.0

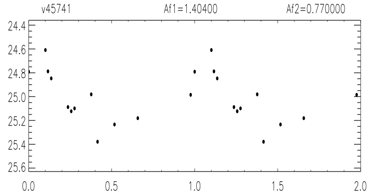
v45741 Af1=1.40400 Af2=0.770000
24.4 24.6 24.8 25.0 25.2 25.4 25.6
0.0 0.5 1.0 1.5 2.0

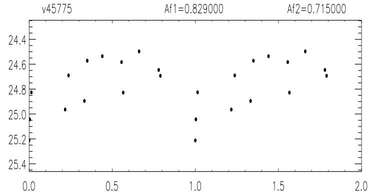
v45775 Af1=0.829000 Af2=0.715000
24.4 24.6 24.8 25.0 25.2 25.4
0.0 0.5 1.0 1.5 2.0

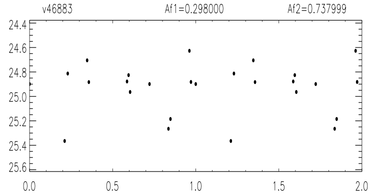
v46883 Af1=0.298000 Af2=0.737999
24.4 24.6 24.8 25.0 25.2 25.4 25.6
0.0 0.5 1.0 1.5 2.0

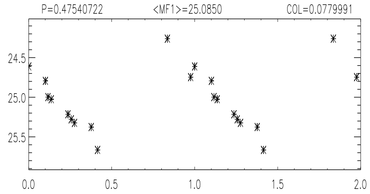
P=0.47540722 <MF1>=25.0850 COL=0.0779991
24.5 25.0 25.5
0.0 0.5 1.0 1.5 2.0

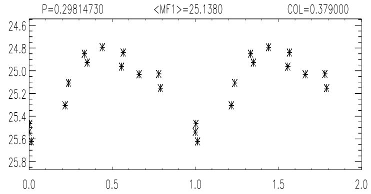
P=0.29814730 <MF1>=25.1380 COL=0.379000
24.6 24.8 25.0 25.2 25.4 25.6 25.8
0.0 0.5 1.0 1.5 2.0

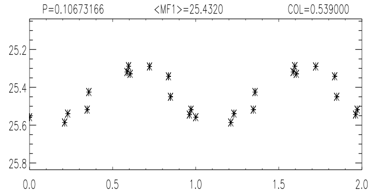
P=0.10673166 <MF1>=25.4320 COL=0.539000
25.2 25.4 25.6 25.8
0.0 0.5 1.0 1.5 2.0

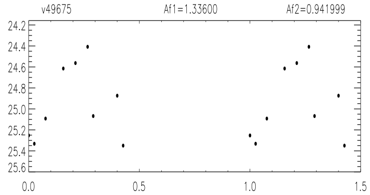
v49675 Af1=1.33600 Af2=0.941999
24.2 24.4 24.6 24.8 25.0 25.2 25.4 25.6
0.0 0.5 1.0 1.5

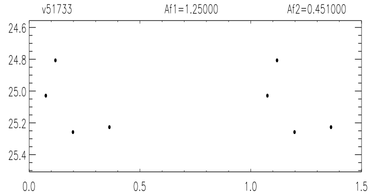
v51733 Af1=1.25000 Af2=0.451000
24.6 24.8 25.0 25.2 25.4
0.0 0.5 1.0 1.5

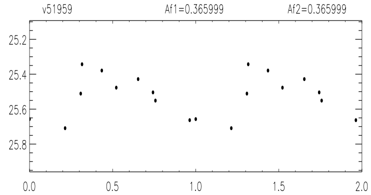
v51959 Af1=0.365999 Af2=0.365999
25.2 25.4 25.6 25.8
0.0 0.5 1.0 1.5 2.0

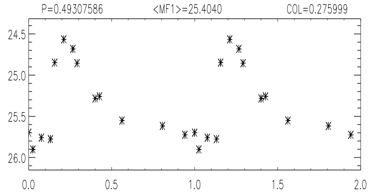
P=0.49307586 <MF1>=25.4040 COL=0.275999
24.5 25.0 25.5 26.0
0.0 0.5 1.0 1.5 2.0

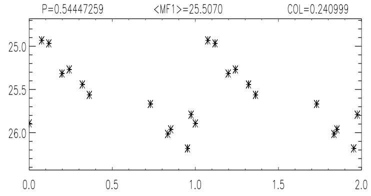
P=0.54447259 <MF1>=25.5070 COL=0.240999
25.0 25.5 26.0
0.0 0.5 1.0 1.5 2.0

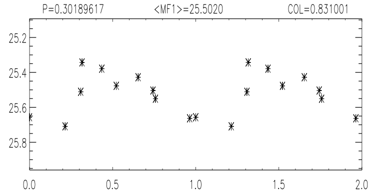
P=0.30189617 <MF1>=25.5020 COL=0.831001
25.2 25.4 25.6 25.8
0.0 0.5 1.0 1.5 2.0

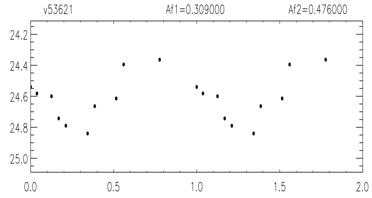
v53621 Af1=0.309000 Af2=0.476000
24.2
24.4
24.6
24.8
25.0
0.0 0.5 1.0 1.5 2.0

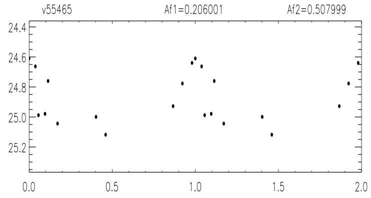
v55465 Af1=0.206001 Af2=0.507999
24.4
24.6
24.8
25.0
25.2
0.0 0.5 1.0 1.5 2.0

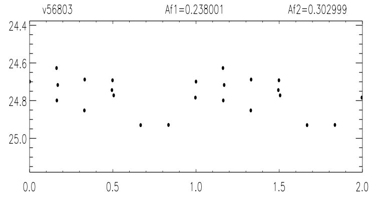
v56803 Af1=0.238001 Af2=0.302999
24.4
24.6
24.8
25.0
0.0 0.5 1.0 1.5 2.0

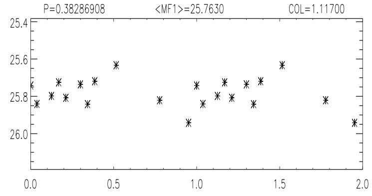
P=0.38286908 <MF1>=25.7630 COL=1.11700
25.4
25.6
25.8
26.0
0.0 0.5 1.0 1.5 2.0

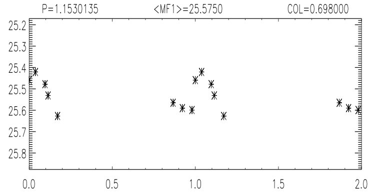
P=1.1530135 <MF1>=25.5750 COL=0.698000
25.2
25.3
25.4
25.5
25.6
25.7
25.8
0.0 0.5 1.0 1.5 2.0

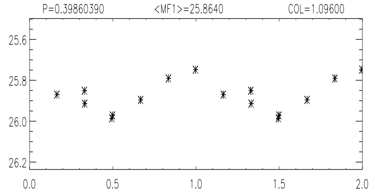
P=0.39860390 <MF1>=25.8640 COL=1.09600
25.6
25.8
26.0
26.2
0.0 0.5 1.0 1.5 2.0

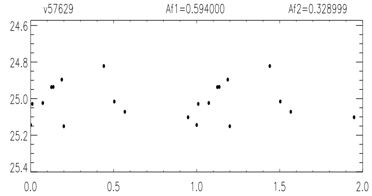
v57629 Af1=0.594000 Af2=0.328999
24.6
24.8
25.0
25.2
25.4
0.0 0.5 1.0 1.5 2.0

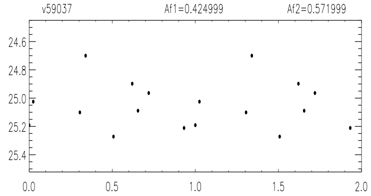
v59037 Af1=0.424999 Af2=0.571999
24.6
24.8
25.0
25.2
25.4
0.0 0.5 1.0 1.5 2.0

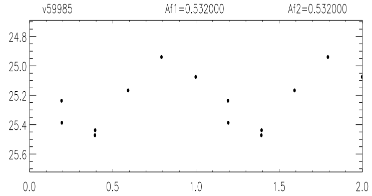
v59985 Af1=0.532000 Af2=0.532000
24.8
25.0
25.2
25.4
25.6
0.0 0.5 1.0 1.5 2.0

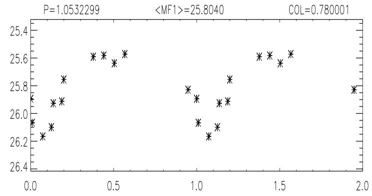
P=1.0532299 <MF1>=25.8040 COL=0.780001
25.4
25.6
25.8
26.0
26.2
26.4
0.0 0.5 1.0 1.5 2.0

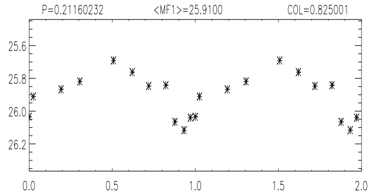
P=0.21160232 <MF1>=25.9100 COL=0.825001
25.6
25.8
26.0
26.2
0.0 0.5 1.0 1.5 2.0

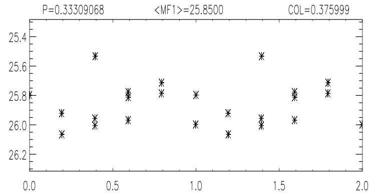
P=0.33309068 <MF1>=25.8500 COL=0.375999
25.4
25.6
25.8
26.0
26.2
0.0 0.5 1.0 1.5 2.0

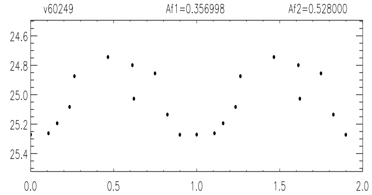
v60249 Af1=0.356998 Af2=0.528000
24.6
24.8
25.0
25.2
25.4
0.0 0.5 1.0 1.5 2.0

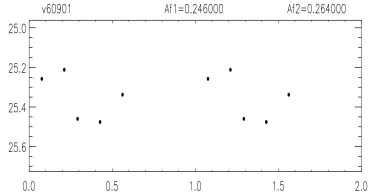
v60901 Af1=0.246000 Af2=0.264000
25.0
25.2
25.4
25.6
0.0 0.5 1.0 1.5 2.0

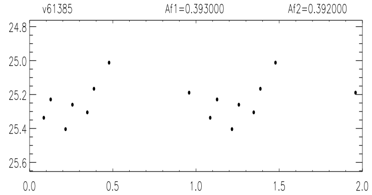
v61385 Af1=0.393000 Af2=0.392000
24.8
25.0
25.2
25.4
25.6
0.0 0.5 1.0 1.5 2.0

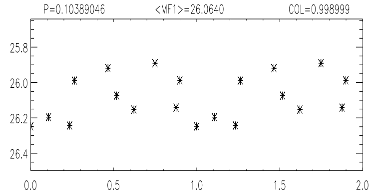
P=0.10389046 <MF1>=26.0640 COL=0.998999
25.8
26.0
26.2
26.4
0.0 0.5 1.0 1.5 2.0

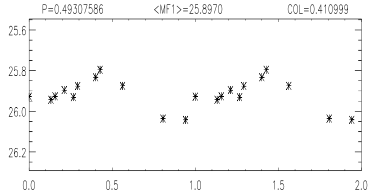
P=0.49307586 <MF1>=25.8970 COL=0.410999
25.6
25.8
26.0
26.2
0.0 0.5 1.0 1.5 2.0

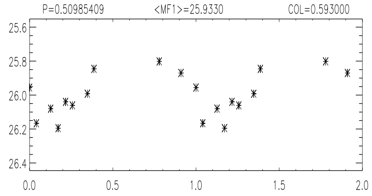
P=0.50985409 <MF1>=25.9330 COL=0.593000
25.6
25.8
26.0
26.2
26.4
0.0 0.5 1.0 1.5 2.0

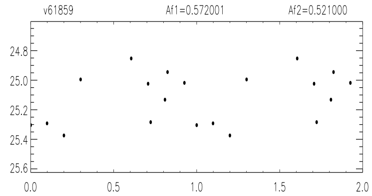
v61859 Af1=0.572001 Af2=0.521000
24.8
25.0
25.2
25.4
25.6
0.0 0.5 1.0 1.5 2.0

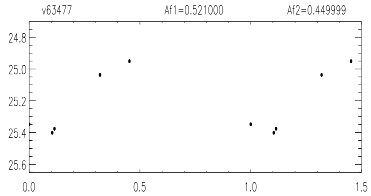
v63477 Af1=0.521000 Af2=0.449999
24.8
25.0
25.2
25.4
25.6
0.0 0.5 1.0 1.5

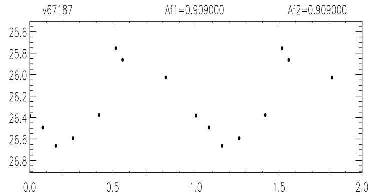
v67187 Af1=0.909000 Af2=0.909000
25.6
25.8
26.0
26.2
26.4
26.6
26.8
0.0 0.5 1.0 1.5 2.0

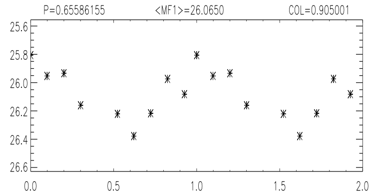
P=0.65586155 <MF1>=26.0650 COL=0.905001
25.6
25.8
26.0
26.2
26.4
26.6
0.0 0.5 1.0 1.5 2.0

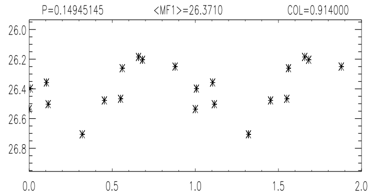
P=0.14945145 <MF1>=26.3710 COL=0.914000
26.0
26.2
26.4
26.6
26.8
0.0 0.5 1.0 1.5 2.0

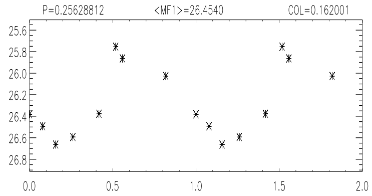
P=0.25628812 <MF1>=26.4540 COL=0.162001
25.6
25.8
26.0
26.2
26.4
26.6
26.8
0.0 0.5 1.0 1.5 2.0

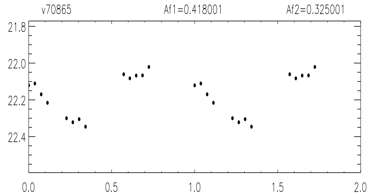
v70865
Af1=0.418001
Af2=0.325001
21.8
22.0
22.2
22.4
0.0
0.5
1.0
1.5
2.0

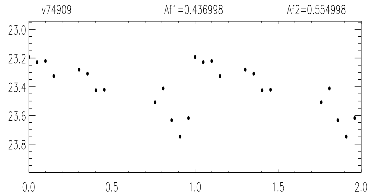
v74909
Af1=0.436998
Af2=0.554998
23.0
23.2
23.4
23.6
23.8
0.0
0.5
1.0
1.5
2.0

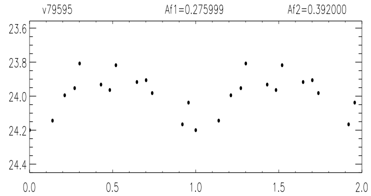
v79595
Af1=0.275999
Af2=0.392000
23.6
23.8
24.0
24.2
24.4
0.0
0.5
1.0
1.5
2.0

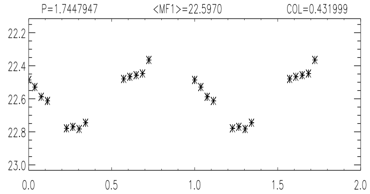
P=1.7447947
<MF1>=22.5970
COL=0.431999
22.2
22.4
22.6
22.8
23.0
0.0
0.5
1.0
1.5
2.0

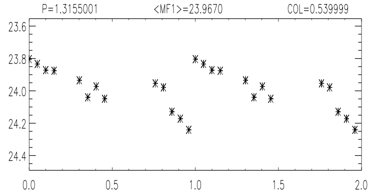
P=1.3155001
<MF1>=23.9670
COL=0.539999
23.6
23.8
24.0
24.2
24.4
0.0
0.5
1.0
1.5
2.0

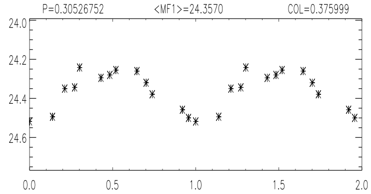
P=0.30526752
<MF1>=24.3570
COL=0.375999
24.0
24.2
24.4
24.6
0.0
0.5
1.0
1.5
2.0

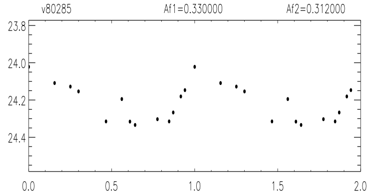
v80285
Af1=0.330000
Af2=0.312000
23.8
24.0
24.2
24.4
0.0
0.5
1.0
1.5
2.0

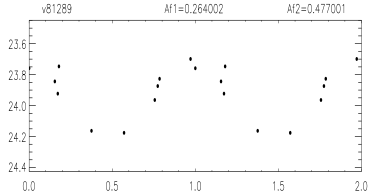
v81289
Af1=0.264002
Af2=0.477001
23.6
23.8
24.0
24.2
24.4
0.0
0.5
1.0
1.5
2.0

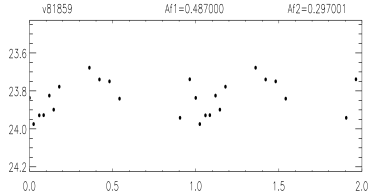
v81859
Af1=0.487000
Af2=0.297001
23.6
23.8
24.0
24.2
0.0
0.5
1.0
1.5
2.0

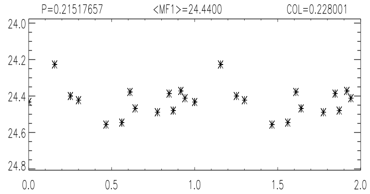
P=0.21517657
<MF1>=24.4400
COL=0.228001
24.0
24.2
24.4
24.6
24.8
0.0
0.5
1.0
1.5
2.0

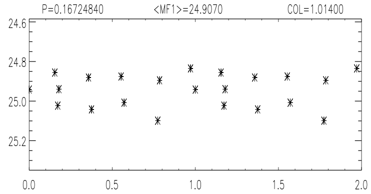
P=0.16724840
<MF1>=24.9070
COL=1.01400
24.6
24.8
25.0
25.2
0.0
0.5
1.0
1.5
2.0

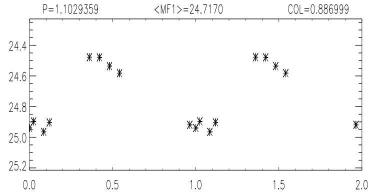
P=1.1029359
<MF1>=24.7170
COL=0.886999
24.4
24.6
24.8
25.0
25.2
0.0
0.5
1.0
1.5
2.0

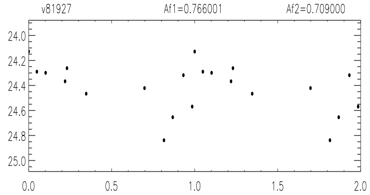
v81927
Af1=0.766001
Af2=0.709000
24.0
24.2
24.4
24.6
24.8
25.0
0.0
0.5
1.0
1.5
2.0

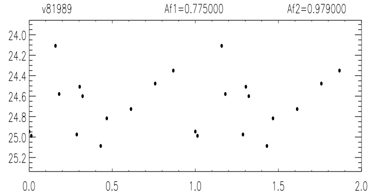
v81989
Af1=0.775000
Af2=0.979000
24.0
24.2
24.4
24.6
24.8
25.0
25.2
0.0
0.5
1.0
1.5
2.0

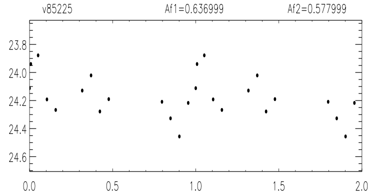
v85225
Af1=0.636999
Af2=0.577999
23.8
24.0
24.2
24.4
24.6
0.0
0.5
1.0
1.5
2.0

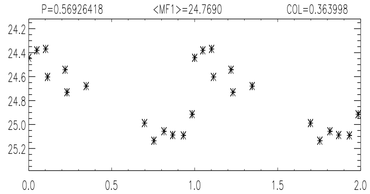
P=0.56926418
<MF1>=24.7690
COL=0.363998
24.2
24.4
24.6
24.8
25.0
25.2
0.0
0.5
1.0
1.5
2.0

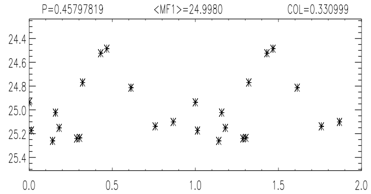
P=0.45797819
<MF1>=24.9980
COL=0.330999
24.4
24.6
24.8
25.0
25.2
25.4
0.0
0.5
1.0
1.5
2.0

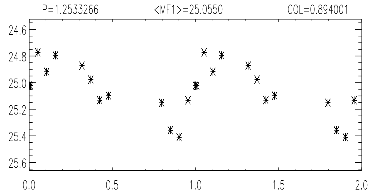
P=1.2533266
<MF1>=25.0550
COL=0.894001
24.6
24.8
25.0
25.2
25.4
25.6
0.0
0.5
1.0
1.5
2.0

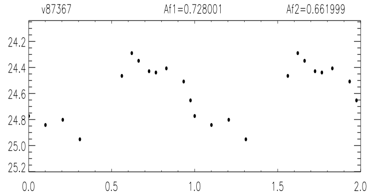
v87367
Af1=0.728001
Af2=0.661999
24.2
24.4
24.6
24.8
25.0
25.2
0.0
0.5
1.0
1.5
2.0

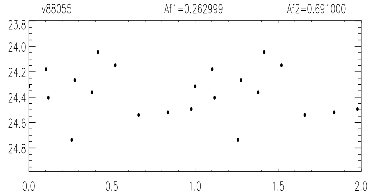
v88055
Af1=0.262999
Af2=0.691000
23.8
24.0
24.2
24.4
24.6
24.8
0.0
0.5
1.0
1.5
2.0

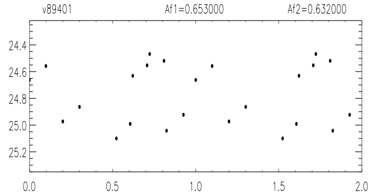
v89401
Af1=0.653000
Af2=0.632000
24.4
24.6
24.8
25.0
25.2
0.0
0.5
1.0
1.5
2.0

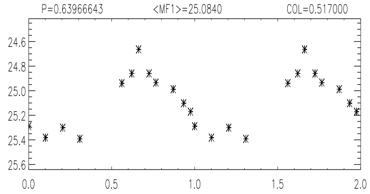
P=0.63966643
<MF1>=25.0840
COL=0.517000
24.6
24.8
25.0
25.2
25.4
25.6
0.0
0.5
1.0
1.5
2.0

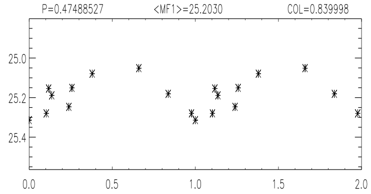
P=0.47488527
<MF1>=25.2030
COL=0.839998
25.0
25.2
25.4
0.0
0.5
1.0
1.5
2.0

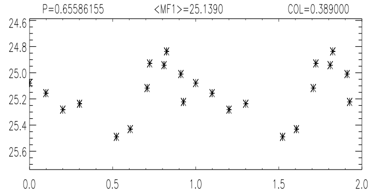
P=0.65586155
<MF1>=25.1390
COL=0.389000
24.6
24.8
25.0
25.2
25.4
25.6
0.0
0.5
1.0
1.5
2.0

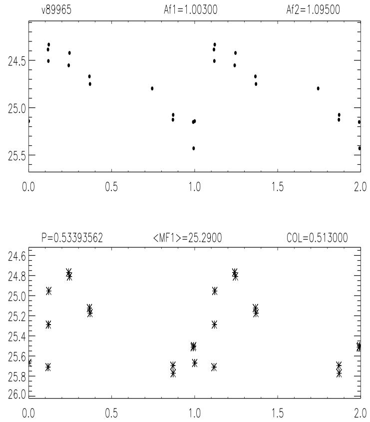
v89965
Af1=1.00300
Af2=1.09500
24.5
25.0
25.5
0.0
0.5
1.0
1.5
2.0
P=0.53393562
<MF1>=25.2900
COL=0.513000
24.6
24.8
25.0
25.2
25.4
25.6
25.8
26.0
0.0
0.5
1.0
1.5
2.0

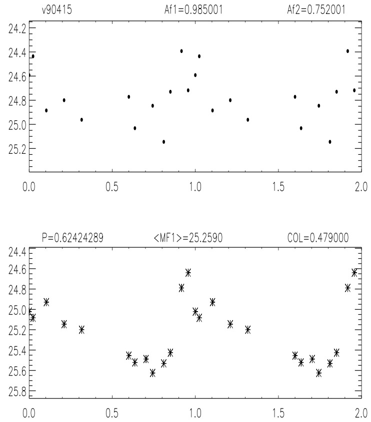
v90415
Af1=0.985001
Af2=0.752001
24.2
24.4
24.6
24.8
25.0
25.2
0.0
0.5
1.0
1.5
2.0
P=0.62424289
<MF1>=25.2590
COL=0.479000
24.4
24.6
24.8
25.0
25.2
25.4
25.6
25.8
0.0
0.5
1.0
1.5
2.0

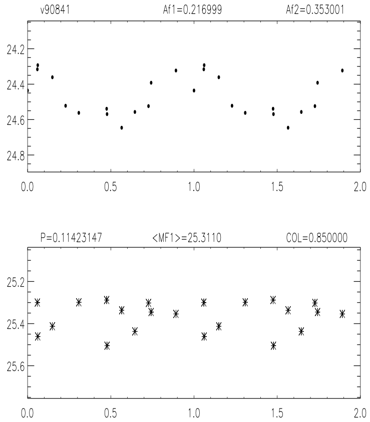
v90841
Af1=0.216999
Af2=0.353001
24.2
24.4
24.6
24.8
0.0
0.5
1.0
1.5
2.0
P=0.11423147
<MF1>=25.3110
COL=0.850000
25.2
25.4
25.6
0.0
0.5
1.0
1.5
2.0

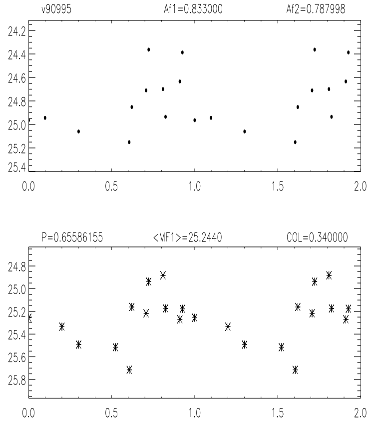
v90995
Af1=0.833000
Af2=0.787998
24.2
24.4
24.6
24.8
25.0
25.2
25.4
0.0
0.5
1.0
1.5
2.0
P=0.65586155
<MF1>=25.2440
COL=0.340000
24.8
25.0
25.2
25.4
25.6
25.8
0.0
0.5
1.0
1.5
2.0

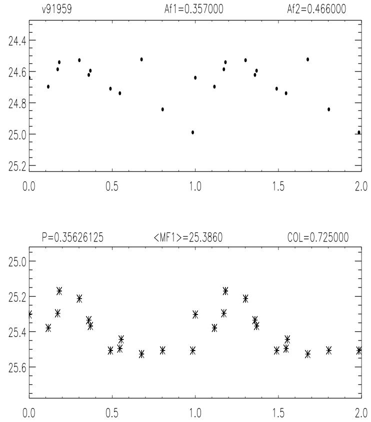
v91959
Af1=0.357000
Af2=0.466000
24.4
24.6
24.8
25.0
25.2
0.0
0.5
1.0
1.5
2.0
P=0.35626125
<MF1>=25.3860
COL=0.725000
25.0
25.2
25.4
25.6
0.0
0.5
1.0
1.5
2.0

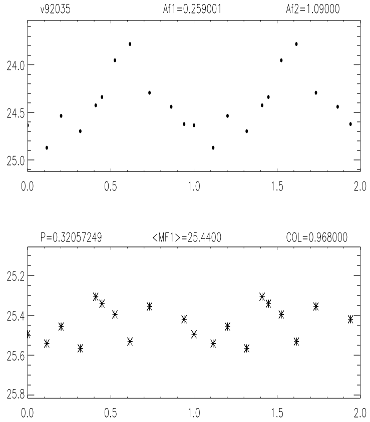
v92035
Af1=0.259001
Af2=1.09000
24.0
24.5
25.0
0.0
0.5
1.0
1.5
2.0
P=0.32057249
<MF1>=25.4400
COL=0.968000
25.2
25.4
25.6
25.8
0.0
0.5
1.0
1.5
2.0

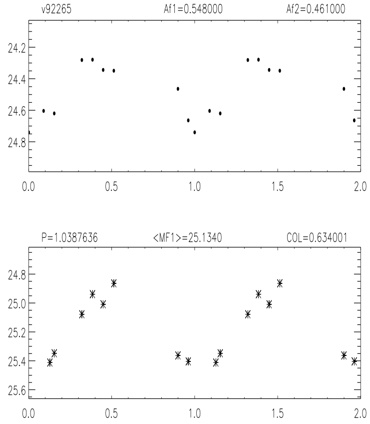
v92265
Af1=0.548000
Af2=0.461000
24.2
24.4
24.6
24.8
0.0
0.5
1.0
1.5
2.0
P=1.0387636
<MF1>=25.1340
COL=0.634001
24.8
25.0
25.2
25.4
25.6
0.0
0.5
1.0
1.5
2.0

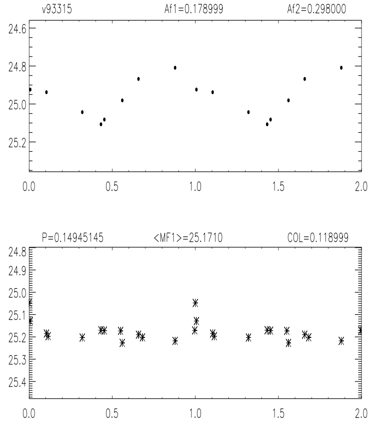
v93315
Af1=0.178999
Af2=0.298000
24.6
24.8
25.0
25.2
0.0
0.5
1.0
1.5
2.0
P=0.14945145
<MF1>=25.1710
COL=0.118999
24.8
24.9
25.0
25.1
25.2
25.3
25.4
0.0
0.5
1.0
1.5
2.0

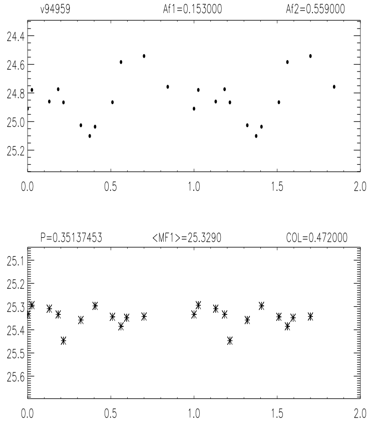
v94959
Af1=0.153000
Af2=0.559000
24.4
24.6
24.8
25.0
25.2
0.0
0.5
1.0
1.5
2.0
P=0.35137453
<MF1>=25.3290
COL=0.472000
25.1
25.2
25.3
25.4
25.5
25.6
0.0
0.5
1.0
1.5
2.0

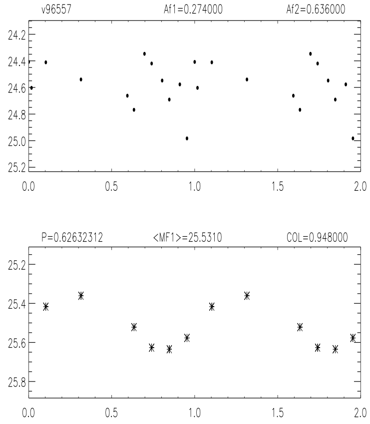
v96557
Af1=0.274000
Af2=0.636000
24.2
24.4
24.6
24.8
25.0
25.2
0.0
0.5
1.0
1.5
2.0
P=0.62632312
<MF1>=25.5310
COL=0.948000
25.2
25.4
25.6
25.8
0.0
0.5
1.0
1.5
2.0

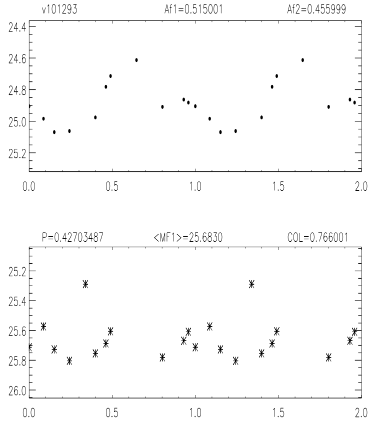
v101293
Af1=0.515001
Af2=0.455999
24.4
24.6
24.8
25.0
25.2
0.0
0.5
1.0
1.5
2.0
P=0.42703487
<MF1>=25.6830
COL=0.766001
25.2
25.4
25.6
25.8
26.0
0.0
0.5
1.0
1.5
2.0

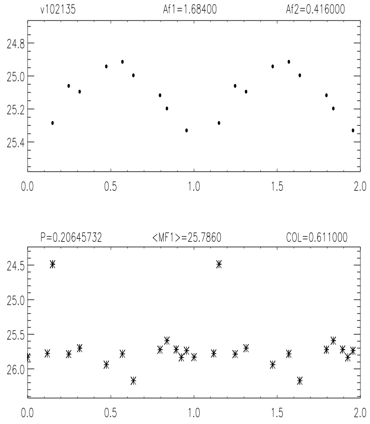
v102135
Af1=1.68400
Af2=0.416000
24.8
25.0
25.2
25.4
0.0
0.5
1.0
1.5
2.0
P=0.20645732
<MF1>=25.7860
COL=0.611000
24.5
25.0
25.5
26.0
0.0
0.5
1.0
1.5
2.0

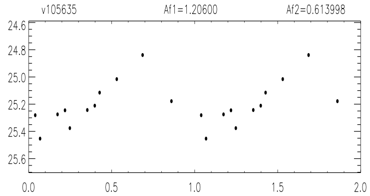
v105635
Af1=1.20600
Af2=0.613998
24.6
24.8
25.0
25.2
25.4
25.6
0.0
0.5
1.0
1.5
2.0

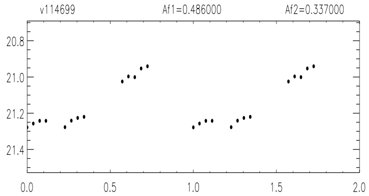
v114699
Af1=0.486000
Af2=0.337000
20.8
21.0
21.2
21.4
0.0
0.5
1.0
1.5
2.0

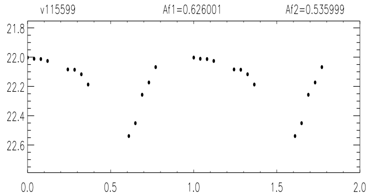
v115599
Af1=0.626001
Af2=0.535999
21.8
22.0
22.2
22.4
22.6
0.0
0.5
1.0
1.5
2.0

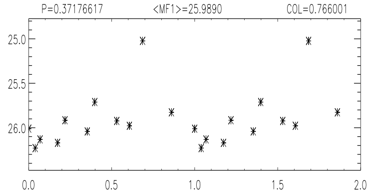
P=0.37176617
<MF1>=25.9890
COL=0.766001
25.0
25.5
26.0
0.0
0.5
1.0
1.5
2.0

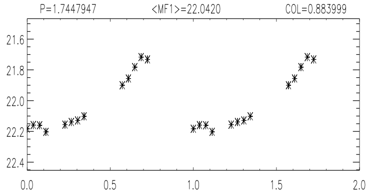
P=1.7447947
<MF1>=22.0420
COL=0.883999
21.6
21.8
22.0
22.2
22.4
0.0
0.5
1.0
1.5
2.0

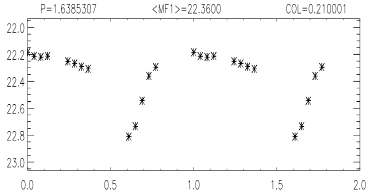
P=1.6385307
<MF1>=22.3600
COL=0.210001
22.0
22.2
22.4
22.6
22.8
23.0
0.0
0.5
1.0
1.5
2.0

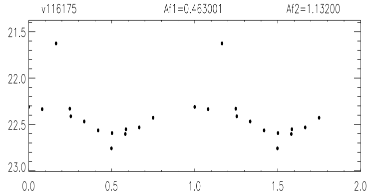
v116175
Af1=0.463001
Af2=1.13200
21.5
22.0
22.5
23.0
0.0
0.5
1.0
1.5
2.0

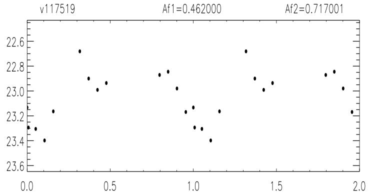
v117519
Af1=0.462000
Af2=0.717001
22.6
22.8
23.0
23.2
23.4
23.6
0.0
0.5
1.0
1.5
2.0

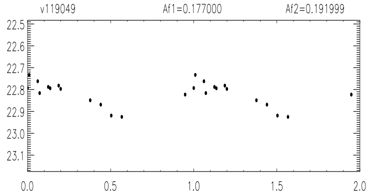
v119049
Af1=0.177000
Af2=0.191999
22.5
22.6
22.7
22.8
22.9
23.0
23.1
0.0
0.5
1.0
1.5
2.0

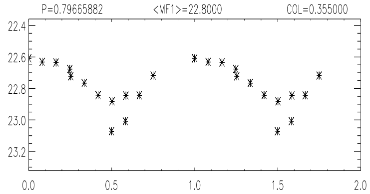
P=0.79665882
<MF1>=22.8000
COL=0.355000
22.4
22.6
22.8
23.0
23.2
0.0
0.5
1.0
1.5
2.0

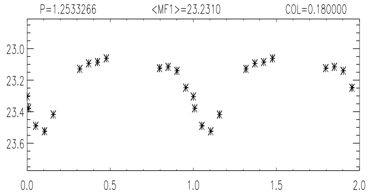
P=1.2533266
<MF1>=23.2310
COL=0.180000
23.0
23.2
23.4
23.6
0.0
0.5
1.0
1.5
2.0

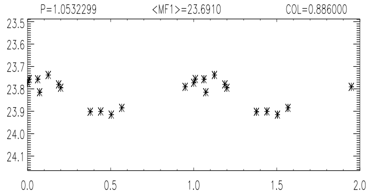
P=1.0532299
<MF1>=23.6910
COL=0.886000
23.5
23.6
23.7
23.8
23.9
24.0
24.1
0.0
0.5
1.0
1.5
2.0

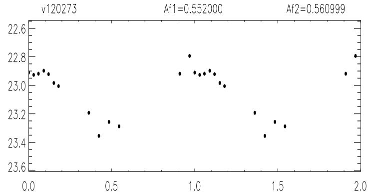
v120273
Af1=0.552000
Af2=0.560999
22.6
22.8
23.0
23.2
23.4
23.6
0.0
0.5
1.0
1.5
2.0

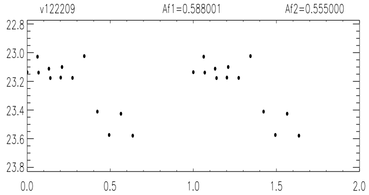
v122209
Af1=0.588001
Af2=0.555000
22.8
23.0
23.2
23.4
23.6
23.8
0.0
0.5
1.0
1.5
2.0

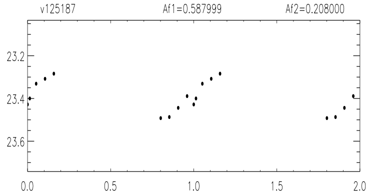
v125187
Af1=0.587999
Af2=0.208000
23.2
23.4
23.6
0.0
0.5
1.0
1.5
2.0

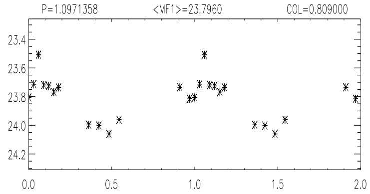
P=1.0971358
<MF1>=23.7960
COL=0.809000
23.4
23.6
23.8
24.0
24.2
0.0
0.5
1.0
1.5
2.0

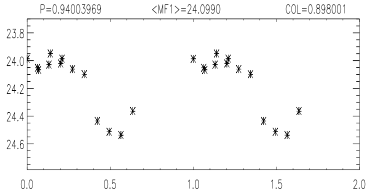
P=0.94003969
<MF1>=24.0990
COL=0.898001
23.8
24.0
24.2
24.4
24.6
0.0
0.5
1.0
1.5
2.0

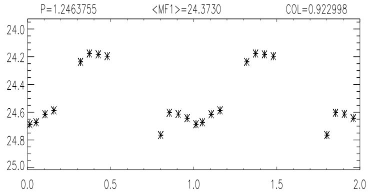
P=1.2463755
<MF1>=24.3730
COL=0.922998
24.0
24.2
24.4
24.6
24.8
25.0
0.0
0.5
1.0
1.5
2.0

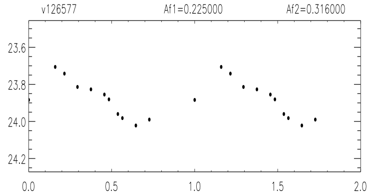
v126577
Af1=0.225000
Af2=0.316000
23.6
23.8
24.0
24.2
0.0
0.5
1.0
1.5
2.0

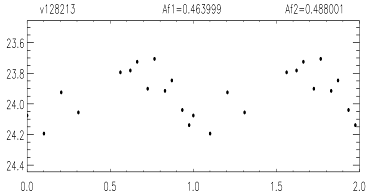
v128213
Af1=0.463999
Af2=0.488001
23.6
23.8
24.0
24.2
24.4
0.0
0.5
1.0
1.5
2.0

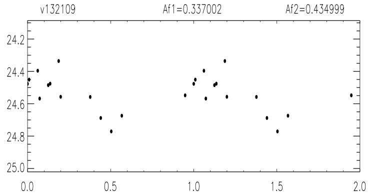
v132109
Af1=0.337002
Af2=0.434999
24.2
24.4
24.6
24.8
25.0
0.0
0.5
1.0
1.5
2.0

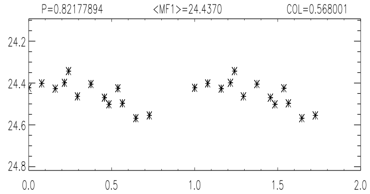
P=0.82177894
<MF1>=24.4370
COL=0.568001
24.2
24.4
24.6
24.8
0.0
0.5
1.0
1.5
2.0

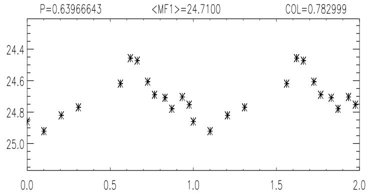
P=0.63966643
<MF1>=24.7100
COL=0.782999
24.4
24.6
24.8
25.0
0.0
0.5
1.0
1.5
2.0

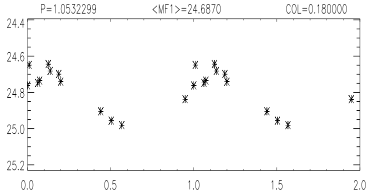
P=1.0532299
<MF1>=24.6870
COL=0.180000
24.4
24.6
24.8
25.0
25.2
0.0
0.5
1.0
1.5
2.0

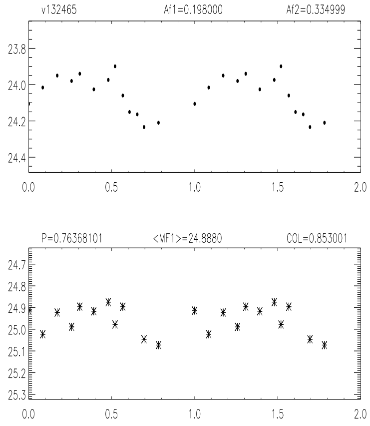
v132465 Af1=0.198000 Af2=0.334999
23.8 24.0 24.2 24.4
P=0.76368101 <MF1>=24.8880 COL=0.853001
24.7 24.8 24.9 25.0 25.1 25.2 25.3
0.0 0.5 1.0 1.5 2.0

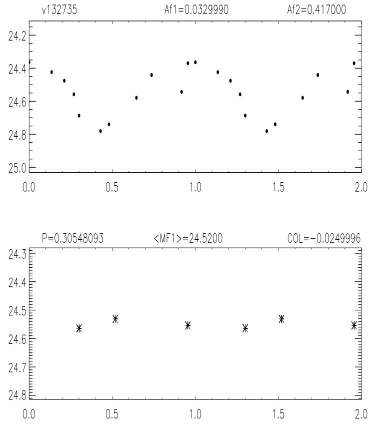
v132735 Af1=0.0329990 Af2=0.417000
24.2 24.4 24.6 24.8 25.0
P=0.30548093 <MF1>=24.5200 COL=-0.0249996
24.3 24.4 24.5 24.6 24.7 24.8
0.0 0.5 1.0 1.5 2.0

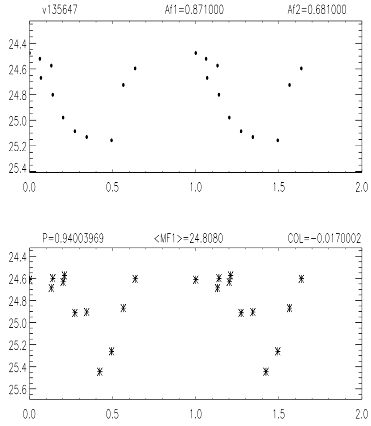
v135647 Af1=0.871000 Af2=0.681000
24.4 24.6 24.8 25.0 25.2 25.4
P=0.94003969 <MF1>=24.8080 COL=-0.0170002
24.4 24.6 24.8 25.0 25.2 25.4 25.6
0.0 0.5 1.0 1.5 2.0

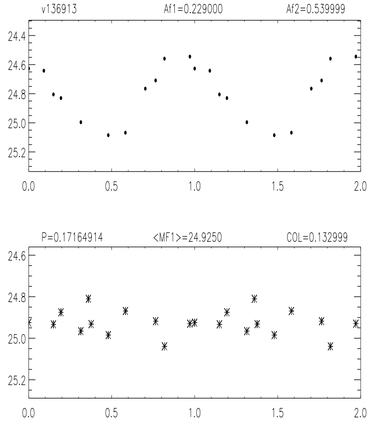
v136913 Af1=0.229000 Af2=0.539999
24.4 24.6 24.8 25.0 25.2
P=0.17164914 <MF1>=24.9250 COL=0.132999
24.6 24.8 25.0 25.2
0.0 0.5 1.0 1.5 2.0

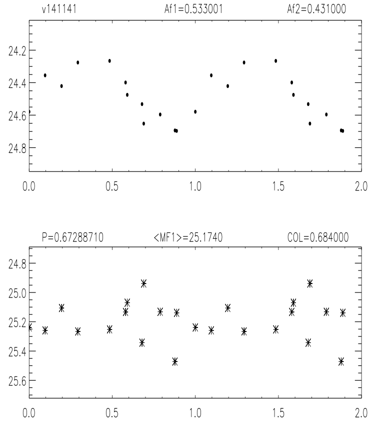
v141141 Af1=0.533001 Af2=0.431000
24.2 24.4 24.6 24.8
P=0.67288710 <MF1>=25.1740 COL=0.684000
24.8 25.0 25.2 25.4 25.6
0.0 0.5 1.0 1.5 2.0

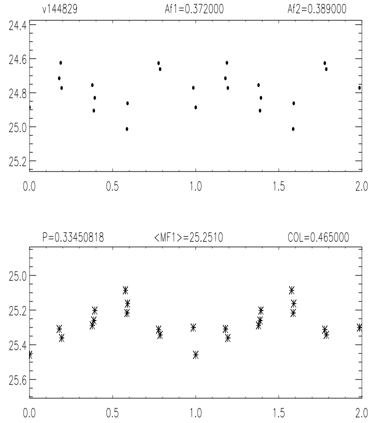
v144829 Af1=0.372000 Af2=0.389000
24.4 24.6 24.8 25.0 25.2
P=0.33450818 <MF1>=25.2510 COL=0.465000
25.0 25.2 25.4 25.6
0.0 0.5 1.0 1.5 2.0

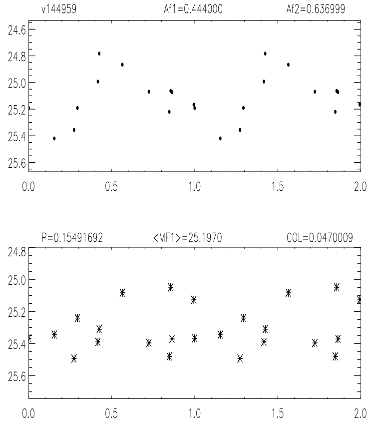
v144959 Af1=0.444000 Af2=0.636999
24.6 24.8 25.0 25.2 25.4 25.6
P=0.15491692 <MF1>=25.1970 COL=0.0470009
24.8 25.0 25.2 25.4 25.6
0.0 0.5 1.0 1.5 2.0

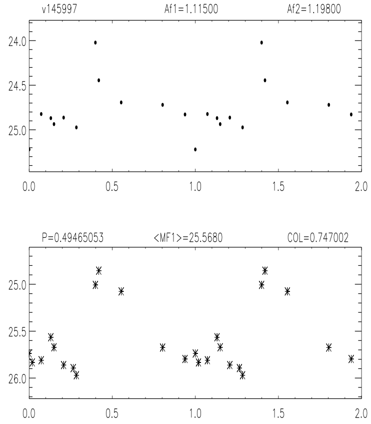
v145997 Af1=1.11500 Af2=1.19800
24.0 24.5 25.0
P=0.49465053 <MF1>=25.5680 COL=0.747002
25.0 25.5 26.0
0.0 0.5 1.0 1.5 2.0

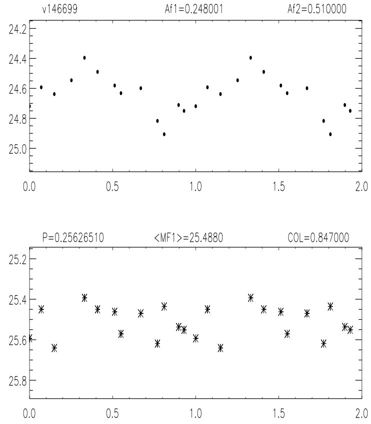
v146699 Af1=0.248001 Af2=0.510000
24.2 24.4 24.6 24.8 25.0
P=0.25626510 <MF1>=25.4880 COL=0.847000
25.2 25.4 25.6 25.8
0.0 0.5 1.0 1.5 2.0

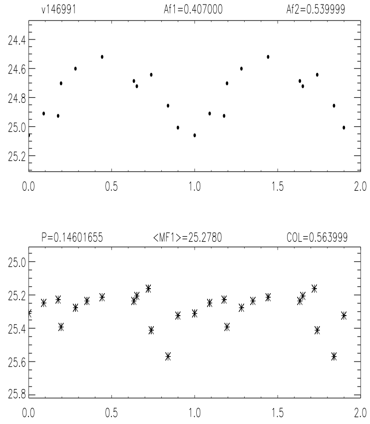
v146991 Af1=0.407000 Af2=0.539999
24.4 24.6 24.8 25.0 25.2
P=0.14601655 <MF1>=25.2780 COL=0.563999
25.0 25.2 25.4 25.6 25.8
0.0 0.5 1.0 1.5 2.0

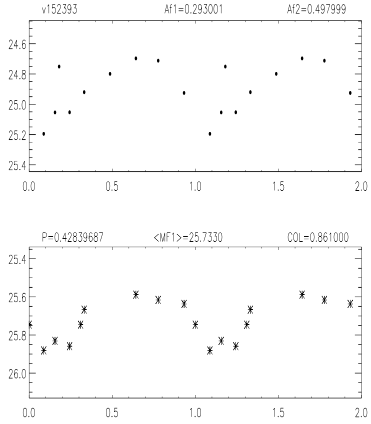
v152393 Af1=0.293001 Af2=0.497999
24.6 24.8 25.0 25.2 25.4
P=0.42839687 <MF1>=25.7330 COL=0.861000
25.4 25.6 25.8 26.0
0.0 0.5 1.0 1.5 2.0

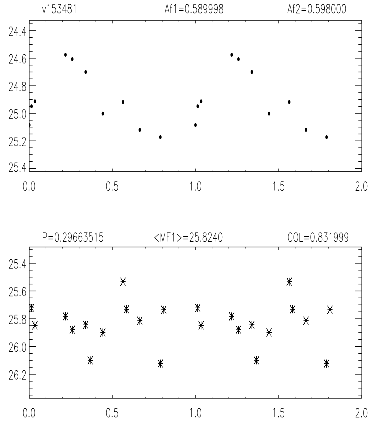
v153481 Af1=0.589998 Af2=0.598000
24.4 24.6 24.8 25.0 25.2 25.4
P=0.29663515 <MF1>=25.8240 COL=0.831999
25.4 25.6 25.8 26.0 26.2
0.0 0.5 1.0 1.5 2.0

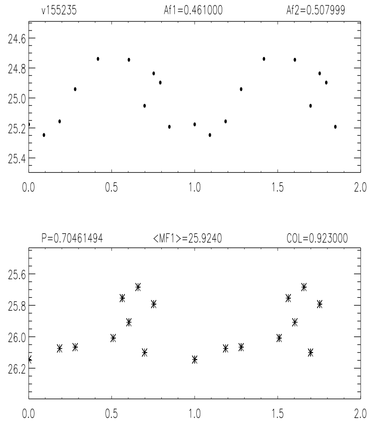
v155235
Af1=0.461000
Af2=0.507999
24.6
24.8
25.0
25.2
25.4
0.0
0.5
1.0
1.5
2.0
P=0.70461494
<MF1>=25.9240
COL=0.923000
25.6
25.8
26.0
26.2
0.0
0.5
1.0
1.5
2.0

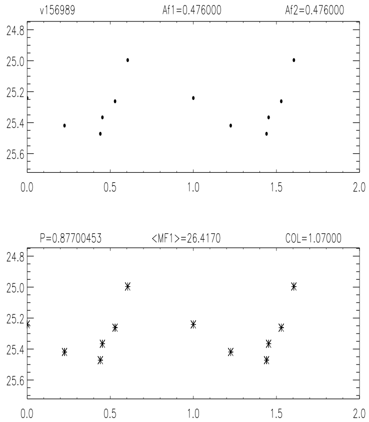
v156989
Af1=0.476000
Af2=0.476000
24.8
25.0
25.2
25.4
25.6
0.0
0.5
1.0
1.5
2.0
P=0.87700453
<MF1>=26.4170
COL=1.07000
24.8
25.0
25.2
25.4
25.6
0.0
0.5
1.0
1.5
2.0

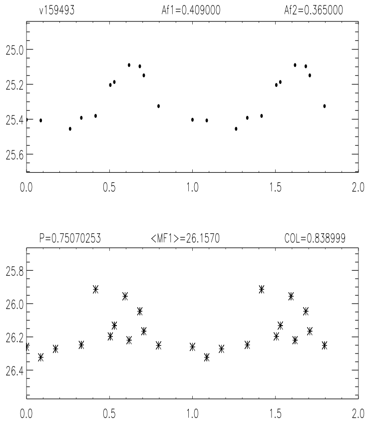
v159493
Af1=0.409000
Af2=0.365000
25.0
25.2
25.4
25.6
0.0
0.5
1.0
1.5
2.0
P=0.75070253
<MF1>=26.1570
COL=0.838999
25.8
26.0
26.2
26.4
0.0
0.5
1.0
1.5
2.0

Chapter 11

Appendix E

ATLAS OF LIGHT CURVES: G105

Atlas of the V,I light curves for candidate variable stars identified in G105. For each variable the upper panel shows the I-band light curve, and the lower panel the V-band light curve. Identification, V and I amplitudes, period, average V magnitude and average V−I color, are provided on top labels of the plots.

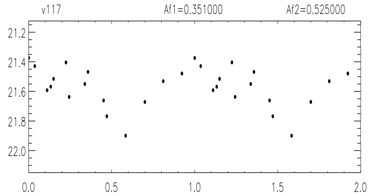
v117
Af1=0.351000
Af2=0.525000
21.2
21.4
21.6
21.8
22.0
0.0
0.5
1.0
1.5
2.0

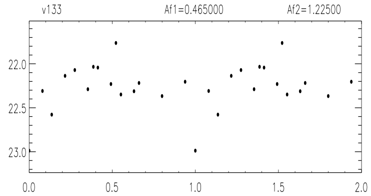
v133
Af1=0.465000
Af2=1.22500
22.0
22.5
23.0
0.0
0.5
1.0
1.5
2.0

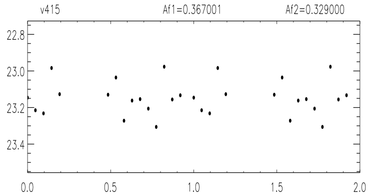
v415
Af1=0.367001
Af2=0.329000
22.8
23.0
23.2
23.4
0.0
0.5
1.0
1.5
2.0

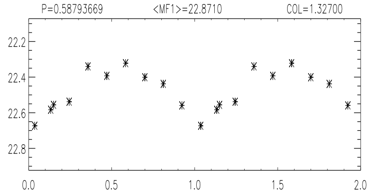
P=0.58793669
<MF1>=22.8710
COL=1.32700
22.2
22.4
22.6
22.8
0.0
0.5
1.0
1.5
2.0

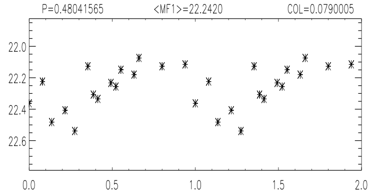
P=0.48041565
<MF1>=22.2420
COL=0.0790005
22.0
22.2
22.4
22.6
0.0
0.5
1.0
1.5
2.0

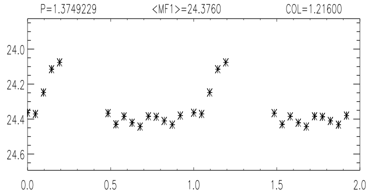
P=1.3749229
<MF1>=24.3760
COL=1.21600
24.0
24.2
24.4
24.6
0.0
0.5
1.0
1.5
2.0

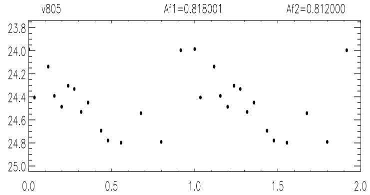
v805
Af1=0.818001
Af2=0.812000
23.8
24.0
24.2
24.4
24.6
24.8
25.0
0.0
0.5
1.0
1.5
2.0

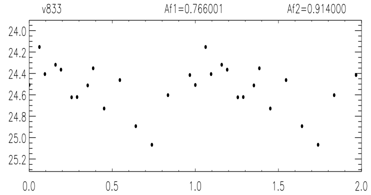
v833
Af1=0.766001
Af2=0.914000
24.0
24.2
24.4
24.6
24.8
25.0
25.2
0.0
0.5
1.0
1.5
2.0

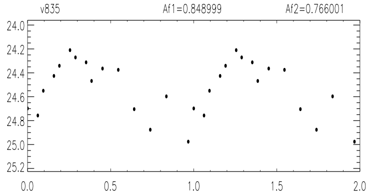
v835
Af1=0.848999
Af2=0.766001
24.0
24.2
24.4
24.6
24.8
25.0
25.2
0.0
0.5
1.0
1.5
2.0

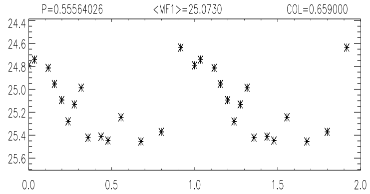
P=0.55564026
<MF1>=25.0730
COL=0.659000
24.4
24.6
24.8
25.0
25.2
25.4
25.6
0.0
0.5
1.0
1.5
2.0

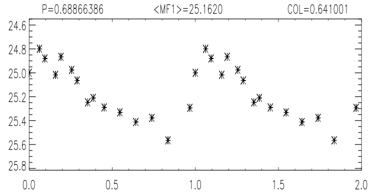
P=0.68866386
<MF1>=25.1620
COL=0.641001
24.6
24.8
25.0
25.2
25.4
25.6
25.8
0.0
0.5
1.0
1.5
2.0

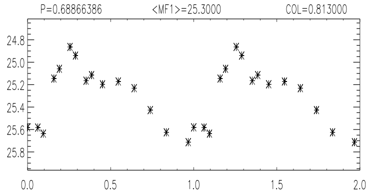
P=0.68866386
<MF1>=25.3000
COL=0.813000
24.8
25.0
25.2
25.4
25.6
25.8
0.0
0.5
1.0
1.5
2.0

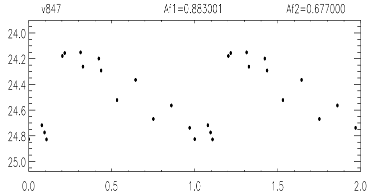
v847
Af1=0.883001
Af2=0.677000
24.0
24.2
24.4
24.6
24.8
25.0
0.0
0.5
1.0
1.5
2.0

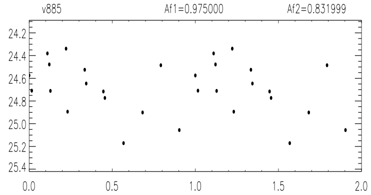
v885
Af1=0.975000
Af2=0.831999
24.2
24.4
24.6
24.8
25.0
25.2
25.4
0.0
0.5
1.0
1.5
2.0

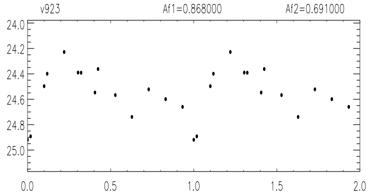
v923
Af1=0.868000
Af2=0.691000
24.0
24.2
24.4
24.6
24.8
25.0
0.0
0.5
1.0
1.5
2.0

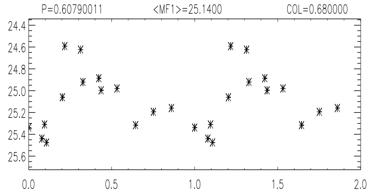
P=0.60790011
<MF1>=25.1400
COL=0.680000
24.4
24.6
24.8
25.0
25.2
25.4
25.6
0.0
0.5
1.0
1.5
2.0

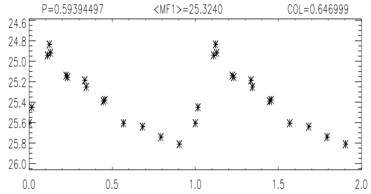
P=0.59394497
<MF1>=25.3240
COL=0.646999
24.6
24.8
25.0
25.2
25.4
25.6
25.8
26.0
0.0
0.5
1.0
1.5
2.0

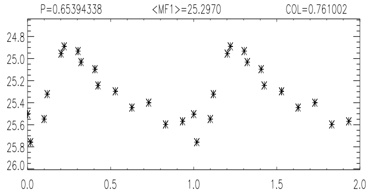
P=0.65394338
<MF1>=25.2970
COL=0.761002
24.8
25.0
25.2
25.4
25.6
25.8
26.0
0.0
0.5
1.0
1.5
2.0

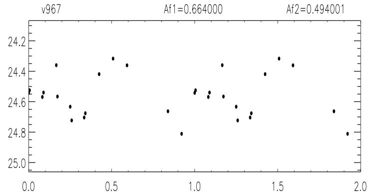
v967
Af1=0.664000
Af2=0.494001
24.2
24.4
24.6
24.8
25.0
0.0
0.5
1.0
1.5
2.0

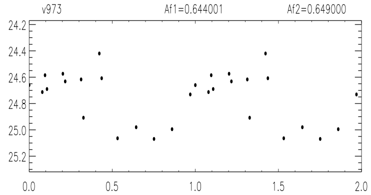
v973
Af1=0.644001
Af2=0.649000
24.2
24.4
24.6
24.8
25.0
25.2
0.0
0.5
1.0
1.5
2.0

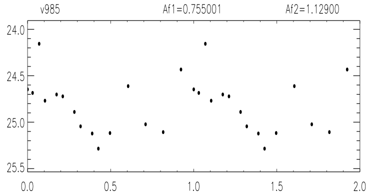
v985
Af1=0.755001
Af2=1.12900
24.0
24.5
25.0
25.5
0.0
0.5
1.0
1.5
2.0

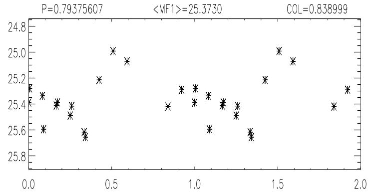
P=0.79375607
<MF1>=25.3730
COL=0.838999
24.8
25.0
25.2
25.4
25.6
25.8
0.0
0.5
1.0
1.5
2.0

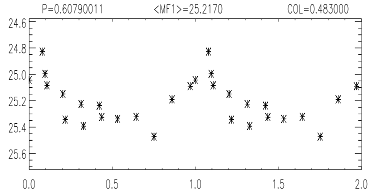
P=0.60790011
<MF1>=25.2170
COL=0.483000
24.6
24.8
25.0
25.2
25.4
25.6
0.0
0.5
1.0
1.5
2.0

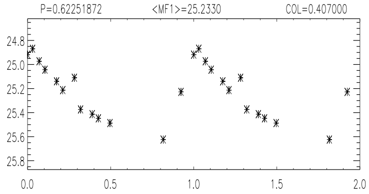
P=0.62251872
<MF1>=25.2330
COL=0.407000
24.8
25.0
25.2
25.4
25.6
25.8
0.0
0.5
1.0
1.5
2.0

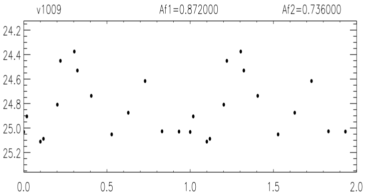
v1009
Af1=0.872000
Af2=0.736000
24.2
24.4
24.6
24.8
25.0
25.2
0.0
0.5
1.0
1.5
2.0

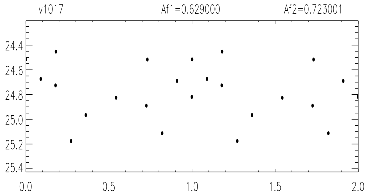
v1017
Af1=0.629000
Af2=0.723001
24.4
24.6
24.8
25.0
25.2
25.4
0.0
0.5
1.0
1.5
2.0

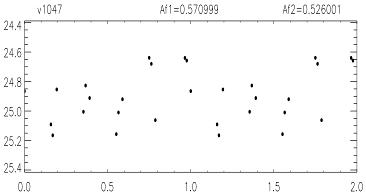
v1047
Af1=0.570999
Af2=0.526001
24.4
24.6
24.8
25.0
25.2
25.4
0.0
0.5
1.0
1.5
2.0

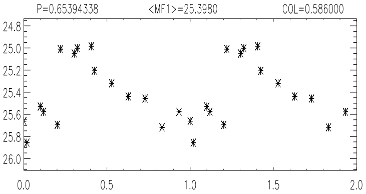
P=0.65394338
<MF1>=25.3980
COL=0.586000
24.8
25.0
25.2
25.4
25.6
25.8
26.0
0.0
0.5
1.0
1.5
2.0

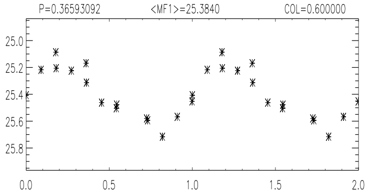
P=0.36593092
<MF1>=25.3840
COL=0.600000
25.0
25.2
25.4
25.6
25.8
0.0
0.5
1.0
1.5
2.0

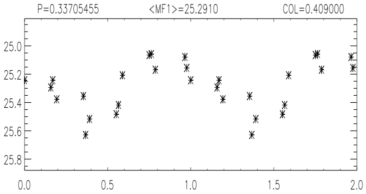
P=0.33705455
<MF1>=25.2910
COL=0.409000
25.0
25.2
25.4
25.6
25.8
0.0
0.5
1.0
1.5
2.0

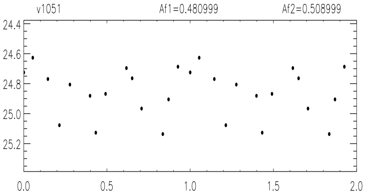
v1051
Af1=0.480999
Af2=0.508999
24.4
24.6
24.8
25.0
25.2
0.0
0.5
1.0
1.5
2.0

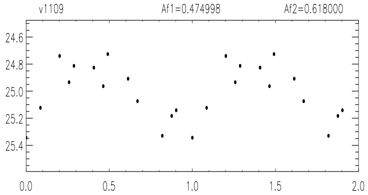
v1109
Af1=0.474998
Af2=0.618000
24.6
24.8
25.0
25.2
25.4
0.0
0.5
1.0
1.5
2.0

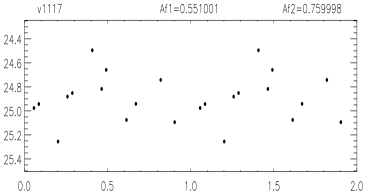
v1117
Af1=0.551001
Af2=0.759998
24.4
24.6
24.8
25.0
25.2
25.4
0.0
0.5
1.0
1.5
2.0

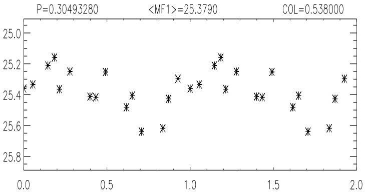
P=0.30493280
<MF1>=25.3790
COL=0.538000
25.0
25.2
25.4
25.6
25.8
0.0
0.5
1.0
1.5
2.0

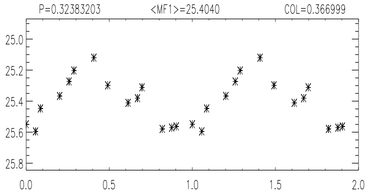
P=0.32383203
<MF1>=25.4040
COL=0.366999
25.0
25.2
25.4
25.6
25.8
0.0
0.5
1.0
1.5
2.0

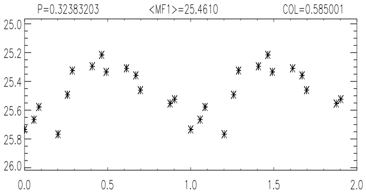
P=0.32383203
<MF1>=25.4610
COL=0.585001
25.0
25.2
25.4
25.6
25.8
26.0
0.0
0.5
1.0
1.5
2.0

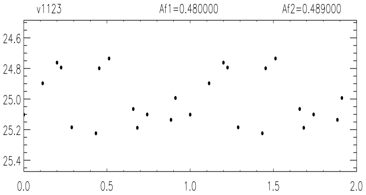
v1123
Af1=0.480000
Af2=0.489000
24.6
24.8
25.0
25.2
25.4
0.0
0.5
1.0
1.5
2.0

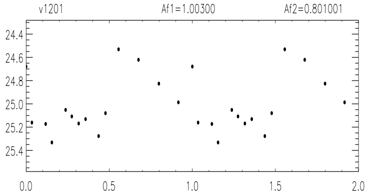
v1201
Af1=1.00300
Af2=0.801001
24.4
24.6
24.8
25.0
25.2
25.4
0.0
0.5
1.0
1.5
2.0

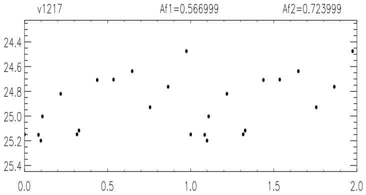
v1217
Af1=0.566999
Af2=0.723999
24.4
24.6
24.8
25.0
25.2
25.4
0.0
0.5
1.0
1.5
2.0

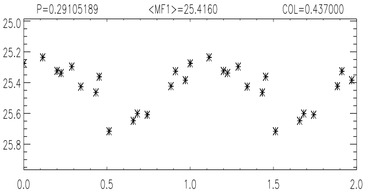
P=0.29105189
<MF1>=25.4160
COL=0.437000
25.0
25.2
25.4
25.6
25.8
0.0
0.5
1.0
1.5
2.0

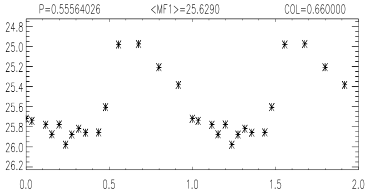
P=0.55564026
<MF1>=25.6290
COL=0.660000
24.8
25.0
25.2
25.4
25.6
25.8
26.0
26.2
0.0
0.5
1.0
1.5
2.0

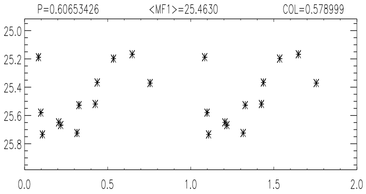
P=0.60653426
<MF1>=25.4630
COL=0.578999
25.0
25.2
25.4
25.6
25.8
0.0
0.5
1.0
1.5
2.0

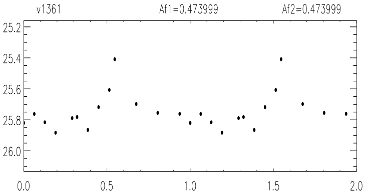
v1361
Af1=0.473999
Af2=0.473999
25.2
25.4
25.6
25.8
26.0
0.0
0.5
1.0
1.5
2.0

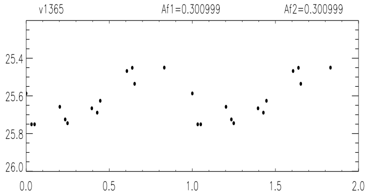
v1365
Af1=0.300999
Af2=0.300999
25.4
25.6
25.8
26.0
0.0
0.5
1.0
1.5
2.0

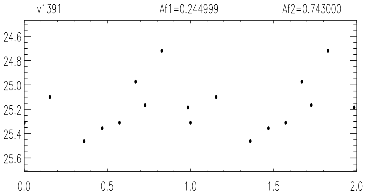
v1391
Af1=0.244999
Af2=0.743000
24.6
24.8
25.0
25.2
25.4
25.6
0.0
0.5
1.0
1.5
2.0

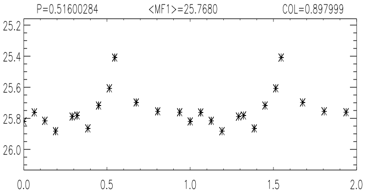
P=0.51600284
<MF1>=25.7680
COL=0.897999
25.2
25.4
25.6
25.8
26.0
0.0
0.5
1.0
1.5
2.0

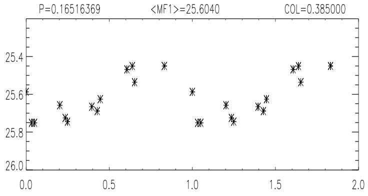
P=0.16516369
<MF1>=25.6040
COL=0.385000
25.4
25.6
25.8
26.0
0.0
0.5
1.0
1.5
2.0

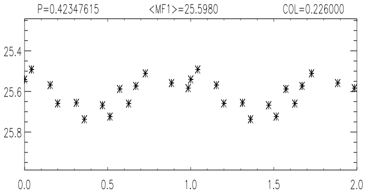
P=0.42347615
<MF1>=25.5980
COL=0.226000
25.4
25.6
25.8
0.0
0.5
1.0
1.5
2.0

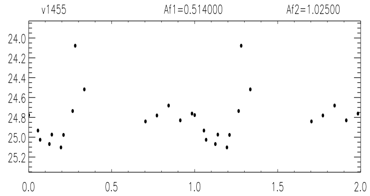
v1455
Af1=0.514000
Af2=1.02500
24.0
24.2
24.4
24.6
24.8
25.0
25.2
0.0
0.5
1.0
1.5
2.0

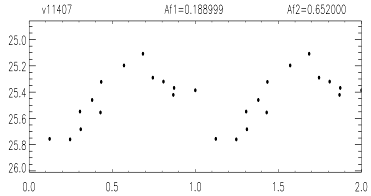
v11407
Af1=0.188999
Af2=0.652000
25.0
25.2
25.4
25.6
25.8
26.0
0.0
0.5
1.0
1.5
2.0

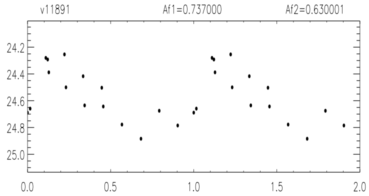
v11891
Af1=0.737000
Af2=0.630001
24.2
24.4
24.6
24.8
25.0
0.0
0.5
1.0
1.5
2.0

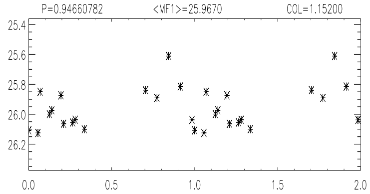
P=0.94660782
<MF1>=25.9670
COL=1.15200
25.4
25.6
25.8
26.0
26.2
0.0
0.5
1.0
1.5
2.0

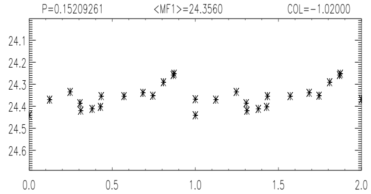
P=0.15209261
<MF1>=24.3560
COL=-1.02000
24.1
24.2
24.3
24.4
24.5
24.6
0.0
0.5
1.0
1.5
2.0

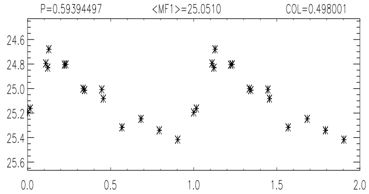
P=0.59394497
<MF1>=25.0510
COL=0.498001
24.6
24.8
25.0
25.2
25.4
25.6
0.0
0.5
1.0
1.5
2.0

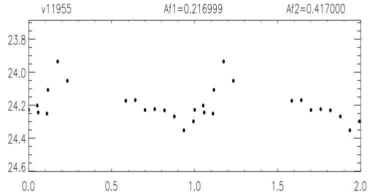
v11955
Af1=0.216999
Af2=0.417000
23.8
24.0
24.2
24.4
24.6
0.0
0.5
1.0
1.5
2.0

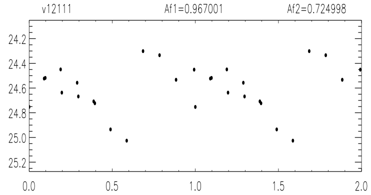
v12111
Af1=0.967001
Af2=0.724998
24.2
24.4
24.6
24.8
25.0
25.2
0.0
0.5
1.0
1.5
2.0

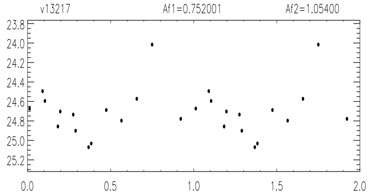
v13217
Af1=0.752001
Af2=1.05400
23.8
24.0
24.2
24.4
24.6
24.8
25.0
25.2
0.0
0.5
1.0
1.5
2.0

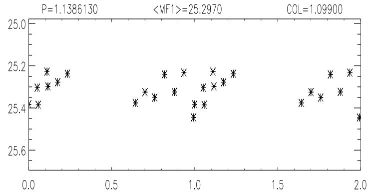
P=1.1386130
<MF1>=25.2970
COL=1.09900
25.0
25.2
25.4
25.6
0.0
0.5
1.0
1.5
2.0

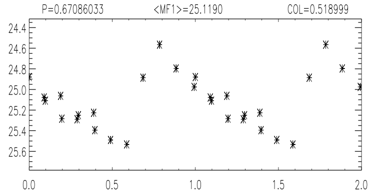
P=0.67086033
<MF1>=25.1190
COL=0.518999
24.4
24.6
24.8
25.0
25.2
25.4
25.6
0.0
0.5
1.0
1.5
2.0

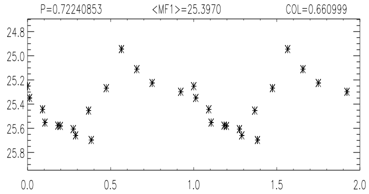
P=0.72240853
<MF1>=25.3970
COL=0.660999
24.8
25.0
25.2
25.4
25.6
25.8
0.0
0.5
1.0
1.5
2.0

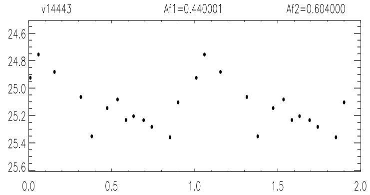
v14443
Af1=0.440001
Af2=0.604000
24.6
24.8
25.0
25.2
25.4
25.6
0.0
0.5
1.0
1.5
2.0

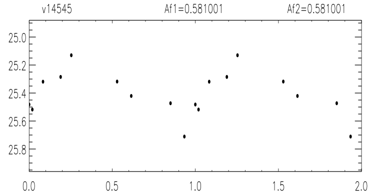
v14545
Af1=0.581001
Af2=0.581001
25.0
25.2
25.4
25.6
25.8
0.0
0.5
1.0
1.5
2.0

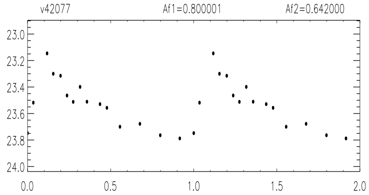
v42077
Af1=0.800001
Af2=0.642000
23.0
23.2
23.4
23.6
23.8
24.0
0.0
0.5
1.0
1.5
2.0

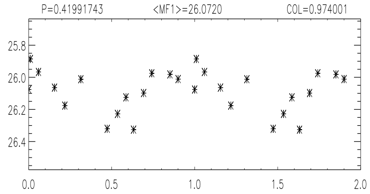
P=0.41991743
<MF1>=26.0720
COL=0.974001
25.8
26.0
26.2
26.4
0.0
0.5
1.0
1.5
2.0

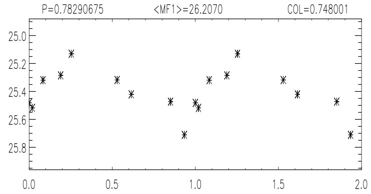
P=0.78290675
<MF1>=26.2070
COL=0.748001
25.0
25.2
25.4
25.6
25.8
0.0
0.5
1.0
1.5
2.0

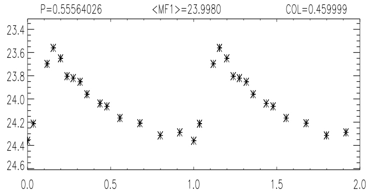
P=0.55564026
<MF1>=23.9980
COL=0.459999
23.4
23.6
23.8
24.0
24.2
24.4
24.6
0.0
0.5
1.0
1.5
2.0

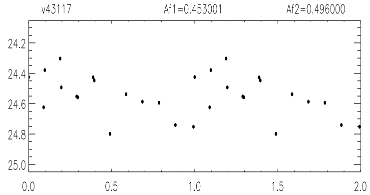
v43117
Af1=0.453001
Af2=0.496000
24.2
24.4
24.6
24.8
25.0
0.0
0.5
1.0
1.5
2.0

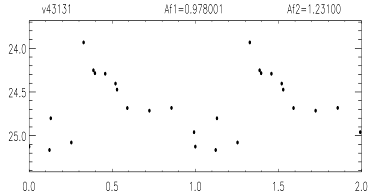
v43131
Af1=0.978001
Af2=1.23100
24.0
24.5
25.0
0.0
0.5
1.0
1.5
2.0

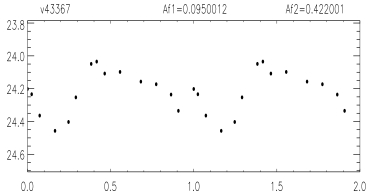
v43367
Af1=0.0950012
Af2=0.422001
23.8
24.0
24.2
24.4
24.6
0.0
0.5
1.0
1.5
2.0

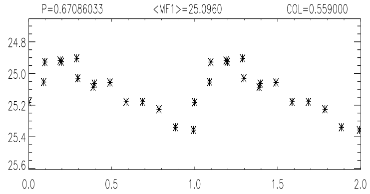
P=0.67086033
<MF1>=25.0960
COL=0.559000
24.8
25.0
25.2
25.4
25.6
0.0
0.5
1.0
1.5
2.0

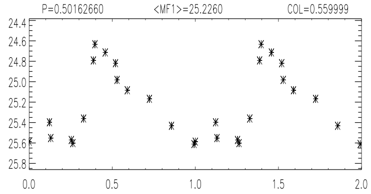
P=0.50162660
<MF1>=25.2260
COL=0.559999
24.4
24.6
24.8
25.0
25.2
25.4
25.6
25.8
0.0
0.5
1.0
1.5
2.0

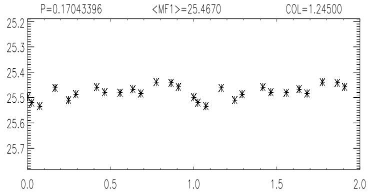
P=0.17043396
<MF1>=25.4670
COL=1.24500
25.2
25.3
25.4
25.5
25.6
25.7
0.0
0.5
1.0
1.5
2.0

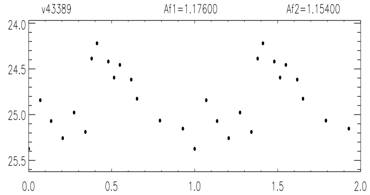
v43389
Af1=1.17600
Af2=1.15400
24.0
24.5
25.0
25.5
0.0
0.5
1.0
1.5
2.0

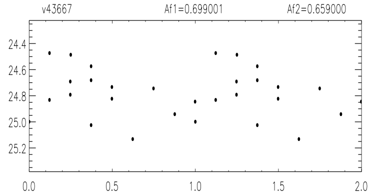
v43667
Af1=0.699001
Af2=0.659000
24.4
24.6
24.8
25.0
25.2
0.0
0.5
1.0
1.5
2.0

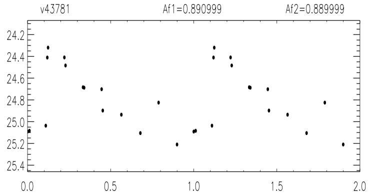
v43781
Af1=0.890999
Af2=0.889999
24.2
24.4
24.6
24.8
25.0
25.2
25.4
0.0
0.5
1.0
1.5
2.0

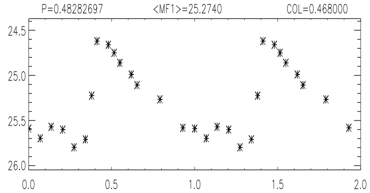
P=0.48282697
<MF1>=25.2740
COL=0.468000
24.5
25.0
25.5
26.0
0.0
0.5
1.0
1.5
2.0

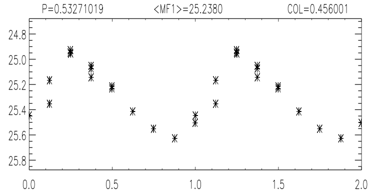
P=0.53271019
<MF1>=25.2380
COL=0.456001
24.8
25.0
25.2
25.4
25.6
25.8
0.0
0.5
1.0
1.5
2.0

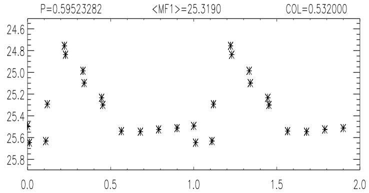
P=0.59523282
<MF1>=25.3190
COL=0.532000
24.6
24.8
25.0
25.2
25.4
25.6
25.8
0.0
0.5
1.0
1.5
2.0

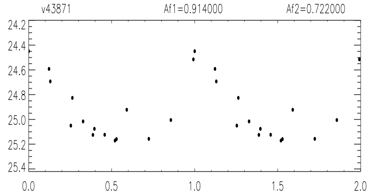
v43871
Af1=0.914000
Af2=0.722000
24.2
24.4
24.6
24.8
25.0
25.2
25.4
0.0
0.5
1.0
1.5
2.0

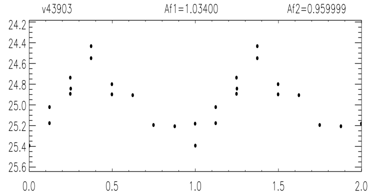
v43903
Af1=1.03400
Af2=0.959999
24.2
24.4
24.6
24.8
25.0
25.2
25.4
25.6
0.0
0.5
1.0
1.5
2.0

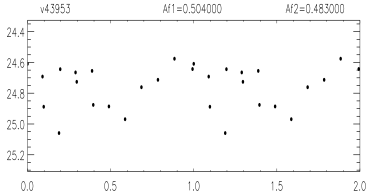
v43953
Af1=0.504000
Af2=0.483000
24.4
24.6
24.8
25.0
25.2
0.0
0.5
1.0
1.5
2.0

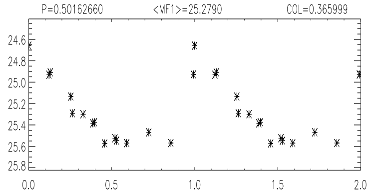
P=0.50162660
<MF1>=25.2790
COL=0.365999
24.6
24.8
25.0
25.2
25.4
25.6
25.8
0.0
0.5
1.0
1.5
2.0

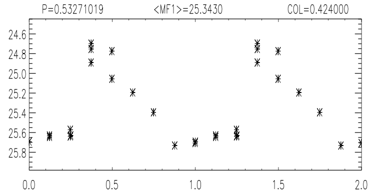
P=0.53271019
<MF1>=25.3430
COL=0.424000
24.6
24.8
25.0
25.2
25.4
25.6
25.8
0.0
0.5
1.0
1.5
2.0

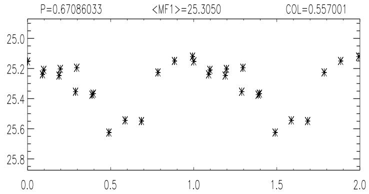
P=0.67086033
<MF1>=25.3050
COL=0.557001
25.0
25.2
25.4
25.6
25.8
0.0
0.5
1.0
1.5
2.0

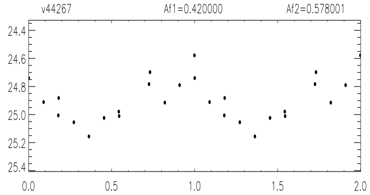
v44267
Af1=0.420000
Af2=0.578001
24.4
24.6
24.8
25.0
25.2
25.4
0.0
0.5
1.0
1.5
2.0

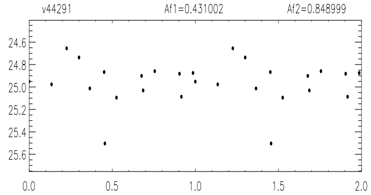
v44291
Af1=0.431002
Af2=0.848999
24.6
24.8
25.0
25.2
25.4
25.6
0.0
0.5
1.0
1.5
2.0

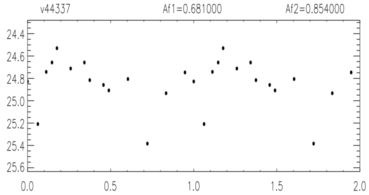
v44337
Af1=0.681000
Af2=0.854000
24.4
24.6
24.8
25.0
25.2
25.4
25.6
0.0
0.5
1.0
1.5
2.0

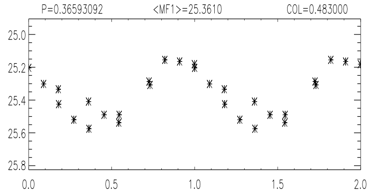
P=0.36593092
<MF1>=25.3610
COL=0.483000
25.0
25.2
25.4
25.6
25.8
0.0
0.5
1.0
1.5
2.0

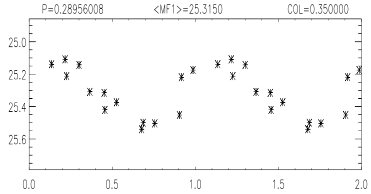
P=0.28956008
<MF1>=25.3150
COL=0.350000
25.0
25.2
25.4
25.6
0.0
0.5
1.0
1.5
2.0

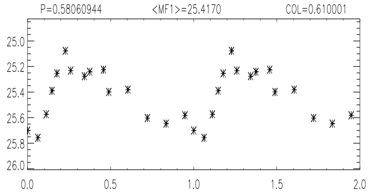
P=0.58060944
<MF1>=25.4170
COL=0.610001
25.0
25.2
25.4
25.6
25.8
26.0
0.0
0.5
1.0
1.5
2.0

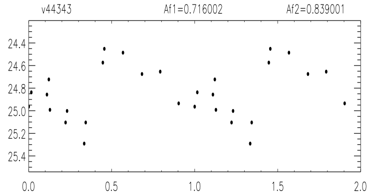
v44343
Af1=0.716002
Af2=0.839001
24.4
24.6
24.8
25.0
25.2
25.4
0.0
0.5
1.0
1.5
2.0

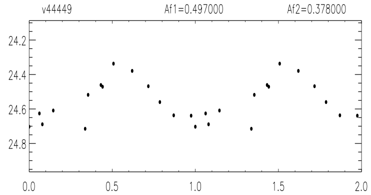
v44449
Af1=0.497000
Af2=0.378000
24.2
24.4
24.6
24.8
0.0
0.5
1.0
1.5
2.0

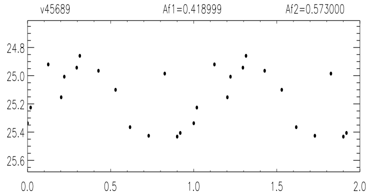
v45689
Af1=0.418999
Af2=0.573000
24.8
25.0
25.2
25.4
25.6
0.0
0.5
1.0
1.5
2.0

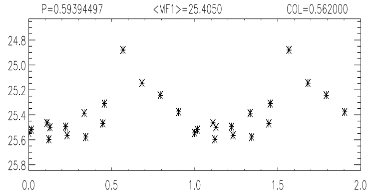
P=0.59394497
<MF1>=25.4050
COL=0.562000
24.8
25.0
25.2
25.4
25.6
25.8
0.0
0.5
1.0
1.5
2.0

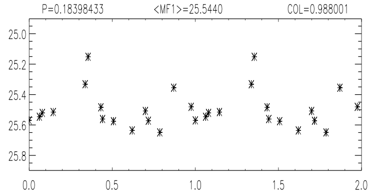
P=0.18398433
<MF1>=25.5440
COL=0.988001
25.0
25.2
25.4
25.6
25.8
0.0
0.5
1.0
1.5
2.0

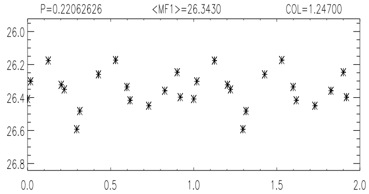
P=0.22062626
<MF1>=26.3430
COL=1.24700
26.0
26.2
26.4
26.6
26.8
0.0
0.5
1.0
1.5
2.0

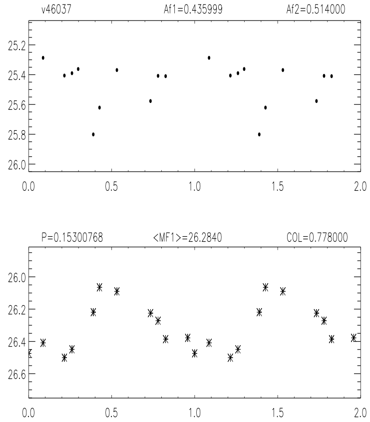
v46037
Af1=0.435999
Af2=0.514000
P=0.15300768
<MF1>=26.2840
COL=0.778000

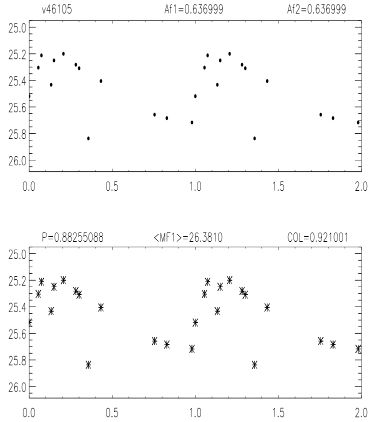
v46105
Af1=0.636999
Af2=0.636999
P=0.88255088
<MF1>=26.3810
COL=0.921001

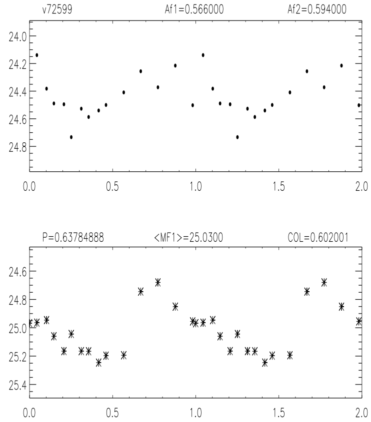
v72599
Af1=0.566000
Af2=0.594000
P=0.63784888
<MF1>=25.0300
COL=0.602001

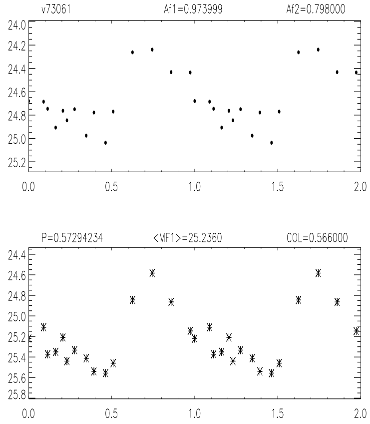
v73061
Af1=0.973999
Af2=0.798000
P=0.57294234
<MF1>=25.2360
COL=0.566000

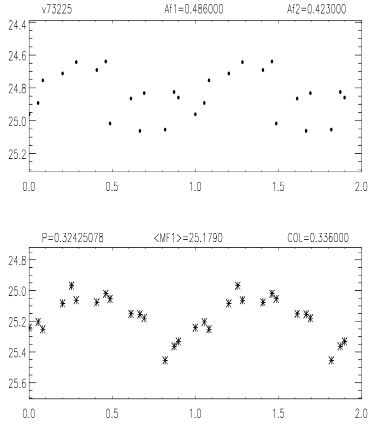
v73225
Af1=0.486000
Af2=0.423000
P=0.32425078
<MF1>=25.1790
COL=0.336000

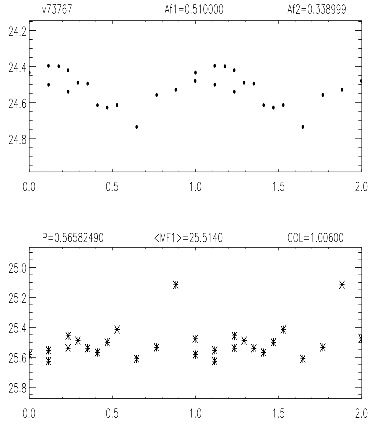
v73767
Af1=0.510000
Af2=0.338999
P=0.56582490
<MF1>=25.5140
COL=1.00600

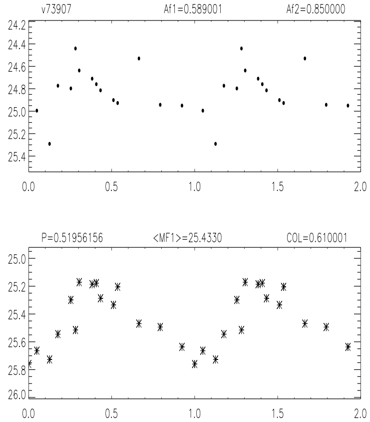
v73907
Af1=0.589001
Af2=0.850000
P=0.51956156
<MF1>=25.4330
COL=0.610001

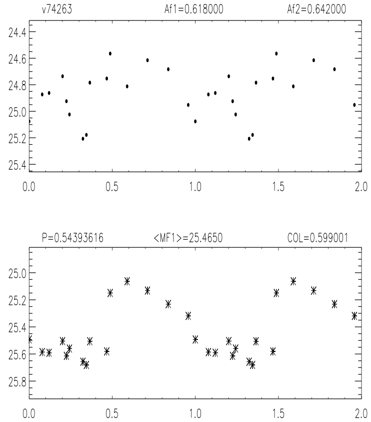
v74263
Af1=0.618000
Af2=0.642000
P=0.54393616
<MF1>=25.4650
COL=0.599001

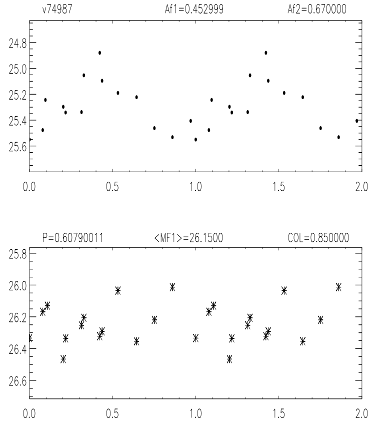
v74987
Af1=0.452999
Af2=0.670000
P=0.60790011
<MF1>=26.1500
COL=0.850000

Chapter 12

Appendix F

ATLAS OF LIGHT CURVES: G322

Atlas of the V,I light curves for candidate variable stars identified in G322. For each variable the upper panel shows the I-band light curve, and the lower panel the V-band light curve. Identification, V and I amplitudes, period, average V magnitude and average V−I color, are provided on top labels of the plots.

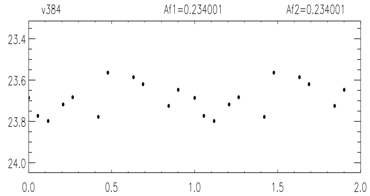
v384
Af1=0.234001
Af2=0.234001
23.4
23.6
23.8
24.0
0.0
0.5
1.0
1.5
2.0

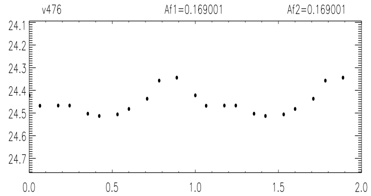
v476
Af1=0.169001
Af2=0.169001
24.1
24.2
24.3
24.4
24.5
24.6
24.7
0.0
0.5
1.0
1.5
2.0

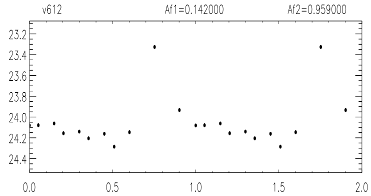
v612
Af1=0.142000
Af2=0.959000
23.2
23.4
23.6
23.8
24.0
24.2
24.4
0.0
0.5
1.0
1.5
2.0

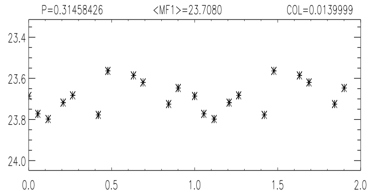
P=0.31458426
<MF1>=23.7080
COL=0.0139999
23.4
23.6
23.8
24.0
0.0
0.5
1.0
1.5
2.0

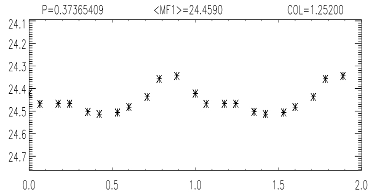
P=0.37365409
<MF1>=24.4590
COL=1.25200
24.1
24.2
24.3
24.4
24.5
24.6
24.7
0.0
0.5
1.0
1.5
2.0

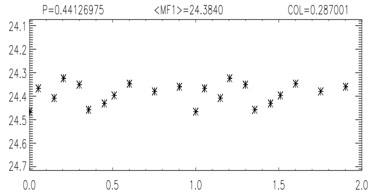
P=0.44126975
<MF1>=24.3840
COL=0.287001
24.1
24.2
24.3
24.4
24.5
24.6
24.7
0.0
0.5
1.0
1.5
2.0

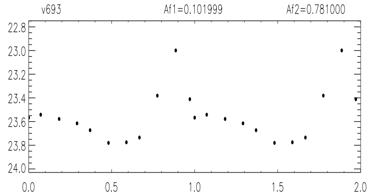
v693
Af1=0.101999
Af2=0.781000
22.8
23.0
23.2
23.4
23.6
23.8
24.0
0.0
0.5
1.0
1.5
2.0

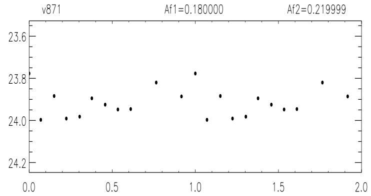
v871
Af1=0.180000
Af2=0.219999
23.6
23.8
24.0
24.2
0.0
0.5
1.0
1.5
2.0

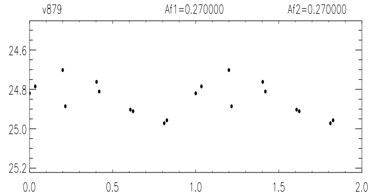
v879
Af1=0.270000
Af2=0.270000
24.6
24.8
25.0
25.2
0.0
0.5
1.0
1.5
2.0

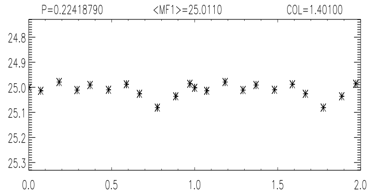
P=0.22418790
<MF1>=25.0110
COL=1.40100
24.8
24.9
25.0
25.1
25.2
25.3
0.0
0.5
1.0
1.5
2.0

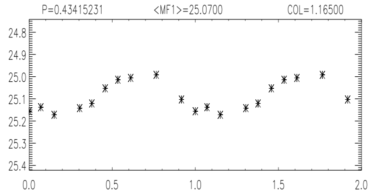
P=0.43415231
<MF1>=25.0700
COL=1.16500
24.8
24.9
25.0
25.1
25.2
25.3
25.4
0.0
0.5
1.0
1.5
2.0

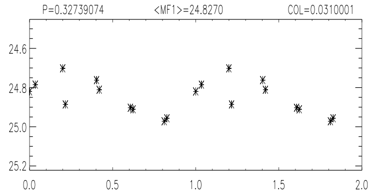
P=0.32739074
<MF1>=24.8270
COL=0.0310001
24.6
24.8
25.0
25.2
0.0
0.5
1.0
1.5
2.0

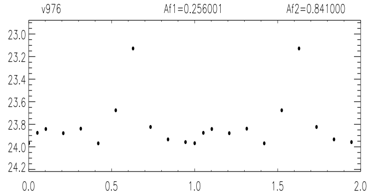
v976
Af1=0.256001
Af2=0.841000
23.0
23.2
23.4
23.6
23.8
24.0
24.2
0.0
0.5
1.0
1.5
2.0

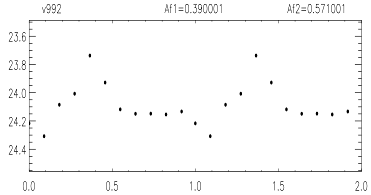
v992
Af1=0.390001
Af2=0.571001
23.6
23.8
24.0
24.2
24.4
0.0
0.5
1.0
1.5
2.0

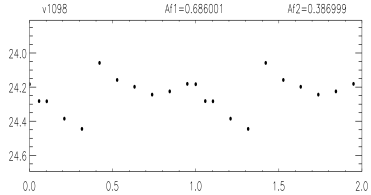
v1098
Af1=0.686001
Af2=0.386999
24.0
24.2
24.4
24.6
0.0
0.5
1.0
1.5
2.0

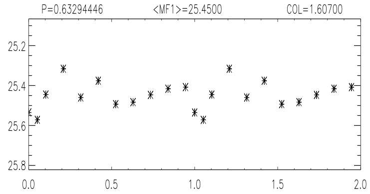
P=0.63294446
<MF1>=25.4500
COL=1.60700
25.2
25.4
25.6
25.8
0.0
0.5
1.0
1.5
2.0

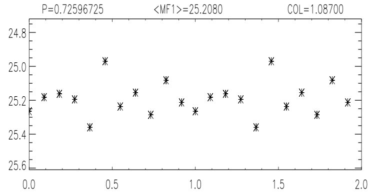
P=0.72596725
<MF1>=25.2080
COL=1.08700
24.8
25.0
25.2
25.4
25.6
0.0
0.5
1.0
1.5
2.0

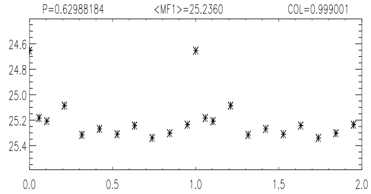
P=0.62988184
<MF1>=25.2360
COL=0.999001
24.6
24.8
25.0
25.2
25.4
0.0
0.5
1.0
1.5
2.0

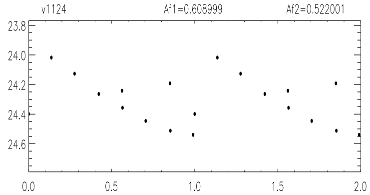
v1124
Af1=0.608999
Af2=0.522001
23.8
24.0
24.2
24.4
24.6
0.0
0.5
1.0
1.5
2.0

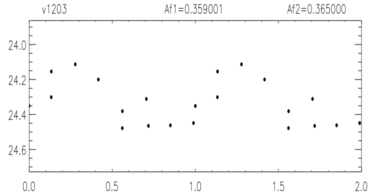
v1203
Af1=0.359001
Af2=0.365000
24.0
24.2
24.4
24.6
0.0
0.5
1.0
1.5
2.0

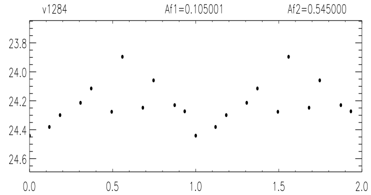
v1284
Af1=0.105001
Af2=0.545000
23.8
24.0
24.2
24.4
24.6
0.0
0.5
1.0
1.5
2.0

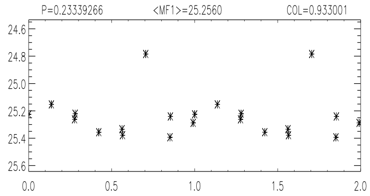
P=0.23339266
<MF1>=25.2560
COL=0.933001
24.6
24.8
25.0
25.2
25.4
25.6
0.0
0.5
1.0
1.5
2.0

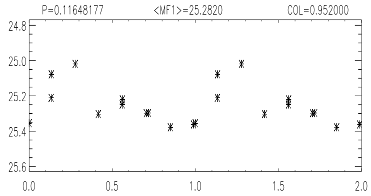
P=0.11648177
<MF1>=25.2820
COL=0.952000
24.8
25.0
25.2
25.4
25.6
0.0
0.5
1.0
1.5
2.0

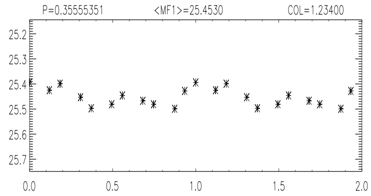
P=0.35555351
<MF1>=25.4530
COL=1.23400
25.2
25.3
25.4
25.5
25.6
25.7
0.0
0.5
1.0
1.5
2.0

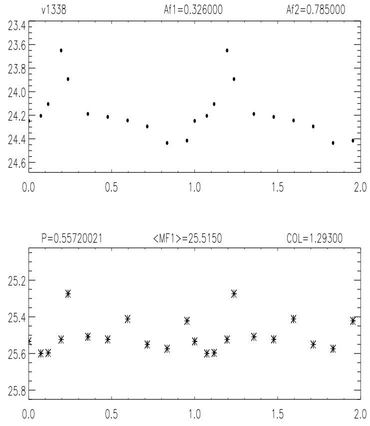
v1338 Af1=0.326000 Af2=0.785000
23.4 23.6 23.8 24.0 24.2 24.4 24.6
0.0 0.5 1.0 1.5 2.0
P=0.55720021 <MF1>=25.5150 COL=1.29300
25.2 25.4 25.6 25.8
0.0 0.5 1.0 1.5 2.0

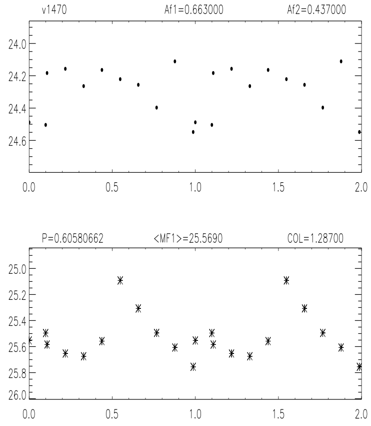
v1470 Af1=0.663000 Af2=0.437000
24.0 24.2 24.4 24.6
0.0 0.5 1.0 1.5 2.0
P=0.60580662 <MF1>=25.5690 COL=1.28700
25.0 25.2 25.4 25.6 25.8 26.0
0.0 0.5 1.0 1.5 2.0

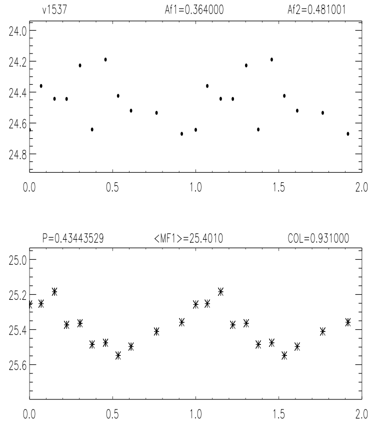
v1537 Af1=0.364000 Af2=0.481001
24.0 24.2 24.4 24.6 24.8
0.0 0.5 1.0 1.5 2.0
P=0.43443529 <MF1>=25.4010 COL=0.931000
25.0 25.2 25.4 25.6
0.0 0.5 1.0 1.5 2.0

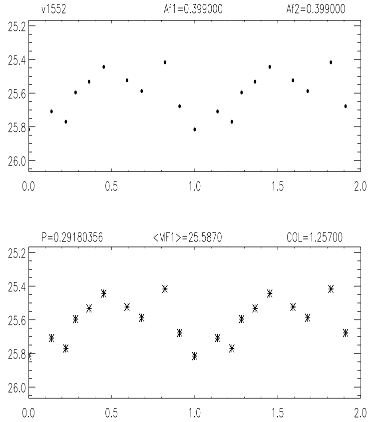
v1552 Af1=0.399000 Af2=0.399000
25.2 25.4 25.6 25.8 26.0
0.0 0.5 1.0 1.5 2.0
P=0.29180356 <MF1>=25.5870 COL=1.25700
25.2 25.4 25.6 25.8 26.0
0.0 0.5 1.0 1.5 2.0

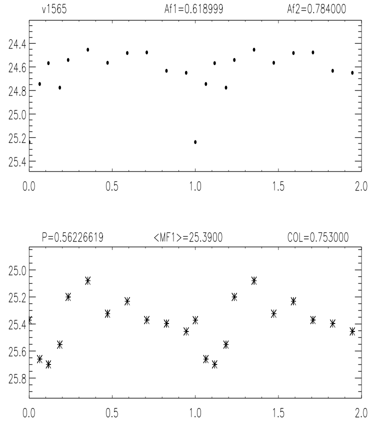
v1565 Af1=0.618999 Af2=0.784000
24.4 24.6 24.8 25.0 25.2 25.4
0.0 0.5 1.0 1.5 2.0
P=0.56226619 <MF1>=25.3900 COL=0.753000
25.0 25.2 25.4 25.6 25.8
0.0 0.5 1.0 1.5 2.0

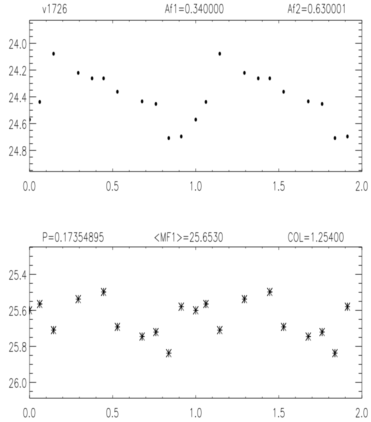
v1726 Af1=0.340000 Af2=0.630001
24.0 24.2 24.4 24.6 24.8
0.0 0.5 1.0 1.5 2.0
P=0.17354895 <MF1>=25.6530 COL=1.25400
25.4 25.6 25.8 26.0
0.0 0.5 1.0 1.5 2.0

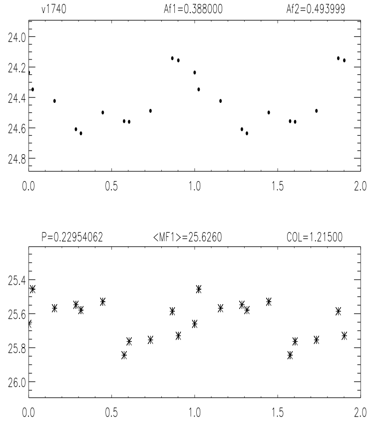
v1740 Af1=0.388000 Af2=0.493999
24.0 24.2 24.4 24.6 24.8
0.0 0.5 1.0 1.5 2.0
P=0.22954062 <MF1>=25.6260 COL=1.21500
25.4 25.6 25.8 26.0
0.0 0.5 1.0 1.5 2.0

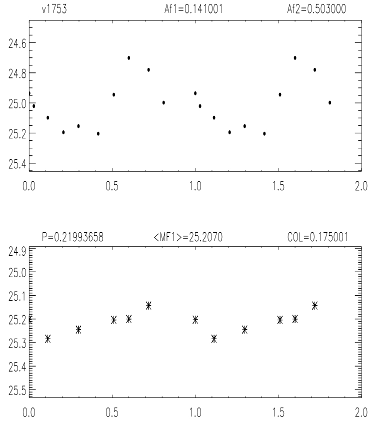
v1753 Af1=0.141001 Af2=0.503000
24.6 24.8 25.0 25.2 25.4
0.0 0.5 1.0 1.5 2.0
P=0.21993658 <MF1>=25.2070 COL=0.175001
24.9 25.0 25.1 25.2 25.3 25.4 25.5
0.0 0.5 1.0 1.5 2.0

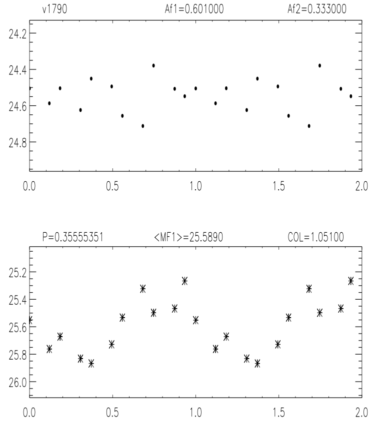
v1790 Af1=0.601000 Af2=0.333000
24.2 24.4 24.6 24.8
0.0 0.5 1.0 1.5 2.0
P=0.35555351 <MF1>=25.5890 COL=1.05100
25.2 25.4 25.6 25.8 26.0
0.0 0.5 1.0 1.5 2.0

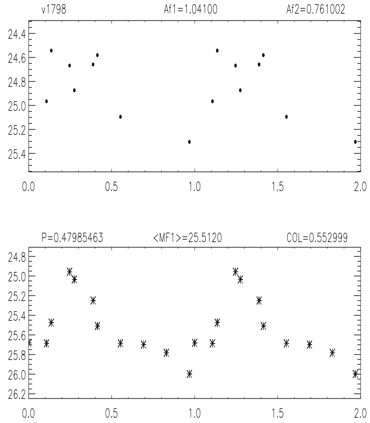
v1798 Af1=1.04100 Af2=0.761002
24.4 24.6 24.8 25.0 25.2 25.4
0.0 0.5 1.0 1.5 2.0
P=0.47985463 <MF1>=25.5120 COL=0.552999
24.8 25.0 25.2 25.4 25.6 25.8 26.0 26.2
0.0 0.5 1.0 1.5 2.0

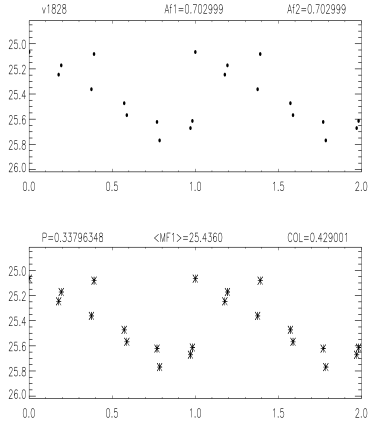
v1828 Af1=0.702999 Af2=0.702999
25.0 25.2 25.4 25.6 25.8 26.0
0.0 0.5 1.0 1.5 2.0
P=0.33796348 <MF1>=25.4360 COL=0.429001
25.0 25.2 25.4 25.6 25.8 26.0
0.0 0.5 1.0 1.5 2.0

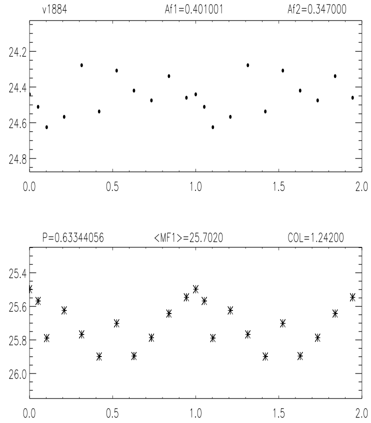
v1884 Af1=0.401001 Af2=0.347000
24.2 24.4 24.6 24.8
0.0 0.5 1.0 1.5 2.0
P=0.63344056 <MF1>=25.7020 COL=1.24200
25.4 25.6 25.8 26.0
0.0 0.5 1.0 1.5 2.0

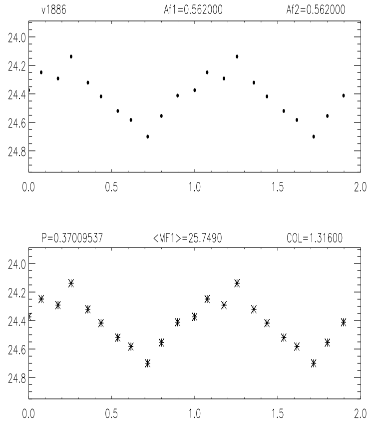
v1886 Af1=0.562000 Af2=0.562000
P=0.37009537 <MF1>=25.7490 COL=1.31600

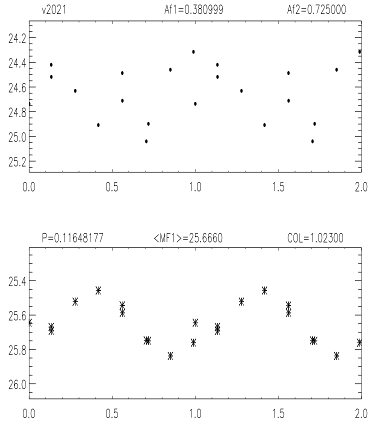
v2021 Af1=0.380999 Af2=0.725000
P=0.11648177 <MF1>=25.6660 COL=1.02300

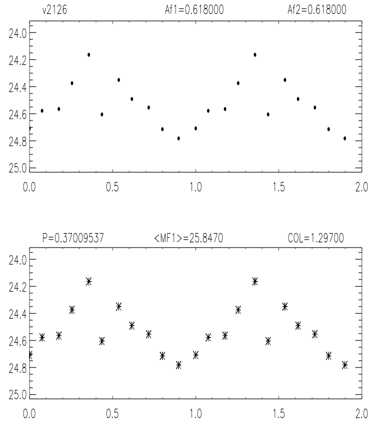
v2126 Af1=0.618000 Af2=0.618000
P=0.37009537 <MF1>=25.8470 COL=1.29700

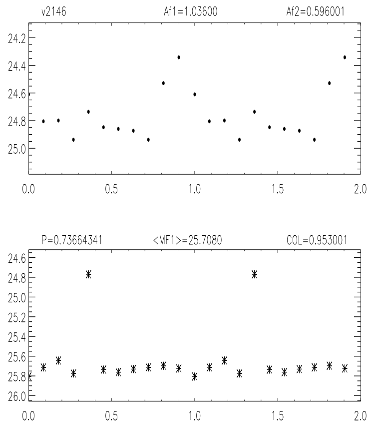
v2146 Af1=1.03600 Af2=0.596001
P=0.73664341 <MF1>=25.7080 COL=0.953001

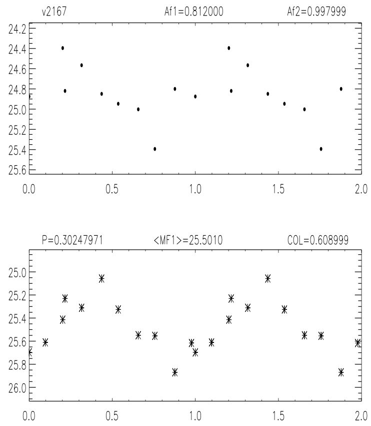
v2167 Af1=0.812000 Af2=0.997999
P=0.30247971 <MF1>=25.5010 COL=0.608999

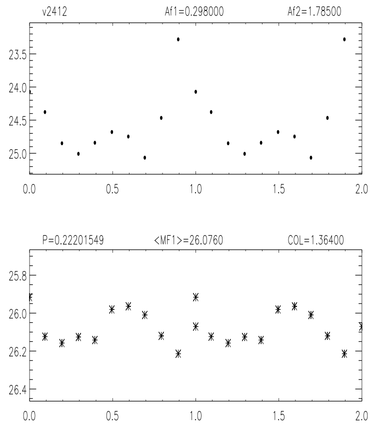
v2412 Af1=0.298000 Af2=1.78500
P=0.22201549 <MF1>=26.0760 COL=1.36400

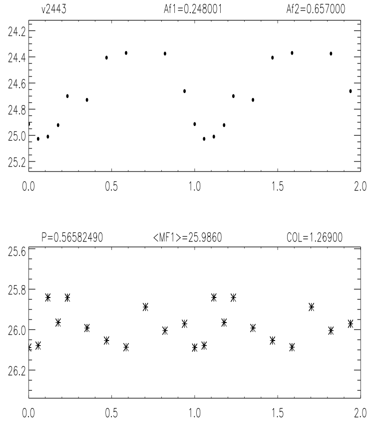
v2443 Af1=0.248001 Af2=0.657000
P=0.56582490 <MF1>=25.9860 COL=1.26900

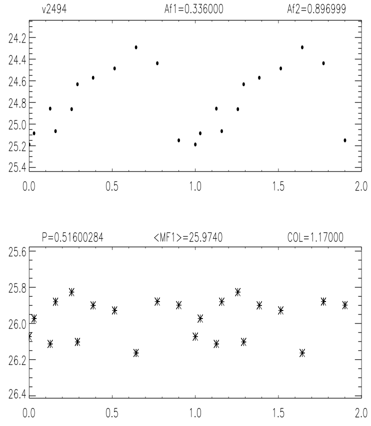
v2494 Af1=0.336000 Af2=0.896999
P=0.51600284 <MF1>=25.9740 COL=1.17000

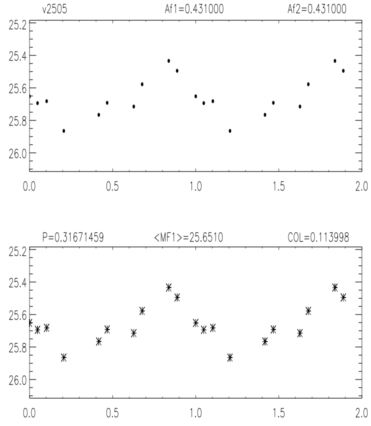
v2505 Af1=0.431000 Af2=0.431000
P=0.31671459 <MF1>=25.6510 COL=0.113998

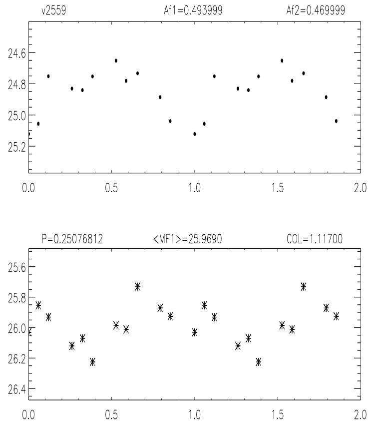
v2559 Af1=0.493999 Af2=0.469999
P=0.25076812 <MF1>=25.9690 COL=1.11700

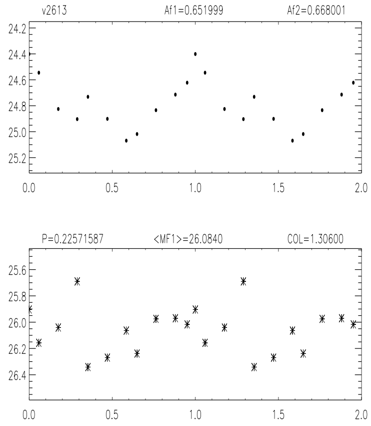
v2613 Af1=0.651999 Af2=0.668001
P=0.22571587 <MF1>=26.0840 COL=1.30600

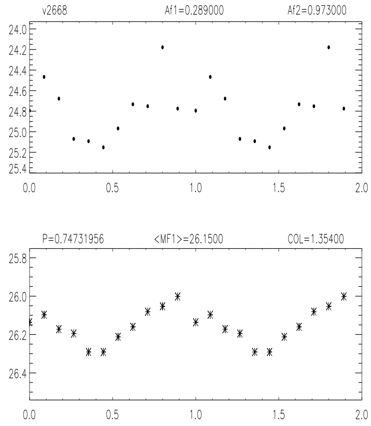
v2668 Af1=0.289000 Af2=0.973000
P=0.74731956 <MF1>=26.1500 COL=1.35400

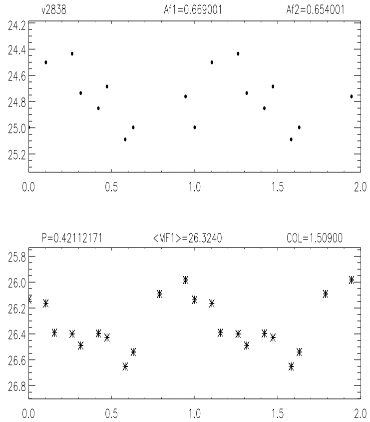
v2838
Af1=0.669001
Af2=0.654001
24.2
24.4
24.6
24.8
25.0
25.2
P=0.42112171
<MF1>=26.3240
COL=1.50900
25.8
26.0
26.2
26.4
26.6
26.8
0.0
0.5
1.0
1.5
2.0

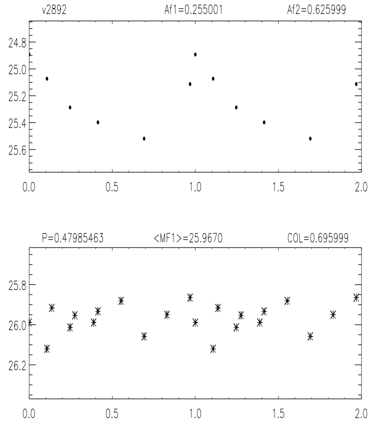
v2892
Af1=0.255001
Af2=0.625999
24.8
25.0
25.2
25.4
25.6
P=0.47985463
<MF1>=25.9670
COL=0.695999
25.8
26.0
26.2
0.0
0.5
1.0
1.5
2.0

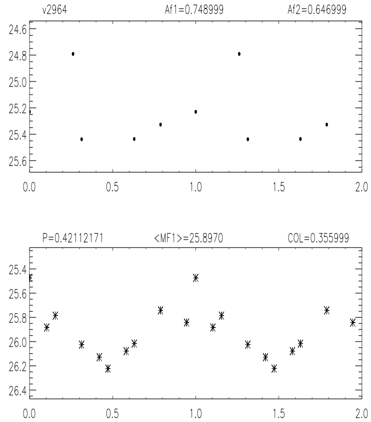
v2964
Af1=0.748999
Af2=0.646999
24.6
24.8
25.0
25.2
25.4
25.6
P=0.42112171
<MF1>=25.8970
COL=0.355999
25.4
25.6
25.8
26.0
26.2
26.4
0.0
0.5
1.0
1.5
2.0

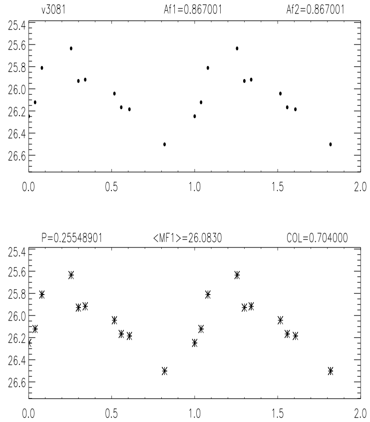
v3081
Af1=0.867001
Af2=0.867001
25.4
25.6
25.8
26.0
26.2
26.4
26.6
P=0.25548901
<MF1>=26.0830
COL=0.704000
25.4
25.6
25.8
26.0
26.2
26.4
26.6
0.0
0.5
1.0
1.5
2.0

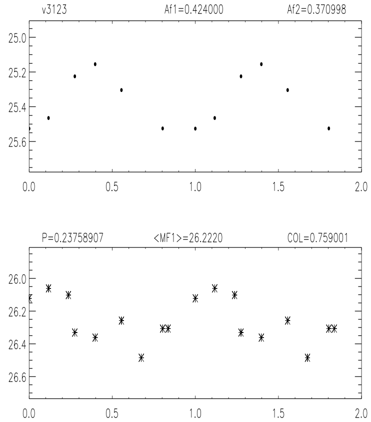
v3123
Af1=0.424000
Af2=0.370998
25.0
25.2
25.4
25.6
P=0.23758907
<MF1>=26.2220
COL=0.759001
26.0
26.2
26.4
26.6
0.0
0.5
1.0
1.5
2.0

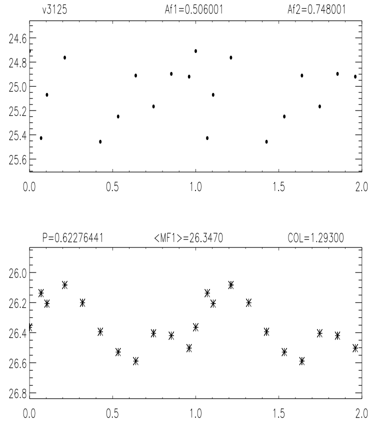
v3125
Af1=0.506001
Af2=0.748001
24.6
24.8
25.0
25.2
25.4
25.6
P=0.62276441
<MF1>=26.3470
COL=1.29300
26.0
26.2
26.4
26.6
26.8
0.0
0.5
1.0
1.5
2.0

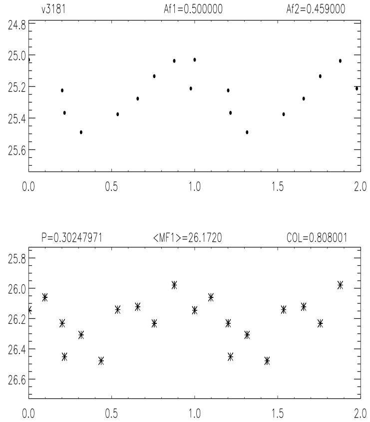
v3181
Af1=0.500000
Af2=0.459000
24.8
25.0
25.2
25.4
25.6
P=0.30247971
<MF1>=26.1720
COL=0.808001
25.8
26.0
26.2
26.4
26.6
0.0
0.5
1.0
1.5
2.0

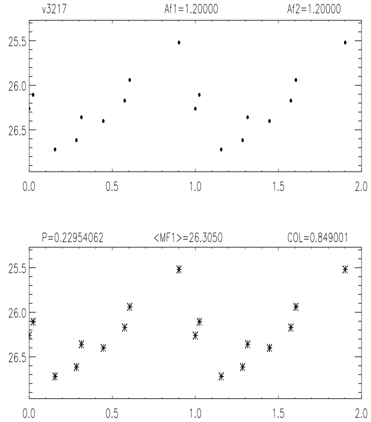
v3217
Af1=1.20000
Af2=1.20000
25.5
26.0
26.5
P=0.22954062
<MF1>=26.3050
COL=0.849001
25.5
26.0
26.5
0.0
0.5
1.0
1.5
2.0

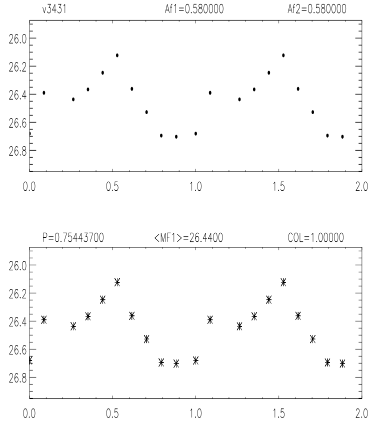
v3431
Af1=0.580000
Af2=0.580000
26.0
26.2
26.4
26.6
26.8
P=0.75443700
<MF1>=26.4400
COL=1.00000
26.0
26.2
26.4
26.6
26.8
0.0
0.5
1.0
1.5
2.0

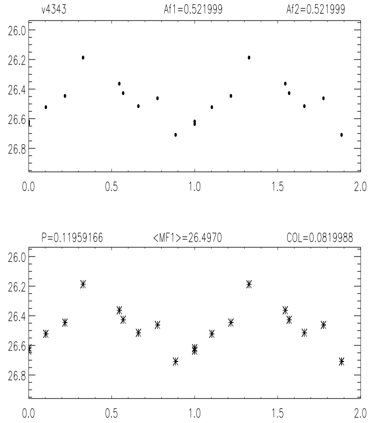
v4343
Af1=0.521999
Af2=0.521999
26.0
26.2
26.4
26.6
26.8
P=0.11959166
<MF1>=26.4970
COL=0.0819988
26.0
26.2
26.4
26.6
26.8
0.0
0.5
1.0
1.5
2.0

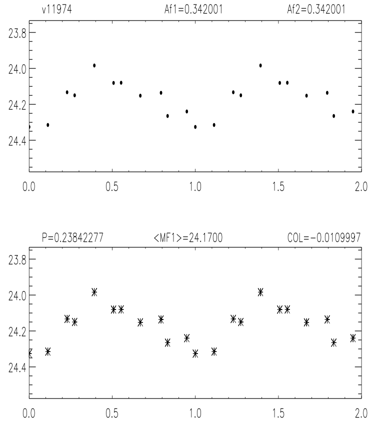
v11974
Af1=0.342001
Af2=0.342001
23.8
24.0
24.2
24.4
P=0.23842277
<MF1>=24.1700
COL=-0.0109997
23.8
24.0
24.2
24.4
0.0
0.5
1.0
1.5
2.0

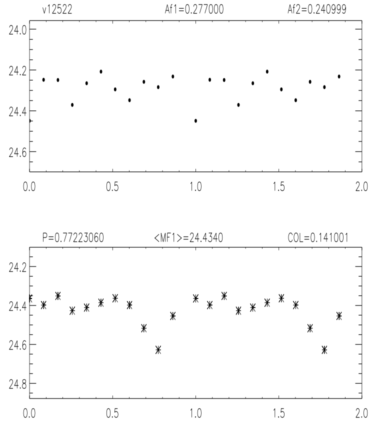
v12522
Af1=0.277000
Af2=0.240999
24.0
24.2
24.4
24.6
P=0.77223060
<MF1>=24.4340
COL=0.141001
24.2
24.4
24.6
24.8
0.0
0.5
1.0
1.5
2.0

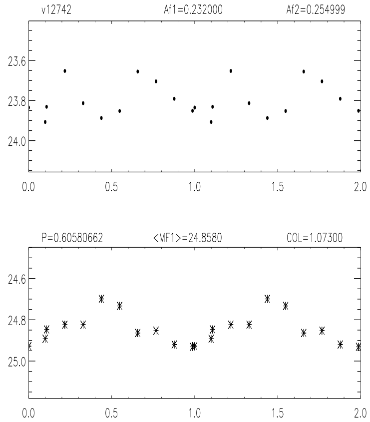
v12742 Af1=0.232000 Af2=0.254999
23.6
23.8
24.0
0.0 0.5 1.0 1.5 2.0
P=0.60580662 <MF1>=24.8580 COL=1.07300
24.6
24.8
25.0
0.0 0.5 1.0 1.5 2.0

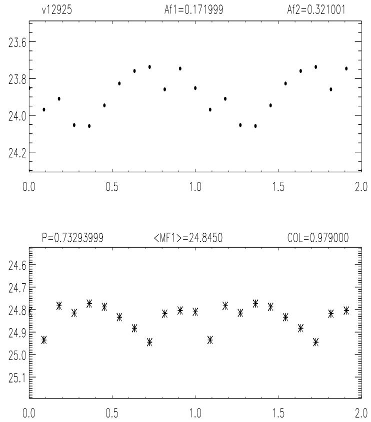
v12925 Af1=0.171999 Af2=0.321001
23.6
23.8
24.0
24.2
0.0 0.5 1.0 1.5 2.0
P=0.73293999 <MF1>=24.8450 COL=0.979000
24.6
24.7
24.8
24.9
25.0
25.1
0.0 0.5 1.0 1.5 2.0

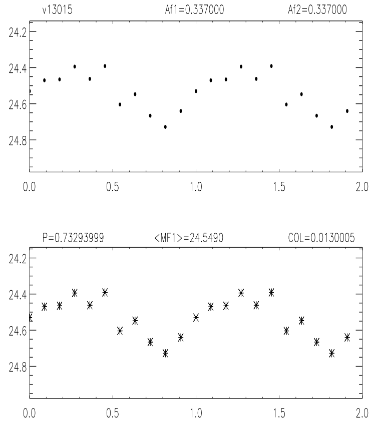
v13015 Af1=0.337000 Af2=0.337000
24.2
24.4
24.6
24.8
0.0 0.5 1.0 1.5 2.0
P=0.73293999 <MF1>=24.5490 COL=0.0130005
24.2
24.4
24.6
24.8
0.0 0.5 1.0 1.5 2.0

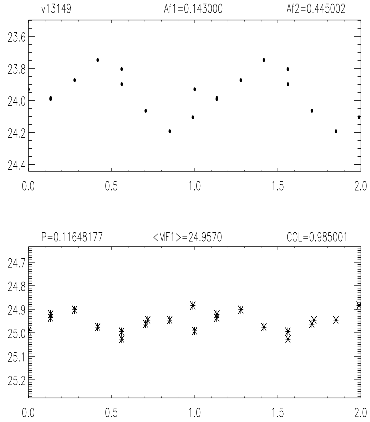
v13149 Af1=0.143000 Af2=0.445002
23.6
23.8
24.0
24.2
24.4
0.0 0.5 1.0 1.5 2.0
P=0.11648177 <MF1>=24.9570 COL=0.985001
24.7
24.8
24.9
25.0
25.1
25.2
0.0 0.5 1.0 1.5 2.0

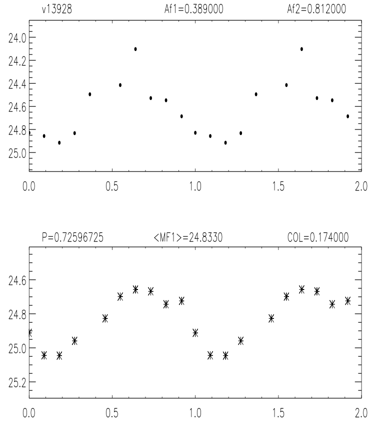
v13928 Af1=0.389000 Af2=0.812000
24.0
24.2
24.4
24.6
24.8
25.0
0.0 0.5 1.0 1.5 2.0
P=0.72596725 <MF1>=24.8330 COL=0.174000
24.6
24.8
25.0
25.2
0.0 0.5 1.0 1.5 2.0

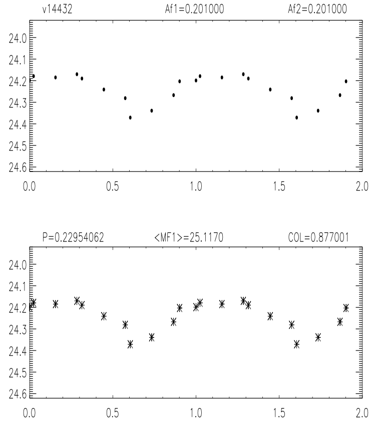
v14432 Af1=0.201000 Af2=0.201000
24.0
24.1
24.2
24.3
24.4
24.5
24.6
0.0 0.5 1.0 1.5 2.0
P=0.22954062 <MF1>=25.1170 COL=0.877001
24.0
24.1
24.2
24.3
24.4
24.5
24.6
0.0 0.5 1.0 1.5 2.0

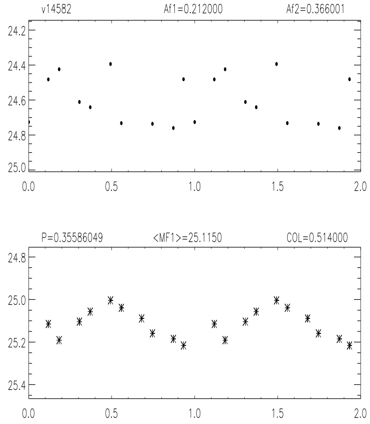
v14582 Af1=0.212000 Af2=0.366001
24.2
24.4
24.6
24.8
25.0
0.0 0.5 1.0 1.5 2.0
P=0.35586049 <MF1>=25.1150 COL=0.514000
24.8
25.0
25.2
25.4
0.0 0.5 1.0 1.5 2.0

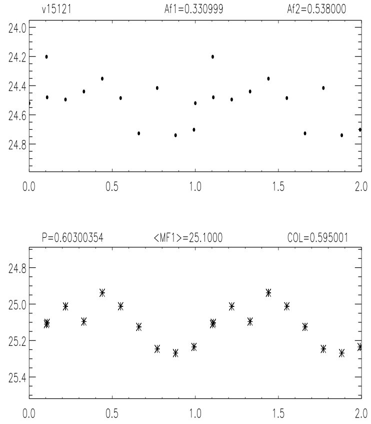
v15121 Af1=0.330999 Af2=0.538000
24.0
24.2
24.4
24.6
24.8
0.0 0.5 1.0 1.5 2.0
P=0.60300354 <MF1>=25.1000 COL=0.595001
24.8
25.0
25.2
25.4
0.0 0.5 1.0 1.5 2.0

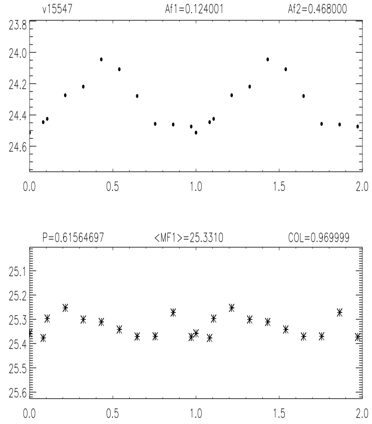
v15547 Af1=0.124001 Af2=0.468000
23.8
24.0
24.2
24.4
24.6
0.0 0.5 1.0 1.5 2.0
P=0.61564697 <MF1>=25.3310 COL=0.969999
25.1
25.2
25.3
25.4
25.5
25.6
0.0 0.5 1.0 1.5 2.0

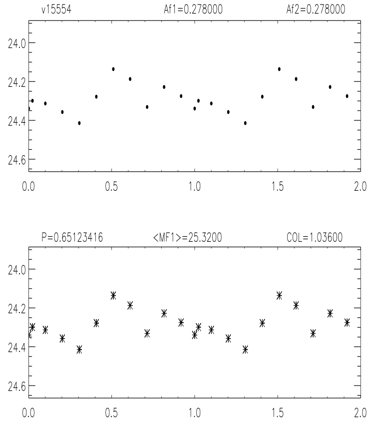
v15554 Af1=0.278000 Af2=0.278000
24.0
24.2
24.4
24.6
0.0 0.5 1.0 1.5 2.0
P=0.65123416 <MF1>=25.3200 COL=1.03600
24.0
24.2
24.4
24.6
0.0 0.5 1.0 1.5 2.0

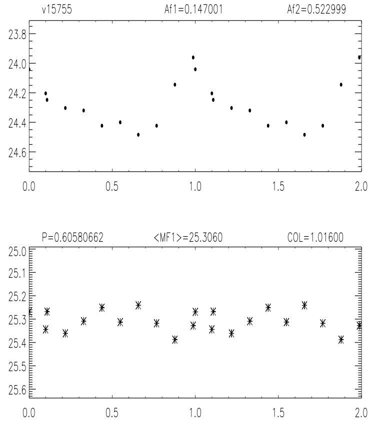
v15755 Af1=0.147001 Af2=0.522999
23.8
24.0
24.2
24.4
24.6
0.0 0.5 1.0 1.5 2.0
P=0.60580662 <MF1>=25.3060 COL=1.01600
25.0
25.1
25.2
25.3
25.4
25.5
25.6
0.0 0.5 1.0 1.5 2.0

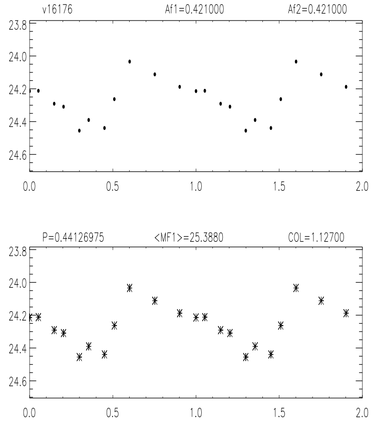
v16176 Af1=0.421000 Af2=0.421000
23.8
24.0
24.2
24.4
24.6
0.0 0.5 1.0 1.5 2.0
P=0.44126975 <MF1>=25.3880 COL=1.12700
23.8
24.0
24.2
24.4
24.6
0.0 0.5 1.0 1.5 2.0

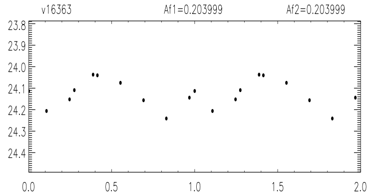
v16363 Af1=0.203999 Af2=0.203999
23.8 23.9 24.0 24.1 24.2 24.3 24.4
0.0 0.5 1.0 1.5 2.0

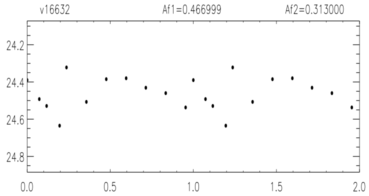
v16632 Af1=0.466999 Af2=0.313000
24.2 24.4 24.6 24.8
0.0 0.5 1.0 1.5 2.0

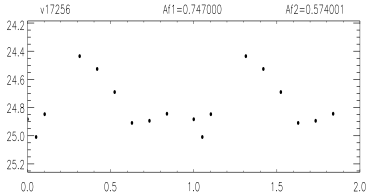
v17256 Af1=0.747000 Af2=0.574001
24.2 24.4 24.6 24.8 25.0 25.2
0.0 0.5 1.0 1.5 2.0

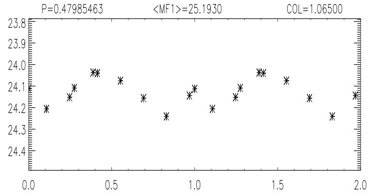
P=0.47985463 <MF1>=25.1930 COL=1.06500
23.8 23.9 24.0 24.1 24.2 24.3 24.4
0.0 0.5 1.0 1.5 2.0

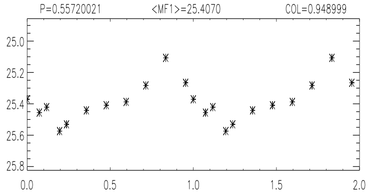
P=0.55720021 <MF1>=25.4070 COL=0.948999
25.0 25.2 25.4 25.6 25.8
0.0 0.5 1.0 1.5 2.0

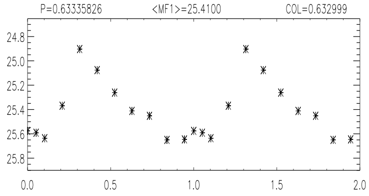
P=0.63335826 <MF1>=25.4100 COL=0.632999
24.8 25.0 25.2 25.4 25.6 25.8
0.0 0.5 1.0 1.5 2.0

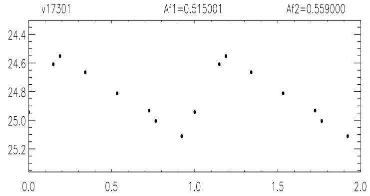
v17301 Af1=0.515001 Af2=0.559000
24.4 24.6 24.8 25.0 25.2
0.0 0.5 1.0 1.5 2.0

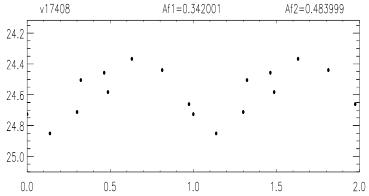
v17408 Af1=0.342001 Af2=0.483999
24.2 24.4 24.6 24.8 25.0
0.0 0.5 1.0 1.5 2.0

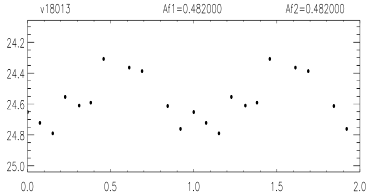
v18013 Af1=0.482000 Af2=0.482000
24.2 24.4 24.6 24.8 25.0
0.0 0.5 1.0 1.5 2.0

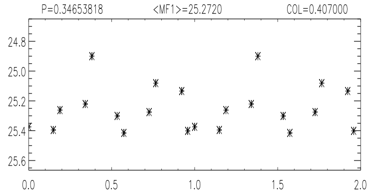
P=0.34653818 <MF1>=25.2720 COL=0.407000
24.8 25.0 25.2 25.4 25.6
0.0 0.5 1.0 1.5 2.0

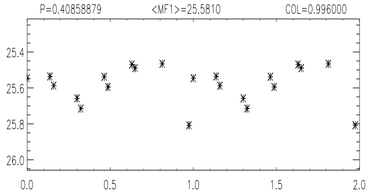
P=0.40858879 <MF1>=25.5810 COL=0.996000
25.4 25.6 25.8 26.0
0.0 0.5 1.0 1.5 2.0

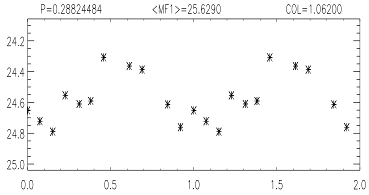
P=0.28824484 <MF1>=25.6290 COL=1.06200
24.2 24.4 24.6 24.8 25.0
0.0 0.5 1.0 1.5 2.0

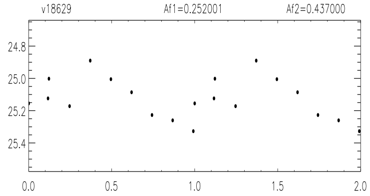
v18629 Af1=0.252001 Af2=0.437000
24.8 25.0 25.2 25.4
0.0 0.5 1.0 1.5 2.0

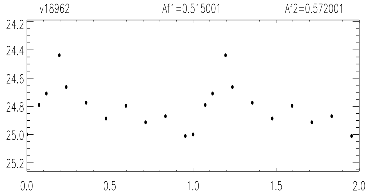
v18962 Af1=0.515001 Af2=0.572001
24.2 24.4 24.6 24.8 25.0 25.2
0.0 0.5 1.0 1.5 2.0

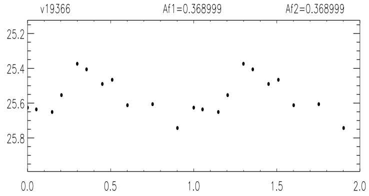
v19366 Af1=0.368999 Af2=0.368999
25.2 25.4 25.6 25.8
0.0 0.5 1.0 1.5 2.0

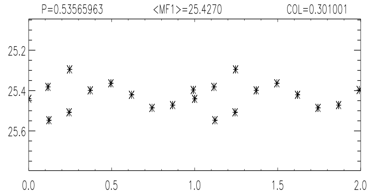
P=0.53565963 <MF1>=25.4270 COL=0.301001
25.2 25.4 25.6
0.0 0.5 1.0 1.5 2.0

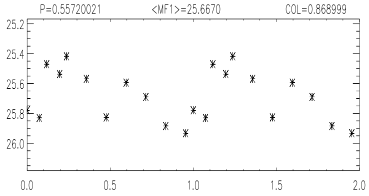
P=0.55720021 <MF1>=25.6670 COL=0.868999
25.2 25.4 25.6 25.8 26.0
0.0 0.5 1.0 1.5 2.0

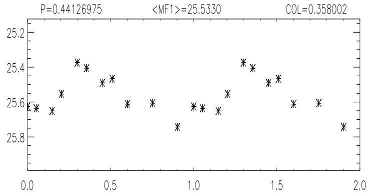
P=0.44126975 <MF1>=25.5330 COL=0.358002
25.2 25.4 25.6 25.8
0.0 0.5 1.0 1.5 2.0

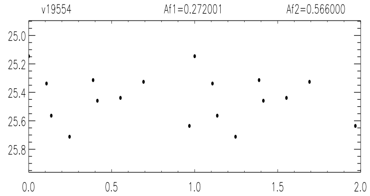
v19554 Af1=0.272001 Af2=0.566000
25.0 25.2 25.4 25.6 25.8
0.0 0.5 1.0 1.5 2.0

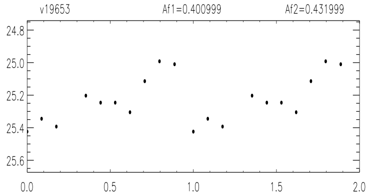
v19653 Af1=0.400999 Af2=0.431999
24.8 25.0 25.2 25.4 25.6
0.0 0.5 1.0 1.5 2.0

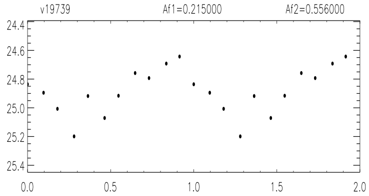
v19739 Af1=0.215000 Af2=0.556000
24.4 24.6 24.8 25.0 25.2 25.4
0.0 0.5 1.0 1.5 2.0

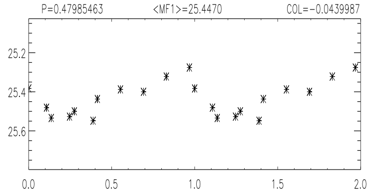
P=0.47985463 <MF1>=25.4470 COL=-0.0439987
25.2 25.4 25.6
0.0 0.5 1.0 1.5 2.0

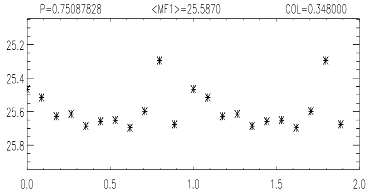
P=0.75087828 <MF1>=25.5870 COL=0.348000
25.2 25.4 25.6 25.8
0.0 0.5 1.0 1.5 2.0

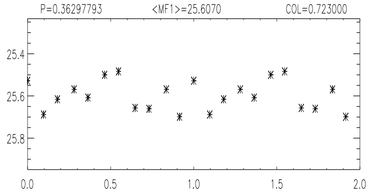
P=0.36297793 <MF1>=25.6070 COL=0.723000
25.4 25.6 25.8
0.0 0.5 1.0 1.5 2.0

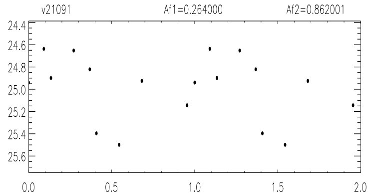
v21091
Af1=0.264000
Af2=0.862001
24.4
24.6
24.8
25.0
25.2
25.4
25.6
0.0
0.5
1.0
1.5
2.0

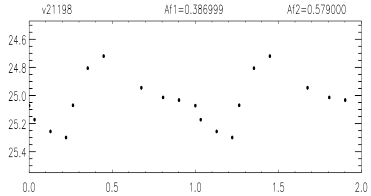
v21198
Af1=0.386999
Af2=0.579000
24.6
24.8
25.0
25.2
25.4
0.0
0.5
1.0
1.5
2.0

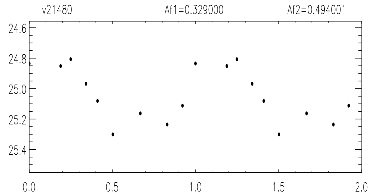
v21480
Af1=0.329000
Af2=0.494001
24.6
24.8
25.0
25.2
25.4
0.0
0.5
1.0
1.5
2.0

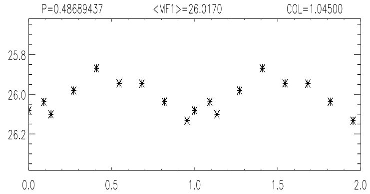
P=0.48689437
<MF1>=26.0170
COL=1.04500
25.8
26.0
26.2
0.0
0.5
1.0
1.5
2.0

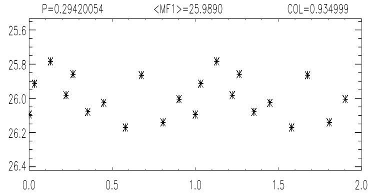
P=0.29420054
<MF1>=25.9890
COL=0.934999
25.6
25.8
26.0
26.2
26.4
0.0
0.5
1.0
1.5
2.0

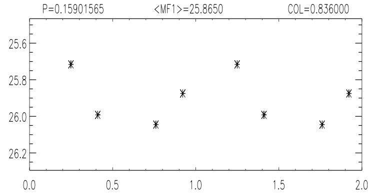
P=0.15901565
<MF1>=25.8650
COL=0.836000
25.6
25.8
26.0
26.2
0.0
0.5
1.0
1.5
2.0

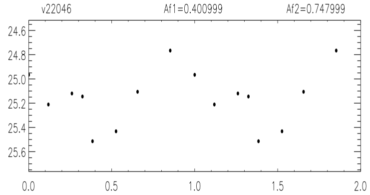
v22046
Af1=0.400999
Af2=0.747999
24.6
24.8
25.0
25.2
25.4
25.6
0.0
0.5
1.0
1.5
2.0

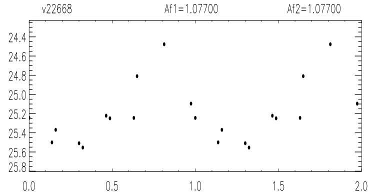
v22668
Af1=1.07700
Af2=1.07700
24.4
24.6
24.8
25.0
25.2
25.4
25.6
25.8
0.0
0.5
1.0
1.5
2.0

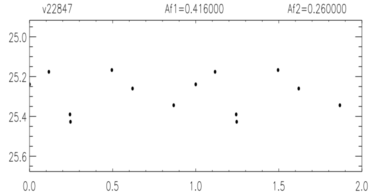
v22847
Af1=0.416000
Af2=0.260000
25.0
25.2
25.4
25.6
0.0
0.5
1.0
1.5
2.0

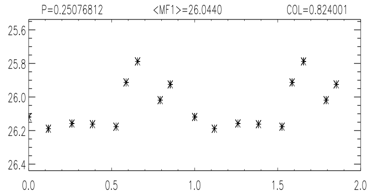
P=0.25076812
<MF1>=26.0440
COL=0.824001
25.6
25.8
26.0
26.2
26.4
0.0
0.5
1.0
1.5
2.0

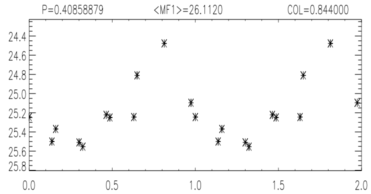
P=0.40858879
<MF1>=26.1120
COL=0.844000
24.4
24.6
24.8
25.0
25.2
25.4
25.6
25.8
0.0
0.5
1.0
1.5
2.0

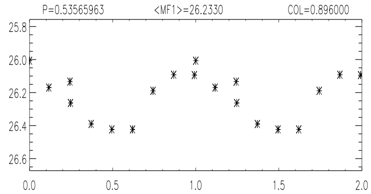
P=0.53565963
<MF1>=26.2330
COL=0.896000
25.8
26.0
26.2
26.4
26.6
0.0
0.5
1.0
1.5
2.0

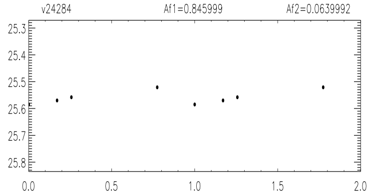
v24284
Af1=0.845999
Af2=0.0639992
25.3
25.4
25.5
25.6
25.7
25.8
0.0
0.5
1.0
1.5
2.0

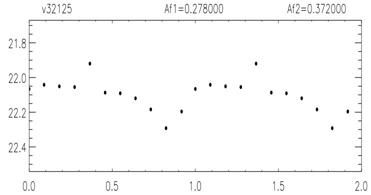
v32125
Af1=0.278000
Af2=0.372000
21.8
22.0
22.2
22.4
0.0
0.5
1.0
1.5
2.0

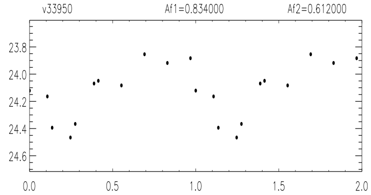
v33950
Af1=0.834000
Af2=0.612000
23.8
24.0
24.2
24.4
24.6
0.0
0.5
1.0
1.5
2.0

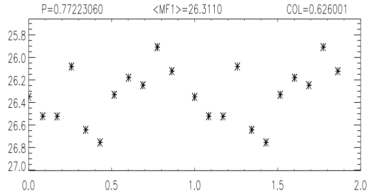
P=0.77223060
<MF1>=26.3110
COL=0.626001
25.8
26.0
26.2
26.4
26.6
26.8
27.0
0.0
0.5
1.0
1.5
2.0

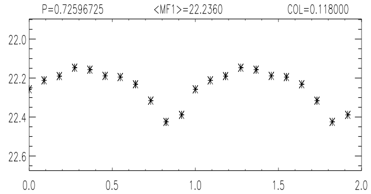
P=0.72596725
<MF1>=22.2360
COL=0.118000
22.0
22.2
22.4
22.6
0.0
0.5
1.0
1.5
2.0

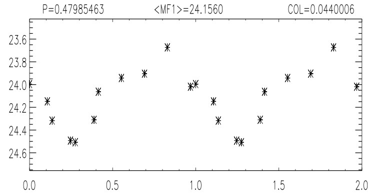
P=0.47985463
<MF1>=24.1560
COL=0.0440006
23.6
23.8
24.0
24.2
24.4
24.6
0.0
0.5
1.0
1.5
2.0

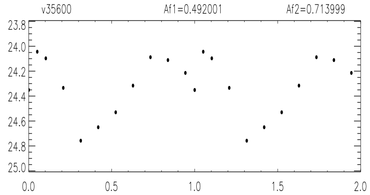
v35600
Af1=0.492001
Af2=0.713999
23.8
24.0
24.2
24.4
24.6
24.8
25.0
0.0
0.5
1.0
1.5
2.0

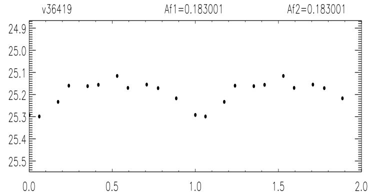
v36419
Af1=0.183001
Af2=0.183001
24.9
25.0
25.1
25.2
25.3
25.4
25.5
0.0
0.5
1.0
1.5
2.0

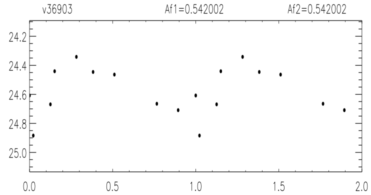
v36903
Af1=0.542002
Af2=0.542002
24.2
24.4
24.6
24.8
25.0
0.0
0.5
1.0
1.5
2.0

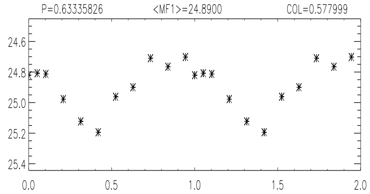
P=0.63335826
<MF1>=24.8900
COL=0.577999
24.6
24.8
25.0
25.2
25.4
0.0
0.5
1.0
1.5
2.0

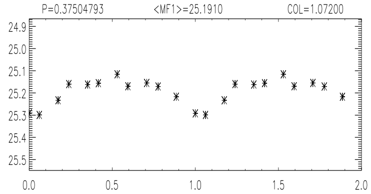
P=0.37504793
<MF1>=25.1910
COL=1.07200
24.9
25.0
25.1
25.2
25.3
25.4
25.5
0.0
0.5
1.0
1.5
2.0

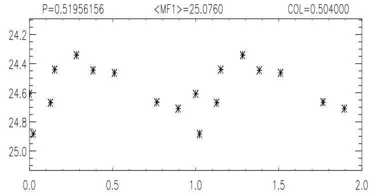
P=0.51956156
<MF1>=25.0760
COL=0.504000
24.2
24.4
24.6
24.8
25.0
0.0
0.5
1.0
1.5
2.0

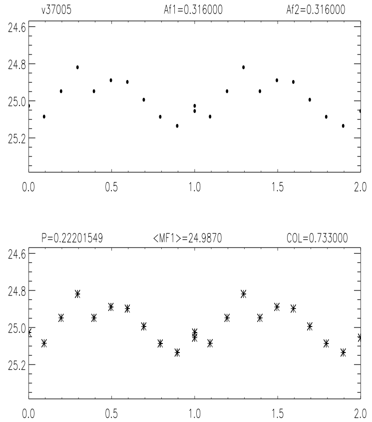
v37005
Af1=0.316000
Af2=0.316000
24.6
24.8
25.0
25.2
0.0
0.5
1.0
1.5
2.0
P=0.22201549
<MF1>=24.9870
COL=0.733000
24.6
24.8
25.0
25.2
0.0
0.5
1.0
1.5
2.0

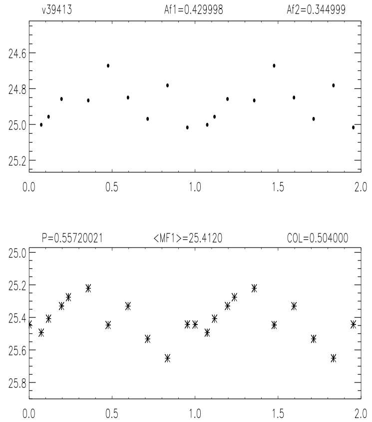
v39413
Af1=0.429998
Af2=0.344999
24.6
24.8
25.0
25.2
0.0
0.5
1.0
1.5
2.0
P=0.55720021
<MF1>=25.4120
COL=0.504000
25.0
25.2
25.4
25.6
25.8
0.0
0.5
1.0
1.5
2.0

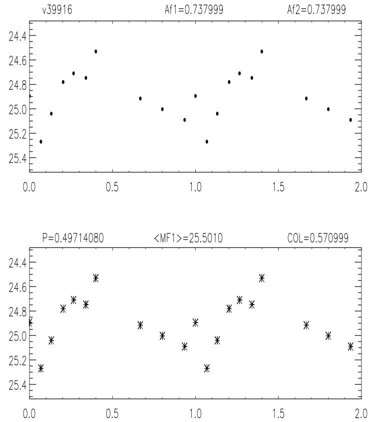
v39916
Af1=0.737999
Af2=0.737999
24.4
24.6
24.8
25.0
25.2
25.4
0.0
0.5
1.0
1.5
2.0
P=0.49714080
<MF1>=25.5010
COL=0.570999
24.4
24.6
24.8
25.0
25.2
25.4
0.0
0.5
1.0
1.5
2.0

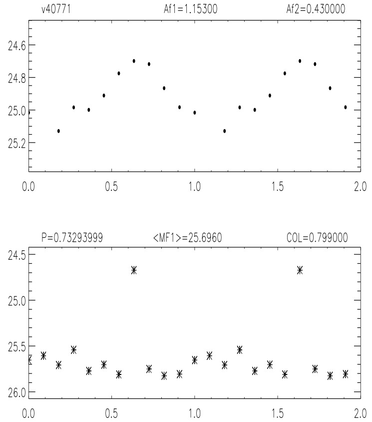
v40771
Af1=1.15300
Af2=0.430000
24.6
24.8
25.0
25.2
0.0
0.5
1.0
1.5
2.0
P=0.73293999
<MF1>=25.6960
COL=0.799000
24.5
25.0
25.5
26.0
0.0
0.5
1.0
1.5
2.0

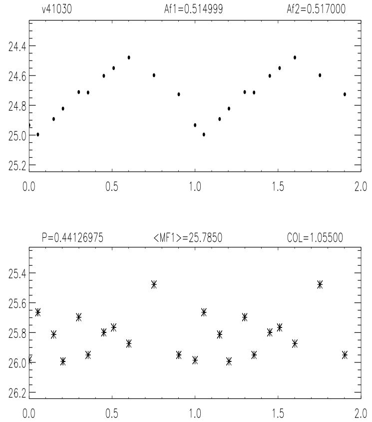
v41030
Af1=0.514999
Af2=0.517000
24.4
24.6
24.8
25.0
25.2
0.0
0.5
1.0
1.5
2.0
P=0.44126975
<MF1>=25.7850
COL=1.05500
25.4
25.6
25.8
26.0
26.2
0.0
0.5
1.0
1.5
2.0

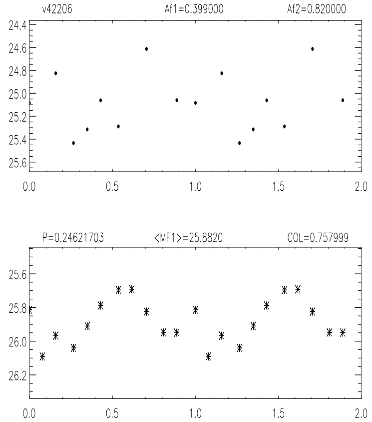
v42206
Af1=0.399000
Af2=0.820000
24.4
24.6
24.8
25.0
25.2
25.4
25.6
0.0
0.5
1.0
1.5
2.0
P=0.24621703
<MF1>=25.8820
COL=0.757999
25.6
25.8
26.0
26.2
0.0
0.5
1.0
1.5
2.0

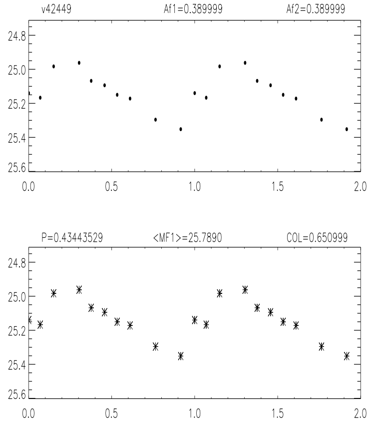
v42449
Af1=0.389999
Af2=0.389999
24.8
25.0
25.2
25.4
25.6
0.0
0.5
1.0
1.5
2.0
P=0.43443529
<MF1>=25.7890
COL=0.650999
24.8
25.0
25.2
25.4
25.6
0.0
0.5
1.0
1.5
2.0

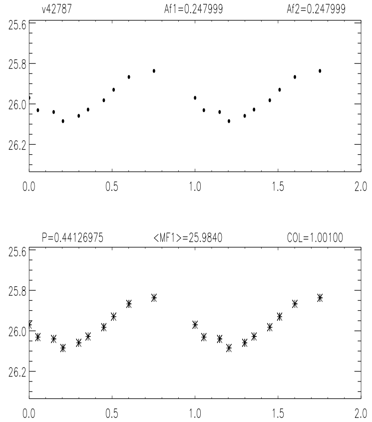
v42787
Af1=0.247999
Af2=0.247999
25.6
25.8
26.0
26.2
0.0
0.5
1.0
1.5
2.0
P=0.44126975
<MF1>=25.9840
COL=1.00100
25.6
25.8
26.0
26.2
0.0
0.5
1.0
1.5
2.0

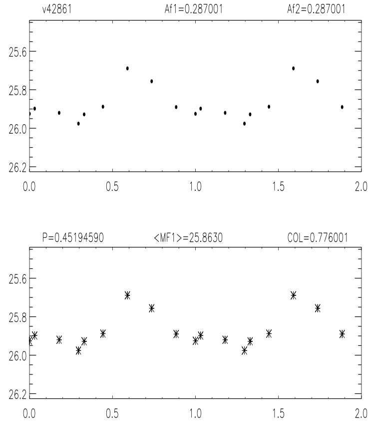
v42861
Af1=0.287001
Af2=0.287001
25.6
25.8
26.0
26.2
0.0
0.5
1.0
1.5
2.0
P=0.45194590
<MF1>=25.8630
COL=0.776001
25.6
25.8
26.0
26.2
0.0
0.5
1.0
1.5
2.0

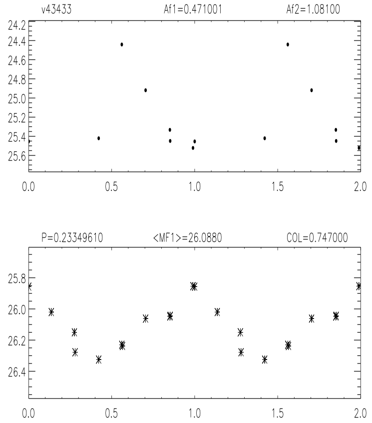
v43433
Af1=0.471001
Af2=1.08100
24.2
24.4
24.6
24.8
25.0
25.2
25.4
25.6
0.0
0.5
1.0
1.5
2.0
P=0.23349610
<MF1>=26.0880
COL=0.747000
25.8
26.0
26.2
26.4
0.0
0.5
1.0
1.5
2.0

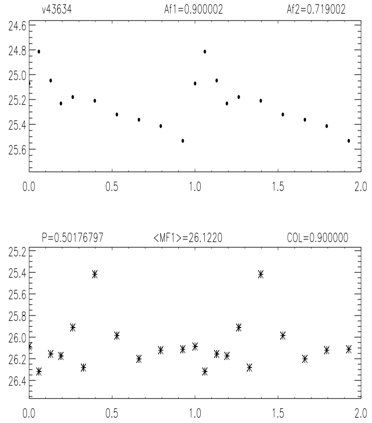
v43634
Af1=0.900002
Af2=0.719002
24.6
24.8
25.0
25.2
25.4
25.6
0.0
0.5
1.0
1.5
2.0
P=0.50176797
<MF1>=26.1220
COL=0.900000
25.2
25.4
25.6
25.8
26.0
26.2
26.4
0.0
0.5
1.0
1.5
2.0

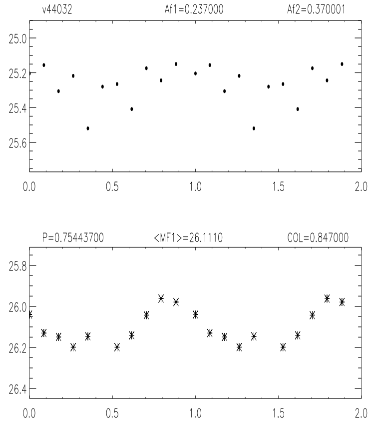
v44032
Af1=0.237000
Af2=0.370001
25.0
25.2
25.4
25.6
0.0
0.5
1.0
1.5
2.0
P=0.75443700
<MF1>=26.1110
COL=0.847000
25.8
26.0
26.2
26.4
0.0
0.5
1.0
1.5
2.0

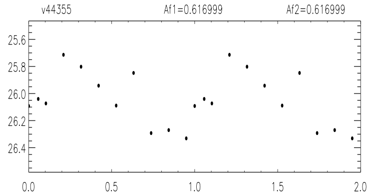
v44355
Af1=0.616999
Af2=0.616999
25.6
25.8
26.0
26.2
26.4
0.0
0.5
1.0
1.5
2.0

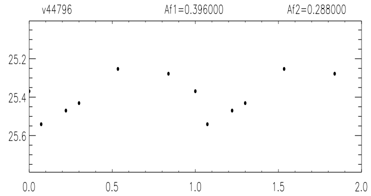
v44796
Af1=0.396000
Af2=0.288000
25.2
25.4
25.6
0.0
0.5
1.0
1.5
2.0

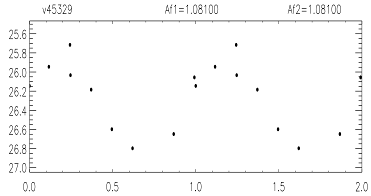
v45329
Af1=1.08100
Af2=1.08100
25.6
25.8
26.0
26.2
26.4
26.6
26.8
27.0
0.0
0.5
1.0
1.5
2.0

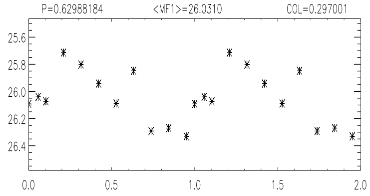
P=0.62988184
<MF1>=26.0310
COL=0.297001
25.6
25.8
26.0
26.2
26.4
0.0
0.5
1.0
1.5
2.0

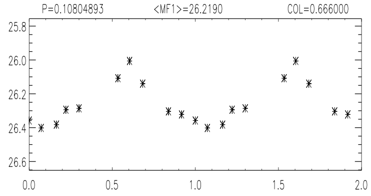
P=0.10804893
<MF1>=26.2190
COL=0.666000
25.8
26.0
26.2
26.4
26.6
0.0
0.5
1.0
1.5
2.0

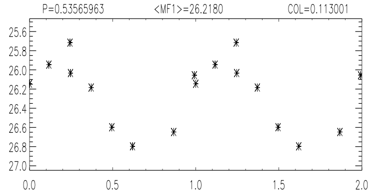
P=0.53565963
<MF1>=26.2180
COL=0.113001
25.6
25.8
26.0
26.2
26.4
26.6
26.8
27.0
0.0
0.5
1.0
1.5
2.0

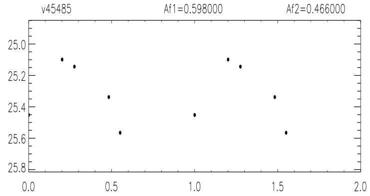
v45485
Af1=0.598000
Af2=0.466000
25.0
25.2
25.4
25.6
25.8
0.0
0.5
1.0
1.5
2.0

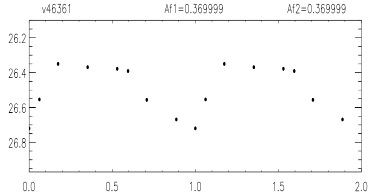
v46361
Af1=0.369999
Af2=0.369999
26.2
26.4
26.6
26.8
0.0
0.5
1.0
1.5
2.0

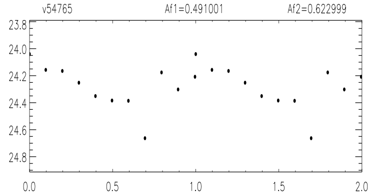
v54765
Af1=0.491001
Af2=0.622999
23.8
24.0
24.2
24.4
24.6
24.8
0.0
0.5
1.0
1.5
2.0

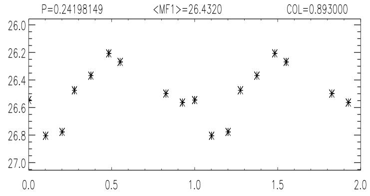
P=0.24198149
<MF1>=26.4320
COL=0.893000
26.0
26.2
26.4
26.6
26.8
27.0
0.0
0.5
1.0
1.5
2.0

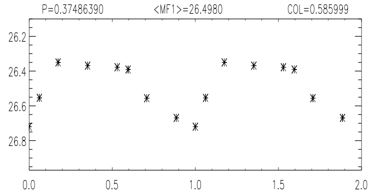
P=0.37486390
<MF1>=26.4980
COL=0.585999
26.2
26.4
26.6
26.8
0.0
0.5
1.0
1.5
2.0

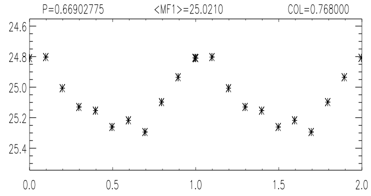
P=0.66902775
<MF1>=25.0210
COL=0.768000
24.6
24.8
25.0
25.2
25.4
0.0
0.5
1.0
1.5
2.0

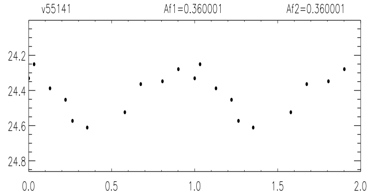
v55141
Af1=0.360001
Af2=0.360001
24.2
24.4
24.6
24.8
0.0
0.5
1.0
1.5
2.0

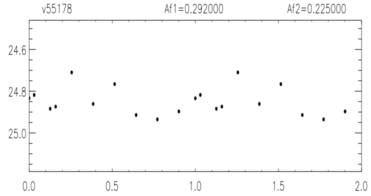
v55178
Af1=0.292000
Af2=0.225000
24.6
24.8
25.0
0.0
0.5
1.0
1.5
2.0

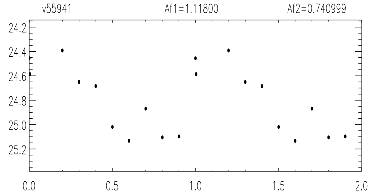
v55941
Af1=1.11800
Af2=0.740999
24.2
24.4
24.6
24.8
25.0
25.2
0.0
0.5
1.0
1.5
2.0

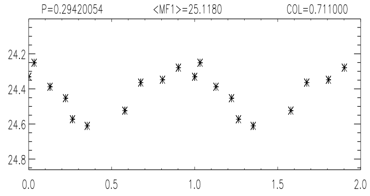
P=0.29420054
<MF1>=25.1180
COL=0.711000
24.2
24.4
24.6
24.8
0.0
0.5
1.0
1.5
2.0

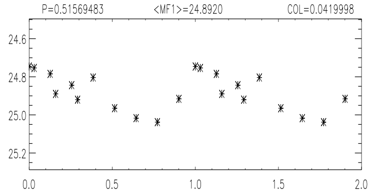
P=0.51569483
<MF1>=24.8920
COL=0.0419998
24.6
24.8
25.0
25.2
0.0
0.5
1.0
1.5
2.0

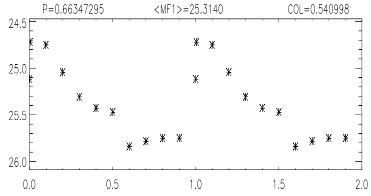
P=0.66347295
<MF1>=25.3140
COL=0.540998
24.5
25.0
25.5
26.0
0.0
0.5
1.0
1.5
2.0

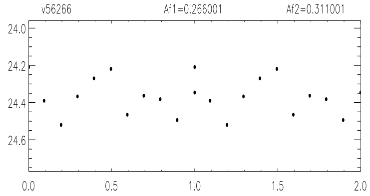
v56266
Af1=0.266001
Af2=0.311001
24.0
24.2
24.4
24.6
0.0
0.5
1.0
1.5
2.0

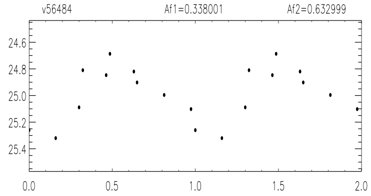
v56484
Af1=0.338001
Af2=0.632999
24.6
24.8
25.0
25.2
25.4
0.0
0.5
1.0
1.5
2.0

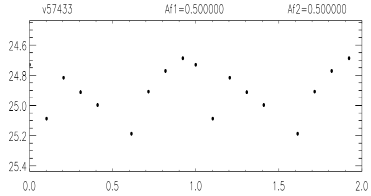
v57433
Af1=0.500000
Af2=0.500000
24.6
24.8
25.0
25.2
25.4
0.0
0.5
1.0
1.5
2.0

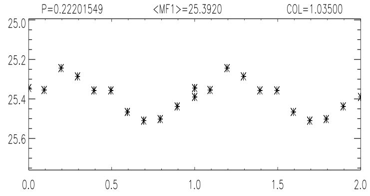
P=0.22201549
<MF1>=25.3920
COL=1.03500
25.0
25.2
25.4
25.6
0.0
0.5
1.0
1.5
2.0

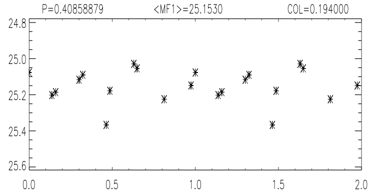
P=0.40858879
<MF1>=25.1530
COL=0.194000
24.8
25.0
25.2
25.4
25.6
0.0
0.5
1.0
1.5
2.0

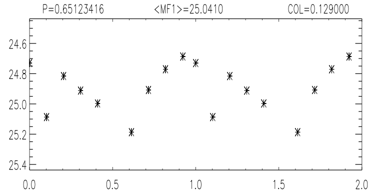
P=0.65123416
<MF1>=25.0410
COL=0.129000
24.6
24.8
25.0
25.2
25.4
0.0
0.5
1.0
1.5
2.0

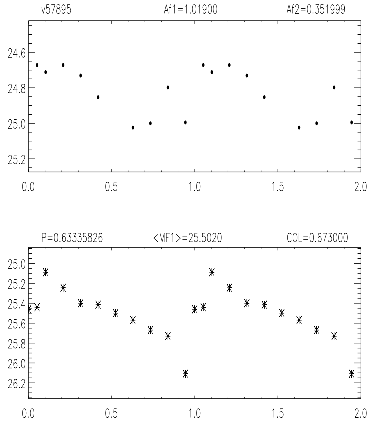
v57895 Af1=1.01900 Af2=0.351999
24.6
24.8
25.0
25.2
P=0.63335826 <MF1>=25.5020 COL=0.673000
25.0
25.2
25.4
25.6
25.8
26.0
26.2
0.0
0.5
1.0
1.5
2.0

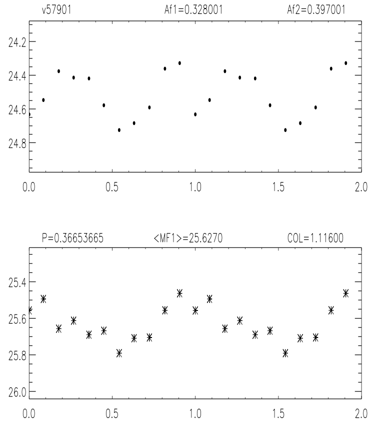
v57901 Af1=0.328001 Af2=0.397001
24.2
24.4
24.6
24.8
P=0.36653665 <MF1>=25.6270 COL=1.11600
25.4
25.6
25.8
26.0
0.0
0.5
1.0
1.5
2.0

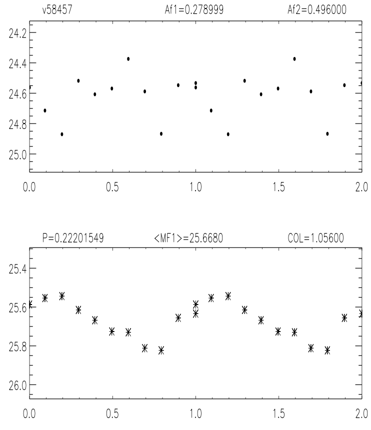
v58457 Af1=0.278999 Af2=0.496000
24.2
24.4
24.6
24.8
25.0
P=0.22201549 <MF1>=25.6680 COL=1.05600
25.4
25.6
25.8
26.0
0.0
0.5
1.0
1.5
2.0

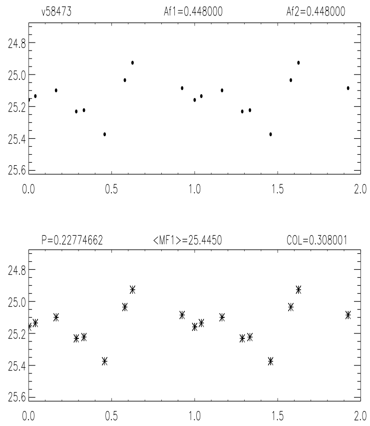
v58473 Af1=0.448000 Af2=0.448000
24.8
25.0
25.2
25.4
25.6
P=0.22774662 <MF1>=25.4450 COL=0.308001
24.8
25.0
25.2
25.4
25.6
0.0
0.5
1.0
1.5
2.0

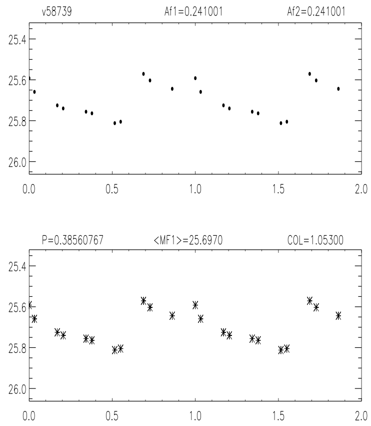
v58739 Af1=0.241001 Af2=0.241001
25.4
25.6
25.8
26.0
P=0.38560767 <MF1>=25.6970 COL=1.05300
25.4
25.6
25.8
26.0
0.0
0.5
1.0
1.5
2.0

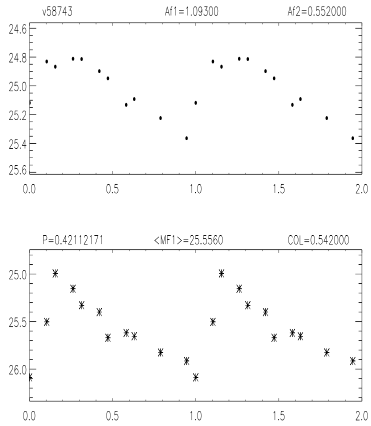
v58743 Af1=1.09300 Af2=0.552000
24.6
24.8
25.0
25.2
25.4
25.6
P=0.42112171 <MF1>=25.5560 COL=0.542000
25.0
25.5
26.0
0.0
0.5
1.0
1.5
2.0

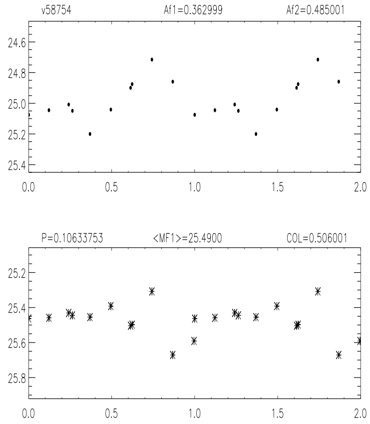
v58754 Af1=0.362999 Af2=0.485001
24.6
24.8
25.0
25.2
25.4
P=0.10633753 <MF1>=25.4900 COL=0.506001
25.2
25.4
25.6
25.8
0.0
0.5
1.0
1.5
2.0

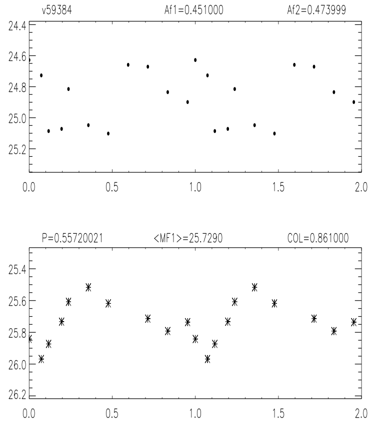
v59384 Af1=0.451000 Af2=0.473999
24.4
24.6
24.8
25.0
25.2
P=0.55720021 <MF1>=25.7290 COL=0.861000
25.4
25.6
25.8
26.0
26.2
0.0
0.5
1.0
1.5
2.0

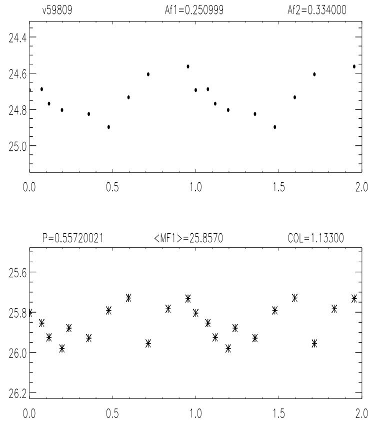
v59809 Af1=0.250999 Af2=0.334000
24.4
24.6
24.8
25.0
P=0.55720021 <MF1>=25.8570 COL=1.13300
25.6
25.8
26.0
26.2
0.0
0.5
1.0
1.5
2.0

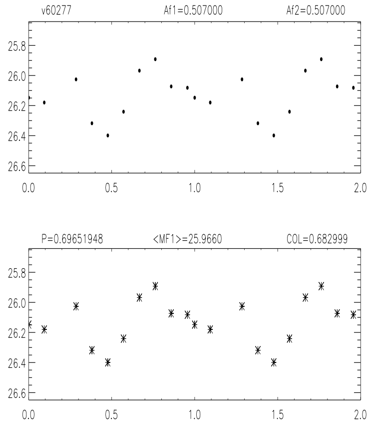
v60277 Af1=0.507000 Af2=0.507000
25.8
26.0
26.2
26.4
26.6
P=0.69651948 <MF1>=25.9660 COL=0.682999
25.8
26.0
26.2
26.4
26.6
0.0
0.5
1.0
1.5
2.0

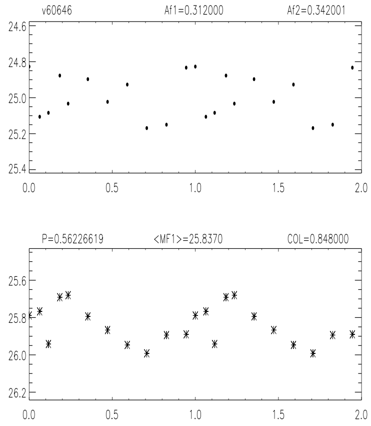
v60646 Af1=0.312000 Af2=0.342001
24.6
24.8
25.0
25.2
25.4
P=0.56226619 <MF1>=25.8370 COL=0.848000
25.6
25.8
26.0
26.2
0.0
0.5
1.0
1.5
2.0

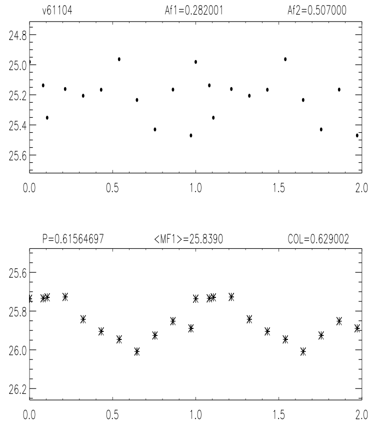
v61104 Af1=0.282001 Af2=0.507000
24.8
25.0
25.2
25.4
25.6
P=0.61564697 <MF1>=25.8390 COL=0.629002
25.6
25.8
26.0
26.2
0.0
0.5
1.0
1.5
2.0

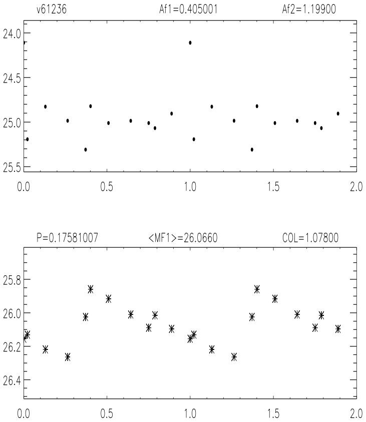
v61236
Af1=0.405001
Af2=1.19900
24.0
24.5
25.0
25.5
0.0
0.5
1.0
1.5
2.0
P=0.17581007
<MF1>=26.0660
COL=1.07800
25.8
26.0
26.2
26.4
0.0
0.5
1.0
1.5
2.0

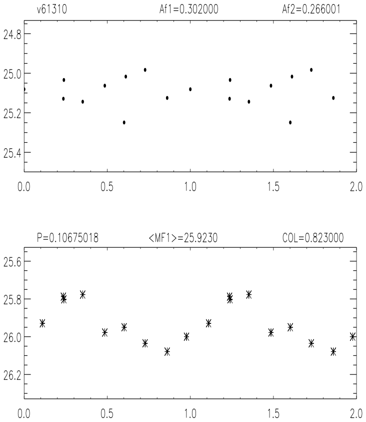
v61310
Af1=0.302000
Af2=0.266001
24.8
25.0
25.2
25.4
0.0
0.5
1.0
1.5
2.0
P=0.10675018
<MF1>=25.9230
COL=0.823000
25.6
25.8
26.0
26.2
0.0
0.5
1.0
1.5
2.0

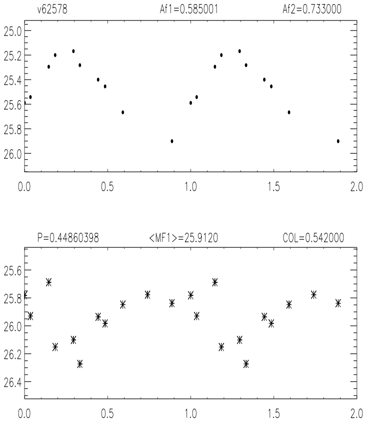
v62578
Af1=0.585001
Af2=0.733000
25.0
25.2
25.4
25.6
25.8
26.0
0.0
0.5
1.0
1.5
2.0
P=0.44860398
<MF1>=25.9120
COL=0.542000
25.6
25.8
26.0
26.2
26.4
0.0
0.5
1.0
1.5
2.0

Chapter 13

Appendix G

ATLAS OF LIGHT CURVES: S2 Chip 1

Atlas of light curves in B-band differential flux, for the candidate variable stars in CCD1 of field S2. For each candidate variable identification and period are provided on top of the plot.

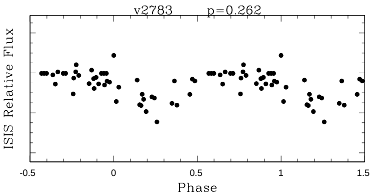
v2783 p=0.262
ISIS Relative Flux
-0.5
0
0.5
1
1.5
Phase

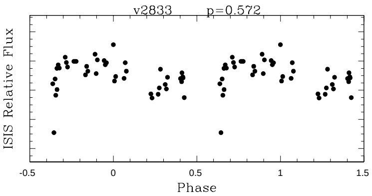
v2833 p=0.572
ISIS Relative Flux
-0.5
0
0.5
1
1.5
Phase

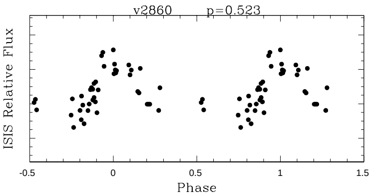
v2860 p=0.523
ISIS Relative Flux
-0.5
0
0.5
1
1.5
Phase

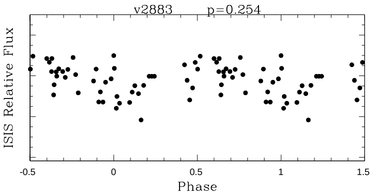
v2883 p=0.254
ISIS Relative Flux
-0.5
0
0.5
1
1.5
Phase

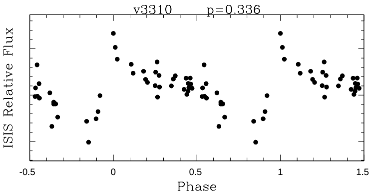
v3310 p=0.336
ISIS Relative Flux
-0.5
0
0.5
1
1.5
Phase

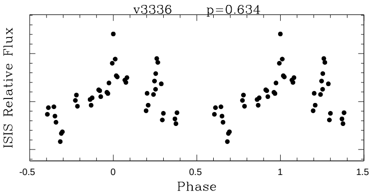
v3336 p=0.634
ISIS Relative Flux
-0.5
0
0.5
1
1.5
Phase

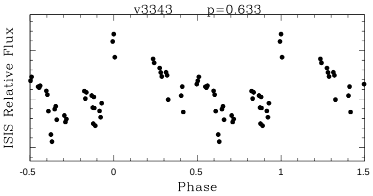
v3343 p=0.633
ISIS Relative Flux
-0.5
0
0.5
1
1.5
Phase

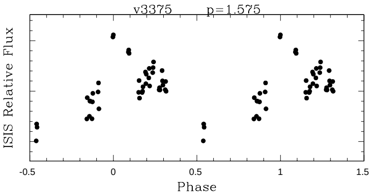
v3375 p=1.575
ISIS Relative Flux
-0.5
0
0.5
1
1.5
Phase

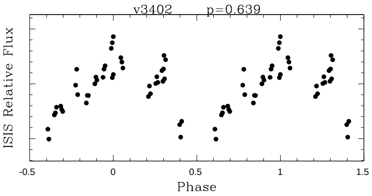
v3402 p=0.639
ISIS Relative Flux
-0.5
0
0.5
1
1.5
Phase

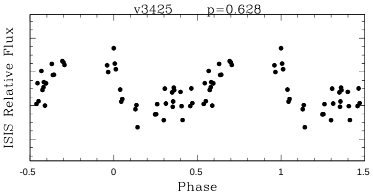
v3425 p=0.628
ISIS Relative Flux
-0.5
0
0.5
1
1.5
Phase

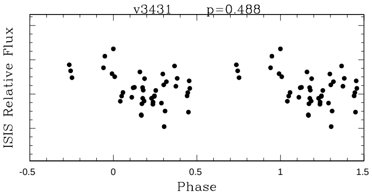
v3431 p=0.488
ISIS Relative Flux
-0.5
0
0.5
1
1.5
Phase

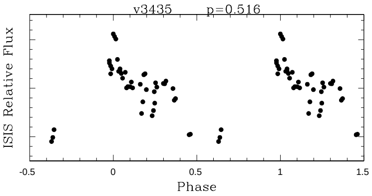
v3435 p=0.516
ISIS Relative Flux
-0.5
0
0.5
1
1.5
Phase

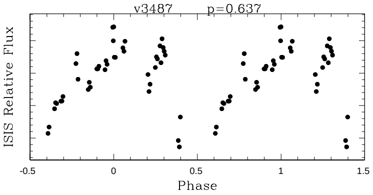
v3487 p=0.637
ISIS Relative Flux
-0.5
0
0.5
1
1.5
Phase

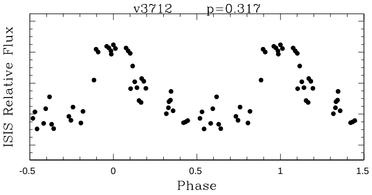
v3712 p=0.317
ISIS Relative Flux
-0.5
0
0.5
1
1.5
Phase

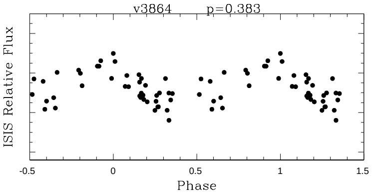
v3864 p=0.383
ISIS Relative Flux
-0.5
0
0.5
1
1.5
Phase

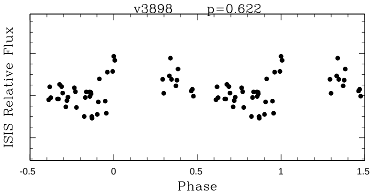
v3898 p=0.622
ISIS Relative Flux
-0.5
0
0.5
1
1.5
Phase

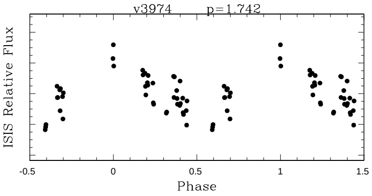
v3974 p=1.742
ISIS Relative Flux
-0.5
0
0.5
1
1.5
Phase

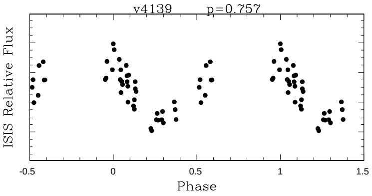
v4139 p=0.757
ISIS Relative Flux
-0.5
0
0.5
1
1.5
Phase

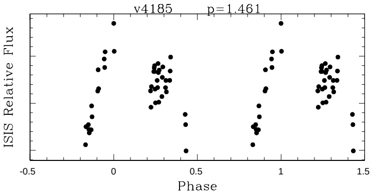
v4185 p=1.461
ISIS Relative Flux
-0.5
0
0.5
1
1.5
Phase

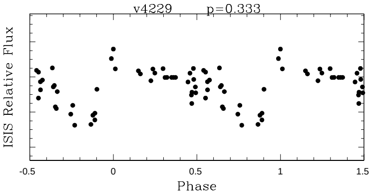
v4229 p=0.333
ISIS Relative Flux
-0.5
0
0.5
1
1.5
Phase

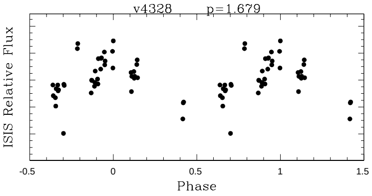
v4328 p=1.679
ISIS Relative Flux
-0.5
0
0.5
1
1.5
Phase

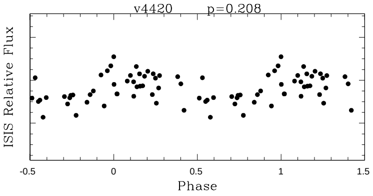
v4420 p=0.208
ISIS Relative Flux
-0.5
0
0.5
1
1.5
Phase

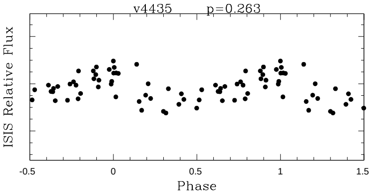
v4435 p=0.263
ISIS Relative Flux
-0.5
0
0.5
1
1.5
Phase

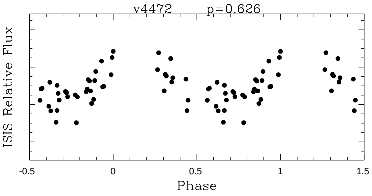
v4472 p=0.626
ISIS Relative Flux
-0.5
0
0.5
1
1.5
Phase

v4475 p=0.390

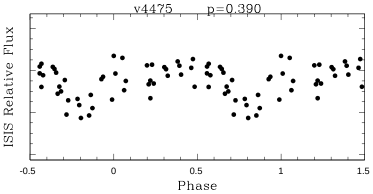

v4562 p=9.501

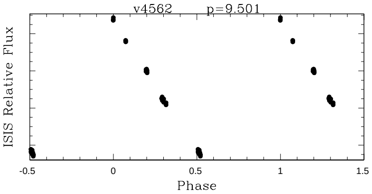

v4564 p=0.622

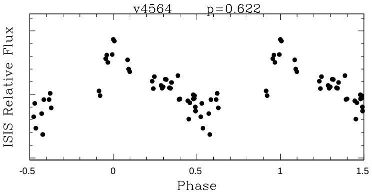

v4578 p=0.334

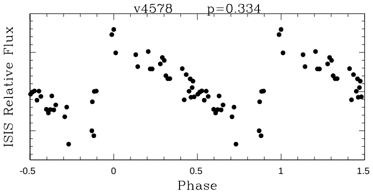

v4592 p=0.264

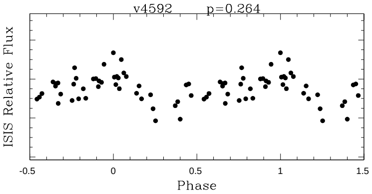

v4623 p=1.502

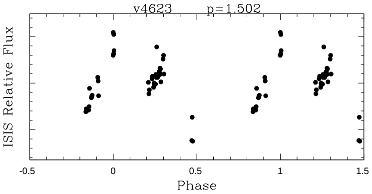

v4705 p=2.625

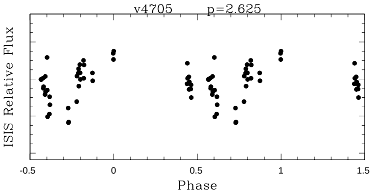

v4809 p=0.381

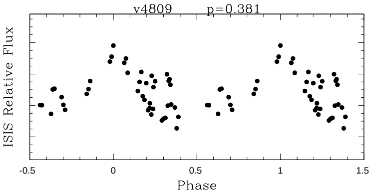

v4875 p=0.565

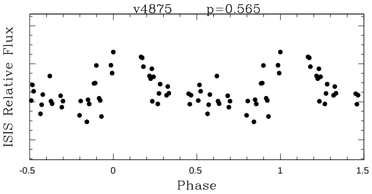

v4936 p=0.570

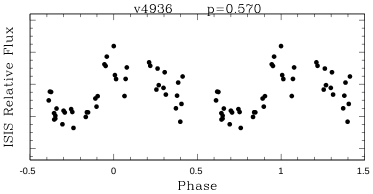

v5033 p=0.205

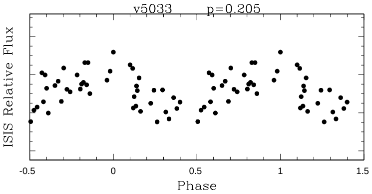

v5089 p=0.601

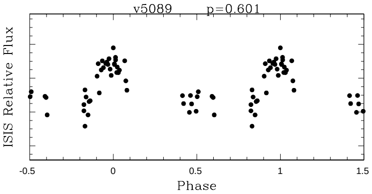

v5093 p=0.355

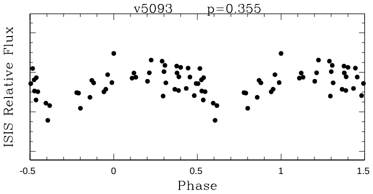

v5169 p=1.682

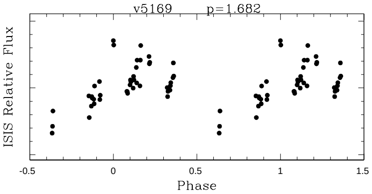

v5202 p=0.513

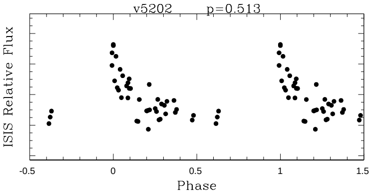

v5205 p=0.335

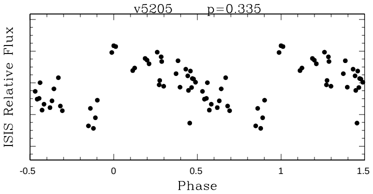

v5305 p=0.335

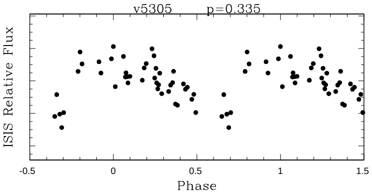

v5384 p=0.333

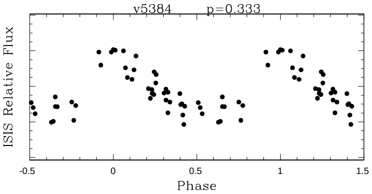

v5385 p=0.638

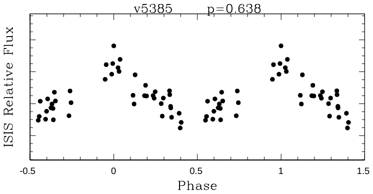

v5510 p=0.408

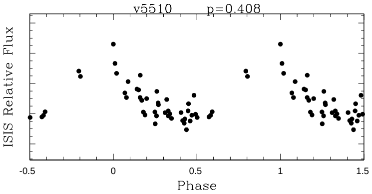

v5512 p=0.809

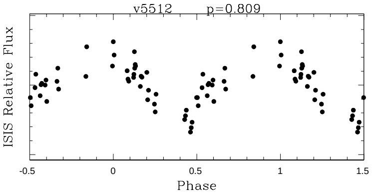

v5847 p=0.450

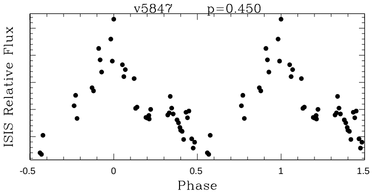

v5850 p=0.569

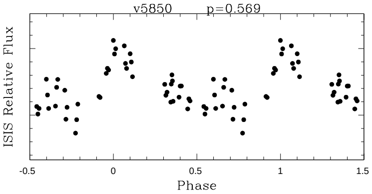

v6191 p=1.151

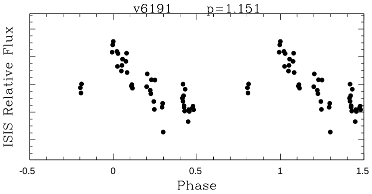

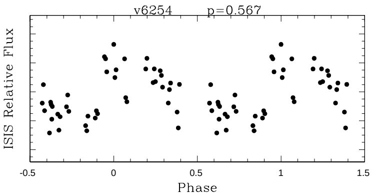
v6254 p=0.567

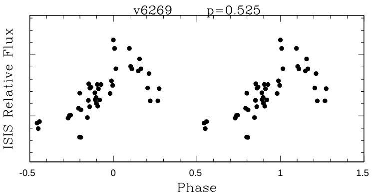
v6269 p=0.525

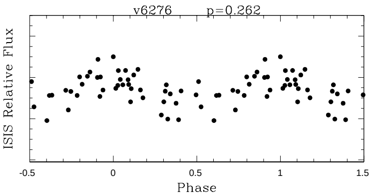
v6276 p=0.262

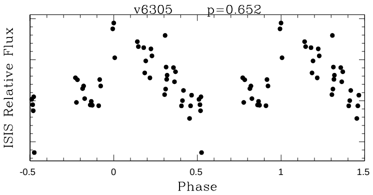
v6305 p=0.652

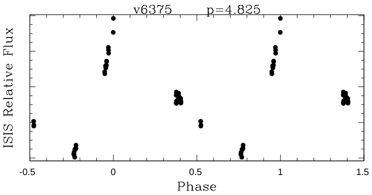
v6375 p=4.825

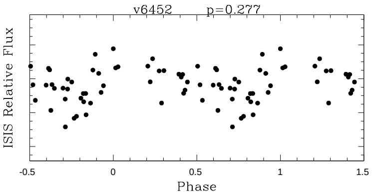
v6452 p=0.277

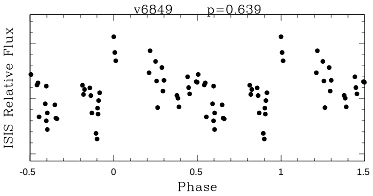
v6849 p=0.639

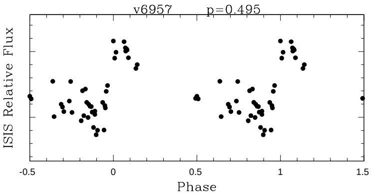
v6957 p=0.495

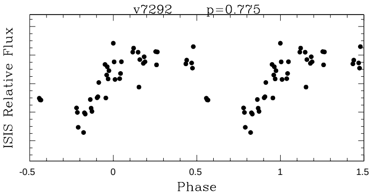
v7292 p=0.775

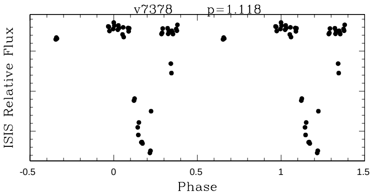
v7378 p=1.118

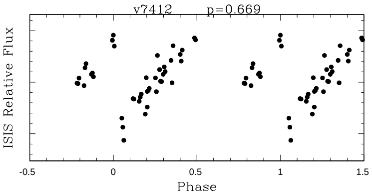
v7412 p=0.669

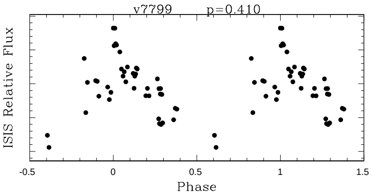
v7799 p=0.410

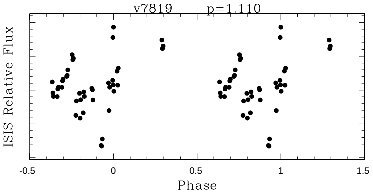
v7819 p=1.110

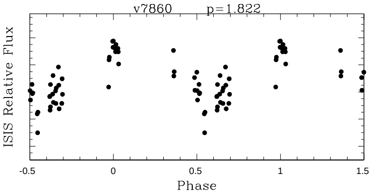
v7860 p=1.822

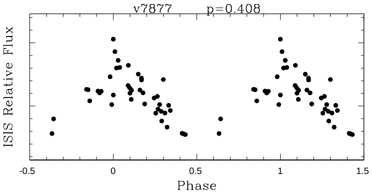
v7877 p=0.408

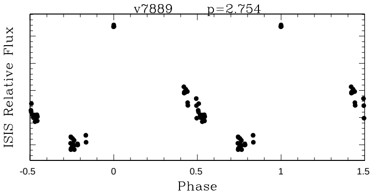
v7889 p=2.754

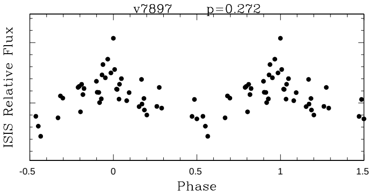
v7897 p=0.272

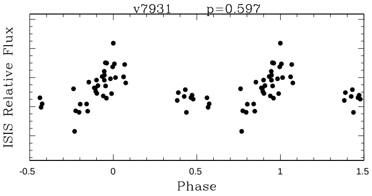
v7931 p=0.597

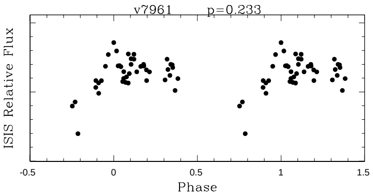
v7961 p=0.233

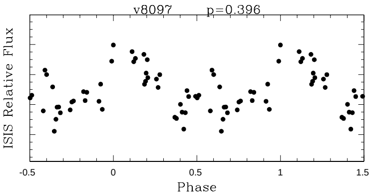
v8097 p=0.396

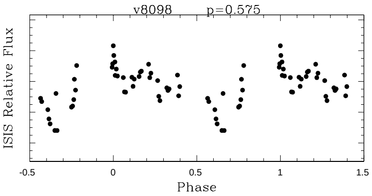
v8098 p=0.575

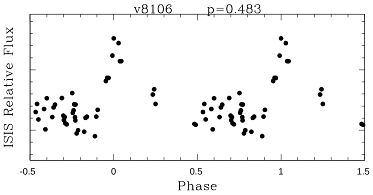
v8106 p=0.483

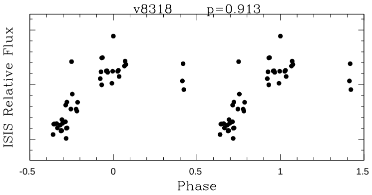
v8318 p=0.913

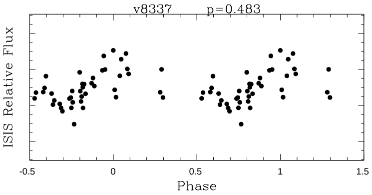
v8337 p=0.483

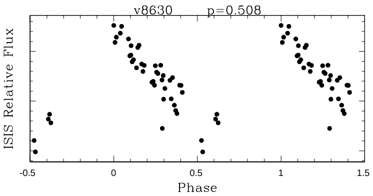
v8630 p=0.508
ISIS Relative Flux
-0.5
0
0.5
1
1.5
Phase

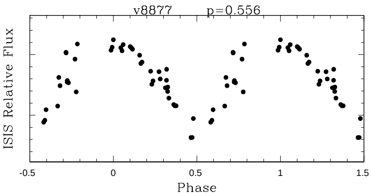
v8877 p=0.556
ISIS Relative Flux
-0.5
0
0.5
1
1.5
Phase

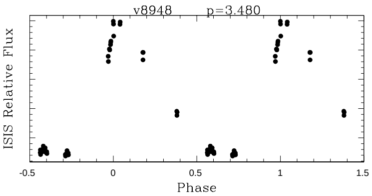
v8948 p=3.480
ISIS Relative Flux
-0.5
0
0.5
1
1.5
Phase

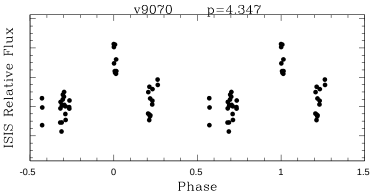
v9070 p=4.347
ISIS Relative Flux
-0.5
0
0.5
1
1.5
Phase

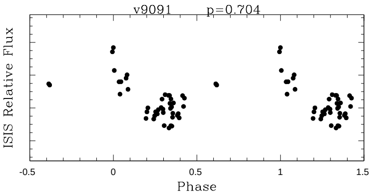
v9091 p=0.704
ISIS Relative Flux
-0.5
0
0.5
1
1.5
Phase

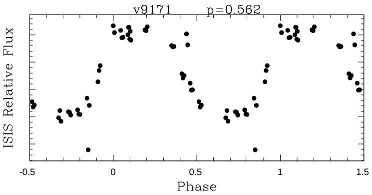
v9171 p=0.562
ISIS Relative Flux
-0.5
0
0.5
1
1.5
Phase

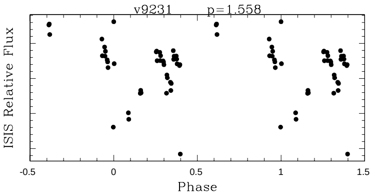
v9231 p=1.558
ISIS Relative Flux
-0.5
0
0.5
1
1.5
Phase

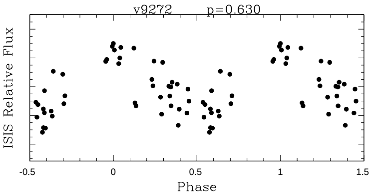
v9272 p=0.630
ISIS Relative Flux
-0.5
0
0.5
1
1.5
Phase

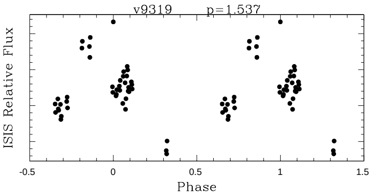
v9319 p=1.537
ISIS Relative Flux
-0.5
0
0.5
1
1.5
Phase

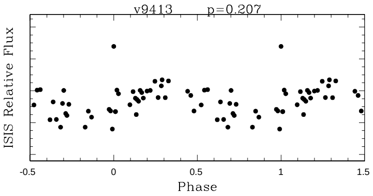
v9413 p=0.207
ISIS Relative Flux
-0.5
0
0.5
1
1.5
Phase

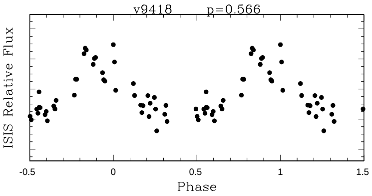
v9418 p=0.566
ISIS Relative Flux
-0.5
0
0.5
1
1.5
Phase

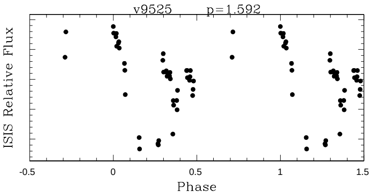
v9525 p=1.592
ISIS Relative Flux
-0.5
0
0.5
1
1.5
Phase

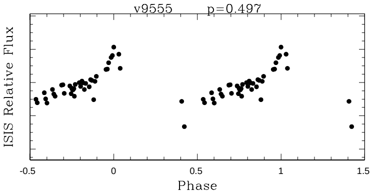
v9555 p=0.497
ISIS Relative Flux
-0.5
0
0.5
1
1.5
Phase

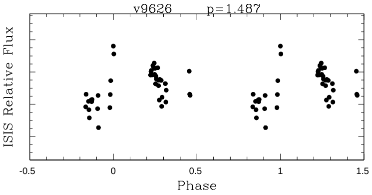
v9626 p=1.487
ISIS Relative Flux
-0.5
0
0.5
1
1.5
Phase

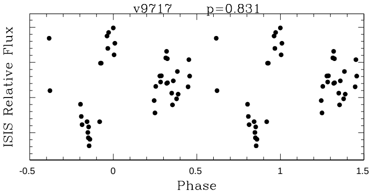
v9717 p=0.831
ISIS Relative Flux
-0.5
0
0.5
1
1.5
Phase

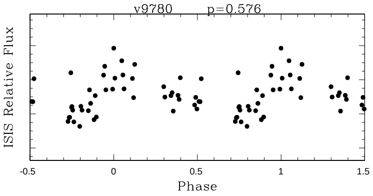
v9780 p=0.576
ISIS Relative Flux
-0.5
0
0.5
1
1.5
Phase

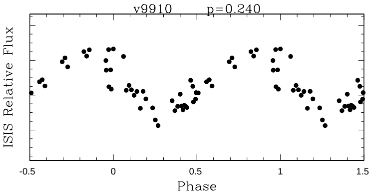
v9910 p=0.240
ISIS Relative Flux
-0.5
0
0.5
1
1.5
Phase

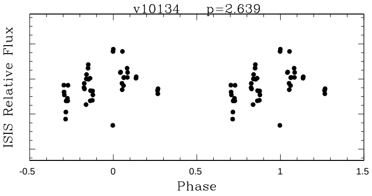
v10134 p=2.639
ISIS Relative Flux
-0.5
0
0.5
1
1.5
Phase

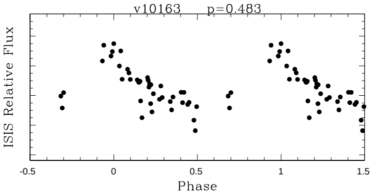
v10163 p=0.483
ISIS Relative Flux
-0.5
0
0.5
1
1.5
Phase

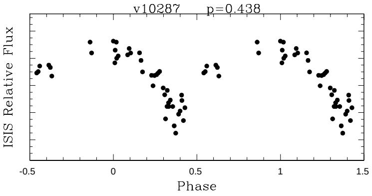
v10287 p=0.438
ISIS Relative Flux
-0.5
0
0.5
1
1.5
Phase

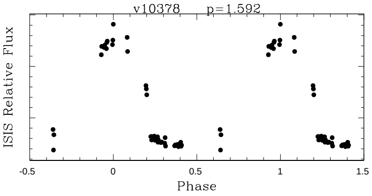
v10378 p=1.592
ISIS Relative Flux
-0.5
0
0.5
1
1.5
Phase

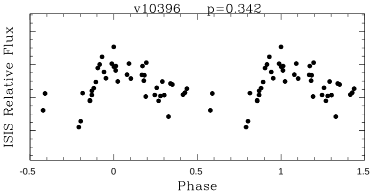
v10396 p=0.342
ISIS Relative Flux
-0.5
0
0.5
1
1.5
Phase

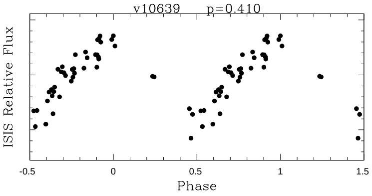
v10639 p=0.410
ISIS Relative Flux
-0.5
0
0.5
1
1.5
Phase

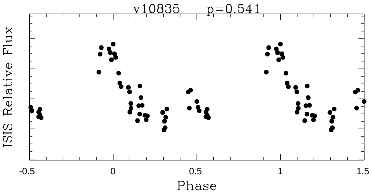
v10835 p=0.541
ISIS Relative Flux
-0.5
0
0.5
1
1.5
Phase

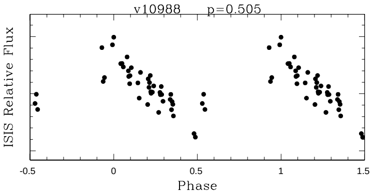
v10988 p=0.505
ISIS Relative Flux
-0.5
0
0.5
1
1.5
Phase

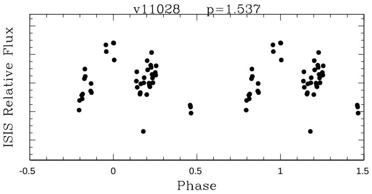
v11028 p=1.537
ISIS Relative Flux
-0.5
0
0.5
1
1.5
Phase

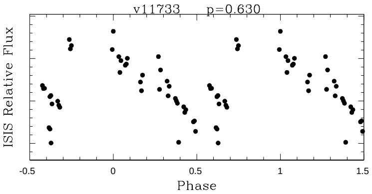
v11733 p=0.630
ISIS Relative Flux
-0.5
0
0.5
1
1.5
Phase

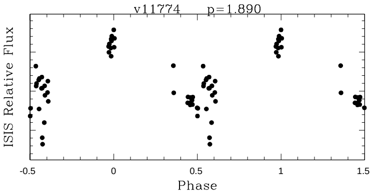
v11774 p=1.890
ISIS Relative Flux
-0.5
0
0.5
1
1.5
Phase

Chapter 14

Appendix H

ATLAS OF LIGHT CURVES: S2 Chip 2

Atlas of light curves in B-band differential flux, for the candidate variable stars in CCD2 of field S2. For each candidate variable identification and period are provided on top of the plot.

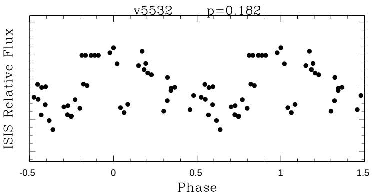
v5532 p=0.182
ISIS Relative Flux
Phase
-0.5
0
0.5
1
1.5

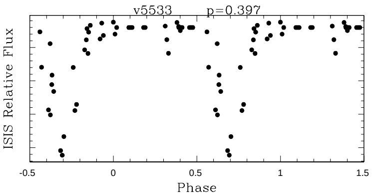
v5533 p=0.397
ISIS Relative Flux
Phase
-0.5
0
0.5
1
1.5

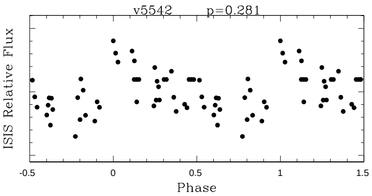
v5542 p=0.281
ISIS Relative Flux
Phase
-0.5
0
0.5
1
1.5

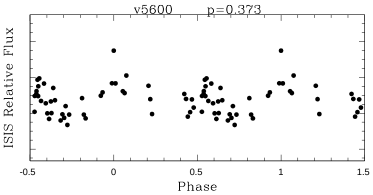
v5600 p=0.373
ISIS Relative Flux
Phase
-0.5
0
0.5
1
1.5

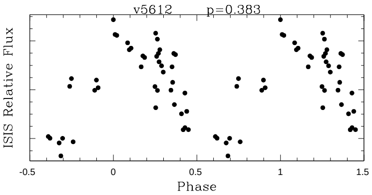
v5612 p=0.383
ISIS Relative Flux
Phase
-0.5
0
0.5
1
1.5

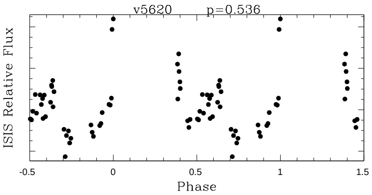
v5620 p=0.536
ISIS Relative Flux
Phase
-0.5
0
0.5
1
1.5

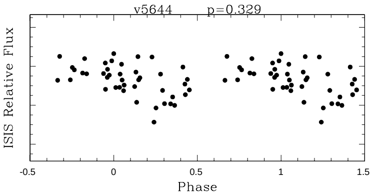
v5644 p=0.329
ISIS Relative Flux
Phase
-0.5
0
0.5
1
1.5

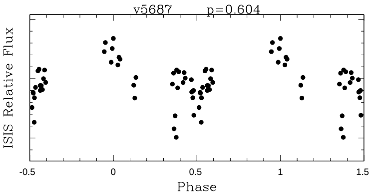
v5687 p=0.604
ISIS Relative Flux
Phase
-0.5
0
0.5
1
1.5

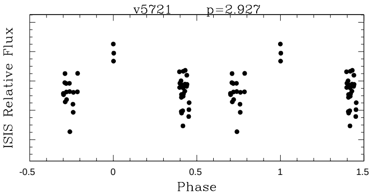
v5721 p=2.927
ISIS Relative Flux
Phase
-0.5
0
0.5
1
1.5

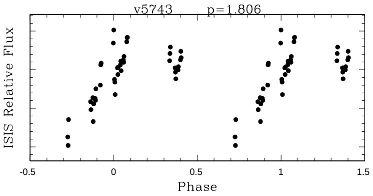
v5743 p=1.806
ISIS Relative Flux
Phase
-0.5
0
0.5
1
1.5

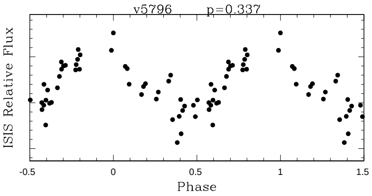
v5796 p=0.337
ISIS Relative Flux
Phase
-0.5
0
0.5
1
1.5

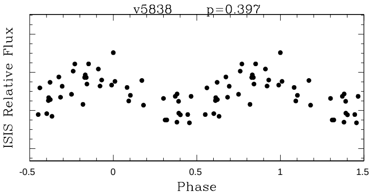
v5838 p=0.397
ISIS Relative Flux
Phase
-0.5
0
0.5
1
1.5

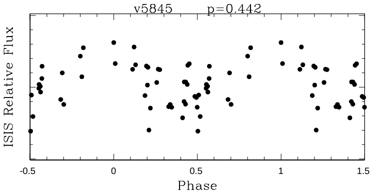
v5845 p=0.442
ISIS Relative Flux
Phase
-0.5
0
0.5
1
1.5

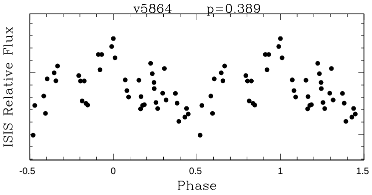
v5864 p=0.389
ISIS Relative Flux
Phase
-0.5
0
0.5
1
1.5

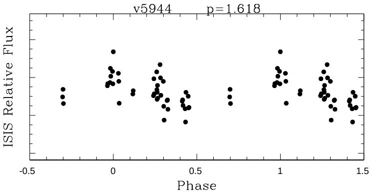
v5944 p=1.618
ISIS Relative Flux
Phase
-0.5
0
0.5
1
1.5

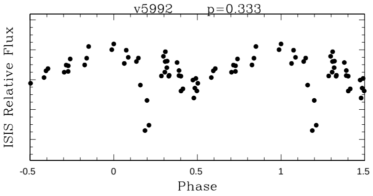
v5992 p=0.333
ISIS Relative Flux
Phase
-0.5
0
0.5
1
1.5

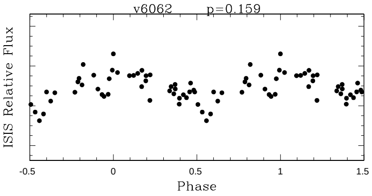
v6062 p=0.159
ISIS Relative Flux
Phase
-0.5
0
0.5
1
1.5

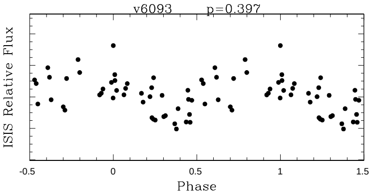
v6093 p=0.397
ISIS Relative Flux
Phase
-0.5
0
0.5
1
1.5

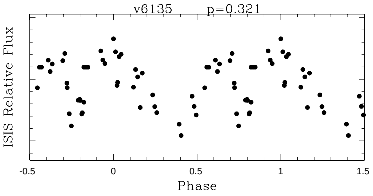
v6135 p=0.321
ISIS Relative Flux
Phase
-0.5
0
0.5
1
1.5

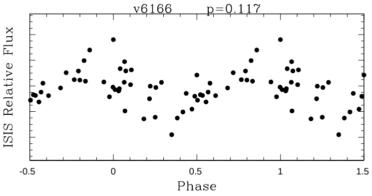
v6166 p=0.117
ISIS Relative Flux
Phase
-0.5
0
0.5
1
1.5

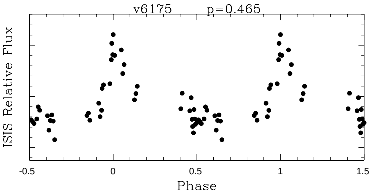
v6175 p=0.465
ISIS Relative Flux
Phase
-0.5
0
0.5
1
1.5

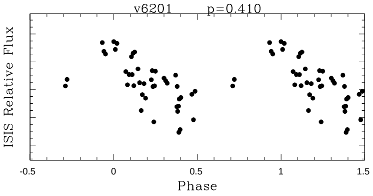
v6201 p=0.410
ISIS Relative Flux
Phase
-0.5
0
0.5
1
1.5

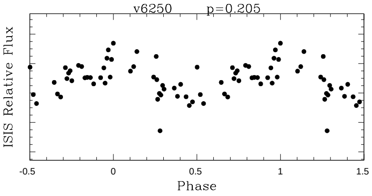
v6250 p=0.205
ISIS Relative Flux
Phase
-0.5
0
0.5
1
1.5

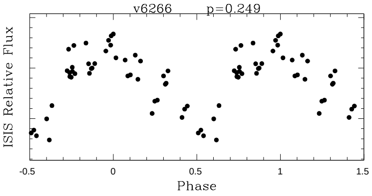
v6266 p=0.249
ISIS Relative Flux
Phase
-0.5
0
0.5
1
1.5

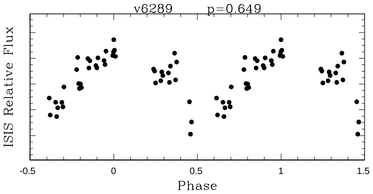
v6289 p=0.649
ISIS Relative Flux
-0.5
0
0.5
1
1.5
Phase

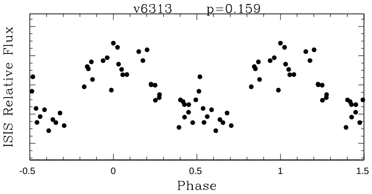
v6313 p=0.159
ISIS Relative Flux
-0.5
0
0.5
1
1.5
Phase

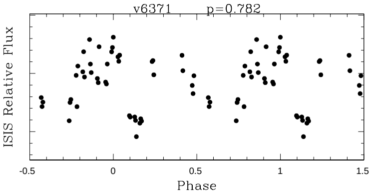
v6371 p=0.782
ISIS Relative Flux
-0.5
0
0.5
1
1.5
Phase

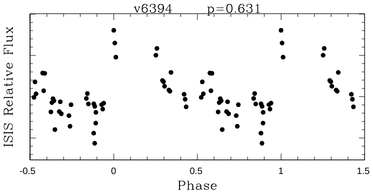
v6394 p=0.631
ISIS Relative Flux
-0.5
0
0.5
1
1.5
Phase

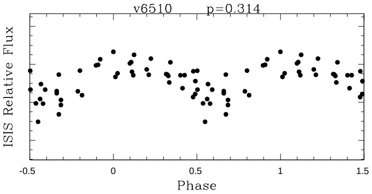
v6510 p=0.314
ISIS Relative Flux
-0.5
0
0.5
1
1.5
Phase

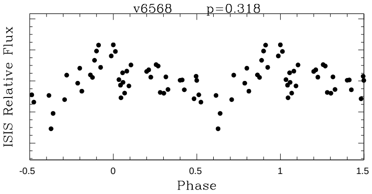
v6568 p=0.318
ISIS Relative Flux
-0.5
0
0.5
1
1.5
Phase

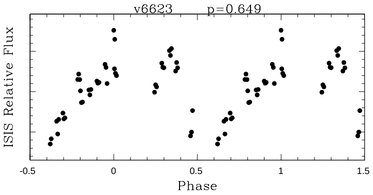
v6623 p=0.649
ISIS Relative Flux
-0.5
0
0.5
1
1.5
Phase

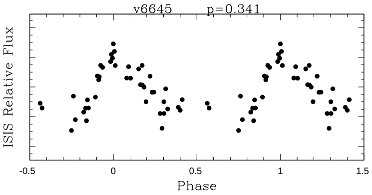
v6645 p=0.341
ISIS Relative Flux
-0.5
0
0.5
1
1.5
Phase

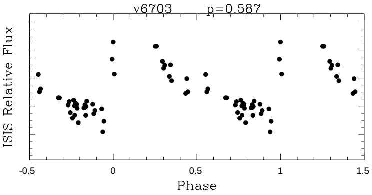
v6703 p=0.587
ISIS Relative Flux
-0.5
0
0.5
1
1.5
Phase

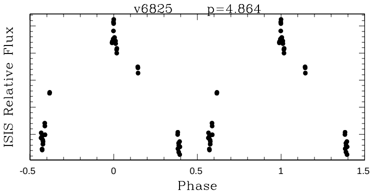
v6825 p=4.864
ISIS Relative Flux
-0.5
0
0.5
1
1.5
Phase

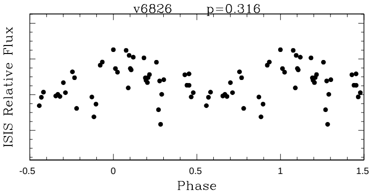
v6826 p=0.316
ISIS Relative Flux
-0.5
0
0.5
1
1.5
Phase

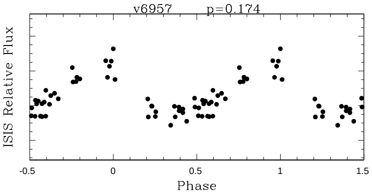
v6957 p=0.174
ISIS Relative Flux
-0.5
0
0.5
1
1.5
Phase

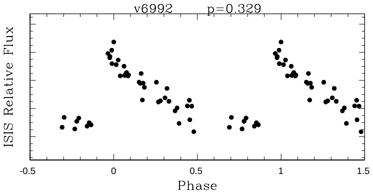
v6992 p=0.329
ISIS Relative Flux
-0.5
0
0.5
1
1.5
Phase

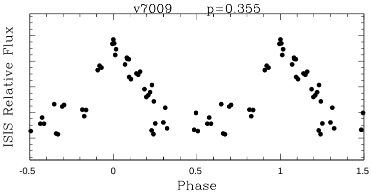
v7009 p=0.355
ISIS Relative Flux
-0.5
0
0.5
1
1.5
Phase

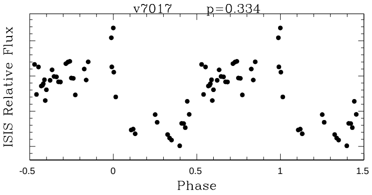
v7017 p=0.334
ISIS Relative Flux
-0.5
0
0.5
1
1.5
Phase

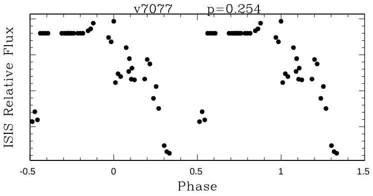
v7077 p=0.254
ISIS Relative Flux
-0.5
0
0.5
1
1.5
Phase

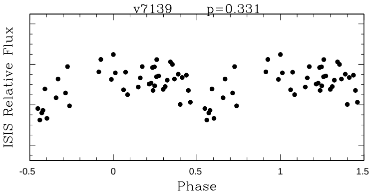
v7139 p=0.331
ISIS Relative Flux
-0.5
0
0.5
1
1.5
Phase

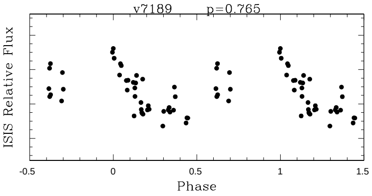
v7189 p=0.765
ISIS Relative Flux
-0.5
0
0.5
1
1.5
Phase

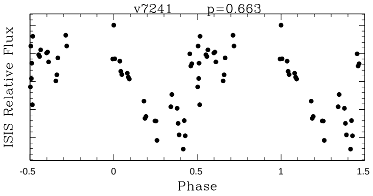
v7241 p=0.663
ISIS Relative Flux
-0.5
0
0.5
1
1.5
Phase

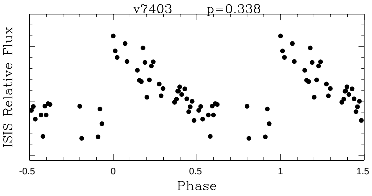
v7403 p=0.338
ISIS Relative Flux
-0.5
0
0.5
1
1.5
Phase

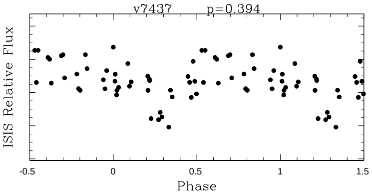
v7437 p=0.394
ISIS Relative Flux
-0.5
0
0.5
1
1.5
Phase

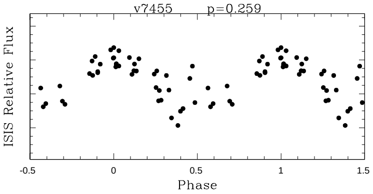
v7455 p=0.259
ISIS Relative Flux
-0.5
0
0.5
1
1.5
Phase

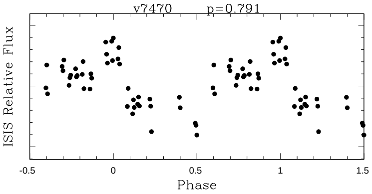
v7470 p=0.791
ISIS Relative Flux
-0.5
0
0.5
1
1.5
Phase

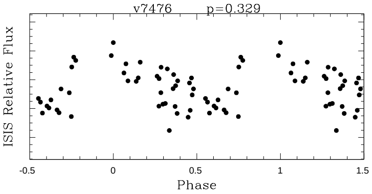
v7476 p=0.329
ISIS Relative Flux
-0.5
0
0.5
1
1.5
Phase

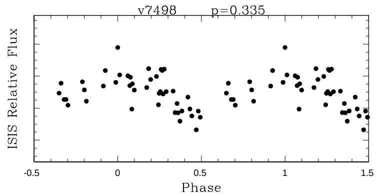
v7498 p=0.335

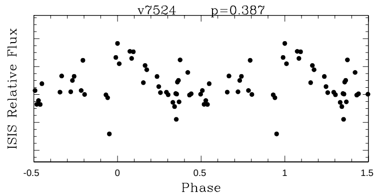
v7524 p=0.387

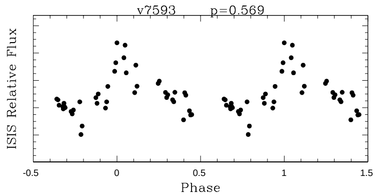
v7593 p=0.569

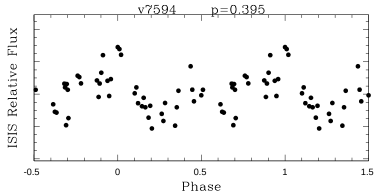
v7594 p=0.395

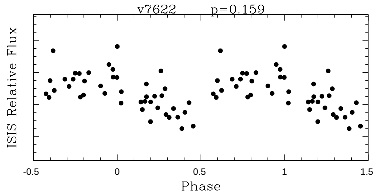
v7622 p=0.159

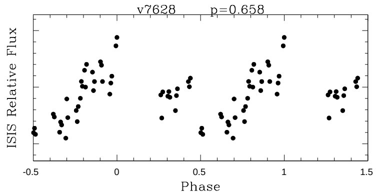
v7628 p=0.658

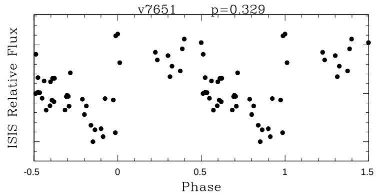
v7651 p=0.329

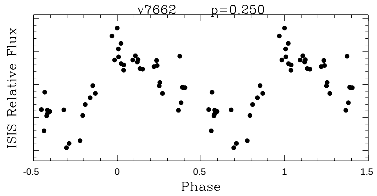
v7662 p=0.250

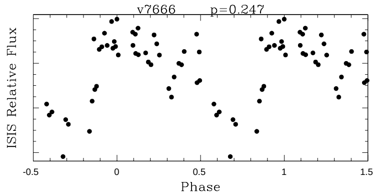
v7666 p=0.247

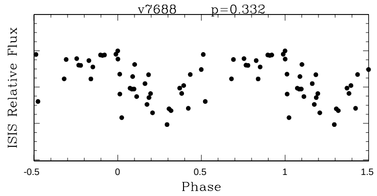
v7688 p=0.332

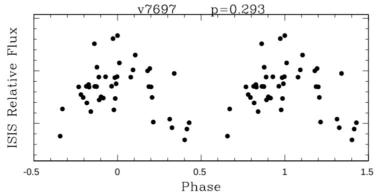
v7697 p=0.293

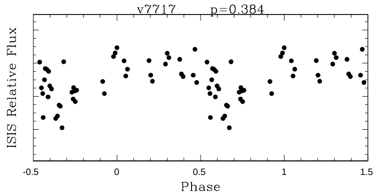
v7717 p=0.384

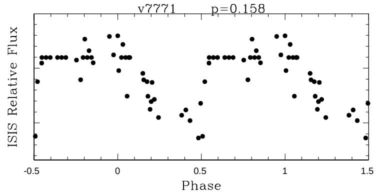
v7771 p=0.158

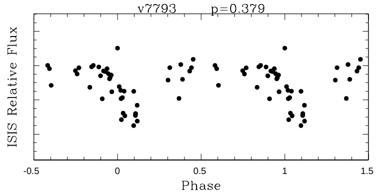
v7793 p=0.379

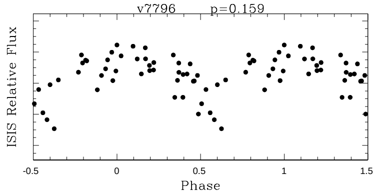
v7796 p=0.159

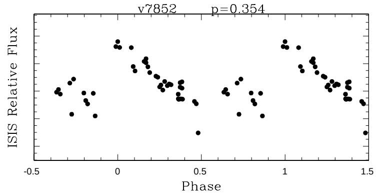
v7852 p=0.354

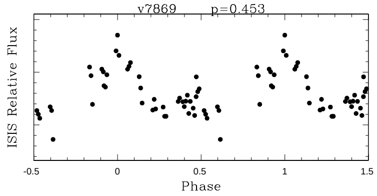
v7869 p=0.453

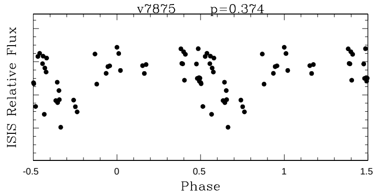
v7875 p=0.374

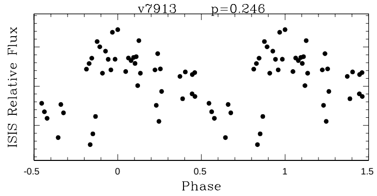
v7913 p=0.246

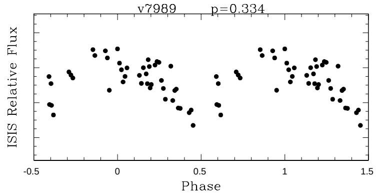
v7989 p=0.334

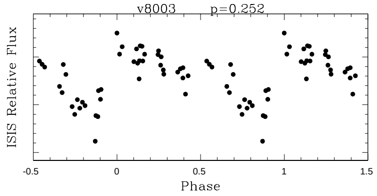
v8003 p=0.252

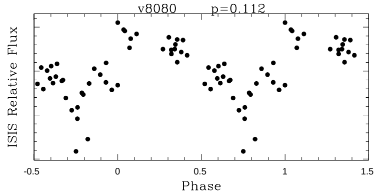
v8080 p=0.112

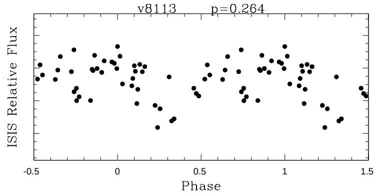
v8113 p=0.264

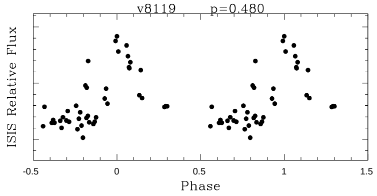
v8119 p=0.480

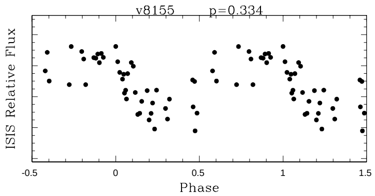
v8155 p=0.334
ISIS Relative Flux
-0.5
0
0.5
1
1.5
Phase

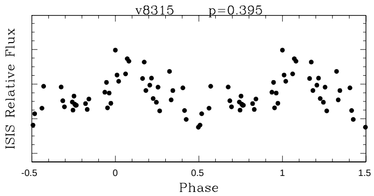
v8315 p=0.395
ISIS Relative Flux
-0.5
0
0.5
1
1.5
Phase

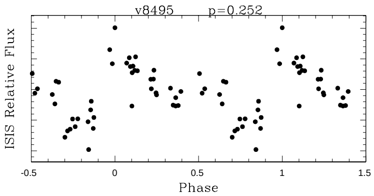
v8495 p=0.252
ISIS Relative Flux
-0.5
0
0.5
1
1.5
Phase

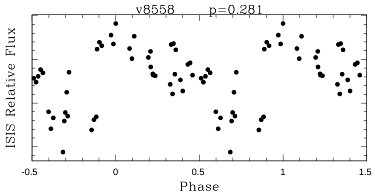
v8558 p=0.281
ISIS Relative Flux
-0.5
0
0.5
1
1.5
Phase

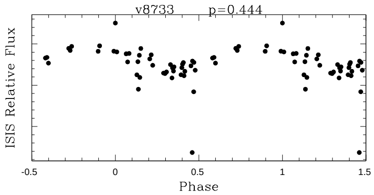
v8733 p=0.444
ISIS Relative Flux
-0.5
0
0.5
1
1.5
Phase

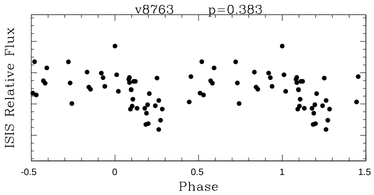
v8763 p=0.383
ISIS Relative Flux
-0.5
0
0.5
1
1.5
Phase

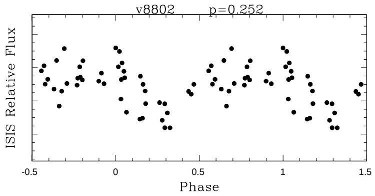
v8802 p=0.252
ISIS Relative Flux
-0.5
0
0.5
1
1.5
Phase

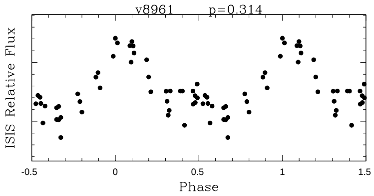
v8961 p=0.314
ISIS Relative Flux
-0.5
0
0.5
1
1.5
Phase

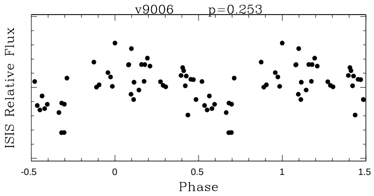
v9006 p=0.253
ISIS Relative Flux
-0.5
0
0.5
1
1.5
Phase

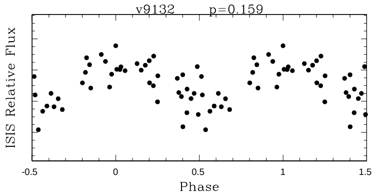
v9132 p=0.159
ISIS Relative Flux
-0.5
0
0.5
1
1.5
Phase

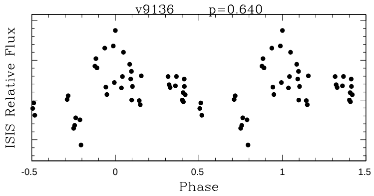
v9136 p=0.640
ISIS Relative Flux
-0.5
0
0.5
1
1.5
Phase

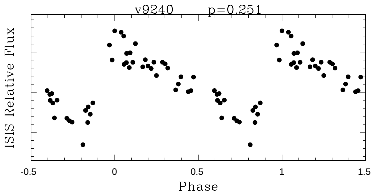
v9240 p=0.251
ISIS Relative Flux
-0.5
0
0.5
1
1.5
Phase

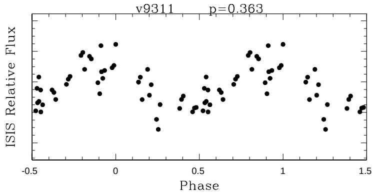
v9311 p=0.363
ISIS Relative Flux
-0.5
0
0.5
1
1.5
Phase

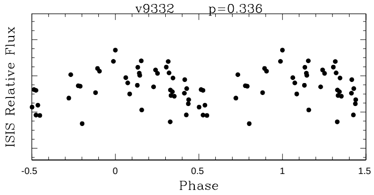
v9332 p=0.336
ISIS Relative Flux
-0.5
0
0.5
1
1.5
Phase

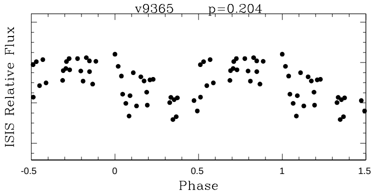
v9365 p=0.204
ISIS Relative Flux
-0.5
0
0.5
1
1.5
Phase

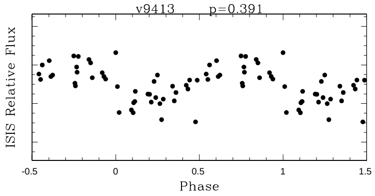
v9413 p=0.391
ISIS Relative Flux
-0.5
0
0.5
1
1.5
Phase

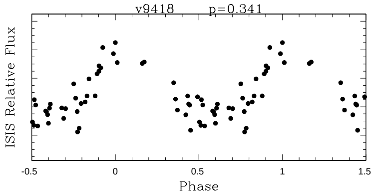
v9418 p=0.341
ISIS Relative Flux
-0.5
0
0.5
1
1.5
Phase

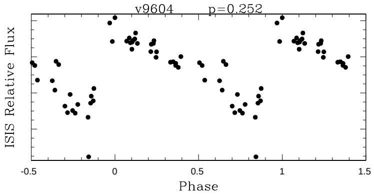
v9604 p=0.252
ISIS Relative Flux
-0.5
0
0.5
1
1.5
Phase

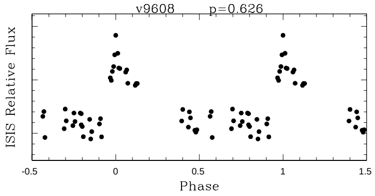
v9608 p=0.626
ISIS Relative Flux
-0.5
0
0.5
1
1.5
Phase

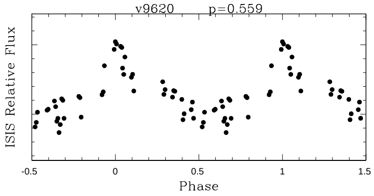
v9620 p=0.559
ISIS Relative Flux
-0.5
0
0.5
1
1.5
Phase

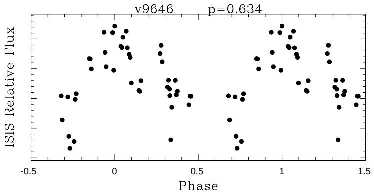
v9646 p=0.634
ISIS Relative Flux
-0.5
0
0.5
1
1.5
Phase

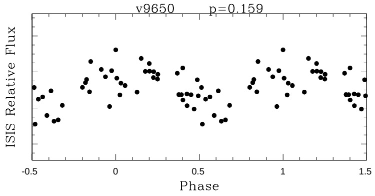
v9650 p=0.159
ISIS Relative Flux
-0.5
0
0.5
1
1.5
Phase

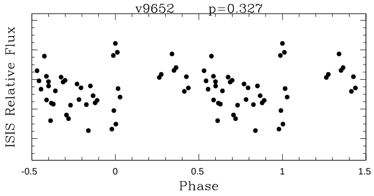
v9652 p=0.327
ISIS Relative Flux
-0.5
0
0.5
1
1.5
Phase

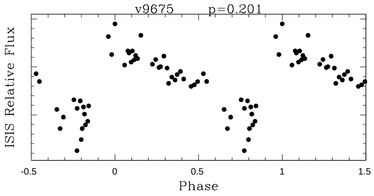
v9675 p=0.201
ISIS Relative Flux
-0.5
0
0.5
1
1.5
Phase

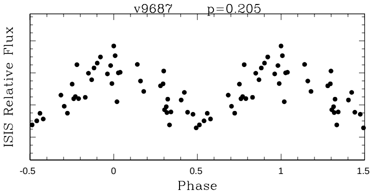
v9687 p=0.205
ISIS Relative Flux
Phase
-0.5 0 0.5 1 1.5

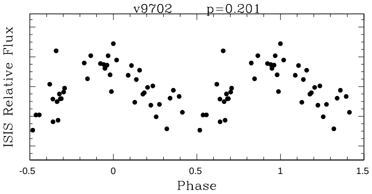
v9702 p=0.201
ISIS Relative Flux
Phase
-0.5 0 0.5 1 1.5

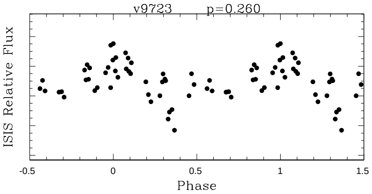
v9723 p=0.260
ISIS Relative Flux
Phase
-0.5 0 0.5 1 1.5

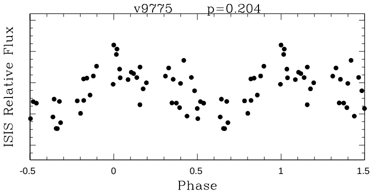
v9775 p=0.204
ISIS Relative Flux
Phase
-0.5 0 0.5 1 1.5

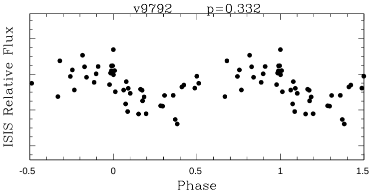
v9792 p=0.332
ISIS Relative Flux
Phase
-0.5 0 0.5 1 1.5

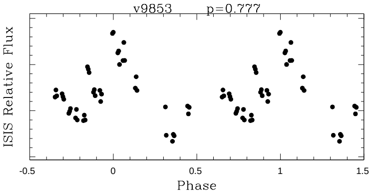
v9853 p=0.777
ISIS Relative Flux
Phase
-0.5 0 0.5 1 1.5

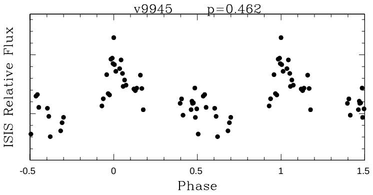
v9945 p=0.462
ISIS Relative Flux
Phase
-0.5 0 0.5 1 1.5

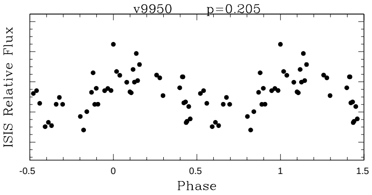
v9950 p=0.205
ISIS Relative Flux
Phase
-0.5 0 0.5 1 1.5

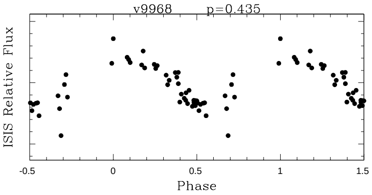
v9968 p=0.435
ISIS Relative Flux
Phase
-0.5 0 0.5 1 1.5

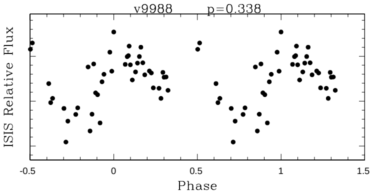
v9988 p=0.338
ISIS Relative Flux
Phase
-0.5 0 0.5 1 1.5

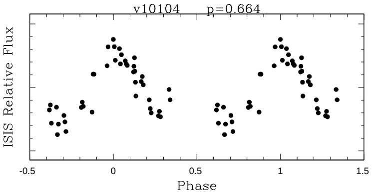
v10104 p=0.664
ISIS Relative Flux
Phase
-0.5 0 0.5 1 1.5

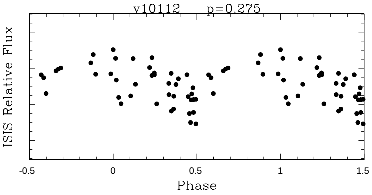
v10112 p=0.275
ISIS Relative Flux
Phase
-0.5 0 0.5 1 1.5

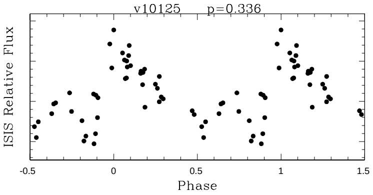
v10125 p=0.336
ISIS Relative Flux
Phase
-0.5 0 0.5 1 1.5

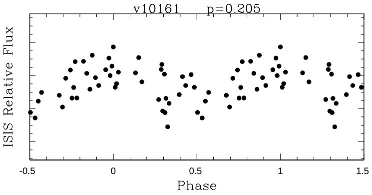
v10161 p=0.205
ISIS Relative Flux
Phase
-0.5 0 0.5 1 1.5

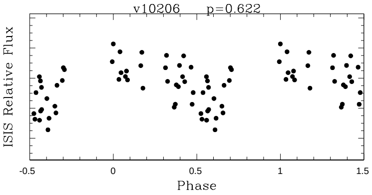
v10206 p=0.622
ISIS Relative Flux
Phase
-0.5 0 0.5 1 1.5

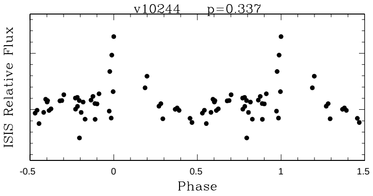
v10244 p=0.337
ISIS Relative Flux
Phase
-0.5 0 0.5 1 1.5

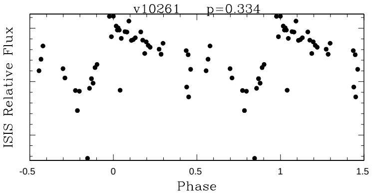
v10261 p=0.334
ISIS Relative Flux
Phase
-0.5 0 0.5 1 1.5

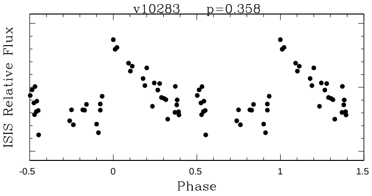
v10283 p=0.358
ISIS Relative Flux
Phase
-0.5 0 0.5 1 1.5

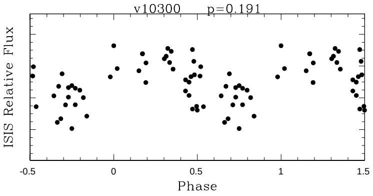
v10300 p=0.191
ISIS Relative Flux
Phase
-0.5 0 0.5 1 1.5

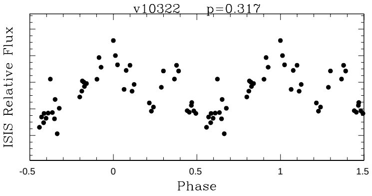
v10322 p=0.317
ISIS Relative Flux
Phase
-0.5 0 0.5 1 1.5

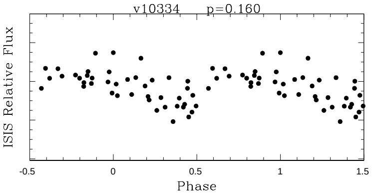
v10334 p=0.160
ISIS Relative Flux
Phase
-0.5 0 0.5 1 1.5

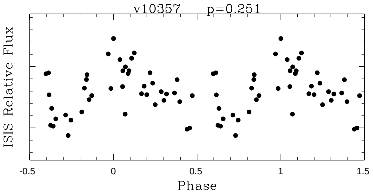
v10357 p=0.251
ISIS Relative Flux
Phase
-0.5 0 0.5 1 1.5

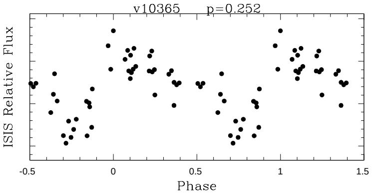
v10365 p=0.252
ISIS Relative Flux
Phase
-0.5 0 0.5 1 1.5

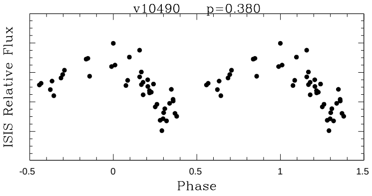
v10490 p=0.380
ISIS Relative Flux
Phase
-0.5 0 0.5 1 1.5

v10494 p=0.636

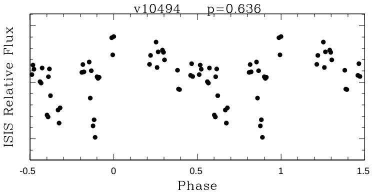

v10506 p=0.449

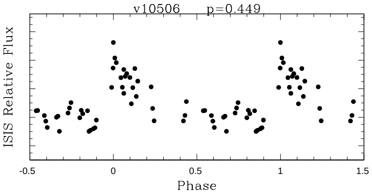

v10515 p=0.530

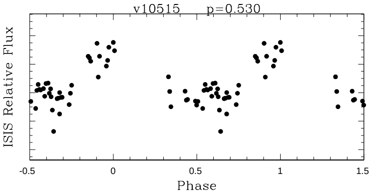

v10525 p=0.204

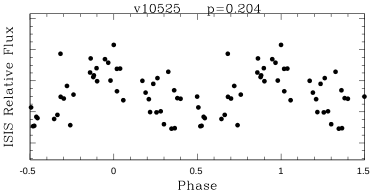

v10536 p=1.759

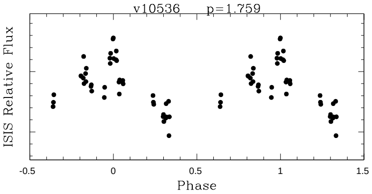

v10577 p=0.637

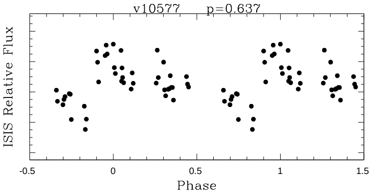

v10626 p=0.329

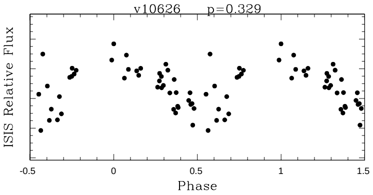

v10648 p=0.249

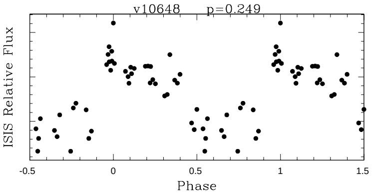

v10653 p=0.333

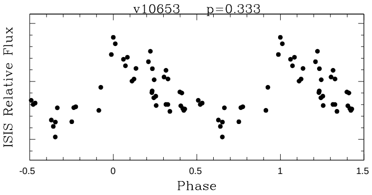

v10666 p=0.120

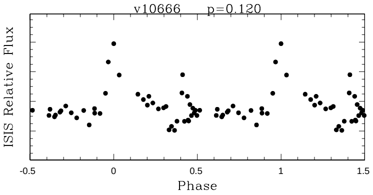

v10680 p=0.218

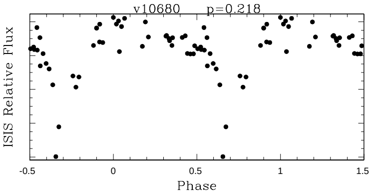

v10688 p=0.376

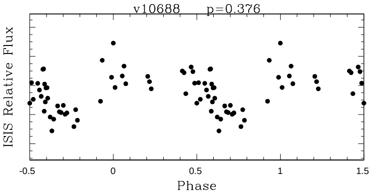

v10756 p=0.254

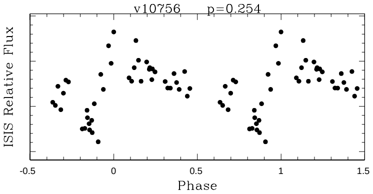

v10780 p=0.339

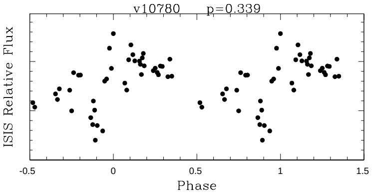

v10791 p=0.673

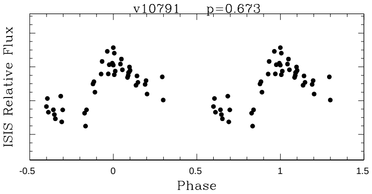

v10800 p=0.204

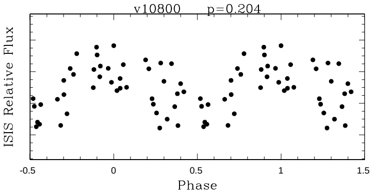

v10992 p=0.335

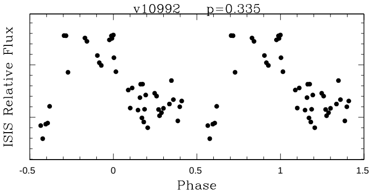

v10995 p=0.316

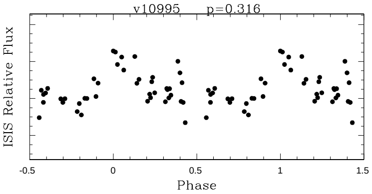

v11082 p=4.306

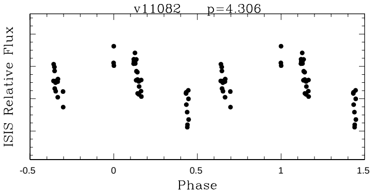

v11106 p=0.862

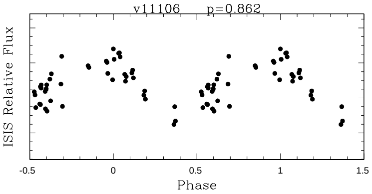

v11211 p=0.691

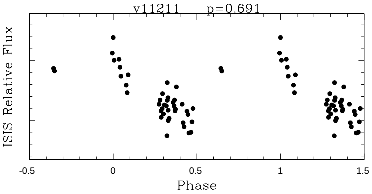

v11282 p=0.149

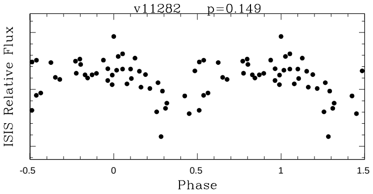

v11291 p=0.379

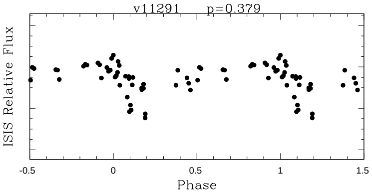

v11329 p=0.519

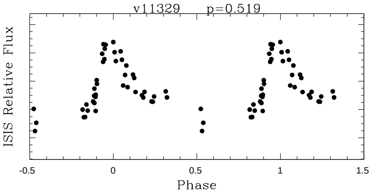

v11383 p=0.513

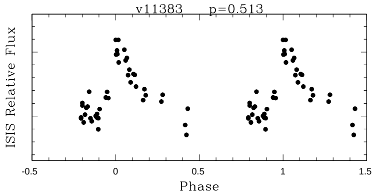

v11492 p=0.664

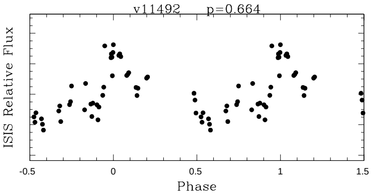

v11497 p=0.533

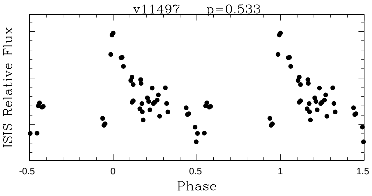

v11588 p=0.380

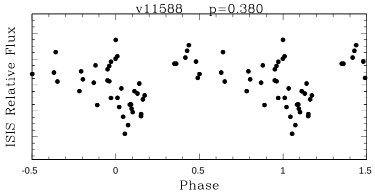

v11681 p=2.846

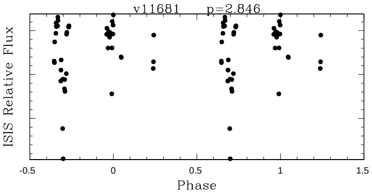

v11763 p=0.457

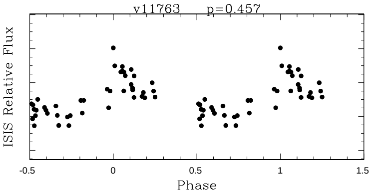

v11812 p=0.268

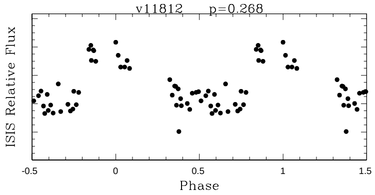

v11858 p=0.347

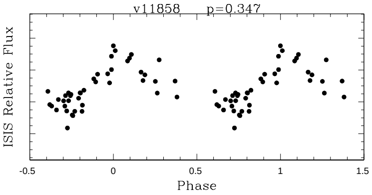

v11892 p=0.649

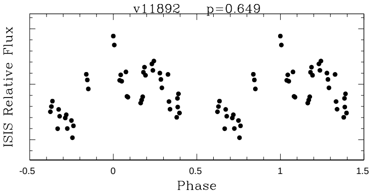

v11935 p=0.252

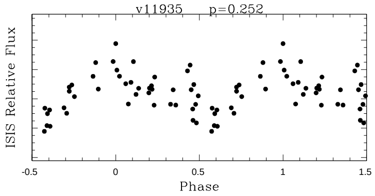

v11955 p=0.472

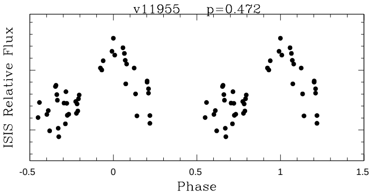

v12000 p=0.815

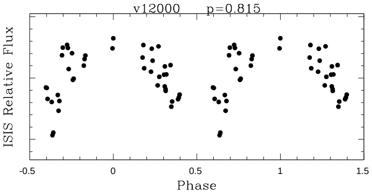

v12124 p=0.115

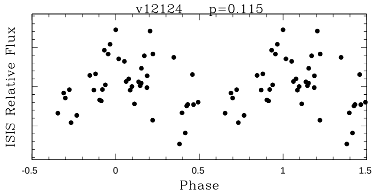

v12158 p=0.493

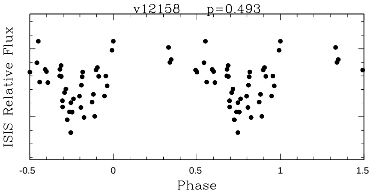

v12214 p=0.331

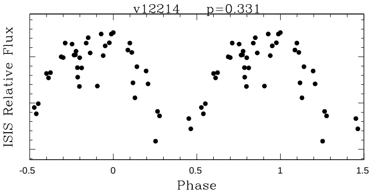

v12291 p=0.394

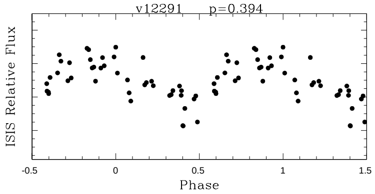

v12408 p=0.533

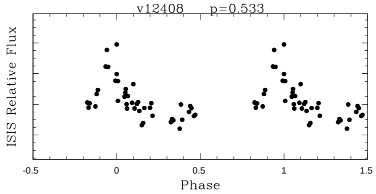

Chapter 15

Appendix I

ATLAS OF LIGHT CURVES: H1 Chip 2

Atlas of light curves in B-band differential flux, for the candidate variable stars in CCD2 of field H1. For each candidate variable identification and period are provided on top of the plot.

v728 p=0.315

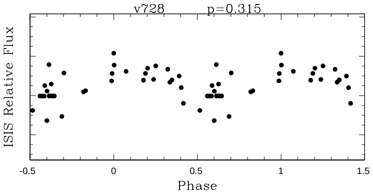

v730 p=0.844

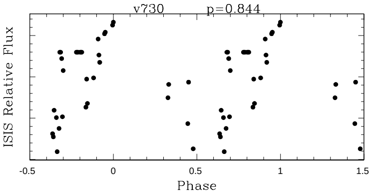

v1128 p=0.320

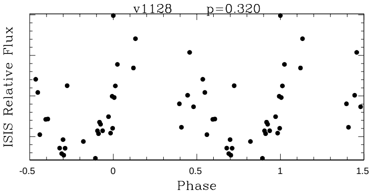

v1184 p=0.690

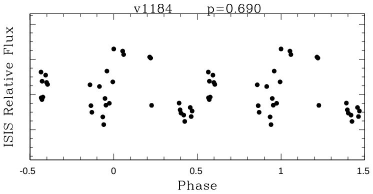

v1212 p=0.241

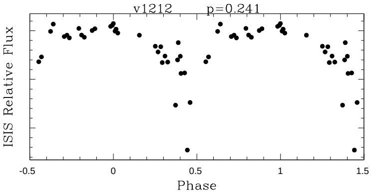

v1224 p=0.462

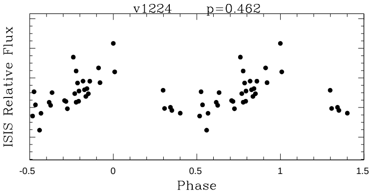

v1225 p=0.253

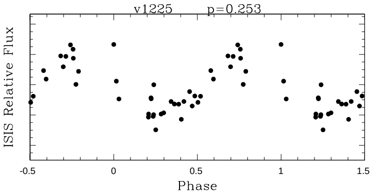

v1349 p=0.241

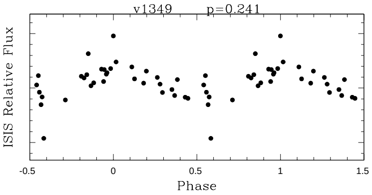

v1565 p=0.437

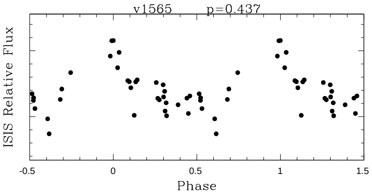

v1570 p=0.248

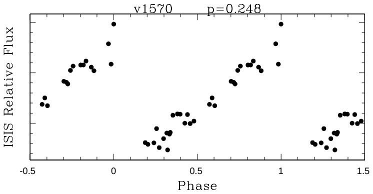

v1578 p=0.322

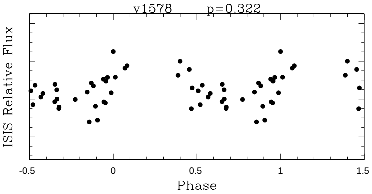

v1856 p=0.437

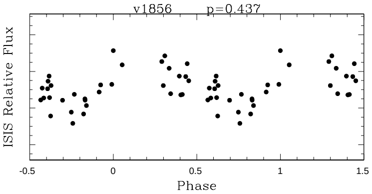

v1881 p=1.355

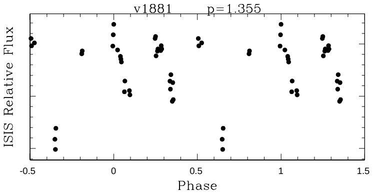

v1882 p=0.253

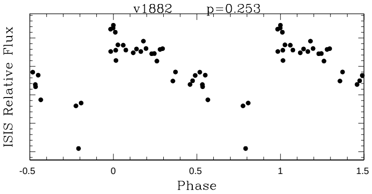

v2647 p=0.244

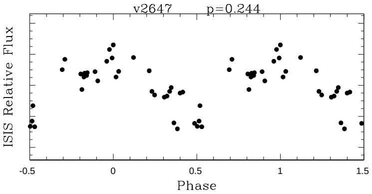

v3046 p=0.316

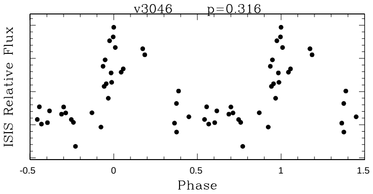

v3798 p=0.337

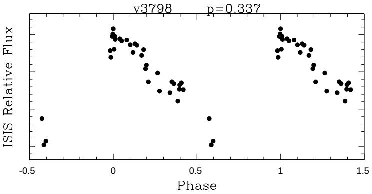

v3821 p=0.553

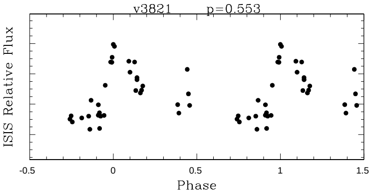

v3938 p=0.607

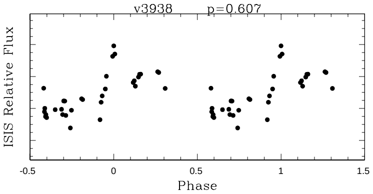

v4054 p=0.248

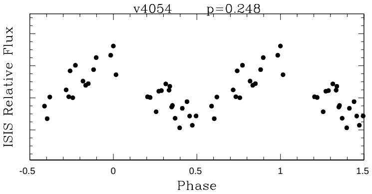

v4115 p=0.448

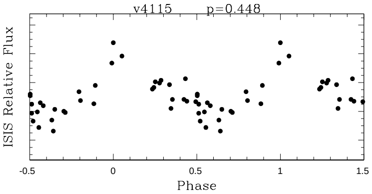

v4149 p=0.256

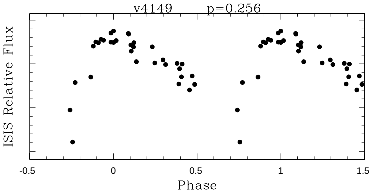

v4520 p=0.320

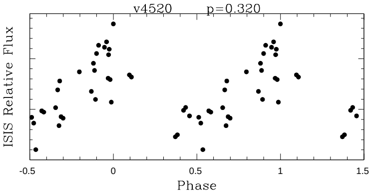

v4547 p=0.244

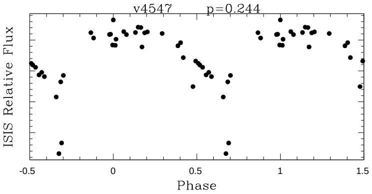

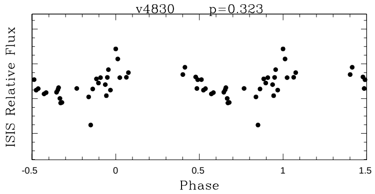
v4830 p=0.323

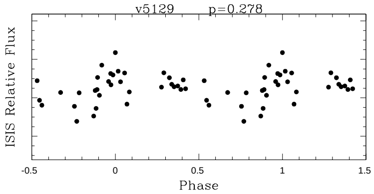
v5129 p=0.278

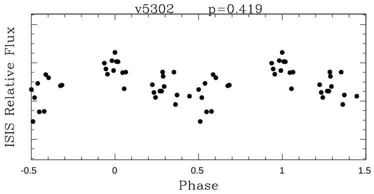
v5302 p=0.419

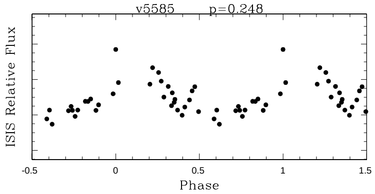
v5585 p=0.248

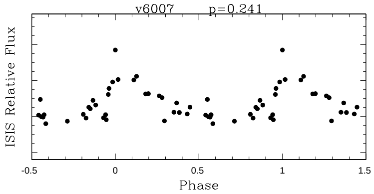
v6007 p=0.241

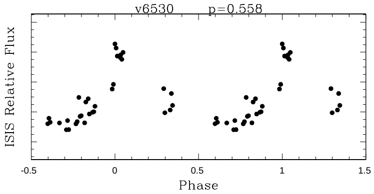
v6530 p=0.558

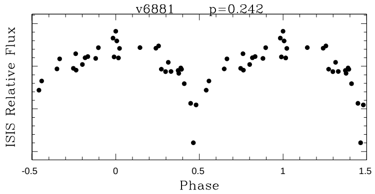
v6881 p=0.242

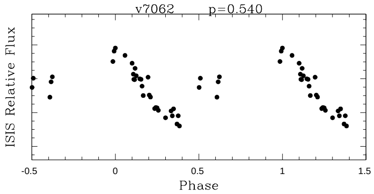
v7062 p=0.540

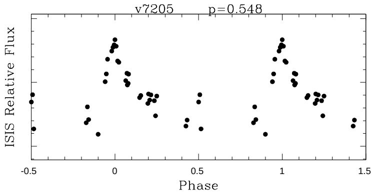
v7205 p=0.548

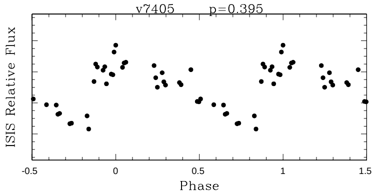
v7405 p=0.395

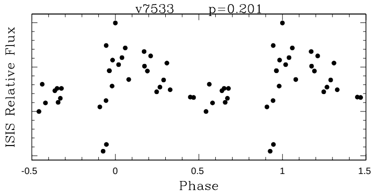
v7533 p=0.201

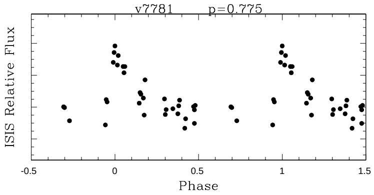
v7781 p=0.775

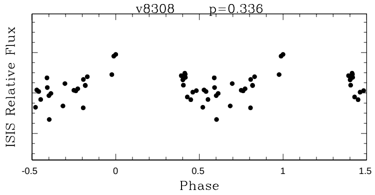
v8308 p=0.336

Bibliography

Alard, C. 2000, A&AS, 144, 363

Alcock, C., et al. 1996, AJ, 111, 1146

Alcock, C., et al. 1998, AJ, 115, 1921

Alcock, C., et al. 2000, AJ, 119, 2194

Alonso-García, J., Mateo, M., & Worthey, G. 2004, AJ, 127, 868

Alves-Brito, A., Forbes, D. A., Mendel, J. T., Hau, G. K. T., & Murphy, M. T. 2009, MNRAS, 395, L34

Aoki, W., et al. 2009, A&A, 502, 569

Barmby, P., & Huchra, J. P. 2001, AJ, 122, 2458

Barmby, P., Huchra, J. P., & Brodie, J. P. 2001, AJ, 121, 1482

Barmby, P., et al. 2006, ApjL, 650, L45

Barmby, P., McLaughlin, D. E., Harris, W. E., Harris, G. L. H., & Forbes, D. A. 2007, AJ, 133, 2764

Barning, F. J. M. 1963, BAN, 17, 22

Beasley, M. A., Brodie, J. P., Strader, J., Forbes, D. A., Proctor, R. N., Barmby, P., & Huchra, J. P. 2005, AJ, 129, 1412

Beaton, R. L., et al. 2007, ApjL, 658, L91

Beccari, G., et al. 2007, A&A, 476, 193

Bellazzini, M., Ferraro, F. R., & Ibata, R. 2003a, AJ, 125, 188

Bellazzini, M., Cacciari, C., Federici, L., Fusi Pecci, F., & Rich, M. 2003, A&A, 405, 867

Beers, T. C., & Christlieb, N. 2005, ARA&A, 43, 531

Belokurov, V., et al. 2006, ApjL, 647, L111

Belokurov, V., et al. 2006, ApjL, 647, L111

Belokurov, V., et al. 2007, ApJ, 654, 897

Belokurov, V., et al. 2008, ApjL, 686, L83

Belokurov, V., et al. 2009, MNRAS, 397, 1748

Belokurov, V., et al. 2010, ApjL, 712, L103

Bertin, E., & Arnouts, S. 1996, A&AS, 117, 393

Block, D. L., et al. 2006, Nature, 443, 832

Bono, G., Caputo, F., Castellani, V., & Marconi, M. 1995, ApjL, 448, L115

Bono, G., Caputo, F., Santolamazza, P., Cassisi, S., & Piersimoni, A. 1997, AJ, 113, 2209

Bono, G., Caputo, F., Castellani, V., & Marconi, M. 1997, A&AS, 121, 327

Bono, G., Marconi, M., & Stellingwerf, R. F. 1999, ApJS, 122, 167

Bono, G., Groenewegen, M. A. T., Marconi, M., & Caputo, F. 2002, ApjL, 574, L33

Brown, T. M., Ferguson, H. C., Smith, E., Kimble, R. A., Sweigart, A. V., Renzini, A., Rich, R. M., & VandenBerg, D. A. 2003, ApjL, 592, L17

Bono, G., Caputo, F., Castellani, V., Marconi, M., Storm, J., & Degl'Innocenti, S. 2003, MNRAS, 344, 1097

Brown, T. M., Ferguson, H. C., Smith, E., Kimble, R. A., Sweigart, A. V., Renzini, A., & Rich, R. M. 2004, AJ, 127, 2738

Brown, T. M., Smith, E., Ferguson, H. C., Rich, R. M., Guhathakurta, P., Renzini, A., Sweigart, A. V., & Kimble, R. A. 2006, ApJ, 652, 323

Brown, T. M., et al. 2008, ApjL, 685, L121

Buonanno, R., Buscema, G., Fusi Pecci, F., Richer, H. B., & Fahlman, G. G. 1990, AJ, 100, 1811

Cacciari, C., Corwin, T. M., & Carney, B. W. 2005, AJ, 129, 267

Caputo, F., Tornambe, A., & Castellani, V. 1978, A&A, 67, 107

Caputo, F. 1998, AAPR, 9, 33

Caputo, F., Marconi, M., & Musella, I. 2000, A&A, 354, 610

Caputo, F., Castellani, V., Marconi, M., & Ripepi, V. 2000, MNRAS, 316, 819

Caputo, F., Castellani, V., Degl'Innocenti, S., Fiorentino, G., & Marconi, M. 2004, A&A, 424, 927

Carollo, D., et al. 2007, Nature, 450, 1020

Castellani, V., Cignoni, M., Degl'Innocenti, S., Petroni, S., & Prada Moroni, P. G. 2002, MNRAS, 334, 69

Catelan, M. 2009, Ap&SS, 320, 261

Christlieb, N., Reimers, D., & Wisotzki, L. 2004, The Messenger, 117, 40

Cignoni, M., Tosi, M., Bragaglia, A., Kalirai, J. S., & Davis, D. S. 2008, MNRAS, 386, 2235

Clement, C. M., & Shelton, I. 1999, ApjL, 515, L85

Clement, C. M., & Rowe, J. 2000, AJ, 120, 2579

Clementini, G., et al. 2000, AJ, 120, 2054

Clementini, G., Federici, L., Corsi, C., Cacciari, C., Bellazzini, M., & Smith, H. A. 2001, ApjL, 559, L109

Clementini, G., Gratton, R., Bragaglia, A., Carretta, E., Di Fabrizio, L., & Maio, M. 2003, AJ, 125, 1309

Clementini, G., et al. 2004, IAU Colloq. 193: Variable Stars in the Local Group, 310, 60

Clementini, G., et al. 2009, ApjL, 704, L103

Clementini, G. 2010, Variable Stars, the Galactic halo and Galaxy Formation, Proceedings of an international conference held in Zvenigorod, Russia, 12-16 October 2009. Published by Sternberg Astronomical Institute of Moscow University, Russia., 107

Contreras, R., Catelan, M., Smith, H. A., Pritzl, B. J., & Borissova, J. 2005, ApjL, 623, L117

Corbin, M. R., O'Neil, E., & Rieke, M. J. 2001, AJ, 121, 2549

Corwin, T. M., Catelan, M., Smith, H. A., Borissova, J., Ferraro, F. R., & Raburn, W. S. 2003, AJ, 125, 2543

Christy, R. F. 1966, ApJ, 144, 108

Dall'Ora, M., et al. 2006, ApjL, 653, L109

De Angeli, F., Piotto, G., Cassisi, S., Busso, G., Recio-Blanco, A., Salaris, M., Aparicio, A., & Rosenberg, A. 2005, AJ, 130, 116

Demarque, P., & Hirshfeld, A. W. 1975, ApJ, 202, 346

Demers, S., & Harris, W. E. 1974, AJ, 79, 627

de Vaucouleurs, G. 1958, ApJ, 128, 465

Di Criscienzo, M., Caputo, F., Marconi, M., & Cassisi, S. 2007, A&A, 471, 893

Dolphin, A. E. 2000, PASP, 112, 1383

Dolphin, A.E., Saha, A., Claver, J., Skillman, E.D., Cole, A.A., Gallagher, J.S., Tolstoy, E., Dohm-Palmer, R.C., & Mateo, M. 2002, AJ, 123, 3154

Dolphin, A. E., Saha, A., Olszewski, E. W., Thim, F., Skillman, E. D., Gallagher, J. S., & Hoessel, J. 2004, AJ, 127, 875

Durrell, P. R., Harris, W. E., & Pritchet, C. J. 2001, AJ, 121, 2557

Durrell, P. R., Harris, W. E., & Pritchet, C. J. 2004, AJ, 128, 260

Eggen, O. J., Lynden-Bell, D., & Sandage, A. R. 1962, ApJ, 136, 748

Elmegreen, B. G., & Efremov, Y. N. 1996, ApJ, 466, 802

Evans, N. W., Wilkinson, M. I., Guhathakurta, P., Grebel, E. K., & Vogt, S. S. 2000, ApjL, 540, L9

Federici, L., Bellazzini, M., Galleti, S., Fusi Pecci, F., Buzzoni, A., & Parmeggiani, G. 2007, A&A, 473, 429

Ferguson, A. M. N., & Johnson, R. A. 2001, ApjL, 559, L13

Ferguson, A. M. N., Irwin, M. J., Ibata, R. A., Lewis, G. F., & Tanvir, N. R. 2002, AJ, 124, 1452

Ferraro, F. R., Messineo, M., Fusi Pecci, F., de Palo, M. A., Straniero, O., Chieffi, A., & Limongi, M. 1999, AJ, 118, 1738

Ferraro, F. R., et al. 2009, Nature, 462, 483

Fiorentino, G., et al. 2010, ApJ, 708, 817

Font, A. S., Johnston, K. V., Guhathakurta, P., Majewski, S. R., & Rich, R. M. 2006, AJ, 131, 1436

Forbes, D. A., Brodie, J. P., & Larsen, S. S. 2001, ApjL, 556, L83

Frebel, A., Simon, J. D., Geha, M., & Willman, B. 2010, ApJ, 708, 560

Freedman, W. L. 1988, ApJ, 326, 691

Freedman, W. L., et al. 2001, ApJ, 553, 47

Freeman, K., & Bland-Hawthorn, J. 2002, ARA&A, 40, 487

Fusi Pecci, F., Bellazzini, M., Cacciari, C., & Ferraro, F. R. 1995, AJ, 110, 1664

Fusi Pecci, F., Bellazzini, M., Buzzoni, A., De Simone, E., Federici, L., & Galleti, S. 2005, AJ, 130, 554

Galleti, S., Bellazzini, M., Federici, L., & Fusi Pecci, F. 2005, A&A, 436, 535

Galleti, S., Federici, L., Bellazzini, M., Buzzoni, A., & Pecci, F. F. 2006, ApjL, 650, L107

Giallongo, E., et al. 2008, A&A, 482, 349

Gingold, R. A. 1976, ApJ, 204, 116

Gingold, R. A. 1985, Memorie della Societa Astronomica Italiana, 56, 169

Gilmore, G., & Wyse, R. F. G. 1998, AJ, 116, 748

Girardi, L., Bressan, A., Bertelli, G., & Chiosi, C. 2000, A&AS, 141, 371

Greco, C., et al. 2007, IAU Symposium, 241, 343

Greco, C., et al. 2008, ApjL, 675, L73

Grillmair, C. J., Freeman, K. C., Irwin, M., & Quinn, P. J. 1995, AJ, 109, 2553

Grillmair, C. J. 2006, ApjL, 645, L37

Grillmair, C. J. 2009, ApJ, 693, 1118

Guhathakurta, P., et al. 2006, AJ, 131, 2497

Habing, H. J., et al. 1984, ApjL, 278, L59

Helmi, A., White, S. D. M., de Zeeuw, P. T., & Zhao, H. 1999, Nature, 402, 53

Helmi, A., et al. 2006, ApjL, 651, L121

Holtzman, J. A., Burrows, C. J., Casertano, S., Hester, J. J., Trauger, J. T., Watson, A. M., & Worthey, G. 1995, PASP, 107, 1065

Hubble, E. 1932, ApJ, 76, 44

Huxor, A., Tanvir, N. R., Irwin, M., Ferguson, A., Ibata, R., Lewis, G., & Bridges, T. 2004, Satellites and Tidal Streams, 327, 118

Huxor, A. P., Tanvir, N. R., Irwin, M. J., Ibata, R., Collett, J. L., Ferguson, A. M. N., Bridges, T., & Lewis, G. F. 2005, MNRAS, 360, 1007

Huxor, A. P., Tanvir, N. R., Ferguson, A. M. N., Irwin, M. J., Ibata, R., Bridges, T., & Lewis, G. F. 2008, MNRAS, 385, 1989

Ibata, R. A., Gilmore, G., & Irwin, M. J. 1994, Nature, 370, 194

Ibata, R. A., Gilmore, G., & Irwin, M. J. 1995, MNRAS, 277, 781

Ibata, R., Irwin, M., Lewis, G., Ferguson, A. M. N., & Tanvir, N. 2001, Nature, 412, 49

Ibata, R., Chapman, S., Ferguson, A. M. N., Irwin, M., Lewis, G., & McConnachie, A. 2004, MNRAS, 351, 117

Ibata, R., Chapman, S., Ferguson, A. M. N., Lewis, G., Irwin, M., & Tanvir, N. 2005, ApJ, 634, 287

Ibata, R., Martin, N. F., Irwin, M., Chapman, S., Ferguson, A. M. N., Lewis, G. F., & McConnachie, A. W. 2007, ApJ, 671, 1591

Irwin, M., & Hatzidimitriou, D. 1995, MNRAS, 277, 1354

Irwin, M. J., et al. 2007, ApjL, 656, L13

Joshi, Y. C., Narasimha, D., Pandey, A. K., & Sagar, R. 2009, arXiv:0912.5415

Kalirai, J. S., et al. 2006, ApJ, 648, 389

Kirby, E. N., Simon, J. D., Geha, M., Guhathakurta, P., & Frebel, A. 2008, ApjL, 685, L43

Kleyna, J. T., Wilkinson, M. I., Evans, N. W., & Gilmore, G. 2005, ApjL, 630, L141

Klypin, A., Kravtsov, A. V., Valenzuela, O., & Prada, F. 1999, ApJ, 522, 82

Klypin, A., Zhao, H., & Somerville, R. S. 2002, ApJ, 573, 597

Kraft, R. P., & Schmidt, M. 1963, ApJ, 137, 249

Krauss, L. M., & Chaboyer, B. 2003, Science, 299, 65

Kuehn, C., et al. 2008, ApjL, 674, L81

Lafler, J., & Kinman, T. D. 1965, ApJS, 11, 216

Lauer, T. R., et al. 1993, AJ, 106, 1436

Lauer, T. R., et al. 1996, ApjL, 471, L79

Lee, J.-W., & Carney, B. W. 1999, AJ, 118, 1373

Lee, Y.-W., Demarque, P., & Zinn, R. 1990, ApJ, 350, 155

Leon, S., Meylan, G., & Combes, F. 2000, A&A, 359, 907

Lomb, N. R. 1976, Ap&SS, 39, 447

Mackey, A. D., et al. 2006, ApjL, 653, L105

Mackey, A. D., et al. 2007, ApjL, 655, L85

Majewski, S. R., Ostheimer, J. C., Patterson, R. J., Kunkel, W. E., Johnston, K. V., & Geisler, D. 2000, AJ, 119, 760

Majewski, S. R., et al. 2002, Modes of Star Formation and the Origin of Field Populations, 285, 199

Majewski, S. R., Skrutskie, M. F., Weinberg, M. D., & Ostheimer, J. C. 2003, ApJ, 599, 1082

Mancone, C., & Sarajedini, A. 2008, AJ, 136, 1913

Marconi, M., Fiorentino, G., & Caputo, F. 2004, A&A, 417, 1101

Martin, N. F., Ibata, R. A., Bellazzini, M., Irwin, M. J., Lewis, G. F., & Dehnen, W. 2004, MNRAS, 348, 12

Martin, N. F., et al. 2009, ApJ, 705, 758

Massey, P., Olsen, K. A. G., Hodge, P. W., Strong, S. B., Jacoby, G. H., Schlingman, W., & Smith, R. C. 2006, AJ, 131, 2478

Mateo, M. 1996, Formation of the Galactic Halo...Inside and Out, 92, 434

Mateo, M. L. 1998, ARA&A, 36, 435

Mateo, M. 2000, IAU Colloq. 176: The Impact of Large-Scale Surveys on Pulsating Star Research, 203, 187

Mateu, C., Vivas, A. K., Zinn, R., Miller, L. R., & Abad, C. 2009, AJ, 137, 4412

Mathewson, D. S., Cleary, M. N., & Murray, J. D. 1974, ApJ, 190, 291

McConnachie, A. W., Irwin, M. J., Ibata, R. A., Ferguson, A. M. N., Lewis, G. F., & Tanvir, N. 2003, MNRAS, 343, 1335

McConnachie, A. W., Irwin, M. J., Lewis, G. F., Ibata, R. A., Chapman, S. C., Ferguson, A. M. N., & Tanvir, N. R. 2004, MNRAS, 351, L94

McConnachie, A. W., Irwin, M. J., Ferguson, A. M. N., Ibata, R. A., Lewis, G. F., & Tanvir, N. 2005, MNRAS, 356, 979

McConnachie, A. W., et al. 2009, Nature, 461, 66

Meylan, G., Sarajedini, A., Jablonka, P., Djorgovski, S. G., Bridges, T., & Rich, R. M. 2001, AJ, 122, 830

Moretti, M. I., et al. 2009, ApjL, 699, L125

Morrison, H. L., Harding, P., Perrett, K., & Hurley-Keller, D. 2004, ApJ, 603, 87

Mould, J., & Kristian, J. 1986, ApJ, 305, 591

Musella, I., et al. 2009, ApjL, 695, L83

Norris, J., & Zinn, R. 1975, ApJ, 202, 335

Odenkirchen, M., et al. 2001, ApjL, 548, L165

Odenkirchen, M., et al. 2003, AJ, 126, 2385

Oosterhoff, P. T. 1939, The Observatory, 62, 104

Oosterhoff, P. T. 1944, BAN, 10, 55

Ostheimer, J. C., Jr. 2003, Ph.D. Thesis,

Peñarrubia, J., Navarro, J. F., & McConnachie, A. W. 2008, ApJ, 673, 226

Perina, S., Federici, L., Bellazzini, M., Cacciari, C., Fusi Pecci, F., & Galleti, S. 2009, A&A, 507, 1375

Piotto, G., et al. 2002, A&A, 391, 945

Pritchet, C. J., & van den Bergh, S. 1987, ApJ, 316, 517

Pritchet, C. J. 1988, The Extragalactic Distance Scale, 4, 59

Pritchet, C. J., & van den Bergh, S. 1994, AJ, 107, 1730

Pritzl, B., Smith, H. A., Catelan, M., & Sweigart, A. V. 2000, ApjL, 530, L41

Pritzl, B. J., Smith, H. A., Catelan, M., & Sweigart, A. V. 2002, AJ, 124, 949

Pritzl, B. J., Smith, H. A., Stetson, P. B., Catelan, M., Sweigart, A. V., Layden, A. C., & Rich, R. M. 2003, AJ, 126, 1381

Pritzl, B. J., Armandroff, T. E., Jacoby, G. H., & Da Costa, G. S. 2004, AJ, 127, 318

Pritzl, B. J., Armandroff, T. E., Jacoby, G. H., & Da Costa, G. S. 2005, AJ, 129, 2232

Reitzel, D. B., Guhathakurta, P., & Gould, A. 1998, AJ, 116, 707

Renzini, A., Mengel, J. G., & Sweigart, A. V. 1977, A&A, 56, 369

Rich, R. M., Corsi, C. E., Cacciari, C., Federici, L., Fusi Pecci, F., Djorgovski, S. G., & Freedman, W. L. 2005, AJ, 129, 2670

Richardson, J. C., et al. 2008, AJ, 135, 1998

Saha, A., & Hoessel, J. G. 1990, AJ, 99, 97

Saha, A., Hoessel, J. G., & Krist, J. 1992, AJ, 103, 84

Saha, A. 1999, Ap&SS, 267, 193

Saha, A., Sandage, A., Tammann, G. A., Dolphin, A. E., Christensen, J., Panagia, N., & Macchetto, F. D. 2001, ApJ, 562, 314

Sandage, A., Katem, B., & Sandage, M. 1981, ApJS, 46, 41

Sandage, A. 1993, AJ, 106, 687

Sarajedini, A., & Van Duyne, J. 2001, AJ, 122, 2444

Sarajedini, A., Barker, M. K., Geisler, D., Harding, P., & Schommer, R. 2006, AJ, 132, 1361

Sarajedini, A., Mancone, C. L., Lauer, T. R., Dressler, A., Freedman, W., Trager, S. C., Grillmair, C., & Mighell, K. J. 2009, AJ, 138, 184

Sarajedini, A., & Yang, S.-C. 2010, Variable Stars, the Galactic halo and Galaxy Formation, Proceedings of an international conference held in Zvenigorod, Russia, 12-16 October 2009. Published by Sternberg Astronomical Institute of Moscow University, Russia., 101

Sawyer, H. B. 1944, Publications of the David Dunlap Observatory, 1, 294

Schechter, P. L., Mateo, M., & Saha, A. 1993, PASP, 105, 1342

Schlegel, D. J., Finkbeiner, D. P., & Davis, M. 1998, ApJ, 500, 525

Schwarzschild, M., Haumlrm, R. 1970, ApJ, 160, 341

Searle, L., & Zinn, R. 1978, ApJ, 225, 357

Siegel, M. H. 2006, ApjL, 649, L83

Simon, J. D., & Geha, M. 2007, ApJ, 670, 313

Sirianni, M., et al. 2005, PASP, 117, 1049

Smith, H. A., & Wehlau, A. 1985, ApJ, 298, 572

Sollima, A., Cacciari, C., & Valenti, E. 2006, MNRAS, 372, 1675

Soszynski, I., et al. 2003, Acta Astronomica, 53, 93

Soszynski, I., et al. 2008, Acta Astronomica, 58, 293

Stellingwerf, R. F. 1978, ApJ, 224, 953

Stetson, P. B. 1987, PASP, 99, 191

Stetson, P. B. 1994, PASP, 106, 250

Stetson, P. B. 1996, PASP, 108, 851

Stobie, R. S. 1971, ApJ, 168, 381

Tolstoy, E., Hill, V., & Tosi, M. 2009, ARA&A, 47, 371

Tremaine, S. 1995, AJ, 110, 628

Unavane, M., Wyse, R. F. G., & Gilmore, G. 1996, MNRAS, 278, 727 van Albada, T. S., & Baker, N. 1971, ApJ, 169, 311

van Albada, T. S., & Baker, N. 1973, ApJ, 185, 477

van den Bergh, S. 1992, A&A, 264, 75

van den Bergh, S. 1993, MNRAS, 262, 588

van den Bergh, S. 1994, AJ, 108, 2145

van den Bergh, S. 2000, PASP, 112, 529

van den Bergh, S. 2000, The galaxies of the Local Group, by Sidney Van den Bergh. Published by Cambridge, UK: Cambridge University Press, 2000 Cambridge Astrophysics Series Series, vol no: 35, ISBN: 0521651816.

van den Bergh, S. 2006, The Local Group as an Astrophysical Laboratory, 1

Vilardell, F., Jordi, C., & Ribas, I. 2007, A&A, 473, 847

Vilardell, F., Ribas, I., & Jordi, C. 2006, A&A, 459, 321

Villanova, S., et al. 2007, ApJ, 663, 296

Wallerstein, G. 1970, ApJ, 160, 345

Wallerstein, G. 2002, PASP, 114, 689

Wallerstein, G., & Cox, A. N. 1984, PASP, 96, 677

Walsh, S. M., Jerjen, H., & Willman, B. 2007, ApjL, 662, L83

Watkins, L. L., et al. 2009, MNRAS, 398, 1757

Watkins, L. L., Evans, N. W., & An, J. 2010, arXiv:1002.4565

Willman, B., et al. 2005a, AJ, 129, 2692

Willman, B., et al. 2005b, ApjL, 626, L85

Worthey, G., España, A., MacArthur, L. A., & Courteau, S. 2005, ApJ, 631, 820

Yang, S.-C., & Sarajedini, A. 2010, ApJ, 708, 293

Yanny, B., et al. 2003, ApJ, 588, 824

Yoon, S.-J., & Lee, Y.-W. 2002, Science, 297, 578

York, D. G., et al. 2000, AJ, 120, 1579

Zaritsky, D., Kennicutt, R. C., Jr., & Huchra, J. P. 1994, ApJ, 420, 87

Zinn, R. 1980, ApJS, 42, 19

Zinn, R. 1993, The Globular Cluster-Galaxy Connection, 48, 38

Zinn, R., & Dahn, C. C. 1976, AJ, 81, 527

Zinn, R., & West, M. J. 1984, ApJS, 55, 45

Zucker, D. B., et al. 2006a, ApjL, 643, L103

Zucker, D. B., et al. 2006, ApjL, 650, L41